THE UNIVERSITY OF
SYDNEY

OVERCOMING PRIMARY AND ACQUIRED ERLOTINIB RESISTANCE WITH EPIDERMAL GROWTH FACTOR RECEPTOR (EGFR) AND PHOSPHOINOSITIDE 3-KINASE (PI3K) CO-INHIBITION IN PANCREATIC CANCER

SUBMITTED IN FULFILLMENT OF THE REQUIREMENTS

FOR ADMISSION TO THE DEGREE

DOCTOR OF PHILOPSOPHY

UNIVERSITY OF SYDNEY

MATTHEW H WONG (311260888)

SYDNEY MEDICAL SCHOOL

Sep 2015

DEDICATION

This thesis is dedicated to my wife Wendy Ho; my two beautiful daughters, Tiffany and Nadia Wong; and to my parents, Andy and Tammy Wong for their love, faith and patience these three years as I pursue the challenges of post-graduate research.

DECLARATION AND CONTRIBUTION

The work in this thesis was performed by the candidate, except where due acknowledge has been made.

This work was undertaken at the Department of Cancer Surgery, Kolling Institute of Medical Research, The University of Sydney, Royal North Shore Hospital. I declare that no part of this work has been submitted previously for the purpose of obtaining a degree or diploma in any other universities.

The *in-vitro* work was independently designed and performed by myself (MW), with advice and assistance to methods development by supervisors and lab technicians. The *in-vivo* work was a group project undertaken by the whole of Cancer Surgery group. Planning of experiments, preparation of drugs and statistical analyses were independently performed by myself, the surgical and drug administration procedures were shared (AX, SJ, MW, RM); H&E was primarily undertaken by SJ and IHC undertaken by AX to maintain quality control, with some assistance provided by myself.

Matthew Wong

ACKNOWLEDGMENT

I would like to thank my Primary supervisor, **Professor Ross Smith**, for his guidance, supervision, support and funding for this research work to be completed. He is not only an outstanding researcher, but also a caring surgeon and a great friend. He always has time for his students, and he will strive his very best to make our dreams happen.

I also like to thank my co-supervisor **Professor Rob Baxter** for his guidance and advice throughout the planning and execution of this research project. His immense knowledge in the IGF1R and PI3K pathways and his many years of experience in research has helped me solidify my concepts and translate them into practice. I especially like to thank him for the many hours he put in to edit my research to publication qualities for conference and the Clinical Cancer Research paper.

I very much thank my co-supervisor **A/Professor Nick Pavlakis** for his many years of support of me as his advanced trainee, research fellow and now staff specialist in Medical Oncology. His expertise and experience in Medical Oncology, Clinical Trials and his associations with Core research groups and pharmaceutical companies have been instrumental to the progress of this research work, and I thank him for the way I have become as a researcher, as a doctor and as a person.

A special thanks extends to my co-supervisor **Dr. Aiqun Xue**, for the countless hours she has put in to develop my research skills and laboratory skills, and help me design the appropriate experiments for this project. It must be tiring teaching a doctor with little previous research experience the basics of *in vitro* and *in vivo* experiments. I certainly could not achieve this research project without Aiqun's help.

I also like to thank **Dr. Sohel Julovi,** post-doc scientist in our CanSur Research Group. His help and assistance to the directions of my project is much appreciated. I particularly like to thank his help in the designing, planning and teaching me in regards to the animal experiments.

I would like to give a special thanks to **A/Prof Jas Samra**, a great teacher, pancreatic surgeon and partner in pancreatic cancer research. His help with the animal studies and providing the surgical specimen are most crucial to the success of this large scale *in vivo* study. I thank him for the constant support and advice he gives me for the pancreatic cancer patients whom I share care.

I also need to thank **Dr Tom Hugh**, our liver surgeon and great teacher in upper GI research. I thank him for his constant support of me and my project, and the great lengths of time he put in for assisting with grant applications.

Here I should express my appreciation to **Mr. Lyndsay Peters,** the manager for the flow cytometer in Kolling Institute. I thank him for his expert advice and assistance for the operation of the flow cytometer, which has occupied much of my research and time in the first 2 years of my study.

I also thank **Dr. Sergey Kurdyukov**, the manager for confocal microscopy and genomic facility. His assistance is vital for ensuring the quality of my research with immunofluorescence and PCR.

I also like to thank **A/Professor Anthony Gill**, head of Cancer diagnosis and pathology, for his valuable assistance and advice on surgical pathology, histopathology and immunohistochemistry, which is crucial to this project.

I like to thank **Dr. Mike Lin** very much for his support and advice in many of my *in vitro* experiments, particularly the confocal microscopy and western blotting techniques.

I would like to thank **Joy McPherson**, secretary of Professor Ross Smith, who has looked after me for many years before me undertaking research. I thank her for her for organising meetings and her involvement in the many funding functions for CanSur.

I greatly appreciate my funding partners: **Amgen Research Scholarship, Royal North Shore Staff Specialist Scholarship, Ramsey Scholarship, Pink Ladies and Cancer Surgery Foundation, and CanSur**. Without them I would not be able to complete this project within the 3 year time frame.

I also like to thank **Novartis Pharmaceuticals** for providing BYL-719 and BEZ-235 targeted therapies, and their assistance for my clinical trial proposal.

TABLE OF CONTENTS

SUMMARY

Pancreatic ductal adenocarcinoma (PDAC) is a deadly disease with multiple genetic aberrations and limited treatment options, with EGFR inhibitor erlotinib being the only clinically proven targeted therapy with marginal benefit in survival when combined with gemcitabine. Better targeted treatment strategies as well as predictive biomarkers remain unmet needs for clinical research in pancreatic cancer. This study first explores the protein and genetic mechanisms of primary (*de novo)* and acquired erlotinib resistance in PDAC using 5 primary PDAC cell lines as well as 2 sub-cultured erlotinib resistance lines. It then utilizes multiple *in vitro* assays and synergy analyses to examine 4 horizontal combined blockade combinations of the Epidermal Growth Factor Receptor (EGFR)/ Insuling Growth Factor Receptor (IGF1R), EGFR/ Phosphoinositide 3-kinase (PI3K), EGFR/ PI3K/ mammalian target of rapamycin (mTOR) and Methyl ethyl ketone (MEK)/ PI3K/mTOR tyrosine kinase inhibitors (TKI). Finally, the study took the two best combinations and established its pre-clinical efficacy using two robust *in vivo* primary patient xenograft models.

In summary, this project found that the PI3K/Akt/mTOR (PAM) pathway was over-expressed in primary erlotinib resistance, and was further over-activated via the downstream mTOR pathway in acquired erlotinib resistance. This occurred in both genetic and protein expression levels. This, in turn, suggested that combined blockade of EGFR and PAM pathway could possibly overcome erlotinib resistance. Indeed, the combined blockade of these two pathways significantly down-regulated downstream signalling of each pathway more than each drug alone. Erlotinib (ERL) acts synergistically with PI3Kα inhibitor BYL-719 (BYL) and dual PI3K/mTOR inhibitor BEZ-235 (BEZ), with superior effect observed in downstream compared to upstream blockades. Of note, treatment of erlotinib resistant cell lines with PI3K inhibitor-based combination caused significant G1 cell cycle arrest, inhibition of colony formation, and

necrosis and apoptosis, more so compared to parent cell lines. Erlotinib plus BYL (PI3Kα inhibitor), and erlotinib plus BEZ (dual PI3K/mTOR inhibitor) were taken forward to *in-vivo* study. In primary patient-derived tumor subrenal capsule and subcutaneous xenografts, Erlotinib plus BYL significantly reduced tumor volume (P=0.005). Strong pEGFR and pAkt immunostaining (2+/3+) was correlated with high and low responses respectively to both erlotinib and erlotinib plus BYL.

Overall, the research project has been successful in demonstrating the efficacy of co-inhibition of EGFR/ PI3K pathway in PDAC, and is leading to an ongoing phase I/ II study proposal of erlotinib plus BYL in metastatic PDAC in second-line setting. Importantly, this study captured the principle of oncogenic dependence or addiction. Despite their molecular and genetic heterogeneity, PDAC cells appear to have a propensity to escape and depend on a specific pathway (PI3K/Akt) in the face of drug pressure (erlotinib), which renders them hypersensitive to EGFR/PI3K co-inhibition. This suggests that oncogenic dependence can be targeted, and identifies pEGFR and pAkt as candidate biomarkers for further translational research. This may be a step in advance in personalising treatment for up to 70% PDAC patients with over-activated PAM pathway.

LIST OF PUBLICATIONS

Original Paper, Clinical Cancer Research

Wong M, Xue A, Julovi S, Pavlakis N, Samra J, Hugh T, Gill A, Peters L, Baxter R and Smith R. Co-targeting of epidermal growth factor receptor (EGFR) and PI3K overcomes PI3K/Akt oncogenic dependence in pancreatic ductal adenocarcinoma. Clinical Cancer Research, published online June 3, 2014. URL at http://clincancerres.aacrjournals.org/content/early/2014/05/31/1078-0432.CCR-13-3377.abstract

Original Paper, submitted to Pancreatology

Xue A, Julovi S, Hugh T, Samra J, **Wong M**, Gill A, Toon C, and Smith R. Establishment of patient-derived subrenal capsule xenografts of pancreatic cancer in NOD/SCID mice: potential models for guidance of gemcitabine responsiveness (submitted to pancreatology)

Australasian Pancreatic Club Annual Meeting 2012 (Oral)

Adelaide, 2012

Wong M, Xue A, Julovi S, Pavlakis N, Samra J, Hugh T, Gill A, Peters L, Baxter R and Smith R. EGFR/ PI3K co-inhibition in pancreatic ductal adenocarcinoma model.

Australasian Pancreatic Club Annual Meeting 2012 (Oral)

Adelaide, 2012

Wong M, Xue A, Julovi S, Pavlakis N, Samra J, Hugh T, Baxter R and Smith R. PI3K and EGFR co-targeting in pancreatic ductal adenocarcinoma: integrating novel drug and biomarker discovery in a phase Ib/ II clinical trial with a biomarker feasibility sub-study.

Australasian Pancreatic Club Annual Meeting 2012 (Oral)

Adelaide, 2012

Xue A, Hugh T, Samra J, Julovi S, Gill A, Toon C, Sioson L, **Wong M**, and Smith R. Establishment of patient-derived tumour xenografts of pancreatic cancers: potential models for drug response of personalised chemotherapy.

Australasian Gastro-Intestinal Trial Group Meeting (Oral and Poster)

Sydney, 2012

Wong M, Lee A, Hugh T, Maher R, Harrington T, Pavlakis N. Post-treatment: pre-treatment Alpha-Feto Protein (AFP) ratio as a predictive marker for Trans-Arterial Chemo-Embolization (TACE) therapy in Hepatocellular Carcinoma (HCC).

28th Annual RNSH UTS USYD SRM (Poster)

Sydney, 2012

Julovi S, Xue A, Hugh T, Samra J, Gill A, **Wong M**, Supramaniam S, Moghaddam M and Smith R. Apolipoprotein A-I improves the uptke of lipid by pancreatic cells in culture and pancreatic cancer tissue engrated in subrenal capsule of NOD/SCID Mice. RNSH/UTS/ USYD SRM; O100

27th Annual RNSH UTS USYD SRM (Oral and Poster) ***Sydney, 2011***

Wong M, Xue A., Baxter R. et al. Synergy with combined IGF1R/ EGFR inhibitors and upregulation of akt as a possible resistance mechanisn in pancreatic cancer in vitro". 28th RNSH/UTS/ USYD SRM; O19: 33

Australia/ Asia Pacific Clinical Oncology Research Development (Oral)

Sunshine Coast, 2010

Wong M and Pavlakis N. Figitumumab (Fig, CP-751,871) and the pan-HER inhibitor PF-00299804 (PF) as treatment of progressive metastatic pancreatic adenocarcinoma (mPA) following first line chemotherapy.

ABBREVIATIONS

AEW	NVP-AEW541
AIHW	Australian Institute of Health and Welfare
ANOVA	Analysis of Variance
ATCC	American Type Culture Collection
BYL	NVP-BYL719
BEZ	NVP-BEZ235
CF	Cystic Fibrosis
CI	Confidence Interval
CRC	Colorectal Cancer
Ct	Threshold Cycle
CV	Coefficient of Variation
CB	Combined blockade
EGF	Epidermal Growth Factor
EGFR	Epidermal Growth Factor Receptor
EMT	Epithelial-Mesenchymal Transition
ER	Erlotinib resistant
ERL	Erlotinib
FBS	Fetal Bovine Serum
FISH	Fluorescence In-Situ Hybridisation
G1	Grade 1, well differentiated
G2	Grade 2, moderately differentiated

G3	Grade 3, poorly differentiated
GBM	Glioblastoma Multiforme
H&E	Haematoxylin and Eosin
Hh	Hedgehog pathway
IC_{50}	Half maximal Inhibitory Concentration
IGF	Insulin-growth Factor
IGF1R	Insulin-growth Factor-1 receptor (IGF1R) up-regulation
IHC	Immunohistochemistry
JAK	Janus Kinase
MW	Molecular Weight
kDa	Kilo Dalton
mTOR	Mammalian Target Of Rapamycin
MAPK	Mitogen-Activated Protein Kinase
MEK	Methyl ethyl ketone
NSCLC	Non-small Cell Lung Cancer
NT	No treatment
OS	Overall Survival
PAM	PI3K/ Akt/ mTOR pathway
PD	PD-98059
PDAC	Pancreatic Ductal Adenocarcinoma
PDTT	Patient Derived Tumour Tissue
PFS	Progression Free Survival
PI3K	Phosphoinositide 3-kinase

PPE	Personal Protective Equipment
PV	Proportional Viability
qRT-PCR	Quantitative Real Time Polymerase Chain Reaction
RR	Response Rate
RT	Reverse Transcription
SB	Single Blockade
SEM	Standard of the Mean
SI	Synergy Index
SHh	Sonic Hedgehog
SPF	S-Phase Fraction
STAT	Signal Transducer and Activator of Transcription
T_m	Temperature of melting
TKI	Tyrosine Kinase Inhibitor
TTF	Time to Treatment Failure

List of Tables

Chapter 1

Chapter 2

Chapter 3

Chapter 4

Chapter 5

Chapter 6

List of Figures

Chapter 1

Chapter 2

Chapter 3

Chapter 4

Chapter 5

Chapter 6

CHAPTER 1:

LITERATURE REVIEW

1.1 Epidemiology of Pancreatic Cancer

1.1.1 Incidence and Survival

Worldwide, pancreatic cancer is the 12th most common cancer, with an age-standardised rate of 4.4 / 100,000 people. The incidence of pancreatic cancer is almost 3 times higher in the developed countries than under-developed countries, with standardised rate if 10.7/ 100,000 in Australian and 12.2/ 100,000 in the United States.[2,3] In Australia, the incidence rate of pancreatic cancer is steadily increasing over the last 30 years. Crude incidence rate in Australia has increased by 50% from 6 per 100,000 (1972) to 11 per 100,000 people (2007), with 2546 patients diagnosed in 2009 **(figure 1.1)**. The increase in incidence trend is not simply a consequence of improved diagnostics. It has been hypothesised that the increased incidence may be related to the aging population, as well as the epidemic of smoking. Smoking in males peaked in 1940s and in females peaked in 1970s, and the long term effects are thought to affect pancreatic cancer incidence after a lag time of 30-40 years.[4]

Most pancreatic cancer patients have a short survival, such that mortality rate is almost equivalent to incidence rate worldwide (4.2/ 100,000). The resulting 5-year prevalence rate is relatively lower compared to other cancers, at 2.7/ 100,000.[5] In Australia, mortality trend also closely juxtaposes the incidence trend **(figure 1.2)**, with 2248 deaths in Australia in 2009.[4,6] Similarly, in the US over the last 70 years there is a steady rise in pancreatic cancer mortality proportional to incidence trends **(figure 1.3)**. Pancreatic cancer contributes to the top five causes of cancer mortality in Australia, with a 5-year relative survival of only 4.6%, and 75% of patients dead within 1 year of diagnosis.[2,4,6] Unfortunately, the poor prognosis has not changed over the years, with 5-year survival of 2% (1975-77), 3% (1984-86) and 5% (1996-2003).[7] With the little progress in treating this deadly cancer over the last half century, combined with the rising incidence of this disease, pancreatic cancer is becoming a serious public health problem.

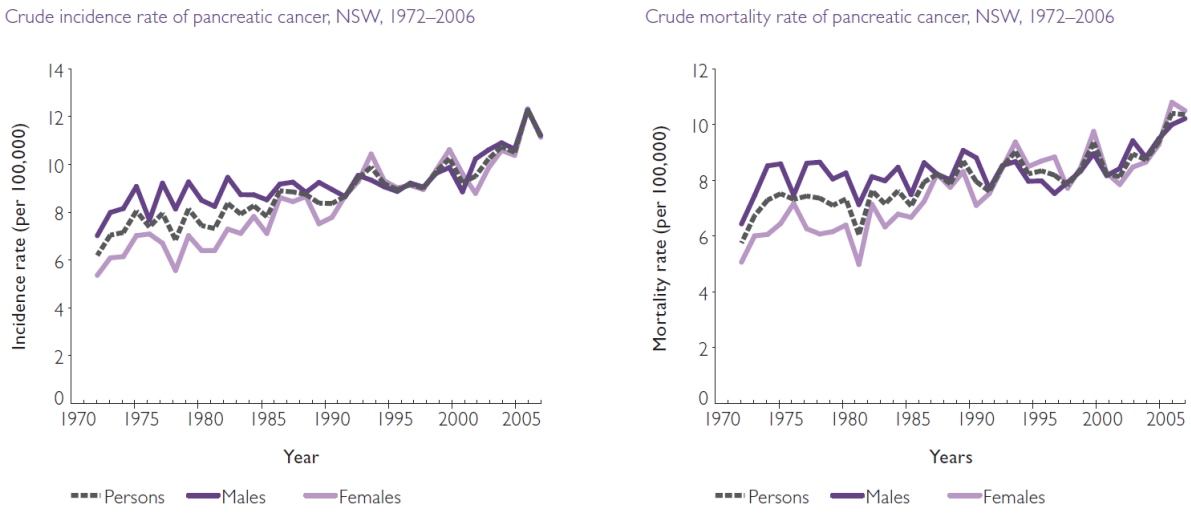

Figure 1.1: Crude incidence and mortality rates of pancreatic cancer, 1972-2006. From Creigton et al. (2010) Pancreatic Cancer in NSW.[4]

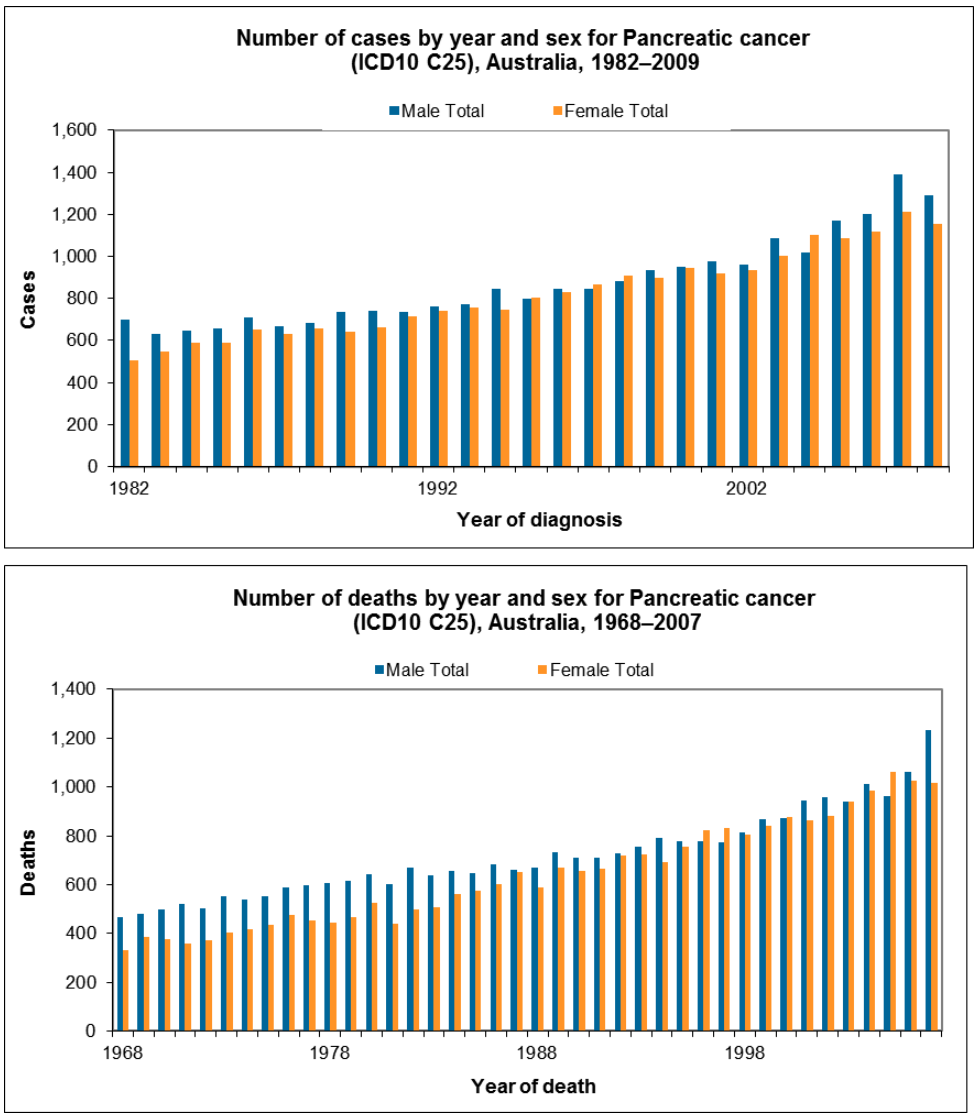

Figure 1.2: Number of pancreatic cancer cases and deaths by year by sex in Australia (2012) AIHW.[6]

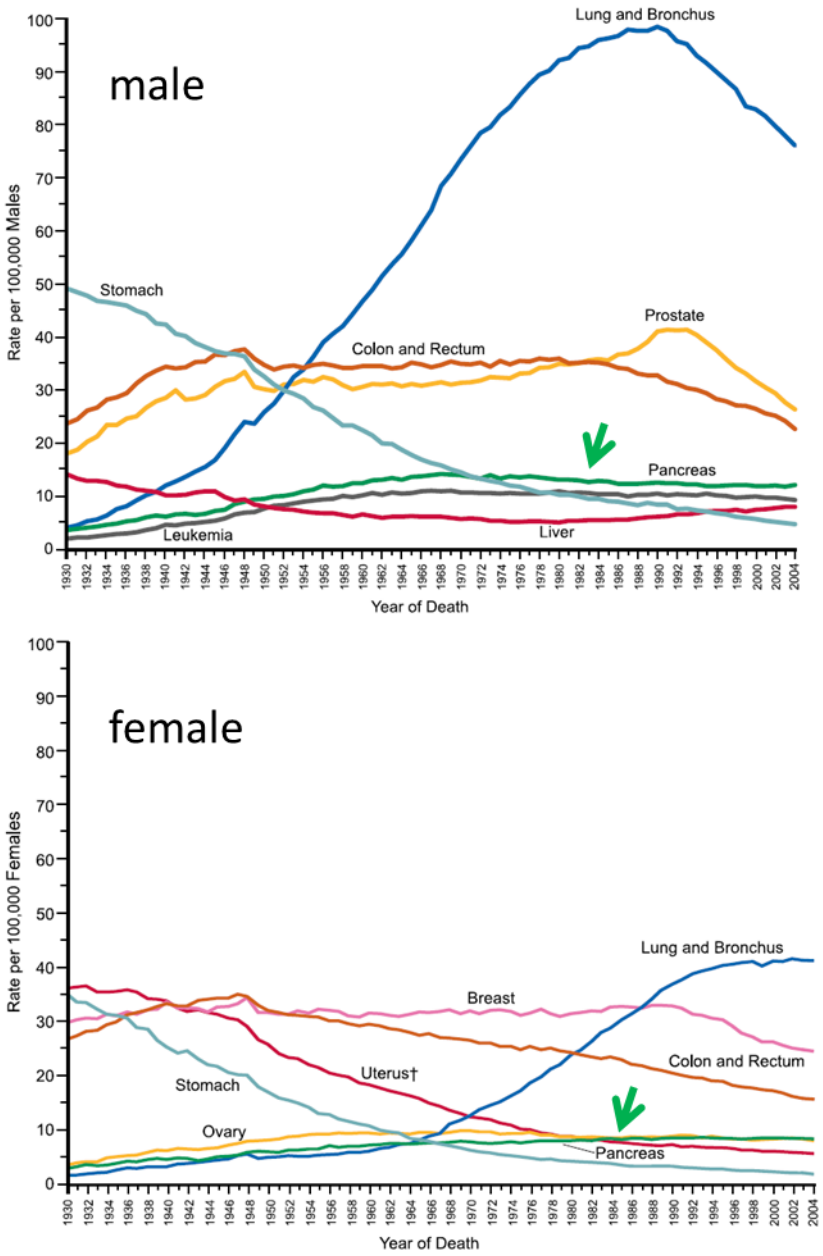

Figure 1.3: Age standardised mortality rate of selected cancers in males and females in US, 1930-2004. From Jemal et al. (2008) Global Cancer Statistics.[7]

1.1.2 Causes of Pancreatic cancer

The causes of pancreatic cancer have yet to be fully elucidated. However, there are a number of risk factors that may predispose to the development of pancreatic cancer.

Age and gender: The risk of pancreatic cancer increases with age. The median age of diagnosis of pancreatic cancer is 66 years old for males and 71 for females. The risk of men and women aged 80-84 years-old diagnosed with pancreatic cancer is 10 and 15 times higher than those aged 50-54 years-old, respectively **(Figure 1.4)**.[4] As well as being a risk factor, age is also an important prognostic factor. The mortality rate for the 80-84 year age group is 11 and 17-fold higher than the 50-54 age group **(Figure 1.4)**.[4] Pancreatic cancer more commonly affects males, which is particularly the case in developed countries **(Figure 1.5)**.[5] Males are found to have 30% higher incidence of pancreatic cancer than females. There is no strong evidence suggesting hormonal or reproductive factors are protective for women. On the other hand, the higher incidence in males is more likely due to smoking habits.[4]

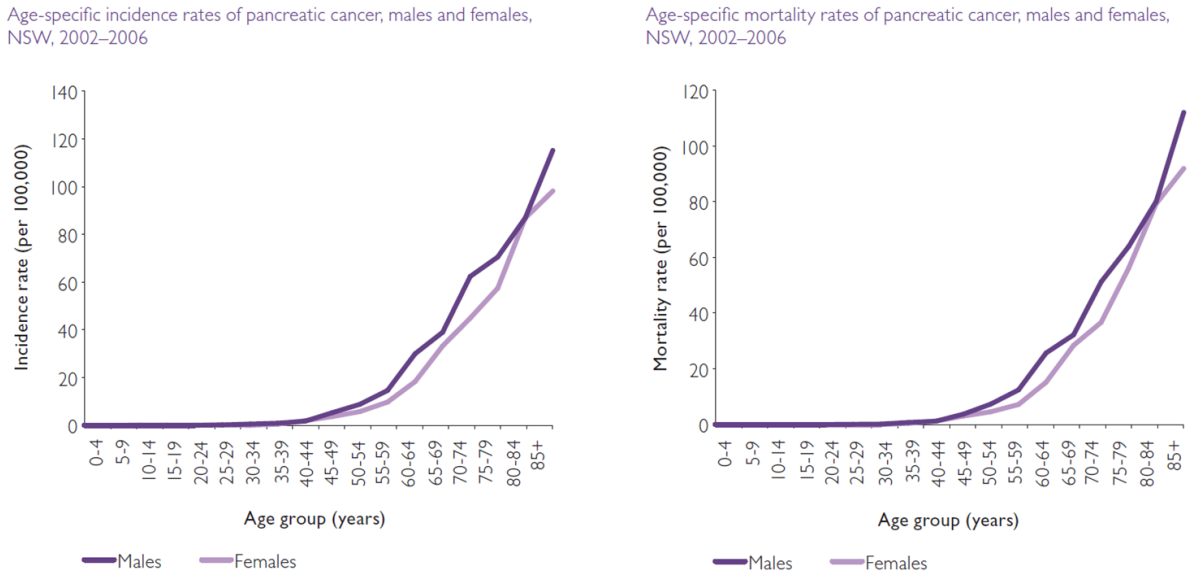

Figure 1.4: Incidence and mortality rates of pancreatic cancer by age in NSW. From Creigton et al. (2010) Pancreatic Cancer in NSW.[4]

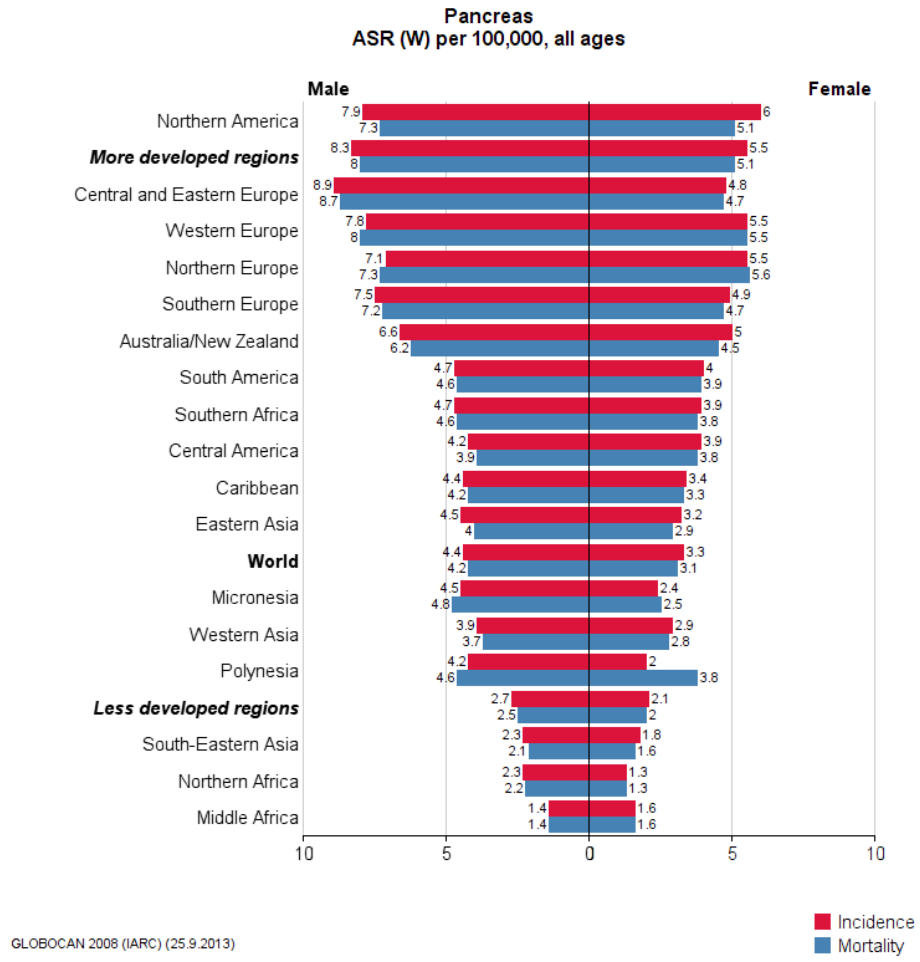

Figure 1.5: Incidence of Pancreatic Cancer worldwide. From GLOBOCAN (2008)[5]

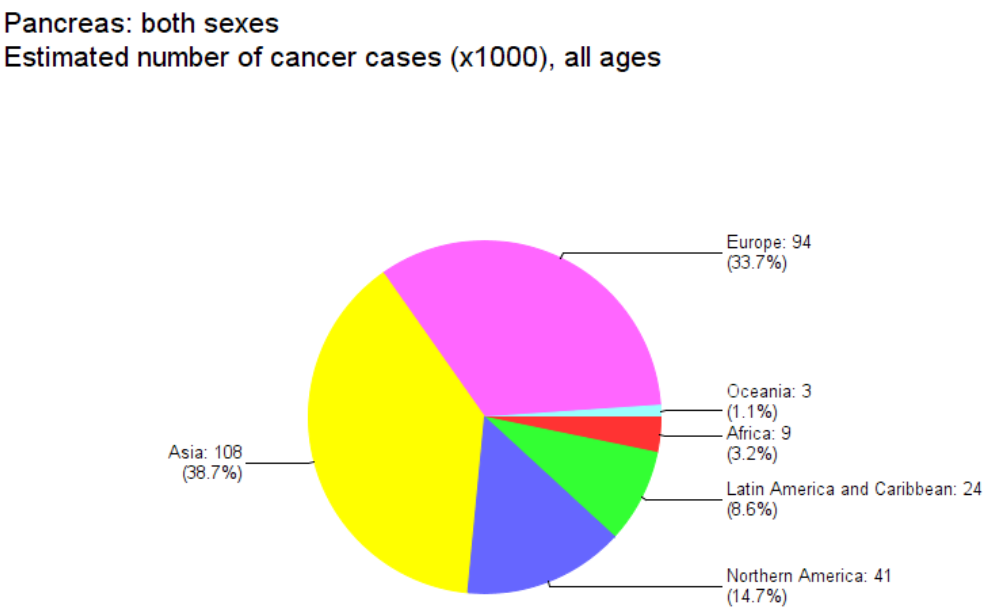

Figure 1.6: Incidence of Pancreatic Cancer by continents. From GLOBOCAN (2008)[5]

Geography and race: Pancreatic cancer has an uneven distribution around the world. By continents, Asia and Europe together contribute 70% of the burden of pancreatic cancer worldwide **(Figure 1.6)**. Approximately 60% of pancreatic cancer occurs in developed countries. The age standardised rates for males and females are 3 and 5 per 100,000 higher in developed than developing countries **(Figure 1.5)**.[5,8] Smoking habits in developed, industrialised countries over the last 3-4 decades have been attributed to the higher incidence of pancreatic cancer, but other factors may include genetic polymorphism by race and lower access to diagnostic facilities in underdeveloped countries.[9,10]

Hereditary factors: Pancreatic cancer is estimated to be inheritable in 5-10% of cases.[9] Hereditary pancreatitis is passed on in an autosomal dominant inheritance with incomplete inheritance. The risk of pancreatic cancer is increased by 50- to 60-fold, and is typically diagnosed in clusters of family with early onset pancreatic cancer (20 years old) [11,12] BRCA mutation carriers are also at risk of developing pancreatic cancer, with a 2-fold increase in risk for BRCA-1 and 3-4-fold increase in risk for BRCA-2 carriers. These patients present a decade earlier than those without family history, and have a male predominance of 2:1 ratio.[13]

Lifestyle risk factors: Smoking is clearly a risk factor for developing pancreatic cancer. A large cohort study in 1993 of 17,633 men found a dose-response effect of smoking, with a 4-fold higher risk for current heavy smokers (RR 3.9, CI= 1.5- 10.3).[14] In Australia, the cancer prevention study by the Australian Institute of Health and Welfare (AIHW) found that both male and female smokers had a 2.3-fold relative risk of developing pancreatic cancer, with a population attributable risk of 17% and 12% respectively.[15] No difference is found between tobacco smokers or chewers, suggesting that pancreatic cancer is caused by both ingesting and inhaling tobacco.[16] Consumers of more than 10 alcohol units per month were also found to have an increased risk of pancreatic cancer, by 3-fold.[14] It is currently thought that alcohol only becomes a risk factor if it leads to chronic pancreatitis.[17] The role of diet has been extensively investigated in pancreatic cancer. Caloric restriction and antioxidants have been suggested to confer a protective effect, but the challenge has been the difficulty validating

these in large-scale cohort studies and obtaining accurate diet exposure data.[9,18] Insulin resistance or diabetes may increase the risk of pancreatic cancer, but may also be secondary to pancreatic cancer, so it is unclear at this stage whether it is a true causative factor.[17]

Chronic pancreatitis: Chronic pancreatitis, like other chronic inflammatory conditions such as chronic gastritis, has been implicated as a precursor to pancreatic cancer. Probably less than 5% of pancreatic cancer is attributed to chronic pancreatitis.[19] Chronic pancreatitis may be related to chronic alcoholism, cystic fibrosis; but can be hereditary or idiopathic.[9] Patients with alcoholic or idiopathic pancreatitis have a 15-fold increased risk of pancreatic cancer.[19]

Overall then, after taking into account of the attributable risk factors of smoking (10-15%), chronic pancreatitis (5%) and family history (5-10%), there still remain 70-80% of cases where no apparent causes are found. There is therefore an urgent need to understand more about the aetiology and biology of this very aggressive tumour type.

1.2 Tumour Biology in Pancreatic cancer

1.2.1 Multiple genetic alterations in Pancreatic cancer

For a long time, it has been known that pancreatic ductal adenocarcinoma is one of the most complex cancers with extensive genetic and molecular alterations.[20,21] Chromosomal aberrations are more complicated than those of other cancer types, with losses in multiple chromosomal arms including 1p, 3p, 4q, 6q, 8p, 9p, 12q, 17q, 18q and 21q as well as gains in 8q and 20q.[22] As well as these, loss of heterozygosity (LOH) has also been identified between 6q and 17p, 12q and 18q, and 12q, 17p and 18q.[23] On the gene level, significant alterations have been detected in oncogenes (K-Ras), tumour suppressor genes (P53, P16, DCC), over-expression of growth factors (EGF, TGF, FGF) and their receptors (EGFR, TGF-

β receptors).[21] Some of these- K-Ras, GNAS, telomere shortening- are identified early in the pancreatic carcinogenesis pathways; while others such as P53, SMAD4 loss and inactivation of DUSP6 are later events **(Figure 1.7)**.[23,24] Telomere shortening and reduction in signal, in particular, has been demonstrated in 96% of pancreatic intraepithelial neoplasia (PanIN), but not in inflammatory or atrophic lesions, suggesting it as one of the earliest events in pancreatic carcinogensis.[25] Furthermore, epigenetic alterations involving methylation-induced silencing of biologically relevant genes are also common in pancreatic cancer. Among these are silencing of P16 (14-33% of cases), Hedgehog interacting protein (40-50%) and SPARC (88-94% of cases).[26]

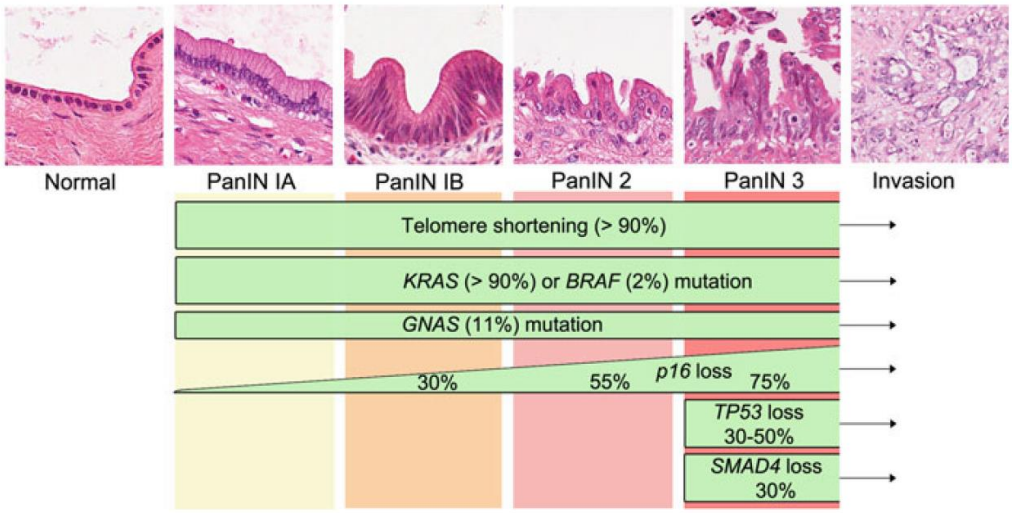

Figure 1.7: Pancreatic carcinogenesis. From Simone and Maitra (2013) Molecular genetics of Pancreatic cancer.[24]

To unravel the complexity of cancer genome, the International Cancer Genome Consortium (ICGC) was set up in 2008 following the launch of the Cancer Genome Project in UK and The Cancer Genome Atlas in US. This is a large-scale global initiative that aims at identifying a full range of somatic mutations and high-definition cataloguing of genomic abnormalities in 50 different cancer types.[27] The pancreatic cancer arm of the ICGC has been led by a network of institutions in Australia and Canada. The Australian Pancreatic Cancer Genome Initiative (APGI) currently has 11 active clinical sites and over 150 clinical and scientific staff involved.

It has been tasked with the prospective accrual of 400 patients with primary resected tumours and performing deep genome sequencing with complete clinical annotation. Additional integrated projects that arise from this global program include xenograft experiments, pathway analyses, epidemiological and clinical trial programs such as the IMPaCT trial.[27,28]

In a seminal paper published in Nature, Biankin *et al.* published the first 142 cases of the APGI program.[29] By using a combination of deep sequencing and capturing system on 142 stage I and II PDAC and correlating these information with detailed clinical-pathological phenotypes –of which 99 had adequate cellularity to be informative, the group identified 16 significantly mutated genes, including some known mutations (*K-Ras, P53, CDKN2A, SMAD4, MLL3, TGFBR2, ARID1A and SF3B1*); and uncovering novel mutations in chromatin modification (EPC1, ARID2), DNA damage repair (*ATM*), and axonal guidance genes (*ROBO2, 3*). Importantly, the detailed analysis identified 2016 non-silent mutations and 1628 copy-number variations with an average of 26 mutations detected per patient, suggesting substantial heterogeneity **(table 1.1)**.[29] Using two independent sleeping beauty mutagenesis models and a short hairpin RNA (shRNA) screen, the investigators further confirmed the functional relevance of *K-Ras, P53, CDKN2A* and *SMAD4* mutations, implying their putative roles as driver mutations. The pathways identified to be significant included G1/S checkpoint, apoptosis, angiogenesis and TGF-β signalling in this study.[29]

Mutations in pancreatic ductal adenocarcinoma ($n = 99$)

Mutation class	Total
Missense	1,684
Nonsense	99
Splice site	89
Insertion/deletion	144
Non-silent	2,016
Silent	611

Table 1.1: mutations found on genome wide sequencing of 99 patients. From Biankin (2012) Pancreatic cancer genomes reveal aberrations in axon guidance pathway genes.[29]

As for metastatic pancreatic cancer, genomic signature is less known, possibly because of the challenges in acquiring sufficient tissue for fine needle aspirate (FNA) or endoscopic ultrasound (EUS) biopsy. Campbell *et al.* was able to sequence multiple metastases from 10 PDAC patients by means of autopsy study, and they found that it had a distinctive pattern of genomic instability characterised by deletions (22%) and fold-back inversions (16%).[30] This, in turn, suggests that a significant disruption in the G1-S cell cycle and repair mechanism.[30] In another study from Nature, Yachida's group studied both the primary and secondaries of 8 pancreatic cancer patients at autopsy. They found that all parental clones already accumulated the common driver ("founder") mutations (*K-Ras, P53, SMAD4*); and metastases had additionally acquired 20-30 highly varied passenger ("progressor") mutations.[31]

1.2.2 Clonal heterogeneity, driver mutations and actionable targets

Gene sequencing studies have thus far identified the extreme complexity of pancreatic cancer. To complicate further, cancer is increasingly recognised as an evolutionary process. The concept of clonal heterogeneity was actually proposed in 1976, and described the evolutionary process where clones acquire "successive somatic mutations that allow for sequential selection of fitter subclones" **(Figure 1.8)**.[32] However, it is only until now when single cell sequencing technologies become available that this concept can be tested. A number of major studies with deep sequencing multiple tissues from the same patient/ cell line have been published in the last few years, and they invariably identified significant variations arising in subclonal populations from a single cancer cell.[30,31,33-35] In the most famous publication from Nature, Swanton's group performed multiple gene sequencing on 8-10 core biopsy sites of nephrectomy and metastatectomy specimen in 4 renal cell carcinoma patients. They identified 128 somatic mutations by multi-region sequencing, but only 40 of which (or 31%) could be detected across all regions. In addition, 26 of the 30 tumour sampling specimens had divergent

allelic-imbalance profile, and ploidy heterogeneity was also observed. This suggested that there was extensive intra-tumoural heterogeneity, and that a single biopsy could only capture 55% of all mutations detected in the entire tumour.[35] The issue of intra-tumoural heterogeneity therefore poses a considerable challenge to the use of targeted therapies, because the decision to targeted treatment often hinges on the concept of discovering "actionable targets" from limited core or FNA biopsy, which may not represent the whole picture if there is significant intra-tumoural heterogeneity.[32]

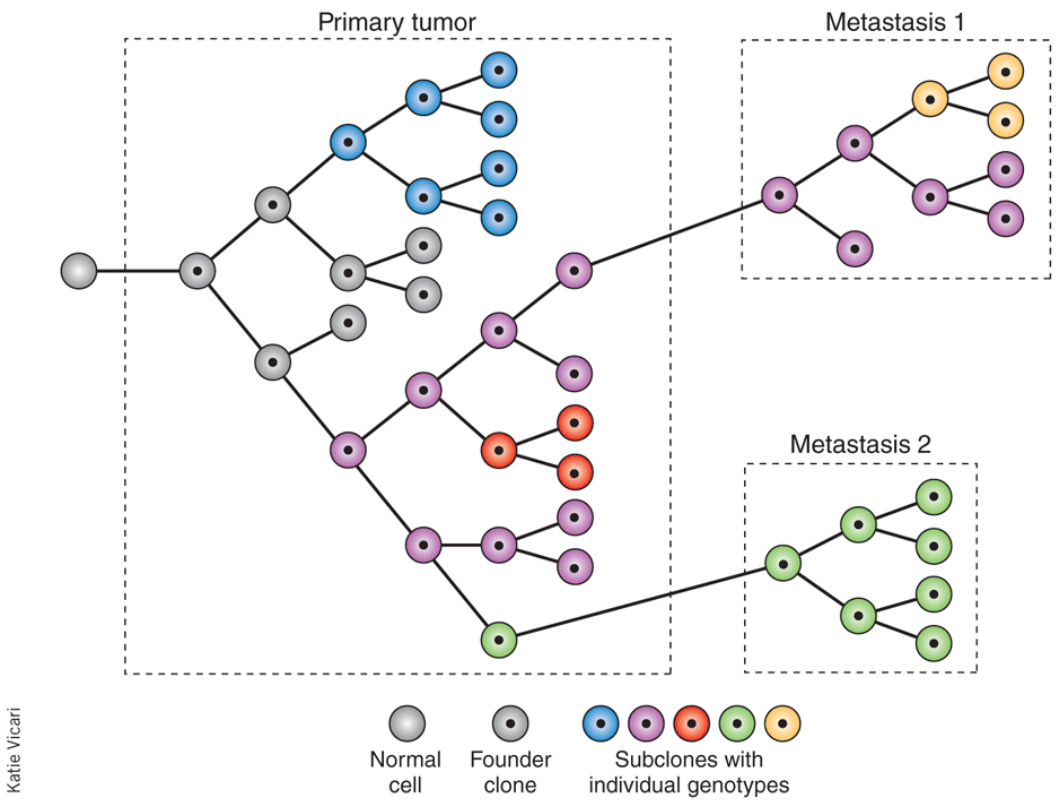

Figure 1.8: clonal expansion in primary and metastatic tumour. From Caldas (2012) Cancer sequencing unravels clonal evolution.[32]

Whilst intra-tumoural heterogeneity may be challenging, it "may not be insurmountable barrier to cancer therapy if treatments can be designed to target mutations present in all cells".[32] There is now a plethora of literature demonstrating the significance of "founder or driver mutations". In Campbell *et al*'s study, eight rearrangements were found in all PDAC metastases of one patient and not in the primary tumour.[30] In Yachida's study, the vast majority

of homozygous mutations (89%) already existed in the parental clone of PDAC, and deleterious mutations were more commonly found in parent than subclones (12.6% vs. 8.1%).[31] These findings have significant therapeutic implications. Whilst extensive gene alterations make it difficult to differentiate “driver mutations” from “passenger mutations”,[36] there is an intrinsic order to these genetic alteration; clonal ordering can be tracked by phylogenetic tree, and suggests that identifying common mutations at the trunk of the phylogenetic tree to be a strategy to develop more robust biomarkers and therapy.[35]

Importantly, these driver mutations can now be mapped to distinctive molecular pathways by means of integrative genomic analyses platforms.[37-39] In fact, by means of complex bioinformatics models, the Cancer Genome Atlas network has now catalogued 291 high-confidence drivers among 11 tumour types. Only 2 high-confidence genes (*P53* and *PIK3CA*) and 51 other gene have protein affecting mutations universally in more than 10% of pan-cancer samples. Of note, these genes are found to originate from 5 distinct pathways: chromatin remodelling, mRNA processing, cell signalling/ proliferation, cell adhesion and DNA repair/ cell cycle.[38] Using this approach, a median of only 4 protein affecting mutations is found among the 11 cancer types, where at least 1 of these are high confidence genes in 94% of tumour types.[38] In other words, in most tumour types there are potentially many gene mutations, some driver mutations but only a few protein-affecting mutations; and these are probably the real actionable targets that matter.

In summary, with the rapidly expanding field of genomics science propelled by the advent of gene sequencing and bioinformatics technology, we are only beginning to understand the extensive tumour complexity and heterogeneity. Yet, within these considerable changes, gene mutations occur in an orderly evolutionary process, and protein-affecting mutations are likely finite. Importantly, these genetic changes appear to conform to common molecular pathways. This suggests that studying specific pathway activation to determine actionable targets may be a more optimal strategy to overcome a disease with such extensive genetic alterations.

1.2.3 Core molecular pathways in pancreatic cancer

In the early 2000s, K-Ras, CDKN2A/P16, P53 and SMAD4 have been identified as the core molecular pathways in pancreatic ductal adenocarcinoma, also known as the "big 4 mountains of the genomic landscape.[20,24,40] Through the advances in gene sequencing and bioinformatics technology, 12 core biological pathways are now identified as core signalling in PDAC **(Figure 1.9)**.[24,41] Importantly, many of these pathways are well-established hallmarks of cancer as identified by Hanahan and Weinberg.[42] It is impossible for this thesis to cover the scope of all the core signalling pathways. Thus, only the pertinent signalling pathways will be described here.

Growth Signalling (K-Ras and PI3K): Ras/Raf/MEK/ERK and PI3K/PTEN/Akt/mTOR pathways are signalling cascades of phosphorylating kinases that play critical roles in cancer growth and proliferation.[43] K-Ras is an important member of a multi-gene Ras family (Ki-Ras, N-Ras, H-Ras), and is particularly important for PDAC carcinogenesis. It has been shown that K-Ras somatic mutations (usually at codon 12, 13 or 61) are present in increasing rates in advanced stages of pancreatic intra-epithelial neoplasia (PanIN)- the precursor of PDAC- from 30-38% (PanIA), 31-44% (PanIB), 73% (PanIN2) to 83% (PanIN3); and are prevalent in over 90% of PDAC.[20] Furthermore, K-Ras is also responsible in promoting and continuing tumour growth. K-Ras activates downstream signalling Raf (B-Raf, Raf-1, A-Raf), ERK and MEK.[43] Activated ERK can translocate into cell nucleus, regulate transcription factors, altered gene expression with the end results of promoting cell growth **(Figure 1.10)**. This so-called mitogenic-activated protein kinases (MAPKs) pathway is constitutively activated by mutated K-Ras through the intrinsic binding of GTPs.[23] K-Ras codon 12 mutation has been shown to be negatively prognostic in advanced PDAC, predicting for higher stage, liver metastases and a survival of 3.9 (K-Ras mutant) versus 10.2 months (K-Ras wild type) (HR 7.39, $P<0.001$).[44]

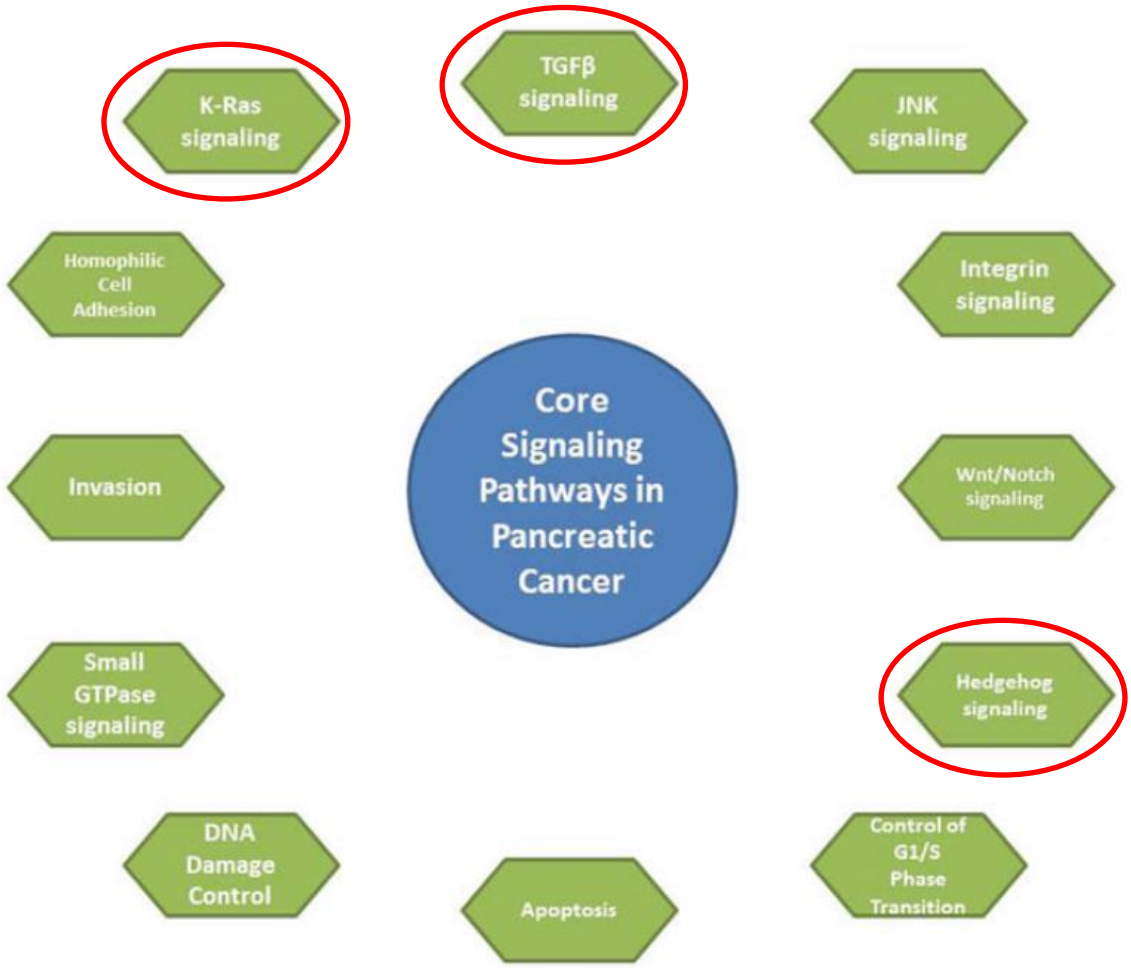

Figure 1.9 Core signalling pathways in pancreatic cancer. From Simone and Maitra (2013) Molecular genetics of Pancreatic cancer.[24] *The highlighted pathways will be described in more detail.*

PI3K/Akt/mTOR –often abbreviated as the PAM pathway- are an integral pathway in cell growth and survival, responsible for important cellular functions such as protein synthesis, cell cycle progression, proliferation and survival.[45,46] In cancer, multiple components of the pathway is known to be disrupted, including *PIK3CA, AKT, PTEN* mutations, *PIK3CA, AKT1, AKT2* gene amplifications, and loss of tumour suppressor gene expression (*PTEN*).[47] The PI3K family consists of three classes. Class I PI3-kinase is highly over-expressed in 70% of pancreatic ductal adenocarcinoma.[48] Class I PI3K isoforms are activated by interacting with Ras and p85 regulatory units.[45] Once activated, PI3K catalyses the transformation of phosphatidylinositol 4,5-bisphosphate to phosphatidylinositol 3,4,5-trisphosphate, which in turn recruits PKB/Akt to the cellular surface. Akt is activated by dual binding of PDK1 to Thr308

and PDK2 to Ser473 regulatory binding sites, which in turn relieves the inhibitor effect of TSC-1 and TSC-2 on mTORC-1 and -2 complexes. mTORC-1 complex is one of the major components of the translational machinery in cancer. It up-regulates direct downstream S6 and 4EBP-1, which are intricately involved in cell cycle and mRNA translation.[49,50] Other downstream signals activated by the PI3K/Akt system include GSK-3, cyclin-D1, Forkhead and BAD, which together regulate a wide range of cellular processes **(Figure 1.10)**.[45,51,52] PI3K, particularly the class IB isoform (p110γ) is over-expressed in 70% of PDAC.[48] Akt, the direct downstream signal of the PI3K complex, is also consistently activated in PDAC cell lines.[53] Close to half of PDAC patients had high total Akt-2 (43%) and phosphorylated Akt (46%) in a study of 65 patients.[54] High pAkt expression has also be shown to be an independently negative prognostic marker, with 5 year survival of 57% for patients with low pAkt expression in the tumour versus 14% for those with high expression ($P<0.05$).[54]

Critical to the function of these two pathways is the myriad of upstream regulators including epidermal growth factor receptor (EGFR), insulin growth factor receptor (IGF1R) and many others (HGF, HER2, HGF, VEGF-R, PDGF-R, Kit); as well as the significant interaction at multiple levels of these signalling pathways.[43,47] EGFR is involved in an autocrine positive feedback loop with the Ras and Raf, as well as the PAM pathway leading to altered transcription of genes such as HCCR.[55,56] Whilst EGFR mutation is rare (<5%) and typically silent in PDAC, it is over-expressed in >40% of PDAC.[57-60] IGF1R, on the other hand, is over-expressed in 50% of PDAC[61], and it also mediates growth and survival via both MAPK and PAM pathways.[62] Importantly, cross-talks have also been demonstrated between these cell surface receptors,[61,63] possibly through EGFR-IGF1R heterodimerization or survivin expression.[64] Cross-talks also exist on multiple levels between the MAPK and PAM pathways, with interactions reported for K-Ras/ GSK3β (a downstream effector of Akt), K-Ras/ PTEN via TGF-β, and K-Ras/ PI3K and PDK1.[65-68] The multiple interactions and feedback loops certainly add a layer of complexity to the biology of these pathways, and suggest that these signalling

cascades should be viewed as a “signalling network” rather than a “simple linear, unidirectional cascade”.[56]

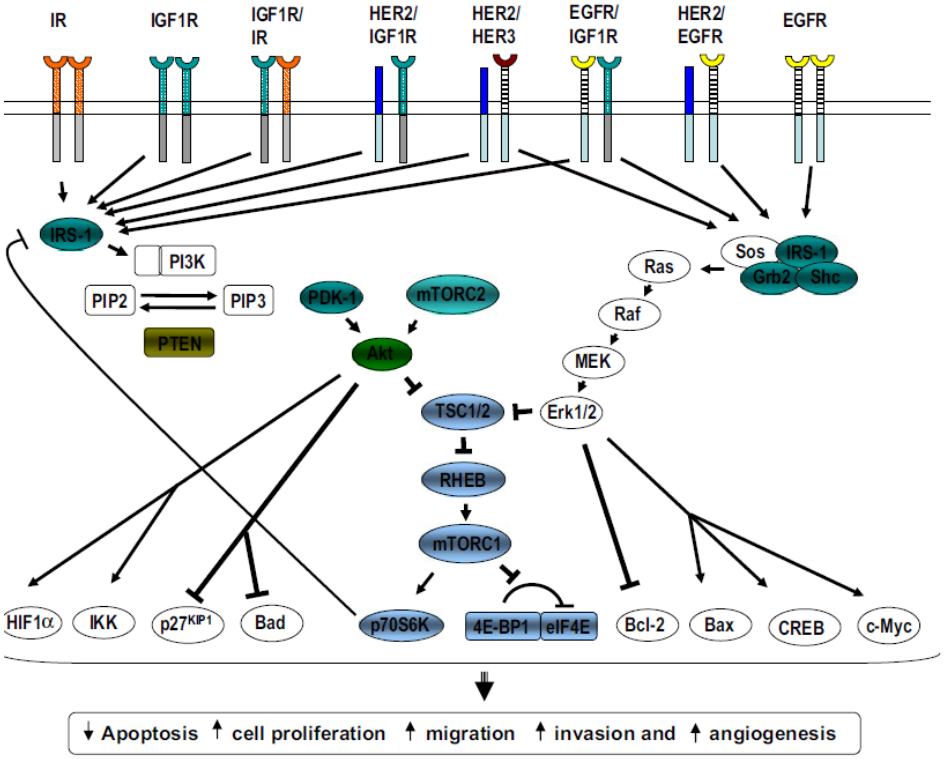

Figure 1.10 MAPK and PAM pathways. From Jin and Esteva (2008) Cross-talk between the HER and insulin-like growth factor receptor signalling pathway.[52]

<u>Epithelial-mesenchymal transition (TGF-β and SMAD-4):</u> Epithelial-mesenchymal Transition (EMT) is a normal development and embryogenesis process that is hijacked by cancer cells for migration and progression.[69] It is a complicated process that is facilitated by TGF-β through either SMAD-4 dependent or SMAD-4 independent (non-canonical) pathway, via transcription factors such as SNAIL, SLUG, ZEB1 and TWIST.[70] Other factors that help orchestrate this process included growth factors and cytokines, miRNAs as well as interaction with microenvironment.[71] This eventually leads to a loss of E-cadherin and gain of vimentin, which transform an epithelial to spindle-shaped mesenchymal cell morphology.[72] The central players of this process are SMAD-4, a family of cytoplasmic transcription factors that are directly activated by serine phosphorylation at their cognate receptors; and TGF-β, which

functions as tumour suppressor normally but may paradoxically induce proliferation in cancer, particularly in the later stages of cancer.[73]

EMT appears to be a central pathophysiologic mechanism in PDAC. Nearly 80% of PDAC tumours have active expression of the EMT transcription factors SNAIL or SLUG.[74] In PDAC with functional SMAD-4, TGFβ binds to a type 2 TGFβ-receptor (TβRII), which phosphorylates the SMAD2 and SMAD3 via ALK5. These in turn form heterodimers with SMAD-4, which mediates EMT, proliferation, migration and invasion.[72] In 55% of PDAC with deleted or inactivated SMAD-4, typically in more advanced stages, the anti-proliferative properties of TGF-β may be lost, which confers survival advantage to the cell.[75] **(Figure 1.11).** That said, TGF-β may continue to have an inhibitory effect on cell proliferation via SMAD-4 independent inhibition of ERK.[76] EMT can still occur in SMAD-4 deleted tumours, but this occurs through MAPK, PI3K, NF-κb, Hedgehog and other non-canonical pathways.[72,77,78] Importantly, Ras/Raf/ERK is not only a crucial activating step by TGF-β in either pathway for EMT,[79] *K-Ras* itself is also known to constitutively induce EMT in transfection experiments.[80] To complicate this further, even among the *K-Ras* mutant cell lines, only those that became independent to *K-Ras* lost expression of E-cadherin gained vimentin and became mesenchymal in morphology, whereas others that remained addicted to *K-Ras* continued to display epithelial morphology.[81]

Aside from tumour migration, EMT has long been implicated in cancer stem cells and drug resistance in PDAC.[82] EMT and drug resistance appeared to go hand in hand. Cancer cells that have undergone EMT are more drug resistant; and cells that survived in the presence of a drug are more likely to undergo EMT.[72] EMT has been studied in the context of erlotinib resistance. In NSCLC, a multigene signature of EMT was found to be a determinant of erlotinib resistance in 42 cell lines.[83] In PDAC, an animal model that utilised 11 cell lines had found that mesenchymal cell lines were much more resistant to erlotinib also.[84] EMT may not be exclusively a marker of EGFR inhibitor resistance. It is also found to be involved in gemcitabine resistance in PDAC,[85] and IGF1R inhibitor resistance in PDAC and hepatocellular

carcinoma.[86,87] At this stage, it is thought that EMT may be reversible. Down-regulation of EMT related pathways such as NOTCH and ZEB/Rho with SiRNA appeared to at least partially reverse EMT.[88,89] Clinical trials targeting NOTCH, Wnt and Hedgehog pathways are now underway in pancreatic cancer.[90]

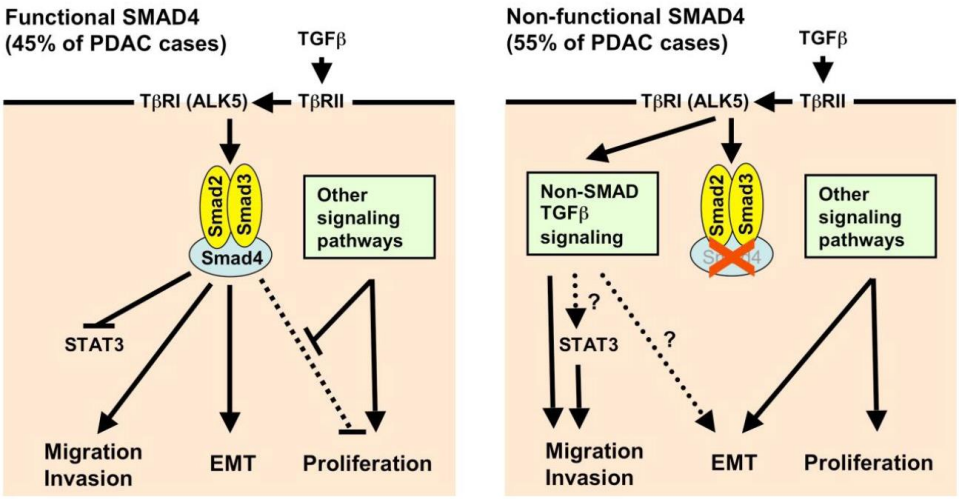

Figure 1.11: SMAD pathway. From Maier et al. (2010) Epithelial-mesenchymal transition in pancreatic carcinoma.[72]

Desmoplasia (Hedgehog): The Hedgehog (Hh) pathway consists of the ligand receptor Patched1 (PTCH) with 3 known ligands: Sonic Hedgehog (SHh), Indian Hedgehog and Desert Hedgehog. When a ligand binds the PTCH, this releases the normal repressive activity it has on the transmembrane protein Smoothened (SMO), leading to activation of a number of transcription factors such as GLI1 and HIP resulting in the transcription of genes.[91] Current evidence suggests that Hh is a downstream target of K-Ras, with NF-κβ suggested as an intermediary between Ras and Hh.[91] Hh activation is actually important for the normal development of the gastrointestinal system during embryogenesis; with the exception being the pancreas, where the down-regulation of Hh is critical for the normal development of pancreas in embryos and functioning of pancreas in adults.[91]

The association between Hh and tumourigenesis in PDAC was first described in PDAC in two papers in Nature simultaneously in 2003.[92,93] In a genomic analysis of 24 pancreatic cancers in 2008, hedgehog pathway is found to be up-regulated in 67-100% of PDAC.[41] SHh is also

found to be increased by 46-fold in PDAC stem cells which occupy the invasive front of pancreatic cancer.[94] Importantly, Hh has been demonstrated to be an important stimulating factor of desmoplasia *in vivo*, a reaction referring to the recruitment of fibroblasts, endothelial cells and many stromal cells. This is a particularly important feature in PDAC as this results in enrichment in the tumour microenvironment and creating barrier to delivery of therapeutic drugs to the tumour cells.[91] The reaction appears to be dependent on the paracrine system between tumour cells and microenvironment. In an experiment of co-transplanting SHh-positive human tumour cells and mouse fibroblasts, SMO knockout mice fibroblasts have been shown to be lead to smaller tumours than SMO- wild type fibroblasts.[95] In another experiment, inhibition of the Hh pathway practically abrogates the metastatic potential of PDAC without affecting tumour volume. Active efforts are continuing to research the therapeutic potentials of combining Hh antagonists with chemotherapy to improve drug delivery in PDAC.[94]

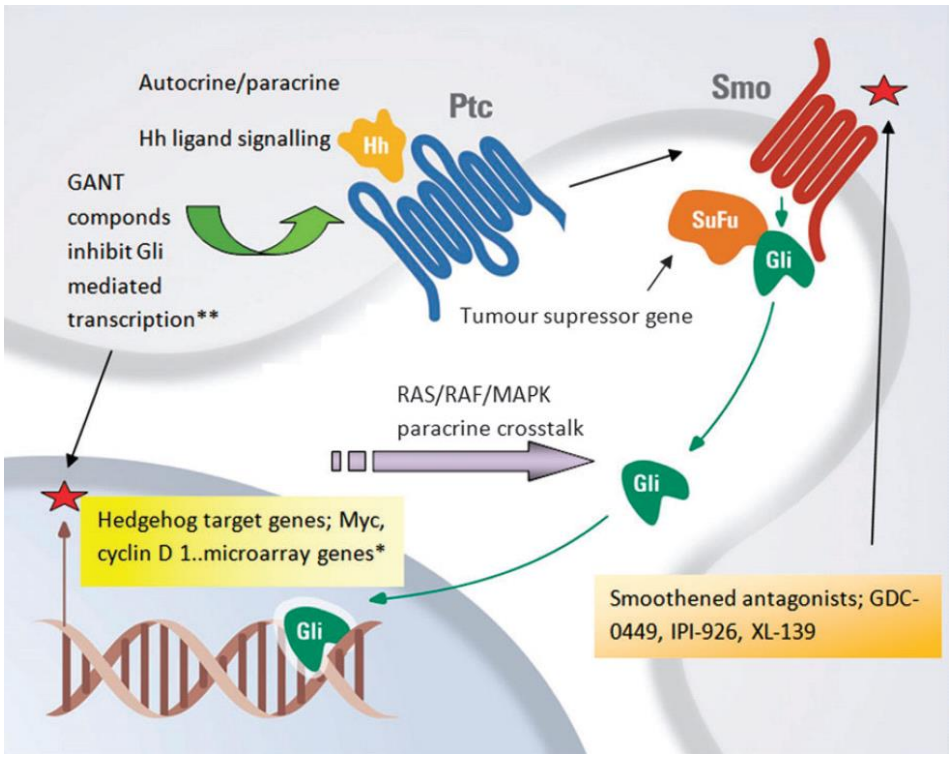

Figure 1.12: Sonic Hedgehog pathway. From Kelleher (2010) Hedgehog signalling therapeutics in pancreatic cancer.[94]

JAK Pathway: Janus Kinase (JAK)/ Signals Transducers and Activators of Transcription (STAT) pathway is a key signalling process of multiple cytokines and growth factors regulating numerous developmental and homeostatic processes.[96,97] It consists of 3 families of genes, including 4 members in the JAK or Janus family, 7 in the STAT family and 8 genes within the Suppressors of Cytokine Signaling (SOCS) family.[96-98] The binding of extracellular ligand to the receptor leads to intracellular JAKs phosphorylating each other, and STATS molecules dimerizing with each other; the STAT molecules then enter the nucleus and regulate transcription.[97] The SOCS molecules, on the other hand, act as negative feedback suppressing JAK/STAT pathway activation.[97] **(Figure 1.13)** Although the canonical JAK/ STAT pathway is relatively direct, it is also known to cross-talk with the MAPK and PAM pathways across multiple levels.[98] Since 2005, several JAK2 mutations and translocations have been described to be the mechanism of leukemia and myeloproliferative disorders.[99,100] Aside from haematological cancers, the JAK/ STAT pathway has also been implicated in the progression of pancreatic cancer;[41,101] and STAT3 over-expression has been shown to be obligatory for the development of acinar-to-ductal metaplasia- an early event of PDAC initiation.[102] Recently, pancreatic cancer-induced cachexia is found to be dependent on JAK2.[103] There is now emerging interest to target JAK1/2 and STAT3 in PDAC.[101,102] In a randomised phase II study recently reported in ASCO 2014, JAK1/2 inhibitor ruloxitinib was explored in the second-line setting of metastatic pancreatic cancer patients. 127 patients were randomised to receive either ruloxitinib 15mg BD plus capecitabine 1000mg/ m^2 days 1-14 every 3 weeks, or placebo plus capecitabine with the same dose. The primary endpoint was overall survival (OS), with secondary endpoints of PFS and overall response rate (ORR).[104] Whilst the primary analysis was negative, in subgroup analysis patients with high CRP (>13 mg/L) were seen to have superior OS (HR 0.47, P=0.01). Ruloxitinib is now being investigated in a multi-centred international phase III study in metastatic pancreatic cancer patients who either fail first-line or are intolerable to first-line chemotherapy.

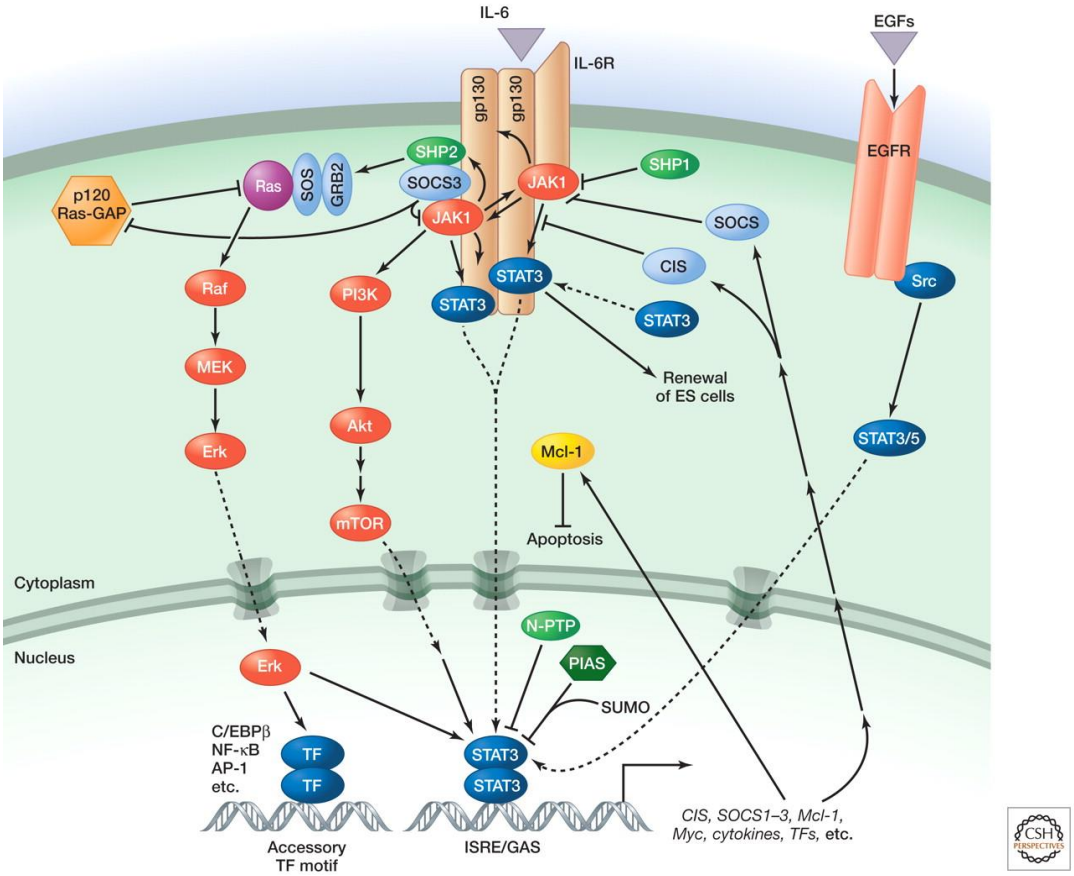

Figure 1.13: JAK/ STAT Pathway. From Harrison (2012) the JAK/ STAT Pathway.[96]

1.3 Treatment Options in Advanced and Metastatic PDAC

1.3.1 Chemotherapies and Targeted therapies

Despite numerous clinical trials and extensive research in advanced and metastatic pancreatic cancer, treatments remain limited and prognosis is unchanged at 6-12 months. Aside from complete resection, all other treatment can only be regarded as palliative. In this next section, the key trials in the area of chemotherapy and targeted therapies are summarised **(table 1.2)**. Chemoradiotherapy is usually reserved for locally advanced disease, and remains controversial due to a number of negative trials including ESPAC-1 and LAP-07.[105] It has little relevance to the background of this thesis, so it will not be discussed here.

Study	Setting/ Pt	Treatment	Response	PFS	OS
Burris *et al.* (1998)[106]	First-Line (n=126)	Gemcitabine vs. 5FU	5 vs. 0%	**2.3 vs. 0.9m (P=0.0002)**	**5.6 vs. 4.4m (P=0.003)**

Tempero *et al.* (2003)[107]	First-Line (n=96)	FDR Gem vs. Gemcitabine #	6 vs. 9%	3.4 vs. 1.9m (P=0.68)	**8.0 vs. 5.0m (P=0.013)**
Moore *et al.* (2007)[108]	First-Line (n=569)	Gem-erlotinib vs. Gem	9 vs. 8%	**3.8 vs. 3.6m (HR 0.77, P=0.004)**	**6.2 vs. 5.9m (HR 0.82, P=0.038)**
Cunningham *et al.* (2009)[109]	First-Line (n=533)	Gem-CAP vs. Gemcitabine	19 vs. 12% (P=0.03)	**5.3 vs. 3.8m (HR 0.78, P=0.004)**	7.1 vs. 6.2m (HR 0.86, P=0.08)*
Conroy *et al.* (2010)[110]	First-Line (n=342)	FOLFIRNOX vs. Gem	32 vs. 9% (P<0.001)	**6.4 vs. 3.3m (HR 0.47, P<0.001)**	**11.1 vs. 6.8m (HR 0.57, P<0.001)**
Von Hoff *et al.*(2013)[111]	First-Line (n=842)	Gem-Abraxane vs. Gem	23 vs. 7% (P<0.0001)	**5.5 vs. 3.7m (HR 0.69, P<0.0001)**	**8.5 vs. 6.7m (HR 0.72, P<0.0001)**
Jacobs *et al.* (2004)[112]	Second-Line (n=46)	OFF vs. BSC^	-	5.3 vs. 2.5m (P not reported)	**4.8 vs. 2.3m (P=0.008)**
Oettle *et al.* (2005)[113]	Second-Line (n=168)	OFF vs. FF	-	3.3 vs. 2.2m (P=0.012)	**6.5 vs. 3.3m (P=0.014)**

Table 1.2: Randomised clinical trials of chemotherapies and targeted therapy with positive results in overall survival. #FDR (Fixed dose rate): 10mg/m^2/ minute, *Meta-analysis of 3 studies with n=935 showed significant OS benefit (HR 0.86, P=0.02).[109] ^OFF: Oxaliplatin-5FU- folinic acid (similar to FOLFOX). BSC= best supportive care

Chemotherapy: In 1998, the landmark randomised controlled trial compared gemcitabine (given 7 out of 8 weeks) against the previous standard 5-FU in advanced pancreatic cancer in 126 patients. The primary endpoint of the trial was actually clinical benefit, a composite endpoint of debilitating symptoms and signs of pain, weight loss and functional impairment.[106] This was fulfilled by demonstrating 24% patients on gemcitabine deriving clinical benefit, compared to only 6% on 5-FU (P=0.002). In addition, gemcitabine significantly improved PFS (P=0.0002) and OS (P=0.003) compared to 5FU. Whilst gemcitabine resulted in higher rates of grade 3-4 neutropenia (26% vs. 5%, P<0.001), no serious infections were observed in either group, and both treatments were otherwise reasonably well tolerated.[106] Gemcitabine was therefore accepted as the new standard of care since the late 1990s. Over the next 10 years, efforts were invested to improve median OS beyond 6 months. Tempero *et al.* researched on more efficient ways of drug delivery. The fixed dose rate (FDR) gemcitabine, given at 10mg/m^2/ min, resulted in a linear and higher serum accumulation of the active compound,

and led to a significant improvement of median (P=0.013), 1-year (P=0.014) and 2-year survivals (P=0.007).[107] However, the FDR strategy could not be widely adopted due to a doubling of grade 3-4 neutropenia, leukopenia and thrombocytopenia to a rate of around 40%.[107] Others have researched on gemcitabine-based combinations to provide additional benefits to gemcitabine alone. The phase III trials on Gem + 5FU and Gem + cisplatin unfortunately did not show significant benefit in OS and only marginal benefit in PFS.[114,115] In 2009, Cunningham *et al.* reported the large GEM-CAP study of 533 patients from 75 hospitals in the UK. Gemcitabine plus capecitabine- an oral pro-drug of 5FU, resulted in a significant improvement in PFS (P=0.004) and a strong trend to improvement in OS (P=0.08). Cunningham *et al.* combined with the results of 2 other RCT in a meta-analysis, and reported a significant benefit in OS (HR 0.86, P=0.02) with no statistical heterogeneity (I^2 =0%). Yet, even then the median survival still remains at 7.1 months. It was only until the ACCORD-11 trial by Conroy *et al.* and MPACT trial by Von Hoff *et al.* reported in the last 3 years that the landscape of chemotherapy in metastatic pancreatic cancer has started to change. The ACCORD-11 trial studied a potent 3-drug combination of 5FU, oxaliplatin and irinotecan in 342 patients at 48 French centres. For the first time, clinical trial was stopped early due to benefit instead of futility. A clinical meaningful benefit of +3.1 (to 6.4 m) and +4.3 months (to 11.1 m) in median PFS and OS was demonstrated in addition to statistical significance (both P<0.001), and fewer patients had worsened quality of life at 6 months (HR 0.47, P<0.001).[110] There were initial concerns over the significantly higher rates of grade 3 and 4 neutropenia (46 vs. 21%), diarrhoea (13 vs. 2%) and sensory neuropathy (9 vs. 0%); but subsequent real-life data showed that the protocol could be safely given in its modified version (without bolus 5FU) without compromising its efficacy.[116] In early 2013, the MPACT trial comparing gemcitabine + abraxane was also reported, showing a significant improvement of PFS and OS of +1.8 (to 5.5 m) and +2.8 (to 8.8 m) respectively.[111] Abraxane has a therapeutic advantage over other chemotherapies, since it is designed as paclitaxel chemotherapy bound in albumin. The albumin coating allows it to bypass the demoplastic structures shielding the tumour and reach the tumour micro-environment readily, and *in vivo* it is shown to cause

stromal collapse and thereby increasing drug bioavailability.[94] Importantly, the combination is well tolerated and patients could receive 75-80% of the proposed dose intensity.[111] Therefore, both FOLFIRINOX and Gem-abraxane can now be considered as acceptable standards for patients who are of good performance status.[117]

Second-line treatment options in PDAC are very limited, with no existing standard of care. Many advanced pancreatic cancer patients are poor candidates for clinical trials after failing first-line treatment. As a result, most second-line clinical trials are either retrospective or single arm phase II trials only, with small sample size of 15-25 in phase II series.[118,119] Most chemotherapy regimens can only produce a response rate of 0-20%, and the progression free and overall survivals are consistently around 1-2 months and 3-4 months respectively regardless of the agents.[118] There are few available phase III trials in second line setting. Oxaliplatin plus 5-FU/ Folinic acid (OFF) improves survival from 13 weeks to 26 weeks over best supportive care (BSC) (P=0.008), and 3.3 to 6.5 months over FF (P=0.014); and Rubitecan, which significantly improves PFS (from 1.6 to 1.9m, P=0.003) but not OS (from 3.0 to 3.6m, P=0.63).[112,113,120] Another trial recently reported is the AIO-PK0104 trial, which randomised advanced or metastatic patients to gemcitabine +erlotinib versus capecitabine+ erlotinib first-line, with planned cross-over to the arm without erlotinib second-line, in a 1:1 ratio with non-inferiority design. Focusing on the second-line analysis, 51% of patients were able to receive salvage therapy. In a post-hoc analysis, gemcitabine appears to be superior to capecitabine in second-line with time to treatment failure 2 cross over (TT2c) of 2.5 vs. 2.0 m (P=0.00005).[121] Clearly some patients may benefit from salvage therapy, and there is thus a great need in clinical trial research to establish a standard in the second-line setting.

Targeted therapies: There has been emerging interest in the use of targeted therapies in cancer treatment. Targeted therapies exploit the fact that some cancers are addicted to certain aberrant molecular pathways for growth and metastases. By blocking the dominant pathway in a particular cancer, targeted therapies result in remarkable control of tumour and promote tumour kill when used in combination with chemotherapy.[122] In pancreatic cancer, the only

targeted therapy with proven efficacy to date is EGFR tyrosine kinase inhibitor (TKI) erlotinib in the PA.3 trial. In this trial, gemcitabine plus erlotinib delays progression by 23% (P=0.004) and improves overall survival by 18% (P=0.038). However, the absolute benefit is exceedingly small, with +0.2 months and +10 days in median PFS and OS.[108]

The development of other targeted therapies including bevacizumab (vascular endothelin growth factor inhibitor), cetuximab (epidermal growth factor inhibitor), tipifarnib (K-Ras inhibitor) and marimastat (matrix metalloproteinase inhibitor) has all been disappointing.[123-126] The latest failure to add to this growing list is ganitumab (IGF1R inhibitor). A phase II trial was reported in 2010, randomizing patients to gemcitabine + conatumumab (death receptor 5 agonist), or gemcitabine + ganitumab (IGF1R inhibitor, Amgen) or gemcitabine + placebo. This resulted in superior median PFS for Gem+ ganitumumab (5.1 m) and Gem+ conatumumab (4.0 m) compared to Gem + placebo (2.1 m), with a borderline significant P-value of 0.072 and 0.082 respectively. The study was not powered for analysis of OS, which was not significantly different between the 3 arms at this stage (Gem+ G: 8.7 vs. 5.9m, P=0.12; Gem+ C: 7.5 vs. 5.9m, P=0.59).[127,128] The promising results in phase II setting prompted a large multi-centre, double-blinded phase III trial development. Unfortunately, in Aug 2012, AMGEN released a statement announcing termination of its phase III trial in PDAC for futility.[129] Currently, there are a number of ongoing phase I/II trials examining the possible utility of novel targeted therapies including Ras, Src, KIT, Hedgehog and proteasome inhibitors.[130,131] However, with the repeated occurrence of promising phase II data only to be rejected by disappointing phase III trial results, investigators must start to look at novel combination of targeted therapies, addressing drug resistance and selecting patients by biomarkers in order to continue forward in this area of unmet need.[132-134]

1.3.2 Comparison of EGFR Drug Clinical Trials in PDAC, CRC and NSCLC

As discussed, EGFR tyrosine kinase inhibitors erlotinib is the only proven targeted therapy in PDAC to date. However, the small clinical benefit observed in OS and the challenge in finding a predictive biomarker have made it difficult to implement erlotinib in routine clinical practice. On the other hand, EGFR inhibitors and antibodies have well established roles in metastatic NSCLC and CRC. By comparing the difference in the trials of these cancer types, the aim was to explore better strategies to continue development of these drugs in PDAC. EGFR TKI erlotinib and gefitinib have been studied across different solid tumours, but the bulk of phase III studies were conducted in metastatic non-small cell lung cancer (NSCLC). At the time of preparing this thesis, the promising data of afatinib has just started to emerge in NSCLC with EGFR mutation, and it certainly corresponds well with other gefitinib and erlotinib studies.[135] EGFR antibodies cetuximab and panninitumab have mainly been studied in metastatic colorectal cancer (CRC). Whereas the emphasis in NSCLC and CRC clinical trials is to select EGFR treatment by predictive biomarkers, the focus of phase III studies in PDAC has only been incorporating EGFR inhibitors/ antibodies into standard chemotherapy in unselected population thus far. **Table 1.3** summarises the important randomised controlled clinical trials in these three cancers using EGFR inhibitor or antibody:

Clinical Trial	Cancer type	Line of Rx	Experimental	Comparator	RR (EGFRi/ab)	PFS	OS
PA.3 (2007)[108]	mPDAC	1st	Erlotinib + gemcitabine	Gemcitabine	RR 9% SD 49%	**3.8 v 3.6m (HR 0.77, P=0.004)**	**6.2 v 5.9m (HR=0.82, P=0.038)**
AIO-PK0104 (2013)[121]	mPDAC	1st / 2nd	Erlotinib + capecitabine → Gemcitabine	Erlotinib + Gemcitabine → Capecitabine	RR 16% SD 38%	TTF2 4.2 v 4.2m (HR 1.00, P=1.0)	6.2 v 6.9m (HR 1.02, P=0.90)
AVITA (2008)[136]	mPDAC	1st	Erlotinib+ gemcitabine + bevacizumab	Erlotinib + gemcitabine	RR 14% SD 67%	**4.6 v 3.6m (HR 0.73, P=0.0002)**	7.1 v 6.0m (HR=0.89, P=0.21)
SWOG S0205 (2010)[124]	mPDAC	1st	Cetuximab + gemcitabine	Gemcitabine	RR 14% SD 37%	**3.4 v 3.0m (HR=1.07, P=0.006)**	6.2 v 5.9m (HR=1.06, P=0.23)
NCT00079066 (2008)[137]	mCRC	2nd or later	Cetuximab + irinotecan	Irinotecan	RR 13% in *K-Ras* WT	**3.7 v 1.9m *in K-Ras* WT (HR**	**9.5 v 4.8m *K-Ras* WT**

						0.40, P<0.001)	**(HR 0.55, P<0.001)**
CRYSTAL (2009)[138]	mCRC	1st	Cetuximab + FOLFIRI	FOLFIRI	RR 59% in *K-Ras* WT	**9.9 v 8.7m in *K-Ras* WT (HR 0.70, P=0.001)**	**23.5 v 20.0m in *K-Ras* WT (HR 0.80, P=0.0093)**
Peters *et al.* (2009)[139]	mCRC	2nd or later	Pannitumuab+ FOLFIRI	FOLFIRI	RR 35% in *K-Ras* WT	**5.9 v 3.9m *K-Ras* WT (HR 0.73, P=0.004)**	14.5 v 12.5m *K-Ras* WT (HR 0.85, P=0.12)
BR.21 (2005)[140]	mNSCLC	2nd/3rd	Erlotinib	Placebo	RR 9% SD 34%	**2.2 v 1.8m (HR 0.61, P<0.001)**	**6.7 v 4.7m (HR 0.70, P<0.001)**
FLEX (2009)[141,142]	mNSCLC	1st	Chemotherapy	Chemo + Cetuximab	RR 36%	4.8 v 4.8m (HR 0.94, P=0.39)	**11.3 v 10.1m (HR 0.87, P=0.044)***
SATURN (2010)[143]	mNSCLC	Maintenance	Erlotinib	Placebo	RR 12% SD 58%	**3.1 v 2.8m (HR 0.71, P<0.0001)**	**12.0 v 11.0m (P=0.009)**
IPASS (2010)[144]	mNSCLC	1st	Gefitinib	Carboplatin/ Paclitaxel	RR 43%	**HR 0.48, P<0.0001 in EGFR mut**	21.9 vs 21.6 (HR 1.00, P=0.99) in EGFR mut
OPTIMAL (2010)[145,146]	mNSCLC (EGFR mut)	1st	Erlotinib	Carboplatin/ Gemcitabine	RR 58% SD 22%	**13.1 v 4.6m (HR=0.16, P<0.0001)**	HR 1.065 (P=0.68)
EURTAC (2012)[147]	mNSCLC (EGFR mut)	1st	Erlotinib	Carboplatin/ Gemcitabine	RR 82% SD 14%	**9.4 v 5.2m (HR 0.37, P<0.0001)**	19.3 v 19.5m (P=0.87)

Table 1.3: List of EGFR inhibitors (erlotinib, gefitinib) and EGFR antibody (cetuximab, pannitumumab) trials in PDAC, CRC and NSCLC. *Bolded indicates significant difference observed (P<0.05). *The updated analysis of the FLEX trial stratified by EGFR expression shows a more significant benefit in OS with tumours of high EGFR expression (HR 0.73, P=0.011).TTF denotes time to treatment failure*

There is certainly a discernible difference in EGFR treatment response rate in patients with tumours selected by a positive predictive marker compared to the unselected population. In clinical trials that study NSCLC patients with EGFR mutation such as OPTIMAL and EURTAC, and in a clinical trial (IPASS) that has a concentrated proportion of patients with EGFR mutation, the response rate (RR=CR/PR) ranges from 43% to 82%.[144-147] If disease control rate (DCR =CR/PR + SD) is considered, this is even as high as 96% (EURTAC).[147] Likewise, the RR of cetuximab approaches 60% in the first-line setting in the selected group of patients

with *K-Ras* WT tumours.[137] In the setting where these drugs are used in an unselected population, the response rates are much lower, in the order of 8-30% (ISEL, INTACT-2), 12% (SATURN) and 9% (BR.21) in first-, maintenance and second-line settings in lung cancer.[143,148-150] In unselected population in PDAC, the response rate of erlotinib is even lower. In the PA.3 trial, the response rate of gemcitabine plus erlotinib is 8.6% which is no different to the 8.0% with gemcitabine alone. DCR between gemcitabine and gemcitabine plus erlotinib are higher but not significantly different (58% vs. 49%, P=0.07).[108] Similarly, in the phase III AVITA trial, the combination of erlotinib, bevacizumab and gemcitabine yields a response rate only slightly higher at 14% compared to 9% in the arm of gemcitabine plus erlotinib (P=0.057) and no difference in DCR 62 vs. 59%.[151] Finally, the AIO-PK0104 trial demonstrates that gemcitabine +erlotinib appears more active than capecitabine+ erlotinib first-line (16% vs. 5%), and both chemo agents alone have low response in second-line (gem: 6%, cap: 3%). The DCR is higher in gemcitabine+ erlotinib at 51% compared to capecitabine+ erlotinib at 38%.[121] From these studies, gemcitabine is likely the main active drug; erlotinib and bevacizumab only add slightly more stable disease and partial response respectively. Currently the exact response rate of erlotinib alone cannot be determined, since there have not been any RCTs with erlotinib only compared to placebo.

With regards also to PFS analysis, there have been proven significant delays in progression in phase III trials of all 3 cancers. The only clinical trial with no demonstrable PFS benefit was the FLEX trial, which compared chemotherapy with chemotherapy plus cetuximab. That said, the time to treatment failure in the FLEX trial was significantly better with the combination therapy (HR 0.86, P=0.015).[142] Importantly, subgroup analyses of the EGFR mutation positive NSCLC and *K-Ras* WT CRC showed a much greater magnitude of PFS advantage of EGFR therapy compared to control with HR as great as 0.16 (P<0.0001) in the OPTIMAL study.[145] For PDAC trials, gemcitabine plus erlotinib or cetuximab demonstrated superior PFS than the respective comparator arm, but the absolute magnitude of PFS benefit appeared to be small, in the order of 0.4 to 1.0 months.[108,124,136] The AIO trial suggests that gemcitabine with erlotinib

may be superior to capecitabine with erlotinib (Time to failure first-line: 3.2 vs. 2.2 m, P=0.003).[121] In all treatment arms, however, the median PFS reported remains between 3-5 months, far less than that observed in first-line NSCLC and CRC trials.

5 phase III trials actually shows an overall survival (OS) advantage for these targeted therapies despite PFS advantage in all trials (NCT00079066, CRYSTAL, PA.3, BR.21, SATURN).[108,137,138,140,143] The absolute benefit in OS is appreciable in the mCRC trial selected for *K-Ras* WT, but in the NSCLC and PDAC trials the magnitude of OS difference in modest at best, in the order of 0.3 months (PA.3) and 2.0 months (BR.21). It has been argued- especially in the first-line NSCLC trials- that OS is a less reliable endpoint than PFS, as patients often receive multiple lines of therapies after end of study. Since EGFR inhibitors are available as an option in the second or third-line setting, and a fair proportion of patients who did not receive the experimental treatment end up being treated with it after first-line, any potential OS advantages may have been diluted by this cross-over effect. For the PDAC trials, only BR.21 reports a significant difference in OS, and median OS are all consistently at the realms of 5-7 months.

In summary, EGFR therapy is clearly active in some cancers. Whilst there are probably mechanistic difference between EGFR inhibitors and EGFR antibodies, all these drugs appear to stabilise disease and have the capability of delaying progression. Although cross-trial comparison is not statistically sound, it appears that these therapies are consistently more active in first-line than subsequent lines settings in advanced and metastatic NSCLC and CRC. Only few clinical trials actually resulted in significant OS benefit, which may be because of cross-over of EGFR inhibitors in the case of NSCLC trials. In general, the median survivals of PDAC regardless of experimental treatment are much shorter than the other two cancers, probably reflecting the aggressive nature of PDAC, poorer functional status of these patients, more treatment-related complications necessitating dose modifications, and a lack of second- and subsequent-line therapy.[108,118] Importantly, the above comparison elucidated a much more favourable outcome when these targeted drugs can be applied on selected populations

(EGFR inhibitors in EGFR mutated NSCLC or EGFR antibodies in *K-Ras* mutation WT CRC). Together, this suggests a strong need to discover predictive markers for EGFR drugs in advanced PDAC so that it can be used upfront.

1.3.3 Resistance in EGFR targeted treatment in Cancer

Before turning to describing strategies to optimise targeted therapies in cancer, the unavoidable problem with targeted drugs- drug resistance- must be explored. Although these drugs were active initially, cancers soon developed resistance to these drugs, probably due to the multiple collateral pathways present.[152] A plethora of translational studies examine the different types of resistance in NSCLC, but increasingly also in other cancer types including colorectal cancers, head and neck cancers, and glioblastoma multiforme.[153-157] The study of EGFR treatment resistance in PDAC is currently much more limited.

In general terms, drug resistance is divided into primary resistance and acquired resistance. Primary resistance describes the de novo properties of cancer which predetermines resistance to a particular therapy, and this is often used as a "negative biomarker" to guide treatment. The definition of acquired drug resistance, on the other hand, is less clear. The most acceptable definition of acquired resistance is both molecular (previous treatment with single agent inhibitor with development of a new genetic mutation) and clinical (progression of disease whilst on inhibitor with no intervening therapy between cessation of inhibitor and initiation of new therapy).[158] This distinction, although only widely adopted in the study of NSCLC treatment, is very important in translational research as well as clinical practice. This is because mechanisms of primary and acquired resistance are often very different, and strategies to overcome them may also vary.[134,159] In lung cancer, primary resistance has been well described with common gene abnormalities such as *EGFR*, *K-Ras* and *B-RAF* mutations. Acquired resistance, on the other hand, can occur due to EGFR modification such as T790M (occurring in over 50% of acquired EGFR inhibitor resistance in NSCLC) and EGFR variant vIII; activation of alternate pathways such as *MET, HER2, NF-κβ, PI3K*; or histologic

transformation such as small cell transformation and epithelial-mesenchymal transition **(table 1.4)**.[132,134,160] Regardless of the cancer type, there is now increasing evidence that acquired resistance may be related to emergence of cancer stem cells.[82] This complexity and diversity of acquired resistance probably reflects clonal evolution in the presence of drug pressure, and therefore requires novel strategies to overcome it. Some of these strategies include intercalating targeted therapies with other treatment modalities (such as chemotherapies) and combining targeted therapies to overcome targeted drug resistance.[161,162]

	Lung (EGFR TKIs)	Colon (EGFR mAbs)	Head and neck (cetuximab)
Primary resistance	*EGFR* exon 20 insertion[7,a] *BIM* deletion[32,a] *EGFR* T790M[41,179]	*KRAS*[47,48,a] *PIK3CA* exon 20 (refs. 47,48)[a] *BRAF* mutation[47,48,a] *PTEN* deletion[47,48,a]	
Acquired resistance			
EGFR modification	T790M[82,a]	S492R[42,a]	*EGFRvIII*[181]
Alternative pathway activation	*BRAF*[51,a] *CRKL*[65] *DAPK*[182] *FGF*[69–71] *HER2* (ref. 45)[a] *HER3* (ref. 68) *IGF*[183,184] *JAK2* (ref. 72) *MED12* (ref. 185) *MET*[44,a] NF-κB[186,a] *PTEN* loss[63,64] *PUMA*[114] *ROR1* (ref. 113) *VEGF*[187]	*HER2* (ref. 46)[a] *IGF*[189,a] *KRAS*[49,50,a] *MET*[190]	*Aurora*[191] *HER2* *HER3* *MET*[192]
Histologic transformation	Acquisition of stem cell properties[73] EMT (AXL, Notch-1 or TGF-β activation)[57–60,185,a] Small cell lung cancer transformation[188,a]		EMT[193,194]

[a]Mechanisms have also been identified in patient tumors.

Table 1.4: Overview of EGFR resistance mechanisms. From Chong and Janne (2013) The quest to overcome resistance to EGFR-targeted therapies in cancer.[134]

In PDAC, several *in-vitro* studies suggested that mesenchymal cell phenotype and loss of dependency on EGFR-HER3 to be major determinants of erlotinib resistance in PDAC.[84,163,164] However, due to the limited utility of erlotinib given its small clinical benefit in survival, much of the research on EGFR signalling and EGFR inhibitor resistance in PDAC has been neglected.[165]

It is interesting to note that there appears to be subtle differences in the resistance mechanisms between EGFR inhibitors and antibodies. Some of the mechanisms described for EGFR inhibitors include change in conformation of EGFRvIII, heterodimerisation of surface receptors, and oncogenic shift to alternate pathways such as IGF1R and Akt/mTOR pathway; whereas mechanisms of EGFR antibodies include EGFR mutations, unbiquination and internalisation and altered VEGF expression.[132] Among these, activation of IGF1R and Akt/mTOR pathways appears to be of particular relevance in EGFR TKI resistance. A number of studies have demonstrated in GBM and NSCLC that EGFR inhibitor resistant tumours express high levels of pIGF1R in association with PI3K, along with loss of IGF-binding protein-3, which results in sustained signalling via PI3K/Akt and rpS6.[153,155] The high rates of IGF1R and PI3K/Akt over-expression (50%, 70%) in PDAC suggest that the association between these and erlotinib resistance should be further explored.[48,54,61]

Altogether, the study of EGFR therapy resistance in NSCLC and other cancer types have been instrumental, though the study in PDAC is still preliminary and limited at this stage. From the current literature, it appears that there are mechanistic differences between primary and acquired resistance, EGFR treatment resistance in different tumour types, and even differences between EGFR TKI and antibody resistance. The oncogenic shift to IGF1R and PI3K/Akt/mTOR pathways is a major mechanism of resistance to EGFR TKI, and is of particular relevance for this thesis. Further examination of these pathways in PDAC is therefore warranted.

1.4 Strategies to improve targeted therapies efficacy

1.4.1 Novel targeted therapies

This thesis will focus on the pre-clinical assessment of novel targeted therapies in the MAPK, IGF1R and PI3K/Akt/mTOR (or PAM) pathways in addition to EGFR inhibitors in PDAC. Whilst the individual compounds will be introduced in **section 2.1.4**, here the history of pre-clinical and clinical development of these novel compounds is outlined.

IGF1R inhibitors and antibodies: Insulin growth factor 1-receptor (IGF-IR), a transmembrane receptor like EGFR with tyrosine kinase activity, activates downstream phosphatidylinositol 3-kinases (PI3K) serine-threonine protein kinase (Akt) proteins resulting in cell proliferation and survival.[166] IGF1R is expressed in 50% of pancreatic cancer and is also important in both its development and progression.[63,167-169] Manipulation of the IGF-IR system is shown to inhibit pancreatic cancer cell growth both *in-vitro* and *in-vivo*.[170,171] There are currently about 8 Insulin Growth Factor antibodies and 3 small molecule tyrosine kinase inhibitors produced by various pharmaceutical companies.[172] Figitumumab (CP-751,871) is a selective fully human IgG2 monoclonal antibody and the first IGF1R targeted therapy to reach randomized phase III clinical trial. In Phase I and II setting, figitumumab showed promising results in NSCLC, prostate cancer and recurrent head and neck cancer.[173-175] When added to carboplatin and paclitaxel, figitumumab resulted in overall response rate of 64% compared to 41% in chemotherapy only arm, including 1 complete response and 7 with striking partial response (50-80% tumour reduction by cycle 2).[175] However, in the phase III randomized controlled trial in NSCLC, the combination of chemotherapy and figitumumab was shown to be harmful 8.5m vs. 10.3m, HR 1.23, p=0.051), with serious adverse events including dehydration, hyperglycaemia and haemoptysis.[176] Post-hoc analysis showed that patients with high pre-treatment IGF-1 level (IGF1 > 145 ng/mL) may have improved overall survival (OS) from chemotherapy + figitumumab (HR = 0.62, p = 0.13).[177] Whilst this compound from Pfizer has been discontinued for clinical development, other companies have continued developing

their IGF1R inhibitor. Most notable example was the AMGEN compound Ganitumab, which in randomised phase II trial improved median PFS from 2.1 to 5.1 months, with borderline statistical significance P=0.072. [127,128] At the time of initiating this research project, the proposed phase III trial from AMGEN was one of the major drivers of our study of EGFR-IGF1R inhibition in pre-clinical study in PDAC. Unfortunately, the phase III trial was discontinued in Aug 2012, putting pressure on any other companies attempting to develop IGF1R targeted treatment further.[129]

PI3K and AKT inhibitors: PI3K in an excellent actionable target, because it responds to EGFR, IGF1R and K-Ras signaling, and it in turn controls a wide range of cellular processes which are major driving forces in cancer progression.[55,178,179] The first-generation PI3K inhibitors were widely used for many pre-clinical experiments. The pan-PI3K inhibitor LY-294002 was able to induce apoptosis *in-vitro* and induce tumour shrinkage *in-vivo.*[53] However, this and others such as GDC-0941 and XL-147 were limited by weak PI3K inhibition and off-target effects.[180] Over the last decade, major advances in biochemistry have resulted in discovery of new compounds such as PI-103, which is a highly selective Class I PI3K inhibitor with extreme potency but solubility limitations; and PI-520 and PI-620, which are Class I PI3K inhibitors with slightly less potency but better pharmacokinetics and pharmacodynamics properties.[180] These inhibitors tend to be isoform specific: NVP-BYL719 has been developed as a class I PI3K inhibitor with a high selectivity of p110α, whilst CAL-101 is a p110δ specific. These inhibitors are expected to produce greater target inhibition with fewer adverse effects.[47] Other inhibitors of this class in early development include allosteric AKT inhibitors (MK-2206) and catalytic AKT inhibitors (GDC-0068 and GSK-690693), with allosteric inhibitors appearing to be more AKT-specific **(Figure 1.14)**.[47] The side effects of these PI3K and AKT inhibitors appear to be manageable, including mild rash, diarrhoea, stomatitis and hyperglycaemia. However, the biggest hurdle in the clinical development of these drugs is the modest activity it has on cancer as monotherapy, as opposed to the use of EGFR, ALK or B-RAF inhibitors on tumours with these driver mutations (EGFR, B-RAF) or translocations (ALK).

Pharmacodynamics studies showed that these drugs are hitting the right targets. Currently, it is thought that their limited efficacy may be related to co-existing mutations relating to resistance such as K-Ras, intra-tumoural heterogeneity, or the use of non-standardized or unvalidated assays for alterations in this pathway.[47]

mTOR and dual PI3K/ mTOR inhibitors: Rapalogues were the first mTORC1 allosteric inhibitors developed, and included everolimus and temsirolmus which had proven single-agent efficacy in renal cell carcinoma (both), neuro-endocrine tumours (everolimus) and mantle cell lymphoma (temsirolimus).[47] The most impressive data on the rapalogues, however, came from combined strategy trial. BOLERO-2 was a randomised phase III trial examined the effect of exemestane plus everolimus or placebo in 724 women with oestrogen receptor (ER) positive recurrent or metastatic breast cancer who previously had a non-steroidal aromatase inhibitor. Median PFS was improved from 4.1 to 10.6 months with a substantial magnitude of effect of HR of 0.36 ($P<0.001$).[181] In other words, the addition of everolimus to aromatase inhibitors appeared to reverse endocrine resistance at least partially, suggesting cross-talk signalling between ER and mTORC pathways.[182]

More recently, the dual PI3K/ mTORC inhibitors were developed based on the structural homologies in the catalytic domain of mTOR and p110 subunit of PI3K, providing the advantage of vertical blockade of the PAM pathway at two levels.[47] BEZ-235 is one of the first compounds of this class, showing good *in-vitro* and *in-vivo* anti-tumour activity in multiple cancer types including pancreatic cancer.[183-186] Early pre-clinical data also suggests that dual PI3K/ mTORC inhibitors are capable of over-riding transfected breast cancer cells with EGFR inhibitor resistance, supporting PAM pathway as an escape route.[187] Recently, there is also pre-clinical data suggesting synergistic effect of BEZ-235 with radiation in glioblastoma, suggesting a role of this drug as a radiosensitizer in the treatment of brain cancer.[188] Interestingly, these inhibitors are known for off-targets such as fatigues and liver dysfunction, but are not associated with the usual metabolic side effects of rapalogues such as

hyperlipidaemia as well as pneumonitis.[47] The safety and efficacy of these drugs are currently investigated in early phase I and II clinical trials.

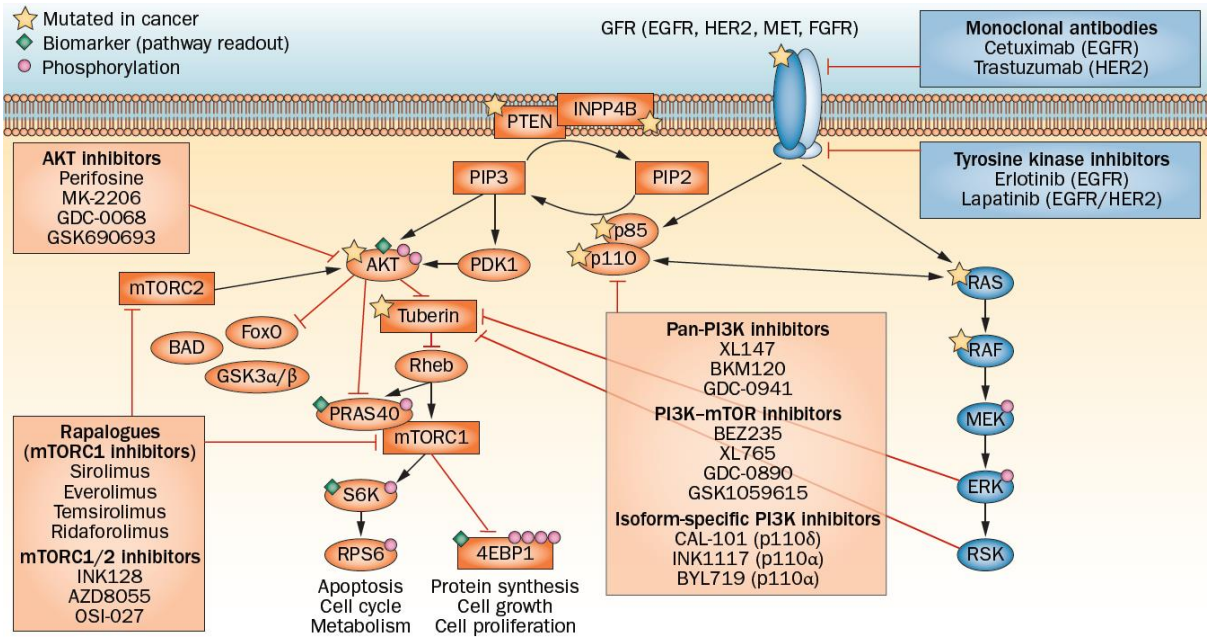

Figure 1.14: Inhibitors of the PAM pathway. From Rodon et al. (2013): Development of PI3K inhibitors: lessons learned from early clinical trials[47]

MEK inhibitors: Targeting MEK is especially useful in cancer therapy, since MEK is a major downstream component of the MAPK (Ras/RAF/MEK/ERK) cascade which is a convergent point of many upstream signalling pathways.[56,189] Whilst *MEK1* and *MEK2* genes are rarely mutated, over-activation of MEK usually occurs in the setting of upstream gain-of-function mutation of Ras and RAF.[190] In contrast to other inhibitors, MEK inhibitors are all non-competitive inhibitors of the ATP binding pocket of MEK that confer higher specificity.[189] However, MEK inhibitors tend to be cytostatic rather than cytotoxic.[191] PD-98059 and U0126, the first MEK drugs, predominantly prevent activation of MEK instead of inhibiting its activity directly. These drugs were limited to *in-vitro* mechanistic studies due to issues with solubility and potency.[192] CI-1040 was the first MEK inhibitor to succeed *in-vivo* and was subsequently assessed in a phase I and II settings. Unfortunately, this drug- whilst relatively non-toxic, demonstrated little clinical efficacy and its development was therefore terminated.[192] The second-generation MEK inhibitors PD 0325901 and AZA6244, produced from changes in the

side chains of the compounds, resulted in >90 folds increase in potency and around 30-fold improvement in *in-vivo* efficacy. Both these drugs have entered into clinical development, with promising clinical activity of 30-50% stable disease rate for a median duration of 3-5 months. At this stage, the dose limiting toxicities for these drugs appear to be grade 3 rash, diarrhoea and a small chance of congestive cardiac failure.[192]

In recent years, oncogenic dependence of downstream MAPK pathways have been discovered in Ras and RAF- mutant tumours, which display enhanced sensitivity to MEK inhibitors compared to wild type tumours.[193,194] Importantly, whilst the mechanism of Ras and RAF mutations are different, both are associated with activated state of MEK, which in turn can be exploited by novel MEK inhibitors.[194] In clinical trials, many have examined the roles of combining MEK inhibitors with other cancer therapies. The most notable example is combined vertical blockade (upstream and downstream) of the MAPK pathways in B-RAF mutated melanoma. A phase II trial demonstrates remarkable response rate of 56% by combining RAF and MEK inhibitors (dabrafenib and trametinib), as well as superior efficacy compared to conventional chemotherapy decarbazine (median PFS 9.4 versus 5.8 months, HR 0.39, P<0.0001).[195] In K-Ras mutated metastatic CRC, a phase I/II study combining MEK inhibitor pimasertib with standard FOLFIRI chemotherapy is ongoing.[196] For pancreatic cancer, whilst there are yet to be clinical trials researching the role of MEK inhibitor, this is certainly recognized as an area of active ongoing research given that virtually all PDAC are K-Ras mutated.[189]

1.4.2 Combined blockade targeted therapies

The drug development of novel targeted therapies has been hampered by the complexity of molecular pathways and existence of escape or bypass pathways. Combining targeted therapies as a strategy has a number of advantages: firstly, by targeting similar cellular pathways synergy may be achieved, where the combined anti-tumoural effects of two agents

exceed the additive effects of each drug. Secondly, combined blockade may circumvent escape pathways that contribute to drug resistance. Thirdly, it may overcome intra-tumoural heterogeneity in advanced disease where there are multiple metastatic clones with different genomic profiles and molecular activity.[197] Lastly, combined blockade may potentially take advantage of synthetic lethality in cancer cells.[198,199] In synthetic lethality, one mutated gene is compatible with viability but two mutated genes result in death. By targeting a gene that is synthetically lethal in cancer cells that have already mutated one gene, the normal cells may be spared.[200] As our understanding of cancer genetics and gene-gene interactions expand, in the future we may be able to identify drug targets which exploit synthetic lethality and design cancer-specific drug combinations with enhanced therapeutic indices.[199]

Combined blockade can take one of three strategies: horizontal blockade (blocking parallel oncogenic pathways), vertical blockade (upstream and downstream of the same pathway), and the so-called "super-inhibition" (maximising blockade of single target).[161,201] Horizontal blockade aims at achieving selective tumour cytotoxicity whilst minimising overlapping toxicities by using different classes of agents, whilst vertical blockade maximises pathway inhibition by shutting down regulatory feedback loops which may give rise to drug resistance.[161] Super-inhibition aims at the complete inhibition of a single target thereby enhancing "on-target" effects, and is utilised in cancer types that are highly dependent on a single oncogenic driver.[202] An example is HER2 antibody (Herceptin) plus EGFR/HER2 dimerising antibody (pertuzumab) in HER2+ metastatic breast cancer (CLEOPATRA).[203]

The strategy of combined therapies has actually existed for a very long time in oncology history. Many chemotherapy regimens have been designed by combining multiple cytotoxic agents with presumably different mechanism of action and non-overlapping toxicities.[198] Examples of these include most adjuvant chemotherapy regimes in solid cancer malignancies (FOLFOX in colorectal cancer, AC-T in breast cancer) and a wide range of regimens used in haematological malignancies. However, there are some notable differences in studying chemotherapy versus targeted therapy combinations **(table 1.5)**. Firstly, chemotherapy

combinations are traditionally studied only after single agents have been assessed as having high clinical efficacy, whereas some targeted therapies have little single-agent efficacy but may be synergistic when combined.[161] Secondly, chemotherapy combinations are limited by non-specific toxicities on rapidly cycling normal tissues (e.g. myelotoxicity), whereas targeted therapies offer greater biochemical selectivity. The potential benefit for this is that there may be fewer overlapping toxicities in targeted therapy combinations, such that therapeutic index is widened allowing for higher dose or more frequent schedules to be adopted.[198]

	Cytotoxic approaches*	Targeted approaches‡
Characteristics	Drugs are individually active against the tumour in question, causing measurable tumour regressions	Agents have therapeutic effects on growth-inhibiting molecular pathways *in vivo*
Mechanism of action	Drugs have different mechanisms of action to minimize resistance	Agents produce complementary effects on multiple forms of the same target, on other targets in the same pathway or on pathways with extensive molecular crosstalk that are involved in growth control; agents target different survival pathways that are required for tumour progression
Toxicity	Drugs have different clinical toxicities to allow full-dose therapy	Non-overlapping toxicities with cytotoxic agents or other molecularly-targeted anticancer agents; toxicity following chronic administration of the combination is tolerable
Dose schedule	Intermittent intensive treatment preferred to continuous low-dose treatment for cytoreduction and to minimize immunosuppression	Agents can be administered in either high-dose intermittent schedules or low-dose continuous schedules as needed to maximize target inhibition

Table 1.5: Combined cytotoxic and targeted therapy combination approaches. From Kummar et al. Utilizing targeted cancer therapeutic agents in combination: novel approaches and urgent requirements (2010)[198]

In view of hundreds of targeted therapies in development, there are essentially an unlimited number of targeted therapy combinations for investigation.[198] In 2006, the US National Cancer Institute (NCI) proposed a set of strategies for development of targeted therapy combinations, and prioritised renal cell carcinoma, melanoma and glioblastoma as the three tumours for further development of this strategy. A total of 15 phase I and II trials were proposed as a result, and emphasis was placed on developing VEGF super-inhibition, VEGF/ mTOR and

VEGF/ EGFR horizontal blockades.[198,199] After this, this approach has also been extended to colorectal and lung cancers.[198] Of recent times, probably the most notable success of combined blockade strategy was the phase III CLEOPATRA trial, where super-inhibition with herceptin and pertuzumab along with docetaxel chemotherapy resulted in a significant improvement in PFS from 12.4 to 18.5m (HR 0.62, P<0.001) compared with Herceptin plus docetaxel and placebo in women with HER2 positive metastatic breast cancer.[203] Another exciting development was the phase II study combining B-Raf and MEK inhibition in B-Raf mutated melanoma and the phase III RCT COMBI that followed.[195] However, not all targeted therapy combinations trials are met with success. Both PAACE and CAIRO2 were phase III metastatic colorectal cancer trials that showed inferior PFS when standard chemotherapy (PAACE: oxaliplatin or irinotecan-based, CAIRO-2: CAPOX) plus VEGF antibody bevacizumab was combined with EGFR antibody (PAACE: pannitumumab, CAIRO-2: cetuximab) whilst increasing toxicity[204,205] At this stage it is uncertain whether this unexpected result was due to reduced dose intensity of chemotherapy, excess toxicity or negative synergy between two targeted therapies.[206] Clearly, empirical combinations have a fair chance of failure; a better understanding in the molecular cross-talks and escape pathways is therefore needed to design biologically rational targeted therapy combinations.[198]

Combined blockade of the MAPK and PAM pathways present itself as an attractive strategy given their relatively high frequencies of gene alteration and extensive cross-talk between the two signalling cascades.[47,207,208] In fact, the relative low potency of the PI3K inhibitors and the apparent cytostaticity of MEK inhibitors may be in part related to the cross-talks between these two pathways, suggesting benefits in the horizontal blockade strategy.[191,207] Pre-clinical studies have already demonstrated synergy of combining Raf and Akt/mTOR inhibitors in B-Raf mutated melanoma, as well as MEK and PI3K inhibition in K-Ras mutated CRC, PTEN deleted ovarian cancer, lung cancer and triple negative breast cancer;[207] and this strategy has been shown to suppress feedback loop associated with reactivation of reciprocal pathway.[208] Ongoing clinical development for PI3K inhibitors is presently focused on combination

strategies, with targeted therapy, chemotherapy or hormone therapy **(Figure 1.15)**.[47] In pancreatic cancer, there is certainly a strong rationale to co-inhibit the MAPK and PAM pathways, given the extremely high rates of K-Ras mutation and its downstream signalling effects on both network.[191] There is early pre-clinical evidence combining PI3K and MEK inhibition in this cancer, but further development for this combination is warranted.[191]

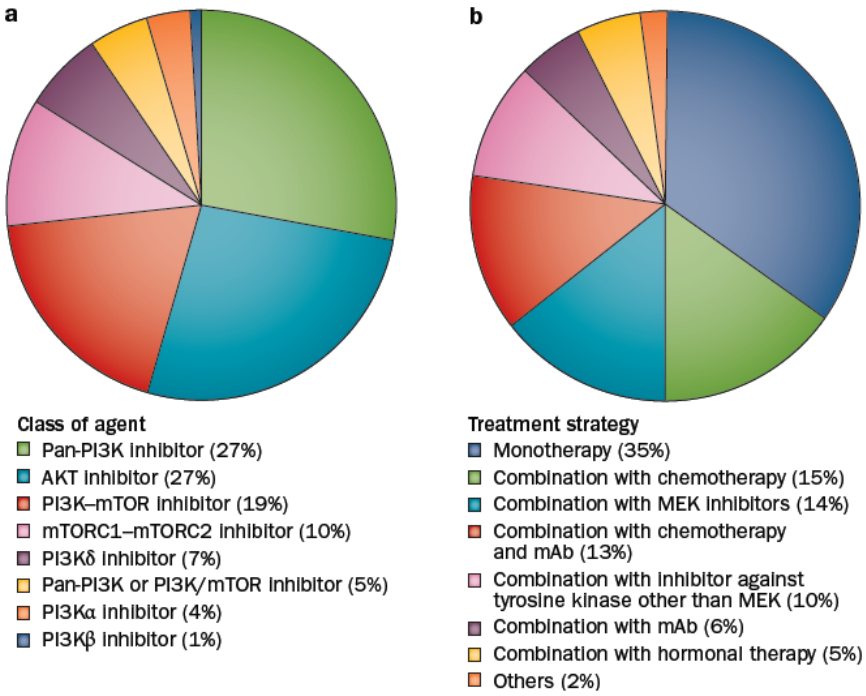

Figure 1.15: Ongoing Clinical Trial strategies of PI3K inhibitors. From Rodon et al. (2013): Development of PI3K inhibitors: lessons learned from early clinical trials[47]

Nevertheless, many challenges remain in the clinical development of drug combination trials, as suggested by the recent Institute of Medicine workshop. These include "developing and applying appropriate preclinical and clinical experiments, prioritising relevant drug combinations, identifying relevant biomarkers, avoiding or managing the overlapping toxicities of multiple agents, and overcoming legal, cultural, and regulatory barriers that impede collaboration of pharmaceutical companies, academia and government institutions."[197] In particular, defining optimal dosing and schedules for the drug combination whilst optimising metabolic interactions and minimising overlapping toxicities in clinical studies can be exceedingly complex, and frequently a phase I study may take more than a year and at

significant costs to complete.[161] To address these challenges, drug combinations should be selected based on "known biologic mechanism for which an assay is available, with activity or target engagement at clinical relevant doses, and validated biomarkers for patient selection".[197] Pre-clinical evidence of a strong biological rationale of the specific drug combination is critical for it to be taken forward to clinical development. During early clinical development, novel combinatory designs such as flexible dose escalation and de-escalation rules, multiple parallel cohorts and Bayesian models of dose escalation should be adopted to reach an optimal recommend phase II dose (R2PD) efficiently.[161] In addition, pharmacokinetic/ pharmacodynamics as well as biomarker studies should be incorporated early in phase I/ II studies. Finally, collaboration between regulatory authorities, pharmaceutical companies and academic institutions is paramount to co-develop multiple drugs from different origins whilst ensuring intellectual property and funding issues are dealt with appropriately.[161]

1.4.3 Biomarkers in EGFR and PI3K inhibitor therapies

A third general strategy to improve targeted therapy treatment is to discover positive predictive biomarkers which may identify patients who will benefit from these treatments. Of recent times, probably the most topical biomarker in PDAC is the Human Equilibrative Nucleoside Transporter (hENT-1)- a bi-directional transporter of pyrimidine nucleosides into cells, where low hENT-1 predicts for gemcitabine resistance and poorer survival.[209-211] On the other hand, discovering biomarkers for targeted therapies in a disease with extensive genetic alterations proves most challenging, and genetic profiling is likely needed in early phase development of these drugs and combinations to enable researchers to tailor drug dosing for each patient.[197] Here current literature informing possible biomarkers in EGFR and PI3K inhibitor therapies is described.

EGFR inhibitors: In PDAC, the study of erlotinib and biomarkers are somewhat limited. Pre-clinical studies implicate HER-3 mediated PI3K/ Akt pathway activation and quasi-

mesenchymal status as negative predictive markers for erlotinib treatment.[163,212] However, in clinical studies, Akt over-activation and K-Ras mutation are only recognized as negative prognostic markers at this stage, whilst their predictive values remained unproven.[44,54] There are two translational studies based on large phase III clinical trials published to date. In the sub-study from the investigator of the PA.3 trial, *K-Ras* mutation status and EGFR gene copy numbers (by FISH) were retrospectively analysed.[213] Unfortunately, as PA.3 trial did not mandate tissue biopsy in its eligibility criteria, only 32% patient samples (181/569) could be retrieved for further analysis, of which only 26% *K-Ras* mutation status and 15% EGFR FISH results were available. The result was inconclusive, with no significant interactions reported for *K-Ras* mutation (P=0.38) or EGFR high polysomy (P=0.32), and OS was not significant different between patients with *K-Ras* mutant and *K-Ras* wild type tumours (7.4 vs. 4.5m, HR=0.68, P=0.30) or between EGFR FISH positive and FISH negative tumours (6.7 vs. 5.3m, HR=1.07, P=0.83). As the investigators rightly pointed out, the study limitations (retrospective design and small sample size) may have influenced the potential prognostic and predictive values of individual markers.[213] In the AIO-PK0104 study, the investigators prospectively collect tissue and analyse K-Ras mutations on fixed paraffin embedded tissue.[121] They also retrospectively analysed EGFR over-expression, *EGFR* gene amplification, intron 1 and exon 13 polymorphism and PTEN over-expression.[60] To the credit of the investigators, they were able to collect tumour blocks in 74% (208/281) and successfully performed *K-Ras* mutation testing on 61% (173/281) cases. The prevalence of *K-Ras* mutation was lower than reported in literature (70%), whilst EGFR gene was found to be overexpressed in 46% by FISH, EGFR over-expressed in 49% by IHC and PTEN over-expressed in 18% by IHC. Patients with *K-Ras* wild type appear to have a longer OS than those with *K-Ras* mutated tumours (7.9 vs. 5.7 m, HR 1.68, P=0.005), but there is no correlation between *K-Ras* status and other study endpoints. Loss of *PTEN* was associated with shorter (Time- to- treatment failure) TTF1 and TTF2 (P=0.02, P=0.04), but none of the EGFR related markers are co-related with differences in any study endpoints, nor are they co-related with each other.[60] From this analysis, *K-Ras* status and PTEN expression may represent important markers in PDAC, though whether they

have prognostic or predictive value remain to be seen. EGFR or *EGFR* gene have limited value, and the authors suggest that further translational research should focus on downstream signalling pathway networks PI3K-PTEN-AKT and RAS-MAPK-MEK-ERK.[60] One other study examined *EGFR* mutation, copy number and *K-Ras* mutation in 66 consecutive patients with PDAC. Whilst presence of *K-Ras* mutation was adversely prognostic (P=0.03), *EGFR* mutation or copy number were not.[214]

Despite the apparent lack of utility of EGFR as a predictive marker for erlotinib sensitivity and resistance in translational studies, there certainly appears that EGFR signalling continues to have a vital role in the tumour biology of PDAC. Although EGFR mutation is rare in PDAC (1.5%) and is typically silent, it can certainly co-exist with *K-Ras* mutation in PDAC.[58,213-215] *EGFR* gene is in fact over-amplified in 42% cases and EGFR tyrosine kinase is over-expressed in 77% of cases.[59] EGFR over-expression, whilst not shown to be prognostic, was strongly correlated with metastasis to lymph nodes and distant organs.[165,216] A seminal paper in Cell found evidence through *in vivo* gene knockout models that EGFR signalling is absolutely vital for PDAC carcinogenesis and progression, and that K-Ras oncogenic driven lesions remain dependent on EGFR signalling.[165] This stands in sharp contrast to our understanding of NSCLC and CRC tumours, where K-Ras and EGFR mutations are mutually exclusive.[58,165] The group further found that EGFR co-operate with K-Ras by activating the AKT and STAT3 pathways, suggesting the need of compound inhibition of all 4 pathways to abrogate progression of PDAC tumours.[165] Based on these findings, EGFR, Ras and PI3K/Akt signalling should all be evaluated as biomarkers in further translational studies, and this probably requires multiple platforms evaluating both genetic and molecular markers.

PI3K/Akt inhibitors: PI3K/ Akt inhibitors have only just entered into early clinical development at this stage. There is active research into evaluating candidate biomarkers for PI3K/ Akt inhibitors; but suffice to say, there are much conflicting results in the early stages of this translational research. Biomarkers for the PI3K/ Akt inhibitors have generally been evaluated under three groups: pharmacodynamics (molecular) markers, metabolic markers and genetic

markers.[47] Pharmacodynamic markers refer to indicators of whether the drugs are hitting the target, and current development focuses on testing phosphorylation of key molecular signals (e.g. Akt, S6, 4EBP-1) in surrogate tissue such as serum, skin or hair through serial sampling. Whilst the strategy appears innovative, this strategy is currently limited by variability in measurements and lack of correlation between surrogate and tumour tissue levels **(table 1.6)**.[47] Metabolic markers are another interesting concept, given that PI3K is intricately involved in glucose metabolism.[46] Attempts have been made to assess dose-response relationship with fasting serum glucose, insulin and C-peptide, but these are limited by normal diurnal variations.[47] ^{18}F-flurodeoxyglucose (FDG)- PET scans appear to correlate strongly with PAM inhibitor treatment response in early pre-clinical studies, suggesting a role of PET as an imaging biomarker for PAM inhibitors treatment.[217,218] This is now a focus of ongoing phase I trial research in this area.[47] Lastly, genetic markers such as PIK3CA mutations and PTEN loss have been assessed in clinical trials with PAM inhibitors, in an attempt to identify predictive biomarkers that may be used to enrich future study populations.[47] In a translational study of a phase I study of 217 patients with advanced tumours, Janku *et al.* found that PIK3CA was mutated in 11.5% of patients, with the highest frequency in endometrial cancer (21%), followed by ovarian (17%), colorectal (17%), breast (14%), cervical (13%) and lung (11%) cancers. Among the patients who received a PAM inhibitors as part of their treatment, response rate was significantly higher for patients with PIK3CA mutation than those without documented mutations (35% vs. 6%, P=0.001). Furthermore, the duration of response for these patients was at least 9 weeks, and as long as 59 weeks by censoring.[219] Despite these encouraging results, identifying genomic markers for PI3K inhibitors prove more challenging than for EGFR or BRAF targeted therapies, due to coexistence of gene mutations (45% of patients with PIK3CA mutation also harbour K-Ras mutation), conflicting preclinical data on the activity of PAM inhibitors in specific molecular setting as well as continuing issues with assays detecting PI3K alterations.[47,219] Certainly, more work is needed to validate these potential biomarkers and translate them into clinical practice.

Table 2 | Pharmacodynamic markers explored in the first clinical trials with PI3K/AKT/mTOR inhibitors

Agent	PD imaging FDG–PET	PD effects on surrogate tissue (% of decrease from baseline)	PD effects on tumour tissue (% of decrease from baseline)
Pan-PI3K			
XL147[9]	Not presented	Decreased levels of pRPS6 in skin (in selected cases)	Decreased levels of pAKT Thr308 (40–80%), p4EBP1 (60–70%), pERK (40–60%), and Ki-67 (in selected cases)
BKM120[7]	Yes (9/19 patients had a metabolic PR)	Decreased levels of pRPS6 in skin in >40% patients (11/14 at MTD); increased levels of C-peptide (dose-dependent)	Decreased levels of pRPS6, pAKT, p4EBP1 and Ki-67 (in selected cases)
GDC-0941[11]	Yes (6/17 patients had a metabolic PR)	Decreased levels of pAKT Ser473 in PRP	Decreased levels of pRPS6 (in selected cases)
BAY80-6946[49]	Yes (selected cases)	Not presented	Not presented
PX-866[44]	Not presented	Decreased levels of RPS6 ribosomal protein and mTOR phosphorylation in PBMCs	Not presented
CH5132799[110]	Yes (selected cases)	Decreased levels of pAKT in PRP (up to 80%)	Not presented
PI3K–mTOR			
XL765[8]	Not presented	Not presented	Decreased levels of pAKT Thr308 (50–80%), p4EBP1 (60–80%), and pERK (50–80%) in selected cases
BEZ235[36]	Yes (8/37 patients had a metabolic PR with QD dosing and 4/9 with BID dosing)	Increased levels of C-peptide, and decreased levels of pRPS6 in skin and sVEGFR2 (dose-dependent)	Decreased levels of pRPS6 (in selected cases)
GDC-0980[12]	Yes (5/6 patients had a metabolic PR)	Decreased levels of pAKT (>90% compared with baseline)	Not presented
mTORC1/2			
OSI-027[111]	Not presented	Decreased levels of p4EBP1 Thr37/Thr46 in PBMCs (>60% compared with baseline)	Not presented
AZD2014[112]	Not presented	Decreased levels of pAKT Ser473 in PRP, p4EBP1 Thr37/Thr46 in PBMCs	Decreased levels of pRPS6 Ser235/Ser236 (average 38%, 8/10 samples), pAKT Ser473 (average 40%, 3/6 samples), and Ki-67 (selected cases)
CC-223[113]	Not presented	pRPS6 (B cells), p4EBP1(T cells) and pAKT (monocytes)	Not presented
MLN-128 (INK128)[114]	Not presented	Decreased levels of p4EBP1 in PMBCs, and decreased levels of p4EBP1, pRPS6 and pPRAS40 in skin in 60–100% of patients	Not presented
AKT			
MK-2206[13]	Not presented	Sustained decreased levels of pPRAS40 Thr246/total PRAS40 ratio (median 48%) in hair follicles (QD regimen)	Decreased levels of pAKT Ser473 (40–95%, median 89%, in 9 patients at MTD–QD regimen)
GDC-0068[33]	Not presented	Decreased levels of pGSK3β in PRP (dose-dependent) of >70% compared with baseline	Decreased levels of pPRAS40 (>50%) and cyclin D1 (dose-dependent)
GSK795[32]	Yes (7/8 patients had a metabolic PR)	Not presented	Decreased levels of pPRAS40 (30–70%), Increased levels of pAKT (in selected patients)
PI3Kδ			
CAL-101[10]	Not presented	Decreased levels of pAKT Thr308 in CCL cells of >90% compared with baseline	Not presented

Abbreviations: BID, twice a day; CCL, chronic lymphocytic leukaemia; FDG–PET, ^{18}F-fluorodeoxyglucose PET; MTD, maximum tolerated dose; p4EBP1, phosphorylation of eukaryotic translation initiation factor 4E-binding protein 1; PBMCs, peripheral blood mononuclear cells; PD, pharmacodynamic; pGSK3b, phosphorylation of glycogen synthase kinase-3 beta; PR, partial response; PRP, platelet-rich plasma; pPRAS40, phosphorylation of proline-rich AKT1 substrate 1; pRPS6, phosphorylation of 40S ribosomal protein S6; QD, every day; QW, once a week; sVEGFR2, soluble VEGFR2.

Table 1.6: Pharmacodynamic markers of PI3K inhibitors. From Rodon et al. (2013): Development of PI3K inhibitors: lessons learned from early clinical trials[47]

1.5 Study Hypotheses and Aims

To summarise, PDAC is a deadly disease that is often diagnosed late, and for which there are few treatment options available. Targeted therapies, whilst becoming an important armamentarium in a number of cancers such as NSCLC, CRC, breast cancer and renal cell carcinoma, have unfortunately little role in PDAC yet. The genetically heterogeneous nature means that clearly empirical testing of targeted therapy in unselected population will bound to fail;[220] unless biological rational *in vitro* and *in vivo* combination treatment models are developed there is a high probability that the wrong drug/s will be tested in the wrong molecular setting.[198] This current research program was designed 4 years ago, to dissect the tumour biology of EGFR inhibitor resistance, leading to *in-vitro and in-vivo* and clinical testings of EGFR/ PI3K combined blockade. The first 3 stages will be covered in chapter 3, 4, 5 of this thesis, and these findings are now leading to study proposal for a phase I/ II study. **(Figure 1.16)**.

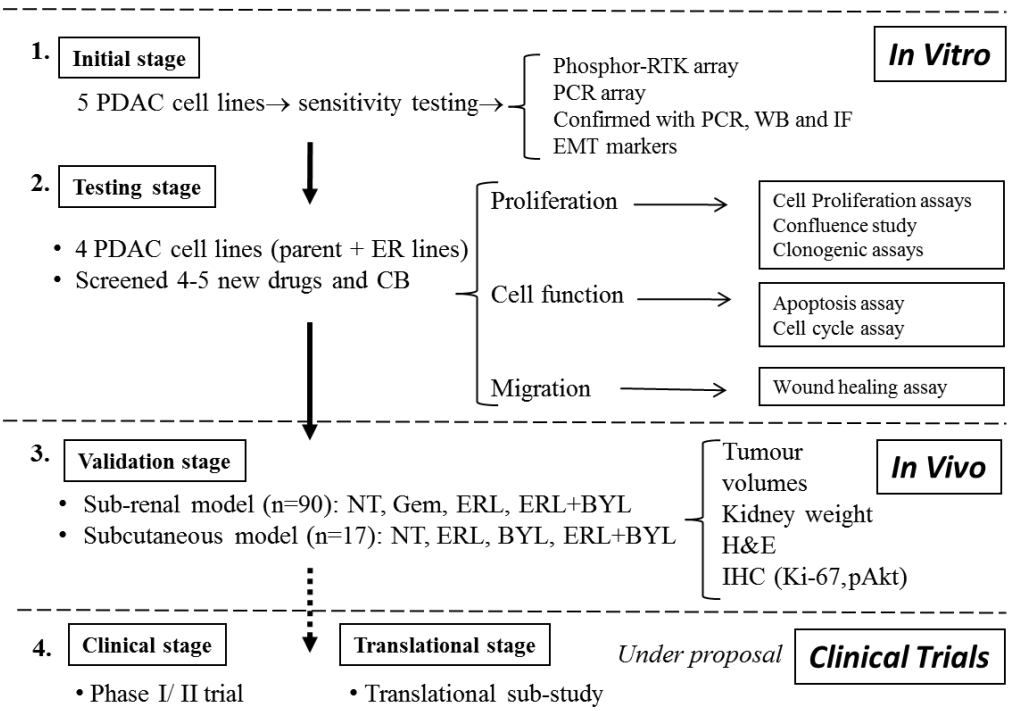

Figure 1.16: Summary of Methods in the Research Program. *ER denotes erlotinib resistant cell lines

The overall objective of this project is to establish pre-clinical evidence of combined blockade of co-dependent pathways to inhibit pancreatic cancer based on the concept of synthetic lethality, for it to be recommended for clinical development. The hypotheses and aims for the chapters to come are as follows **(table 1.6 and 1.7)**, and will be developed at the beginning of the respective chapters.

Chapters	Chapter Hypotheses
Chapter 3: genetic and molecular characterisation of primary and acquired erlotinib resistance **(initial stage)**	1. The lack of clinical benefit of erlotinib in PDAC may be due to development of resistance 2. There is a distinction between primary and acquired resistance 3. Based on current knowledge, there is a high probability that erlotinib resistance is associated in over-activation of reciprocal pathways (EGFR, IGF1R, MAPK or PAM)
CHAPTER 4: dual blockade versus single blockade of EGFR and PI3K/mTOR in-vitro **(testing stage)**	1. Given findings of chapter 3 that downstream MAPK and PAM pathways are involved in erlotinib resistance, combined horizontal blockade is likely synergistic and more effective than single blockade 2. Downstream horizontal blockade is likely more effective than upstream horizontal blockade
CHAPTER 5: dual blockade of EGFR and PI3K in-vivo **(validation stage)**	1. The subrenal patient xenograft tumour tissue model may reflect tumour mechanisms in human beings in a more realistic way 2. The model may be used to test drug combinations, discover predictive biomarkers and develop resistance models.

Table 1.6: Hypotheses of the research project

Chapters	Chapter Aims
Chapter 3: genetic and molecular characterisation of primary and acquired erlotinib resistance **(initial stage)**	1. To assess erlotinib sensitivity in 5 PDAC cell lines 2. To develop PDAC cell lines with acquired resistance to erlotinib 3. To study molecular properties for primary and acquired erlotinib resistance 4. To propose treatment strategies that may exploit the knowledge of erlotinib resistance
CHAPTER 4: combined blockade versus single blockade of EGFR and PI3K/mTOR in-vitro **(testing stage)**	1. To compare the effect of combined blockade (CB) versus single blockade (SB), and to establish synergy 2. To propose the "best" CB combination for pancreatic cancer to take to in-vivo study 3. To explore onocogenic dependence by comparing differential response to CB between parent and resistant cell lines
CHAPTER 5: combined blockade of EGFR and PI3K in-vivo **(validation stage)**	1. To establish and validate a pancreatic cancer xenograft model for drug testing 2. To test the in-vivo efficacy of EGFR and PI3K dual blockade

Table 1.7: Summary of chapters and chapter aims

CHAPTER 2:

MATERIALS AND METHODS

2.1 Materials

2.1.1 Cell Lines

BxPC-3 and CAPAN-2 were purchased from ATCC (Manassas, VA), CFPAC-2 and PANC-1 were gifts from St George and MiaPACA-2 from Royal North Shore Hospitals. Cell lines were typed and they conformed to the ATCC reference standards (CellBank, Westmead, NSW). All 5 cell lines except for BxPC-3 are *K-Ras* mutated. The genetic, phenotype characteristics and erlotinib sensitivities of these cell lines are illustrated in **table 1.**

BxPC-3 (ATCC CRL-1687) (ATCC: the American Type Culture Collection, Manassas, VA, USA) is an epithelial type PDAC derived from the body of the pancreas from a 61 year-old female.[221,222] It has a poorly differentiated grade and is known to have a rapid doubling time of 24 hours.[223] The tumorigenicity of this cell line was proven by xenograft in nude mice, and it differentially expressed carcinoembryonic antigen, human pancreas-cancer associated antigen and human pancreas-specific antigen.[223] Unlike most PDAC cell lines, BxPC-3 is *K-Ras* wild type. It is also wild type for p16, but is mutated for p53 (codon 220 Cys) and deleted for SMAD4/DPC-4.[224] It has a 69% inhibition with erlotinib 10μM *in-vitro*,[163] and is the most erlotinib sensitive among 12 PDAC cell lines studied *in-vivo*.[84]

CFPAC-1 (ATCC CRL-1918) is derived from a PDAC liver metastasis of a 26 year-old Caucasian male with cystic fibrosis (CF).[225] The cells show epithelial morphology and polarisation with apical microvilli. It is well differentiated, and has a doubling time of 32 hours. It has been stable for over 80 passages.[225] CFPAC-1 is *K-Ras* mutated (codon 12 Val), p53 mutated (codon 242 Arg), p16 methylated and SMAD-4/DPC-4 deleted.[226] Additionally, it displays a phenylalanine-508 deletion, the commonest form of CF mutation.[225] *In-vitro,* it is inhibited by 51% with erlotinib 10μM.[163] *In-vivo,* it is found to be sensitive to erlotinib.[84]

CAPAN-2 (ATCC HTB-80) originated from a 56-year old male with PDAC, whose primary tumour involved the head of pancreas and invaded the duodenal wall distal to ampulla.[227,228] The allozyme phenotypic profile of CAPAN-2 was determined in eight genetically determined loci, and it showed characteristics of ductal epithelium ultrastructurally.[139,222] CAPAN-2 has an exceedingly long doubling time of 96 hours. It is *K-Ras* mutated (codon 12 Val); but is wild type for p53, p16 and SMAD-4/DPC-4.[228] It is inhibited by 50% with erlotinib 10µM *in*-vitro,[163] but is only moderately sensitive to erlotinib *in-vivo.*[84]

MiaPACA-2 (ATCC CRL-1420) is a PDAC cell line isolated from a 65 year-old Caucasian male in 1975.[229] The tumour was poorly differentiated and involved the body and tail of the pancreas that had invaded the periaortic area.[228] This cell line has a mesenchymal morphology and displayed both mesenchymal and amoeboid motility.[222,230] MiaPACa-2 was first reported to have a doubling time of 40 hours,[229] but a doubling time as short of 19 hours has been reported.[223] MiaPACA-2 is *K-Ras* mutated (codon 12 Cys), p53 mutated (248 Trp) and p16 deleted, but it is wild type for SMAD-4/DPC-4.[226] It is insensitive to erlotinib *in-vitro* with only 9% inhibition with erlotinib 10µM and it is also insensitive *in-vivo.*[84,163]

PANC-1 (ATCC CRL-1469) was from an epithelioid PDAC carcinoma from a 56 year-old male, whose primary tumour originated from the head of the pancreas, and invaded the duodenal wall and metastasized to peripancreatic lymph node.[228,231] PANC-1 has a mixed population of epithelial and mesenchymal cell type,[222,232] but is known only to express mesenchymal marker vimentin and not epithelial marker e-cadherin.[84] It is poorly differentiated, has a doubling time of 52 hours and displays glucose-6-phosphate dehydrogenase deficiency (G6PD) activity of the B-type slow mobility.[231] PANC-1 is *K-Ras* mutated (codon 12 Asp), p53 mutated (codon

273 His) and p16 deleted, but it is wild type for SMAD-4/DPC-4.[226] Like MiaPACA-2, it is not sensitive to erlotinib *in-vitro* (8% inhibition with erlotinib 10μM) and *in-vivo.*[84,163]

Cell Lines	**BxPC-3**	**CFPAC-1**	**CAPAN-2**	**MiaPACA-2**	**PANC-1**
Origin	Body of Pancreas Primary	Liver Metastasis	Head of Pancreas Primary	Body/tail of Pancreas Primary	Head of Pancreas Primary
Cell Type	Epithelial	Epithelial	Epithelial	Mesenchymal	Mixed
Doubling Time	24hr	32hr	96hr	40hr (18hr has been reported)	52hr
Differentiation	Moderate	Well	Well	Poor	Poor
E-Cadherin	+	+	+	-	-
Vimentin	-	-	-	+	+
K-Ras	**WT**	12Val	12Val	12Cys	12Asp
p16	WT	WT	WT	del	del
p53	220Cys	242Arg	WT	248Trp	273His
SMAD-4*	1659del	del	WT	WT	WT
ERLOTINIB SENSITIVITY	**VERY HIGH**	**HIGH**	**MODERATE**	**LOW**	**LOW**

Table 2.1: Genetic, morphological characteristics and erlotinib sensitivities of 5 PDAC cell line used for in-vitro experiments. *Number denotes the position of the gene codon where the mutation occurs, resulting in the translation of an incorrect amino acid. WT- wild type. Del- deleted. Val- valine, Cys- cysteine, Asp- aspartic acid, Arg- arginine, Trp- tryptophan, His- histidine.*[84,226,228]

2.1.2 Media for Cell Culture

Dulbecco's Modified Eagle's Medium (DMEM)

DMEM medium (Hyclone, Thermo scientific Fisher, NSW, Australia) with 2mM L-glutamine, supplemented with 10% Fetal Bovine Serum (FBS) Ausgene X, QLD, Australia) and 1% L-glutamine (Thermo Scientific Fisher) was used for cell culture for MiaPACA-2 and PANC-1 cell lines. It was also used for PANC-ER, a cell line derived from PANC-1 and made resistant to erlotinib.

RPMI 1640 Medium

BxPC-3, CFPAC-1 and CAPAN-2 cell lines were cultured in RPMI 1640 solution (Thermo Scientific Fisher), supplemented with 10% FBS and 2mM L-glutamine. It was also used for BxPC-ER, a cell line derived from BxPC-3 and made resistant to erlotinib.

2.1.3 Novel Tyrosine Kinase Inhibitors (inhibitor)

Erlotinib ($C_{21}H_{21}N_3O_4$.HCl, MW 415.87) is an oral epidermal growth factor receptor/ human epidermal growth factor type 1 (EGFR/ HER1) tyrosine kinase inhibitor (TKI) with a half-life of 36 hours.[233] EGFR is expressed on cell surface of normal cells and epithelial type cancer cells; erlotinib inhibits phosphorylation of EGFR tyrosine kinase in these cells with nanomolar potency.[233] It is currently TGA approved for the indication for the treatment of locally advanced or metastatic PDAC in combination with gemcitabine, first-line in NSCLC with EGFR mutation, and subsidised by the Pharmaceutical Benefits Scheme (PBS) for NSCLC after prior platinum based doublet chemotherapy due to progression or intolerance of chemotherapy.[234] Erlotinib was used in both *in-vitro* and *in-vivo* studies in this project. For *in-vitro* experiments, erlotinib was purchased from Selleckchem, Houston, TX (cat no: S2205), and was diluted with 100% DMSO to 20mM stock. Final concentration tested for *in-vitro* experiments ranged from 5 to 30µM, as initial optimisation experiments had found that erlotinib concentration higher than 30µM could not be completely dissolved in medium resulting in crystallisation. For *in-vivo*

experiments, 150mg erlotinib tablets for clinical use (Roche) were homogenized in 6 mg/ml 0.5% methylcellulose prepared fresh twice weekly for gavaging, and stored at -20ºC for a maximum of 7 days.

Gefitinib ($C_{22}H_{24}ClFN_4O_3$, MW 446.90) is an oral selective EGFR inhibitor with EGFR inhibitory IC_{50} of 0.03µM and a half-life of 41 hours.[233,235] *In-vitro,* it has a cellular inhibitory IC_{50} as low as 0.2 to 0.4µM in colon cancers, breast cancers and ovarian cancers, but only significantly reduces cell proliferation at concentration above 20µM in pancreatic cancer.[236,237] Although gefitinib is active across many tumour types *in-vivo*,[235] gefitinib has only been extensively investigated in NSCLC clinical trials, and its clinical efficacy in PDAC is unproven. Gefitinib is used alongside erlotinib in *in-vitro* studies to assess sensitivities of cell lines to EGFR inhibitors. Gefitinib was purchased from Selleckchem, Houston, TX (cat no: S1025), and was diluted with 100% DMSO to 10mM stock. Final concentration tested for *in-vitro* experiments ranged from 5 to 30µM.

NVP-AEW541 ($C_{27}H_{29}N_5O$, MW 439.55) is an IGF1R inhibitor belonging to the pyrrolo [2,3-d]pyrimidine class family of compounds, with equipotent inhibition activity against IGF1R (IC_{50}=0.15µM) and Insulin Receptor (Ins-R) (IC_{50}=0.14µM) on kinase activity assays, and highly specific cellular inhibitory activity for IGF1R (IC_{50} = 0.086µM) which is 27-fold higher than Ins-R and other kinases. It also has activity against Akt and MAPK signalling pathway.[238] It has *in-vivo* activity against various tumour types including pancreatic cancer, colorectal cancers and sarcoma, but has not yet been studied in clinical settings.[238-240] NVP-AEW541 was purchased from Selleckchem (cat no: S1034) used for *in-vitro* studies only. It was dissolved in 100% DMSO as a 2mM stock and frozen in -20ºC refrigerator.

LY-294002 ($C_{19}H_{17}NO_3$, MW 307.34) has been extensively studied in preclinical studies as a pan-PI3K inhibitor with inhibitory IC_{50} of PI3K-p110α, p110δ, and p110β of 0.5, 0.57 and 0.97µM, resulting in a dose-dependent inhibition of Akt.[241,242] LY-294002 is in fact not a very

specific PI3K inhibitor, as it also binds to other non-lipid kinases such as CK2, mTOR and GSK3β, though all these kinases may indirectly relate back to PI3K.[243] It is also not very potent, as it only inhibits PI3K with micromolar potency.[180] LY-294002 has proven *in-vivo* efficacy in pancreatic cancers, colorectal cancers, hepatoblastoma and ovarian cancers among many others.[53,242,244,245] In this project, LY-294002 was purchased from Selleckchem (cat no: S1106) and was used *in-vitro* to compare with specific PI3Kα inhibitor NVP-BYL719. It was dissolved in 100% DMSO as a 2mM stock and frozen in -20ºC refrigerator.

NVP-BYL719 is a novel specific class I PI3Kα inhibitor currently being developed by Novartis and donated by Novartis for these experiments (Basel, Switzerland). It has been tested *in-vitro*, *in-vivo* with plans for clinical development.[246] Due to privacy agreement with the pharma company, details of previous studies could not be provided in this thesis. NVP-BYL719 was used for both *in-vitro* and *in-vivo* studies. For *in-vitro* studies, it was dissolved in 100% DMSO as 2mM stock and stored in 4ºC refrigerator upon advice from Novartis. For *in-vivo* studies, NVP-BYL719 was prepared fresh twice weekly and homogenized in 6 mg/ml 0.5% methylcellulose for oral gavaging, and stored at -20ºC for a maximum of 7 days.

NVP-BEZ235 is a novel dual PI3K/ mTOR inhibitor also currently developed by Novartis. It has an inhibitor IC_{50} of 75nM against Class I PI3K, and also has nanomolar potency against mTOR (IC_{50} =20nM). It has strong anti-proliferative activity with an average GI_{50} of 10 to 12nM, and also strong anti-tumour activity *in-vivo* at 25mg/kg twice daily.[183] Whilst NVP-BEZ235 was only a recently developed inhibitor over the last few years, it already had established *in-vivo* activity against pancreatic cancers, ovarian cancers, renal cell carcinomas, and is now being developed in phase I clinical trial.[184-186] NVP-BEZ235 was initially purchased from Biochempartner (Shanghai, China) and later supplied by Novartis. For *in-vitro* studies, it was dissolved in 100% DMSO as a 40μM stock and frozen in -20ºC refrigerator. For *in-vivo* studies,

it was homogenized in 6 mg/ml 0.5% methylcellulose prepared fresh twice, and stored at -20ºC for a maximum of 7 days.

PD-98059 ($C_{16}H_{13}NO_3$, MW 267.28) is the first and oldest synthetic inhibitor of the MAPK pathway via selective MEK inhibition (IC_{50} =2µM).[247] Over the years, it has been extensively studied in cancers *in-vitro*, predominantly to illustrate connections of MAPK/MEK/ERK pathways to other systems.[248-251] More recently, it has been investigated in various combination strategies with chemotherapy, IGF1R inhibitors, mTOR inhibitors and PI3K inhibitors.[252-255] PD-98059 was purchased from Selleckchem (cat no: S1177) and dissolved in 100% DMSO as a 4µM stock and frozen in -20ºC refrigerator for *in-vitro* experiments.

Other targeted therapies used in this PhD project were IGF1R inhibitor OSI-906 ($C_{26}H_{23}N_5O$, MW 421.49, Selleckchem) and IGF1R antibody Figitumumab (CP751,871; Pfizer, Conneticut, USA). These drugs were used initially in preliminary experiments, and were later superseded by the more potent NVP-AEW541. Data for these were not shown.

2.1.4 Chemotherapeutic agents

Gemcitabine ($C_9H_{11}F_2N_3O_4$.HCl, MW: 299.66) is a pyrimidine analogue that is primarily cytotoxic for cell undergoing DNA synthesis (S-phase). It is given intravenously in patients with a half- life between 42 to 94 minutes. It is used clinically in a wide range of cancer types including breast cancers, lung cancers, pancreatic cancers and ovarian cancers.[233] It was used predominantly *in-vivo* in the studies given that it is the standard first-line therapy in advanced and metastatic PDAC. Gemcitabine was purchased as powder (Hospira) and reconstituted in sterile normal saline 0.9% into 10mg/ml solution for intra-peritoneal injection *in-vivo*.

Mitomycin ($C_{15}H_{18}N_4O_5$. MW: 334.3) is an antibiotic that has cytotoxic properties. At low concentration, it inhibits DNA synthesis; and at high concentration, it also suppresses RNA and protein synthesis.[233] It was purchased as powder (Bristol-Myers Squibb), reconstituted in sterile normal saline to produce 0.2mg/ml stock, and was used as a cytostatic agent in migration assays.

2.1.5 Antibodies

The primary antibodies p-EGFR, EGFR, p-IGF1R, IGF1R, p-Erk, Erk, p-Akt, Akt, p-S6, S6, p-4EBP1, 4EBP1 and β-actin were purchased from Cell Signalling. Conventional secondary antibodies goat anti-rabbit, goat anti-mouse and human anti-goat, were from Santa Cruz. Fluorescent secondary antibodies goat anti-rabbit (733nM- red), goat anti-mouse (488nM-green) and human anti-goat (733nM- red) were from Cell Signalling. Antibodies were used for western blotting, immunofluorescence and immunohistochemistry experiment (**Table 2a-c**).

Western Blotting Experiments

Primary Antibody	Size (kda)	Optimised Concentration for Primary Antibody	Optimised Concentration for Secondary Antibody
pEGFR $_{Tyr1068}$	175	1:1000	1:1000 (anti-rabbit)
pEGFR $_{Tyr845}$	175	1:1000	1:1000 (anti-rabbit)
EGFR	175	1:1000	1:1000 (anti-rabbit)
pIGF1R $_{Tyr1135}$	95	1:1000	1:1000 (anti-rabbit)
IGF1R	95	1:1000	1:1000 (anti-rabbit)
pERK $_{Thr202/Tyr204}$	42, 44	1:1000	1:1000 (anti-rabbit)
ERK	42, 44	1:1000	1:1000 (anti-rabbit)
pAkt $_{Ser473}$	60	1:1000	1:1000 (anti-rabbit)
pAkt $_{Thr308}$	60	1:1000	1:1000 (anti-rabbit)
Akt	60	1:1000	1:1000 (anti-rabbit)
pS6 kinase $_{Thr398}$	70	1:1000	1:1000 (anti-rabbit)
pS6 kinase	70	1:1000	1:1000 (anti-rabbit)
p4E-BP1 $_{Thr37/46}$	15-20	1:1000	1:1000 (anti-rabbit)
4EBP1	15-20	1:1000	1:1000 (anti-rabbit)
Cleaved Caspase-3	17, 19	1:1000	1:1000 (anti-rabbit)
E-cadherin	110	1:1000	1:1000 (anti-mouse)
Vimentin	58	1:1000	1:1000 (anti-goat)
B-actin	45	1:3000	1:3000 (anti-mouse)

Immunofluorescence Experiments

Primary Antibody	Optimised Concentration for Primary Antibody	Optimised Concentration for Secondary Antibody
pERK (mouse)	1:125	1:1000 (anti-mouse)
pERK (rabbit)	1:125	1:1000 (anti-rabbit)
ERK	1:100	1:1000 (anti-rabbit)
pAkt $_{Ser473}$	1:125	1:1000 (anti-rabbit)
Akt	1:125	1:1000 (anti-rabbit)
Cleaved Capase-3	1:100	1:1000 (anti-rabbit)
E-cadherin	1:150	1:1000 (anti-mouse)
Vimentin	1:150	1:1000 (anti-goat)

Immunohistochemistry Experiments

Primary Antibody	Optimised Concentration for Primary Antibody	Optimised Concentration for Secondary Antibody
Cytokeratin 7	1:100	1:1000 (anti-rabbit)
Cytokerain 20	1:100	1:1000 (anti-rabbit)
p-Akt	1:100	1:1000 (anti-rabbit)
Akt	1:100	1:1000 (anti-rabbit)
Ki-67	1:300	1:1000 (anti-rabbit)

Table 2.2 a-c) Optimised concentration for primary and secondary antibodies for Western blotting (WB), Immunofluorescence (IF) and Immunohistochemistry (IHC).

2.1.6 Primers

Table 3 shows the list of primers used for quantitative real time PCR (qRT-PCR). These primers cover for genes from the PI3K/ Akt pathways as well as alternate pathways such as MAPK, TLR-4 and HER3 pathways. All of these were kiCqStart pre-made sYBR Green primers (Sigma), with the exception of NF-kb1A, Rel and GAPDH which were TaqMan probes (Applied Biosystems). TaqMan probes were used for these because no suitable SYBR Green primers were found for NF-kb system for the PDAC cell lines in this study. GAPDH was used as the reference gene for Taqman assay, and 18S for SYBR Green assay. SYBR Green Primers were obtained in pairs (forward and reverse primers), and different variants of the same gene were obtained to improve the sensitivity of the results. The primer pair, reference codes, exon size, description, position and sequences are shown below:

Primer Pair	Unigene	Ref Seq	Exon	Description
Gene Position		**Sequence (5'-3')**		
PIK3CA_1	Hs.553498	NM_006218	9-10	Phosphoinositide-3-kinase, catalytic, alpha polypeptide
3q26.3		Forward: GAGTAACAGACTAGCTAGAGAC Reverse: AGAAAATCTTTCTCCTGCTC		
PIK3CG_1	Hs.32942	NM_002649	6-8	Phosphoinositide-3-kinase, catalytic, gamma polypeptide
7q22.3		Forward: CAGATTCTACGAATCATGGAG Reverse: TCCTATTTTGTCACCAGTTG		
PIK3CG_2	Hs.32942	NM_002649	10-11	Phosphoinositide-3-kinase, catalytic, gamma polypeptide
7q22.3		Forward: TCAGGACATCTGTGTTAAGG Reverse: GCATCCCGGATATATTCAATG		
AKT2_1	Hs.631535	NM_001243027	2-3	V-akt murine thymoma viral oncogene homolog 2, AKT2
19q13.1-q13.2		Forward: CACCATGAATGAGGTGAATAC Reverse: CTACGGAGAAGTTGTTTAAGG		
AKT2_2	Hs.631535	NM_001243027	1-3	V-akt murine thymoma viral oncogene homolog 2, AKT2
19q13.1-q13.2		Forward: GAAACACAAGGAAAGGGAAC Reverse: AGGTCTTGATGTATTCACCTC		

MAPK1_1	Hs.431850	NM_002745	n/a	Mitogen-activated protein kinase 1. ERK2
22q11.21		Forward: TAACATCTGGAGACTGTGAG Reverse: TGAAGTTAGTGGTTTCATGC		
MAPK1_2	Hs.431850	NM_002745	n/a	Mitogen-activated protein kinase 1. ERK2
22q11.21		Forward: TACCAAAATAACACAGCACC Reverse: TAAACAAGTTACCACATGC		
ERBB3_1	Hs.118681	NM_001982	27-28	V-erb-b2 erythroblastic leukemia viral oncogene homolog 3, HER3
12q13		Forward: ATACACACCTCAAAGGTACTC Reverse: ATCTTCTTCTTCAGTACCCAG		
FOS_1	Hs.728789/ Hs.731317	NM_005252	3-4	FBJ murine osteosarcoma viral oncogene homolog. Fos
14q24.3		Forward: GGAGACAGACCAACTAGAAG Reverse: GTTTTTCCTTCTCCTTCAGC		
TLR4_2	Hs.174312	NM_138557	1-2	Toll-like receptor 4
9q33.1		Forward: TGGAGGTGTGAAATCCAG Reverse: CTTGARAGRCCAGAAAAGGC		
NF-kb1A	Hs00765730_m1	n.a.	n.a.	Nuclear factor- kappa B P50
		Not disclosed by company		
Rel-A	Hs01042010_m1	n.a.	n.a.	Nuclear factor- kappa B P65 (Rel A)
		Not disclosed by company		
18S	X3205.1	HSRRN18S	-	Ribosomal 18S
		Forward: GCCCGAAGCGTTTACTTT Reverse: TCCATTATTCCTAGCTGCGGTATC		
GAPDH	Hs99999905_m1	n.a.	n.a.	glyceraldehyde-3-phosphate dehydrogenase
		Not disclosed by company		

Table 2.3 Primers used in qRT-PCR experiments

2.2 Methods

2.2.1 Cell Culture Protocols

BxPC-3, CFPAC-1, CAPAN-2 and BxPC-ER were cultured in T75 flasks with RPMI medium supplemented with 10% FBS and 1% L-glutamine. MiaPACA-2, PANC-1 and PANC-ER were cultured in T75 flasks with DMEM supplemented with 10% FBS and 1% L-glutamine. Every 3 days old medium would be discarded and fresh medium added. When cells reached 80% confluence, cells were passaged into new T75 flasks. Briefly, cells were rinsed twice using Dulbecco's phosphate buffer saline (dPBS, GIBCO, BRL), after which 2-4mL 0.25% (w/v) trypsin/0.03% (w/v) EDTA solution was added to the flask and incubated at 37^{o}C for 5 to 10 minutes. The cells were inspected under inverted microscope (x40, Olympus, Diagnostic Instruments, NSW, Australia) to check if the cell layer was detached. Once cells were trypsinized, the flask content was added aseptically to a new 15mL tube with 5mL growth medium with 10% FBS, and centrifuged at 1200g for 5 minutes (Eppdendorf Centrifuge 5702, NSW, Australia). After discarding the supernatant, 5mL of fresh medium with 10% FBS was added to the tube and the solution resuspended. At this stage, 10µL of mixture could be added to the haemocytometer for cell counting if new experiments were being set up. Otherwise, the cells were transferred to a new flask at a ratio of 1 to 3 and grown at 37^{o}C in 5% CO_2 in air atmosphere.

Two erlotinib-resistant (ER) cell lines (BxPC-ER and PANC-ER) were subcultured from BxPC-3 and PANC-1 respectively after prolonged treatment daily with graduating concentrations of erlotinib from 10µM to 30µM over a 10-month period, as per a protocol described previously.[64] Cells were not sub-cultured in erlotinib concentration higher than 30µM as crystallisation appeared above this concentration indicating saturation of the drug. Resistant cells were passaged approximately every 10 days with a seeding ratio of 1:2, with the aim of maintaining confluence at less than 20%. Each month after the 4th month, the IC_{50} to erlotinib for inhibition of cell proliferation was calculated, and a small portion of ER cells were cryopreserved as

reserve. At the completion of subculturing cell lines, both BxPC-ER and PANC-ER were tested against erlotinib and a wide range of inhibitor to assess erlotinib resistance and cross resistance to other inhibitors. They were also tested for any mycoplasma contamination and for stability, after which they were stored in liquid nitrogen as per cell storage protocol below. The progress results for the subculturing of ER cell lines were discussed further in **Chapter 3**.

2.2.2 Cell Cryopreservation and Thawing Frozen Cells Protocols

Cells were trypsinised and harvested at 3-5 x10^6 per mL of fresh complete medium with 10% FBS. After centrifuge, supernatant was discarded and an equal volume of complete medium and freezing solution containing 20% heat-inactivated FBS, 20% sterilised DMSO (Sigma-Aldrich, NSW) and 60% appropriate medium was added drop wise with gentle mixing. Cells were aliquoted at 800µL each to pre-label sterile freeing vials, and placed in coolcell racks (Biocision, CA) in -80^{o}C fridge overnight resulting in a rate of approximately 1^{o}C drop per minute. The cells were then transferred to liquid nitrogen tank storage (-196^{o}C).

Frozen cells were removed from liquid nitrogen tank using full personal protective equipment (PPE). The vial was thawed in 37^{o}C water bath by gentle agitation for one to two minutes, and sprayed and cleaned with 70% ethanol. The content of the thawed vial was transferred to a 15mL tube containing 5mL of fresh growth medium with 10% FBS in cell culture cabinet, and then centrifuged at 1200g for 5 minutes. Supernatant was discarded and cells resuspended in 3mL medium, and then transferred to T75 flask with 7mL medium. The culture flask was incubated at 37^{o}C with 5% CO_2 in air atmosphere.

2.2.3 Cell Proliferation (MTT Colorimetric Assay)

The colorimetric MTT assay [3-(4,5-Dimethylthiazol-2-yl)-2,5-diphenyltetrazolium bromide] was used to measure cell proliferation *semi-quantitatively* for cells on treatment compared to control. Cells were seeded at 2 x 10^3 density in 100µL final volume in 96 well plate. The next

day, old medium was discarded and cells were treated with varying concentrations of inhibitor in medium supplemented with 10% FBS in biological triplicates. Cells with complete medium and cells with complete medium plus 0.3% DMSO were used as controls in the initial experiments, since all drugs stock were dissolved with DMSO with final concentration up to 0.3%. In the subsequent experiments, only cells with complete medium were used as control, since it was found that DMSO at 0.3% did not adversely affect cell proliferation. Initial optimisation tested treatment durations for 24, 48, 72 and 96 hours, and had found that 72 hours of inhibitor treatment yielded the most optimal results. After completion of 72 hours treatment, 5mg/ml Thiazolyl Blue Tetrazolium Bromide (Sigma-Aldrich, NSW) was added to medium and results read after 2 hours with colorimeter at 570 (test) and 630nM (reference) wavelengths (Biotek synergy HT, VT, US) Absorbance was calculated as the difference between the test and reference wavelength values. All Cell Proliferation assays were performed in at least six independent experiments to allow for accurate statistical analysis.

2.2.4 Cell Proliferation Assay (Incucyte)

Incucyte Live Cell Imager is a combined incubator and imaging system (Essen Bioscience, VIC) developed to accurately produce *semi-quantitative* measure of cell proliferation. For these experiments, the Essen ImageLock 96-well plates (Essen Bioscience, VIC) were used as fiducial marks at the bottom of each well allowed the camera to lock on the same location of each well and capture accurate images. Cells were seeded in the same density and treated in the same way as in the MTT assay. The ImageLock plate was then transferred to the Incucyte Imaging System, which incubated the plate in 37^{o}C and 5% CO_2 in air atmosphere. Camera was set on phase contrast to capture images of each well every 2 hours for 72 hours. The absolute quantitative measure of confluence was calculated by the Incucyte system as the density of cells in a particular image. The results appeared as a plot of confluence against

time for each treatment. Each experiment was designed with biological triplicate, and four cell proliferation (incucyte) experiments were performed.

2.2.5 Clonogenic Assay (anchorage dependent)

The cell ability to form colonies after exposure to inhibitor was measured by anchorage-dependent clonogenic assay, and the protocol has been described previously.[256] Cells were seeded at 2 x 10^5 in 12-well plates. After 24 hours, these were treated with inhibitor for 72 hours, trypsinised and counted on a haemocytometer. 2000 live cells were reseeded on a new 6-well plate with complete medium (10% FBS). Every 4 days, medium was changed. The 6-well plate was observed under inverted microscope daily, and colonies were defined as a group of more than 50 cells. When confluence reached about 10%, or when there were sufficient colonies observed under the microscopy (typically after 7-10 days of reseeding), 0.05% crystal violet was added for 5 minutes after discarding medium. The plate was washed and air-dried, and images were taken on the LAS-3000 (Fujifilm, NSW). Colonies were counted using Colony v1.1 software (Fujifilm, NSW), and were represented as a percentage of colonies in untreated controls. Biological duplicates were performed in each experiment, and three independent experiments were performed for each comparison.

2.2.6 Phospho- RTK Array

Phospho-RTK array (Cell Signalling, QLD) is a slide-based antibody array kit that allowed simultaneous detection of 39 proteins (28 receptor tyrosine kinases and 11 important signalling nodes), and represents a rapid screening methods of differences in activated signalling pathways between several cell lines. In this study, phospho-RTK array was used to compare basal and EGF-stimulated pathways between ER and respective parent cell lines. For this experiment, 1 x10^5 cells for BxPC-3, BxPC-ER, PANC-1 and PANC-ER were seeded

in 12 well plates in duplicate. After plating overnight, old medium was discarded and serum free medium was added for at least 4 hours. One sample of each cell line was treated with EGF stimulation (10ng/ml) for 15 minutes, and the other untreated. All samples were harvested with Cell Lysis Buffer provided by the kit supplemented with 1mM phenylmethylsulfonyl fluoride (PMSF). Protein Concentration assay (Thermo Fisher Scientific, VIC) was used to equalise amount of proteins between samples and to adjust the final concentration to 0.5mg/mL. For the array procedure, the manufacturer's instructions for the PathScan RTK Signalling Antibody Array Kit were strictly followed. The glass slide and multi-well gasket were first assembled, followed by addition of array blocking buffer for 15minutes, diluted lysate for 2 hours, detection antibody cocktail for 1 hour, and HRP-Linked Streptavidin for 30 minutes, with washing procedures in between each step. For readout, the slide was dissembled and covered with LumiGlo/ peroxide reagent, and read on high-resolution setting on the LAS-4000 imaging system. Graphical representation of 39 phospho-proteins were tested. The chemiluminescence intensity was first quantified with Multigauge software (Fujifilm, NSW), adjusted to both negative and positive controls, and graphed as per manufacturer's recommendations. Western blotting was used to validate phospho-RTK array results.

2.2.7 Western blotting

Western blotting experiments were conducted as previously described.[257] All western blotting experiments were performed three times. Representative blots, and average and standard error of the mean (SEM) of triplicate experiments are provided.

2.2.7.1 Preparing Cell Lysates

As per phospho-RTK array, 1 x10^5 cells were seeded in 12-well plate per sample. All samples were conditioned with serum free medium for at least 4 hours after overnight set down. For drug inhibition studies, inhibitor was added for 60 minutes followed by 15 minutes of growth factor stimulation. For EGFR or MEK inhibitors studies, EGF (10ng/ml) was added. For IGF1R,

PI3K or mTOR inhibitors studies, IGF (50ng/ml) was added. For combined blockade studies, EGF, IGF or both were added in optimisation experiments. In subsequent experiments, EGF and IGF were added together whenever combined blockade (CB) was used to maintain consistency across all experiments. After inhibitor inhibition and growth factor stimulation, cells were washed twice with PBS and lysed with either RIPA buffer containing 1% NP-40, 0.1% Sodium doccyl sulphate (SDS, BDH), 150µL complete protease inhibitors (Roche) and 0.5% sodium deoxycholate (BDH) in PBS; or Laemmli buffer containing 62.5mM Tris, 2% SDS, 10% glycerol, 50mM DTT and 0.01% bromphenol blue. Laemmli buffer was preferred over RIPA buffer, and used whenever possible since the higher concentration of SDS ensured that all protein lysate could be detached from the well and collected. When protein concentration assay was needed as an additional step, however, RIPA buffer was used as Laemmli buffer dyed the lysate blue making it incompatible with protein concentration assay. Lysates were collected in 1mL microtubes and immediately placed on ice. They were then sonicated at 40% Amp for 30 seconds (Vibracell, CT, USA) and centrifuged at 8000g for 10 minutes at 4^{o}C (Beckman Coulter, NSW, Australia). Lysates were stored in -20^{o}C freezer until use.

2.2.7.2 Adjusting Protein Concentration

Protein concentration assay (Thermo Fisher Scientific, VIC) was used whenever western blotting experiments involved comparison across different cell lines or if inhibition studies more than two hours were performed. In the latter case, proteins needed to be adjusted between samples since cells began to die within two hours of inhibitors treatment. Instructions for the Protein Concentration Assay were strictly followed. Eight diluted BSA standards were first prepared from kit ranging from 0 to 200µg/mL. Micro BCA working reagent was prepared by mixing 25 part A with 24 part B and 1 part C. 100µL of lysates or BSA standards and 100µL of Micro BCA working reagent were added to a 96 well microplate in duplicate. After two hours of incubation in 37^{o}C air atmosphere, the absorbance was measured on the plate reader at 562nM. A standard curve was fitted by plotting the average BSA standard absorbance reading and the known concentration (Excel 2010). Protein concentrations of the unknowns were

estimated from the absorbance values on the fitted curve. This information was then used to dilute samples prior to electrophoresis.

2.2.7.3 Electrophoresis

The NuPAGE gels (Bis-Tris 12%, Invitrogen, NSW) were used for electrophoresis. 10-well, 12-well and 15-wells were all used depending on the number of samples to be compared. After removing gel from packaging, the tape at the bottom of the cassette and the comb from the top of the cassette were carefully removed, and it was rinsed with 1x NuPAGE SDS running buffer (Invitrogen, NSW). The mini-cell gel apparatus (Invitrogen, NSW) was set up with both upper and lower chambers filled with 1x running buffer. 15-45µL of sample was added to the well depending on the size of the gel, with 5µL protein molecular weight pageruler (Invitrogen) added on either side of the gel. If protein concentrations needed to be equalised across samples, they were diluted with PBS according to the BCA protein concentration assay. Electrophoresis was run at 180V for 60-90 minutes when the pageruler was observed to reach full length down to the bottom of the gel. For longer gels (20 or 25 well), self-customised gels were used with the Galileo system. Resolving gel was made by combining 3.75ml 1M tris (pH 8.8), 100µL 10% SDS, 4ml 30% 29:1 acrylamide, 100µL 10% APS, 10µL Temed and 2.05ml ddH_2O to a final volume of 10mL. This was inserted between the glass apparatus and left to set for 5 minutes. Stacking gel was made by combining 1.25ml tris (pH6.8) 100µL 10% SDS. 1.6ml 30% 29:1 arcrylamide, 100µL 10% APS, 10µL Temed and 6.95ml ddH_2O to a final volume of 10ml. This was added on top of the resolving gel after it had set, and a 20-well or 25-well comb was inserted between the glasses to create the well. After another 5 minutes of setting, samples could be loaded into these long gels. For these long gels, electrophoresis was run on the Galileo apparatus at 100V for 90-120 minutes.

2.2.7.4 Preparing Various Buffers

Transfer Buffer 10x, TBS 10x were prepared in batches and stored in 4°C refrigerator. When a new western blotting experiment was run, transfer buffer 1x, TBST 1x and 5% Skim milk were prepared fresh. The buffer constituents were listed below:

Transfer buffer 10x (1L): 14.4g Glycine/L, 3.03g Tris Base/L (BDH) in 1L Milli-Q water

Transfer buffer 1x (1L): 100mL Transfer Buffer 10x, 200mL 20% methanol (BDH) and 700mL Milli-Q water to make 1L of Transfer Buffer 1x

Tris Buffered saline (TBS) 10x (1L): 2.42g Tris Base/L, 8.0g NaCl/ L (BDH) in 1L Milli-Q water, adjusted to pH 7.6

TBS-Tween (TBST) 1x (1L): 100mL TBS 10x, 900mL Milli-Q water and 0.5mL Tween to make 1L of TBST 1x

5% Skim milk in TBST: 5g skim milk powder in 100mL TBST

2.2.7.5 Transferring Membrane

After electrophoresis, the cassette was carefully opened and gel immediately placed in freshly prepared Transfer Buffer 1x. Polyvinylidene difluoride (PVDF) membrane (Millipore, MA) was wet in methanol for 1 minute and then transferred to Transfer Buffer 1x. Electroblotting apparatus was assembled from bottom to top with Sponge, 3x layers filter paper, NuPAGE gel, PVDF membrane, 3x layers filter paper and sponge. The apparatus was closed and sealed with white clasp. An ice pack was placed in the apparatus, and it was then filled with 1L Transfer Buffer 1x up to the top of apparatus. The equipment was run at 85V for 2 gels for 90 minutes at room temperature. Long gels were transferred with both gels and membrane placed in the Galileo Transfer system separated by 3x filer papers in a sandwich configuration. Current was set at 0.36mAmp for 120 minutes for a complete transfer.

2.2.7.6 Immunoblotting

After transfer was completed, it was checked to see if Pageruler ladder appeared on either side of the PVDF membrane. This was further checked by placing the PVDF in Ponceau S solution 5% w/v (Sigma, NSW). With good transfer, dark bands representing different proteins should appear on the membrane upon Ponceau exposure. At this stage the membrane could be divided so that different portions of the membrane could be incubated with different primary antibodies simultaneously. The dark bands that appeared on ponceau X was easily reversible by washing the membrane a couple of times with TBST. Membrane was then blocked with 5% skim milk TBST for 1 hour, and then incubated with primary antibody. Primary antibody incubation was performed with 50mL tubes and a roller to conserve amount of antibody needed. For example, 5µL of primary antibody was added in 5mL of 5% skim milk, as according to the optimised primary antibody concentration listed on **Table 2.2b**. Different portions of the membrane were then inserted in the corresponding tubes with the correct primary antibodies. The tubes were then placed on the roller and incubated in the cold room (4^{o}C). In this way, 2 membranes incubated with up to 3 primary antibodies (typically pEGFR at 165 dKa, pAkt at 60 dKa, and pERK at 42 and 44 dKa) could be read simultaneously the next day. After overnight primary antibodies incubation, the membranes were then washed 4x with TBST, and incubated with corresponding secondary antibodies in the same way for 1 hour at room temperature. After 4x further washes with TBST, the membranes were ready to be exposed for imaging.

2.2.7.7 Membrane exposure

ECL (GE Healthcare Life Science, NSW) was used to bring out chemilluminescence of the membrane. All membrane portions were incubated with ECL mixture for 3 minutes in dark. Images were then taken with LAS-3000 at high resolution, with exposure time as determined by the camera.

2.2.7.8 Membrane stripping

Since each membrane portion might have to be incubated several times with different primary antibody, all membrane portions were stripped with stripping solution (Invitrogen, NSW) for 15 minutes in 37ºC. After stripping, the membrane portions were washed at least 4x, after which primary antibody incubation could be repeated **(2.2.6.5).** Membrane portions could be stripped up to three times, after which the bands often became too faint on chemilluminescence to be reliable. If more information was required, a separate western blotting experiment would then need to be run.

2.2.8 Immunofluorescence (Confocal Microscopy)

Confocal Microscopy (Leica TCS SP5, NSW) was used for all immunofluorescence experiments as the tight control on laser emission microscope improved specificity and limited the amount of auto-fluorescence, while the tiny pinhole mounted on a 63x objective allowed cells to be scanned in cross sections down to a few microns thick.[258] All experiments were performed in triplicates. Representative images, averages and SEM were provided, and additionally samples were statistically analysed with 2-sample t-test.

2.2.8.1 Samples preparation and treatment duration

Prior to cells seeding, 10mm diameter coverslips were placed at the bottom of each well in a 12-well plate. 1.5 x 10^5 cells were seeded on top of the coverslips of each well. Serum free medium replaced old medium after cells set down overnight. For the studies of phosphorylated ERK and Akt, EGF stimulation (10ng/ml) was added for 15 minutes as in western blotting experiments. No growth factor stimulation was required if basal level of e-cadherin, vimentin or total proteins were studied. For caspase-3 inhibitor studies, inhibitor in 10% FBS serum was added to samples for various times from 6 to 36 hours after overnight plating, and later on at 16-24 hours after the timing was optimised.

2.2.8.2 Fixing and Permeabilising

Cells were washed with PBS twice, after which they were fixed with 3% formaldehyde and permeabilised with 0.2% Triton X-100 for 15 minutes each, with two PBS washings in between each procedure.

2.2.8.3 Antibody Incubation

The coverslips were lifted from the wells and transferred to a plastic wrap placed inside a cassette box. They were blocked with 2% BSA for 1 hour, and incubated with 60µL e-cadherin, vimentin (1:150); p-ERK, p-Akt (1:125); ERK, Akt (1:100); or capase-3 (1:100) in 2% BSA in dark at 4^{o}C overnight, followed by incubation with secondary fluorescent antibody 1:1000 in dark for 1 hour at room temperature. PBS washings x3 were performed after antibody incubation. DAPI was added to slides, and the coverslips were placed face down on the slides and stored in dark at room temperature. Incubation with DAPI was for at least 30 minutes, but mostly the incubation was for overnight. For each experiment, a positive control and negative control were always included.

2.2.8.4 Confocal Microscopy

Before viewing slides under confocal microscopy, coverslips were sealed on the slides by applying acetone on the side for at least 30 minutes. 4 lasers from the Leica Confocal Microscopy system (blue diode, argon, DPSS, HeNe) were switched on at power of at least 20% to allow for laser excitation to occur at a range from 405 to 633nM. Slides were viewed with x63 objective under oil immersion. All images were captured with the LAS-AF program (Leica). The anti-rabbit, anti-mouse and anti-goat secondary antibodies were of 633nM, 488nM and 633nM respectively, and appeared red, green and red upon exposure to laser emission. Positive control and negative control were first viewed, so that gain parameters could be adjusted. To assess objectively, 5 random images were taken at the top right, top left, bottom right, bottom left and centre of the coverslips for each sample. After all images were captured, the 3 strongest signals of each image were measured for colour intensity,

expressed numerically as mean grey value (MGV) by the program. This means that for each sample 15 highest signals would be obtained in each experiment. As all experiments were repeated in triplicate, a total of 45 values were collected. This then allowed 2- sample t-test to be objectively performed between samples, in addition to providing the usual averages and SEM data.

2.2.9 PCR Array

PI3K PCR Array was a customised 384-well plate that allowed simultaneous analysis of 96 genes (84 genes related to PI3K pathway, 5 housekeeping genes and 7 control genes) between 4 samples (Qiagen). It utilised the same equipment (7900HT) and methodology of qRT-PCR. This was performed twice to compare genetic differences in PI3K pathway between the two pairs of parent and ER cell lines (BxPC-3, BxPC-ER, PANC-1, PANC-ER). Standard RNA extraction, reverse transcription and mastermixes protocols from the company were strictly followed.

2.2.9.1 RNA extraction and purification

RNeasy Mini kit (Qiagen, VIC) was used for RNA extraction. 1.5 x 10^6 cells were seeded as a monolayer in T75 flasks and harvested at the log growth phase two days after seeding. They were first trypsinised and centrifuged in 15ml tubes at 1200g for 5 minutes; then washed with PBS. After second centrifuge, supernatant was discarded and 350µL of buffer RLT was added to lyse pelleted cells. Lysates were homogenised by brief vortexing, and then pipetted to QIAshredder spin column in 2ml collection tubes, before centrifuging at 12,000g for 2 minutes. Equal volume of ethanol was then added to the homogenized lysate for RNA precipitation, and the total volume was centrifuged in RNeasy spin column for 15s at 12,000g so that concentrated RNA was isolated at the spin column. At this stage, DNase digestion was performed as an additional step to remove foreign DNA and improve RNA purification. After 3 washing steps with buffer RPE, 30µL water was added to the spin column and the RNA content was eluted into 1.5ml collection tube. RNAs were stored in -80^{o}C freezer until use.

2.2.9.2 RNA Quantification and Quality Control

Nanodrop spectrophotometer (Thermo Scientific Fisher, NSW, Australia) was used to assess the quantity and quality of RNA. After appropriate dilution, 1µL of RNA from each sample was added to the Nanodrop machine and compared to H_2O blanks. Quantification of the RNA was calculated as an average of two consecutive measurement from Nanodrop after adjustment to the dilutional factor (ng/µL). Quality of the RNA was assessed by the A260:280 ratio (between 1.8 to 2.0 was optimal) and the shape of the mass spectrometry curve (only one peak with low baseline was optimal).

2.2.9.3 Reverse Transcription

Reverse Transcription (RT) was performed with RT^2 First Strand Kit (Qiagen). After diluting all RNA samples to 400ng, the genomic DNA elimination mix of each sample was produced by mixing this with 2µL Buffer GE and making up to 10µL total volume with RNase-free water. After heating this at 42^{o}C for 5 minutes using the Thermal Cycler (Biorad), 10µL of RT mix containing 4µL Buffer BC3 5x, 1µL Control P2, 2µL RE3 RT mix and 3µL RNase-free water was added to produce a 20µL mixture. RT reaction was conducted by incubating this mixture at 42^{o}C for exactly 15 minutes and stopping reaction by 95^{o}C for 5 minutes. Finally, 91µL RNase-free water was added to each reaction, and this was placed on ice for the PCR protocol.

2.2.9.4 Quantitative Real Time PCR

1300µL of PCR component mix was produced by mixing 102µL of cDNA synthesis reaction with 650µL SYBR Green Mastermix and 548µL RNase-free water. The 384-well plate had the following configuration, and already had different primers preloaded in each well.

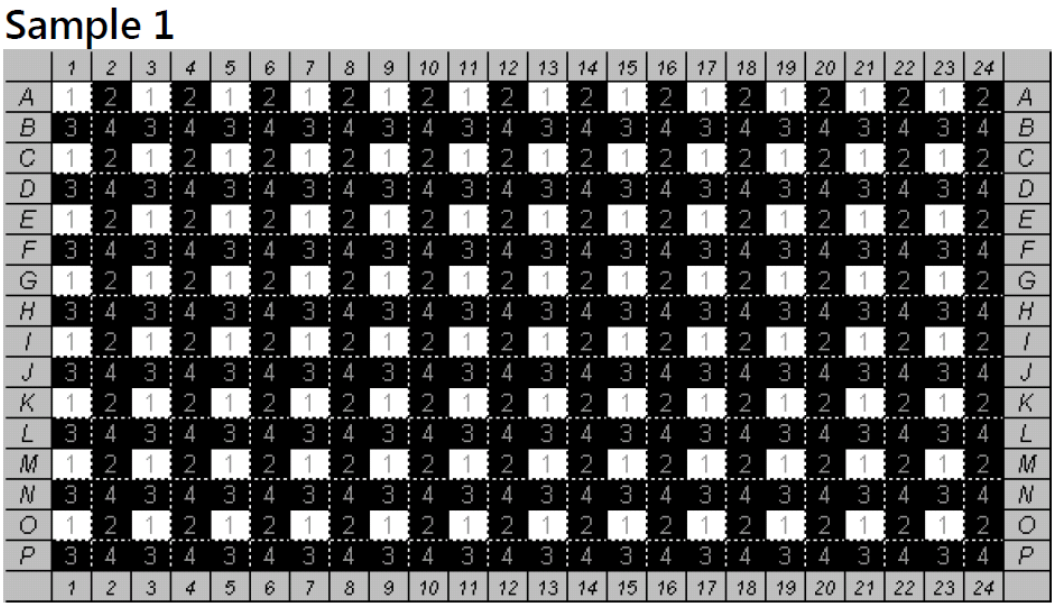

Figure 2.1: Configuration of 384-well PCR array used in the PI3K array experiment

Mastermix/ sample mixtures were robotically dispensed 10µL in each well for sample 1, followed by samples 2, 3 and 4 (EP Motion 5070, Eppendorf). The Qiagen primers were already preloaded in the 384-well array and came with the packing. ROX was built in as the reference dye. After sealing and centrifuging, qRT-PCR was run on the 7900HT system (Applied Biosystems, Australia) with the following cycling condition.

Cycles	Duration	Temperature	Comments
1	10 min	95°C	HotStart DNA *Taq* Polymerase is activated by this heating step.
40	15 s	95°C	
	1 min	60°C	Perform fluorescence data collection.

Table 2.4: qRT-PCR cycling setup

The Qiagen primers had undergone extensive Q.A., and claimed to be “internally validated”. As such, no technical replicates were needed. Instead, PCR array was performed on biological

duplicate (run on two independent experiments), and sought to validate the Genes of Interest (GOI) with standard qRT-PCR.

2.2.9.5 Data Analysis

After setting baseline and threshold for the qRT-PCR data at the exponential phase of the amplification plots, average C_t data for each experiment was exported in excel file and analysed with the web-based program provided by Qiagen. For quality control, RT efficiency as assessed by built-in controls, distribution of C_t ranges and melting curves of key genes were reported. The combined data of two experiments were compared between BxPC-3 and PANC-1, and between each pair of parent and ER cell lines. All results with greater than 3-fold changes were reported. Additionally, scattergram, 3D-plots, clustergrams and histograms were used to present genomic differences between cell lines.

2.2.10 Quantitative Real-time PCR (qRT-PCR)

qRT-PCR was used to confirm results for the PI3K PCR array among the 2 pairs of parent and ER cell lines in the study of acquired erlotinib resistance, as well as to study key genes in the other ATCC cell lines that may be attributable to primary erlotinib resistance. The same method of RNA extraction and RNA quantification was used on all 7 cell lines (5 parent cell lines, 2 ER cell lines) as described in the previous section. For reverse transcription, the Sigma Reverse Transcriptase kit (ReadyScript™ cDNA Synthesis Mix) was used. This kit utilised a blend of oligoDT and random hexamers offering higher sensitivity. Since the predesigned SYBR Green primers may be less specific than Qiagen customised SYBR-based primers or Taqman probes, it was recommended to use this Reverse Transcriptase kit to optimise the cDNA product for qRT-PCR.

2.2.10.2 Standard curve optimisation experiments for SYBR Green primers

For SYBR Green primers, specificity of the primers were tested first by standard curve experiments with 5 points of 10 fold dilution for samples. PCR efficiency was assessed by calculating for slope, efficiency [E= 10 $^{(-1/slope)}$] and R squares of each standard curve, as previously described.[259] Melting curves were also analysed to assess the specificity of the SYBR Green primers. Gel electrophoresis was not performed however, since melting curve analysis is a more accurate method for screening specificity of primers.[260] Standard curve and melting curve analyses were not necessary for the highly specific Taqman probes.

2.2.10.3 Quantitative Real Time PCR

Real Time PCR for validation was conducted with 96 well plates in the same 7900HT system. This protocol was also slightly different than that for PCR array, in that 20µL total volume was used for 96 well plates. For SYBR green primers, each 20µL of PCR Master mix contained 0.4µL (0.2µM) each of forward and reverse primer, 0.2µL SYBR Green primer 0.1x, 0.2µL (10nM) fluorescein as reference dye (BioRad, NSW, Australia), 10µL SuperMix-UDG Mastermix 2x (Invitrogen), 5µL of cDNA sample, and 3.8µL of RNA free water. 18S was chosen as the reference gene. The samples for 18S were diluted 10,000 fold, as 18S is a ubiquitous gene and serial dilutions were needed to bring C_t value back from 9-10 to 14-15 cycles. For Taqman probes, each 20µL of PCR Master mix contained 9µL cDNA, 10µL of universal PCR mix (uPCR, Appied biosystems) and the respective Taqman probe. Standard cycling set ups were used for SYBR and taqman based probes.

2.2.10.3 Data Analysis

For the core experiments, C_t values were acquired and analysed and cross-validated with DataAssist 3.0 (SA Bioscience) and excel 2010 (Microsoft). Intra- and inter-assay precision [Coefficient of Variation (CV) <5%] were measured. Relative quantification (delta-delta C_t or $\Delta\Delta C_t$) method was used, where the calculations for the parameters are as follows:[261]

Delta C_t values (ΔC_t) = $C_{t\ GOI} - C_{t\ Ref}$, where GOI and Ref are gene of interest and reference. In the case of SYBR Green assay, 18S was the chosen Reference Gene; in the case of Taqman assay, GAPDH was the chosen Reference Gene

$\Delta\Delta C_t = \Delta C_{t\ Cell\ Line} - \Delta C_{t\ Ref\ Cell\ Line}$, in these experiments BxPC-3 was reference cell line

Fold change = $2^{(-\Delta\Delta C_t)}$

Standard error = $(SD_{GOI}^2 + SD_{Ref}^2)^{1/2} / n$

All results were reported as fold change to reference cell line BxPC-3, with standard error bars shown. Biological triplicate experiments are performed, and P-values calculated by two-way analysis of variance (ANOVA) of the delta C_t adjusted for experiments. All results showing greater than 2-fold change and P-value <0.05 were considered significant results.[262]

2.2.11 Cell Cycle (Flow Cytometry)

Cell cycle analysis was used to study the effect of different inhibitor and drug combinations on cell cycle arrests in cell lines. Three independent experiments were performed for each comparison. 4 x 10^5 cells were plated on 6 well plates. After seeding overnight, cells were treated with various drugs for 24 and 48 hours. After treatment, cells were trypsinised, fixed, permeabilised and washed as previously described.[263] 300µL each of flow cytometry cell cycle mixture -consisting of 50 µg/ml of propidium iodide (PI), 25 µg/ml of fresh boiled RNase and 0.2% Triton X-100 in PBS- was added to the samples once supernatants were discarded from centrifuged samples. The mixture was resuspended by vortexing, and incubated in dark at room temperature for 30 minutes, then on ice for another 30 minutes. After further vortexing, samples were transferred to FACS tubes, and analysed by the 2-laser 4-colour FACSCaliburs (BD Bioscience, California, USA) on the FL2-A channel (designated to DNA mass by PI). DNA histogram was constructed by Modfit (Verity, Topshem, USA). The endpoint for cell cycle

analysis was S-phase fraction (SPF) between treated cells and untreated controls,[264] but any irregular changes in the DNA histogram were also reported.

2.2.12 Apoptotic Assay (Flow Cytometry)

A local protocol utilising DiLC5 and PI was used to study apoptosis due to various inhibitor or drug combinations.[265] After seeding $2x10^5$ cells in 12-well plates, they were treated with inhibitor for 48 and 72 hours from day 2. After treatment, the samples were trypsinised, centrifuged and resuspended in 300µL of PBS. To each sample 2µL of 2µM DiLC5 was added for 30 minutes to stain for mitochondria, followed by 2µL of 10mg/ml PI for another 30 minutes. Apoptotic Assay was read by FACSCaliburs and analysed on CellQuest (BD Bioscience, California). DiLC5 fluorescence was excited at 633nM laser and detected in the FL-4 channel, and PI was excited at 488 nm and detected in the FL-2 or FL-3 channel. Live cells were located on the upper left quadrant in the apoptotic scatterplot as they accumulated DiLC5 dye in the intact mitochondria but were not stained with PI because of intact membrane. Apoptotic cells had a clear loss of mitochondrial signal but retained an intact membrane, and were located on the lower left quadrant. Necrotic cells had lost mitochondrial signal and was stained with PI because of disrupted membranes, and were located in the lower right quadrant. Apoptotic and necrotic cells were analysed together in a cumulative column graph as they were usually found on a continuum of cell stress and cell death. To accurately estimate apoptosis and necrosis, five independent experiments were performed for apoptotic assay. To validate this particular apoptotic assay, caspase-3 western blotting and immunofluorescence were performed.

2.2.13 Migration Assay (Incucyte)

Cells ($8x10^5$) were seeded in 96-well plates to achieve 100% confluence. After overnight plating, cells were first pre-treated with mitomycin (10µg/ml) as an anti-proliferation agent for at least 3 hours.[266] Essen Bioscience 96-pin wound maker (Essen Bioscience) was then used on the plate to make a uniform scratch in each well. After three washings, the cells were incubated in a fresh medium mixture consisting of 10%FBS, 10µg/ml mitomycin and varying concentrations of inhibitor. The plate was inserted into the Incucyte Imager, where photographs were taken every 2 hours for 48 hours using high definition scratch wound phase-contrast imaging. Cell migration kinetics was quantified using relative migration density as calculated by the software provided. Triplicate experiments were performed and results are presented as average time plots with SEM provided.

2.2.14 General Methods of Animal Experiment

Detailed methodology of the Animal Experiment will be described in Chapter 5. Animal experiments were undertaken as a group work (RS, SJ, AX, SS, MW), with tumour engraftment surgery and tumour harvest primarily performed by AX and SS to ensure quality control. For the core experiments sub-renal transplantation of first-generation xenograft were used. For supplementary experiments, a subcutaneous model of fourth to fifth generation xenografts was utilised. These methods and the rationales for each method will be discussed in more detail in chapter 5.

Briefly, for sub-renal model, patient-derived tumour tissue (PDTT) was harvested from pancreatic cancer parenchyma in patients undergoing Whipple's surgery, and engrafted under both renal capsules of NOD/SCID mice (male, 6-8 week-old; Animal Resources Centre, WA, Australia) in multiple 1 x 2 x 2 mm^3 segments within 2 hours of tumour retrieval, as per methodology described previously.[267,268] In pilot studies, this animal model was validated by demonstrating an engraftment rate >90%, similar histopathology and immunohistochemistry

between xenografts and original tissue, and confirming the effectiveness of standard intra-peritoneal (IP) gemcitabine compared to control. For subcutaneous model, xenograft was passaged using sub-renal engraftment over several generations of mice- a group of 4-5 mice in each generation. The tumour that grew the fastest each time would be chosen and passaged to a new generation. After 4-5 generations, the tumours chosen by "natural selection" were highly pathogenic, and could thus be studied in mice using traditional subcutaneous methods. As with the sub-renal model, tumours were cut into multiple small segments, but were inserted subcutaneously after a small cut was made in the mice's back. After tumour insertion, the edges of the skin were apposed and dermabond glue (Ethicon, NSW) applied.

After engraftment in either model, animals were given standard post-op care for 4 weeks. Animals were then randomly divided into 3-4 treatment groups consisting of control and various drug treatments. Oral medications were gavaged, and IP medications were inserted aseptically with a 30-gauge needle. After 4 weeks of treatment, mice were sacrificed and the kidneys removed and weighed. Lymph nodes, lungs, livers, kidneys, spleens, and bone (femur) of the hosts were also removed, fixed and examined for metastases. The primary endpoint was tumour volume based on the modified ellipsoid formula ½ (Length × $Width^2$),[269,270] and secondary endpoints were kidney weight, metastatic disease and IHC of Ki-67. Animal study was approved by local animal and human ethics committee at Northern Sydney Central Coast Area Health, Sydney, in April 2011 (Reference numbers:1011-015A, 0909-227M)

2.2.15 Haematoxylin and Eosin Staining (H&E) and Immunohistochemistry (IHC)

2.2.15.1 H&E Protocol

H&E and IHC (Cytokerain 7, 20, Ki-67) were performed on all original tumour specimens as well as tumour xenografts upon animal sacrifice, according to standard methods.[271] Tumour tissue was cut, preserved in formalin 10% overnight, and then 70% ethanol. For slide preparation, tissue was paraffin embedded (Leica EG1150H), prepared (Thermo Scientific Fisher), trimmed in 6 µm and then sectioned in 4µm slices (Leica RM2245), and then mounted on standard histology slides (HD scientific Supplies, NSW, Australia). Slides were dried at 65^{o}C for 30 minutes (Labec, Australia) and deparaffinised in two changes of xylene. This was followed by graded series of alcohol immersion (100%, 95%, 75%) and washing in distilled water for 2 minutes. The slides were stained in Harris Hematoxylin for 5 minutes and washed, followed by differentiation in 1% acid alcohol briefly. After this, the slides were stained with Scott's blue and counter-stained with Eosin, with washings in between each procedure. After a series of dehydration in alcohol immersion (75%, 95%, 100%), the slides were again put in two changes of xylene, and further air-dried in 40^{o}C incubator for 5 minutes. Finally, coverslips were mounted on the slide after oil immersion, and left overnight to dry. H&E slides were inspected on inverted microscope (Olympus BX60, NJ, US) to determine the existence of tumours on each xenograft, so that engraftment rate (%) could be determined.

2.2.15.2 IHC Protocol

IHC was performed on all xenografts with tumour present on corresponding H&E sections. New paraffin embedded slides were deparaffinised and immersed in graded series of alcohol as before. The slides were then boiled in buffer (pH 9) at 98^{o}C for 20 minutes, cooled for 15 minutes, washed then blocked with 0.3% H_2O_2 followed by 10% horse serum in slide cassettes. Overnight, slides were incubated with mouse anti-human cytokeratin 7, cytokeratin 20 or ki-67 in humidifier chamber at 4^{o}C (Thermoline Scientific, NSW). The primary antibody

concentration was optimised in initial experiments based on positive labelling of tumour cells against negative background of adjacent stromal tissue, and were listed in **Table 2.2 c**. The slides were washed three times with TBS the next day, and incubated with rabbit anti-mouse IgG-HRP (Dakopatts, Glostrup, Denmark) for 30 minutes at room temperature. After another two washings with TBS, the slides were developed with 3,3' diaminobenzidine (DAB, Dakopatts) for 5-10 minutes. For negative control, primary antibody was omitted. Cytokeratin 7 and 20 staining of slides were inspected under light microscopy to ensure that the staining patterns were similar between original tumour and xenograft tumour treated with control, so to validate the existing animal model. Ki-67 was expressed as a percentage of positively stained cells over all cells observed under 40x objective to the closest 5% by senior pathologist (AG) at Royal North Shore Hospital. pAkt was scored 0, 1+, 2+ or 3+.

2.2.16 General Statistical Analysis

For *in-vitro* experiments, raw results of all experiments were expressed as a percentage to untreated control, except for apoptotic assay where total % of necrosis and apoptosis was expressed (baseline apoptosis and necrosis rate were close to 0%), and in migration and cell proliferation incucyte experiments where absolute values (relative migration density and confluence) were measured by the program. These percentages were combined and expressed as average and SEM. In cell proliferation (MTT) and western blotting experiments, IC_{50} of cell were calculated and expressed as mean IC_{50}, mean IC_{50} +/- SEM. Where appropriate, paired t-tests were performed with P-values calculated to assess for statistical significance. This primarily applied to qRT-PCR and immunofluorescence data, which were discussed in more detail in the relevant sections.

Synergy of 2 inhibitors was studied by cell proliferation and western blotting experiments. 3-D dose reponse curve, synergy index and isobolograms were used.[272] A 6x6 matrix of doubling concentration of drug A and drug B was performed in cell proliferation experiments. Three-

dimensional dose-response curves were fitted with spline interpolation using SAS version 9.2 as described previously (SAS, Cary, NC).[272] A concave contour map with a steep slope from top left to bottom right suggests synergistic effect of the two drugs. A convex or flat contour map with small gradient suggests antagonistic effect. Synergy Index (S.I.) was calculated using PROC NLIN in SAS v.9.2 with the Bliss synergism/ antagonism formula.[272] A S.I. >1 indicates synergism, where the result was *more than* effects of each drug combined; and S.I. <1 indicates antagonism, where the result was *less than* effects of each drug combined. Isobolograms were used to assess synergy in western blotting experiments, where the placement of observed inhibitory IC_{50} of combined inhibitors below the estimated additivity line indicates synergy. These methodologies will be explained in more detail in Chapter 4.

For *in-vivo* studies, tumour volumes between each treatment group were compared using two-way analysis of variance (ANOVA) after adjusting for experiments (SAS v9.2), since tumours xenografts from one patient was used on all mice in each experiment. Tumour volumes data were log transformed as raw data did not conform to the normality assumption.[273] Boxplots of tumour volumes from each group were presented. Ki-67% was categorised with standard quantitative scoring methods (<10%, 10-25%, 25-50%, 50-75%, >75%) prior to statistical analysis.[274,275]

CHAPTER 3:

GENETIC AND MOLECULAR CHARACTERISATION OF PRIMARY AND ACQUIRED ERLOTINIB RESISTANCE

3.1 Introduction

3.1.1 Chapter Background

Erlotinib resistance is an unmet area in pancreatic cancer research. HER-3 mediated PI3K/ Akt pathway activation has been implicated in EGFR inhibitor resistance, and other pathways such as loss of IGFBP3 and MET amplification have also been speculated from studies of other cancer types.[153,154,163,209] However, there is a dearth of research specifically for pancreatic cancer. In recent years, there has only been a small number of *in-vitro* studies on erlotinib resistance in pancreatic cancer,[84,163] and only one translational study on investigating possible predictive biomarkers for this drug, based on a sub-study of the PA.3 phase III clinical trial.[213] Further molecular characterisation of erlotinib resistance is therefore urgently needed in PDAC.

This chapter explores the distinct molecular characteristics of erlotinib resistance. A specific distinction is made between primary (*de* novo) and acquired erlotinib resistance, because the two are not necessarily synonymous and they often harbour different genetic mechanisms.[159] This was achieved by comparing the molecular profiles of 5 PDAC cell lines stratified by erlotinib sensitivity and 2 cell lines made resistant to erlotinib. A particular focus was placed at the interaction of EGFR and IGF1R activity with the MAPK and PAM pathways **(Figure 3.1)**. These two pathways are the principal mechanisms for controlling "cell survival, differentiation, proliferation, metabolism, and motility in response to extracellular cues"; and there are significant cross-talks between them.[276] Importantly, in pancreatic cancer *K-Ras* is mutated in over 90%,[20] whilst PI3K and Akt are overexpressed in 70% and 50% respectively,[48,54] suggesting that both pathways are active in this cancer.

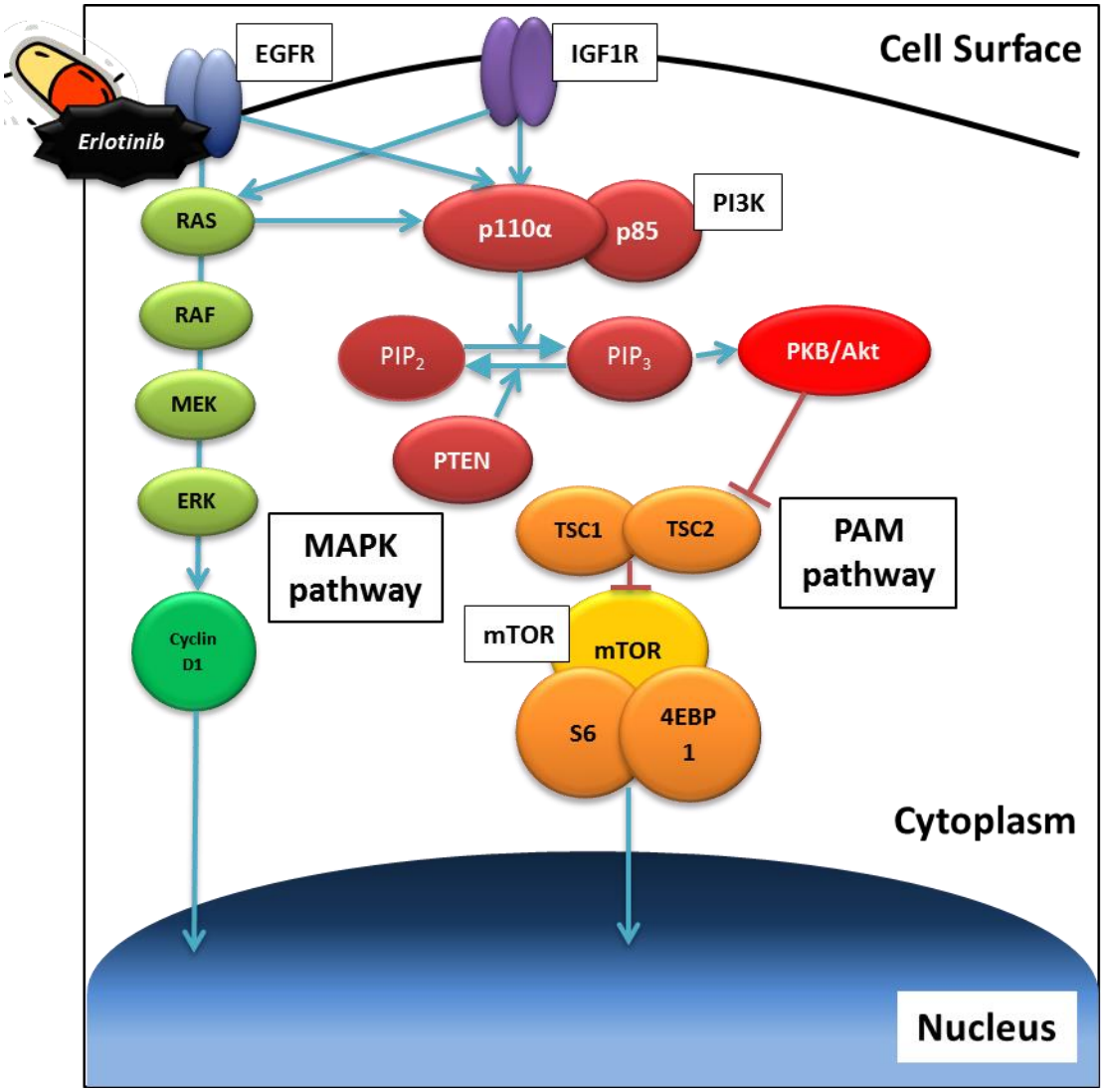

Figure 3.1: EGFR/ MAPK and IGF1R/ PI3K/Akt/mTOR pathways: molecular cross-talks

3.1.2 Chapter Aims

1. To assess erlotinib sensitivity in 5 PDAC cell lines
2. To develop PDAC cell lines with acquired resistance to erlotinib
3. To study molecular properties for primary and acquired erlotinib resistance
4. To propose treatment strategies that may exploit the knowledge of erlotinib resistance

3.1.3 Chapter Methods

In the first part of this chapter, erlotinib sensitivity among 5 PDAC cell lines (BxPC-3, CFPAC-1, CAPAN-2, MiaPACA-2 and PANC-1) is determined, with the aim of confirming earlier published reports.[84,277] 2 EGFR TKIs erlotinib and gefitinib with gemcitabine were used to assess if this was a class effect or a drug-specific effect. Erlotinib sensitivity was studied by means of cell proliferation (MTT assay) and clonogenic assay.

After erlotinib sensitivity was established in these cell lines, the most innately sensitive (BxPC-3) and most resistant (PANC-1) cell lines were chosen and they were sub-cultured in condition with graduating daily erlotinib concentration from 10μM to 30μM, for a period of 10 months. The detailed methodology was already discussed in **Methods 2.2.1**. The complete change in the morphology of these cells (BxPC-ER, PANC-ER) signalled the completion of erlotinib resistant (ER) cell lines. These results for the progress are illustrated in **section 3.3.**

To study primary or *de novo* erlotinib resistance, molecular characteristics of the 5 cell lines were compared, after stratifying into erlotinib sensitive and erlotinib insensitive groups. Western blotting, immunofluorescence and qRT-PCR were performed. To study acquired erlotinib resistance, the two pairs of parent versus ER cell lines (BxPC-3 and BxPC-ER; PANC-1 and PANC-ER) were compared. Phospho-RTK array and PCR array were first used for larger-scale molecular and gene discovery. Western blotting, immunofluorescence and PCR were then used to validate the findings. The specific mechanisms that will be focused include epithelial-mesenchymal status, EGFR, IGF1R, PI3K pathways.

For the purpose of this thesis, erlotinib insensitivity (EI) was used interchangeably as primary erlotinib resistance. Erlotinib resistance (ER) was used to refer to acquired erlotinib resistance.

3.2 Measuring Erlotinib Sensitivity in 5 PDAC Cell Lines

3.2.1 Cell Proliferation Results to Erlotinib and Gefitinib Single Agent

***Key Finding:* Cell Proliferation differentiated two groups of cell lines (erlotinib sensitive and erlotinib insensitive), and erlotinib sensitivity closely correlated with pattern of sensitivity to MEK inhibition also.**

MTT assay is one of the most established method in studying cell proliferation, based on the cleavage of yellow MTT (tetrazolium) to a soluble blue formazan product by mitochondrial enzymes.[278] However, several parameters have been found to affect cell metabolism and hence produced false positive and negative results.[278] In addition, reporting of treatment concentration ranges (erlotinib 0- 100μM), treatment time (48- 96 hours), and cell numbers (2000- 20000 cells) in erlotinib and gefitinib cell proliferation assays were highly varied in current literature.[164,237,279,280] Thus, before embarking in the main cell proliferation studies, five conditions needed to be optimised: treatment concentration ranges, DMSO concentration, treatment time, cell number and MTT incubation time.

DMSO concentration was a crucial condition to be optimised, because all drugs were dissolved in 100% DMSO as per product information, making final DMSO concentration as high as 0.3% in complete medium. Since DMSO is potentially toxic to cells,[281] and the DMSO concentration varied depending on how much drug working stock was added to the medium, it was pertinent to ensure there was no significant toxicity caused by DMSO. Optimising treatment time and cell number were also paramount, as suboptimal treatment time and cell number would profoundly affect cell proliferation results.

MTT incubation time was also an important parameter that needed to be optimised.[278] Since MTT assay is based on the mitochondrial metabolic activity of cell lines, the results for a slow growing cell line could be falsely over-estimated if the incubation of MTT was too short. Conversely, MTT results for a fast growing cell line may be falsely under-estimated if the incubation of MTT was too long.

The 5 PDAC cell lines varied immensely in their doubling times, from as short as 18 hours for MiaPACA-2 to 96 hours for CAPAN-2. Therefore, all 5 PDAC cell lines were tested independently for optimisation conditions. For brevity, only optimisation results of CFPAC-1 and CAPAN-2 will be shown, since CFPAC-1 was a good representative of all 5 cell lines having an intermediate doubling time of 32 hours, and CAPAN-2 had the longest doubling time and was therefore good as a comparison. Optimisation experiments were performed in duplicate, and R^2 statistics was used to assess the best optimisation condition based on goodness of fit in a log linear regression model. MTT assay results were presented as proportional viability, based on this formula[282,283]:

Proportional Viability	= Net Absorbance$_{treatment}$/ Net Absorbance$_{control}$ x 100%
	= (Abs$_{630nM}$ – Abs$_{570nM}$) $_{treatment}$ / (Abs$_{630nM}$ – Abs$_{570nM}$) $_{control}$ x 100%
	Where Abs$_{630nM}$ and Abs$_{570nM}$ represents reference and test colorimetry values

3.2.1.1 Optimising Cell number and Treatment Time

Gefitinib was used to conduct cell number and treatment time optimisation experiments. Cell numbers of 2000 or 4000 were seeded in the 96-well plate, and they were treated with varying concentration of gefitinib for 24, 48 or 72 hours.

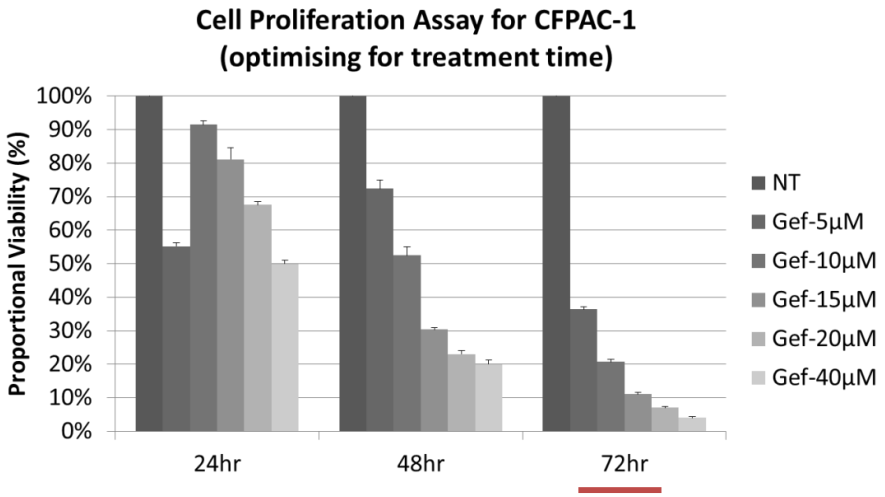

Treatment Time	*R square*
24 hours	0.3275
48 hours	0.9772
72 hours	**0.9830**

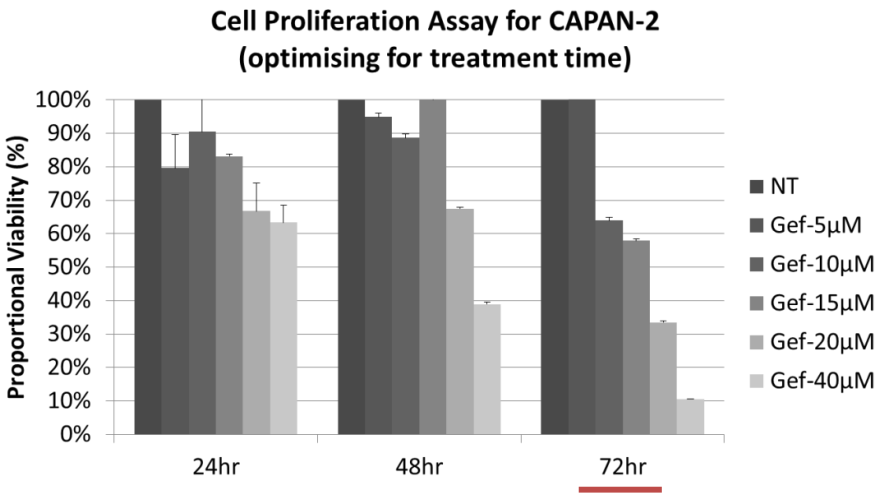

Treatment Time	*R square*
24 hours	0.7816
48 hours	0.6609
72 hours	**0.8448**

Figure 3.2: Cell Proliferation Assay optimising for treatment time

Figure 3.2 shows the optimisation results for treatment time for CFPAC-1 and CAPAN-2. For the moderately fast growing cell line CFPAC-1, both 48 hour and 72 hour treatment appeared to show an excellent dose response to gefitinib. On the other hand, for the slow growing CAPAN-2, there was an unpredictable response at 24 hours and 48 hours treatment. Only at 72 hours treatment was the cell viability proportional to the drug concentration. By fitting these dose response curves, both cell lines demonstrated a good fit at 72 hours treatment (R^2= 0.983 for CFPAC-1 and 0.845 for CAPAN-2). Thus, **72 hours treatment** was chosen as the optimised condition for all cell lines in subsequent studies.

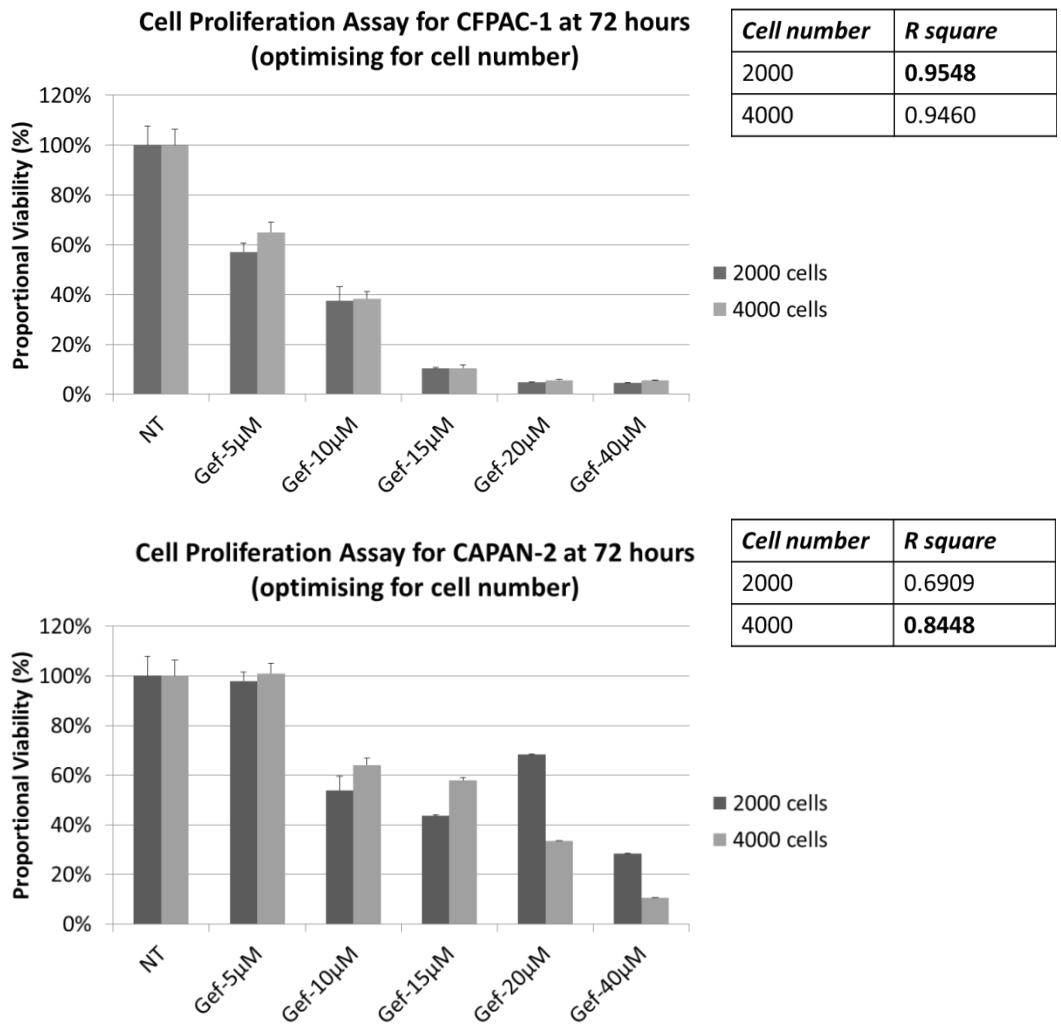

Cell number	*R square*
2000	**0.9548**
4000	0.9460

Cell number	*R square*
2000	0.6909
4000	**0.8448**

Figure 3.3: Cell Proliferation Assay optimising for cell number

Figure 3.3 shows the optimisation results for cell numbers seeding. For CFPAC-1, the cell number of 2000 cells demonstrated a very slightly better fit than 4000 cells ($R^2 = 0.955$). BxPC-3, MiaPAC-2 and PANC-1 were also optimised for 2000 cells (not shown). On the other hand, 4000 cells clearly demonstrated a better fit for *slow-growing* CAPAN-2 ($R^2 = 0.845$). This was clear on visual inspection of the plate. At 72 hours, a plate seeded with 2000 CAPAN-2 cells only would show a very faint colour across the entire plate after MTT / DMSO addition, whereas a plate seeded with 4000 cells would showed a differential changes in colour from dark to faint with increasing drug concentration. Hence, **for CAPAN-2 4000 cells were used** and **for other cell lines 2000 cells** were used in subsequent experiments.

3.2.1.2 Optimising Drug Concentration Ranges and DMSO Concentration

In the previous figures, gefitinib was tested in a range from 0 to 40μM. As is clear in **figure 3.2**, the proportional viability for CFPAC-1 was almost equivocal and very low for gefitinib at 20μM and 40μM. This most likely represented baseline detection threshold by the MTT assay. Similarly, for CAPAN-2 gefitinib 40μM resulted in a viability proportion of <10%, with a net absorbance <0.05, which probably passed the lower threshold of detection by this assay. And since previous reports had estimated PDAC cell lines to have gefitinib IC_{50} mostly between 2.5 to 10μM,[284] there was no need to increase gefitinib concentration above 20μM. Thus, for ongoing experiments **a range of 0 to 20μM gefitinib** was used.

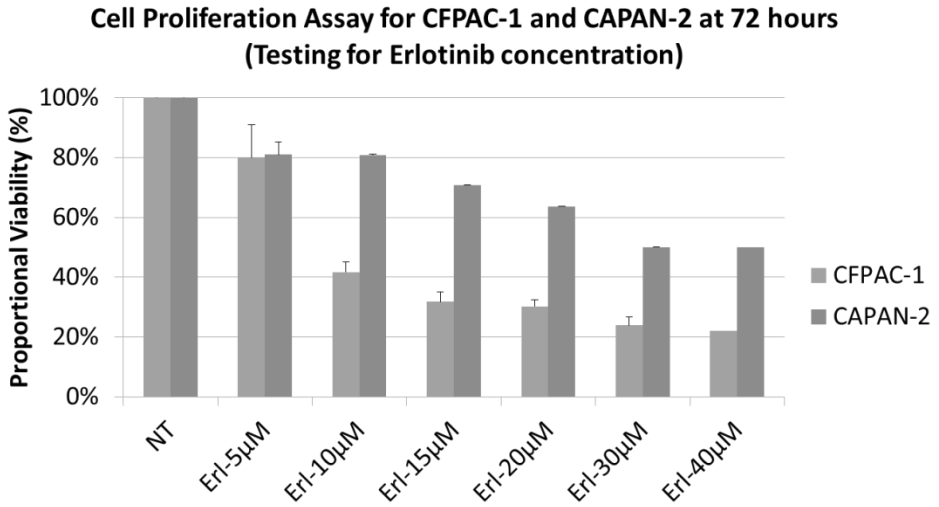

Figure 3.4: Cell Proliferation Assay Testing erlotinib concentration range

Figure 3.4 shows the cell proliferation results of the two cell lines treated with erlotinib from 0 to 40μM. Again, there appeared little difference between the result at the higher drug concentrations (erlotinib 30 and 40μM). Importantly, at concentration above 30μM erlotinib could not be fully dissolved in complete medium- it crystallised instead. The crystals were readily detectable under light microscopy, and could not be dissolved with heating or homogenising. The fact that erlotinib oversaturated above 30μM means that it could not produce reliable results for higher erlotinib concentration. Therefore, for ongoing experiments **a range of 0 to 30μM erlotinib** was used.

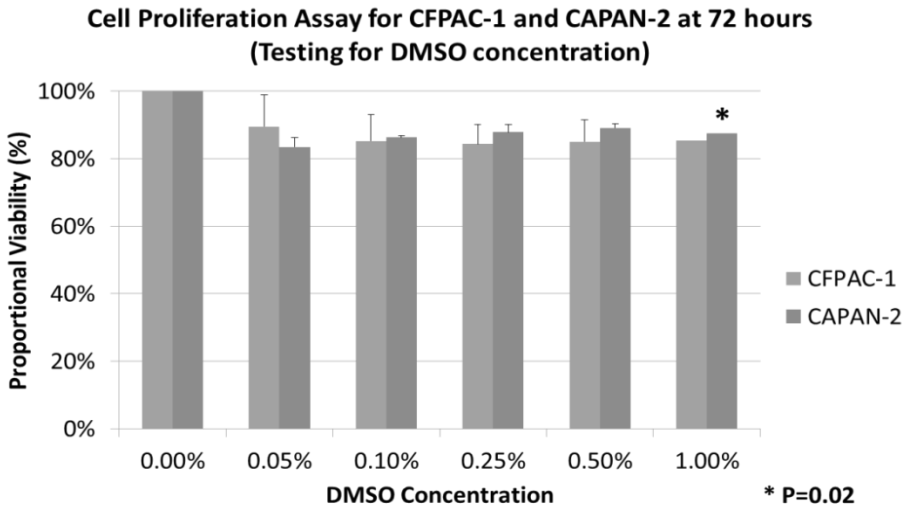

Figure 3.5: Cell Proliferation Assay Testing DMSO concentration. * P=0.02

Next, it must be determined whether DMSO was actually toxic to the PDAC cells. As mentioned before, DMSO concentration up to 0.3% may be present with the higher concentration drugs being dissolved in medium. DMSO concentration was tested from 0 all the way to 1.0% **(Figure 3.5)**. In both cell lines, there was no significant reduction in proportional viability with DMSO concentration below 1.0%. This optimisation experiment gave the reassurance that the cell proliferation results was due to the tested drug alone and not from other constituents. This result was also useful for other *in-vitro* studies that investigated the effect of drug inhibition- such as cell cycle assay or apoptosis assay, since all these assays utilised inhibitors dissolved in DMSO.

3.2.1.3 Optimisation of MTT incubation time

Finally, MTT exposure time needed to be optimised. MTT was the last step of the cell proliferation assay, and studies have shown that the duration MTT is added to the wells for oxidising reaction has a profound impact on results.[278] To optimise MTT assay, cell lines were treated with gefitinib and erlotinib in graduating concentrations in the exact same way in 3 separate plates. After MTT was added to the plates, the first plate was read after discarding medium and adding DMSO, in exactly 1 hour. The second plate was read after 2 hours, and

the third after 3 hours. For brevity, results for the cell line with fastest and slowest doubling times (MiaPACA-2 and CAPAN-2) were shown here:

CAPAN-2

Erlotinib	Absorbance (NT)	Calculated IC_{50}	R square	*Gefitinib*	Absorbance (NT)	Calculated IC_{50}	R square
1hr	0.05	27.9μM	0.93	**1hr**	0.05	20.5μM	0.97
2hr	0.09	23.4μM	0.91	**2hr**	0.09	16.1μM	0.98
3hr	0.11	19.0μM	0.92	**3hr**	0.11	15.3μM	0.98

MiaPACA-2

Erlotinib	Absorbance (NT)	Calculated IC_{50}	R square	*Gefitinib*	Absorbance (NT)	Calculated IC_{50}	R square
1hr	0.40	13.9μM	0.93	**1hr**	0.40	14.0μM	0.97
2hr	0.64	15.4μM	0.94	**2hr**	0.64	16.2μM	0.97
3hr	0.77	19.9μM	0.97	**3hr**	0.77	23.5μM	0.97

Table 3.1: MTT Timing Optimisation Experiments (CAPAN-2, MiaPACA-2)

The absolute measures of absorbance for no treatment were fairly low in CAPAN-2 compared to MiaPACA-2, possibly due to a slower metabolic rate of this cell line. In both cell lines, however, the absorbance increased with time. Goodness of fit was very good (>0.90) for all incubation times in both cell lines. Of interest, the IC_{50} appeared to decrease for the slow-growing CAPAN-2 with longer MTT incubation, and increase for the fast-growing MiaPACA-2. This was probably related to the mathematical artefact when calculating IC_{50}, since IC_{50} was determined by log linear regression curve that was based on the PV against control at different concentrations. With a relatively low absorbance of 0.05 for CAPAN-2 at 1 hour, all PV would appear to be much higher %, thereby falsely predicting a higher IC_{50}. Based on higher absorbance with control (NT) on longer MTT incubation, **2.5 hours** was deemed to be appropriate as the optimal MTT incubation time.

To sum it up, these experiments found that the optimal conditions were seeding **4000 cells for CAPAN-2 and 2000 for others, treating them with gefitinib 0-20μM and erlotinib 0-30μM for 72 hours, and finally incubating with MTT for 2.5 hours before reading**.

3.2.1.4 Erlotinib and Gefitinib Cell Proliferation Studies

To study the effect of erlotinib and gefitinib on the 5 PDAC cell lines, 6 replicate experiments with biological triplicate were carried out for each experiment. The erlotinib treatment concentrations tested were 0, 5, 10, 20 and 30µM, and for gefitinib treatment concentrations were 0, 5, 10 and 20µM. Averages and Standard error of the mean (SEM) were presented below, with best regression line fitted for each cell line.

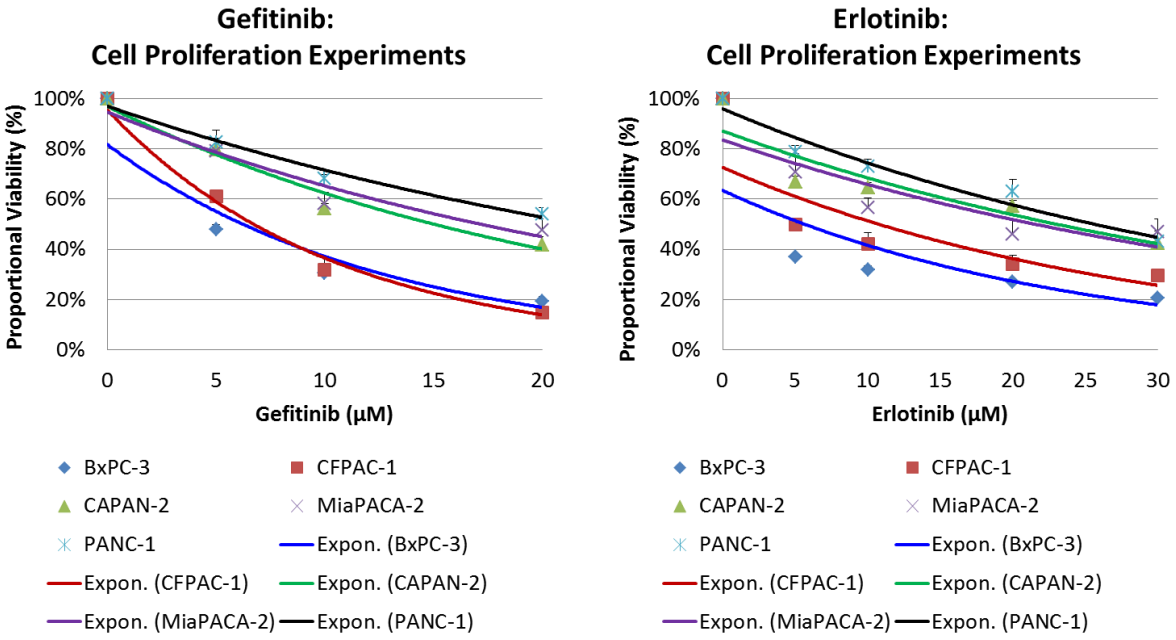

Figure 3.6: Cell Proliferation Assay Proportional Viability Scatterplots for Gefitinib and Erlotinib

From this **figure 3.6**, it was discernible that BxPC-3 and CFPAC-1 were much more sensitive to EGFR inhibitors than CAPAN-2, MiaPACA-2 and PANC-1. For gefitinib, there was even a clearer separation between the highly sensitive and highly insensitive cell lines. This result was in accordance to that reported by Buck *et al.*[84], who assigned BxPC-3 and CFPAC-1 to erlotinib sensitive group, CAPAN-2 to intermediate sensitive group, and MiaPACa-2 and PANC-1 to erlotinib insensitive group. A similar trend was also observed in another study.[277]

To calculate for cytotoxic IC_{50}, a log linear regression formula was calculated from the best fitted curve (SAS 9.2), and the drug concentration corresponding to the 50% proportional viability was extrapolated.

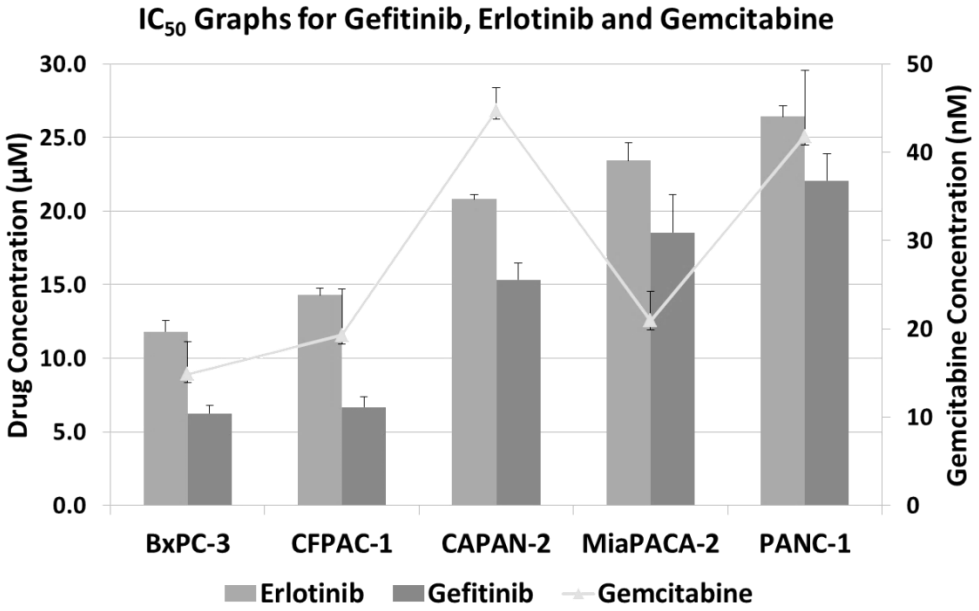

Figure 3.7: Cell Proliferation Assay IC_{50} for Gefitinib and Erlotinib

The cytotoxic IC_{50} of the 5 cell lines (**Figure 3.7**) confirmed the observation in **figure 3.6**, where there was a decreasing effect to EGFR inhibitors in the order BxPC-3 (most sensitive)>CFPAC-1>CAPAN-2>MiaPACA-2>PANC-1 (least sensitive). It also demonstrated that this was actually an EGFR inhibitor class effect, since the results were largely concordant between erlotinib and gefitinib, but followed a different pattern of sensitivity to gemcitabine chemotherapy. These results made sense because BxPC-3 and CFPAC-1 were known to be epithelial cell type, and epithelial tumours were known to have high EGFR expression,[285] thus possibly making them more susceptible to EGFR inhibition.[84] On the other hand, MiaPACA-2 is a true mesenchymal cell type and PANC-1 has a mixed cell type.[222,232] Interestingly, CAPAN-2 is reported to have an epithelial morphology,[222] and yet is only moderately insensitive to EGFR inhibitor. However, as in **section 3.4.1**, a new finding in the epithelial-mesenchymal status of this cell line could explain why this was so.

3.2.1.5 Cell Proliferation Studies on Other inhibitors

Several inhibitors of other classes were tested on the 5 cell lines. This included IGF1R inhibitor NVP-AEW541 (AEW), pan-PI3K inhibitor LY-294002, PI3Kα inhibitor NVP-BYL719 (BYL), dual PI3K/mTOR inhibitor NVP-BEZ235 (BEZ) and MEK inhibitor PD-98059 (PD). These experiments were also repeated six times.

Pathway	EGFR/ ERK/ MEK Pathway			IGF1R/ PI3K/ AKT pathway			PI3K/mTOR
Inhibitor	EGFRi	EGFRi	MEKi	IGF1Ri	PI3Ki	PI3Kαi	PI3K/mTORi
Drugs	***Erlotinib*** (IC_{50}, Mean +/- SE, umol/L)	***Gefitinib*** (IC_{50}, Mean +/- SE, umol/L)	***PD-98059*** (IC_{50}, Mean +/- SE, umol/L)	***NVP-AEW541*** (IC_{50}, Mean +/- SE, umol/L)	***LY-294002*** (IC_{50}, Mean +/- SE, umol/L)	***NVP-BYL719*** (IC_{50}, Mean +/- SE, umol/L)	***NVP-BEZ235*** (IC_{50}, Mean +/- SE, umol/L)
BxPC-3	11.8 (11.0-12.6)	6.2 (5.7-6.8)	26.9 (26.1-27.7)	4.9 (3.8-6.1)	12.6 (10.0-15.2)	4.9 (3.9-5.9)	0.03 (0.02-0.03)
CFPAC-1	14.3 (13.8-14.7)	6.7 (5.9-7.4)	32.5 (24.5-40.6)	3.9 (3.2-4.5)	7.7 (6.2-9.2)	7.6 (6.8-8.5)	0.05 (0.04-0.06)
CAPAN-2	20.8 (20.5-21.1)	15.3 (14.2-16.5)	37.9 (33.4-42.4)	6.0 (4.4-7.6)	17.3 (14.6-19.9)	8.2 (6.9-9.4)	0.14 (0.12-0.17)
MiaPACA-2	**22.4 (21.2-23.6)**	**18.5 (15.9-21.1)**	**38.9 (33.8-44.0)**	2.0 (1.8-2.2)	13.8 (12.8-14.8)	6.9 (6.5-7.2)	0.02 (0.02-0.02)
PANC-1	**26.4 (25.7-27.2)**	**22.7 (21.7-23.7)**	**62.7 (54.5-70.8)**	**10.3 (7.8-12.9)**	**22.0 (18.6-25.3)**	**10.9 (9.9-12.0)**	0.13 (0.12-0.14)

Table 3.2: Cell Proliferation Assay IC_{50} for other inhibitors

Whilst the sensitivities to inhibitors vastly differed between the 5 PDAC cell lines, three patterns were observed. Firstly, the **pattern of sensitivities to MEK inhibition closely correlated to that of EGFR inhibition**. That is, the erlotinib insensitive (EI) cell lines- CAPAN-2, MiaPACA-2 and PANC-1, were also insensitive to PD-98059 (in red, bolded = most highly insensitive). This is comprehensible as MEK lies downstream of EGFR in the Raf-MEK-ERK cascade.[56] It would seem to suggest that the basis of both primary EGFRi and MEKi resistance arose from molecular signals downstream of both EGFR and MEK, possibly ERK. Secondly, **the IGF1R and PI3K inhibitor sensitivity followed a different pattern**. CAPAN-2 and PANC-1 were insensitive (blue), but not MiaPACA-2. Thirdly, **all cell lines remained sensitive to dual PI3K/mTOR inhibition with nanomolar potency**.

3.2.2 Clonogenic Results to Erlotinib and Gefitinib Single Agent

***Key Finding:* Clonogenic results were concordant with cell proliferation assay results**

Clonogenic assay was used as a second assay to confirm EGFR inhibitor sensitivity pattern of the 5 PDAC cell lines. Clonogenic assay was selected, because by the nature of this assay, it is measuring the after-effect of drug inhibition. Cells are treated for 3 days, and after harvesting, they are reseeded in a new plate with fresh complete medium *without* the drug.[256] Therefore, in essence this assay measures if there are any *residual* effects of the drug on colony formation. Thus, combining results from both cell proliferation assay and clonogenic assay, a clear distinction can be made between erlotinib sensitive and erlotinib insensitive cell lines in regarding to the immediate and delayed effects of these inhibitors.

3.2.2.1 Optimising Cell Number, Treatment Concentration and Colony Size

Again, before commencing on the core experiments, a number of conditions needed to be optimised. In the preliminary experiments, the cell numbers, treatment concentration and colony size were optimised using CFPAC-1, CAPAN-2 and PANC-1 given the varying differences between the doubling time and cell properties of these 3 cell lines. The problem with seeding too many cells is that there will be too many overcrowded small colonies instead of fewer but bigger colonies. This essentially defeats the purpose of clonogenic assay, which is to measure their ability of individual cells to build into big colonies. The best treatment concentration was also sought for testing clonogenic assay. Whilst clonogenic assay could technically be performed under several treatment concentrations, there would become too many permutations once several dual inhibitor combination treatments were planned. For optimisation, erlotinib 5μM or 10μM were tested for three days, after which 1000 or 2000 cells were seeded in 6-well plates. An attempt was also made to “optimise” colony size. Historically, a colony in a clonogenic assay is defined by a cluster of more than 50 cells.[256] In reality, however, the plate was photographed under magnification (LAS 3000), and the colonies were automatically counted as pixel by an associated program (Fujifilm Colony) after setting density,

circularity and size of colonies. Clearly, it was impossible to correlate the exact locations of the colonies on a microscope to the crystal violet dots on the plate given the microscopic size of colonies. Thus, in order to make an association between identified pixels with colony size, the plate was viewed under light microscope at high objective (40x) after staining with crystal violet, and was then compared with the results obtained from Colony v1.1.

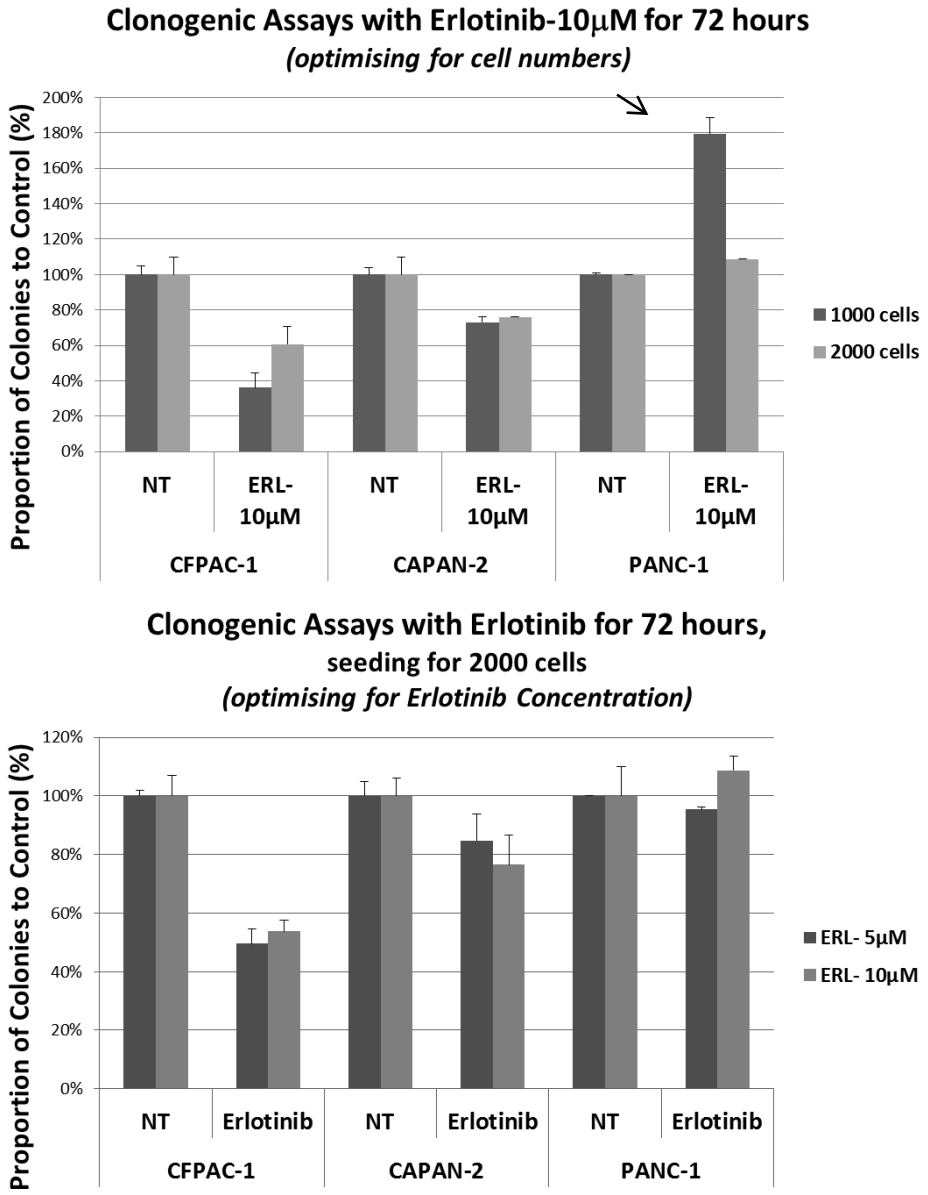

Figure 3.8: Clonogenic assay optimising for cell numbers and erlotinib concentration

Figure 3.8 shows the optimisation results of cell number seeding and erlotinib concentration. The number of colonies identified by seeding 2000 cells was clearly more than that by seeding

1000 cells. For example, given the same treatment with erlotinib 10μM, 138 colonies were identified by seeding 2000 PANC-1 cells, compared to 73 colonies when seeding 1000 cells (not shown). Whilst this theoretically should not affect the results given all results were expressed as a percentage to control, the smaller number of colonies would make the results susceptible to larger errors of variation produced by the automatic pixel counting program. This is particularly the case for cell lines that are resistant to erlotinib. In this case, the error of variation had resulted in an overestimation of proportion of colonies in PANC-1 (PANC-1 treated with erlotinib 10μM having 179% colonies compared to control **(Figure 3.8, arrow)** - 131 colonies compared to 73 colonies), which clearly does not make sense. Thus, from here on **2000 cells were reseeded after drug treatment.**

Clonogenic assay was also assessed with erlotinib 5 versus 10μM for 72 hours, after reseeding 2000 cells. There was not much difference between the two drug concentrations, and here it was shown that at either dose, CFPAC-1 was highly sensitive, CAPAN-2 was moderately so, and PANC-1 was not. For the subsequent experiments, **erlotinib 10μM** for 72 hours was used since this dose was also used as a standard in other *in-vitro* assays. For experiments in Chapter 4 with combined blockade treatment, erlotinib 5μM and 10μM were both used as the dose response with low dose and moderate dose combined blockade treatment needed to be determined.

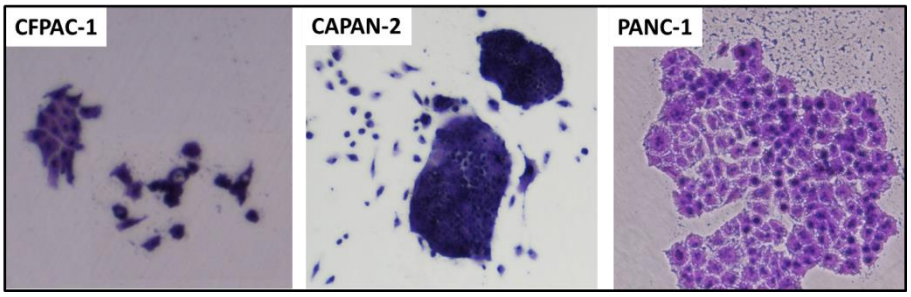

Figure 3.9: Representative photos of clonogenic assay under light microscopy

A general view of the clonogenic assay under light microscopy had shown only small clusters of cells for CFPAC-1 (which does not classify as a “colony” based on the definition of more

than 50 cells), intermediate colonies for CAPAN-2, and large colonies for PANC-1 **(Figure 3.9)**. This corresponded well with the results of optimisation experiments, that is, CFPAC-1 was sensitive, CAPAN-2 was moderately insensitive and PANC-1 was insensitive to erlotinib.

3.2.2.2 Erlotinib and Gefitinib Clonogenic Assay Studies

Triplicate clonogenic assays were then performed for all 5 cell lines, after exposure of erlotinib or gefitinib 10μM for 72 hours. Cells were harvested after 72 hours, and manually counted on haemocytometer. Since both cell proliferation and clonogenic assays exposed cells to inhibitors for 72 hours, the results from counting from 3 experiments were included as a secondary outcome, to assess whether this matched the cell proliferation assay results.

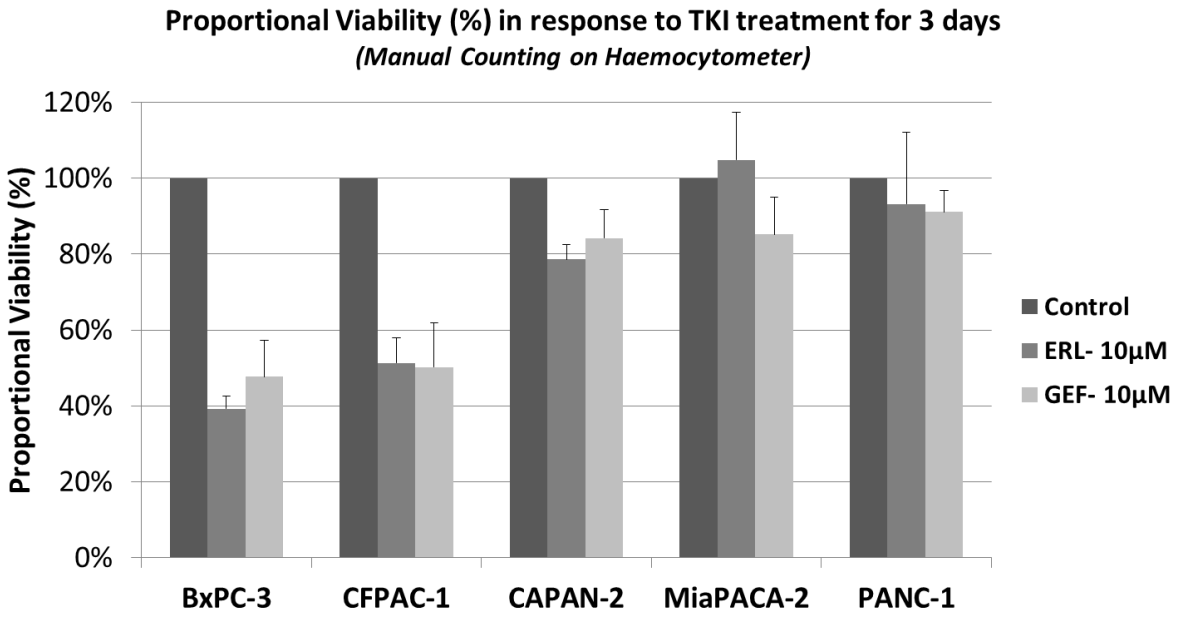

Figure 3.10: Proportional Viability in response to erlotinib/ gefitinib, by manual counting.

As expected, both BxPC-3 and CFPAC-1 were sensitive to erlotinib and gefitinib, CAPAN-2 was only moderately sensitive, and MiaPACA-2 and PANC-1 insensitive to the drugs. Of note, the proportional viability for erlotinib and gefitinib followed very similar trend, further supporting

this observation as an EGFR inhibitor class effect. Overall, the manual counting correlated well with the cell proliferation (MTT) assay results.

After 7-10 days of seeding and growing in new medium, crystal violet 0.025% was added after discarding the medium. After washing and air-drying, photos of the plate were taken on standard resolution setting on the LAS 3000. **Figure 3.11** shows representative photos of the clonogenic assay of the 5 cell lines after erlotinib and gefitinib treatment. The colony size and numbers were clearly smaller with EGFR inhibitor treatment for BxPC-3 and CFPAC-1. With the other 3 cell lines, there were perhaps some minor reduction in the size and number of colonies, but this was not very obvious on visual inspection.

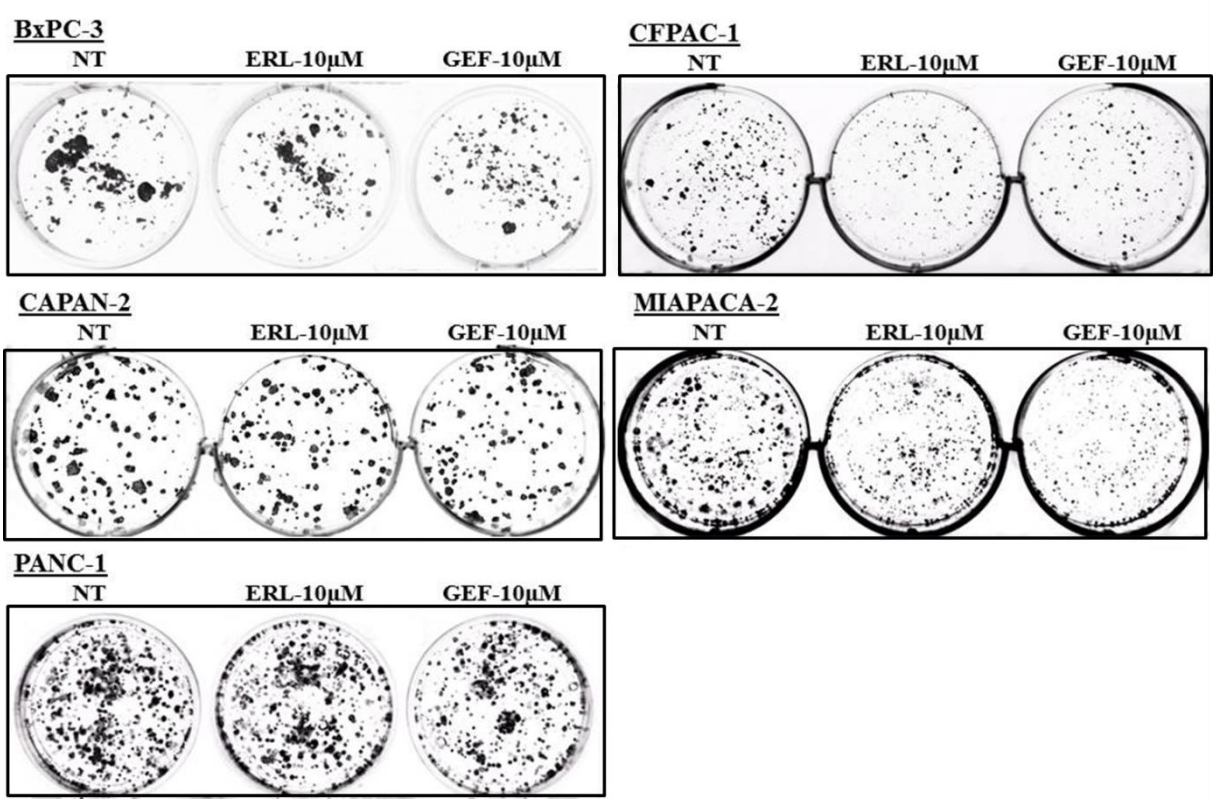

Figure 3.11: Representative photos of the Clonogenic assay with erlotinib and gefitinib

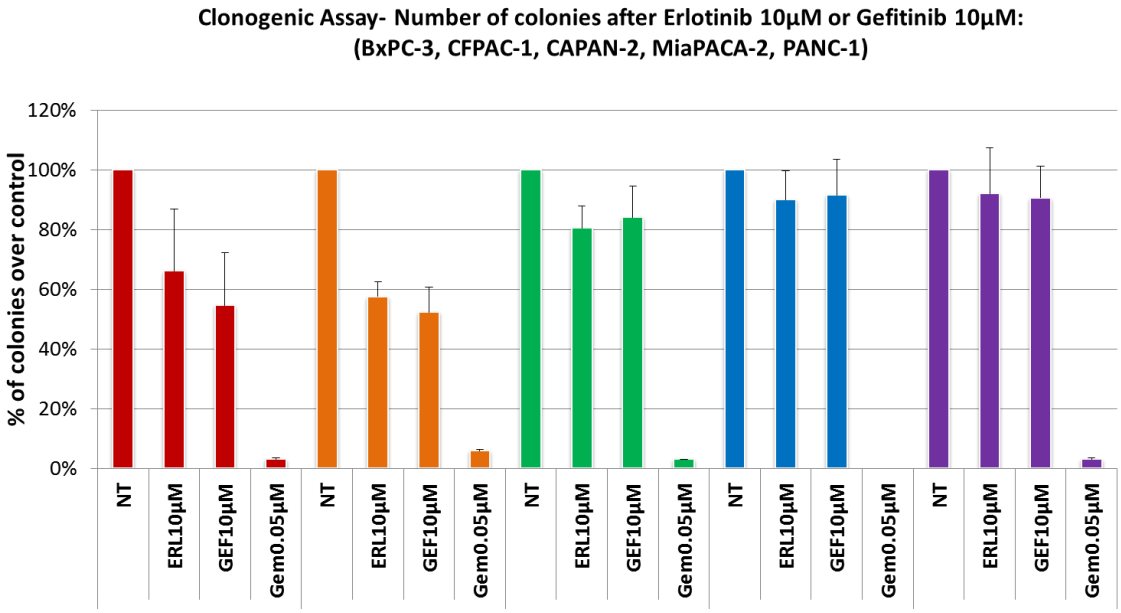

Figure 3.12: Aggregate Clonogenic Assay results with erlotinib and gefitinib treatment

Colony numbers were counted by Colony v1.1, and averages and SEM of triplicate biological experiments of two technical duplicates were presented. Clearly, erlotinib and gefitinib had prolonged effect on the first two cell lines, with colony numbers only 50-60% of control. In contrast, the last three cell lines were little affected by EGFR inhibitors, with only around 10-20% reduction of colony numbers. In keeping with cell proliferation experiments, clonogenic assay also showed marked sensitivity of all cell lines to gemcitabine, at a dose as low as 0.05 µM. Once again, this supports the sensitivity pattern observed for erlotinib as an EGFR inhibitor class effect.

In summary, cell proliferation and clonogenic assays had identified two groups of cell lines **(erlotinib sensitive – BxPC-3 and CFPAC-1; and erlotinib insensitive – CAPAN-2, MiaPACA-2, PANC-1).** The effects of these inhibitors to the cell lines seemed to be prolonged, with definite inhibition of cell proliferation at 72 hours but also continual effect of the drug to colony numbers over 7-10 days after the drugs were withdrawn.

3.3. Sub-culturing acquired erlotinib resistance PDAC Cell Lines

Key Finding: ***2 ER Cell Lines showed significant erlotinib resistance compared to parent cell lines, and were cross-resistant to IGF1R and MEK inhibitors.***

The previous experiments differentiated erlotinib sensitive and erlotinib insensitive cell lines. To create cell lines with acquired erlotinib resistance (ER), the most erlotinib-sensitive cell line (BxPC-3) and most erlotinib-insensitive cell line (PANC-1) were treated daily with graduating concentration of erlotinib, from 10 to 20 to 30μM over a period of 10 months. Three times a week old medium was removed and fresh medium supplemented with the drug was added. The highest subculturing erlotinib concentration was 30μM, because above this dose erlotinib crystallised as previously described. The cells were passaged at a ratio 1:2 whenever confluence reached 10-20%, typically every 10-14 days. This occurred after 4 months of sub-culturing, as discussed below. Below summarises the progress results.

3.3.1 Change of Erlotinib IC_{50} and Morphology over Time

The micrographs of the sub-cultured cell lines (BxPC-ER and PANC-ER) and the time plots of IC_{50}% (compared to control) are presented here.

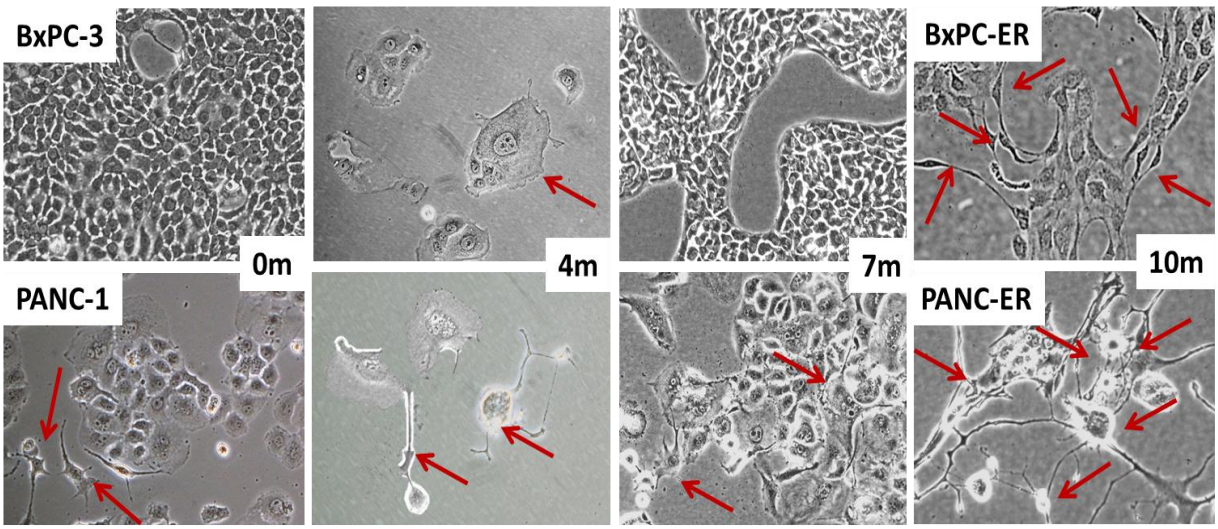

Figure 3.13: Micrographs of subcultured cell lines *(red arrows: mesenchymal cells)*

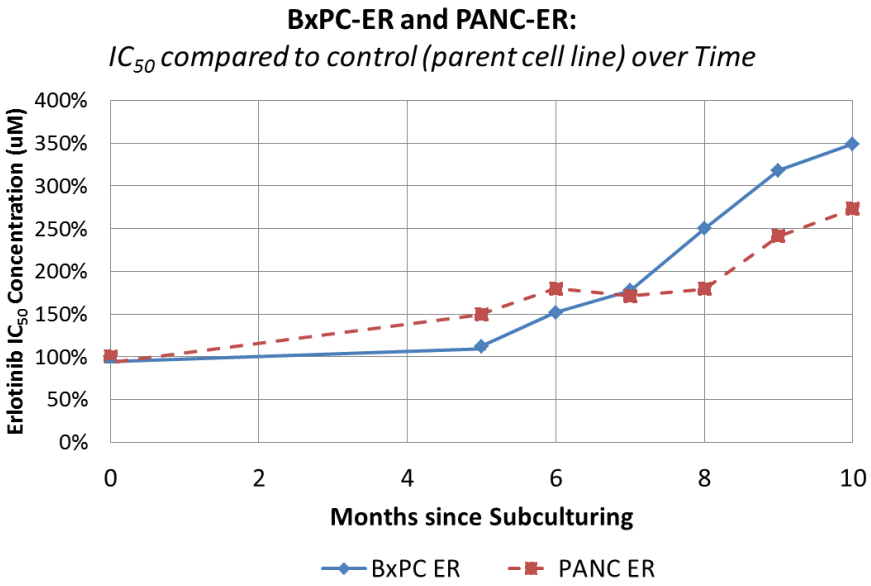

Figure 3.14: IC_{50} time plot of the two sub-cultured cell lines

Before sub-culturing started, BxPC-3 was identified as an epithelial cell type and PANC-1 as a mixture of epithelial and mesenchymal cell type (mesenchymal cells highlighted in red) **(Figure 3.13)**, as previously described.[221,232] In the first 4 months of sub-culturing, BxPC-3 and PANC-1 were treated with erlotinib 10-20μM. The growth of BxPC-3 and PANC-1 were drastically suppressed by the erlotinib, to the point that no passage of cells was done or could be done during this initial period. This may seem somewhat surprising for the PANC-1 cell line, as previously this cell line was shown to be insensitive to erlotinib. However, one needs to make clear the distinction of "insensitivity" and "resistance" here. Even though PANC-1 was labelled as erlotinib insensitive, 40% of cells still died within 3 days of erlotinib exposure on cell proliferation assay **(Figure 3.6)**. And this was an exposure of the drug for 3 days only. At prolonged daily exposure over months, it is perceivable that even erlotinib insensitive cell lines would succumb to the effect of the inhibitor.

Despite the fact that most cells died at 4 months, there remained a small number of cells in both cell lines that appeared to survive under the drug pressure. These cells were very few in number, and they looked different in morphology than the parent cell lines (red arrows) **(Figure 3.13).** They were bigger, irregular and more elongated in shape, and sometimes there were cells with axons that were branching out. At first, these were thought to be apoptotic cells that

were dying from erlotinib, but gradually these types of cells increased in number and actually started to form colonies.

At 5th month, both cell lines finally started growing to a reasonable confluence (10-20%) that allowed them to be passaged. A small volume of cells were tested against parent cell lines BxPC-3 and PANC-1 in cell proliferation assay, and the rest were transferred to new T75 flasks. As expected, there were relatively little changes of IC_{50} of both subcultured cell lines compared to parent cell lines (150% and 112% for BxPC-ER and PANC-ER) **(Figure 3.14)**. Over the next few months, the cell lines continued to grow at a reasonable rate that allowed cell passage to occur every 10-14 days. This also meant that the cells could now be treated daily with the higher erlotinib concentration (30μM). Monthly cell proliferation assay had demonstrated that the IC_{50} of the subcultured cell lines continued to increase gradually against control.

At 7th month, the micrographs of the subcultured cell lines showed that these cells were able to withstand drug pressure and formed reasonable size colonies. The morphology of the cells had changed ever so slightly, with BxPC-ER looking slightly more elongated and irregular and the PANC-ER becoming more stallate in shape (red arrows). The IC_{50} ratio was 177% and 171% for BxPC-ER and PANC-ER.

From 7th to 10th month, there was a sudden change with both cell lines growing at a more rapid rate, necessitating cell passage every 7 days instead of 10-14 days. There was a sudden increase in IC_{50} of both cell lines, with BxPC-ER IC_{50} going above 30μM and PANC-ER IC_{50} going above 50μM. There was also gradual replacement of epithelial to mesenchymal cell type (red arrows), and **epithelial-mesenchymal transition (EMT) was suspected to have occurred.** This initially occurred in the outer edges of the colonies for both cell lines. By 10th month, there was a monoclonal population of mesenchymal cells taking over in both cell lines. At this stage, the sub-culturing process had completed and a large number of these cells were cryopreserved. The final cell proliferation assay was repeated three times, with the final IC_{50} of 35.9μM for BxPC-ER (349% to BxPC-3) and 66.9μM for PANC-ER (273% to PANC-1).

BxPC-ER and PANC-ER were significantly resistant to erlotinib compared to parent cell lines in 6 independent cell proliferation experiments (both P<0.001) **(Table 3.3)**. The cell lines were sent for typing, and also analysed for mycoplasma infection. It confirmed that both BxPC-ER and PANC-ER were derived from original cell lines by ATCC standards, and was negative for mycoplasma contamination.

Cell Lines	Erlotinib (IC_{50}, Mean +/- SEM, μmol/L)	NVP-AEW541 (IC_{50}, Mean +/- SEM, μmol/L)	LY-294002 (IC_{50}, Mean +/- SEM, μmol/L)	NVP-BYL719 (IC_{50}, Mean +/- SEM, μmol/L)	NVP-BEZ235 (IC_{50}, Mean +/- SEM, μmol/L	PD-98059 (IC_{50}, Mean +/- SEM, μmol/L)
BxPC-3	10.3 (9.8-10.8)	5.0 (3.6-6.4)	17.2 (15.1-19.4)	7.5 (5.9-9.1)	0.03 (0.02-0.04)	32.4 (24.1-40.7)
BxPC-ER	35.9 (33.4-38.3)	8.8 (7.3-10.2)	21.4 (15.8-27.0)	9.4 (7.5-11.3)	0.04 (0.04-0.05)	58.8 (49.3-68.2)
IC_{50} %	349%	176%	124%	125%	132%	181%
P-value	<0.001	0.037	0.87	0.27	0.10	0.053
PANC-1	24.5 (23.5-25.5)	9.4 (7.5-11.5)	20.6 (14.1- 27.1)	10.1 (8.4-11.8)	0.16 (0.15-0.17)	58.2 (52.8-63.6)
PANC-ER	66.9 (60.9-73.0)	17.3 (14.9-19.6)	29.2 (25.3-33.1)	9.7 (8.5-11.0)	0.14 (0.14-0.16)	126.0 (112.8-139.1)
IC_{50} %	273%	184%	142%	96%	90%	142%
P-value	<0.001	<0.001	0.42	0.77	0.47	0.006

Table 3.3: Cell proliferation IC_{50} of multiple inhibitor with t-test statistics

3.3.2 Stability of Acquired Erlotinib Resistant Cell Lines

Recent evidence is emerging that chemotherapy or drug resistance could be reversible in cancer, and epigenetic phenomenon is largely implicated for this reversible process.[286] Was erlotinib resistance complete? Or was it reversible in the ER cell lines? This was a fundamental question that must be addressed in this project. If erlotinib sensitivity was indeed restored after drug pressure was removed, then genetic, epigenetic and molecular alterations may be all equally important. More importantly, if drug resistance was not static, then the results of these experiment results would no longer be consistent since it took about 12 months to complete the *in-vitro* work for the ER cell lines.

To assess for stability of the cell lines, each ER cell line was cultured separately in two T25 flasks, one continuing with daily treatment with erlotinib 30μM and one without. After 4 weeks of further culturing, the IC_{50} of parent cell lines, resistant cell lines with and without erlotinib

were assessed on three biological triplicate cell proliferation experiments. The ER cell lines were determined to be stable if the ER cell line that discontinued from erlotinib treatment remained resistant to erlotinib compared to parent cell line.

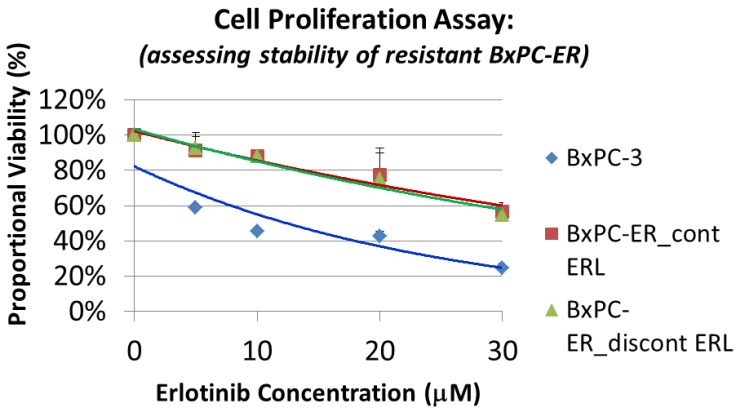

	IC_{50}	v Ctr (%)	P-value
BxPC-3	12.5 μM	-	-
BxPC-ER cont ERL	39.8 μM	319%	0.004
BxPC-ER discontinue d ERL	38.5 μM	307%	0.004

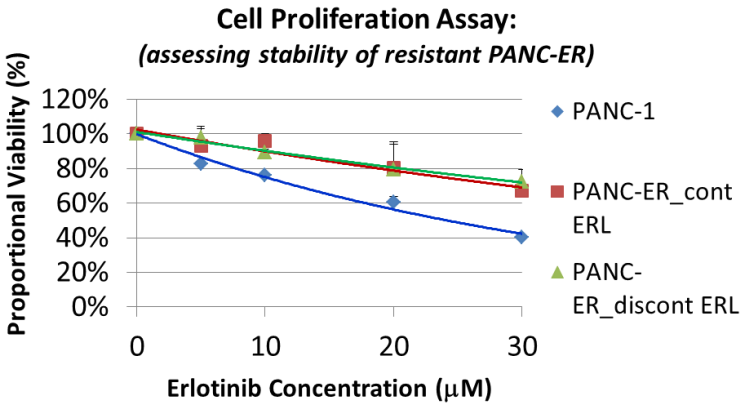

	IC_{50}	v Ctr (%)	P-value
PANC-1	23.9 μM	-	-
PANC-ER cont ERL	55.2 μM	231%	0.004
PANC-ER discontinued ERL	64.0 μM	268%	0.026

Figure 3.15: Cell Proliferation Assay assessing stability of ER cell lines

Averaging from triplicate experiments, both BxPC-ER and PANC-ER with daily erlotinib continued to display significant erlotinib resistance compared to respective parent cell lines (319% and 231% respectively). The BxPC-ER that discontinued erlotinib for at least 4 weeks was still 307% more resistant than BxPC-3. Likewise, PANC-ER that discontinued erlotinib was 268% more resistant than PANC-1. Both these were significantly resistant. Notice that the estimated IC_{50} was slightly higher for PANC-ER that discontinued erlotinib (64.0μM) than PANC-ER that continued erlotinib (55.2μM). Clearly, the graphs looked very similar between the two. This was likely an artefactual error from extrapolation of fitted curve, where the estimated IC_{50} was much higher than the highest erlotinib concentration being tested (30μM).

In any case, both ER cell lines that discontinued erlotinib remained *significantly* resistant to erlotinib. In other words, **the ER cell lines were stable**.

3.3.3 Cross Resistance to IGF1R and MEK inhibition

Next, the ER cell lines were assessed for cross- resistance to other inhibitors. The inhibitor tested included IGF1R inhibitor AEW, pan-PI3K inhibitor LY-294002, PI3K-α inhibitor BYL, dual PI3K/ mTOR inhibitor BEZ and MEK inhibitor PD. These drugs were used to test the cell proliferation of 5 parent cell lines previously, and were also used in different combinations in other *in-vitro* studies, which will be the core subject of **chapter 4.** Cell proliferation inhibition IC_{50} of multiple inhibitors in acquired resistant cell lines versus parent cell lines is presented in **table 3.3** and graphically in **figure 3.16**. 6 experiments were performed, and t-test statistics (paired) was calculated.

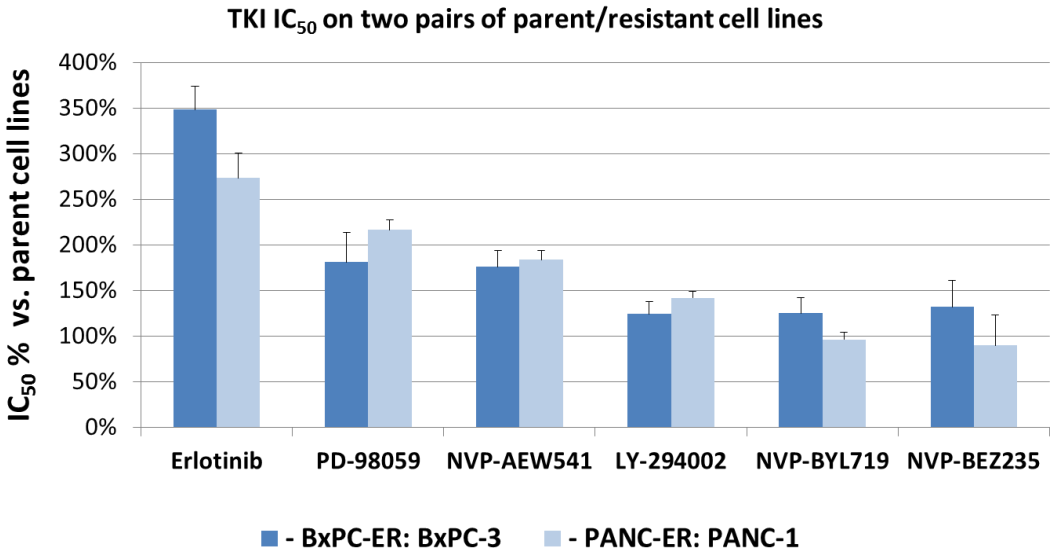

Figure 3.16: Cell proliferation IC_{50} of multiple inhibitors

As described before, both BxPC-ER and PANC-ER were made significantly resistant to erlotinib (BxPC-ER IC_{50} 349% to BxPC-3 and PANC-ER IC_{50} 273% to PANC-1, both $P<0.001$). In addition, both resistant cell lines showed significant cross-resistance to IGF1R inhibitor

NVP-AEW541 (BxPC-ER: 176% of IC_{50}, P=0.037; PANC-ER: 184% of IC_{50}, P<0.001) and MEK inhibitor PD-98059 (PANC-ER: 218% of IC_{50}, P=0.006), with the exception of BxPC-ER reaching near statistical significance to MEK inhibitor resistance (BxPC-ER: 181% of IC_{50}, P=0.053). Notably, **there was no significant cross-resistance to either PI3K inhibitors or the PI3K/mTOR inhibitor**. That is, the ER cell lines remained sensitive to PI3K inhibition. This therefore gave us the first impression of the involvement of PI3K/Akt/mTOR (PAM) pathway in erlotinib resistance, which will be studied in much greater detail in the **section 3.5**.

3.4 Molecular Characterisation for primary erlotinib resistance

After the 5 PDAC cell lines were stratified into erlotinb sensitive group (BxPC-3, CFPAC-1) and EI group (CAPAN-2, MiaPACA-2, PANC-1), molecular characterisation of these cell lines was performed in an attempt to find distinct properties shared in each group of cell lines, that could possibly be attributable to primary or *de novo* erlotinib resistance. Epithelial-mesenchymal status was briefly reviewed, after which the focus was placed on the gene and molecular studies of EGFR, IGF1R, MAPK and PAM related pathways. These findings were correlated with the cell proliferation and clonogenic assay results in **section 3.4.2**, and a detailed discussion will be presented in **section 3.6**.

3.4.1 Epithelial-mesenchymal Status of 5 Cell Lines

***Key Finding:* CAPAN-2 had mixed epithelial and mesenchymal properties. So all three cell lines with some mesenchymal properties (CAPAN-2, MiaPACA-2 and PANC-1) appeared erlotinib-insensitive.**

First, epithelial-mesenchymal status of the 5 cell lines is presented here. This is important mesenchymal morphology has been implicated as a mechanism of erlotinib resistance.[84]

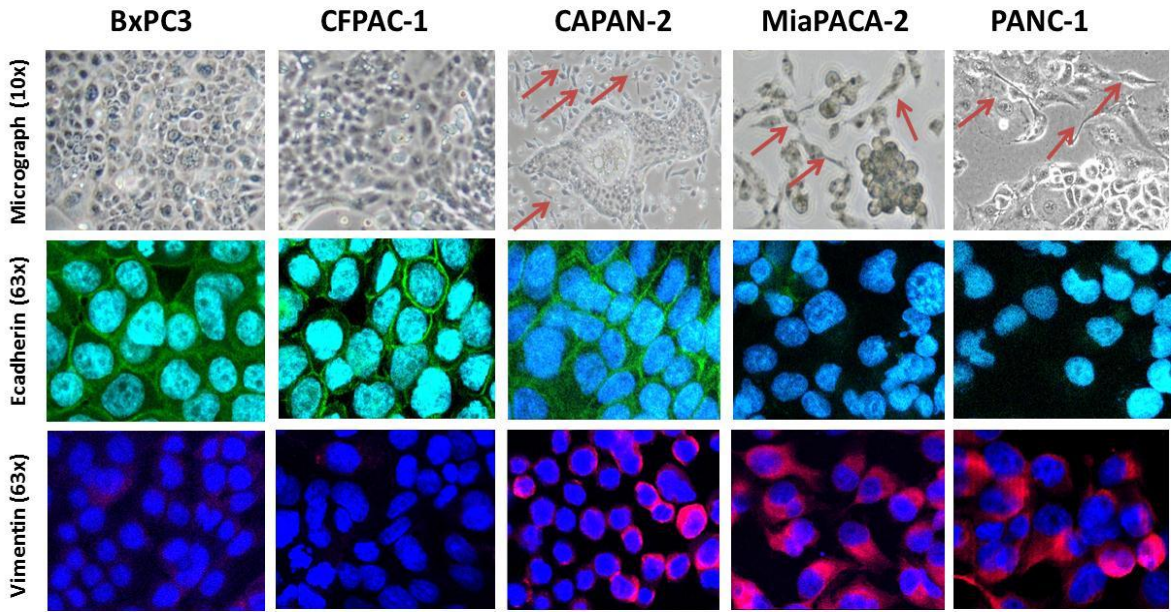

Figure 3.17: Micrographs and e-cadherin/ vimentin (immunofluorescence) of 5 cell lines

The micrographs showed that BxPC-3 and CFPAC-1 had predominantly epithelial morphology as described previously.[221,225] MiaPACA-2 was true mesenchymal. PANC-1 was mixed, showing a mixture of epithelial and spindle-shaped cells.[230,232] CAPAN-2 was reported to be an epithelial cell type,[139] but on micrographs of CAPAN-2 showed a mixture of epithelial and mesenchymal cell types (red arrows) **(Fig 3.17)**. The 5 cell lines had been typed (03/2012) and conformed to ATCC standards. This finding in CAPAN-2 did not necessarily contradict with literature, since epithelial-mesenchymal transition (EMT) is a reversible and transient process that allows for certain plasticity without full commitment to mesenchymal phenotypes.[287]

To study epithelial-mesenchymal status in more detail, the cells were stained for epithelial marker e-cadherin and mesenchymal marker vimentin. On confocal microscopy, vimentin appeared red (633nM) and e-cadherin appeared green (488nM). As expected, epithelial cells BxPC-3 and CFPAC-1 had positive e-cadherin but no vimentin expression. Mesenchymal MiaPACA-2 had positive vimentin but no e-cadherin. PANC-1 was mixed, though it was only positive for vimentin and not for e-cadherin. By contrast, CAPAN-2 was positive for both e-cadherin and vimentin **(Fig 3.17)**.

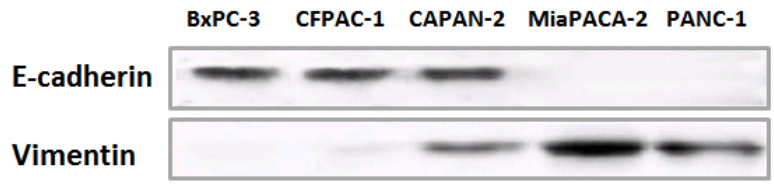

Figure 3.18 E-cadherin/ vimentin (western blotting) of 5 cell lines

To confirm this, e-cadherin and vimentin were confirmed by western blotting. This was consistent with the immunofluorescence findings, in that BxPC-3 and CFPAC-1 showed e-cadherin alone; MiaPACA-2 and PANC-1 vimentin alone, and CAPAN-2 displayed both **(Fig 3.18)**.

Altogether, **cell lines with some mesenchymal properties (as demonstrated by high vimentin) were insensitive to erlotinib**. This was consistent with the existing literature.[84] In

reality, this is an over-simplification, since the EMT program is dependent on a large signalling network of proteins and factors in addition to e-cadherin and vimentin.[69] Moreover, epithelial-mesenchymal status is governed by a dynamic equilibrium of EMT and mesenchymal-epithelial transition (MET).[69] The full study of this process requires interrogation of TGF-stimulated SMAD4 and various transcription factors like Snail, and was clearly beyond the scope of this PhD. Since this PhD focuses on the role of EGFR and PI3K co-inhibition in PDAC, a primary effort was placed on the examination of these signal transduction pathways.

3.4.2 EGFR, IGF1R, PI3K related protein expressions (western blotting)

Key Finding: ***The constitutively active Akt and ERK, the readily activated Akt by both EGF and IGF stimulation, and oncogenic shift of PI3K/Akt and MAPK pathways appeared to contribute to erlotinib insensitivity in PDAC.***

In this sub-section, EGFR, IGF1R, Akt and ERK protein expression were examined by means of western blotting. As discussed previously, Akt is a key regulator of the PI3K pathway, which is part of the larger IGF-stimulated PAM pathway. ERK1/2, on the other hand, is downstream of EGFR in the MAPK cascade. Both EGFR and IGF1R have input in these pathways. [43,288] Current literature suggests significant cross-talk between these two pathways,[43] and transactivation of EGFR or IGF1R by the other receptor via autocrine loop is also known to occur.[289] Hence, to study the molecular mechanisms of these cell lines, the basal expression of these proteins was first assessed, followed by downstream activation by EGF/ IGF, and finally single blockade by EGFR, IGF1R and PI3K inhibitors.

3.4.2.1 Basal Expression of EGFR, IGF1R, ERK and Akt

In this duplicate experiment, the 5 cell lines and the supernatant from residual medium were lysed, adjusted with protein concentration assay, and then immunoblotted in 2 separate 12-well gel, with markers on the last lanes from each side. Both total and phosphorylated proteins were assessed. Below showed the representative blot from one of the experiments:

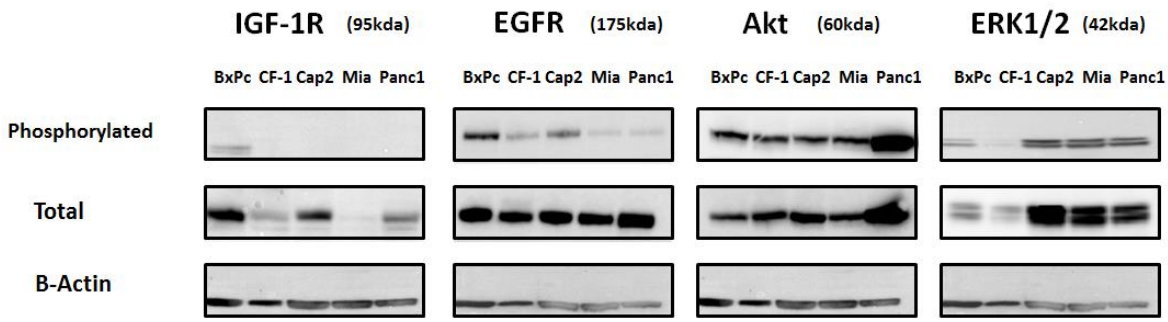

Figure 3.19: Western blotting experiment of basal expression of EGFR, IGF1R, Akt and ERK1/2

In regards to expression of the surface receptors (EGFR and IGF1R) in the 5 cell lines, the most erlotinib-sensitive BxPC-3 had the most constitutively active EGFR and IGF1R. On the other hand, the erlotinib-insensitive MiaPACA-2 and PANC-1 had the most attenuated EGFR and non-existent phosphorylation of IGF1R at baseline. By contrast, in regards to expression of downstream signals (ERK and Akt), these two cell lines and CAPAN-2 had high total and phosphorylated ERK compared to the other two cell lines. Moreover, PANC-1 appeared to have substantially higher expression of both total and phosphorylated Akt, indicating a basally active PI3K/Akt pathway. Also, not shown in the above figure were the blotting results of the supernatant (culture medium) of the 5 PDAC cell lines. EGFR and IGF1R could not be detectedin the supernatant of any cell lines, indicating that EGFR and IGF1R were indeed cell surface receptors and not present as circulating free receptors.

3.4.2.2 EGF- and IGF- stimulated Downstream Signals

The effect of EGF and IGF on downstream signals was studied next. Before this experiment was performed, the conditions for EGF and IGF stimulation needed to be optimised. EGF 10ng/ml and IGF 50ng/ml were used based on literature and previous laboratory experience.[64,289] The timing for growth factor stimulation should be optimised, so that the best signals for both surface receptors and downstream proteins could be achieved. The stimulation time of 5, 15 and 60 minutes was tested on BxPC-3 and CAPAN-2. These two were chosen because theoretically the rapid growth rate of BxPC-3 and the slow growth rate

of CAPAN-2 could result in different signalling rates between these two cell lines by growth factor stimulation.

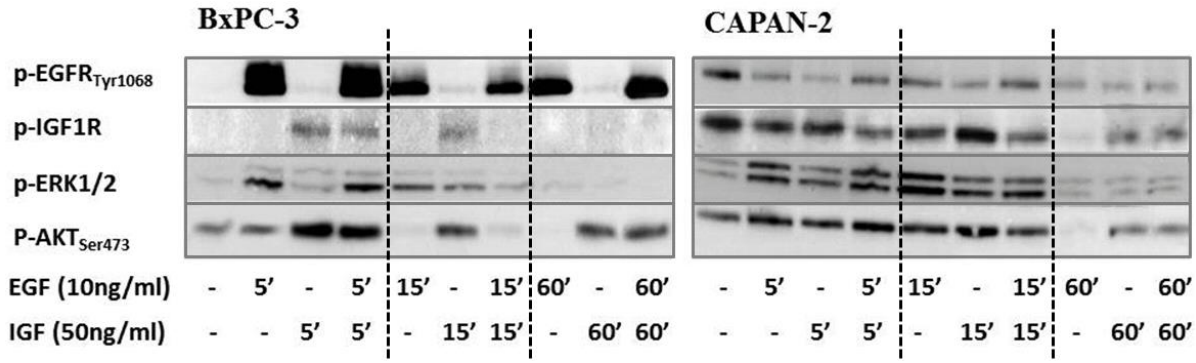

Figure 3.20: Western blotting experiment time optimisation for EGF and IGF

Time optimisation experiments showed that the phosphorylated receptor signalled best at 5 minutes for BxPC-3 and 5 or 15 minutes for CAPAN-2 **(Fig 3.19)**. At 60 minutes, the signals were too attenuated for both cell lines. Interestingly, this optimisation experiment was the first of many to elicit "exclusive signalling" in erlotinib sensitive cell lines. In BxPC-3, EGF only activated pERK and IGF only activated pAkt. By contrast, in CAPAN-2 EGF and IGF both stimulated pAkt and pERK. Note that in this optimisation experiments protein concentration adjustment was not performed. Also, total proteins were not tested for this pilot study. This was not necessary, as it only sought to find the optimal time for the phosphorylated signal. Results from these cell lines were not directly comparable. Since downstream signals were strongest at 5 minutes for BxPC-3 and slightly stronger at 15 minutes for CAPAN-2, **EGF and IGF stimulation for 10 minutes was chosen for subsequent studies.**

After optimisation, the downstream signals ERK and Akt were studied in more detail for the 5 PDAC cell lines. This time protein concentrations were adjusted between samples. These were studied in a long 25-well gel that allowed for simultaneous immunoblotting and exposure of all 20 samples, with markers loaded at the end lane on either side. Phosphorylated and total proteins were both studied. This core experiment was performed 3 times, and below shows a representative western blot.

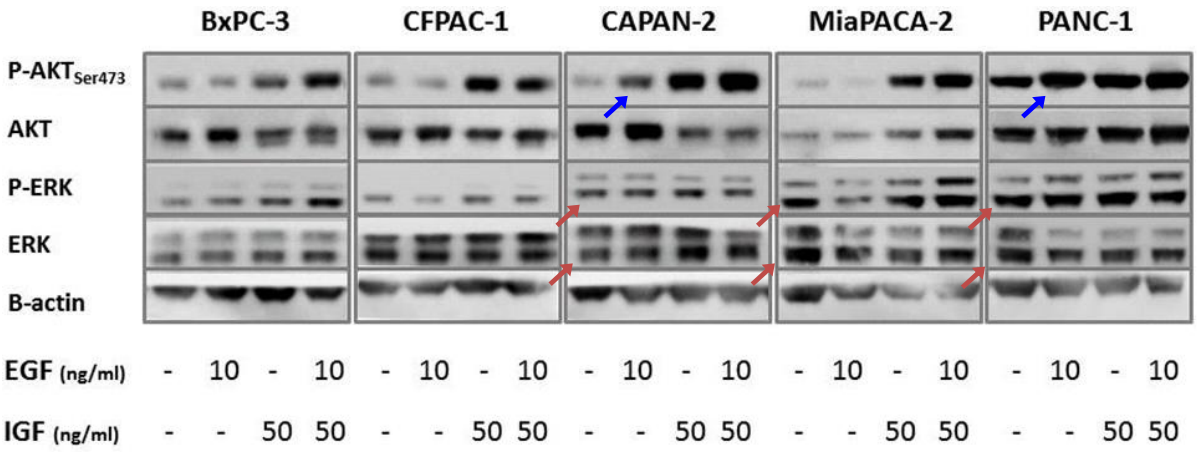

Figure 3.21: Western blotting experiment pAkt and pERK in 5 PDAC cell lines

Two things were of particular interest in this EGF and/or IGF stimulation study. Firstly, erlotinib insensitive cell lines all seemed to have higher basal level of total and phosphorylated ERK (red arrows), suggesting that they had a constitutively active MAPK pathway. PANC-1 also had a more constitutively active pAkt compared to other cell lines, though the total Akt intensities were similar between the cell lines except for MiaPACA-2. Secondly, in 2 of the 3 erlotinib-insensitive cell lines (CAPAN-2 and PANC-1) pAkt was readily activated by IGF as well as EGF (blue arrows), and pAkt signals of these 2 cell lines were also the highest when both EGF and IGF stimulation were applied.

In the pooled analysis of quadruplicate experiments, pAkt and pERK were measured (multiguage v3.0), adjusted to total Akt and ERK protein respectively, and the summary statistics were then calculated. However, the nature of western blotting experiment did not allow for t-statistics to be performed as there was only one raw data per experiment (only 4 data point for 4 experiments). Immunofluorescence experiment by confocal microscopy was used to study total and phosphorylated Akt and ERK, and comparative statistics were calculated based on those next results. These will be presented in the next section (**3.4.3**).

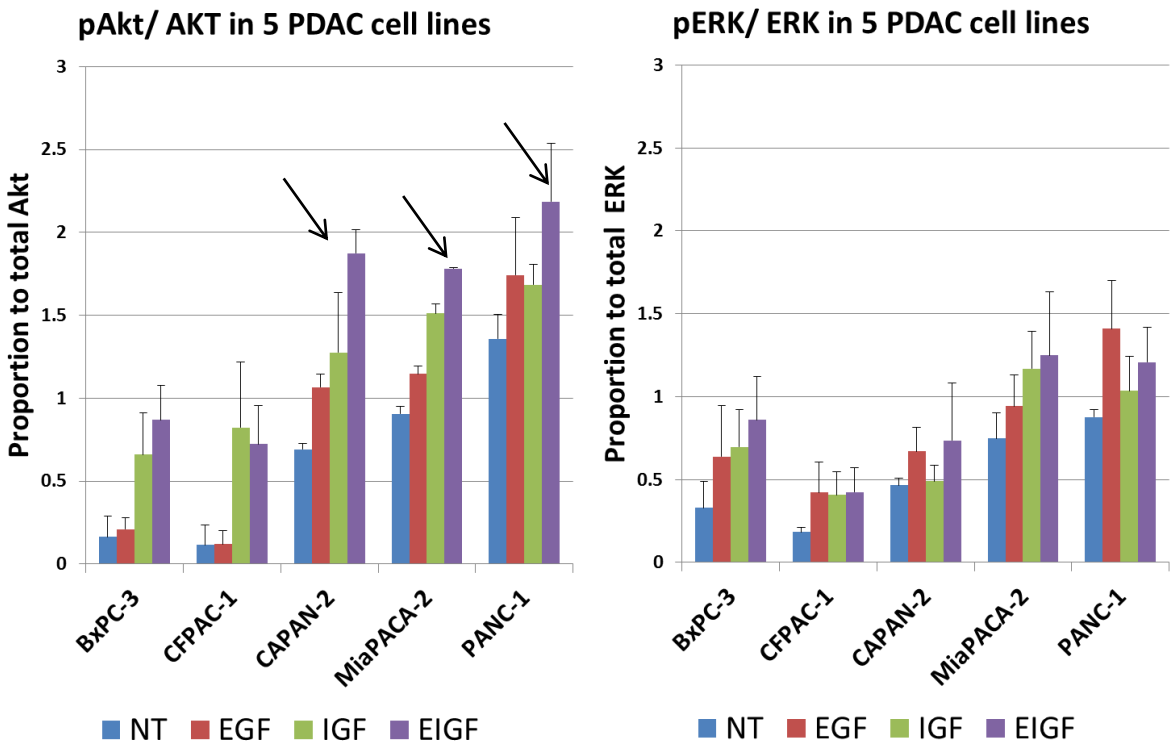

Figure 3.22: Western blotting experiment pAkt and pERK in 5 PDAC cell lines, average of 4 experiments

In the pooled results above, erlotinib insensitive cell lines were confirmed to have constitutively higher level of activation of both pAkt and pERK. EGF stimulated pERK in all cell lines (blue bars, right); but also pAkt in CAPAN-2 MiaPACA-2 and PANC-1 (red bars, left, **figure 3.22**). IGF strongly stimulated pAkt in all cell lines (green bars, left), but pERK in variable extents in the 5 cell lines (green bars, right). The combination of EGF and IGF had a profound effect of Akt and ERK to a lesser extent; and the proportion of pAkt to total Akt was the highest in the erlotinib insensitive cell lines (purple bars, left: black arrows). Therefore, by western blotting methods, **erlotinib insensitive cell lines appeared to be characterised by a more basally active pAkt and pERK system, high pAkt activity upon dual EGF and IGF stimulation.**

3.4.2.3 Response to EGFR, IGF1R or PI3K single drug inhibition

To study the effect of drug inhibition of these pathways, western blotting was performed on erlotinib-sensitive BxPC-3 and erlotinib-insensitive PANC-1 after treatment with EGFR

inhibitor erlotinib, IGF1R inhibitor AEW, pan-PI3K inhibitor LY and PI3K-α inhibitor BYL, in dose response studies. For erlotinib experiments, EGF stimulation was used. For IGF1R or PI3K inhibitor experiments, IGF stimulation was used. Total proteins were not blotted for this condensed experiment, as a more detailed experiment will be covered in **subsection 4.2.3.2**. This experiment had been performed in triplicate:

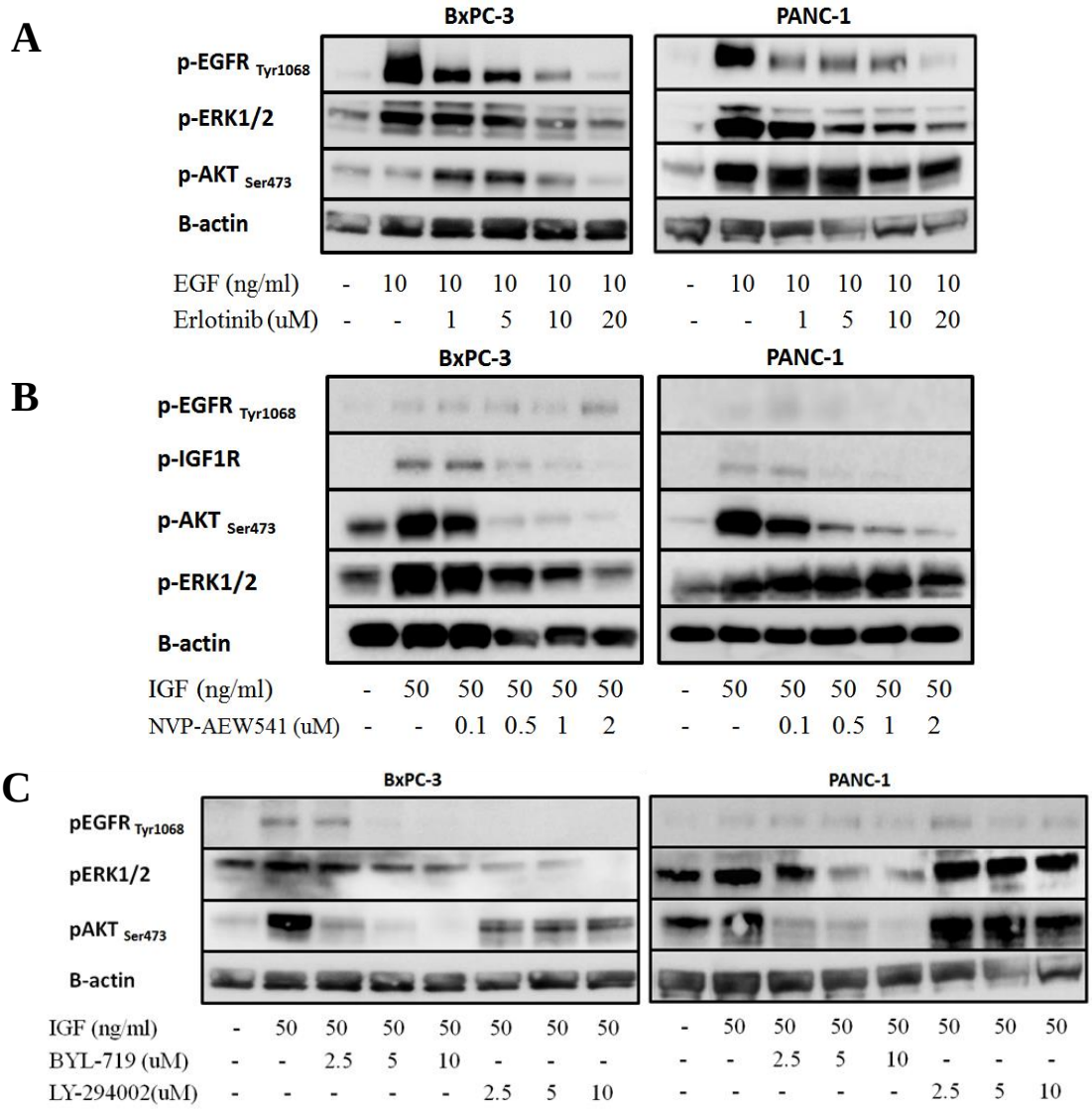

Figure 3.23: Western blotting of BxPC-3 and PANC-1 after EGFR, IGF1R or PI3K inhibition

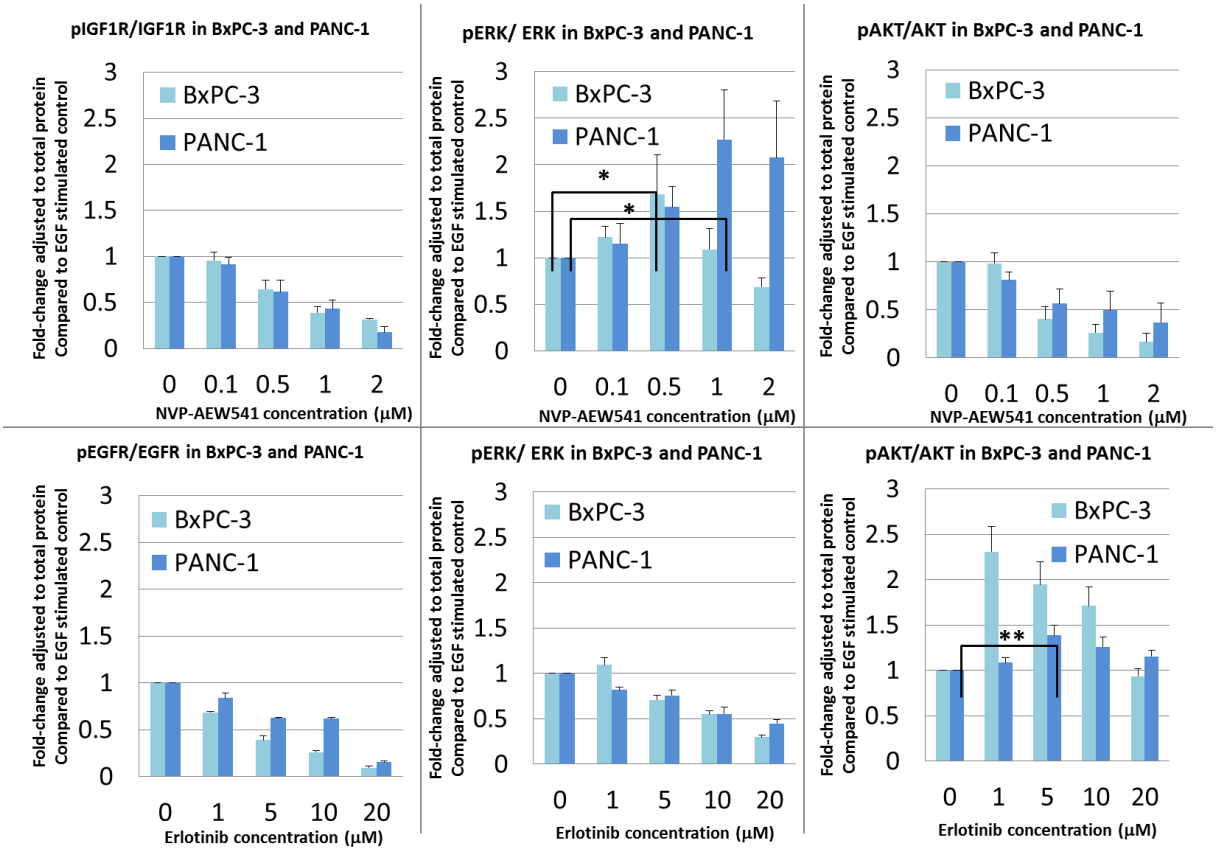

***Figure 3.24: Average and SEM of phosorylated/ total signals of BxPC-3 and PANC-1 in response to erlotinib and NVP-AEW541 (average of 3 experiments)**, * P<0.05, ** P<0.01*

IC50 ERL	pEGFR	pERK	pAkt
BxPC-3	4.0μM (3.6-4.4)	15.7μM (11.3-12.0)	39.3μM (30.3-48.2)
PANC	8.2μM (7.9-8.6)	15.6μM (13.9-18.1)	67.6μM (28.1-106.9)

	BxPC-3		PANC-1	
IC_{50}	pAkt	pERK	pAkt	pERK
AEW-541	0.61μM (0.38-0.84)	0.39μM (0.26-0.52)	0.53μM (0.32-0.73)	NR
LY-294002	5.6μM (3.1-8.1)	29.9μM (21.9-37.8)	21.5μM (17.0-26.0)	NR
BYL-719	1.6μM (0.8-2.3)	25.3μM (15.9-34.6)	4.6μM (3.8-5.3)	22.8μM (21.5-24.2)

Table 3.4: Western blotting estimated IC_{50} for erlotinib, NVP-AEW541, LY294002 and NVP-BYL719

EGF substantially stimulated pAkt in PANC-1 but not BxPC-3 **(figure 3.23)**. For both cell lines, there were appropriate increases in pEGFR and pERK with exposure to EGF, and reduction in these signals with EGFR inhibitor erlotinib. The IC_{50} for pEGFR inhibition was estimated to be 4.0 μM (3.6-4.4 μM) for BxPC-3 and higher at 8.2 μM (7.9-8.6 μM) for PANC-1; and the IC_{50} for pERK inhibition was 15.7 μM (11.3-12.0 μM) and 15.6 μM (13.9-18.1 μM) for BxPC-3 and PANC-1 respectively. Both cell lines, however, paradoxically increased pAkt with erlotinib suggesting oncogenic shift to the alternate pathway (both $P<0.05$). In BxPC-3, after the initial rise pAkt appropriately decreased from 1μM erlotinib. In PANC-1, the trend only decreased from 10μM erlotinib; implying a more resilient mechanism of oncogenic shift in this less sensitive cell line **(figure 3.24)**. Note that all signals were adjusted to EGF-stimulated control, so for PANC-1 which had a much more highly EGF-stimulated pAkt, the relative fold-change with erlotinib inhibition appeared smaller than for BxPC-3. Averaged from three experiments, the IC_{50} for pAkt inhibition was estimated to be 39.3 μM (30.3-48.2) for BxPC-3 and 67.6 μM (28.1-106.9) for PANC-1 **(Figure 3.23a)**.

Next, the two cell lines were treated with IGF1R and PI3K inhibitors. pAkt inhibition IC_{50} for BYL [1.6μM (0.8-2.3) for BxPC-3 and 4.6μM (3.8- 5.3) for PANC-1] was 4-5 times more potent than LY [5.6μM (3.1-8.1) and 21.5μM (17.0-26.0) respectively]. On the other hand, the pAkt inhibition IC_{50} for AEW was the most potent, at 0.61μM (0.38-0.84) for BxPC-3 and 0.53μM (0.32-0.73) for PANC-1 **(Table 3.4)**. Of interest, whilst AEW strongly inhibited pAkt and pIGF1R in both cell lines, there was a paradoxical increase in pERK with increasing concentration of AEW in PANC-1 ($P<0.01$) **(Figure 3.23b)**. In BxPC-3, pERK appropriately decreased from 1μM AEW whilst the trends only decreased from 2μM AEW for PANC-1 **(Figure 3.24)**. pERK in PANC-1 also appeared to be unaffected by LY. Only BYL induced a reduction in p-ERK in both cell lines, with an IC_{50} of 25.3 μM (15.9-34.6) and 22.8 μM (21.3-24.2) in BxPC-3 and PANC-1 **(Figure 3.23c, table 3.4)**. The paradoxical increases in pAkt level in response to EGFR inhibitor and pERK level in response to IGF1R inhibitor suggested that **there was significant cross-talk between MAPK and PI3K/Akt pathways.** When a

stressor is applied to one downstream pathway, the cancer cells rapidly switch to an escape pathway, a process that has been termed “oncogenic shift”.[132] This mechanism appears to be more resilient in the erlotinib insensitive PANC-1 cell line.

3.4.3 ERK and Akt expressions in 5 Cell Lines (Immunofluorescence)

***Key Findings*: All 3 erlotinib insensitive cell lines had significantly increased total and phosphorylated ERK or Akt at baseline, and higher EGF-stimulated pAkt signals.**

Confocal microscopy using Immunofluorescence was used to confirm the western blotting findings of activated downstream pathways and inter-pathway cross-talk. Immunofluorescence had enabled quantification of the intensity of signals, to measure this in multiple cells (and thereby allowing t-test statistics to be calculated), and to study total proteins independently. Immunofluorescence by confocal microscopy utilised laser emission and capture technique that enabled slide sections via ~0.2 micron pinholes, thus permitting high definition of intracellular signals and compartmentalising of cytoplasmic or nuclear signals.[258] In this sub-section, total Akt and ERK was first examined in the 5 cell lines, followed by phosphorylated ERK and Akt signals basally and with EGF. Quadruplicate experiments were performed to allow for robust statistical calculation. Since quantification could be subjected to a variety of measurement bias, a more stringent P-value of 0.01 was used. Exact P values down to 0.0001 were presented.

3.4.3.1 Total ERK and Akt

Total ERK was stained in fluorescent green (488nM) and total Akt in fluorescent red (633nM). The representative set of photos from confocal microscopy is shown below:

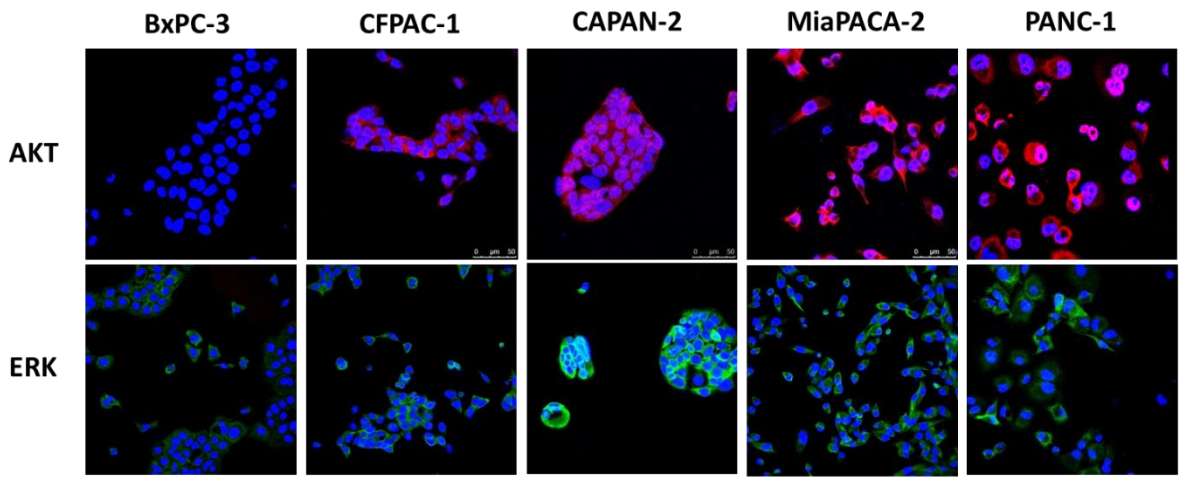

Figure 3.25: Representative photo of total Akt and ERK immunofluorescence in 5 PDAC cell lines

For Akt, PANC-1 clearly expressed the highest signal, followed by MiaPACA-2, CAPAN-2 and CFPAC-1. BxPC-3 hardly expressed any Akt. For ERK, CAPAN-2 showed the highest signal, followed by MiaPACA-2 and PANC-1, CFPAC-1 and BxPC-3 **(Fig 3.25)**. Summary statistics was calculated for 4 experiments, with t-statistics and trend statistics shown below:

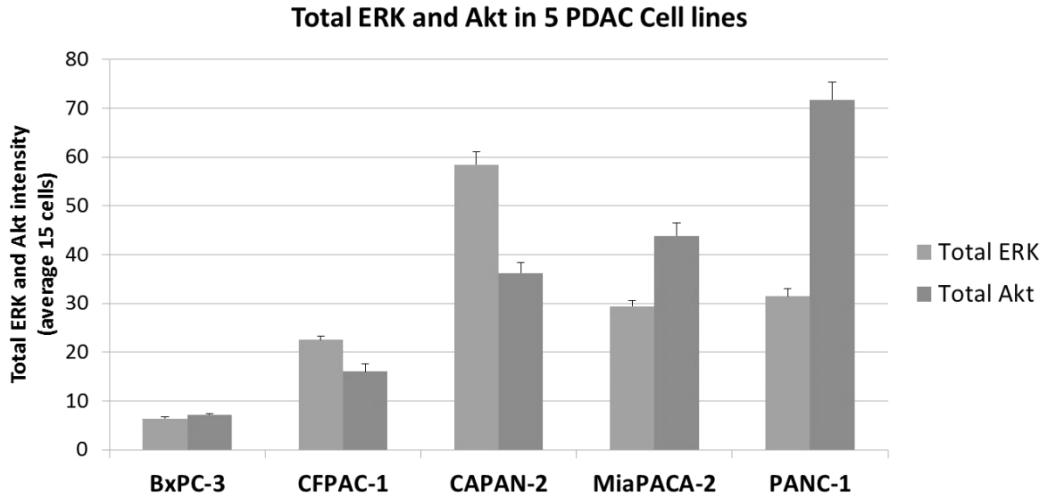

Figure 3.26: Immunofluorescence of total Akt and ERK in 5 cell lines, average of 4 experiments

NT	Akt	p-value	*BxPC-3*	*CFPAC-1*	*CAPAN-2*	*MiaPACA-2*	*PANC-1*
		BxPC-3	-	0.084	<0.0001	<0.0001	<0.0001
		CFPAC-1		-	0.003	<0.0001	<0.0001
		CAPAN-2			-	0.149	<0.0001
		MiaPACA-2				-	0.011
NT	**ERK**	**p-value**	***BxPC-3***	***CFPAC-1***	***CAPAN-2***	***MiaPACA-2***	***PANC-1***
		BxPC-3	-	<0.0001	<0.0001	<0.0001	<0.0001
		CFPAC-1		-	<0.0001	0.066	0.320
		CAPAN-2			-	<0.001	<0.001
		MiaPACA-2				-	0.003

Table 3.5: t-test statistics of total Akt and ERK expression between 5 PDAC cell lines

Concordant to the representative photos, total ERK was highest in CAPAN-2 and total Akt highest in PANC-1. Student paired t-test showed that the erlotinib insensitive cell lines (CAPAN-2, MiaPACA-2 and PANC-1) had significantly higher pAkt than sensitive cell lines (BxPC-3, CFPAC-1) (all P<0.01). For ERK, each cell line was significantly different to another, with the exception of CFPAC-1 and MiaPACA-2 as well as CFPAC-1 and PANC-1. To further summarise these data, trend statistics was performed according to decreasing erlotinib sensitivity in the 5 cell lines after adjusting to each experiment. **A significant trend was present for total Akt (t=2.76, P=0.006) but not in total ERK (t=1.47, P=0.14).**

3.4.3.2 pERK and pAkt at baseline and with EGF stimulation

For phosphorylated signals, pERK and pAkt signals were studied at baseline and with EGF stimulation only; since EGF was the direct ligand of EGFR, and EGF-stimulated pAkt in 2 of the 3 erlotinib insensitive cell lines (CAPAN-2 and PANC-1) on western blotting was of particular interest from **Fig 3.22**. To achieve this, phosphorylated downstream signals upon EGF stimulation were compared with baseline signals.

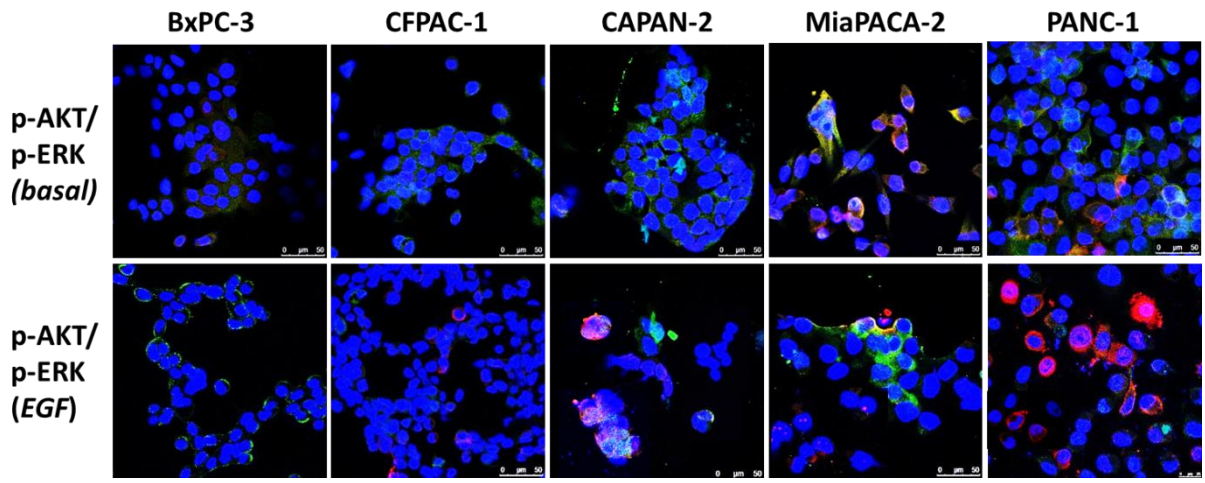

Figure 3.27: Immunofluorescence of pAkt and pERK in 5 cell lines, at baseline and with EGF (10ng/ml, 10 minutes) stimulation.

Again, pAkt was stained in fluorescent red like AKT, and pERK stained in the same fluorescent green as ERK, to maintain consistency. The results from immunofluorescence were very similar to western blotting. CAPAN-2, MiaPACA-2 and PANC-1 had visible pERK and pAkt signalling at baseline. Whilst EGF stimulated pERK and pAkt in all 5 cell lines, the signal intensity was clearly stronger in the latter 3 cell lines. In particular, PANC-1 had a propensity of activating pAkt (red) on EGF stimulation. Combining 4 experiments, the summary statistics and t-statistics are presented below.

NT	pAkt	p-value	*BxPC-3*	*CFPAC-1*	*CAPAN-2*	*MiaPACA-2*	*PANC-1*
		BxPC-3	-	<0.0001	<0.0001	<0.0001	<0.0001
		CFPAC-1		-	0.001	<0.0001	0.001
		CAPAN-2			-	0.738	0.042
		MiaPACA-2				-	0.164
NT	**pERK**	**p-value**	***BxPC-3***	***CFPAC-1***	***CAPAN-2***	***MiaPACA-2***	***PANC-1***
		BxPC-3	-	<0.0001	<0.0001	<0.0001	<0.0001
		CFPAC-1		-	0.002	0.003	0.001
		CAPAN-2			-	0.657	0.661
		MiaPACA-2				-	0.958

EGF	pAkt	p-value	*BxPC-3*	*CFPAC-1*	*CAPAN-2*	*MiaPACA-2*	*PANC-1*
		BxPC-3	-	0.135	<0.0001	<0.0001	<0.0001
		CFPAC-1		-	<0.0001	<0.0001	<0.0001
		CAPAN-2			-	0.289	0.006
		MiaPACA-2				-	0.013
EGF	**pERK**	**p-value**	***BxPC-3***	***CFPAC-1***	***CAPAN-2***	***MiaPACA-2***	***PANC-1***
		BxPC-3	-	0.128	0.0009	<0.0001	0.017
		CFPAC-1		-	<0.0001	<0.0001	0.382
		CAPAN-2			-	0.451	<0.0001
		MiaPACA-2				-	<0.0001

Table 3.6: t-test statistics of pAkt and pERK expression at baseline and with EGF stimulation between 5 PDAC cell lines

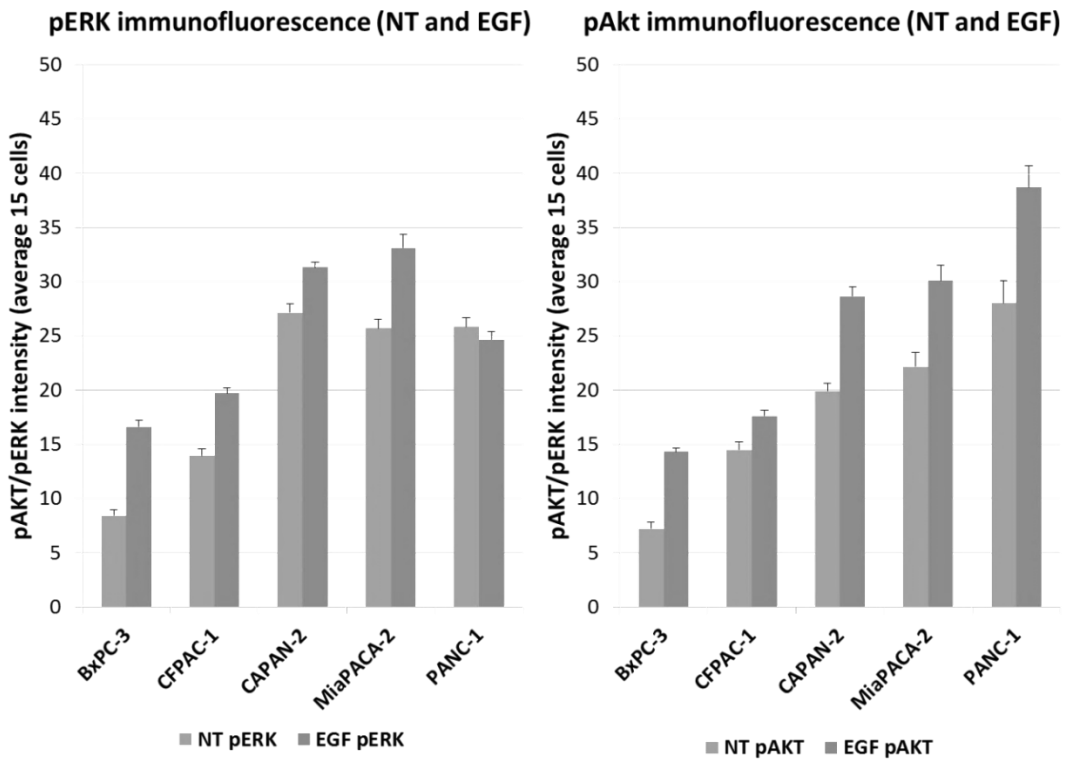

Figure 3.28: Immunofluorescence of pAkt and pERK in 5 cell lines, at baseline and with EGF stimulation, average of 4 experiments

For pERK and pAkt at baseline, CAPAN-2, MiaPACA-2 and PANC-1 had statistically different level of signals than BxPC-3 and CFPAC-1. Likewise, they also had higher levels of pAkt with EGF stimulation than the two erlotinib sensitive cell lines. Only pERK with EGF stimulation did not follow this pattern **(Table 3.5)**. On the graphical representation, pERK was higher in the 3 erlotinib insensitive cell lines, but the levels were similar between them. On the other hand, pAkt clearly followed the incremental erlotinib insensitivity of the 5 PDAC cell lines, at baseline and with EGF stimulation. The trend statistics showed pAkt followed a significant trend of erlotinib insensitivity at baseline ($t=3.11$, $P=0.002$) and with EGF ($t=6.83$, $P<0.0001$). However, pERK was not shown to follow a significant trend at baseline ($t=2.29$, $P=0.023$) and with EGF ($t=1.48$, $P=0.14$), using the stringent criteria of $P<0.01$ to demonstrate statistical significance.

In summary, western blotting and immunofluorescence were largely consistent in showing that the **3 erlotinib-insensitive cell lines tended to have more highly activated downstream pathways.** Both total and phosphorylated proteins were up-regulated. Importantly, **total and pAkt followed a significant trend in erlotinib insensitivity, but not total and pERK.** This implies that the PI3K/Akt system has a more crucial role in EGFR inhibitor insensitivity, as opposed to the MAPK pathways**. Nonetheless, cross talk between the two pathways still takes a major role**, as shown by the ability of "oncogenic shift" between MAPK and PI3K/Akt pathway in PANC-1 when put under drug pressure with low dose inhibitors.

3.4.4 PCR of key Gene Expressions in 5 Cell Lines (qRT-PCR)

***Key Findings:* EGFR and HER3 was significantly down-regulated and AKT-2 was significant up-regulated in erlotinib insensitivity**

qRT-PCR experiments were performed to assess the upstream and downstream-related genes of the two pathways among the 5 PDAC cell lines **(3.4.3.3)**, and later to validate the

gene array results in erlotinib resistant cell lines **(3.5.6)**. For simplicity, the optimisation studies of both experiments were presented below.

3.4.3.2 Optimisation of SYBR Green Primers

The genes of interest (GOI) for the erlotinib insensitivity and (later) erlotinib resistance experiments were *EGFR, IGF1R, HER3 (ERBB3), MAPK1, PI3Kα, PI3Kγ, TLR4, Fos, NFkB* and *RelA*. The control genes tested were *18S, B-actin* and *GAPDH*. *NFkB, RelA* and *GAPDH* were taqman probes, whilst the others were SYBR Green-based primers. Taqman probes are internally validated, so optimisation experiments are generally not needed.

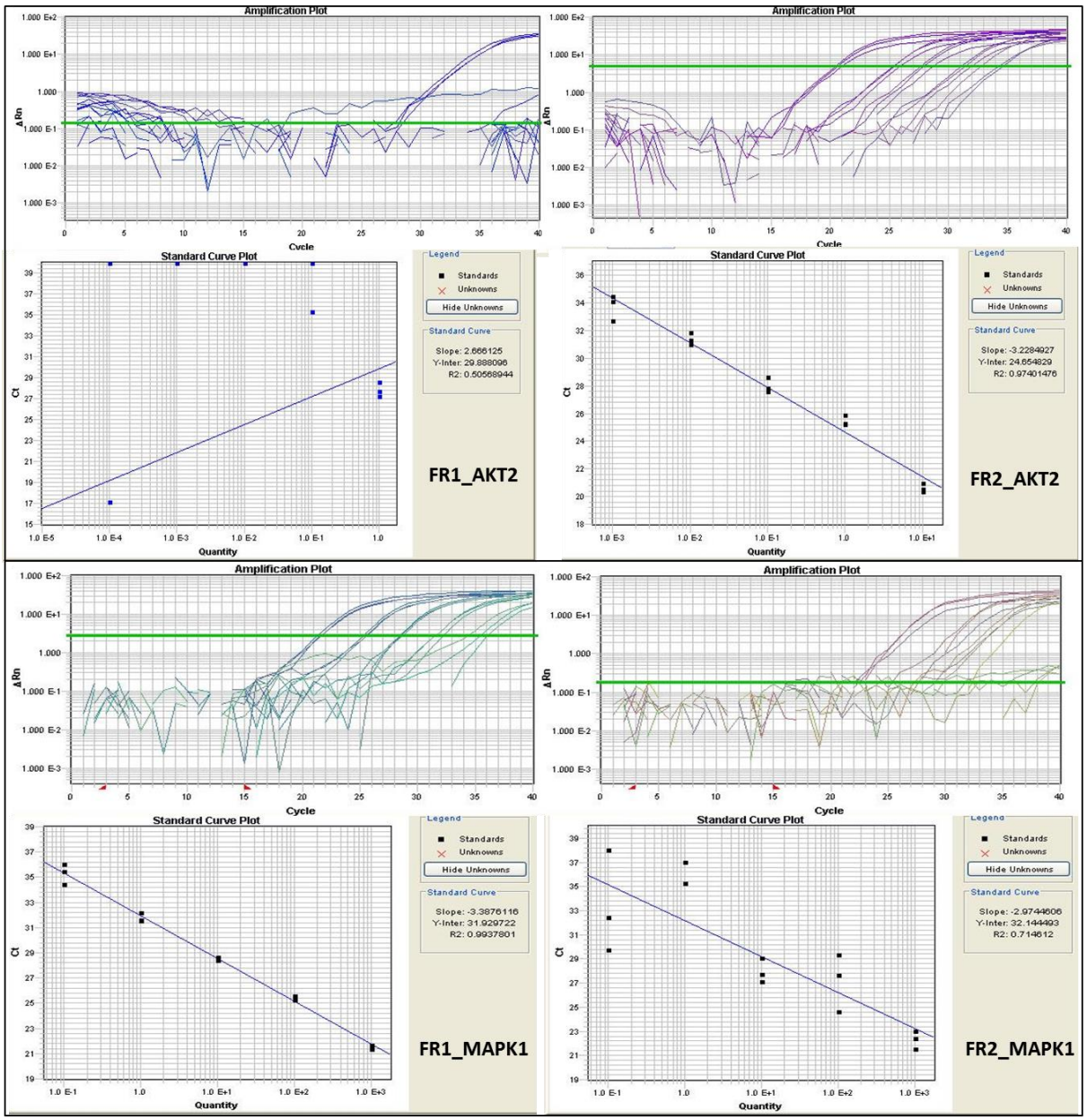

Figure 3.29: Examples of Amplification and Standard curve plots for different variants of AKT2 and MAPK1 SYBR green primers

Genes	Variant	Slope	R^2	Efficiency
AKT2	FR1	2.666	0.509	21%
AKT2	**FR2**	**-3.228**	**0.974**	**102%**
MAPK1	**FR1**	**-3.172**	**0.994**	**99%**
MAPK	FR2	-3.507	0.715	108%
PIK3CA	**FR1**	**-3.388**	**0.988**	**98%**
PIK3CG	**FR1**	**-2.974**	**0.858**	**98%**
PIK3CG	FR2	-3.421	0.978	96%
ERBB3	**FR1**	**-3.396**	**0.992**	**103%**
TLR4	**FR1**	**-3.513**	**0.98**	**95%**
Fos	**FR1**	**-3.563**	**0.995**	**96%**

Table 3.7: Slope, Efficiency and R squares for different variants of SYBR green primers

SYBR Green technologies utilise DNA-binding as opposed to probe-based detection systems for Taqman probes, resulting in preferential binding of GC sequence and reduced specificity.[290-292] The Minimum Information for Publication of Quantitative Real-Time PCR Experiments (MIQE) regards PCR efficiency and primer specificity as essential information for publication.[293] For the SYBR Green primers, 2 variants of each gene were purchased where available, with corresponding forward and reverse primers. These were mixed, diluted and frozen according manufacturer's instructions. Altogether 2 variants of *AKT2*, 2 variants of *MAPK1,* 2 variants of *PI3Kγ*, 1 variant of *PI3Kα*, 1 variant of *HER3*, 1 variant of *TLR4* and 1 variant of *Fos* were obtained. *EGFR* and *IGF1R* primers were previously validated by the CanSur laboratory staff and used in prior publication.[63] Standard curve experiments were performed with 5 10-fold dilution points on all variants, to determine the more specific primer of each gene to take into the core experiments.

Figure 3.29 and **Table 3.7** showed exemplary results of the optimisation experiments, in the study of PCR efficiency. In **Figure 3.29**, the amplification plots and standard curve plots are shown for the two variants for *AKT2* and *MAPK1*. What is immediately obvious is that different variants of the same gene could produce very different efficiency. For *AKT2*, the FR1 variant

could not even detect the PCR product whereas the FR2 variant closely conformed to the standard curve. For *MAPK1*, the FR1 variant showed a good standard curve whereas there was an unacceptable level of variation in the FR2 variant. **Table 3.7** showed the estimated slope and efficiency for each primer. A good reaction should have a slope between -3.10 to -3.58, equivalent to an efficiency between 90 to 110% and ideally as close to 100% as possible, as well as a correlation coefficient (R^2) as close to 0.999 as possible.[294] After these parameters were calculated, most primers were found to have very good efficiency. The final primers chosen for further study were *AKT2 (FR2), MAPK1 (FR1), PIK3CA (FR1), PIK3CG (FR1), ERBB3 (FR1), TLR4 (FR1)* and *Fos (FR1)*.

Next, the specificity of the primers were evaluated by means of melting curves. Melting curves plot the folded fraction of a structure vs. temperature, yielding important thermodynamic information. In highly specific PCR primers, Only one spike should be present for each melting plot, designated as the Temperature of melting (T_m).[260] In **Figure 3.30**, the melting curve examples of 6 gene variant primers are shown. All of these primers showed a single spike indicating high specificity. With this information, it was deemed unnecessary to perform gel electrophoresis to assess primer specificity further. Finally, in this set of standard curve experiments, 18S and GAPDH were selected as the reference genes for subsequent experiments. B-actin, another possible reference gene, had a less specific melting curve plot than the other reference gene primers, so it was not used.

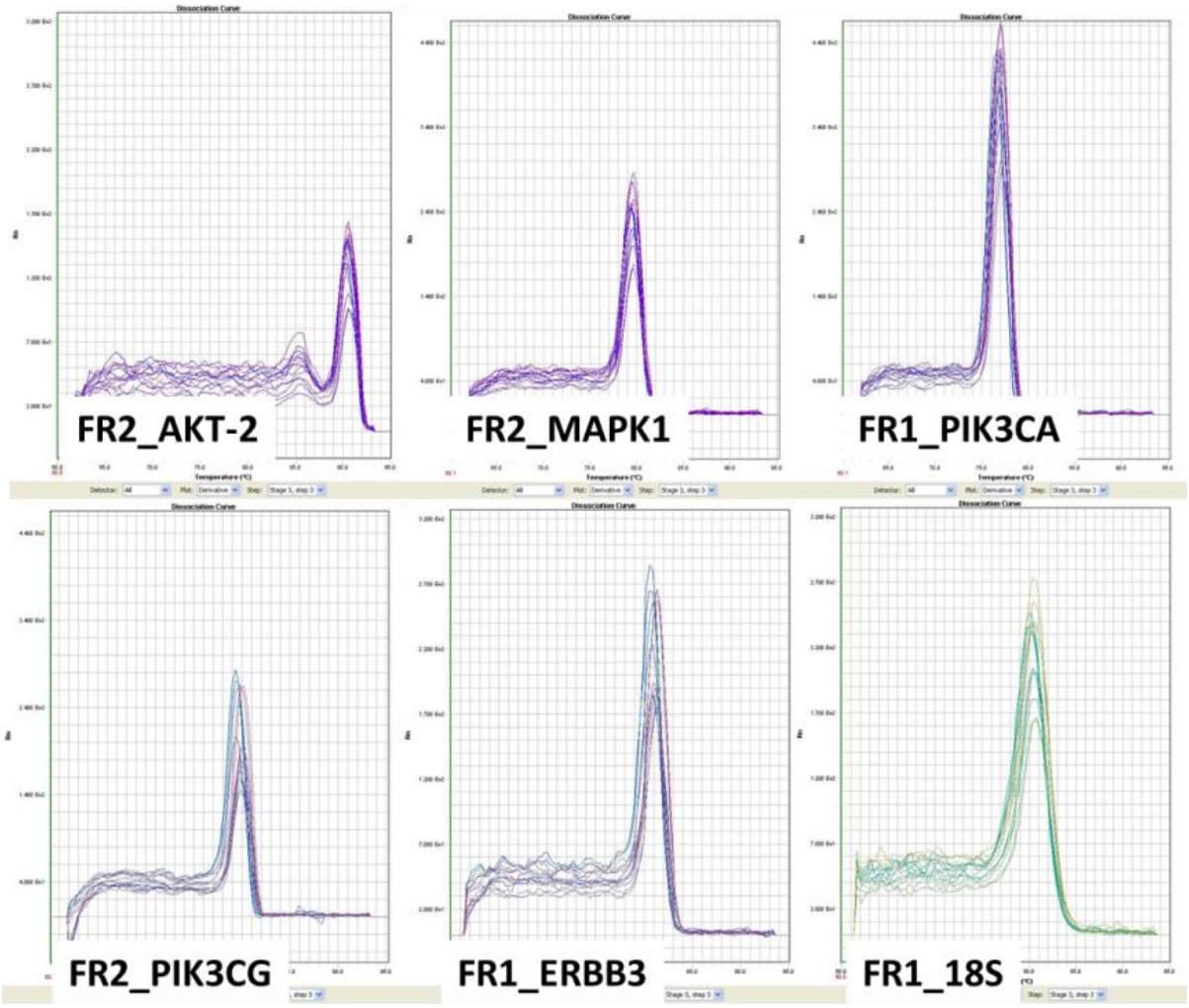

Figure 3.30: Examples of Melting Curves of SYBR green primers tested

3.4.3.3 qRT-PCR results of EGFR and IGF1R/PI3K related genes

The relative quantification method using $\Delta\Delta C_t$ was used for qRT-PCR analysis, with the methodology and calculations already covered in methods **(2.2.10.3)**. BxPC-3 was chosen as the reference cell line. As 18S was an abundant gene among these cell lines, samples were diluted 10,000 fold for 18S to achieve a C_t value of 14-15 (cycle 14-15). This allowed a calculation of fold –regulation with lesser degree of variance, as most other genes had a C_t values from 20-25. This core experiment was performed with technical duplicate in biological triplicate experiments. Pooled results with higher than 2-fold difference (up- or down-regulation) with a P-value less than 0.01 were considered statistically significant.[262] To

evaluate the 5 PDAC cell lines for erlotinib insensitivity, the genes of interest (GOI) *were EGFR, IGF1R, HER3, MAPK1, PI3KCA and AKT2*.

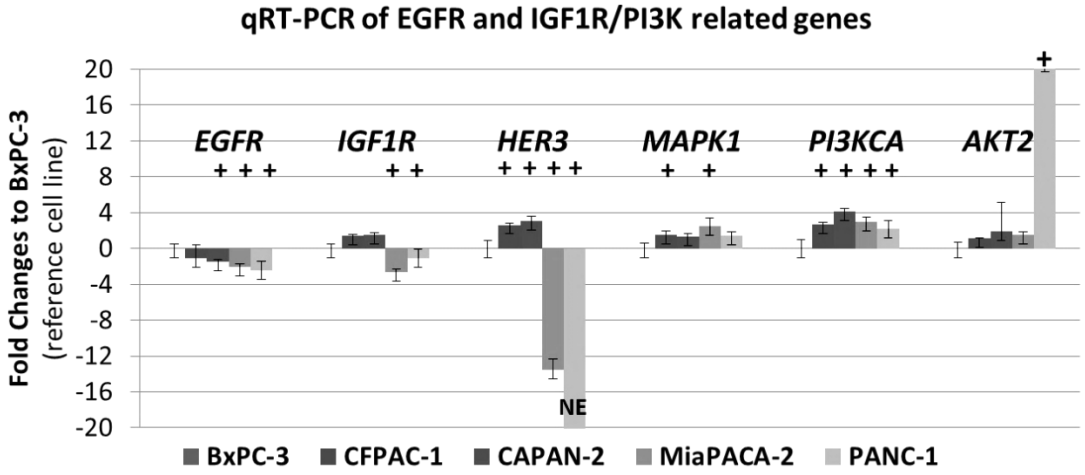

Figure 3.31: qRT-PCR results for EGFR and IGF1R/PI3K related genes in 5 PDAC Cell Line. **NE-not expressed. + P<0.01*

INCREMENTAL Insensitivity

Fold Changes	*EGFR*		*IGF1R*		*HER3*		*MAPK1*		*PI3KCA*		*AKT2*	
	Average	P-value	Average	P-value	Average	P-value	Average	P-value	Average	P-value	Average	P-value
BxPC-3	1.00	-	1.00	-	1.00	-	1.00	-	1.00	-	1.00	-
CFPAC-1	-1.08	0.54	1.44	0.87	**2.61**	**0.0003**	1.54	**0.006**	**2.70**	**<0.0001**	1.10	0.75
CAPAN-2	-1.51	**0.003**	1.52	0.65	**3.07**	**<0.0001**	1.32	0.064	**4.13**	**<0.0001**	1.91	0.039
MiaPACA-2	**-2.09**	**<0.0001**	**-2.64**	**<0.0001**	**-13.54**	**<0.0001**	**2.44**	**<0.0001**	**3.00**	**<0.0001**	1.49	0.19
PANC-1	**-2.45**	**<0.0001**	-1.08	**0.006**	**NE**	**<0.0001**	1.44	**0.018**	**2.16**	**<0.0001**	**20.75**	**<0.0001**
Multiple regression, trend t-statistics	**t=6.85, P<0.0001 Significantly down-regulated**		**t=0.28, P=0.78** Possibly down-regulated		**t=5.86, P<0.0001 Significantly down-regulated**		**t=-0.78, P=0.442** Possibly up-regulated		**t=-1.05, P=0.305** Possibly up-regulated		**t=-5.54, P<0.0001 Significantly up-regulated**	

Table 3.8: Fold up- or down-regulation and P-values for EGFR/MAPK and IGF1R/PI3K related genes in 5 PDAC cell lines, with trend statistics. *Genes with more than +/- 2 fold change AND P< 0.05 are considered significantly different (coded in pink and blue for up and down-regulation).*

In 3 experiments, all 3 erlotinib insensitive cell lines was shown to have some degree of *EGFR* down-regulation (-1.5 to -2.5 fold, all P<0.01), accompanied by up-regulation of varying downstream targeting genes. For CAPAN-2, *PI3KCA* was found to be most strongly up-

regulated among the PDAC cell lines (+4.13 fold compared to BxPC-3, P<0.0001); for MiaPACA-2, *MAPK1* was up-regulated by 2.4 fold (P<0.0001); and for PANC-1, *AKT2* was up-regulated by 20.8 fold (P<0.0001). Interestingly, the two most erlotinib insensitive cell lines also had a substantial down-regulation of HER3 (more than -13.5-fold, both P<0.0001). The standard errors of the gene expression were very acceptable, with an average CV of 1.4% and no CV above 5% across the gene tested. In particular, the CV for *HER3* and *AKT2* were fairly tight (1.1% and 1.9% respectively), suggesting that the substantial down- and up-regulation of these 2 genes were valid results. Trend t-statistics was calculated after adjusting to experiments, with a similar statistical approach as in the immunofluorescence studies. A consistent pattern was observed in the direction of the trend. Upstream targeting genes *(EGFR, IGF1R, HER3)* tended to down-regulate, whereas downstream targeting genes (*MAPK1, PIK3CA, AKT2)* tended to up-regulate in decreasing erlotinib sensitivity. Moreover, a significant trend of *EGFR* and *HER3* down-regulation and *AKT2* up-regulation was observed (all P<0.0001) **(Table 3.8)**.

To sum up this section, **erlotinib insensitivity is associated with downstream MAPK or PI3K/Akt over-activation.** On the gene level, erlotinib insensitivity was correlated with down-regulation of *EGFR* and up-regulation of PI3K/Akt and MAPK-related genes. Each erlotinib insensitive cell line was characterised by a different downstream gene over-expression. **The highest gene signals for CAPAN-2, MiaPCA-2 and PANC-1 were *PIK3CA, MAPK1* and *AKT2* respectively.** These gene over-expressions resulted in a higher total and phosphorylated Akt and ERK molecular signals on the molecular level, as demonstrated by western blotting and immunofluorescence. Importantly, a significant trend was observed for Akt but not in ERK. These results underline the importance of cross-talk of the 2 systems, and perhaps suggests a more critical role of PI3K/Akt in erlotinib insensitivity.

3.5 Molecular Characterisation of Acquired erlotinib resistance

In this next section, the molecular characteristics between parent and acquired erlotinib resistant (ER) cell lines were compared. Technically, BxPC-ER and PANC-ER were the same cell lines as BxPC-3 and PANC-1, except that they were made resistant to erlotinib after chronic drug exposure. Thus, these two pairs of parent versus ER cell lines serve as a powerful tool in the study of acquired erlotinib resistance. One thing to note, however, is that even though both ER cell lines were produced in the same way, they may not necessarily acquire erlotinib resistance via the same mechanism. Furthermore, the driver mechanism of erlotinib could be multiple, and may lie anywhere upstream or downstream, and may even be attributed by entirely different signalling pathways, as already discussed in introduction **(1.5).** For this reason, after the study of epithelial-mesenchymal status of these cell lines was completed, phospho-RTK array and PCR array were performed as a mass screening of genetic and molecular signatures that determined or contributed erlotinib resistance. PCR, western blotting and immunofluorescence were then used to validate these biomarker discovery findings.

3.5.1 Epithelial-mesenchymal Status of Parent versus ER cell lines

***Key Finding:* Both ER cell lines had likely undergone epithelial-mesenchymal transition as demonstrated by increased vimentin.**

3.5.1.1 E-cadherin and Vimentin of Parent versus ER cell lines

Previously, the micrographs of the two pairs of parent and resistant cell lines were shown, and demonstrated that BxPC-ER and PANC-ER had both transformed into a more mesenchymal phenotype, characterised by elongated and almost stellate morphology **(Figure 3.13)**. To validate these findings, e-cadherin and vimentin were studied by immunofluorescence and western blotting. A representative set of photos are shown, where e-cadherin was stained in fluorescent green (488nm) and vimentin stained in fluorescent red (633nm), was shown below:

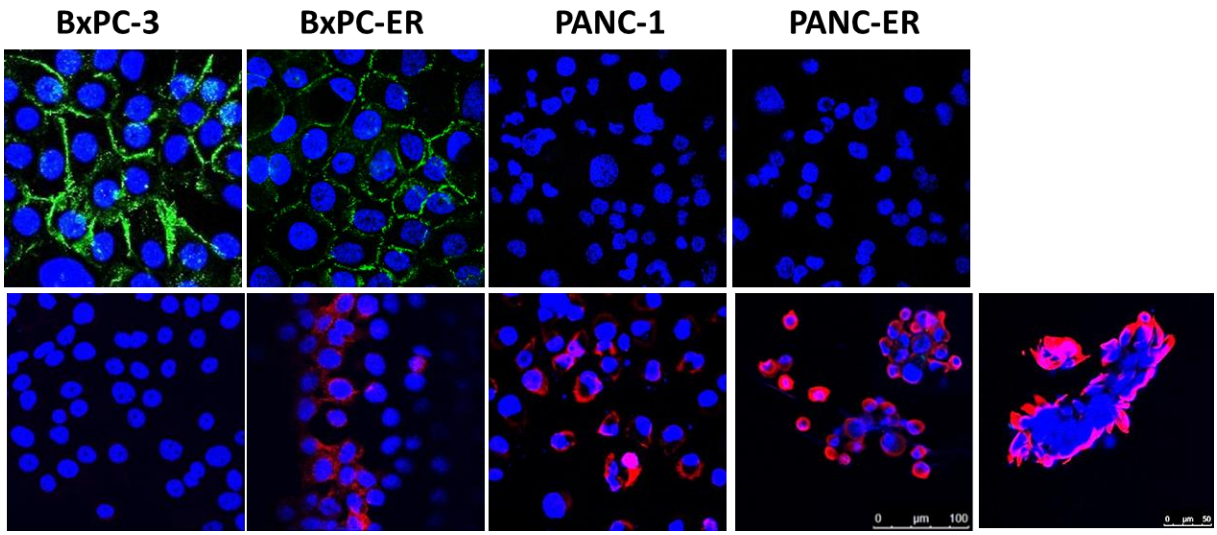

Figure 3.32: Representative photos of immunofluorescence of e-cadherin and vimentin in parent versus resistant cell lines by confocal microscopy

BxPC-3 normally expressed e-cadherin but no vimentin. In the resistant sub-line BxPC-ER, there was a decrease in e-cadherin and corresponding increased expression in vimentin, consistent with the finding of mesenchymal morphology in this cell line. PANC-1 normally expressed vimentin but not e-cadherin. The PANC-ER showed increased expression in vimentin compared to PANC-1 **(Figure 3.32)**. Interestingly, there was also a change in location of vimentin expression. Vimentin expression was scattered throughout PANC-1, which was consistent with its mixed epithelial and mesenchymal phenotype. In PANC-ER, on the other hand, vimentin was found at the edge of the colonies. This also appeared the case for BxPC-ER. Light microscopy showed that mesenchymal cells of BxPC-ER were found at the edges of colonies. The above photo, too, was taken at the periphery of a large colony. Thus, there was a strategic relocation of mesenchymal cells in ER cell lines to facilitate invasion and migration.

To quantitatively measure signal change in e-cadherin and vimentin, the signal intensity was again assessed by LAS3000 and the averages were compared in four experiments:

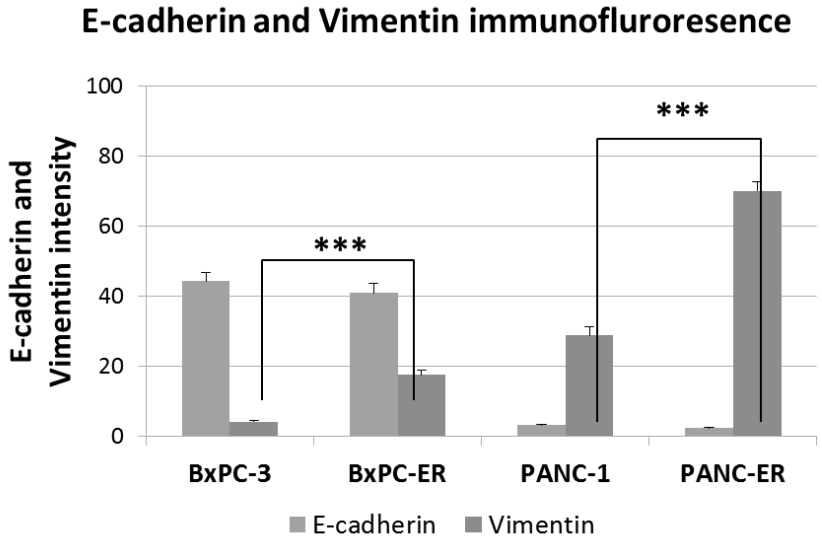

Figure 3.33: Immunofluorescence of e-cadherin and vimentin, average of 3 experiments (P<0.0001)***

Whilst there were no significant changes in e-cadherin expression between parent and resistant cell lines, there was a significant increase in vimentin expression in BxPC-ER and PANC-ER compared to BxPC-3 and PANC-1 (both P<0.0001). In addition, there was a large magnitude increase in vimentin expression from PANC-1 to PANC-ER **(Figure 3.33)**. These results suggested that ER cell lines, like erlotinib insensitive cell lines, also acquired mesenchymal properties. It thus provided a good link between erlotinib resistance and EMT.

3.5.2 Phosphorylated RTK Protein Discovery Array

***Key Finding:* Acquired erlotinib resistance is characterised by the up-regulation of the PAM pathway, with increased pAkt and pS6 activity.**

To study acquired erlotinib resistance in detail, molecular profiling of BxPC-3, BxPC-ER, PANC-1 and PANC-ER was performed using the Phosphorylated Receptor Tyrosine Kinase array (phospho-RTK). The Pathscan phospho-RTK array (cell signalling) is customised for 39 key targets from the EGFR/MAPK, IGF1R/PI3K, FGFR, HGFR, VEGF, PDGFR, EphR families, and is a useful tool for molecular screening between cell lines.[295] The primary aim for this study was to characterise molecular mechanism of acquired erlotinib resistance, by comparing between the two pairs of parent and resistant cell lines (BxPC-ER versus BxPC-3,

and PANC-1 versus PANC-ER). As a secondary comparison. major differences between the molecular signatures of BxPC-3 and PANC-1 were also studied that may contribute to erlotinib insensitivity. However, the results for this secondary aim was understandably of low yield, since BxPC-3 and PANC-1 were two very different cell lines, and the many molecular differences between them may not be specifically related to erlotinib insensitivity.

3.5.2.1 Basal phosphorylated RTK signals between parent and resistant cell lines

The first set of experiment examined the 4 cell lines at baseline. For consistency, $2x10^5$ cells were plated overnight for each cell line. They were washed and conditioned with serum-free medium before lysis using the kit lysis buffer provided. Protein concentrations were then adjusted using BCA assay (thermo scientific fisher) to 0.7mg/ml (array dynamic range: 0.125 - 2 mg/mL) prior to performing array experiment. Below showed the phospho-RTK array set up for comparison of phosphorylated signals at baseline between the 4 cell lines (**Figure 3.35)**, and the target map (**Figure 3.36)**:

	Target	Phosphorylation Site	Family
1	EGFR/ErbB1	pan-Tyr	EGFR
2	HER2/ErbB2	pan-Tyr	EGFR
3	HER3/ErbB3	pan-Tyr	EGFR
4	FGFR1	pan-Tyr	FGFR
5	FGFR3	pan-Tyr	FGFR
6	FGFR4	pan-Tyr	FGFR
7	InsR	pan-Tyr	Insulin R
8	IGF-IR	pan-Tyr	Insulin R
9	TrkA/NTRK1	pan-Tyr	NGFR
10	TrkB/NTRK2	pan-Tyr	NGFR
11	Met/HGFR	pan-Tyr	HGFR
12	Ron/MST1R	pan-Tyr	HGFR
13	Ret	pan-Tyr	Ret
14	ALK	pan-Tyr	LTK
15	PDGFR	pan-Tyr	PDGFR
16	c-Kit/SCFR	pan-Tyr	PDGFR
17	FLT3/Flk2	pan-Tyr	PDGFR
18	M-CSFR/CSF-1R	pan-Tyr	PDGFR
19	EphA1	pan-Tyr	EphR
20	EphA2	pan-Tyr	EphR
21	EphA3	pan-Tyr	EphR
22	EphB1	pan-Tyr	EphR
23	EphB3	pan-Tyr	EphR
24	EphB4	pan-Tyr	EphR
25	Tyro-3/Dtk	pan-Tyr	Axl
26	Axl	pan-Tyr	Axl
27	Tie2/TEK	pan-Tyr	Tie
28	VEGFR2/KDR	pan-Tyr	VEGFR

	Target	Phosphorylation Site	Family
29	Akt/PKB/Rac	Thr308	Akt
30	Akt/PKB/Rac	Ser473	Akt
31	p44/42 MAPK (ERK1/2)	Thr202/Tyr204	MAPK
32	S6 Ribosomal Protein	Ser235/236	RSK
33	c-Abl	pan-Tyr	Abl
34	IRS-1	pan-Tyr	IRS
35	Zap-70	pan-Tyr	Zap-70
36	Src	pan-Tyr	Src
37	Lck	pan-Tyr	Src
38	Stat1	Tyr701	Stat
39	Stat3	Tyr705	Stat

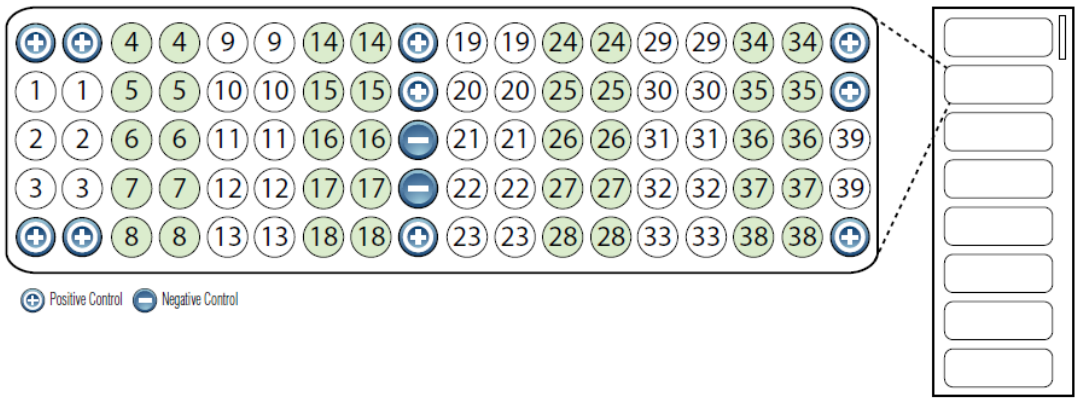

Figure 5. Target map of the PathScan® RTK Signaling Antibody Array Kit (Fluorescent Readout)

Figure 3.35: Target map of phosphorylated RTK tested in the phospho-RTK array. Courtesy of Cell Signalling © 2012

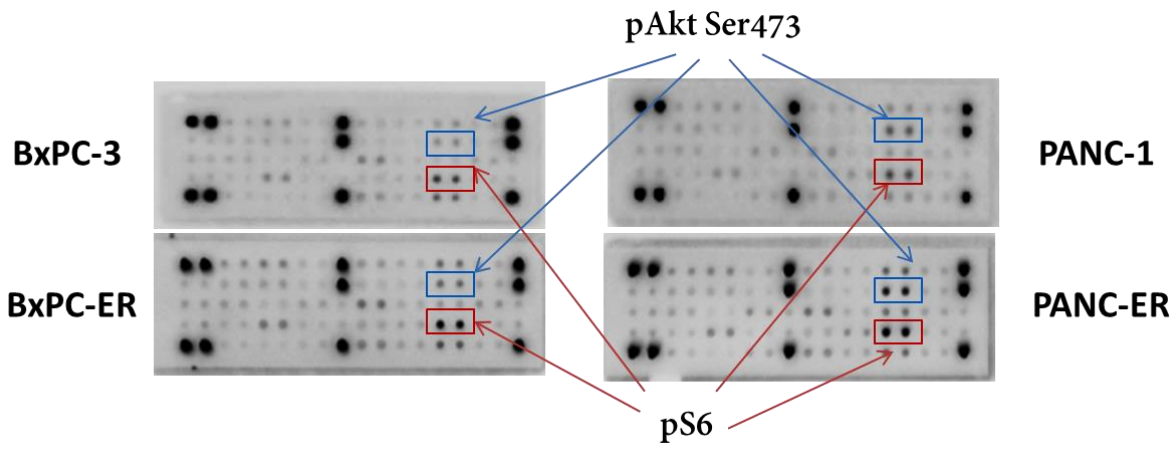

Figure 3.36: Representative phospho-RTK array blotting results (on high resolution)

The above chemilumminescent images were taken on LAS-3000 on high resolution settings. To orientate the reading for the phosphorylated RTK array, one noticed the 10 highly intense (dark) signals in the same area of each array. These were the positive controls, and were located in a specific pattern to allow the correct orientation of other signals. The next highest signals were actually pS6 and pAkt (red and blue boxes: **Figure 3.36**). Importantly, pS6 and pAkt appeared higher in BxPC-ER and PANC-ER compared to BxPC-3 and PANC-1. S6 is one of the two major downstream effectors of mTOR whose activity is dependent of Akt (the other effector being 4E-BP1).[49] This suggested that acquired erlotinib resistance appeared to be at least partly attributable to up-regulation of PI3K/Akt/mTOR or the PAM pathway.

In order to quantify these results, each signal was measured by pixel density (multigauage v3.0) and then adjusted to both positive and negative controls, as per product instruction. The column graphs for BxPC-3 versus PANC-1, BxPC-3 versus BxPC-ER and PANC-1 versus PANC-ER are shown below. The axis scaling was kept the same for these and subsequent comparisons:

A

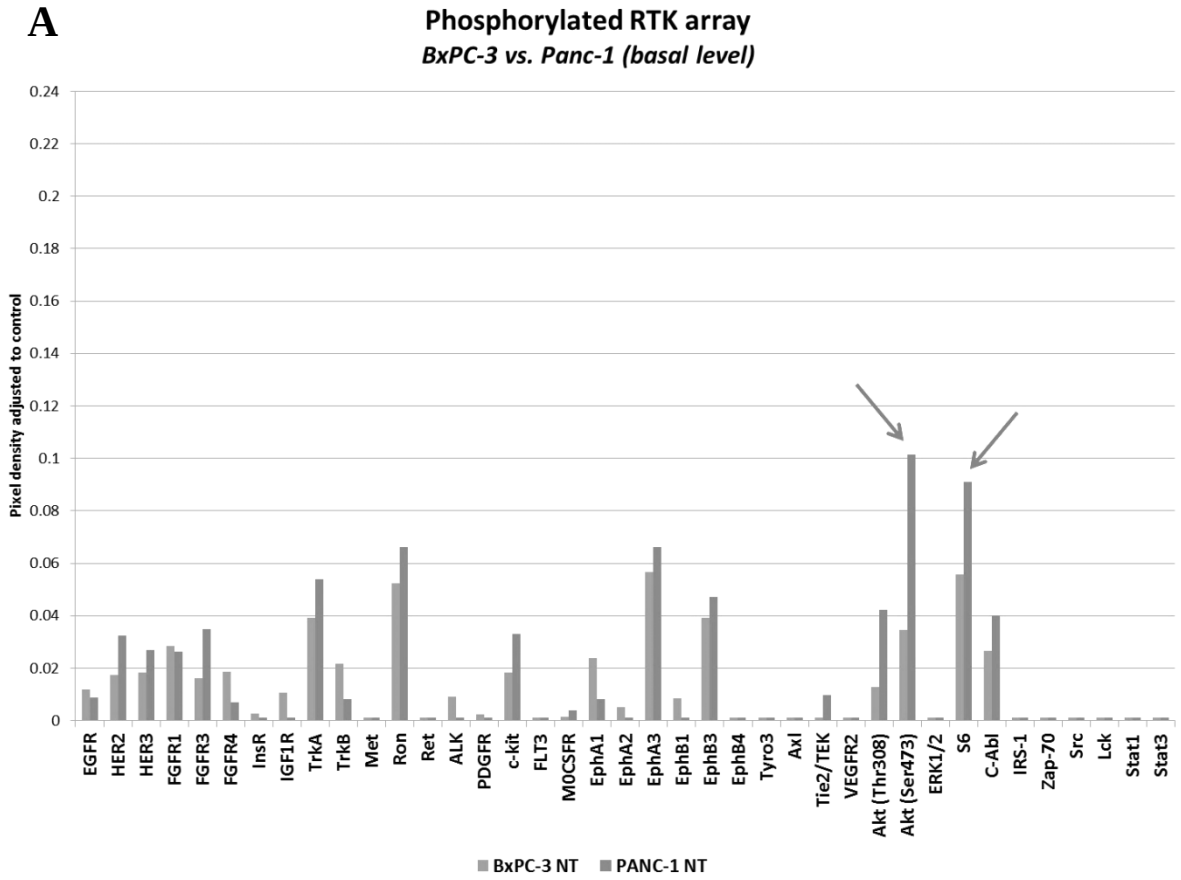
Phosphorylated RTK array
BxPC-3 vs. Panc-1 (basal level)
Pixel density adjusted to control
0.24
0.22
0.2
0.18
0.16
0.14
0.12
0.1
0.08
0.06
0.04
0.02
0
EGFR HER2 HER3 FGFR1 FGFR3 FGFR4 InsR IGF1R TrkA TrkB Met Ron Ret ALK PDGFR c-kit FLT3 M0CSFR EphA1 EphA2 EphA3 EphB1 EphB3 EphB4 Tyro3 Axl Tie2/TEK VEGFR2 Akt (Thr308) Akt (Ser473) ERK1/2 S6 C-Abl IRS-1 Zap-70 Src Lck Stat1 Stat3
BxPC-3 NT
PANC-1 NT

B

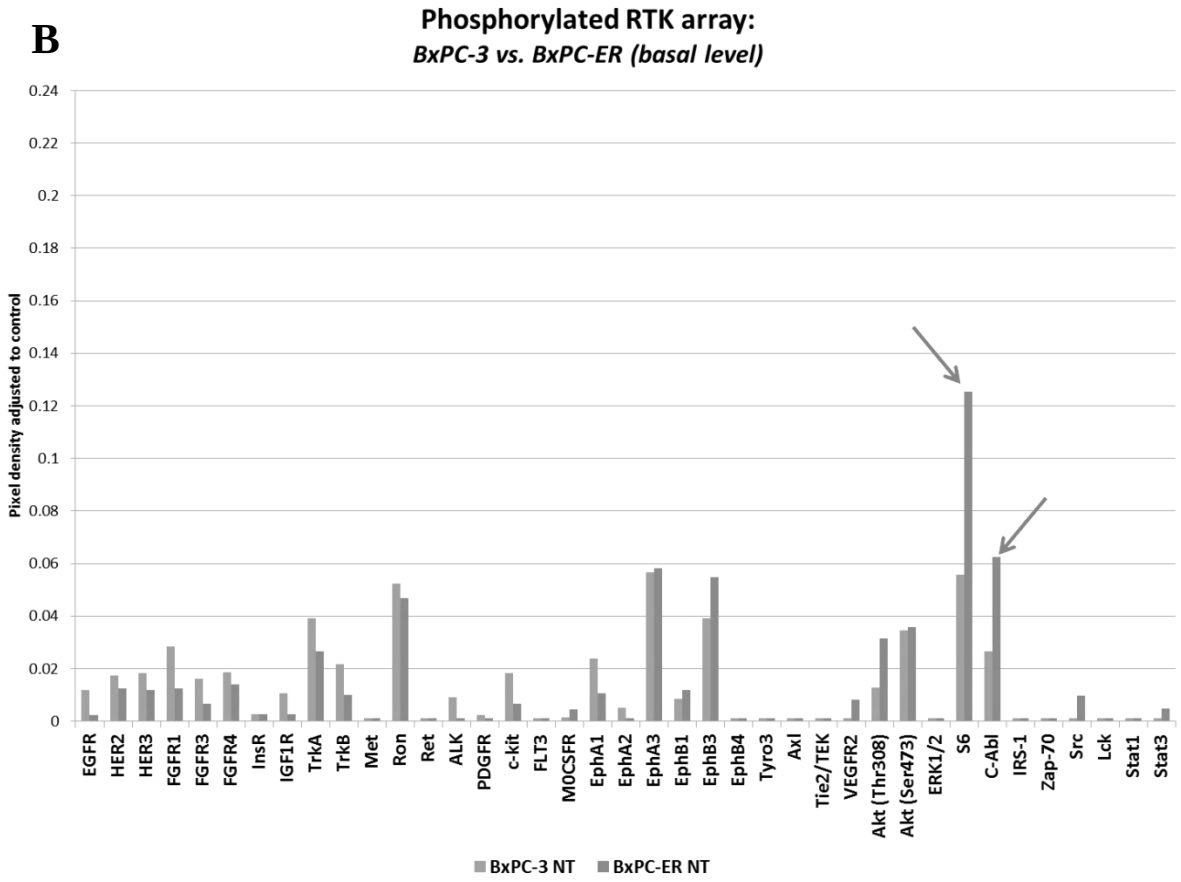
Phosphorylated RTK array:
BxPC-3 vs. BxPC-ER (basal level)
Pixel density adjusted to control
0.24
0.22
0.2
0.18
0.16
0.14
0.12
0.1
0.08
0.06
0.04
0.02
0
EGFR HER2 HER3 FGFR1 FGFR3 FGFR4 InsR IGF1R TrkA TrkB Met Ron Ret ALK PDGFR c-kit FLT3 M0CSFR EphA1 EphA2 EphA3 EphB1 EphB3 EphB4 Tyro3 Axl Tie2/TEK VEGFR2 Akt (Thr308) Akt (Ser473) ERK1/2 S6 C-Abl IRS-1 Zap-70 Src Lck Stat1 Stat3
BxPC-3 NT
BxPC-ER NT

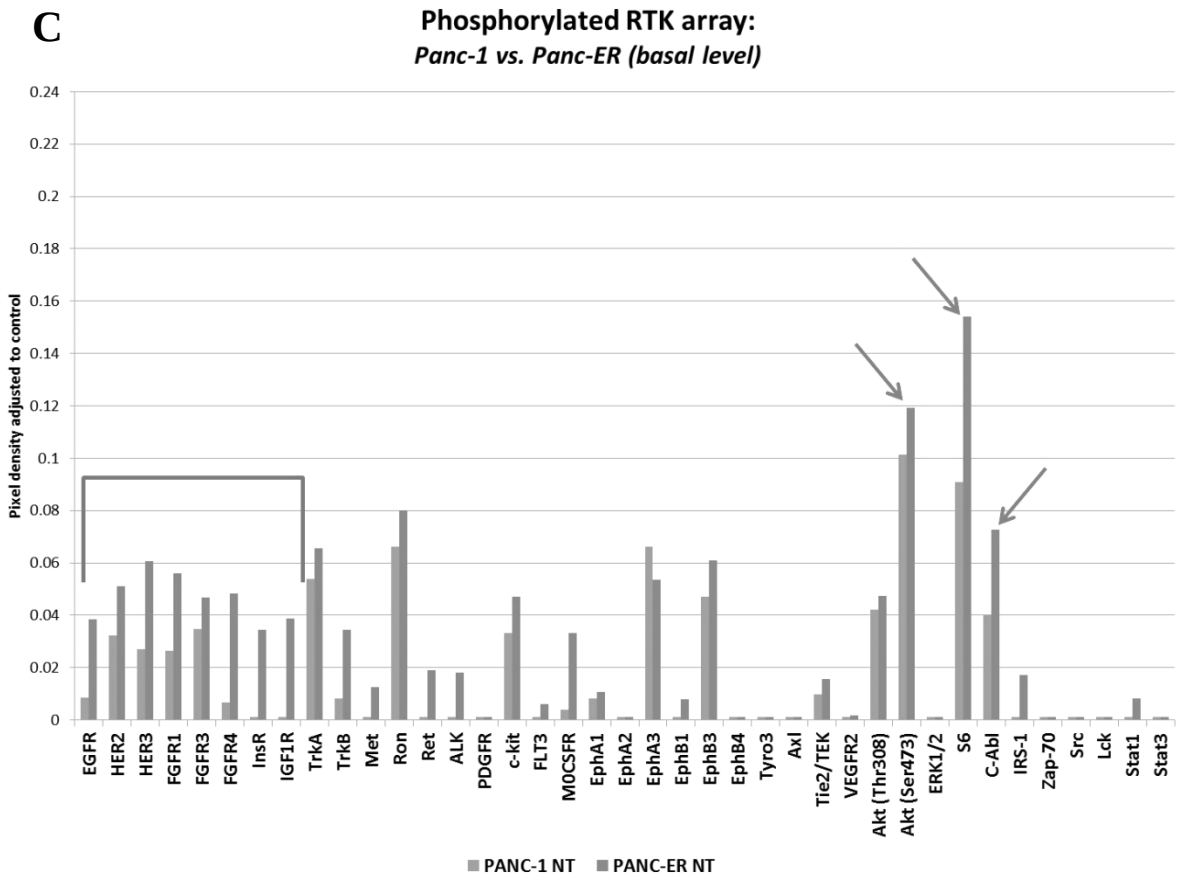

Figure 3.37: Phospho-RTK array result for parent and resistant cell line (baseline)

Between BxPC-3 and PANC-1, there were many molecular differences as expected. However, the greatest differences were pAkt (Ser473) and pS6, which also happened to be the highest intensity signal in PANC-1 (arrows, **figure 3.37a**). This is consistent with the previous western blotting and immunofluorescence finding, that PI3K/ Akt pathway is highly regulated in this cell line. A comparison between BxPC-3 and BxPC-ER showed that pS6 was much more highly up-regulated in BxPC-ER, even above the level observed in PANC-1 (about 0.12 pixel density to positive control, **figure 3.37b**). Another signal that was more active in BxPC-ER was C-abl, a tyroinse kinase in the Abl family that was extensively studied in haematological malignancies including leukemia. Importantly, c-Abl could induce drug resistance by modulating DNA repair mechanism, and was directly activated by the PI3K/Akt pathway.[296] Likewise, PANC-ER also increased pS6 and pC-Abl compared to PANC-1, and pAkt was also slightly increased as well (red arrows, **figure 3.37c**). In addition, PANC-ER also appeared more active in some of the

surface receptors, including the HER, IGF and Fibroblast-growth factor (FGF) families (blue bracket).

3.5.2.1 Phosphorylated RTK signals between parent and resistant cell lines upon EGF stimulation

In the next set of experiment, the effect of 10 minutes of EGF stimulation (10ng/ml) was examined on the 4 cell lines. These samples had protein concentration adjusted together with the baseline samples, and were measured together in single run. Thus, the results for baseline and EGF stimulation were directly comparable:

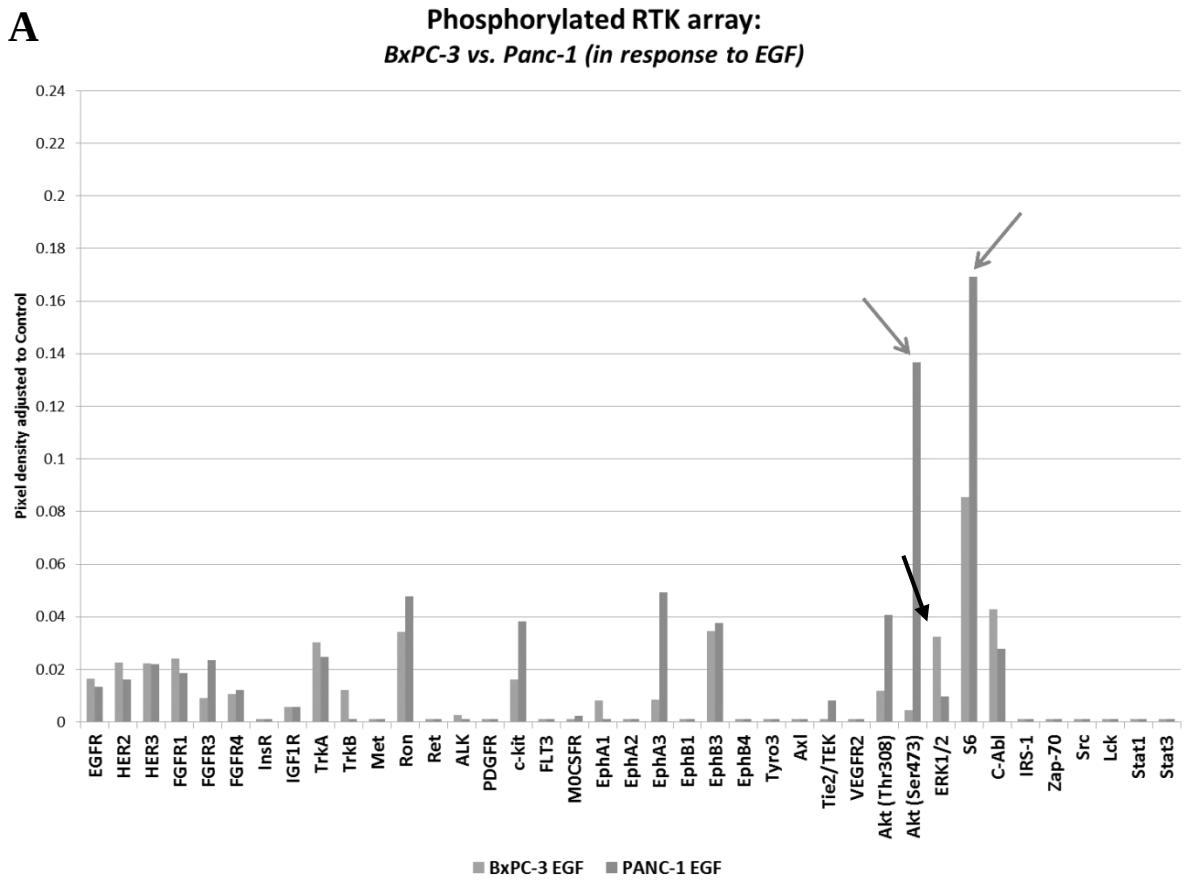

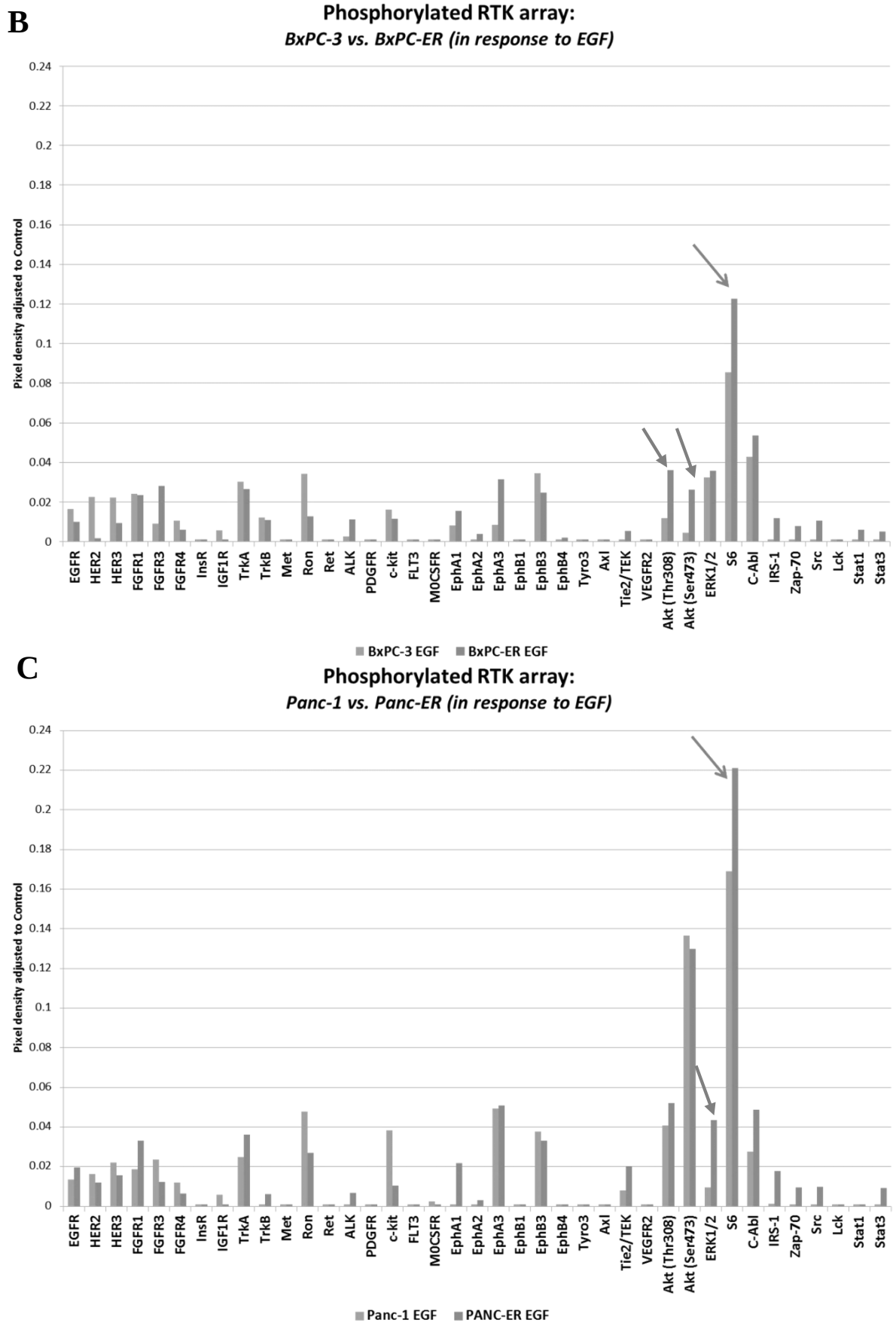

Figure 3.38: Phospho-RTK array result for parent and resistant cell line (with EGF stimulation)

With EGF stimulation, BxPC-3 preferentially activated ERK1/2 in a classical EGFR/ MAPK cascade (black arrow), whereas PANC-1 greatly increased the PAM system via Akt and S6 (grey arrows, **Figure 3.38a**). The intensity for these signals (0.14 and 0.17 of positive control) was much higher than baseline (0.09 and 0.1). In the BxPC-3 versus BxPC-ER and PANC-1 versus PANC-ER comparisons, there were further increases in pS6 and pAkt (Thr308 and Ser473) in BxPC-ER, and pS6 and pERK1/2 in PANC-ER (grey arrows). The highest signal and the greatest difference remained pS6, which was 0.12 of positive control in BxPC-ER, and up to as high as 0.22 of positive control in PANC-ER (**Figure 3.38b-c**).

Hence, PI3K/Akt system was not only implicated in erlotinib insensitivity, but also further manipulated in erlotinib resistance, mediating via the mTOR system. In both ER cell lines, pS6 and to a lesser extent pAkt was up-regulated at baseline. These signals were further increased with EGF stimulation. There were also a slightly more active pERK in the PANC-ER cell line, though this was a much smaller increase compared to the pS6. These findings were of major significance, since this was the first mass screening experiment to show the dominance of PI3K/Akt/mTOR or PAM over other possible molecular targets. In the next section, these findings need to be validated by western blotting and immunofluorescence. In chapter 4, the hypothesis of PI3K/ mTOR system up-regulation contributing to erlotinib resistance will be further tested, by means of single blockade and combined blockade studies using these inhibitors.

3.5.3 Validation for ERK, Akt and S6 of Parent versus ER Cell Lines (Western Blotting)

***Key Finding*: Western blotting supported the findings of phospho-RTK array, in that pS6, pAkt and pERK were all found to be of higher intensity in ER cell lines compared to parent cell lines. In particular, the pAkt and pS6 were the highest in PANC-ER than the other 3 cell lines.**

Western blotting was used to validate the Pathscan phospho-RTK array results. Due to technical difficulties, repeated blotting for S6 on all 5 primary PDAC cell was not performed. A very long gel would need to be made to compare across 7 (5 primary + 2 ER) cell lines. Since the 4 cell lines used in phospho-RTK arrays were BxPC-3, BxPC-ER, PANC-1 and PANC-ER, western blotting was perform on these only. The molecular targets of interest were pAkt, pERK and pS6. Samples were loaded on a 20-well membrane with markers on each side. These were performed as 3 independent experiments.

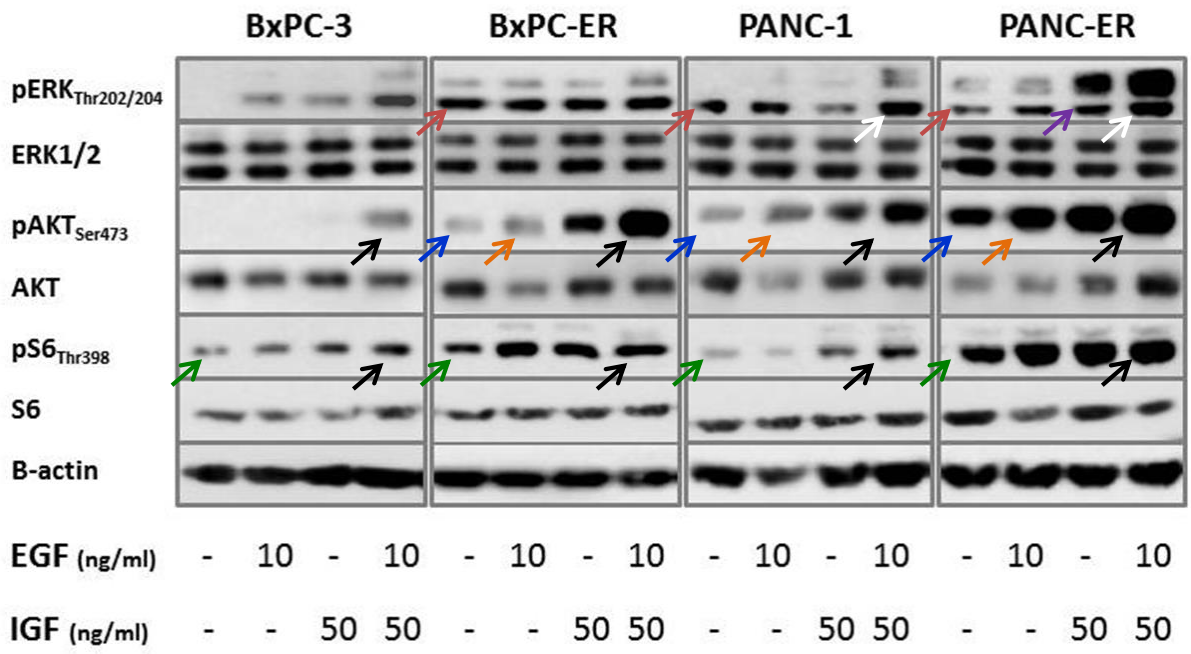

Figure 3.39: Western blotting results of ER versus parent cell line with EGF and IGF stimulation

At baseline, all cell lines expressed pERK (red arrows) and pAkt (blue arrows) except for BxPC-3, though the pAkt signals were much fainter in BxPC-ER and PANC-1 than PANC-ER **(Figure 3.39)**. In addition, both ER cell lines expressed more pS6 than the parent cell line

(green arrows). In **Figure 3.21**, PANC-1 was already shown to have high expression of pAkt at baseline. In this representative blot **(Figure 3.39)**, PANC-ER had even higher pAkt than PANC-1. The exposure was 60 seconds on high exposure setting for the previous blot, but only 4 seconds on standard exposure for this experiment, indicating that PANC-ER had even more up-regulated PAM compared with its parent predecessor which was already active in this pathway. With EGF stimulation, BxPC-3 preferentially activated ERK1/2 in the MAPK pathway. BxPC-ER and PANC-1 possibly stimulated pAkt with EGF, but this was definitely the case for PANC-ER (orange arrows). PANC-ER also appeared to stimulate pERK with IGF (purple arrows). With EGF and IGF stimulation, both ER cell lines appeared to have higher pAkt and pS6 intensity as the parent counterpart (black arrows), and PANC-ER also appeared to have higher pERK than PANC-1 (white arrows).

To sum it up, this representative blot had demonstrated that ER cell lines were more likely to have highly active PI3K/Akt/mTOR pathway as indicated by pAkt and pS6, basally and with growth factor stimulation. In addition, the PANC-ER cell line also had a highly activated MAPK pathway upon growth factor stimulation. These were almost identical results as the phosphor-RTK array.

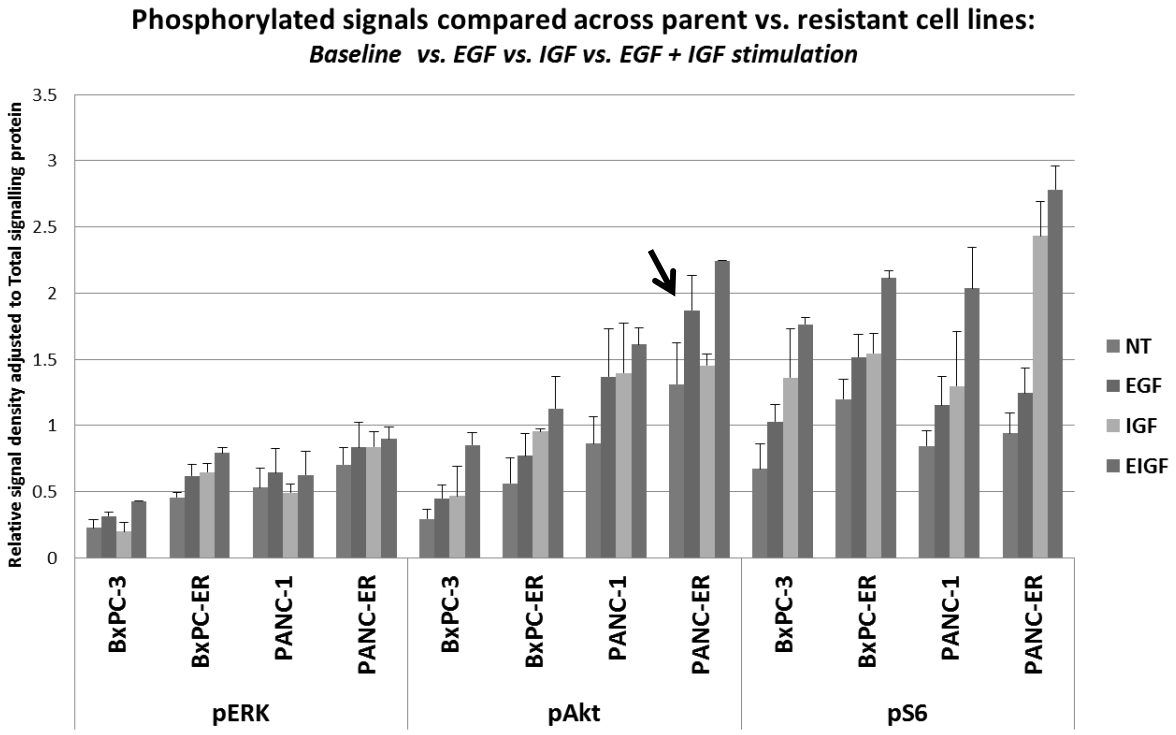

Figure 3.40: Western blotting results of ER versus parent cell line with EGF and IGF stimulation, average of 3 experiments

3 western blotting experiments were pooled together and presented as relative signal intensity to total proteins. After combining the three experiments, one could see graphically that ER cell lines had higher pERK, pAkt and pS6 than parent cell lines, basally as well as with growth factor stimulation. It was clear that the differences were very small for pERK, more prominent for pAkt, and most prominent for pS6- particularly after EGF and IGF dual stimulation (**Figure 3.40**). EGF was slightly better at activating pERK in all 4 cell lines; IGF was slightly better at activating pAkt; and IGF was substantially better at activating pS6. The one exception to this rule was that EGF was actually better than IGF in stimulating pAkt in PANC-ER (black arrow), which was consistent with the representative blot above. Since S6 is an Akt-driven effector of the mTOR complex, PAM pathway was indeed the active mechanism of acquired erlotinib resistance, with the driving force down the mTOR complex through S6.

3.5.4 Validation of ERK and Akt of Parent versus ER Cell Lines (Immunofluorescence)

***Key Finding*: ER cell lines had more highly active pAkt by immunofluorescence, both at baseline and EGF stimulation, and total Akt level was also over-expressed.**

The interaction between EGF and IGF with PAM and MAPK pathways was the central concept of this thesis. Given its relevance and significance, immunofluorescence was used as a second method of validation. Total ERK/ Akt and pERK/ pAkt were again assessed under confocal microscopy. Although S6 was another important signal by the RTK array, a primary pS6 antibody that would function well for immunofluorescence could not be obtained. Given S6 was primarily driven by Akt in the same PAM pathway, the emphasis was placed on Akt instead. Phosphorylated signals were studied at baseline and with EGF stimulation as previous experiments. IGF stimulation was deemed unnecessary given that IGF-pERK was not observed in substantial magnitude in **Figure 3.40**. Again, 4 experiments were performed to allow for statistical analysis.

3.5.4.1 Total ERK and Akt

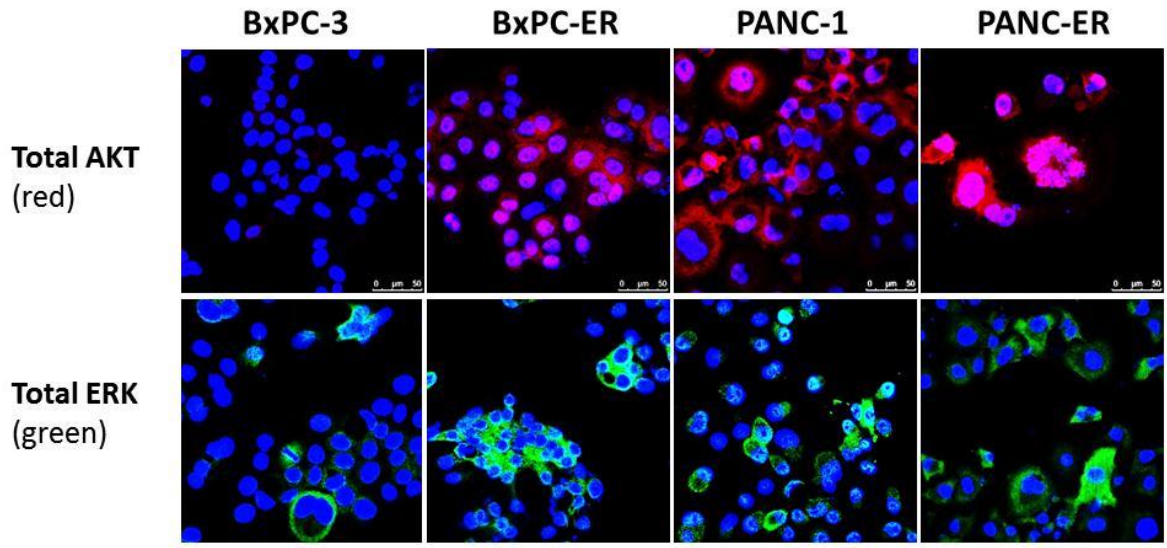

Figure 3.41 Representative photos of immunofluorescence of total Akt and ERK in parent versus resistant cell lines by confocal microscopy

From the previous immunofluorescence studies on total Akt of 5 PDAC cell lines **(3.4.3.1, figure 3.24)**, PANC-1 was already established as having high total Akt expression. PANC-ER appeared to have higher intensity in total Akt than PANC-1 still. BxPC-3 had little Akt expression, and BxPC-ER had slightly gained some Akt expression. Total ERK appeared to be somewhat more intense in BxPC-ER than BxPC-3. However, the difference between PANC-1 and PANC-ER was probably slight at best, and was not appreciated readily in the representative photos.

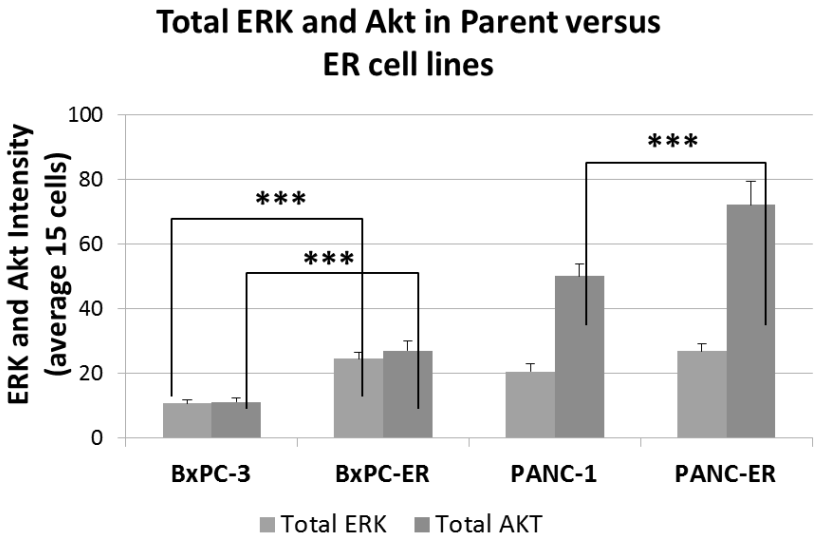

Figure 3.42: Immunofluorescence of total Akt and ERK in parent versus resistant cell lines, average of 3 experiments (P<0.0001)***

Averaged from 3 experiments, total Akt was significantly highly expressed in ER cell lines than parent cell lines (both P<0.0001). Total ERK was also significantly more highly expressed in BxPC-ER than BxPC-3 (P<0.0001, **Figure 3.42**). These findings parallelled that observed in erlotinib insensitive cell lines. Phosphorylated ERK and Akt was studied next to see if they were also significantly *over-activated*, as suggested from phospho-RTK array and western blotting experiments.

3.5.4.2 Phosphorylated ERK and Akt at baseline and EGF stimulation

Again, pERK (green) and pAkt (red) were studied together, at baseline and with EGF stimulation. Below showed the low power and high power representative set of photos:

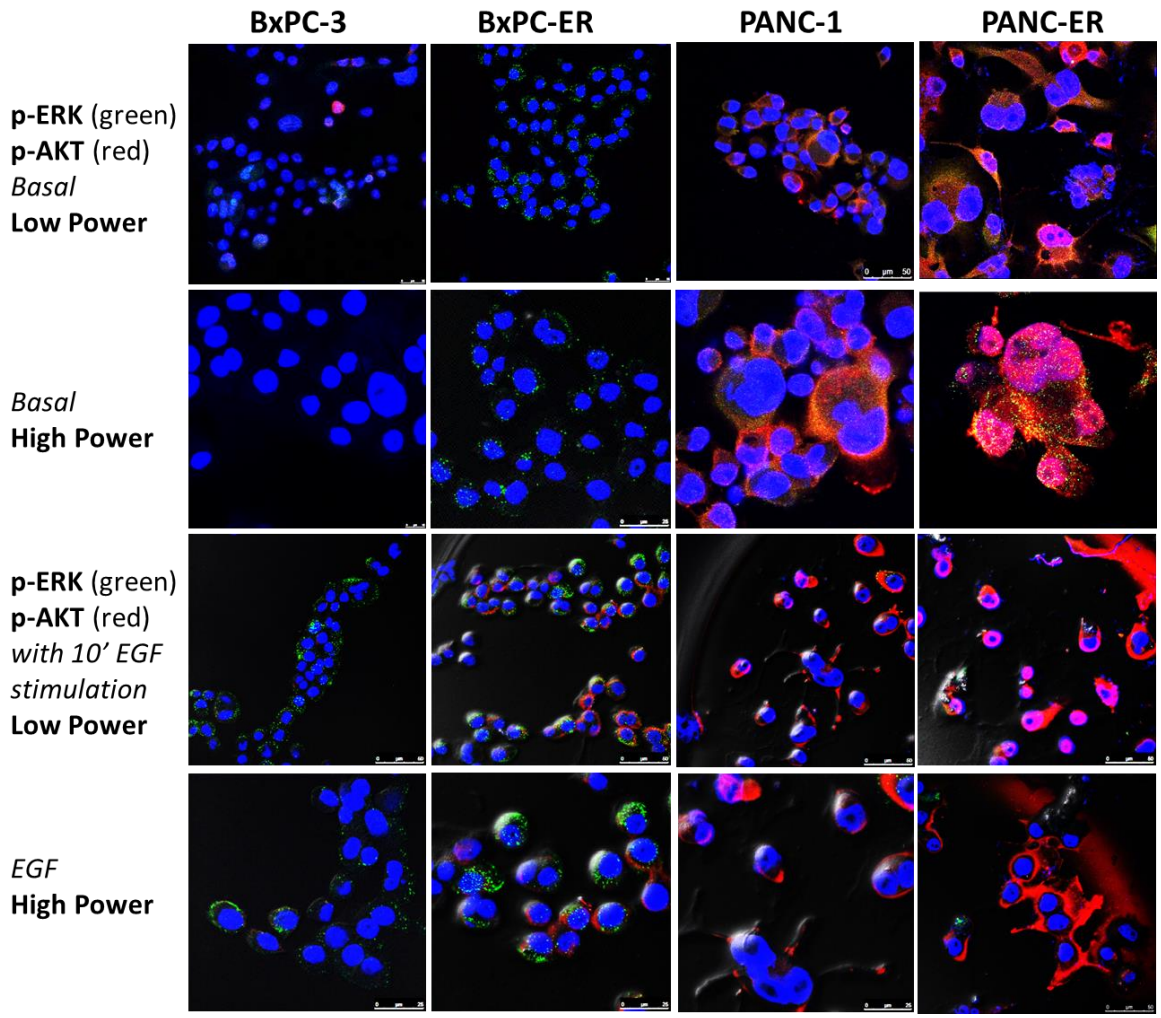

Figure 3.43: Representative photos of immunofluorescence of pAkt and pERK at baseline and with EGF stimulation in parent versus resistant cell lines by confocal microscopy

The basal pERK and pAkt signals were fairly weak for BxPC-3 and BxPC-ER, though on higher power pERK was more detectable in a speckled configuration around the nucleus. By contrast, pAkt signal was high in PANC-1 and even more intense in PANC-ER, indicating that Akt (or PI3K pathway) was constitutively active in these cell lines **(Figure 3.43)**. With EGF stimulation, it was observed that pERK signal increased in BxPC-3. In BxPC-ER, pERK signal increased, as did the pAkt signal. In PANC-1, pAkt (not pERK) was predominantly increased with EGF stimulation. Comparing PANC-1 with PANC-ER, pAkt was further and markedly increased by EGF stimulation, predominantly in the cytoplasmic region of the cells.

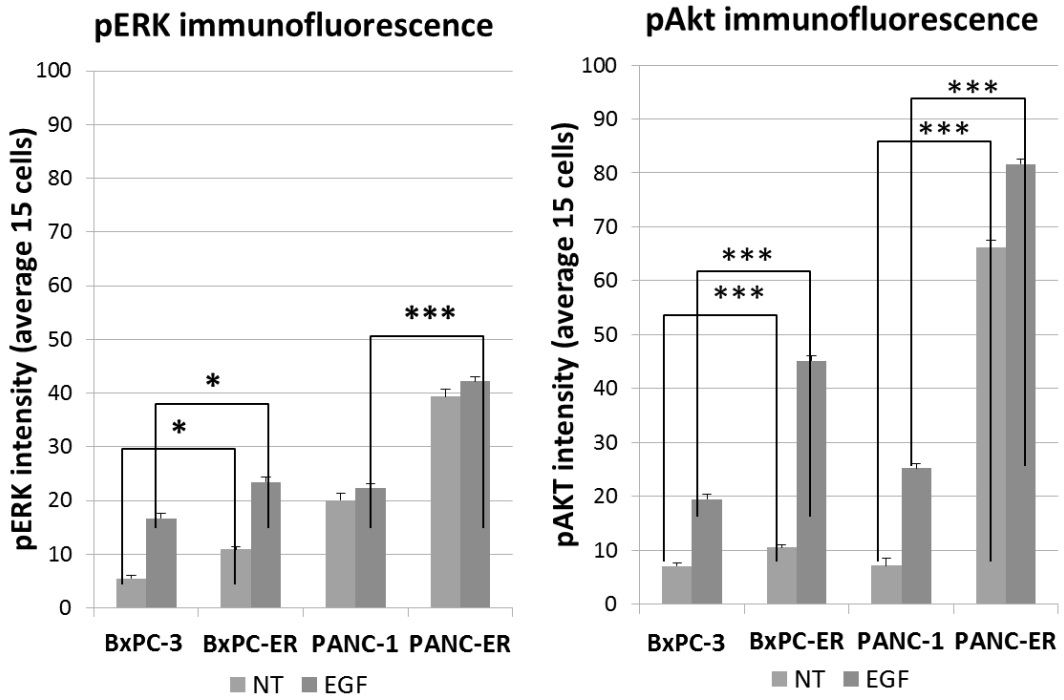

Figure 3.44: Immunofluorescence of pAkt and pERK at baseline and with EGF stimulation, average of 3 experiments ** P< 0.05, *** P<0.0001*

Again, using the stringent criteria of statistical significance of P<0.01, a significant increase in pERK signalling was noted in PANC-ER compared to PANC-1, but only on EGF stimulation (P<0.0001; **Figure 3.44**). By comparison, pAkt signalling were significantly increased in both ER cell lines under both basal or EGF stimulation conditions (all P<0.0001). There was a particularly substantial increase in pAkt in PANC-ER compared to PANC-1 (65 and 80 mean intensity values in NT and EGF). Thus, **western blotting and immunofluorescence results were concordant in showing that over-expression and over-activity of PI3K (not MAPK) pathway was associated with acquired erlotinib resistance.**

3.5.5 Gene Discovery by PI3K PCR Array

Key Finding: ***The two ER cell lines appeared to have derived erlotinib resistance from pathways downstream of PI3K/Akt, as opposed to AKT or S6 genes. NF-kb and c-fos could be the possible driver mechanism in BxPC-ER and PANC-ER respectively.***

In the experiments so far, Akt and S6 were established to be important factors in acquired erlotinib resistance. The drug inhibition and molecular characterisation studies so far have suggested a high possibility that the *entire* PAM pathway was involved in erlotinib resistance, particularly as ER cell lines remained sensitive to PI3K and PI3K/mTOR but not IGF1R or MEK inhibitors. Importantly, it appeared that it was both total Akt and phosphorylated Akt were increased in ER cell lines. In this case, one would expect that *AKT* or related genes to be over-expressed resulting in the transcription of these proteins. To search for an answer, gene discovery study was the next step.

Recent advances in gene technology have introduced methods such as next-generation DNA sequencing (NGS) and DNA microarray for the mass screening of whole human genome.[297,298] Whilst the costs of these techniques have dramatically reduced over the last decade, this was still a substantial cost to the project considering that these gene searching methods needed to be repeated twice at the very least. Since the genes of interest were highly likely located within the PI3K/ mTOR or other related pathways, a focused PI3K PCR array was used for the gene discovery experiment. The RT2 Profiler Array (Qiagen) is a 384-well plate intended for gene discovery of 96 customised genes for 4 simultaneous samples. Among the 96 genes were 84 genes related to PI3K pathway, 5 housekeeping genes and 7 controls. The primers are all preloaded in the array. The dye used is a highly sensitive sYBR green dye with ROX as a reference dye. Detailed methodology had already been described in **subsection 2.2.9**.

In the array experiment, the 2 pair of parent and resistant cell lines (BxPC-3, BxPC-ER, PANC-1, PANC-ER) were simultaneously tested in a single 384-well PCR array for two times, with qRT-PCR used to validate the genes of interest **(subsection 3.5.6)**. Each experiment was independently performed. New cells were thawed, grown, RNA was then extracted, reverse transcribed, and PCR array performed, in two independent experiments.

3.5.5.1 Quality Control of RNA, DNA and PCR

For conciseness, only the most relevant quality control results are shown. RNeasy mini Kit (Qiagen) was used for RNA extraction and purification from the 4 cell lines. The maximum binding capacity for the mini spin column was 100μg. Below shows the RNA *quantity* extracted from each experiment, as measured on mass spectrometer:

	BxPC-3	BxPC-ER	PANC-1	PANC-ER
Exp 1	23.8μg	17.9μg	22.3μg	35.4μg
Exp 2	16.9μg	20.4μg	39.7μg	48.7μg

Table 3.9: RNA quantity for two PCR array experiments

Hence, the total RNA quantities from both experiments were well within the maximum capacity of the RNA extraction kit. Next, the RNA *quality* was assessed by the mass spectrophotometric curve, A_{260}:A_{280} ratio, and A_{260}:A_{230} ratios. UV absorbances at 280nM, 260nM and 230nM are used to measure aromatic amino acids, nucleic acid and contaminants respectively.[299] Thus, A_{260}:A_{280} and A_{260}:A_{230} ratios were used to provide a measure of RNA purity, with acceptable A_{260}:A_{280} ratio being 1.8-2.2 and A_{260}:A_{230} ratio >1.7.[293,299]

	BxPC-3	BxPC-ER	PANC-1	PANC-ER
Exp 1: A_{260}:A_{280}	1.95	1.92	2.05	2.01
Exp 2: A_{260}:A_{280}	1.91	1.82	1.95	1.91
Exp 1: A_{260}:A_{230}	2.03	2.08	2.17	2.17
Exp 2: A_{260}:A_{230}	2.38	2.27	2.07	2.32

Table 3.10: RNA quality for two PCR array experiments **(**A_{260}:A_{280} ratio)

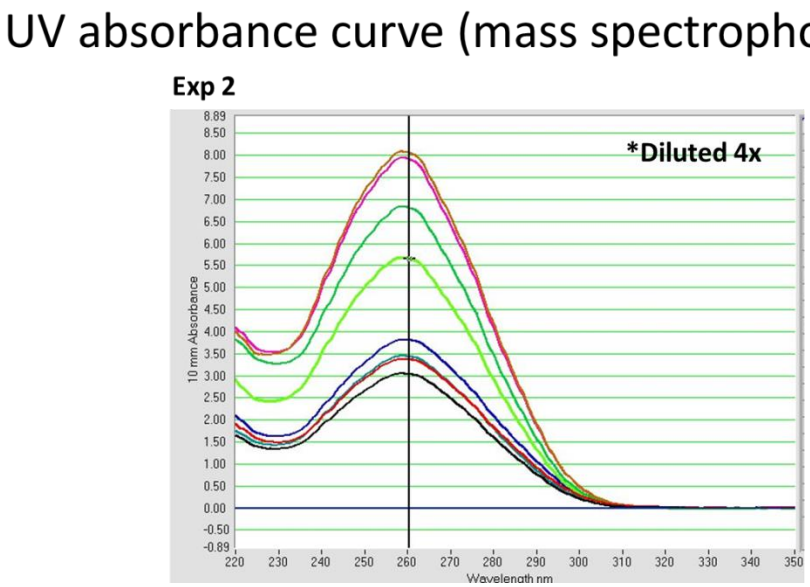

Figure 3.45: Example of a mass spectrophotometric curve in assessing RNA quality

A_{260}:A_{280} ratio, and A_{260}:A_{230} ratios of the 4 cell lines in both experiments were within the acceptable ranges. Shown above was an example of UV absorbance curve for experiment 2. In this case each sample was tested twice; the absorbance curves for each pair were fairly close together. In all samples there was only one peak indicating high purity of RNA. The main disadvantages of using mass spectrophotometry to assess RNA purity are inaccuracy in measuring low-level samples and its inability to distinguish other nucleic acids such as dsDNA and ssDNA.[299] Since the samples for both experiments were of appropriate quantity, and that DNAse was used as an additional step in RNA extraction, it was not necessary to further assess RNA quality by gel electrophoresis (RNA gel).

After adjusting RNA quantity, 400ng of total RNA were reverse transcribed into DNA for each sample. Master mixes were then added to the cDNA, and these were dispensed to the PCR array by robotics. Quality of PCR was assessed a number of ways.

As a screening test, before qRT-PCR was run for the PCR array, the 4 samples were run together with a control sample with known cDNA quantity, and were tested for 18s and β-actin control genes. The results showed that these samples had almost identical amplification rate to control and each other, thus supporting that all 4 samples had similar quantity of DNA.

qRT-PCR was then run on the 384-well plate, according to the protocol in **subsection 2.2.9.** Threshold was set at 10x the standard deviation of the fluorescent value of baseline. The amplification plot and distribution of threshold cycle (C_t) are shown below:

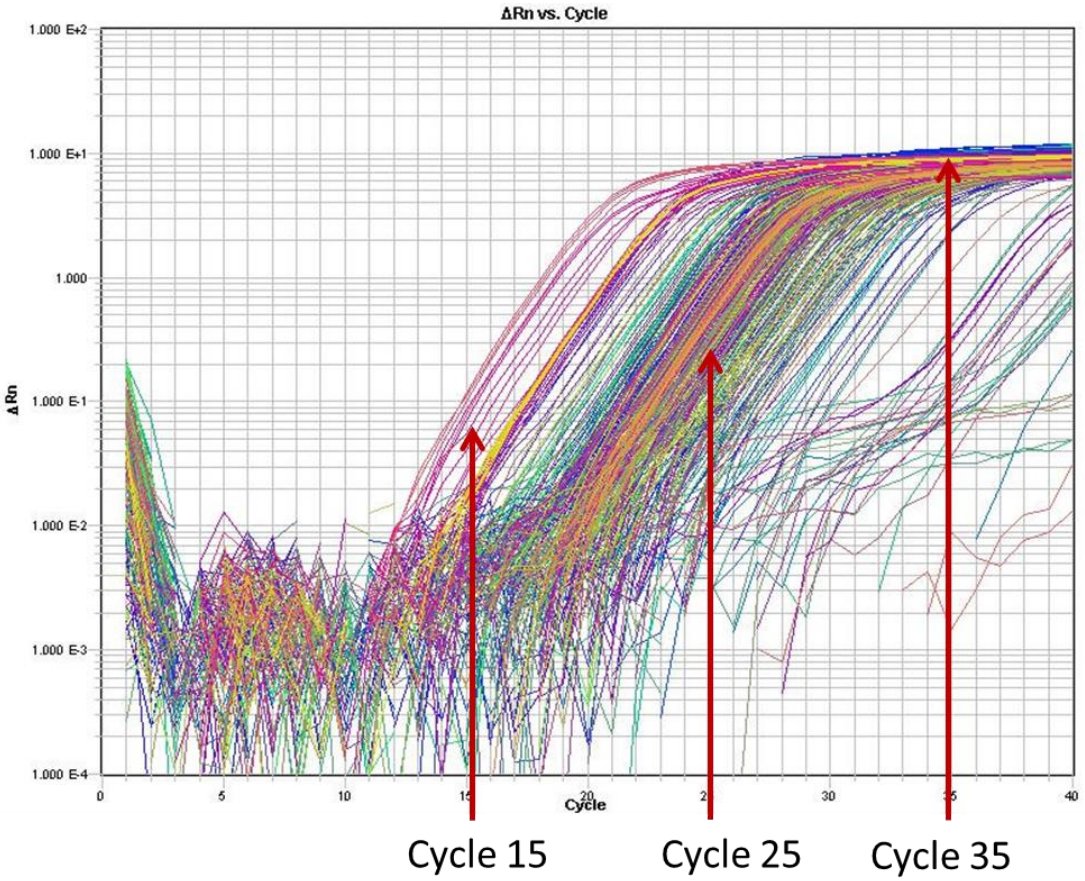

Figure 3.46: Amplification plot for 96 genes * 4 samples in the 384 well PCR array

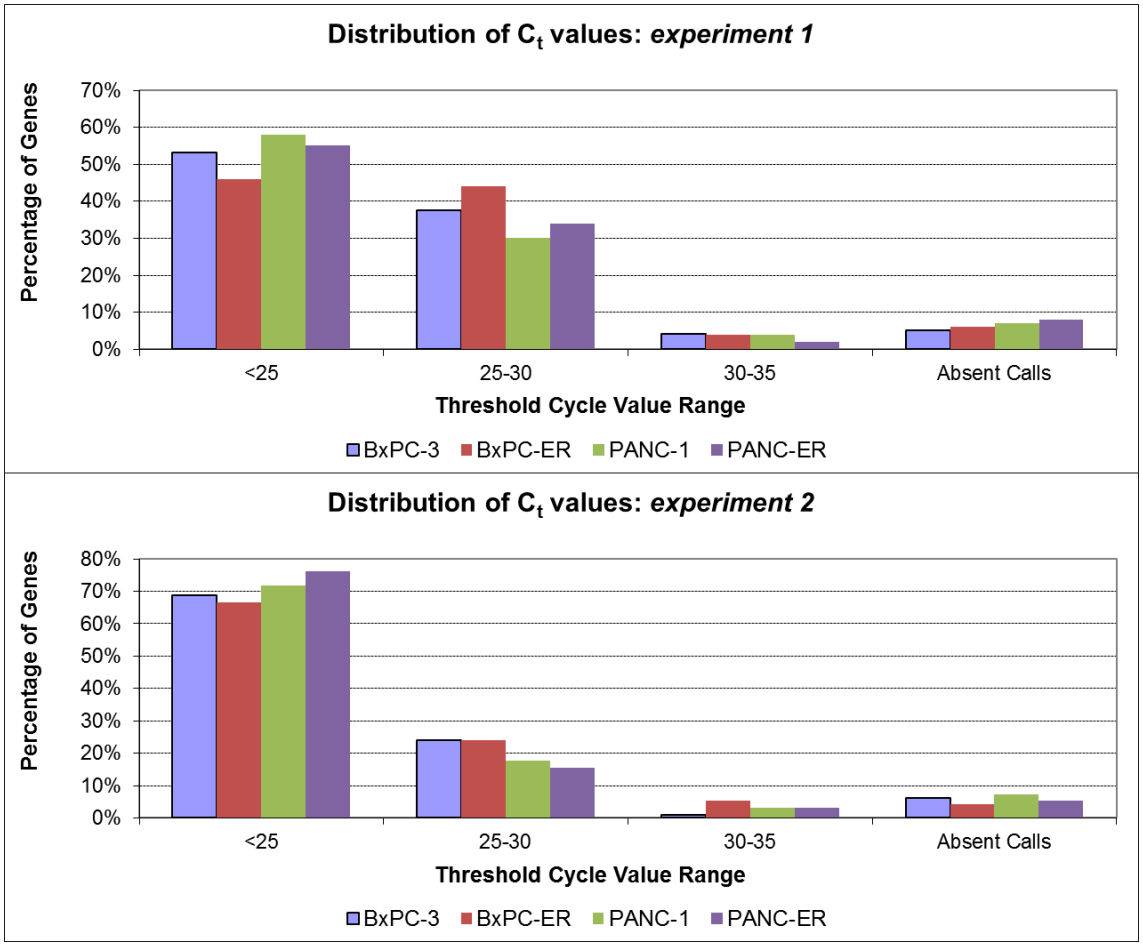

Figure 3.47: Distribution of C_t of 96 genes for 4 samples in 2 experiments

As depicted above, most genes were at the steep part of the amplification by cycles 15-25. In the C_t distribution column graph, most C_t values were before 30 cycles. Only 5-10% of genes had C_t values after 30 cycles, which likely represented genes that were not expressed in the cell lines as opposed to artefactual errors. The average C_t values for each cell line in both experiments were very close together, with a range from 18.6 to 19.5 cycles, with standard deviation of only 0.45-0.59 between experiments. 4 of the 5 control genes tested (β-actin or ACTB, β2-microglobulin, GAPDH and ribosomal protein large P0 or RPLP0) had C_t values ranging from 16 to 20 cycles, while the less commonly used hypoxanthine control gene had C_t values between 23 and 24 cycles. Internal controls with reverse transcription control ($<5C_t$) and genomic DNA contamination ($>35C_t$) were also found to be acceptable.

Finally, the use of SYBR Green probes allowed melting or dissociation curve analysis to be performed. Melting curve analysis was programmed at the end of PCR experiment. Each primer has a temperature of melting (T_m); a melting curve plots the folded fraction of the structure versus temperature, and enables assessment of the specificity of the primers.[260] Clearly, it is impossible to show the melting curves of all 96 genes here. Melting curves of the key genes of interest are presented below:

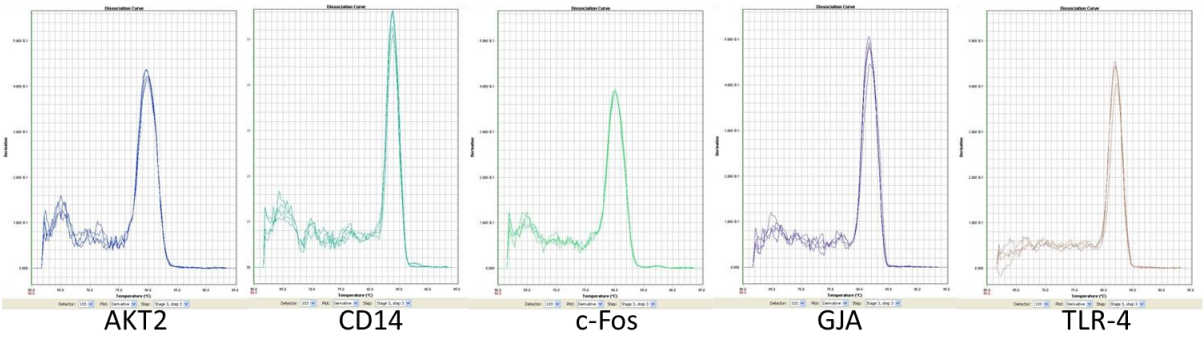

Figure 3.48: Melting curves of some of the key genes in PCR array

In all these genes, melting curves showed only one peak- that is one product only. All 96 melting curves had been checked, and they all showed equivalent results indicating the primers used in this array was specific.

All in all, the quality of RNA, DNA and PCR were suitable for further analysis. Results of the PCR array experiment are now presented, as per the Minimum Information for Publication of Quantitative Real-Time PCR Experiments (MIQE) guidelines.[293]

3.5.5.2 PCR Array Results

As a general overview, the clustergram or heat map of all 96 genes grouped in gene families are shown below. From left to right are PANC-1, PANC-ER, BxPC-3 and BxPC-ER. Green indicates down-regulation, red indicates up-regulation and black indicates average level:

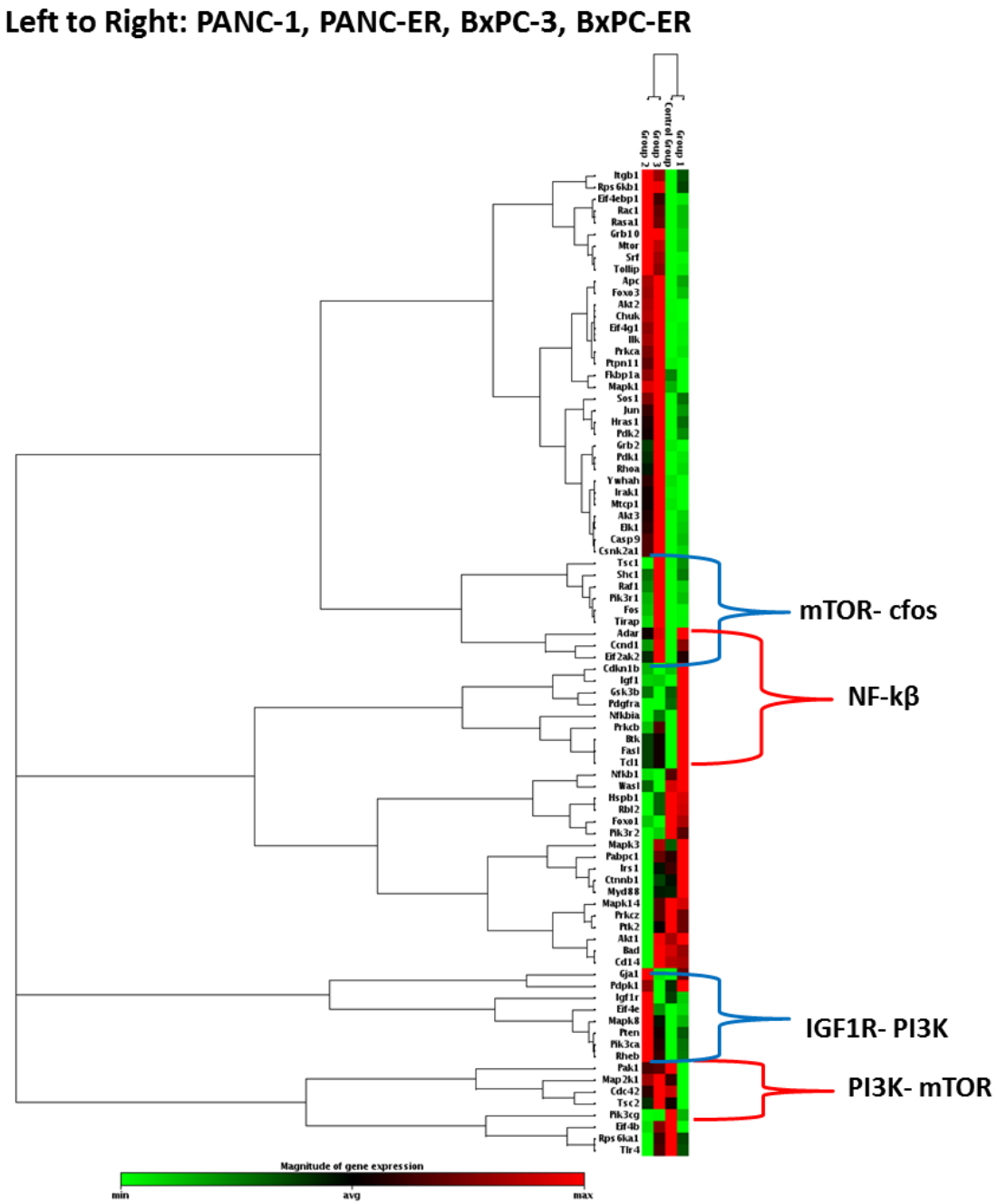

Figure 3.49: Clustergram or heat map for 96 genes on the 4 cell lines, average of 2 experiments (red = up-regulation; green = down-regulation)

Between parent and ER cell lines, most genes were concordant between the two pairs of cell lines. However, there were also distinct groups of genes that were differentially expressed (that is, up-regulated in one cell line and down-regulated in another). These were highlighted in red bracket (BxPC-3 versus BxPC-ER) and blue bracket (PANC-1 versus PANC-ER). Interestingly, these followed specific families of genes in a particular pattern. In BxPC-ER, the genes lying in mTOR to nuclear c-fos pathways were up-regulated, with accompanying down-regulation of genes in the IGF1R – PI3K pathways. In PANC-ER, the genes in the NF-κB family appeared to be up-regulated, and the genes in the PI3K- mTOR pathway were down-regulated. In both cell lines, there appeared to be a silencing of part of the PI3K/Akt/mTOR signals, but accentuation of nuclear or paranuclear signals parallel or downstream of mTOR.

To explore erlotinib resistance in greater detail, two-way comparisons were first made between BxPC-3 and PANC-1; then BxPC-3 and BxPC-ER, and PANC-1 and PANC-ER for acquired erlotinib resistance. Scatterplots of 2^-delta C_t and 3 dimensional column graphs are shown below, with C_t values and fold changes listed in ascending order:

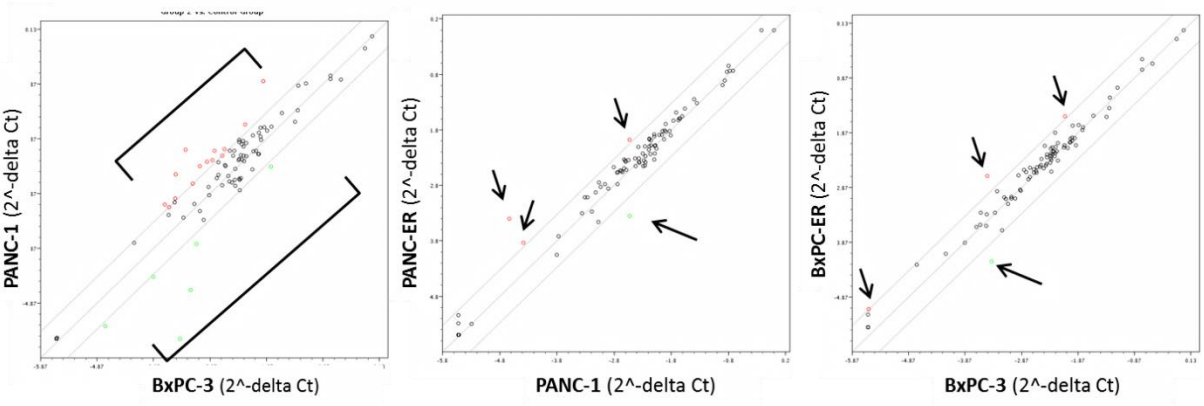

Figure 3.50: Scatter plots of square root of –delta C_t between pairs of cell lines in PCR array. Boundary set at 3 fold difference

A

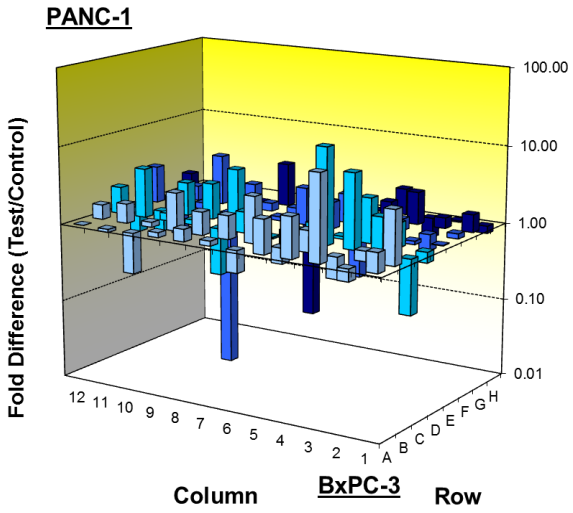

Gene	BxPC-3 average CT	PANC-1 average CT	PANC-1/ BxPC-3 (fold change)
AKT-3	28.01	26.48	+3.33
RHEB	26.16	24.26	+4.31
CHUK	26.57	24.52	+4.78
PDGF	25.68	23.61	+4.87
GJA-1	27.98	25.04	+8.91
AKT-2	22.83	19.40	+12.48
GRB10	27.39	23.54	+16.61
HSP B1	22.38	24.55	-3.90
Foxo1	26.75	29.26	-4.94
Toll-like receptor 4	27.11	32.05	-26.55*
PI3K-γ	27.71	35.00	-134.97*

**This gene's average threshold cycle is relatively high (> 30) in control (BxPC-3), and is reasonably low in the test sample (PANC-1) (< 30).*

B

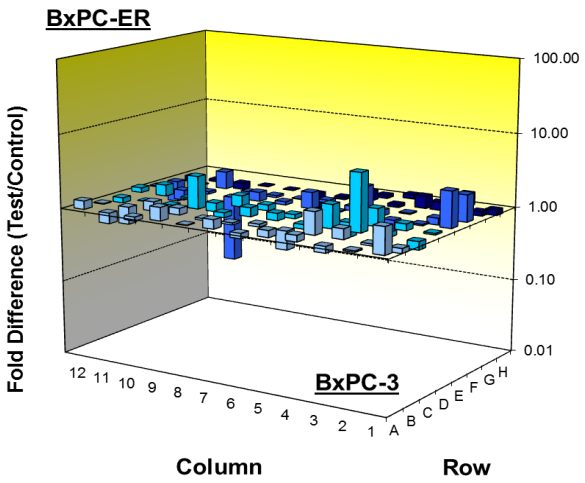

Gene	BxPC-3 average C_t	BxPC-ER average C_t	BxPC-3/ BxPC-ER (fold change)
NFkb- 1A	23.40	22.19	+3.08
GJA-1	27.98	25.80	+6.04
TLR4	27.11	29.11	-3.01
PI3K-γ	27.71	31.01	-7.37

C

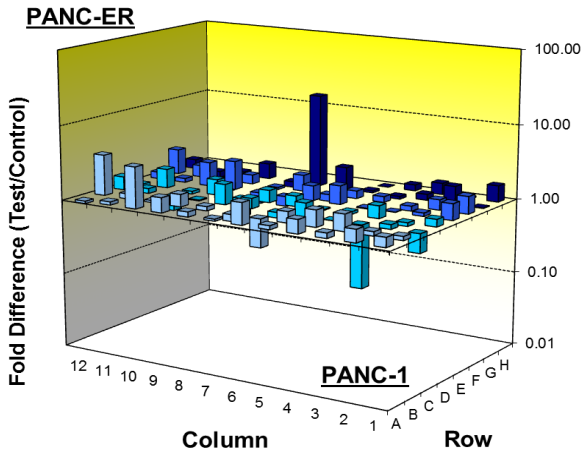

Gene	BxPC-3 average C_t	BxPC-ER average C_t	BxPC-3/ BxPC-ER (fold change)
FOS	25.05	23.32	+3.52
CD-14	31.23	29.47	+3.60
TLR-4	32.05	28.04	+17.13
GJA-1	25.04	27.88	-6.73

Figure 3.51: 3-dimensonal column graphs, C_t values and fold changes between cell lines

The scatterplots and the 3-dimensional column graphs both showed many molecular differences between BxPC-3 and PANC-1, as to be expected from two completely different cell lines. Some genes were highly over-expressed in PANC-1 (+16 fold), while others were most likely not expressed at all (-135 fold). Consistent with the qRT-PCR findings previously **(3.4.4)**, here it is also shown that PANC-1 was up-regulated in *AKT-2* (+12.48 fold) and *AKT-3 genes* (+3.33 fold) **(Figure 3.51a)**.

The two pairs of parent and resistant cell lines were much more similar, as expected. Importantly, there was a small number of genes of interest that were found to be different **(Figure 3.50, 3.51 b-c)**. Two things were noted in these analyses. Firstly, the *AKT* genes were not up-regulated in either ER cell line. After two experiments, it was shown that BxPC-ER only had a +0.96, +0.82, and +1.22 fold up-regulation of *AKT-1, -2* and *-3* genes compared to BxPC-3, whilst PANC-ER had +1.49, +1.17 and +1.53 fold up-regulation (not shown). It was difficult at this stage to assess whether these were significant differences, but less than 2-fold change was not usually considered meaningful in any case.[262]

Secondly, some genes were common between the BxPC-ER: BxPC-3 and PANC-ER: PANC-1 analyses, but the direction of up-regulation and down-regulation were opposite. For example, GJA-1 was up-regulated in BxPC-ER compared to BxPC-3 (+6.04) and down-regulated in PANC-ER compared to PANC-1 (-6.73). TLR-4, on the other hand, was down-regulated in BxPC-ER compared to BxPC-3 (-3.01) and up-regulated in PANC-ER compared to PANC-1 (+17.13). The first column graph appeared to shed some light to this apparent paradox **(figure 3.51 a)**, where it was shown that PANC-1 had much more highly up-regulated GJA-1 gene (+8.91) and down-regulated TLR-4 gene (-26.55) than BxPC-3. That is, it may be that the differences observed were simply due to some unique properties of a parent cell line, not the ER cell line.

To address these issues and filter down the genes of interest in acquired erlotinib resistance, a 4-way comparison of these genes was presented to search for genes that were unique to

one ER cell line only and not the others. Below shows the column graphs of delta C_t, 2 to the power of (-delta C_t) and fold change of the 6 genes of interest revealed in the PCR array. Error bars of two experiments were shown for average delta Ct and (- delta C_t) squared.

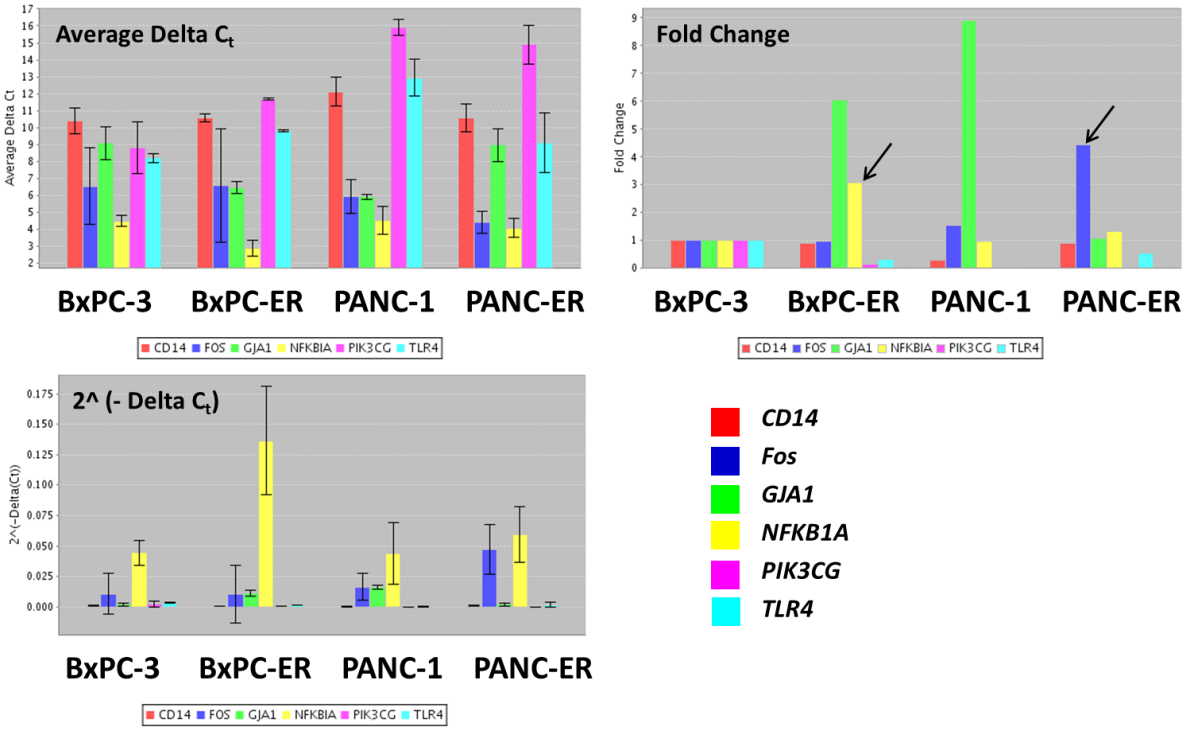

Figure 3.52: 4-way analysis of genes of interest in PCR array

In the 4-way analysis, PI3KCG, TLR4 and CD14 gene expressions did not follow a predictable pattern. The average C_t was higher in BxPC-ER than BxPC-3, and lower in PANC-ER than PANC-1, but the highest average C_t was in PANC-1 **(Figure 3.52, upper left)**. These therefore represented unique properties for PANC-1, and might possibly reflect the artefacts from environmental factors that had affected this cell line. Clearly, this was not the aim of this experiment. The aim here was to search for unique markers of ER cell lines. Instead, the gene of interest must be unique and differentially expressed in either or both ER cell lines, but not in the parent cell lines.

To offset the variability, 2 to the power of –delta C_t was calculated as per product instructions and a column graph was produced. Two distinct markers were now apparent: NFκB1A was the highest in BxPC-ER and not the other three cell lines **(Figure 3.52, bottom left, yellow**

bars), and Fos was highest in PANC-ER and not the other three cell lines (**blue bars**). Finally, fold change was calculated by squaring negative delta-delta Ct, and here NFκB1A was up-regulated by about 3 fold in BxPC-ER, and Fos was up-regulated by about 4 fold in PANC-ER, compared to the other cell lines **(Figure 3.52, upper right, yellow and blue bars, black arrow)**.

Thus, PI3K PCR array found a propensity of ER cell lines to up-regulate alternate pathways further downstream to mTOR. It had also uncovered two possible markers, one for each ER cell lines. To validate this, qRT-PCR was performed to be discussed in the next sub-section.

3.5.6 PCR Validation of Key Genes of Parent versus ER Cell Lines

***Key Finding:* qRT-PCR had reproduced and validated the PCR array results**

In total, 12 genes were tested in this qRT-PCR validation study. Some of these genes had already been tested in the previous experiment on 5 PDAC cell lines (*MAPK, PI3Kα, PI3Kγ, AKT2, ERBB3*. PCR array genes of interest (GOI) were fos, TLR4, NFκB1a (P50) and Rel-A (P65), and these were also assessed in validation study. Rel-A is one of the key sub-unit of the NFκB family complex equipped with a non-homologous transactivation domain.[300] Given its intricate association with NFκB1a, it was also studied here even though it was not included in the PI3K array. Taqman probes were used for NFκB1a and Rel-A- since there were no appropriate SYBR green primers found for these genes. Other GOIs were all detected by SYBR Green primers. The integrity of the SYBR Green primers had already been tested in standard curve experiments in **3.4.3.2**. SYBR Green primers were corrected to 18S as the reference gene as before, and Taqman probes to GAPDH. As before, biological triplicate experiments with technical duplicate were performed.

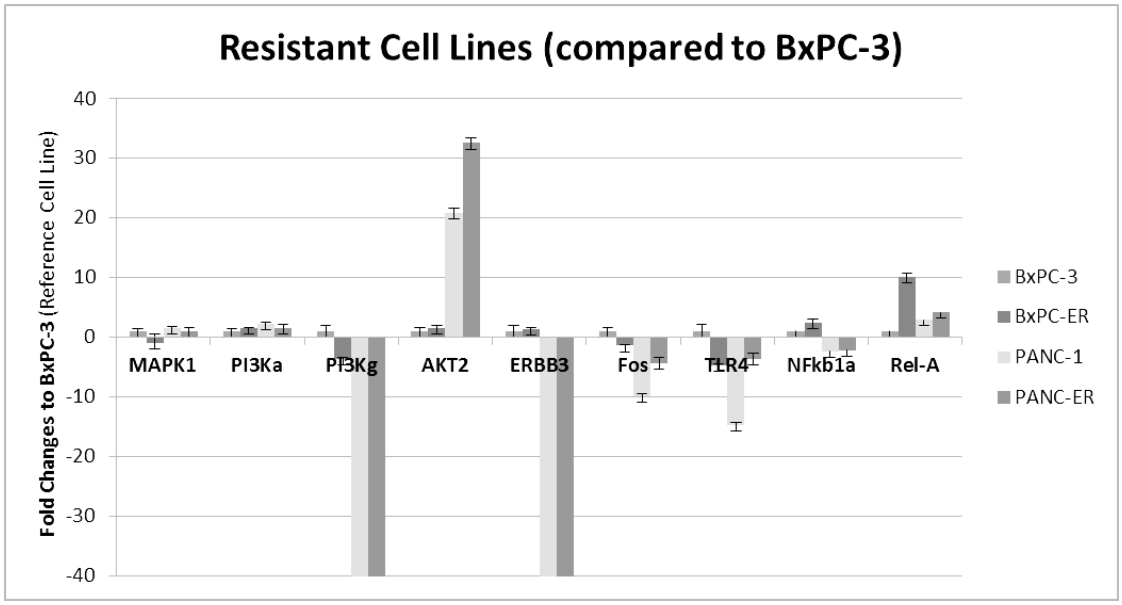

Figure 3.53: qRT-PCR genes of interest results for ER versus parent cell lines

	MAPK1	PI3KCA	PI3KCG	AKT2	ERBB3	Fos	TLR4	NFkb1a	Rel-A
Bx vs Br	-1.00	1.56	**-3.68**	1.45	1.33	-1.43	**-4.81**	**2.40**	**10.10**
P-value	**<0.0001**	**0.024**	**0.029**	**0.016**	0.23	0.24	**0.023**	**0.015**	**0.036**
Bx vs Pa	1.44	**2.16**	**Not Exp***	**20.75**	**Not Exp***	**-9.93**	**-14.77**	**-2.35**	**2.91**
P-value	**0.018**	**<0.0001**	**<0.0001**	**<0.0001**	**0.0049**	**<0.0001**	**0.0002**	0.22	**0.04**
Pa vs Pr	-1.36	-1.41	**7.66**	1.57	1.20	**2.30**	**3.95**	**-2.18**	1.42
P-value	**<0.0001**	**0.0013**	**<0.0001**	**0.0047**	0.45	**0.0018**	**0.044**	0.91	0.67

Table 3.11: Fold up- or down-regulation and P-values for GOI in parent versus ER cell lines

In this new set of qRT-PCR results, the axes were set at ± 40-fold, as opposed to ± 20-fold previously in **Figure 3.31**. As already observed, PANC-1 had substantially up-regulated *AKT2*, and down-regulated PI3Kγ and *EGFR* compared to BxPC-3. Here there were in fact many other significant genetic differences between these two cell lines, with a definite trend of up-regulation of PI3Kα/ AKT2 but down-regulation in other pathways **(Table 3.11).** Between ER and parent cell lines, although both BxPC-ER and PANC-ER had significantly up-regulated *AKT-2* than parent cell line (P<0.05), the fold changes were relatively small to be considered meaningful (BxPC-ER: +1.4 fold, P=0.016; PANC-ER: +1.6 fold, P=0.005). Previous PCR array found other pathways to be active in ER cell lines. In here, the two isoforms of NF-κB (1A and c-rel) were probably up-regulated in BxPC-ER (+2.4 and 10.1-fold respectively,

0.01<P<0.05), whilst *Fos* was up-regulated in PANC-ER (+2.3-fold, P=0.002). *TLR4* and *PI3Kg* were both down-regulated in BxPC-ER (from BxPC-3) and up-regulated in PANC-ER (from PANC-1), and were regarded as artefacts. All in all, these results were almost identical to the PCR array results. To sum it up, there was slight up-regulation in MAPK1 and PI3KCA in ER cell lines, which was somewhat surprising. *AKT2* was further up-regulated in PANC-ER (more than +30-fold to BxPC-3), but the comparative fold change from each pair of ER: parent cell lines were short of 2-fold. Instead, two markers were identified- **NF-κB1a and c-Fos -** which was up-regulated in BxPC-ER (2.4-10.1 fold) and PANC-ER (2.3 fold) respectively. These, in turn, may represent the driver mechanism of erlotinib resistance in these two ER cell lines. Importantly, these genetic markers for erlotinib resistance appeared to arise further downstream to PI3K/Akt/mTOR. This certainly highlighted the exceeding complexity and our limited knowledge of drug resistance, though the above findings remained entirely plausible, given that feedback loops of both NF-κB and c-Fos had certainly been well described in literature and implicated in drug resistance.[301,302]

3.6 Discussion

This chapter explores the mechanism of erlotinib resistance in detail. Although erlotinib is not routinely used in PDAC due to its high cost and marginal benefit in survival, erlotinib resistance remains an important area of research. It helps current understanding about the molecular biology of pancreatic cancer, and may lead to discover novel strategy to target this cancer and overcome drug resistance. A distinction was made between primary (*de novo*) resistance and acquired resistance, since there had already been examples of different mechanisms between primary and acquired erlotinib resistance in NSCLC.[159] The results of chapter 3 are summarised in the following table **(Table 3.12)**:

Studies	Primary (*de novo*) Resistance (BxPC-3, CFPAC-1 vs. CAPAN-2, MiaPACA-2, PANC-1)	Acquired Resistance (BxPC-3 vs. BxPC-ER; PANC-1 vs. PANC-ER)
F(x) studies (clonogenic, cell proliferation)	Erlotinib insensitive cell lines had **cross-resistance to MEK inhibition**. PANC-1 which is particularly activated in PI3K pathway also had cross-resistance to IGF1R and PI3K inhibitor but not PI3K/mTOR inhibitor	ER cell lines were significantly resistant to EGFR, IGF1R and MEK inhibition, but **remained sensitive to PI3K and PI3K/mTOR inhibition**
EMT status (morphology, e-cadherin/ vimentin WB and IF)	All 3 erlotinib insensitive cell consisted of **some mesenchymal properties**, though they were not entirely mesenchymal except for MiaPACA-2	There was a **definite EMT** that occurred in the ER cell lines, accompanied by a significantly up-regulated vimentin.
Protein studies (IF, phos-array, WB)	**Downstream MAPK or PI3K/Akt signalling** pathways were over-expressed (Total ERK and/or Akt, IF) and over-activated (pAkt and/or pERK) at baseline. There was also **more EGF activation of pAkt** in erlotinib insensitive cell lines (WB, IF)	**PI3K/Akt/mTOR pathway** is particularly up-regulated in ER cell lines , as indicated by a very high pS6 (phosphoRTK array, WB), significantly over-expressed total Akt (IF) and over-activated pAkt at baseline and upon EGF stimulation (WB, IF)
Gene studies (PCR array, qRT-PCR)	Upstream targets are down-regulated and downstream targets up-regulated. There is a significant trend of down-regulation in ***EGFR***, and up-regulation of ***PIK3CA*** *(CAPANC-2),* ***MAPK1*** *(MiaPACA-2) or* ***AKT2*** *(PANC-1)* (qRT-PCR)	***AKT2*** is further up-regulated. In addition, mechanism downstream of PI3K/mTOR may be responsible for development of acquired erlotinib resistance (***NF-kb*** in BxPC-ER, ***c-Fos*** in PANC-ER) (PCR array, qRT-PCR)

Table 3.12 Summary of primary and acquired erlotinib resistance results in chapter 3. *WB = western blot, IF = immunofluorescence*

Whilst the experiments that were performed in chapter 3 may seem somewhat repetitive, these experiments in totality had provided an insight in the similar yet subtly different mechanisms of primary and acquired erlotinib resistance. These are illustrated in the next 2 figures under the two respective headings.

3.6.1 Mechanisms of Primary Erlotinib Resistance

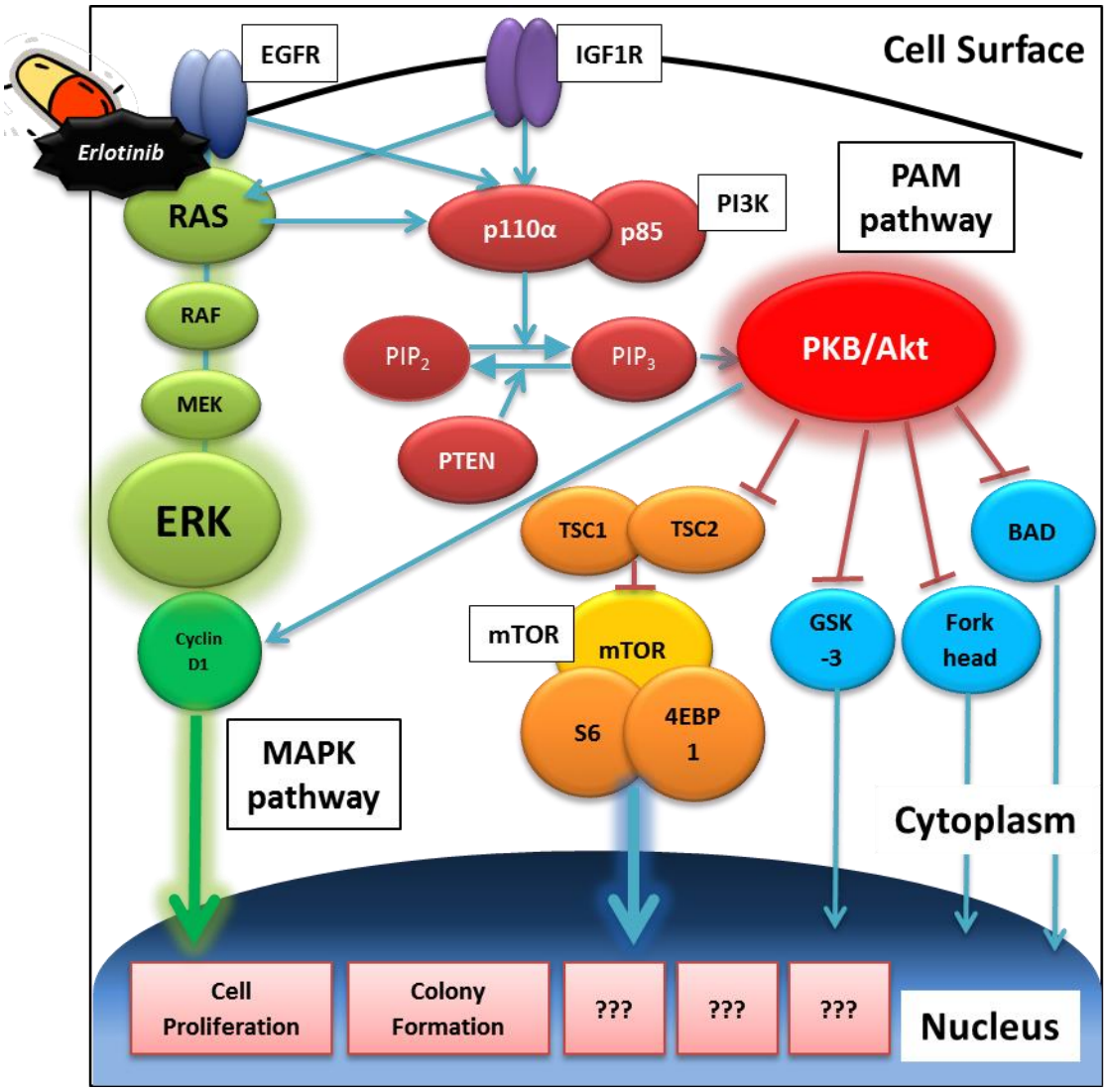

Figure 3.54: Proposed molecular mechanism of erlotinib insensitivity in PDAC

Primary erlotinib resistance or erlotinib insensitivity is characterised by an **up-regulation of pathways downstream of EGFR**. The predominant pathways studied are the direct **downstream MAPK pathway and the PAM pathway**, and **both appear involved (Figure 3.54)**. This is a class effect, since cell proliferation experiments showed a similar pattern of

drug sensitivity for gefitinib and erlotinib but not gemcitabine chemotherapy (**section 3.2**). At baseline, all 3 erlotinib-insensitive cell lines were found to be over-expressed in downstream pathways, with higher total ERK or AKT (IF) **(Figure 3.25)** and pERK and pAkt (IF and WB) **(Table 3.6, Figure 3.22)**. Erlotinib sensitive BxPC-3, on the other hand, has up-regulated pEGFR and pIGF1R compared to other cell lines. This pattern of protein expression was closely associated with the gene expression. From qRT-PCR, erlotinib-insensitive cell lines had either up-regulated *PI3Kα, MAPK1 or AKT2* genes (CAPAN-2, MiaPACA-2 and PANC-1), accompanied by a down-regulation of *EGFR* gene **(Figure 3.31)**. A significant trend of *EGFR* gene down-regulation was observed with incremental erlotinib insensitivity. *AKT-2* also displayed a significant up-regulation trend, though the statistical significance was largely contributed from a 20-fold increase in *AKT-2* in PANC-1 **(Table 3.8)**. Interestingly, the 2 most erlotinib-insensitive cell lines MiaPACA-2 and PANC-1 had substantially down-regulated *ERBB3 (HER3)* compared to the reference standard. In gefitinib-sensitive lung cancer cell lines models, HER3 coupled with EGFR in the activation of the PI3K/Akt pathway; whilst in gefitinib-resistant cell lines MET amplification had a dominant role.[154,303] The demonstration of *HER3* down-regulation in the two highly erlotinib-insensitive cell lines appeared to be consistent with existing literature, suggesting HER3/ EGFR independent downstream activation of the PI3K/Akt axis in mediating de novo erlotinib resistance.

One intriguing observation from these experiments was the responsiveness of PI3K/Akt and significant EGFR/ PI3K pathways cross-talk in erlotinib-insensitive cell lines. Through a series of immunofluorescence and western blotting experiments, erlotinib-insensitive cell lines were found to have equipped with higher total Akt and pAkt at baseline **(Figure 3.26, Figure 3.28)**, pAkt was also more actively stimulated by EGF **(Figure 3.22, table 3.6**). Furthermore, from both here and in the next chapter, PANC-1 was shown to be able to paradoxically activate pAkt upon EGFR inhibition alone, and activate pERK upon IGF1R inhibition alone **(Figure 3.23, Figure 4.13)**. This indicates that erlotinib-insensitive cell lines are active in multiple pathways and is capable of mediating molecular signals via the pathway of the least

"resistance", a process known as "oncogenic shift". This agrees well with the observation of feedback activation of reciprocal pathway by Sos *et al.*, where pERK and pAkt are paradoxically activated by PI3K and MEK inhibitors respectively;[208] and an experimental and mathematical model by Lange *et al.* showing basal Akt phosphorylation and degree of EGF-activated Akt and ERK as a determining factor of erlotinib sensitivity.[304]

Finally, the studies of the 5 PDAC cell lines have yielded interesting observations on *K-Ras*. *K-Ras* mutant PDAC may act differently than in other cancer types. In *K-Ras* mutated colorectal cancer, there is a "constitutive activation of Ras/RAF/MEK/ERK pathway, with loss of EGFR signalling control, rendering EGFR inhibitors (cetuximab and pannitumumab) ineffective."[305] In BRAF mutated melanoma, there is also a constitutive activation of the MEK/ERK signalling pathway.[306] As both *K-Ras* and BRAF lie further upstream than ERK and MEK, this may explain why *K-Ras* mutant colorectal cancers and BRAF mutant melanomas remain sensitive to MEK inhibitors.[195,307] On the other hand, in this project *K-Ras* mutant pancreatic cancer was found to behave somewhat differently. Firstly, *K-Ras* wild type cell line BxPC-3 was much more highly up-regulated in *EGFR*, whilst all *K-Ras* mutant cell lines had significantly highly up-regulated *PI3Kα* **(Table 3.7)**. In addition, cell proliferation experiments showed that erlotinib-insensitive PDAC cell lines (all of which are *K-Ras* mutant) also exhibited the same pattern of insensitivity to PD-98059, a highly specific tyrosine kinase inhibitor of MEK1/2;[56] whilst remaining sensitive to dual PI3K/mTOR inhibitor NVP-BEZ235 **(Table 3.2)**. Further, in chapter 4, by western blotting, pERK was inhibited by PI3K and PI3K/mTOR inhibitors in PANC-1, but ironically was not inhibited by the direct downstream MEK inhibitor **(figure 4.13 and table 4.2)**. These findings in aggregate suggest that *K-Ras* mutant PDAC tumours have a propensity to act via PI3K/Akt/mTOR instead of the classical Ras/RAF/MEK/ERK pathway. Clearly, these experiments so far merely raise this as a hypothesis, which can only be proven in large scale patient tumour studies. In **section 6**, a study proposal for a clinical trial will be discussed as a future direction to prove this concept.

In summary, the current hypothesis is that erlotinib-insensitive tumours likely have **high activity in both MAPK and PAM pathways, with either or both pathways efficiently switched on depending on the situation**. This dynamic shift in molecular pathways of pancreatic cancer may potentially explain the heterogeneity in PDAC and why it has been so difficult to isolate a molecular marker. Based on this premise, the goal for overcoming primary erlotinib resistance is no longer simply finding a specific marker and using a novel targeted drug to inhibit it. Instead, one must think about *combining targeted therapies of multiple pathways* to achieve a complete blockade of the signalling pathways in PDAC, a strategy that has already been well established in many cancer types in trial settings and an approach that is in line with the general directions of American Society of Clinical Oncology 2012.[161] Given the influence of MAPK and PAM pathways in erlotinib insensitivity, the effect of different upstream and downstream combined blockades of EGFR and PI3K pathways in PDAC cell lines will be explored in chapter 4.

3.6.1 Mechanisms of Acquired Erlotinib Resistance

In many ways, acquired erlotinib resistance appeared to be an extension of erlotinib insensitivity in this study. Erlotinib insensitive cell lines had various downstream target pathways activation, whilst erlotinib resistant cell lines further exploited the PI3K/Akt pathways **(Figure 3.55)**. On close examination, 4 important characteristics were found to be unique to acquired erlotinib resistance.

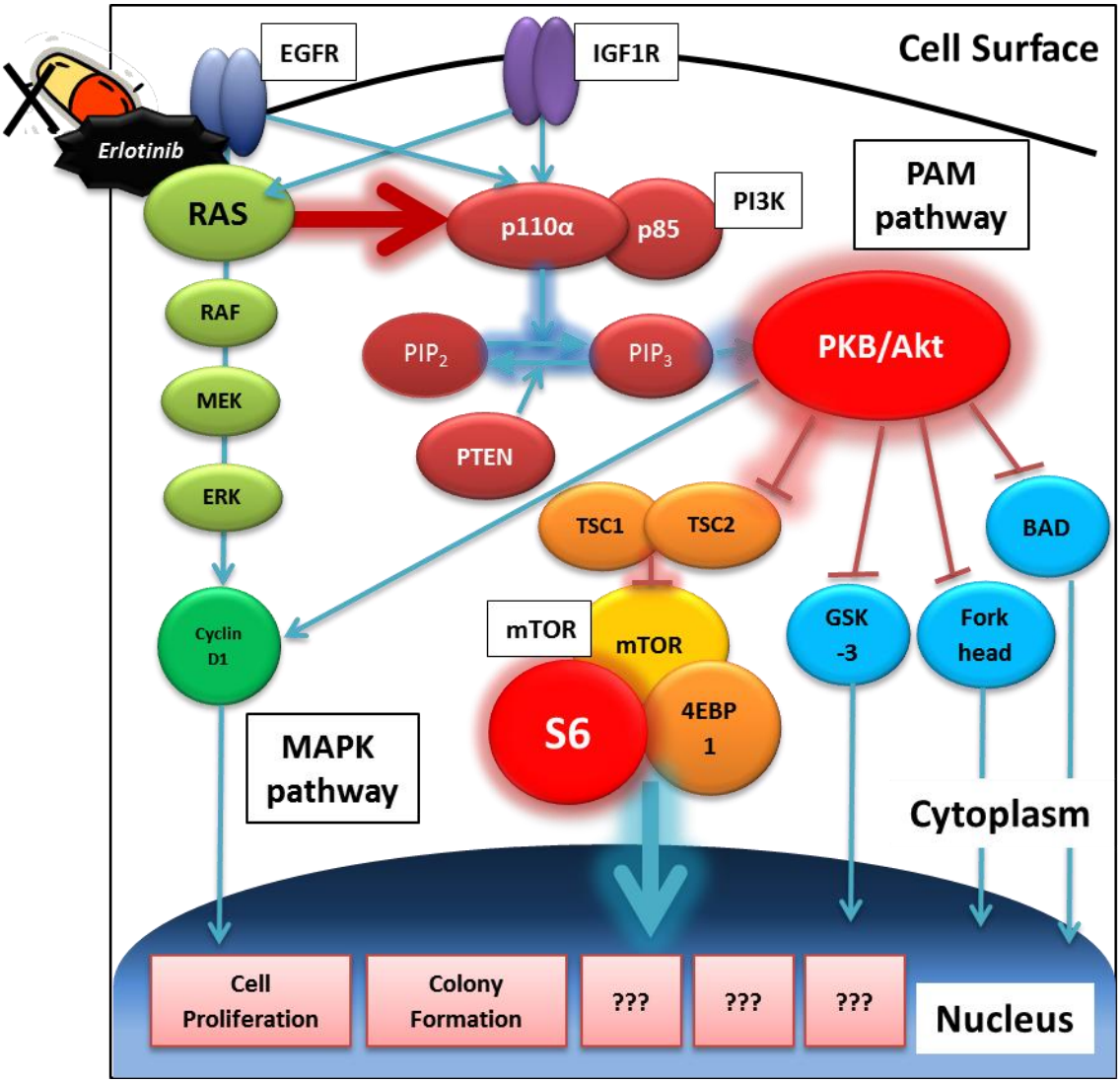

Figure 3.55: Proposed molecular mechanism of acquired erlotinib resistance in PDAC

Firstly, in both ER cell lines there was a dominant shift from the MAPK pathway to the **PI3K/Akt pathway mediating through mTOR**, as demonstrated by western blotting and immunofluorescence **(Figure 3.40, Figure 3.44)**. Of interest, whilst PANC-1 already had up-regulated PI3K/Akt pathway and PANC-ER simply took further advantage of this active system, BxPC-3 had low PI3K/Akt pathway activity to start off with. Yet, like PANC-ER, BxPC-ER also up-regulated this pathway in mediating erlotinib resistance. In particular, Akt-driven pS6 within the mTOR complex was highly up-regulated, as opposed to the many other effectors of Akt **(Figure 3.37, 3.38, 3.44)**. This therefore implies that PI3K/Akt/mTOR pathway confers a natural selective advantage under the erlotinib drug pressure, which in turn suggests a possible role of mTOR inhibition in overcoming erlotinib resistance.

Secondly, **ER cell lines were characterised by epithelial-mesenchymal transition (EMT).** Whilst BxPC-3 was epithelial and PANC-1 mixed epithelial and mesenchymal, a progression from epithelial to mesenchymal morphology was observed in ER cell lines. Of note, there was a strategic relocation of vimentin close to the edges of ER cell colonies. In PDAC TGF-β activates SMAD-4 pathway in mediating EMT, in the so-called "canonical EMT pathway"[71,72] However, BxPC-3 is known to be SMAD-4 deleted,[228] implying that BxPC-ER probably mediated EMT via non-canonical pathways. In support of this, a series of preliminary western blotting experiments that SMAD4 protein was present in PANC-1 and PANC-ER but not BxPC-3 and BxPC-ER. Comparing each ER cell line to parent cell line, pSMAD2/3 was more active in PANC-ER and less active in BxPC-ER. Recent evidence suggested that pathways such as MAPK pathway, c-jun N-terminal kinase (JNK) and PI3K may be involved in EMT.[77] It is possible that EMT is driven by the up-regulated PI3K/Akt/mTOR pathway, such that it represents an "outcome" rather than the "cause" of acquired erlotinib resistance. Note that the focus of this project remains the study of interaction between EGFR, IGF1R, MAPK and PAM, and it is not designed to substantiate EMT and erlotinib resistance. A thorough examination of SMAD and EMT transcription factors (e.g. Snail, Trail) by TGF stimulation will be required for ongoing studies.

Thirdly, **the genetic drivers for acquired erlotinib resistance may possibly lie further downstream of PI3K/Akt/mTOR.** In the case of BxPC-ER, the NF-κB system was involved; for PANC-ER, c-Fos was implicated **(3.5.5 and 3.5.6)**. NF-κB has been found to activate PI3K/Akt as early as 2002, and is now known to stimulate PI3K/Akt through removal of a brake involving the mTOR/S6/IRS1 feedback and down-regulation of PTEN via an intermediary RIP1.[301,308,309] c-Fos, on the other hand, is a transcriptional regulator of many genes, and is known to be induced by both ERK and PI3K/Akt via Elk1.[309] That said, no current data exists that support negative feedback of c-Fos on PI3K/Akt. Whilst these current experiments were only hypothesis-generating at best, it nonetheless highlighted the extensive genetic

heterogeneity, alterations and complex pathway wirings observed in pancreatic cancer,[20,29] and provides a basis for ongoing sequencing experiments of these intriguing cell lines.

Lastly, and importantly, the ER cell lines which were up-regulated in the PAM pathway became significantly cross-resistant to IGF1R and MEK inhibitors whilst remaining sensitive to PI3K and PI3K/mTOR inhibitors as single agents **(Table 3.3)**. In a way this is counter-intuitive, since one would expect that over-activation of PAM pathway should lead to an increased resistance to drugs that are designed to block it. The current hypothesis is that **erlotinib resistant cell lines have not only "shifted" but also become dependent in the PAM pathway.** To investigate oncogenic dependence further, the differential response of ER and parent cell lines to PI3K and mTOR inhibitors across multiple functional assays needs to be studied. So far both **figures 3.54 and 3.55** are incomplete, and have many unknown endpoints denoted by "?". In chapter 4, the results of migration assay, cell cycle assay and apoptosis assay will be presented in addition to cell proliferation and clonogenic assay, and further information will be added to the existing diagrams of proposed molecular mechanisms. This discussion point will be revisited in the **section 4.5**.

In summary, primary erlotinib resistance appears to be determined by active downstream signal activation and cross-talk between multiple pathways (notably EGFR/MAPK and PI3K/Akt pathways), whereas acquired erlotinib resistance results from a dominant shift to PI3K/Akt/mTOR pathway under constant drug pressure. In both cases, cancer cells remained sensitive to PI3K/mTOR inhibitor NVP-BEZ235 and PI3Kα inhibitor NVP-BYL719 to a lesser extent. The next chapter will examine the effect of these inhibitors, erlotinib, MEK inhibitor and IGF1R inhibitors, alone or in combination.

CHAPTER 4:

COMBINED BLOCKADE VERSUS SINGLE BLOCKADE OF EGFR AND PI3K/MTOR IN-VITRO

4.1 Introduction

4.1.1 Chapter Background

In the previous chapter, genomic and molecular characterisation was performed on 5 PDAC cell lines and 2 ER cell lines. Primary or *de novo* erlotinib resistance was found to be contributed by constitutively active downstream signalling pathways and significant cross-talk between EGF/IGF and MAPK/PAM pathways; whereas acquired erlotinib resistance was characterised by an oncogenic shift to the dominant PAM pathway. Yet, at this stage only little was known about the end outcomes of erlotinib resistance, as cell proliferation and clonogenic assays were the only functional assays that were discussed in the last chapter. In the last chapter, there was early evidence that both primary and acquired resistant cell lines remained sensitive to dual PI3K/mTOR inhibitor (BEZ-235) with nanomolar potency. However, an in-depth analysis of the optimal strategy to overcome erlotinib resistance had yet to be explored.

Over the last few years, combined targeted treatment or combined blockade (CB) has rapidly gained momentum in pre-clinical and clinical studies, particularly with the aim of overcoming targeted drug resistance.[310] The concept of CB is to improve the complete blockade of a target by inhibiting on multiple forms of the same target; or to produce complementary effect by blocking different targets in the same pathway".[198] This latter strategy is particular important for cancers with extensive molecular crosstalk- as demonstrated in the erlotinib insensitive PDAC cell lines, since these cancers are often equipped with redundant signalling pathways making them difficult to inhibit by single drug alone.[160] Given the significant interaction between EGFR/ IGF1R/ MAPK/ PAM pathways, 4 horizontal combined blockade strategies ranging from dual upstream to dual downstream blockades were closely examined in their synergy as well as efficacy. The differential sensitivities between parent and resistant cell lines to CB were then scrutinised to explore the concept of oncogenic addiction, whereby cancer cells driven down a molecular pathway are preferentially killed by CB.

4.1.2 Chapter Aims

1. To compare the effect of CB versus single blockade (SB), and to establish synergy
2. To propose the "best" CB combination for pancreatic cancer to take to *in-vivo* study
3. To explore onocogenic dependence by comparing differential response to CB between parent and resistant cell lines

4.1.3 Chapter Methods

In the first half of this chapter, various methods from pharmacology biostatistics are used to demonstrate the important concept of synergy between drug A and drug B. These are used to study the synergistic effect of 4 horizontal CB combinations covering the MAPK and PAM pathways: 1) erlotinib (ERL)* NVP-AEW541 (IGF1Ri: AEW)– both cell surface receptors (dual upstream); 2) ERL* NVP-BYL719 (PI3Kαi: BYL)– upstream plus "midstream" blockade, 3) erlotinib* NVP-BEZ235 (dual PI3K/mTORi: BEZ) – upstream plus downstream blockade; and 4) PD-98059 (MEKi: PD)* BEZ – dual downstream blockades. *"Cytotoxic synergy"* and *"molecular synergy"* were studied by cell proliferation and western blotting respectively. In the second half of this chapter, CB versus SB and the test of 4 CB combinations were then carried out in a wide variety of *functional* assays, including cell cycle, apoptosis assay, clonogenic assay and migration assay. Finally, in the discussion, all results are pooled to make conclusions about the best combination to take to *in-vivo* study, and to generate some theories about molecular functions of erlotinib resistance and logical ways to overcome this.

Building from the diagram from previous chapter, the designed targets of these inhibitors are illustrated in the figure below:

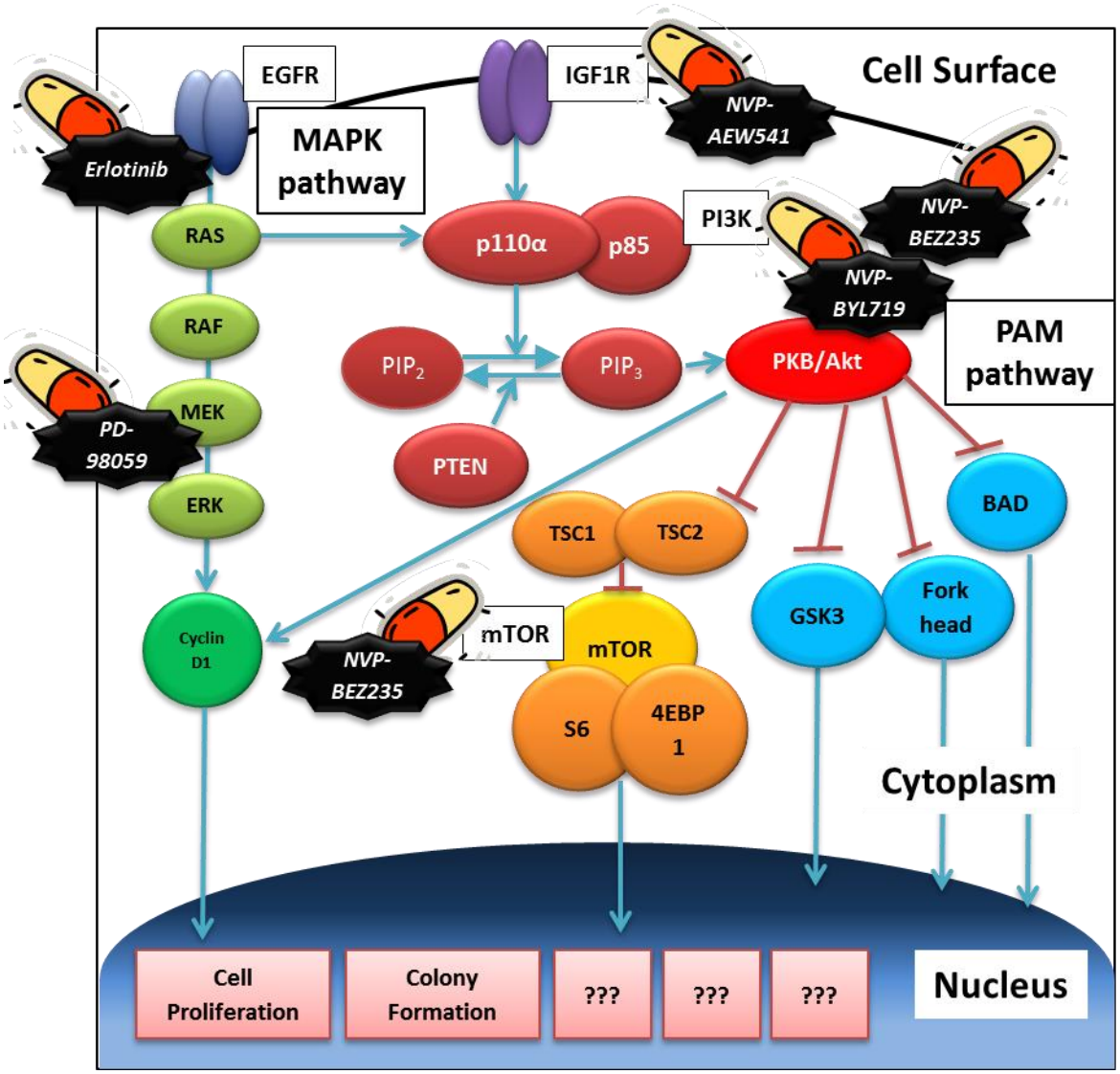

Figure 4.1: Drug Targets on EGFR, IGF1R, MAPK and PAM pathways

The design of these CB combinations took into account that erlotinib resistance was found to be mediated via up-regulated downstream MAPK or PAM pathways with downstream mTOR being intricately involved. If this hypothesis was true, one would expect that combined downstream blockades would be more complete than upstream blockades. That is, the last combination would be more effective than third, than second, than the first combination.

4.2 Establishing Pharmacological Synergy

4.2.1 Statistical analysis of pharmacologic synergy

4.2.1.1 Definition of Synergy

Drug combinations have been studied extensively in pharmacological investigations. The standard way of examining drug combination is the concept of *dose equivalence* or *additivity*, where the combined effect of two drugs are well fitted in the equation predicted by the maximum effect produced by each drug combined.[311] Mathematically, this is expressed by the following formula:

$$E_{ab} = \frac{E_{max}(b + a/R)}{(b + a/R) + C_B}$$

where E_{ab} denotes the effect observed when drug a and drug b are combined, R denotes the ratio of equivalent doses ($R = C_A / C_B$) and E_{max} denotes the upper limit of effect observed in the system.[311] In other words, additivity simply means that the less potent drug is acting as a diluted form of the other drug, and that there are no interactions between the two drugs.[312] Thus, by definition, *synergy* is more than expected for an additive effect and *antagonism* is less than expected for an additive effect.

Whilst the combined effects of two drugs can be easily represented in column graphs, it is often important to quantify synergy mathematically, especially as several CB combinations will be compared against one another. The subject of synergy analysis is exceedingly complex, often requiring complicated mathematical algorithms and advanced pharmacological statistical analysis. In addition, there are in excess of 13 ways to quantify synergy, including isobolograms, combination index plots, combined dose effect curves and many others.[313] As such, the subject of synergy analysis cannot be comprehensively covered in this thesis; nor is it necessary to do so. Instead, the concepts of the 3 most common ways of synergy analysis

(dose response surface plots, isobolograms and synergy index) and their interpretations are described below.

4.2.1.2 Three-dimensional dose response surface plot

The combined dose response of drug A and drug B can be simply explored in a matrix of graded concentrations of drug A times drug B. This is particularly used for cell proliferation experiments, where responses are measured as proportional viability (%), as in this example:

	Dose of NVP-AEW541			
Dose of erlotinib	**0 μM**	**1 μM**	**2 μM**	**4 μM**
0 μM	**100%**	**78%**	**68%**	**54%**
10 μM	**40%**	**8%**	**7%**	**4%**
20 μM	**34%**	**6%**	**5%**	**5%**
30 μM	**31%**	**6%**	**5%**	**4%**

Table 4.1: Raw Data example of combined blockade cell proliferation experiments

This data in **Table 4.1** can then be plotted in a dose response surface plot, where x-axis represents dose of one drug, y-axis the dose of second drug, and z-axis the proportional viability (%). There are then three ways of producing the graph using SAS 9.2, as described elsewhere.[272]

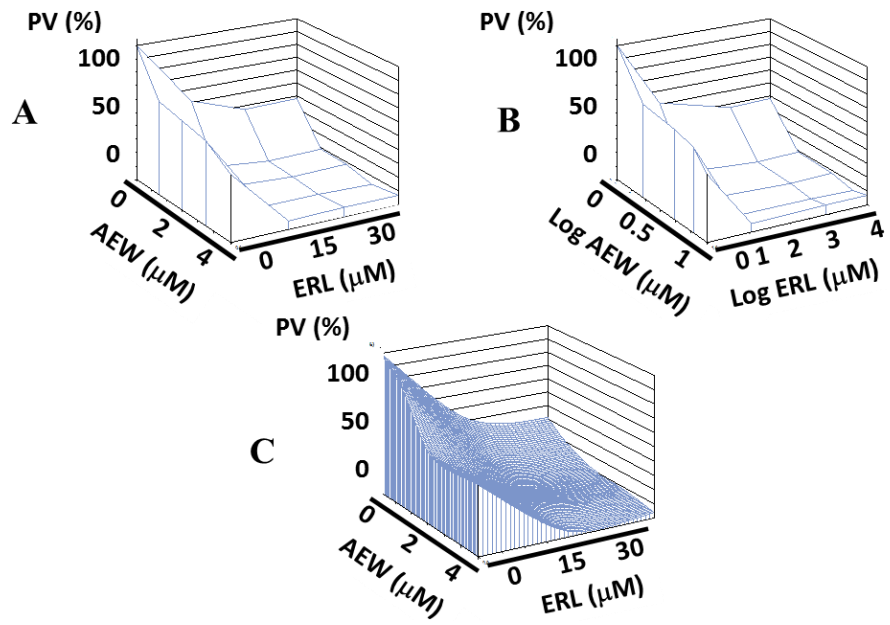

Figure 4.2: Different forms of dose response surface plots

In **figure 4.2 (a)**, the raw proportional viability (PV) data is shown on the surface plot. Whilst all observed data in the 4x4 matrix are presented accurately, there is a lack of appreciation of the "contour" of the dose response because of the small number of data points. In the actual experiments, a 6x 6 matrix of graded concentrations of each drug was used, but despite this, 36 observations were still too few to create a sense of contour. **Figure 4.2 (b)** uses log transformation on the observed data, as recommended by Whitehead *et al.*[272] Presumably this is because tumour growth have been described in log linear models previously.[314] However, the log transformation did not enhance the sense of contour in these experiments, and created unequal distance between each log doses. **Figure 4.2 (c)** shows a fitted curve based on the observed data. The values are fitted using spline interpolation with SAS 9.2, and the resulting curve comprises of 50 x 50 = 2500 expected data points. This closely resembles the raw data surface plot in **figure 4.2 (a)**, and also creates a contour shape that can be easily appreciated.

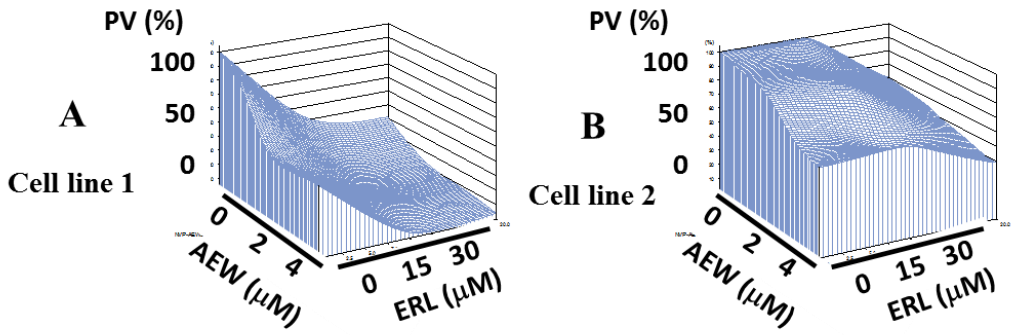

Figure 4.3: Interpretation of fitted dose response surface plots

In terms of the interpretation of fitted dose response surface plots, **figure 4.3 (a)** shows a cell line that is sensitive to both drugs, with PV reduced to more than 50% with each drug alone (x and z-axis).The combination of two drugs at high dose essentially suppress the cells to 0%. This is therefore a synergistic combination, and the resulting surface plot tends to be concave, slanting from the top left corner to the bottom right in a steep slope. On the other hand, an antagonistic combination is usually flat or even convex, with the proportional viability remaining high even at the highest concentrations of both drugs as in **figure 4.3 (b)**. The left and right figures represented the actual experiment results of ERL* AEW combination in BxPC-3 and

PANC-1 respectively. From these results, it is appreciated that this combination is synergistic in BxPC-3 but not in PANC-1.

4.2.1.3 Isobolograms

A very common way of representing drug synergy graphically is isobologram. This is a graph of equally effective dose pairs called isoboles, and is particularly effective in conditions where two agonists have varying potency.[312] Below is an example of isobologram:

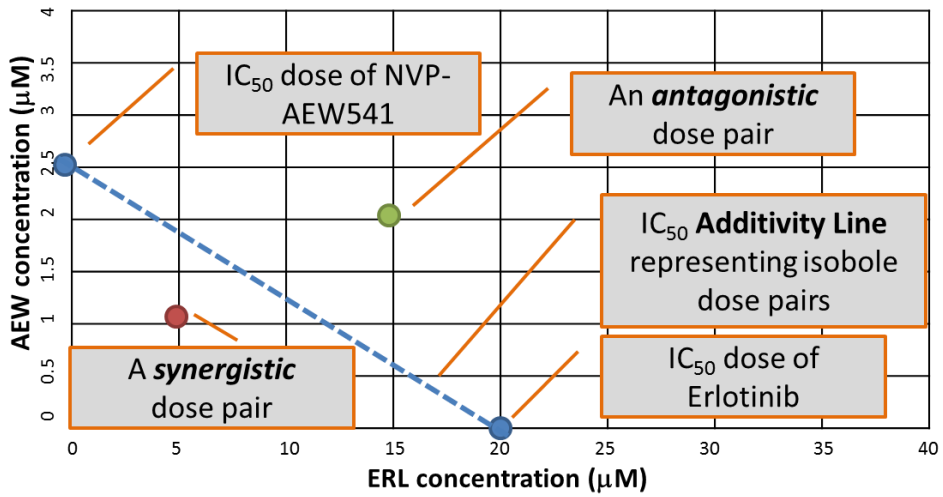

Figure 4.4: Example of an isobologram

A particular effect level is first selected, such as IC_{50}. The doses of drug A and drug B to produce the IC_{50} are plotted on the X and Y-axis. A straight line connecting the two intercepts represents all the possible dose pairs that produce the effect in an additivity combination. This line is called the additivity line, and is expressed by this equation:

$$\frac{a}{A_i} + \frac{b}{B_i} = 1$$

where Ai and Bi represent the IC_{50} of each drug, and all (a,b) points represent the dose pairs that lie on the additivity line.[315]

The observed dose pairs to achieve IC_{50} are then plotted on the same graph. A dose pair that lies below the additivity line represents a synergistic or supra-additive combination, whereas

a dose pair that lies above the additivity line represents an antagonistic or sub-additive combination.[312]

4.2.1.4 Synergy Index

The above two methods only qualitatively assess synergy. It is useful for assessing whether a CB combination is synergistic, but is less useful for comparing whether one CB combination is more synergistic than another. To quantitatively measure synergy, the Bliss synergism/ antagonism model, one of the most popular and robust model for measuring synergy, was implemented.[316] The Bliss model essentially predicts if each individual drug cause growth inhibition by 50%, then two drug combined decrease growth by 1–0.5*0.5, or 75%.[317]

In the modelling part, a four-parameter model was programmed on SAS 9.2 and this model was fitted using PROC NLIN (non-linear regression). This formula has been published elsewhere, but is not included here because of its complexity.[272] The results will be presented in the following way:

	Bliss Synergy/ antagonism model			Departure from model		Conclusion
Cell line	**n**	**S.I.**	**95% C.I.**		**t-value**	**P-value**	
BxPC-3	4	**1.99**	1.43	2.76	t= 0.00	1.00	**Significant synergy**
PANC-1	4	0.96	0.68	1.37	t = 0.07	0.94	Possible antagonism

Table 4.2: Interpretation of Synergy Index

Synergy Index (S.I.) equals to 1 when the observed effect of the dose pair is exactly the same as the combined effect of each drug alone, that is the combined effect is additive only. A S.I. >1 indicates that synergy is present, with higher values representing more synergy. A S.I. <1 indicates that antagonism is present, with lower values (>0) representing less synergy. A 95% confidence interval (C.I.) is calculated. A 95% C.I. that crosses 1 indicates the result is non-significant, whereas a 95% C.I. that excludes value of 1 indicates significant result. That said, a non-significant result did not necessarily exclude synergy, since type II error was high with

this model. Finally, the residuals are used to assess departure from the Bliss model, and the formula had been previously described.[272] A significant P (<0.05) suggests heterogeneous data, resulting from poor iterations and unreliable data. In this case, synergy index cannot be interpreted with confidence. In the above example that studied ERL*AEW combination, the CB was significantly synergistic for BxPC-3 as the 95% C.I. did not cross the null value of 1, and possibly slightly antagonistic for PANC-1 since the C.I. crossed 1.

4.2.2 Study of Cytotoxic Synergy by cell proliferation assays

As described previously, a 6x6 matrix of graded concentration of two drugs from 4 CB combinations (ERL*AEW, ERL*BYL, ERL*BEZ, PD*BEZ) were tested on the 5 PDAC cell lines. For erlotinib, the 6 doses ranged from 0, 5, 10, 15, 20 and 30μM; for NVP-AEW541, this ranged from 0, 0.5, 1, 2, 3 and 4μM; for NVP-BYL719, this ranged from 0, 0.5, 1, 2.5, 5 and 10μM; for NVP-BEZ235, this ranged from 0, 0.01, 0.025, 0.05, 0.1 and 0.2μM; and for PD-98059 this ranged from 0, 5, 10, 20, 30 and 40μM. Biological triplicates were performed for each dose set. Synergy experiments were repeated in at least 4 times, to provide enough statistical power for performing synergy analysis.

4.2.2.1 Synergy analysis of 4 CB combinations in 5 PDAC cell Lines

Key Finding: ***EGFR and IGF1R are synergistic for cell lines with active upstream receptors; whilst EGFR and PI3K are synergistic for cell lines with active downstream pathways.***

Before analysing synergy with the methodologies above, the raw values of an ERL*AEW synergy experiments for 2 combination dose sets are presented as an illustration.

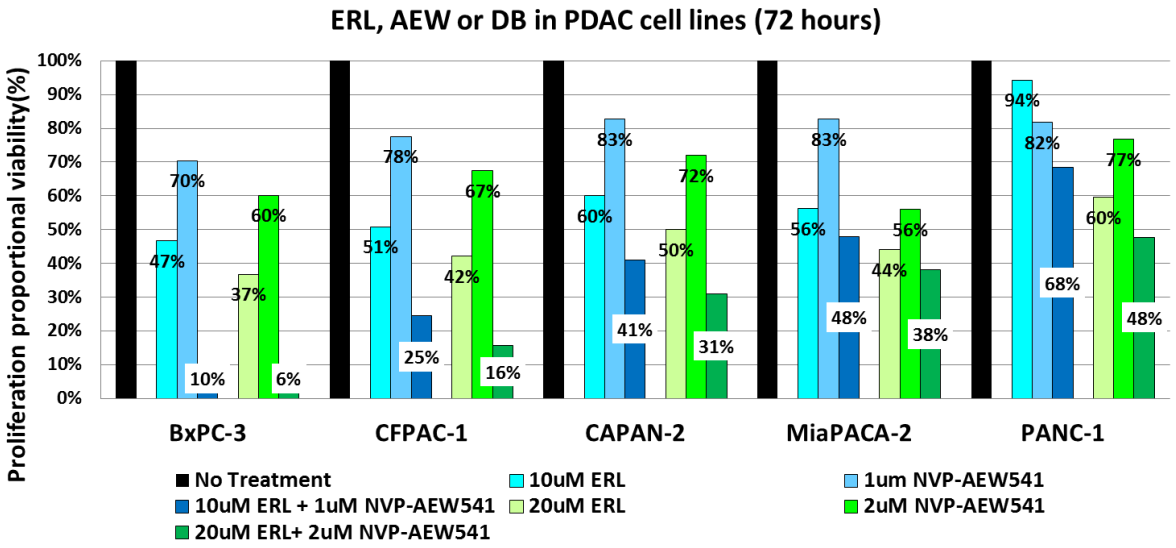

Figure 4.5: An example of raw data for an erlotinib* NVP-AEW541 synergy experiment

In the figure above, the raw data of erlotinib 10 and 20μM, crossed with IGF1R inhibitor AEW 1 and 2μM respectively, are shown for the 5 cell lines. First of all, the most obvious finding was that the responses of these 5 cell lines to CB (dark blue, dark green bars) followed a similar pattern to single drug alone. It roughly followed that BxPC-3<CFPAC-1<CAPAN-2 <MiaPACA-2<PANC-1 in insensitivity. As for synergy, a simple calculation using the bliss model could be done manually. The Bliss synergy/ antagonism model simply predicts that synergy occurs when the observed effect of two drugs combined is more than the product of the expected effect of each drug, as discussed previously. Thus, as an example, the proportional viability (PV) from the effect of ERL 10μM * AEW 1μM on BxPC-3 should be at least 70%*47% = 33%. In this case, the observed PV of erlotinib 10μM * NVP-AEW541 1μM was 10%. In other words, the cell suppression effect of the combination was actually 90%, which was far greater than the expected 1-33%= 67%. Therefore, synergy was likely present for this combination at this dose for this cell line. After simple multiplications, the expected combined PV for ERL 10μM * AEW 1 μM were 33%, 40%, 50%, 46% and 77% for BxPC-3, CFPAC-1, CAPAN-2, MiaPACA-2 and PANC-1; whereas the observed PV were 10%, 25%, 41%, 48% and 68%. At this dose, then, synergy was present for BxPC-3, CFPAC-1, CAPAN-2 and PANC-1 since the observed CB PV was smaller than the expected CB PV (or the

observed cell proliferation suppression effect was greater), whereas antagonism was present for MiaPACA-2 as the observed PV (or the observed cell proliferation suppression effect was smaller). For ERL 20 μM * AEW 2 μM the expected combined PV were 22%, 28%, 36%, 25% and 46%; whereas the observed PV were 6%, 16%, 31%, 38% and 48%. Thus, at a higher dose this combination was synergistic in BxPC-3, CFPAC-1 and CAPAN-2. This time, this combination was antagonistic for both MiaPACA-2 and PANC-1.

Of course, this illustration was far from complete, since only 2 combination dose sets were represented here, and as many as 25 dose sets should be assessed in a 6x6 matrix experiment. Also, as was becoming clear in this illustration, 2 drugs could be synergistic for one dose set and antagonistic in another for the same cell line (PANC-1 in this example). A more robust way of combining these data is needed rather than averaging or performing 2-sample t-test. This is why synergy index is much more powerful to statistically analyse for synergy. Below, the dose response surface plot is presented first before the S.I. data.

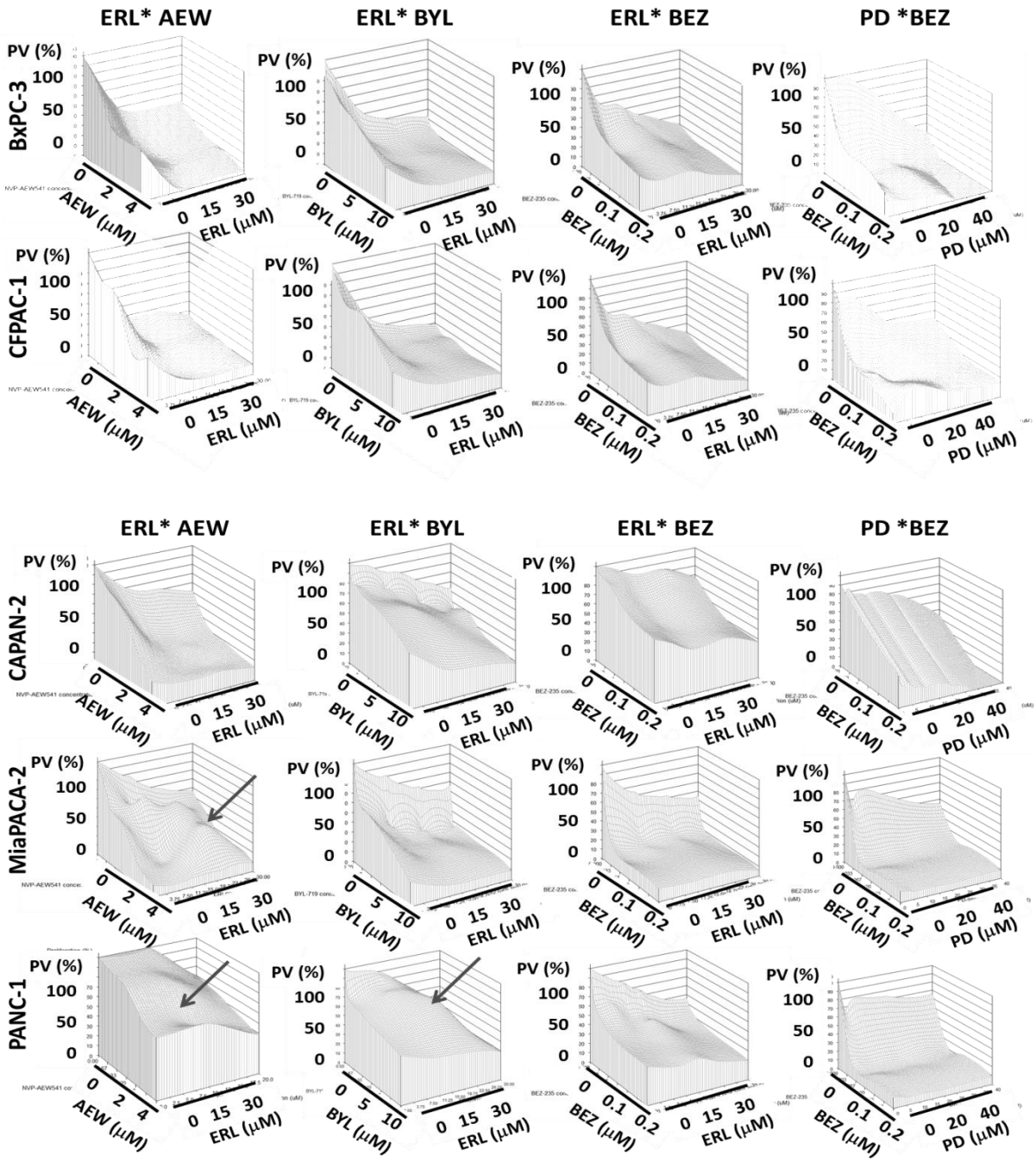

Figure 4.6: Dose response surface plots of 4 CB combinations in 5 PDAC cell lines

Firstly, examining the first column from the left, ERL* AEW CB appeared to be synergistic for BxPC-3, CFPAC-1 and CAPAN-2, consistent with the raw data. In all three surface plots, the contour appeared concave, and there was a steep gradient from the top left to the bottom right. Importantly, the PV at the highest dose set almost reached zero baseline for BxPC-3, indicating that the two drugs together at this dose (ERL 30μM and AEW 4μM) nearly

completely eliminated all cells. For MiaPACA-2 and PANC-1, however, the shapes of the surface plots were clearly different. There was a convexity in the middle of the surface plots for both cell lines (arrows), indicating an unexpectedly high PV (or low effect) as would be predicted by additivity. In addition, for MiaPACA-2 there were many irregular contour "terrains" in addition to the central convexity in PANC-1, and this was reflected in the lower S.I. value (higher antagonism) which is discussed in the next section.

As the surface plots of all 4 CB combinations were examined in all 5 PDAC cell lines, it was clear for most combinations there was a steep concave slope suggesting synergy. The exceptions to this are MiaPACA-2 and PANC-1 for the ERL*AEW combination as discussed above; and PANC-1 for the ERL * BYL (PI3Kα inhibitor) combination (arrows). In all three cases, the apparent convexity appeared at mid-range dose sets, indicating where the antagonism was observed. Importantly, on closer examination, the last 3 cell lines (CAPAN-2, MiaPACA-2 and PANC-1) were relatively insensitive to ERL or PD (MEK inhibitor), as indicated by the small gradient on the z-axes (z-axis corresponds to ERL in the first 3 combination, and PD for the 4^{th} combination). Despite this, the use of BYL and in particular the dual PI3K/ mTOR inhibitor BEZ was mostly capable to reduce the PV synergistically.

Synergy index with 95% confidence interval and statistical testing of model departure was shown below for all 4 CB combinations in 5 PDAC cell line:

Cell Line	ERLOTINIB * NVP-AEW541		ERLOTINIB * NVP-BYL719		ERLOTINIB * NVP-BEZ235		PD-98059 * NVP-BEZ235	
	S.I. (95% C.I)	Model Depart.	S.I. (95% C.I)	Model Depart.	S.I. (95% C.I)	Model Depart.	S.I. (95% C.I)	Model Depart.
BxPC-3	**1.99 (1.43-2.76)**	t=0.00, P=1.00	**1.34 (1.17-1.55)**	t=-0.10, P=0.92	**1.51 (1.21-1.88)**	t=-0.03, P=0.97	**1.46 (1.21-1.75)**	t=0.12, P=0.90
CFPAC-1	**1.55 (1.14-2.14)**	t=0.06, P=0.95	1.15 (0.90-1.47)	t=-0.01, P=0.99	**1.13 (1.00-1.29)**	t=-0.10, P=0.92	1.22 (0.90-1.66)	t=-0.10, P=0.92
CAPAN-2	1.22 (0.82-1.84)	t=-0.03, P=0.98	1.18 (0.86-1.52)	t=0.13, P=0.89	1.12 (0.79-1.58)	t=0.30, P=0.77	1.14 (0.84-1.55)	t=-0.03, P=0.98
MiaPACA-2	0.84 (0.67-1.05)	t=-0.03, P=0.97	1.15 (0.98-1.35)	t=0.12, P=0.90	**1.44 (1.29-1.60)**	t=1.03, P=0.30	1.35 (0.80-2.31)	t=0.14, P=0.89
PANC-1	0.96 (0.68-1.37)	t=0.07, P=0.94	0.85 (0.68-1.07)	t=0.16, P=0.87	**1.27 (1.04-1.54)**	t=0.18, P=0.86	**1.44 (1.13-1.84)**	t=-0.10, P=0.92

Table 4.3: Synergy Index (S.I.) for 4 CB combinations in 5 cell lines with 95% confidence interval (C.I.) and statistics for model departure provided.

For easier inspection, S.I. >1 indicating synergy was coded in red, and S.I. <1 indicating antagonism was coded in blue. A significant result with 95% C.I. not crossing 1 was bolded **(Table 4.3)**. From these analyses, the following observations could be made:

1) The results of S.I. analysis closely corresponded to the dose response surface plots, with synergy indicated for all cell lines except for MiaPACA-2 (ERL*AEW) and PANC-1 (ERL*AEW, ERL*BYL) (blue).

2) For the erlotinib sensitive cell lines, ERL* AEW combination was highly synergistic for BxPC-3 (S.I. = 1.99, 1.43-2.76) and CFPAC-1 (S.I. = 1.55, 1.14-2.14). Other combinations remained synergistic for these 2 cell lines, but were clearly less synergistic than this CB.

3) For the erlotinib insensitive cell lines, ERL* AEW combination was non-significantly antagonistic for MiaPACA-2 (S.I. =0.84, 0.67-1.05) and PANC-1 (S.I. =0.96, 0.68-1.37).

However, ERL* BYL was possibly synergistic for MiaPACA-2 (S.I. = 1.15, 0.98-1.35); and when combined with BEZ, both 3rd/4th CB were highly synergistic, with S.I. from 1.27- 1.44.

4) For the moderately insensitive CAPAN-2, all CB combinations were equally synergistic.

5) Comparing the 4 CB combinations, ERL and BEZ were significantly synergistic with 4 of the 5 cell lines. Significant results could not be demonstrated for CAPAN-2 using any CB combination, since CAPAN-2 was a slow-growing cell line with inherent issues of underestimating the true PV as discussed in chapter 3.

6) None of the results had significant departure from the model, and were all valid results.

Finally, isobolograms were constructed for all 4 CB combinations on the 5 cell lines. However, since the results were largely concordant with the two previous methodologies, only the ones for the most erlotinib-sensitive BxPC-3 and most erlotinib-insensitive PANC-1 are presented here.

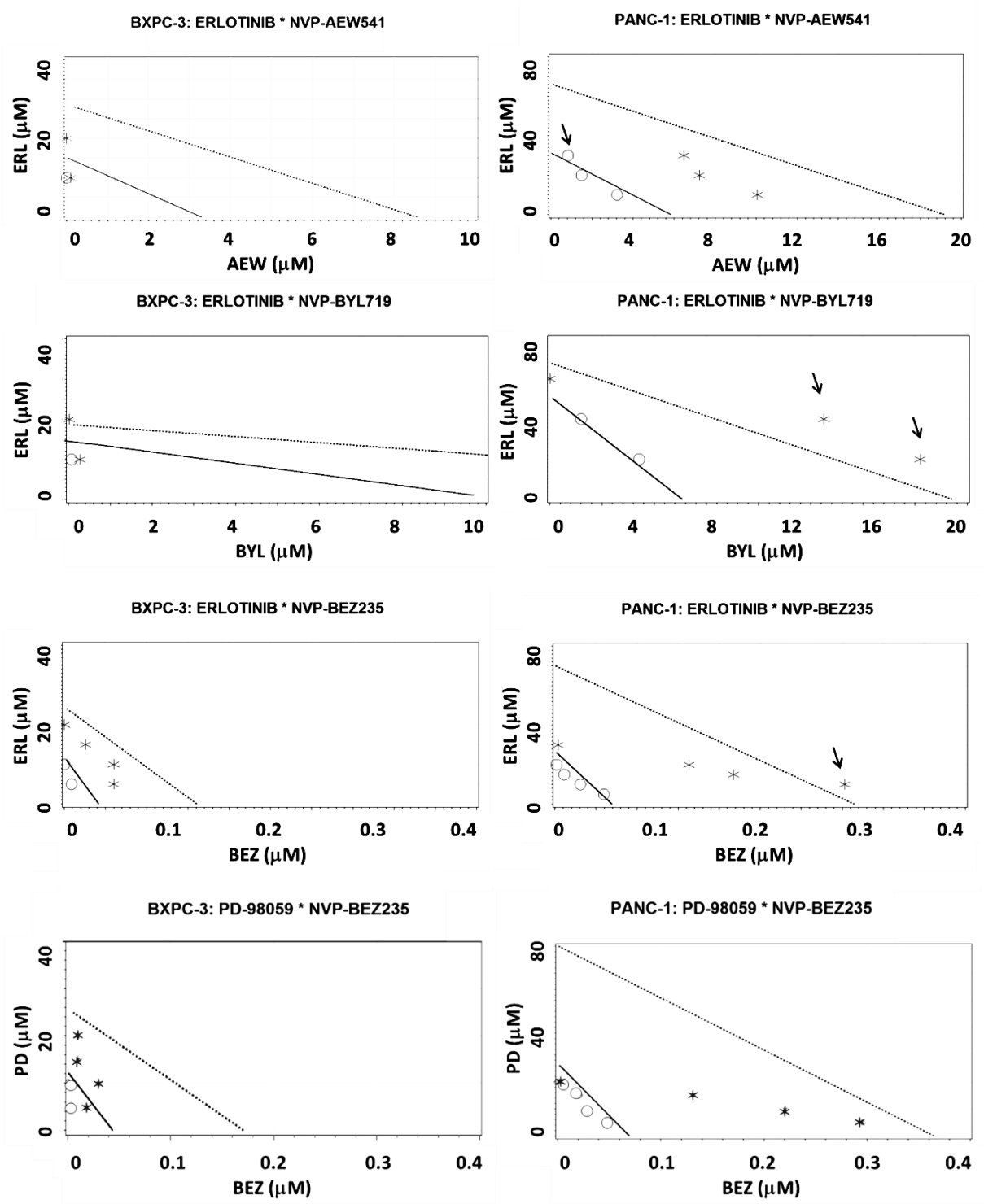

Figure 4.7: Isobolograms of 4 CB combinations in BxPC-3 and PANC-1

In **figure 4.7**, the IC_{50} additivity line was the bolded straight line, and the IC_{75} line was the dotted black line. The circles and stars represented the observed dose sets that were predicted to achieve the same IC_{50} and IC_{75}. They had to be below the bolded straight line and dotted straight line respectively to establish synergy. The black arrows indicated the dose sets

that lied above the additivity line, suggesting antagonism. Notice that the axes are different between BxPC-3 and PANC-1. The Y-axes go up to 40 μM for BxPC-3 and up to 80 μM for PANC-1. The X-axes are also doubled for PANC-1 for the first 2 CB, but are the same for both cell lines for the last 2 BEZ-235 based CB combinations. This is because BEZ remain potent in both cell lines, such that the additivity lines lie appropriately within the axes ranges.

For BxPC-3, the ERL *AEW were very highly synergistic. The observed dose sets were located virtually on the Y-axis. This meant that when this cell line was treated with erlotinib, only very minimal AEW was needed to reach the same IC_{50} that was achieved by SB. Other CB remained synergistic for BxPC-3, since the circles lie below the straight line and stars lied below the dotted line. However, the magnitude of synergy was clearly less than that of the first combination, with these symbols lying further away from the Y-axis.

For PANC-1, the first 3 CB resulted in outlier symbols (above the additivity line) indicating antagonism. The first two isobolograms corresponded well with the S.I. analysis. There was only 1 circle lying above the additivity line for ERL* AEW (S.I. =0.96, just below), whereas there were 2 outliers for ERL* BYL (S.I. =0.85). ERL* BEZ were significantly synergistic in S.I. analysis (1.27), but the isobologram indicates otherwise. PD and BEZ were synergistic for PANC-1 (1.44), which was consistent with the isobologram results.

Overall, then, isobolograms appeared to correspond well with the previous two methodologies with the exception of ERL *BEZ for PANC-1. Here, it must be pointed out that isobologram has a major limitation. Like the raw data first presented, isobolograms here only present a limited view of all the possible dose sets. In this figure, IC_{50} and IC_{75} lines were arbitrarily chosen, but in reality there is an unlimited number of additivity lines that can be selected. S.I. analysis, however, accounts for all possible values, and produces a statistics of significance. Thus, the S.I. remains the most valid and reliable methods of the three.

In summary, the three synergy analyses methods employed were largely concordant, and showed that ERL and IGF1R inhibitor AEW were highly synergistic for BxPC-3 and CFPAC-

1, the two erlotinib-sensitive cell lines. Conversely, these were antagonistic for the highly erlotinib-insensitive MiaPACa-2 and PANC-1. However, when combinations involving downstream PI3K and PI3K/mTOR inhibitors were used, the reverse was true. These combinations were still synergistic for BxPC-3 and CFPAC-1, although less so. On the other hand, these combinations were increasingly synergistic for the erlotinib-insensitive cell line. As discussed previously, the erlotinib-sensitive cell lines – particularly BxPC-3- had a more active upstream receptors (EGFR, IGF1R), whereas MiaPACA-2 and PANC-1 had a highly active downstream MAPK and PI3K/Akt system **(section 3.4)**. This may explain why the downstream CB combinations were much more synergistic in inhibiting the latter two cell lines. From these results, **positive interactions between EGFR and IGF1R were observed in erlotinib-sensitive cell lines, and between EGFR and PI3K or PI3K/mTOR in erlotinib-insensitive cell lines**.

4.2.2.2 Synergy analysis of 4 CB combinations in parent vs. resistant cell lines

Key Finding: ***EGFR and PI3K inhibitors became more synergistic in ER cell lines, suggesting a dominant shift from EGFR-IGF1R interaction to EGFR-PI3K interaction.***

In this next section, the same 6x6 matrix in biological triplicates were performed on ER cell lines, in 4 independent experiments. Synergy of parent versus erlotinib-resistant (ER) cell lines were examined by dose-response surface plots and synergy index only. Isobolograms were not includedin this analysis. ER cell lines, though stably drug-resistant, were subjected to more variability than PDAC cell lines. They were more senile than PDAC cell lines, as they had been sub-cultured over 10 months before frozen, and there was plenty of manipulation and disruption to the environment where these cell lines are grown (changing of medium and drug). In fact, this variability of the ER cell lines between proliferation experiments was reflected by the wide C.I. in the S.I. as shown below. Given all the limitations of isobolograms already discussed, such as variations in assessing synergy based on a number of arbitrary additivity levels, isobolograms are too unreliable to be applied to analysis of ER cell lines. Instead, the

more robust S.I. analysis and the dose response surface plots are presented here **(Figure 4.8)**:

ERLOTINIB * NVP-AEW541

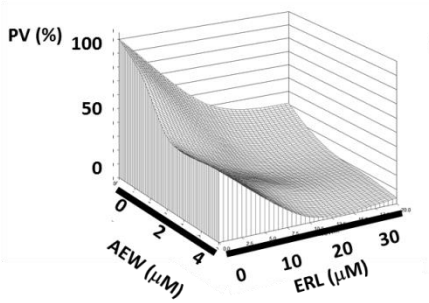

BxPC-3: S.I. = **1.99 (1.43-2.76)**

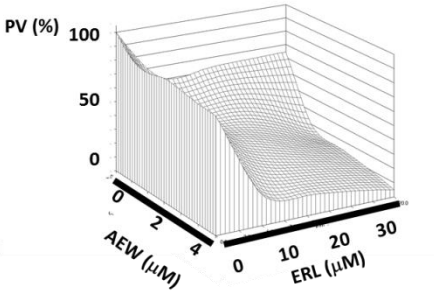

BxPC-ER: S.I. = 1.85 (0.46-7.61)

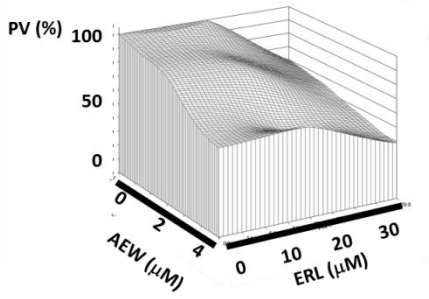

PANC-1: S.I.= 0.96 (0.68-1.37)

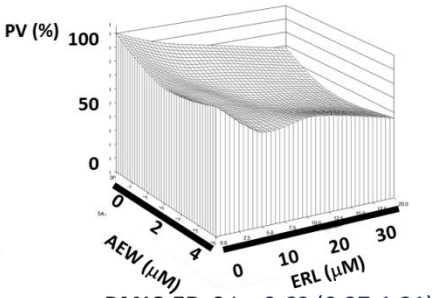

PANC-ER: S.I.= 0.69 (0.37-1.31)

ERLOTINIB * NVP-BYL719

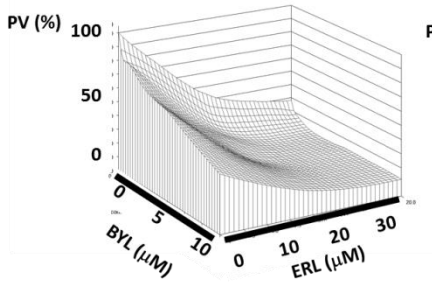

BxPC-3: S.I. = **1.34 (1.17-1.55)**

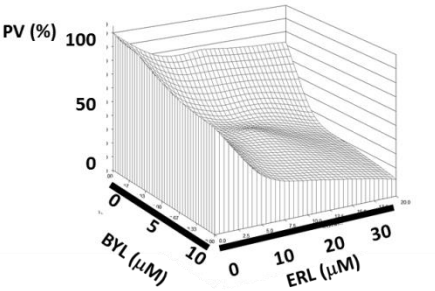

BxPC-ER: S.I. = **1.71 (1.00-2.89)**

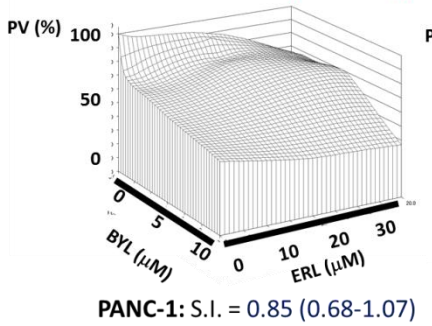

PANC-1: S.I. = 0.85 (0.68-1.07)

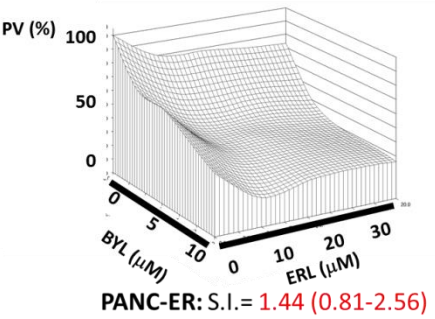

PANC-ER: S.I.= 1.44 (0.81-2.56)

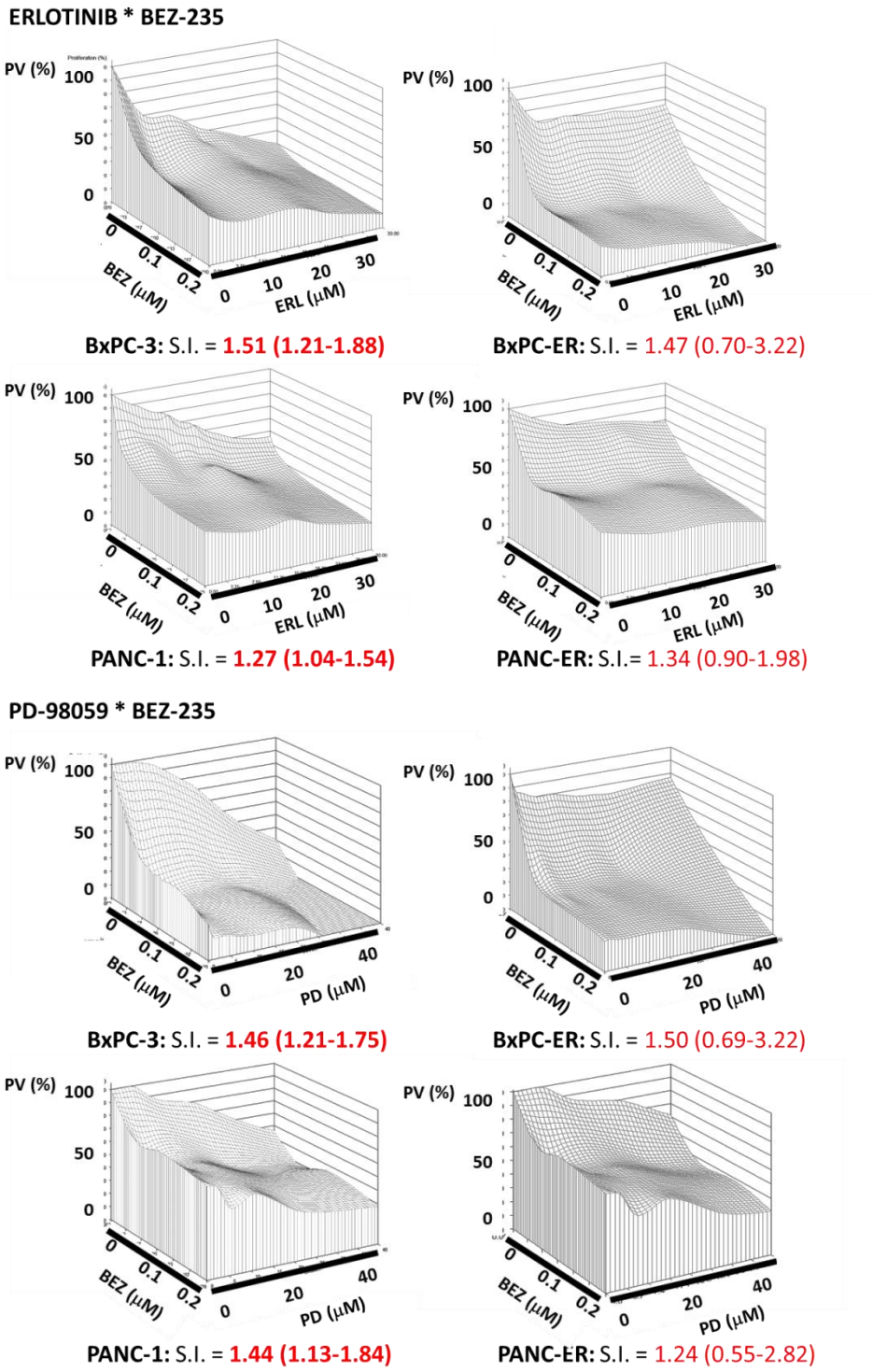

Figure 4.8: Synergy Index and Surface plots for 4 CB combinations in parent versus ER cell lines

First of all, the effect of single drug on ER cell lines can be examined by inspecting the gradient of each axis. By definition, ER cell lines were more resistant to erlotinib compared to parent cell line. This was particularly noticeable in the BxPC-3 versus BxPC-ER comparison, where

the gradient of Z-axis was flat and PV remained high at erlotinib 30μM in BxPC-ER. ER cell lines were also cross-resistant to MEK inhibitor PD and IGF1R inhibitor AEW; but remained moderately sensitive to PI3Kα inhibitor BYL and dual PI3K/mTOR inhibitor BEZ. As for synergy analysis, the S.I. of each pair of parent and resistant cell line was compared. ERL and AEW were synergistic in BxPC-3 [S.I. = 1.99 (1.43-2.76)] and not in PANC-1 [S.I. = 0.96 (0.68-1.37)], as shown previously. The S.I. decreased for both ER cell lines [BxPC-ER: S.I. = 1.85 (0.46-7.61); PANC-ER: S.I. = 0.69 (0.37-1.31)] compared to their parent cell lines. ERL and BYL were synergistic in BxPC-3 [S.I. = 1.34 (1.17-1.55)], but not in PANC-1 [S.I. = 0.85 (0.68-1.07)]. The S.I. for both resistant cell lines increased markedly, with S.I. for BxPC-ER at 1.71 (1.00-2.89)] and for PANC-ER at 1.44 (0.81-2.56). For the last two combinations involving the use of BEZ, both combinations were synergistic across the two pairs of cell lines, and the S.I. were relatively unchanged between parent and ER cell lines. Note, too, that the confidence intervals were much wider in the ER cell lines than the parent cell lines. This reflects the larger inter-experimental variability due to reasons stated above, which was accounted for by the robust S.I. regression model.

To summarise, EGFR and IGF1R inhibitors became less synergistic in the erlotinib resistant cell lines. Conversely, EGFR and PI3K inhibitors became more synergistic. CB using dual PI3K/ mTOR inhibitor were synergistic in ER cell lines, but were not any more or less so than parent cell lines. Thus, it appears that **there was a dominant shift from EGFR-IGF1R interaction to EGFR-PI3K interaction in both acquired erlotinib resistant cell lines.** The fact that the last two CB combinations were equally synergistic in all 4 cell lines, and the fact that CB effect was only slightly more than BEZ-235 alone (X-axes in the last 2 CBs), suggest that it was the main component that exert effect in either CB combination. This drug was likely to be sufficient as a single drug alone, as the dual mechanisms of action in BEZ (PI3Kα and mTOR inhibition) were probably “internally synergistic” in the same drug. Since BEZ was already effective on its own, any drug added to NVP-BEZ235 could only make it a little more

effective. This supports the nanomolar potency observed for this drug on all PDAC and ER cell lines in chapter 3 **(Table 3.2)**.

4.2.2.3 Confluence % by cell imaging proliferation experiments

Key Finding: ***PI3K inhibitors were effective in erlotinib insensitive and resistant cell lines; ER cell lines became "hypersensitive" to PI3K-inhibitor based combined blockade***

The previous synergy analyses, although detailed, were based on one type of experiment- the MTT cell proliferation assay. MTT assay is a widely used cell viability assay, but results can be potentially interfered by compounds that contain polyphenolic hydroxyl groups, culture media types and filter sets.[318] Furthermore, the results of MTT are only semi-quantitative, expressed as proportional viability percentage to control; and are based on measurement of a single time point (72 hours).[319] Since synergy analysis is one of the vital components of this project, a second method was used to validate the MTT assay. The confluence study by the incucyte live imager (Essen Bioscience) was chosen, as this is essentially a time-lapsed microscopy system that allows semi-quantitation of proliferation based on confluence. This system has been increasingly used in cancer research in the last few years.[320-322]

In this experiment, one dose set was selected for each combination, based on the relative equipotency between each drug alone as measured by the MTT assay: ERL 10μM and AEW 1μM (designated as E10A1), ERL 10μM and BYL 5μM (E10Y5), ERL 10μM and BEZ 0.1μM (E10B0.1) and PD 10μM and BEZ 0.1μM (P10B0.1). The first set of experiment compared single blockade (SB) versus CB for the first two combinations. The second set of experiment compared all 4 CB combinations. The cell lines tested were the two pairs of parent versus resistant cell lines. Confluence was measured over 70 hours in 4 experiments; the trend of the average values and its standard errors are presented below.

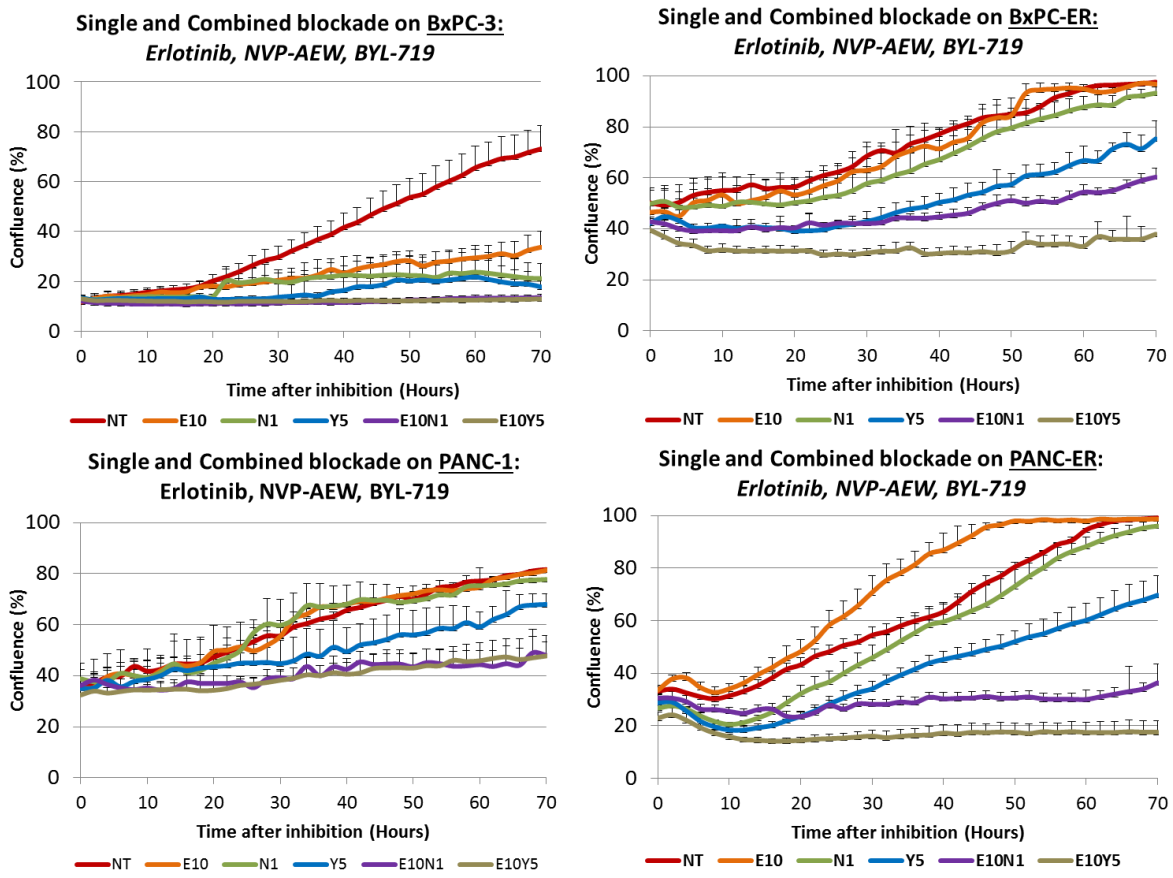

Figure 4.9: Confluence % as measured by Incucyte for erlotinib, NVP-AEW541 and NVP-BYL719, alone or in combination in parent versus resistant cell lines.

In this first set of experiments, a differential response to SB and CB was immediately obvious in the ER compared to parent cell lines, as demonstrated by the divergent plots **(Figure 4.9)**. BxPC-3 had high sensitivity and PANC-1 had low sensitivity to erlotinib as a single drug. Upon treatment with erlotinib 10 µM, there was marked reduction in cell density of BxPC-3 compared to control (orange versus red lines), but no reduction for PANC-1. Importantly, BxPC-ER showed resistance to erlotinib, and PANC-ER was actually growth-stimulated by erlotinib compared to control. In response to other single agents, PANC-1 as well as both acquired ER cell lines showed cross-resistance to AEW (green), but was moderately sensitive to BYL (blue). Whilst both CB (purple and grey) were more effective than SB, in both ER cell lines ERL* BYL showed the most substantial suppression in cell proliferation, and was the only treatment strategy that was clearly cytostatic in all four cell lines.

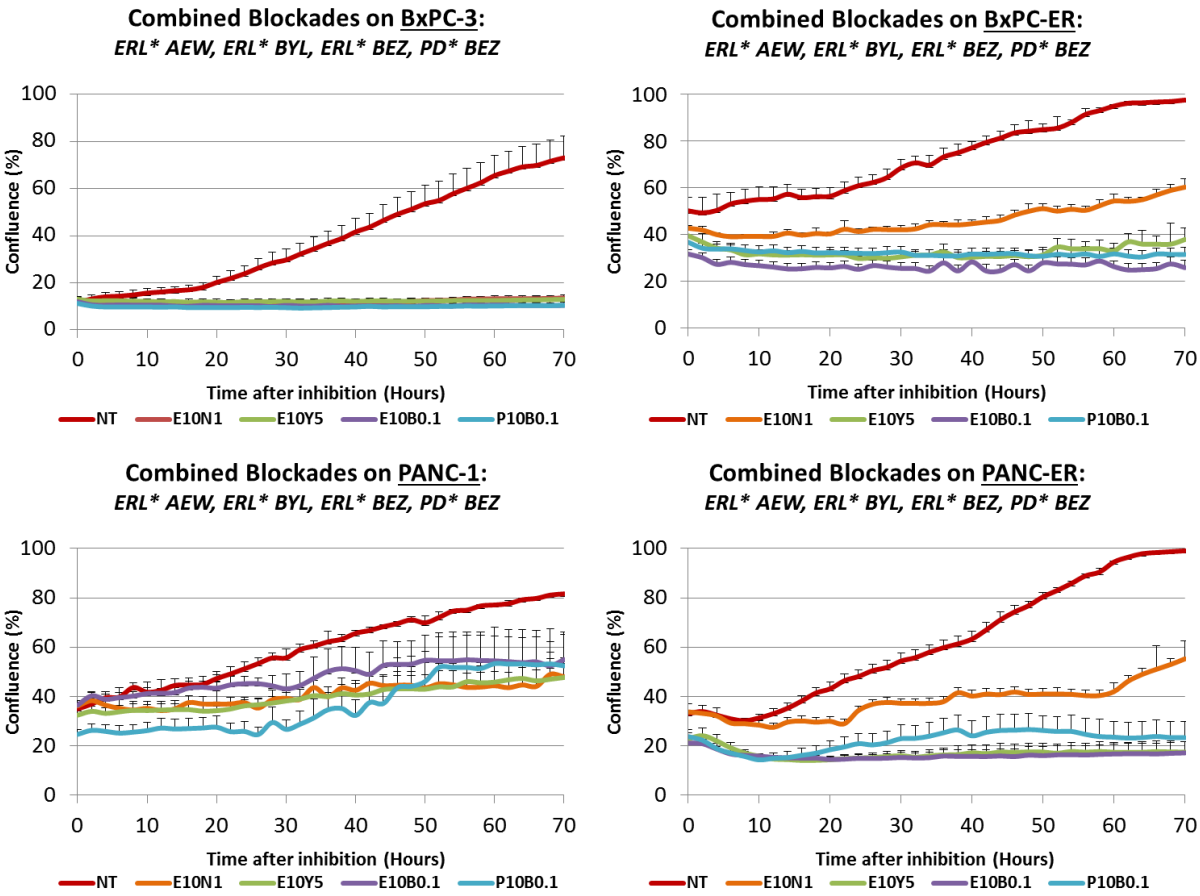

Figure 4.10: Confluence % as measured by Incucyte for 4 CB combinations in parent versus resistant cell lines.

In the second set of experiments, the 4 CB combinations were compared. Although ERL and AEW were previously shown to be more synergistic than other combinations in BxPC-3, the absolute measure of confluence% was completely suppressed by all 4 combinations in BxPC-3. This suggested that synergy is merely a measure of interaction, not efficacy. For PANC-1, there were some increase in confluence with all 4 combinations over 70 hours, but the change was still less than that of control. Whilst all 4 combinations exhibited a similar pattern of cell proliferation suppression in the parent cell lines, the ER cell lines responded to the CB combinations in a different pattern. Once again, both ER cell lines were only moderately sensitive to the EGFR and IGF1R co-inhibition (orange lines), but were sensitive to the other 3 combinations that utilised a PI3K inhibitor or dual PI3K/mTOR inhibitor (blue, purple and grey lines). Importantly, whilst these 3 combinations had a suppressed proliferation in PANC-

1 compared to control, these induced complete cytostaticity on BxPC-ER and PANC-ER. This indicates that ER cell lines exhibited a hyper-sensitivity to CB based on a PI3K or PI3K/mTOR inhibitor.

In summary, PI3K or PI3K/mTOR inhibitors were clearly active in both erlotinib insensitive or resistant cell lines. **While ER cell lines became moderately insensitive to IGF1R plus EGFR inhibitors, they remained sensitive or even became hypersensitive to PI3K based combined blockade.** This is supported by the synergy analyses that dmonstrated a shift from dominant EGFR/ IGF1R interaction to EGFR/ PI3K interaction in ER cell lines. Therefore, these results validated and reinforced the results of the MTT assay.

So far, only cytotoxic synergy was explored at this stage. To fully understand the mechanism of this synergy, the molecular mechanisms of action of this synergy needed to be examined. In the next sub-section, the western blotting results of PDAC cell lines in response to combined blockade are described.

4.2.3 Study of Molecular Synergy by western blotting

In this part of the project, the differential response of PDAC cell lines to combined blockade (CB) versus single blockade (SB) was first established, and then the 4 CB were compared. The membranes were blotted for key tyrosine kinase receptors/ signalling proteins of the EGFR, MAPK and PAM pathways, as suggested from the results in chapter 3. These included EGFR, ERK, Akt, S6 and 4EBP1, the second effector of mTOR (the first being S6). Both total and phosphorylated proteins were studied. Three independent experiments were performed for each comparison unless otherwise specified.

4.2.3.1 Optimisation of EGF/ IGF stimulation in BxPC-3 and PANC-1

***Key Finding*: Significant cross talk of EGF- Akt and IGF- ERK in the erlotinib-insensitive PANC-1**

In the initial optimisation experiment, it needed to determine if drug inhibition studies should be accompanied by EGF, IGF or both. ERL* BYL was used as the CB combination in these optimisation experiments. Cell lines were treated with inhibitor SB or CB for 60 minutes and then stimulated with EGF or IGF alone for 10 minutes, so that the effect of a particular growth factor could be easily discerned. The cell lines used for optimisation were BxPC-3 and PANC-1. Protein quantification was not done so the two cell lines were not directly comparable. This experiment was repeated twice.

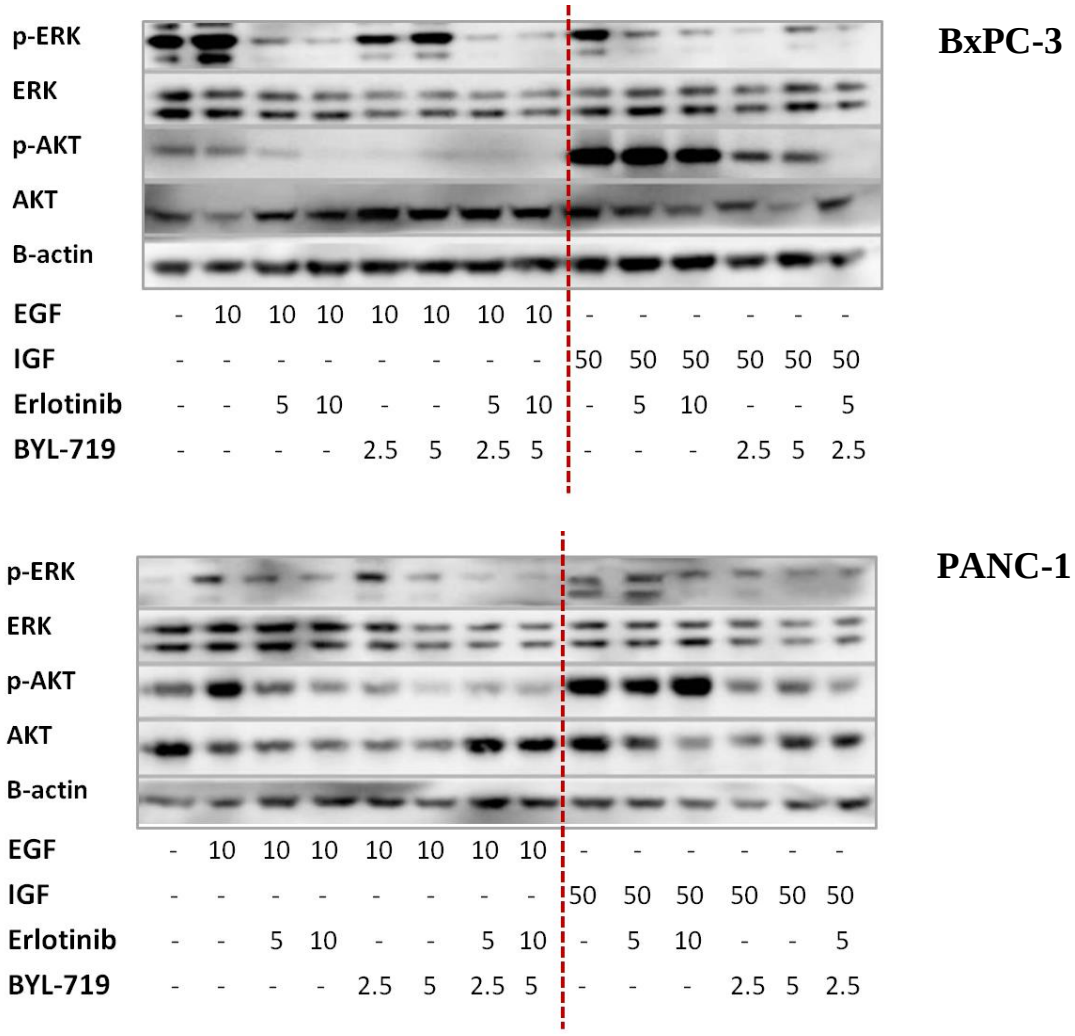

Figure 4.11: Optimisation of EGF or IGF growth factors stimulation in SB and CB studies

Consistent with the previous findings in **sub-section 3.4.2**, extensive cross-talk was found between EGF-pAkt and IGF-pERK with PANC-1 but not in BxPC-3. BxPC-3 followed a strict classical cascade, where EGF predominantly stimulated ERK and IGF predominantly stimulated Akt. PANC-1, on the other hand, was capable of stimulating ERK and Akt in response to either EGF or IGF. Erlotinib was able to strongly inhibit ERK and also EGF-stimulated Akt, but was not so good in inhibiting IGF-stimulated pAkt. BYL was also able to suppress its intended target Akt as well as IGF-stimulated pERK, but was less potent in inhibiting EGF-stimulated pERK. SB inhibition of downstream targets was therefore incomplete. The two drugs together were able to inhibit both ERK and Akt more strongly than either drug alone, even at erlotinib 5μM plus BYL719 2.5μM (low dose), suggesting positive interaction or "molecular synergy" in both cell lines. Thus, in this optimisation experiment **EGF appears to have a stronger influence on pERK, and IGF on pAkt.** In subsequent experiments, the cells were stimulated with EGF if they were treated with EGFR or MEK inhibitor; IGF if they were treated with PI3K or PI3K/mTOR inhibitor; and both EGF and IGF for CB treatment. This was done so that there would remain strong signals for different CB combinations to be compared with each other. Also, there was an early indication that regardless of the cross-talk mechanism of the two cell lines, CB appeared to be an effective strategy that was superior to single agent alone.

4.2.3.2 Combined blockade of 4 inhibitor Combinations in BxPC-3 and PANC-1

***Key Finding*: CB was able to prevent paradoxical activation of alternate pathways that was observed in SB. CB combinations that included the dual PI3K/mTOR inhibitor NVP-BEZ235, appeared to be more effective than other combinations.**

To compare between the 4 CB combinations, cell lines were treated with erlotinb (0, 5, 10, 20μM), NVP-AEW541 (0, 0.5, 1, 2μM), NVP-BYL719 (0, 2.5, 5, 10μM), NVP-BEZ235 (0, 0.05, 0.1, 0.2μM), and PD-98059 (0, 5, 10, 20μM), alone or in combination. These doses were chosen based on previous western blotting experiments on single drug alone. Each cell line

was loaded in a 15-well gel for ERL* AEW and ERL* BYL and 12-well gel for ERL* BEZ and PD* BEZ. For consistency, the samples were loaded in the following way for the first two combinations: no treatment, EGF alone followed by graded concentration of drug A with EGF, IGF alone followed by graded concentration of drug B with IGF, and then EGF plus IGF followed by both drugs in the same graded concentration with EGF and IGF. For the latter two combinations, the experiment was abbreviated (only BEZ SB was tested against ERL* BEZ, and only PD was tested against PD* BEZ) to avoid repetition. All membranes were immunoblotted for phosphorylated and total EGFR, ERK, Akt and S6. In addition, the ERL* AEW was also blotted for IGF1R, since NVP-AEW541 was an IGF1R inhibitor and it needed to be shown whether the inhibitor was acting on its intended target.

Because of the sheer number of permutations of drug inhibition and stimulation combination experiments, it was not possible to test CB on all 5 PDAC cell lines. Instead, BxPC-3 was chosen to represent erlotinib sensitive cell lines, and PANC-1 to represent erlotinib insensitive cell lines. Representative blots of 3 experiments each were shown below:

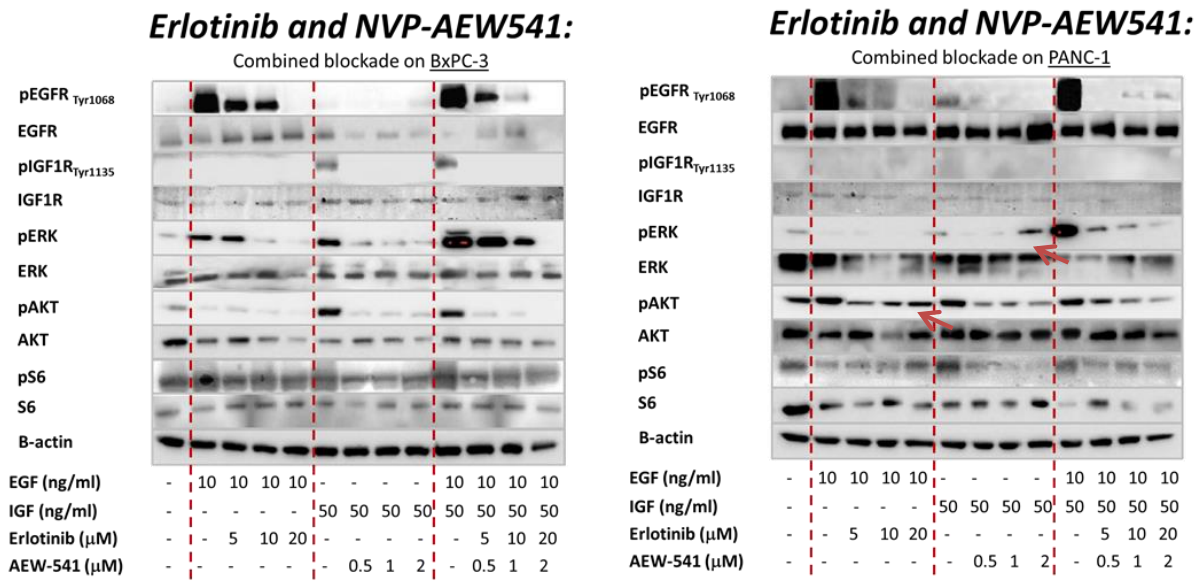

Erlotinib and BYL-719:

Combined blockade on BxPC-3

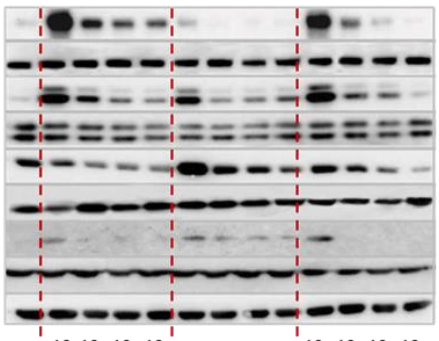

EGF (ng/ml)	-	10	10	10	10	-	-	-	-	10	10	10	10
IGF (ng/ml)	-	-	-	-	-	50	50	50	50	50	50	50	50
Erlotinib (μM)	-	-	5	10	20	-	-	-	-	-	5	10	20
BYL-719 (μ M)	-	-	-	-	-	-	2.5	5	10	-	2.5	5	10

Erlotinib and BYL-719:

Combined blockade on PANC-1

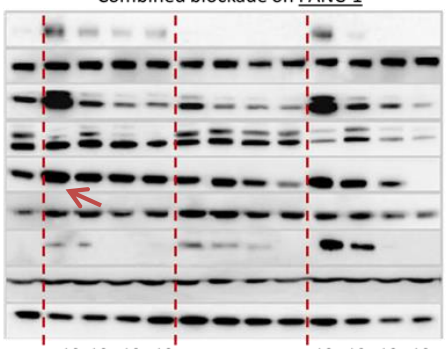

EGF (ng/ml)	-	10	10	10	10	-	-	-	-	10	10	10	10
IGF (ng/ml)	-	-	-	-	-	50	50	50	50	50	50	50	50
Erlotinib (uM)	-	-	5	10	20	-	-	-	-	-	5	10	20
BYL-719 (uM)	-	-	-	-	-	-	2.5	5	10	-	2.5	5	10

Erlotinib and BEZ-235:

Combined Blockade on **BxPC-3**

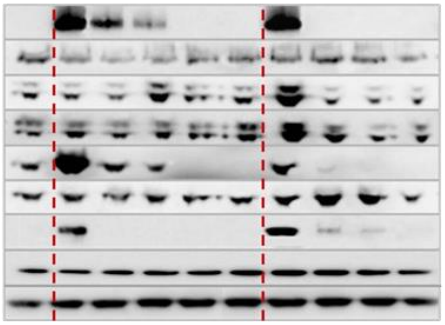

EGF (ng/ml)	-	-	-	-	-	-	10	10	10	10	-	-	-	-	-	-	10	10	10	10
IGF (ng/ml)	-	50	50	50	50	50	50	50	50	50	-	50	50	50	50	50	50	50	50	50
Erlotinib (μM)	-	-	-	-	-	-	-	5	10	20	-	-	-	-	-	-	-	5	10	20
BEZ-235 (nM)	-	-	10	50	100	200	-	50	100	200	-	-	10	50	100	200	-	50	100	200

Erlotinib and BEZ-235:

Combined Blockade on **PANC-1**

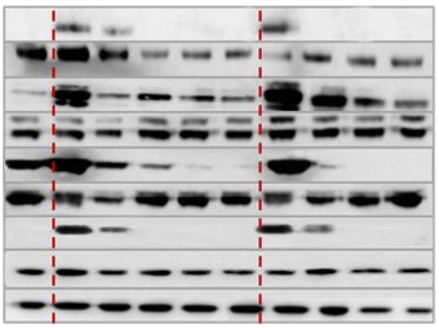

EGF (ng/ml)	-	-	-	-	-	-	10	10	10	10	-	-	-	-	-	-	10	10	10	10
IGF (ng/ml)	-	50	50	50	50	50	50	50	50	50	-	50	50	50	50	50	50	50	50	50
Erlotinib (μM)	-	-	-	-	-	-	-	5	10	20	-	-	-	-	-	-	-	5	10	20
BEZ-235 (nM)	-	-	10	50	100	200	-	50	100	200	-	-	10	50	100	200	-	50	100	200

PD-98059 and BEZ-235:

Combined Blockade on **BxPC-3**

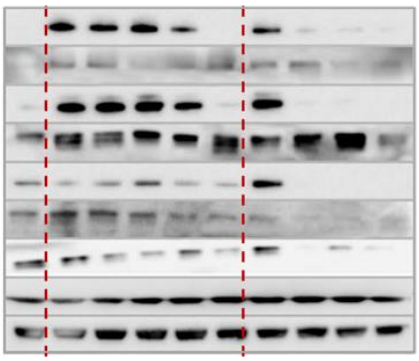

EGF (ng/ml)	-	10	10	10	10	10	10	10	10	10	10	-	-	-	-	-	-	10	10	10	10
IGF (ng/ml)	-	-	-	-	-	-	-	50	50	50	50	-	50	50	50	50	50	50	50	50	50
PD-98059 (μM)	-	-	1	2.5	5	10	20	-	2.5	5	10	-	-	1	2.5	5	10	20	-	2.5	5	10
BEZ-235 (nM)	-	-	-	-	-	-	-	-	50	100	200	-	-	-	-	-	-	-	-	50	100	200

PD-98059 and BEZ-235:

Combined Blockade on **PANC-1**

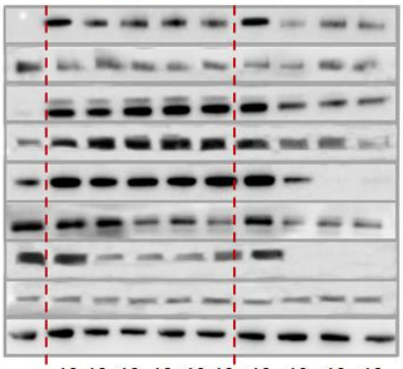

EGF (ng/ml)	-	10	10	10	10	10	10	10	10	10	10	-	-	-	-	-	-	10	10	10	10
IGF (ng/ml)	-	-	-	-	-	-	-	50	50	50	50	-	50	50	50	50	50	50	50	50	50
PD-98059 (μM)	-	-	1	2.5	5	10	20	-	2.5	5	10	-	-	1	2.5	5	10	20	-	2.5	5	10
BEZ-235 (nM)	-	-	-	-	-	-	-	-	50	100	200	-	-	-	-	-	-	-	-	50	100	200

Figure 4.12: Representative blots for SB versus CB for 4 combinations in BxPC-3 and PANC-1

To summarise the exceedingly large amount of information from these 8 representative blots, emphasis was first placed on two dose-response experiments for ERL, AEW and BYL, alone or in combination. In BxPC-3, ERL, AEW and BYL appropriately reduced EGF-stimulated pERK and IGF-stimulated pAkt signals as single agents. CB using either drug in combination with ERL on this cell line was capable of near-complete inhibition of pERK and pAkt in the presence of both EGF and IGF. In PANC-1, however, pAkt was either unaffected or paradoxically increased by ERL, whereas pERK increased after exposure of higher dose of AEW (2μM) (red arrows). Only BYL appropriately decreased downstream signals. The paradoxical effects observed in this cell line were abolished by CB with either AEW or BYL together with ERL, resulting in monotonic inhibition of both pERK and pAkt. Both CB combinations also diminished pS6 in both cell lines; but the ERL* BYL CB appeared to be superior in complete inhibition of this signal. Yet, even at the high dose of ERL 20μM and BYL 10μM, downstream signals did not completely disappear, but were only attenuated.

The last two combinations were interesting because both consisted of the dual PI3K/ mTOR inhibitor BEZ. This drug certainly appeared to hit the intended targets PI3K and mTOR, resulting in diminishing of AKT and disappearing of S6 (downstream of mTORC1) at a dose as low as 10nM. On the other hand, PD was not a very good MEK inhibitor. It only began to decrease ERK (downstream of MEK) at 10 μM for BxPC-3, whilst PANC-1 was completely resistant to its effect on ERK. Despite the fact that PD was inferior to erlotinib in inhibiting the downstream MAPK pathway, either drug combined with BEZ resulted in some reduction in pERK signals in addition to disappearing of pAKT and pS6 in both cell lines. This confirmed the potency of BEZ by itself or in combination with EGFR or MEK inhibitor. Thus, this experiment established the CB as a strategy to overcome cancer cells that have significant cross talk and multiple active pathways, and demonstrate the superiority of CB of downstream targets of EGFR/ MAPK and PAM pathways.

4.3.2.3 Synergy Analysis of 4 CB Combinations in BxPC-3 and PANC-1

***Key Finding*: EGFR and PI3K inhibitors positively interact at the level of S6, downstream of PI3K/mTOR, particularly in ER cell lines. This confirms the up-regulation of PAM pathway in ER cell lines, and supports the strategy of CB to overcome erlotinib resistance.**

Raw data are particularly difficult to interpret in western blotting experiments, because no two blots are the same, and it is difficult to visually detect small differences in signals. To attempt at synergy analysis on western blots, the signal changes were first quantified using multigauge v3.0 a pixel density calculator. Phosphorylated signals were measured in 3 independent experiments, and corrected against total protein (or β-actin in the setting where total protein exposure was inadequate). Since these experiments were performed in a dose response configuration, an IC_{50} for protein inhibition could be calculated by fitting a regression curve after pooling all experiments (SAS 9.2). IC_{50} of CB was calculated in the same way as SB, since both drugs doubled in dose in each dose escalation, but was reported as drug A [X μM] + drug B [y μM]. The averages of all IC_{50} for the key downstream signals pERK, pAkt and pS6 (in μM) for SB and CB as dosing sets were shown below:

E+A	(uM)	ERL	AEW	ERL*AEW_E	ERL*AEW_A	E+N	(uM)	ERL	AEW	ERL*AEW_E	ERL*AEW_A
BxPC-3	pERK	17.06	3.91	13.03	1.303	PANC-1	pERK	16.0	NR	18.97	1.9
	pAKT	39.3	0.613	8.39	0.839		pAKT	67.60	0.552	19.4	1.94
	pS6	30.93	0.239	53.52	0.535		pS6	53.25	0.121	31.64	0.316
E+Y	(uM)	ERL	BYL	ERL*BYL_E	ERL*BYL_Y	E+Y	(uM)	ERL	BYL	ERL*BYL_E	ERL*BYL_Y
BxPC-3	pERK	17.06	25.27	11.67	5.83	PANC-1	pERK	16.0	22.84	26.76	13.38
	pAKT	39.3	1.50	15.77	7.88		pAKT	67.60	4.56	20.4	10.2
	pS6	30.93	42.71	18.75	9.37		pS6	53.25	36.95	24.62	12.31
E+B	(uM)	ERL	BEZ	ERL*BEZ_E	ERL*BEZ_B	E+B	(uM)	ERL	BEZ	ERL*BEZ_E	ERL*BEZ_B
BxPC-3	pERK	17.06	0.286	9.13	0.091	PANC-1	pERK	16.0	0.586	17.92	0.179
	pAKT	39.3	0.215	10.93	0.109		pAKT	67.60	0.109	12.89	0.129
	pS6	30.93	0.164	8.06	0.081		pS6	53.25	0.313	12.93	0.129
P+B	(uM)	PD	BEZ	PD*BEZ_E	PD*BEZ_B	P+B	(uM)	PD	BEZ	PD*BEZ_E	PD*BEZ_B
BxPC-3	pERK	12.03	0.286	7.71	0.193	PANC-1	pERK	NR	0.586	NR	NR
	pAKT	15.19	0.215	9.00	0.225		pAKT	49.17	0.109	31.3	0.78
	pS6	13.80	0.164	5.17	0.13		pS6	5.92	0.313	5.41	0.16

Table 4.4: IC_{50} of single blockade and combined blockade in BxPC-3 and PANC-1. *E+A denotes ERL*AEW; E+Y ERL* BYL; E+B ERL* BEZ; P+B PD* BEZ,. NR "not reached".*

While there was too much data here to go through one by one, there were a number of general observations that could be made. Firstly, in general, each inhibitor was the most potent for inhibiting its direct downstream target (red bolded), as indicated by the lowest IC_{50}. The notable exceptions were AEW, which appeared to reduce pS6 (further downstream) more effectively than pAkt; and PD, which was not able to suppress pERK signal at all in PANC-1 (NR), as mentioned previously. Secondly, PANC-1 was more resistant to have off-targets inhibited than BxPC-3. For example, the IC_{50} of Akt inhibition by erlotinib was estimated to be 39.3 μM in BxPC-3 but 67.6 μM in PANC-1. This also occurred in other inhibitors including pERK for BEZ (0.586 vs. 0.286 μM) and pAkt for PD (15.19 vs. 49.17 μM). This supported the previous study of PANC-1 as a cell line with multiple switched-on pathways and significant cross talks between pathways. Thirdly, regarding combined blockade, the effect of combined treatment was not very effective for EGFR/ IGF1R co-inhibition, but progressively became more effective with downstream inhibitions in the other combinations. For instance, in BxPC-3, the pERK inhibition IC_{50} for erlotinib was 17.06μM and for AEW 3.91μM, but the combined IC_{50} dosing set was only erlotinib 13.03μM and AEW 1.3μM. That is, the CB had only dropped IC_{50} of erlotinib by 25%. By combining erlotinib with BYL or BEZ, the IC_{50} of the erlotinib component in the CB was able to be reduced by 32% (erlotinib 11.67μM plus 5.83μM BYL) and 47% (erlotinib 9.13μM plus 91nM BEZ) respectively (red arrows). In other words, less erlotinib was required when combined with downstream inhibitors to achieve the same IC_{50}. That said, this occurred in BxPC-3 but did not appear to be the case for erlotinib insensitive PANC-1. Hence, the presence of a inhibitor of downstream targets appeared to assist erlotinib in gain better control of its key targets in cell lines already sensitive to erlotinib, but was not able to do so for erlotinib insensitive cell line. To confirm these findings, synergy analysis of these molecular signals was measured.

In assessing synergy for western blotting experiments, it needs to be noted that it was impossible to design a 6x6 matrix as in the case for cell proliferation experiments. Also, the

only quantitative data attained in western blotting was IC_{50}. For these reasons, isobolograms were the only appropriate method for assessing synergy here. There were, however, some minor differences between these isobolograms to the ones shown in cell proliferation. Firstly, only one estimated dose set for CB was produced from these western blotting experiments. Secondly, synergy was suggested when estimated dose set lay below the additivity line; but antagonism was not necessarily suggested when observed dose set lay above the additivity line. This is because of the difference in growth factor stimulation between SB and CB. In SB, either EGF or IGF stimulation was used; in CB, both EGF and IGF stimulation were used. Thus, the estimated dose sets could be above the additivity line simply due to more growth factor stimulation, instead of antagonism between two drugs. With this in mind, the isobolograms are now presented for pERK, pAkt and pS6 inhibition:

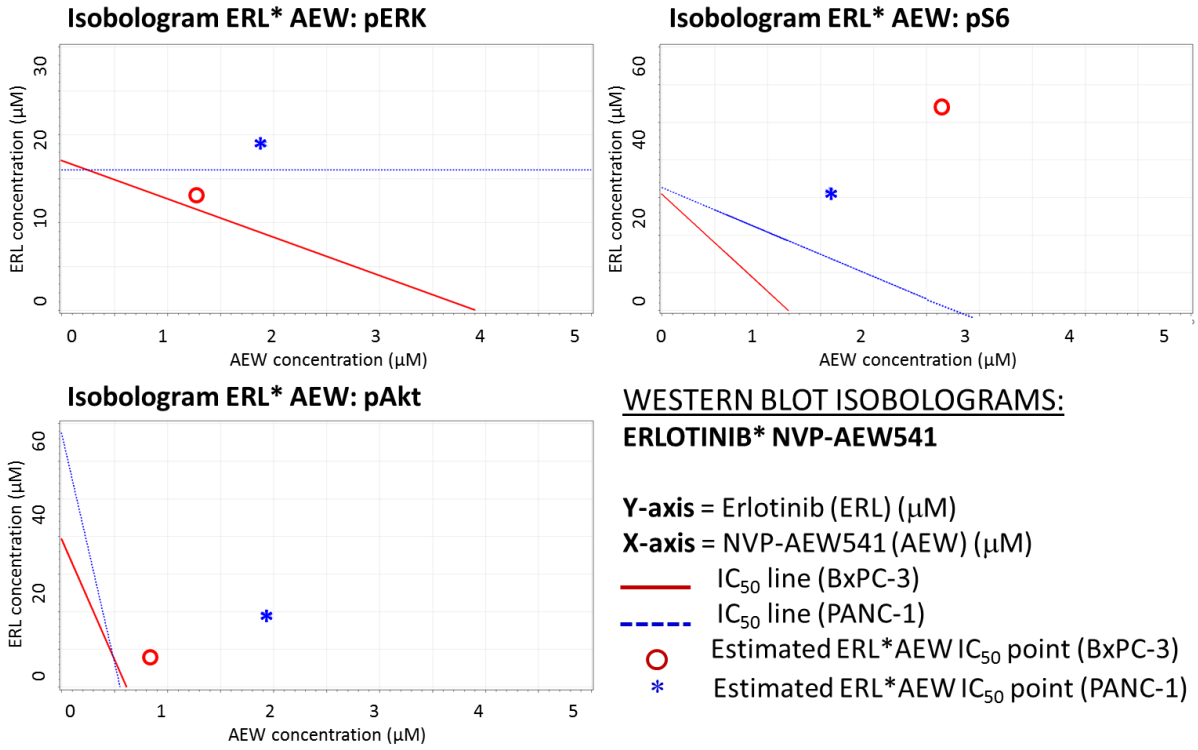

Isobologram ERL* BYL: pERK

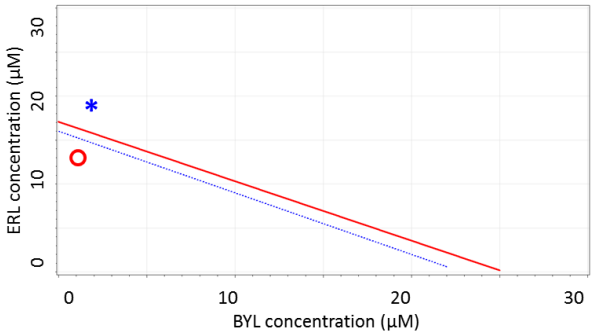

Isobologram ERL* BYL: pS6

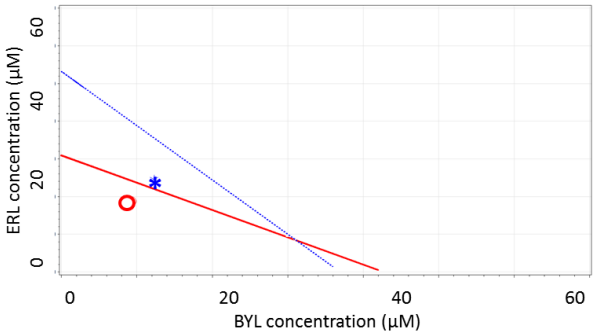

Isobologram ERL* BYL: pAkt

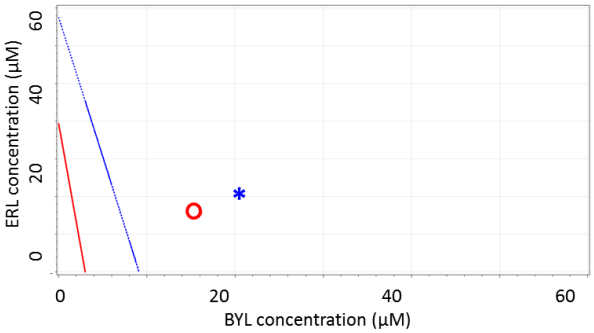

<u>WESTERN BLOT ISOBOLOGRAMS:</u>

ERLOTINIB* BYL-719

Y-axis = Erlotinib (ERL) (µM)

X-axis = NVP-BYL719 (BYL) (µM)

IC_{50} line (BxPC-3)

IC_{50} line (PANC-1)

Estimated ERL*BYL IC_{50} point (BxPC-3)

Estimated ERL*BYL IC_{50} point (PANC-1)

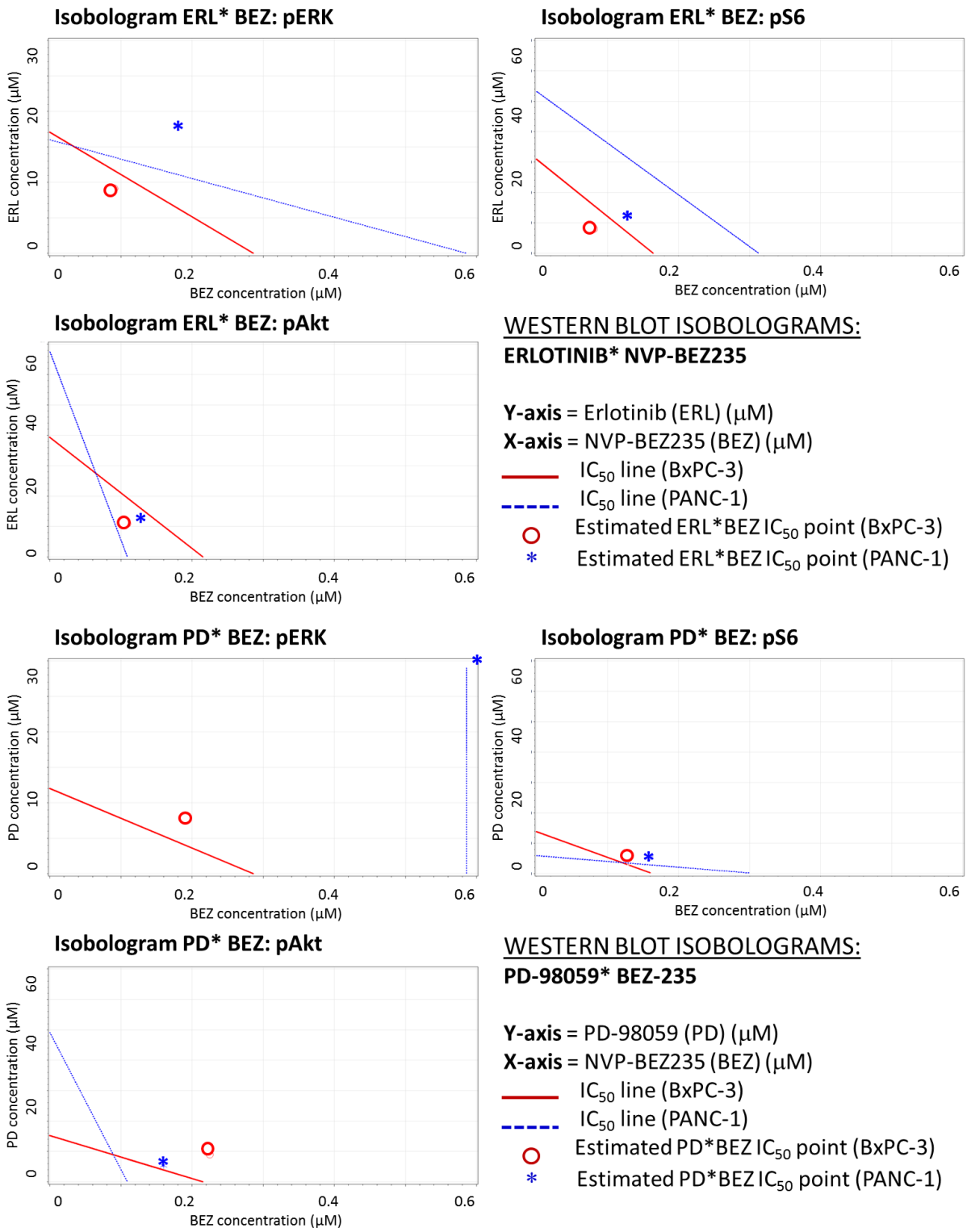

Figure 4.13: Isobolograms for 4CB combinations in BxPC-3 and PANC-1

Regarding to SB of individual drugs, AEW and BEZ were more potent than ERL, PD and BYL. The IC_{50} axes of the former 2 drugs ranged from 0.6 to 5 μM, whereas the latter 3 drugs ranged from 30 to 60 μM. Yet, this could simply relate to the potency of the drugs and affinity to the

targets, and did not necessarily indicate drug resistance. What was more suggestive of drug resistance was when the additivity line appeared as either vertical or horizontal lines, as in the case of the pERK line on PANC-1 for the PD* BEZ isobologram. In this example this means that all tested doses of PD did not inhibit pERK, and IC_{50} for pERK could not be reached for this drug.

The CB isoblograms were studied next. For the ERL* AEW combination, all estimated IC_{50} dose sets for both cell lines lied above the respective additivity line. As discussed before, synergy was not present, but this did not necessarily indicate antagonism. That said, comparing between pERK, pAkt and pS6 isobolograms, the estimated dose sets for pERK were closer to the additivity lines than pAkt and pS6 signals. In the second combination (ERL* BYL), pERK estimated IC_{50} point was also much closer to the additivity line than the pAKT estimated IC_{50} point. In addition, the two drugs were synergistic for inhibiting pS6 signal in both cell lines. In the third combination (ERL* BEZ), the two drugs were also synergistic for inhibiting pS6 signal. Further, the observed IC_{50} point also moved much closer to the additivity line than the previous combinations, suggesting greater synergism. Finally, in the fourth combination, “molecular synergism” was particularly difficult to assess since PD was found to inhibit pS6 much more strongly than erlotinib as a single agent, but was unable to suppress its intended pERK target in PANC-1. Taken altogether, pS6 appeared to be the point of synergism for ERL plus BYL or BEZ.

To assess the previous speculation about the synergistic role of downstream inhibitors with erlotinib in overcoming basal autonomic downstream MAPK pathway activation in erlotinib sensitive cell lines, pERK synergism among the first three combinations was studied in greater detail. In contrast to ERL plus AEW, ERL plus BYL or BEZ were indeed synergistic in BxPC-3 (indicated by the red circle below red line). This, however, did not occur in PANC-1, as all estimated IC_{50} dose sets lied above the additivity line. Overall, this is consistent with the analysis of the crude analysis of the raw data in **Table 4.4**.

In conclusion, erlotinib was more synergistic with downstream than upstream inhibitors. ERL* BEZ was the most synergistic, followed by ERL* BYL, and lastly the ERL* AEW. Synergism of PD plus BEZ235 could not be formally assessed, since PD-98059 behaved as a very different inhibitor than erlotinib. **The level of interaction was located downstream at Akt-driven S6 for both cell lines, and also at ERK for the erlotinib-sensitive BxPC-3.** Altogether, cell proliferation and western blotting experiments demonstrated synergistic activity between erlotinib and PI3K or PI3K/mTOR inhibitors; suggesting the important interaction of EGFR and PI3K/ mTOR in PDAC cell lines.

4.3.2.3 Comparison of CB combinations in parent versus resistant cell lines

Key Finding: ***CB appeared more effective in inhibiting downstream signals in ER cell lines compared to SB. In particular, CB using PI3K or dual PI3K/mTOR inhibitor appeared more effective in ER cell lines.***

In the previous sub-sections, there was a heavy emphasis on using synergy analysis. However, synergy analysis was not possible in comparing CB combinations between parent and ER cell line. To obtain isobolograms in a way that could be comparable between parent and resistant cell lines, each pair of the parent and ER cell lines needed to be loaded in the above format (14 samples each) in one single gel, so that IC_{50} for SB and CB could be simultaneously produced for both cell lines. To do this, a 29 sample loading gel (including 1 lane for marker) would be required as a minimum, but there were no customized gels that had this many loading wells. If the cell lines were loaded in different gels, even if the protein concentration was adjusted, the signals between each cell line pairs may remain incomparable due to inter-blot variability.

Thus, rather than insisting on performing synergy analysis with the associated issues, two simple experiments for CB combination were performed instead. In the first set of experiment, the effect of SB versus CB was examined in a chosen combination (ERL * BYL). In the second

set of experiment, the different CB were compared in the ER versus parent cell lines. To allow for SB and CB to be compared, cell lines were all treated with EGF alone without IGF. The order for the sample loading was no treatment (NT), EGF alone, Erlotinib 20M, BYL-719 10μM, and combined erlotinib and BYL-719 (5 samples) in the first experiment. Each pair of parent and resistant cell lines were loaded together (total 10 samples) in a 12-well gel (2 markers on the side) to allow for valid comparisons. All previous downstream signals (ERK, Akt, S6) plus another mTOR1 target (4E-BP1) were explored:

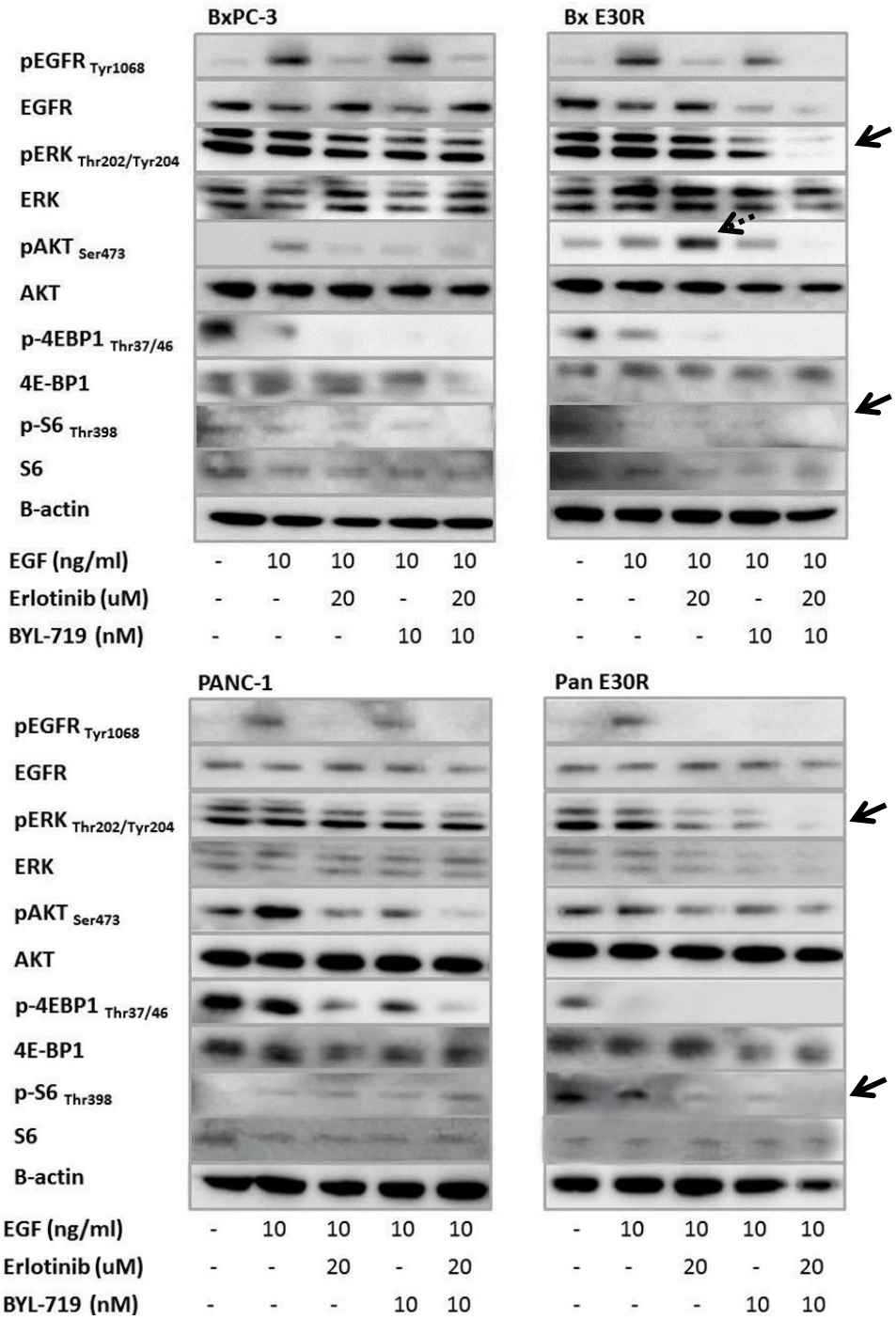

Figure 4.14: Representative blot of CB versus single blockade in parent versus resistant cell lines

Comparing parent and ER cell lines at baseline, there appeared higher pS6 signals in BxPC-ER and PANC-ER than BxPC-3 and PANC-1, though the signals were very faint indeed. On the other hand, p4EBP1 appeared lower in BxPC-ER and PANC-ER. This confirmed phospho-RTK array results earlier that the ER cell lines transduced PI3K/Akt growth signals down S6, and here it was shown that it was likely pS6 that was active in ER lines, as opposed

to the other mTOR effector p4EBP1. In all cell lines, EGF stimulated pEGFR and pAkt (slightly) but was unable to stimulate ERK in this representatibe blot. This was because the EGF stimulation was longer than usual (20 minutes- by accident) in this particular experiment, and previous optimisation experiments **(3.4.2.2)** had shown that EGF-stimulated pERK was short-lived, between 5 to 15 minutes. All cell lines responded to erlotinib with decreased pEGFR, and responded to BYL719 with decreased pAkt, which were the intended target. Paradoxical activation representing alternate pathway escape was again observed with SB alone. This time, this occurred in BxPC-ER, where erlotinib paradoxically increased pAkt (dotted black arrow). The effect of CB was intriguing in this particular blot. CB with erlotinib and BYL-719 reduced pERK and pS6 signals much more in ER cell lines than parent cell lines, though in this particular blot the signal for S6 was much too faint to be appreciated (straight black arrows). To quantify and compare signal changes, the phosphorylated signals were measured and corrected to total protein in three experiments. The NT signals of the parent cell lines were set at 100%, and relative signals to this were shown **(Figure 4.15)**:

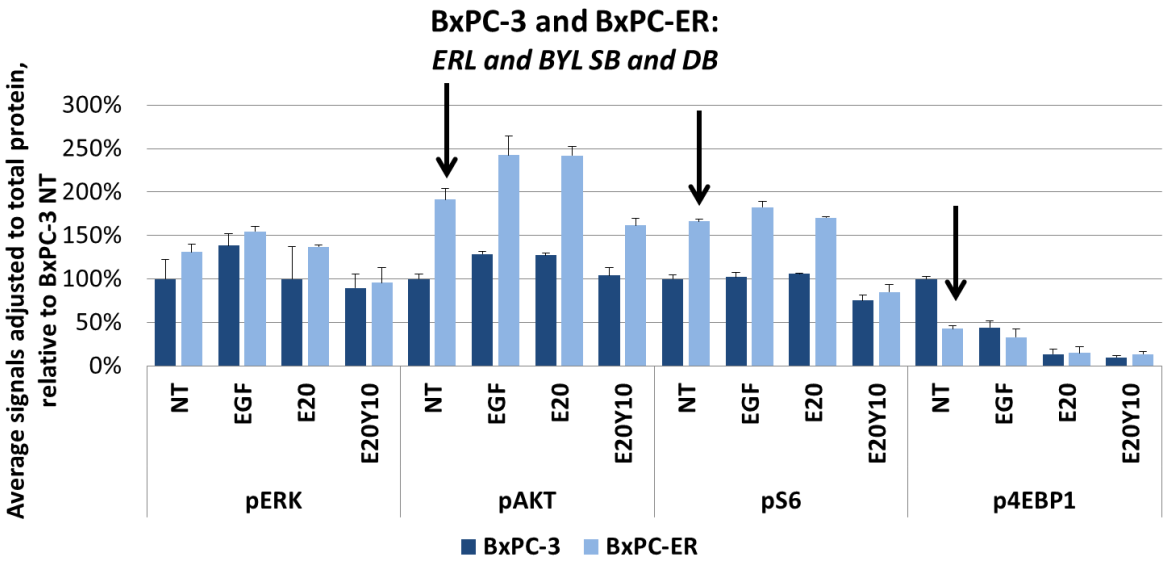

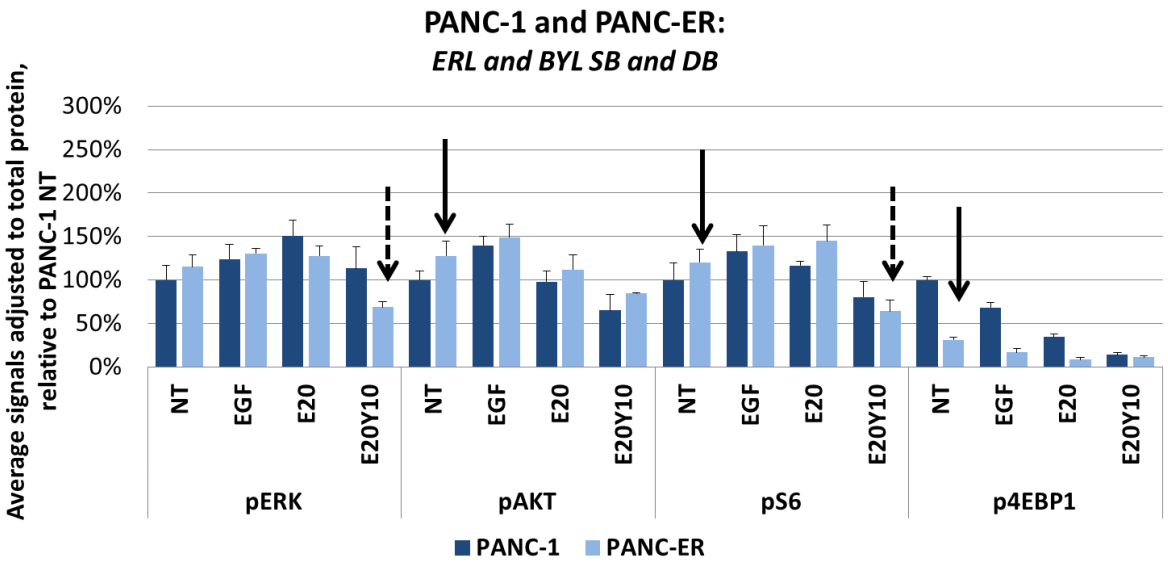

Figure 4.15: Combined blockade versus single blockade in parent versus resistant cell lines in 3 experiments. *E20 denotes erlotinib 20μM, and E20Y10 denotes erlotinib 20μM * NVP-BYL719 10μM*

Comparing each pair of parent and ER cell line at baseline, both ER cell lines had up-regulated pAkt and pS6 but substantially down-regulated p4EBP1 (straight black arrows). In particular, BxPC-ER had a 50% relative increase in pAkt and pS6 than BxPC-3. From previous experiments, PANC-1 had high absolute pAkt and pS6 signals to start off with, and PANC-ER further increased this. EGF also appeared to increase pAkt more than pERK in the ER cell lines, as demonstrated before **(3.4.2.2).** Comparing between CB and SB, there was a clear trend of reduction in all phosphorylated signals in all 4 cell lines. Furthermore, PANC-ER appeared slightly more sensitive to CB than PANC-1. After averaging 3 experiments, both pERK and pS6 were more highly suppressed in PANC-ER than PANC-1 (dotted black arrows).

The second set of experiment sought to compare the efficacy of signal inhibition with 3 CB combinations: ERL* AEW, ERL* BYL and ERL* BEZ. PD* BEZ was not tested here, since erlotinib was the constant here, and this experiment aimed to test the effect of IGF1R, PI3K or PI3K/mTOR inhibitor in combination to erlotinib. To maintain consistency, EGF stimulation only was used. However, 20ng/ml EGF was used here instead of 10ng/ml, such that weaker signals such as pS6 could become strong enough to be accurately detected. p4EBP1 was not

displayed here, since in the last figure it was already shown that the absolute signalling level was too low to be compared between the 3 CB.

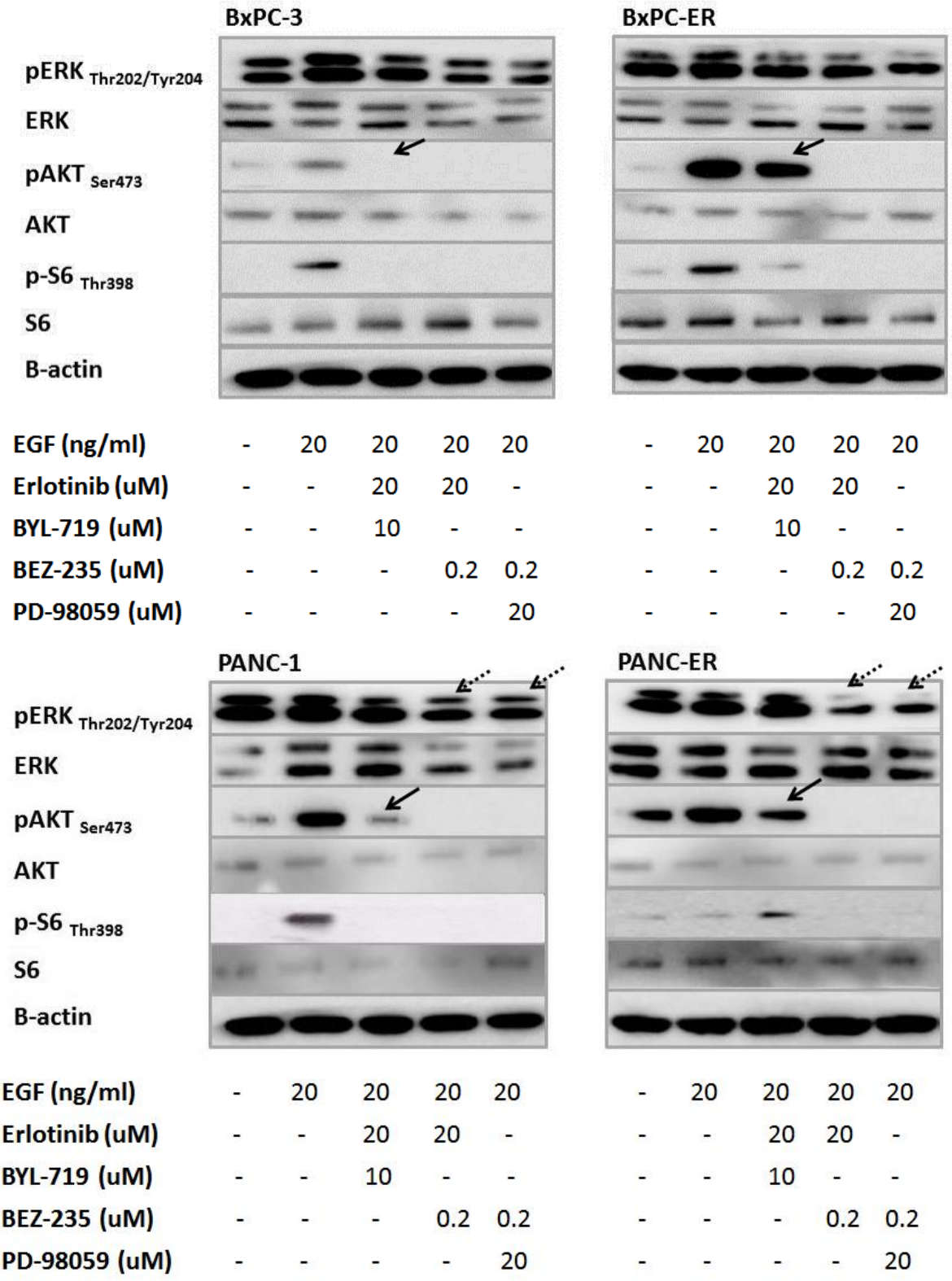

Figure 4.16: Representative blot comparing 3 CB combinations in parent versus resistant cell lines

Firstly, the higher dose of EGF had resulted in more visible signals in pS6. The most striking differences between the three CB was that pAkt and pS6 were attenuated but still present with EGFR/ IGF1R co-inhibition, as compared with complete disappearing of these phosphorylated signals with EGFR/ PI3K and EGFR/ PI3K/ mTOR co-inhibitions. pERK remained present in all 3 CB combination with 20ng/ml EGF stimulation, but again the second and third CB appeared to inhibit it more than ERL* AEW. Interestingly, when comparing between parent and resistant cell line, it was noted that ERL* AEW inhibited downstream signal pAkt less in ER than parent cell lines (straight black arrows). In addition, the CB combination utilising downstream combined blockades were not only able to abrogate pS6 and pAkt, but were also able to attenuate pERK in PANC-ER more strongly than PANC-1 (dotted black arrows). Thus, ERL* AEW was less effective, and ERL* BYL or BEZ were more effective in inhibiting downstream signals in ER cell lines. To summarise these data, phosphorylated signals from the three CB combinations were corrected to EGF stimulation, and the averages and SE were presented below **(Figure 4.17)**.

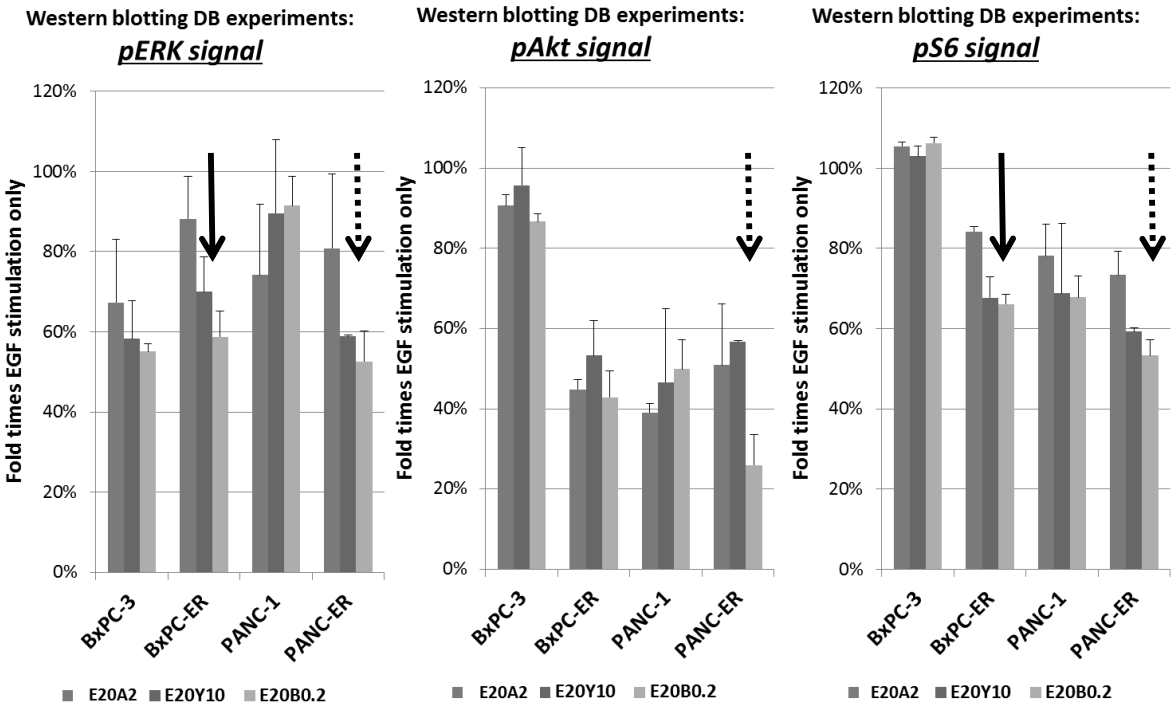

Figure 4.17: Comparison of CB combinations in parent versus resistant cell lines

For BxPC-3, ERL* BEZ was slightly more effective in inhibiting pERK. However, the effect of the 3 CB on pAkt and pS6 signals was difficult to assess. These signals were only weakly activated by EGF in BxPC-3, since there was little EGF-Akt cross-talk in this cell line as described earlier. When the pAkt and pS6 signals in response to CB were compared, the resultant proportion to EGF stimulation was all close to 1 for BxPC-3. For the other cell lines, certainly CB appeared to suppress pAkt signals more than pERK and pS6, in keeping with the direct downstream targeting of PI3K/Akt. Comparing the 3 CB, BxPC-3 appeared to have a much lower pERK and pS6 in response to ERL* BEZ, followed by ERL* BYL (straight black arrows). PANC-ER also appeared to respond markedly in response to ERL* BEZ, with much lower signals for pERK, pAkt and pS6 (dotted black arrows). This suggested a differential sensitivity of PANC-ER to dual PI3K/mTOR inhibition combined with erlotinib. In other words, there appears to be a dependency of this cell line on the PAM pathway through mTOR.

All in all, then, CB was better at inhibiting downstream signals than SB, particularly in ER cell lines. Among the CB combinations downstream ERL* BEZ was especially effective in erlotinib resistance, followed by ERL* BYL. This observation was consistent with the cell proliferation experiments, where a dominant shift to EGFR-PI3K interaction was established. These results were counter-intuitive yet intriguing. In chapter 3 ER cell lines were found to have higher Akt and S6 than parent cell lines. The highly up-regulated in PI3K/Akt/mTOR pathway probably contributed to the erlotinib resistance. If that were the case, one would normally expect ER cell lines to be more resistant to PI3K/mTOR inhibitor and CB involving these drugs, since they were more active in PI3K/mTOR pathway. However, what was observed was the reverse. These cell lines became more strongly inhibited in downstream signals by PI3K and PI3K/mTOR inhibitors, and that these inhibitors were more synergistic with EGFR in these ER cell lines. The only explanation to this was that ER cell lines became *dependent* to an obligatory PI3K/mTOR pathway, a process known as “oncogenic addiction”. To prove this hypothesis, the absolute effects of these CB on ER cell lines must be studied by a variety of functional assays.

4.3 Functional assays of CB and SB

In the first half of this chapter, positive interaction or synergy between various CB combinations was demonstrated. However, as already alluded to, *synergy* is not necessarily same as *efficacy.* To examine efficacy of CB and to prove the concept of "oncogenic addiction", various functional assays including clonogenic, migration, cell cycle and apoptosis key assays were explored. These assays were chosen because PAM pathway has a direct role in cell cycle progression, modulating anti-apoptosis signals and colony formation, and an indirect role in cancer cell migration together with transcription factors, EMT status and molecular signals of other pathways.[45,180,323,324] Importantly, if ER cell lines had onogenic dependence to the PAM pathway, one would expect to see a higher sensitivity of ER cell lines to PI3K- or PI3K/mTOR-based CB treatment, across all types of functional assays. Due to the large number of variable conditions for CB experiments, only 2-3 CB doses were selected for each assay, performed on a selection of primary cell lines, then ER vs. parent lines.

4.3.1 Clonogenic Assays

***Key Finding*: Downstream CB caused highly significant inhibition in colonies in ER compared to parent cell lines, with near-complete loss of colony formation**

Clonogenic assay results for erlotinib and gefitinib single drug treatment have been presented in chapter 3. In this sub-section, the effect of CB versus SB was first examined, and the best of 4 CB combinations in 3 primary lines was then evaluated. After that, CB between parent and ER cell lines was tested to assess any differential responses. Two dosing levels with erlotinib (5μM and 10μM), together with low and medium dosing of other inhibitors, were tested. These doses were decided based on potency observed from CB cell proliferation experiments **(4.2.2)**. Each set of experiment was performed three times. In the first set of experiments, BxPC-3, CAPAN-2 and PANC-1 were chosen among the 5 PDAC cell lines to

represent erlotinib-sensitive, moderately insensitive, and erlotinib-insensitive cell lines respectively.

4.3.1.1 Four CB Combinations in PDAC cell lines

These initial experiments examined combined blockade versus single blockade inhibition. The cells were set up in a consistent pattern with 2 no treatment, 1 drug A, 1 drug B, and 2 drug A*B on each 6 well plate. Low doses and moderate doses treatment were tested in 2 separate plates. All 4 CB combinations were tested against the SB that made up the combination. For brevity and to illustrate a point, the following representative photo showed two sets of CB only (ERL* AEW and ERL* BYL with moderate dosing):

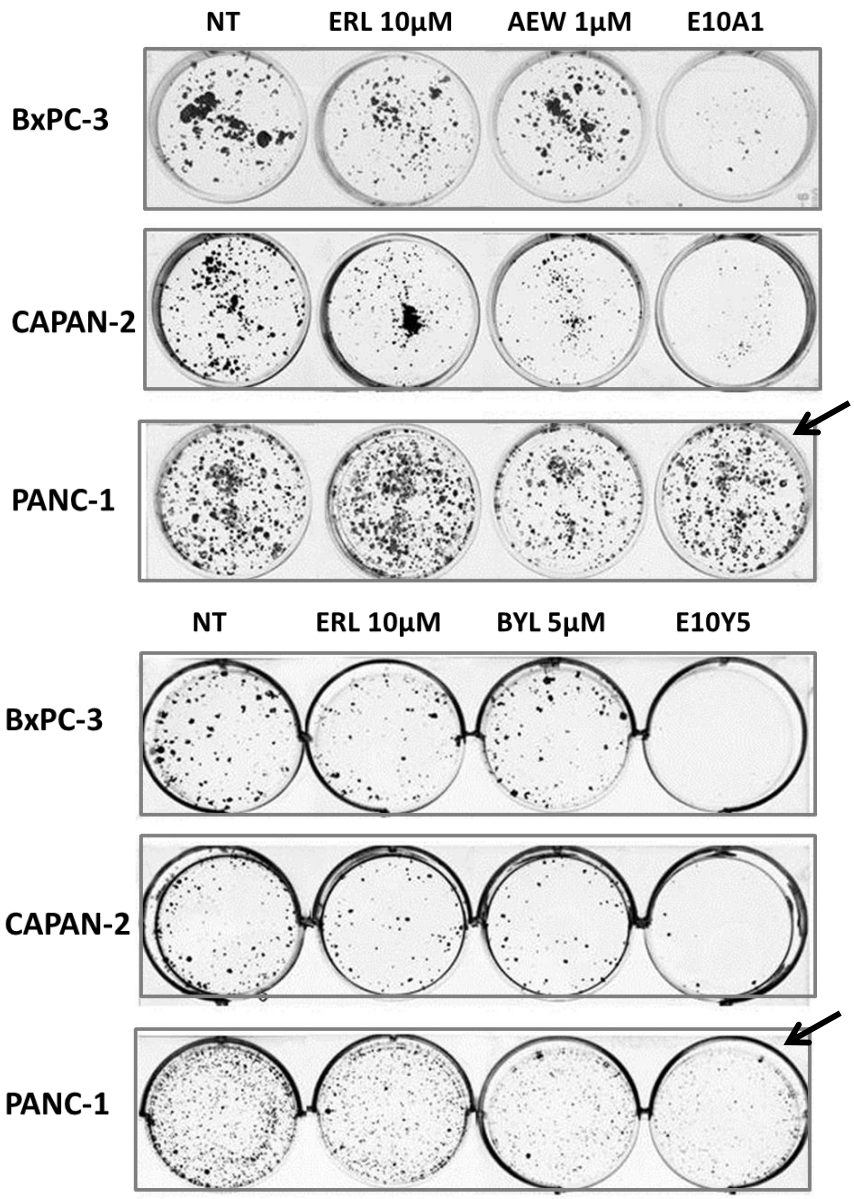

Figure 4.18: Representative photos of CB Clonogenic Assay: E10A1 denotes erlotinib 10μM * NVP-AEW541 1μM, and E10Y5 denotes erlotinib 10μM * NVP-BYL719 5μM.

Here, combined blockade worked better than single blockade. CB with either combination appeared to reduce number of colonies markedly in BxPC-3, and in CAPAN-2 to a lesser extent. However, there was a clear difference between the two CB combinations in PANC-1. In PANC-1, there remained a large formation of colonies after treatment with E10A1, which was not smaller in number than either SB or control. By contrast, the colony size and numbers were evidently suppressed after treatment with BYL 5μM, and even more so for E10Y5 (black arrows). In other words, the EGFR/ PI3K co-inhibition was superior to EGFR/ IGF1R co-inhibition in the erlotinib-insensitive PANC-1.

In determining the best of the 4 CB combinations, the summary results of 3 experiments for the 4 CB combinations in these 3 cell lines are illustrated next, in 4 sets of column graphs. In each set, CB and the SB that makeup the combinations are presented as percentages to control, and low dose and moderate dose SB/CB are presented adjacent to each other:

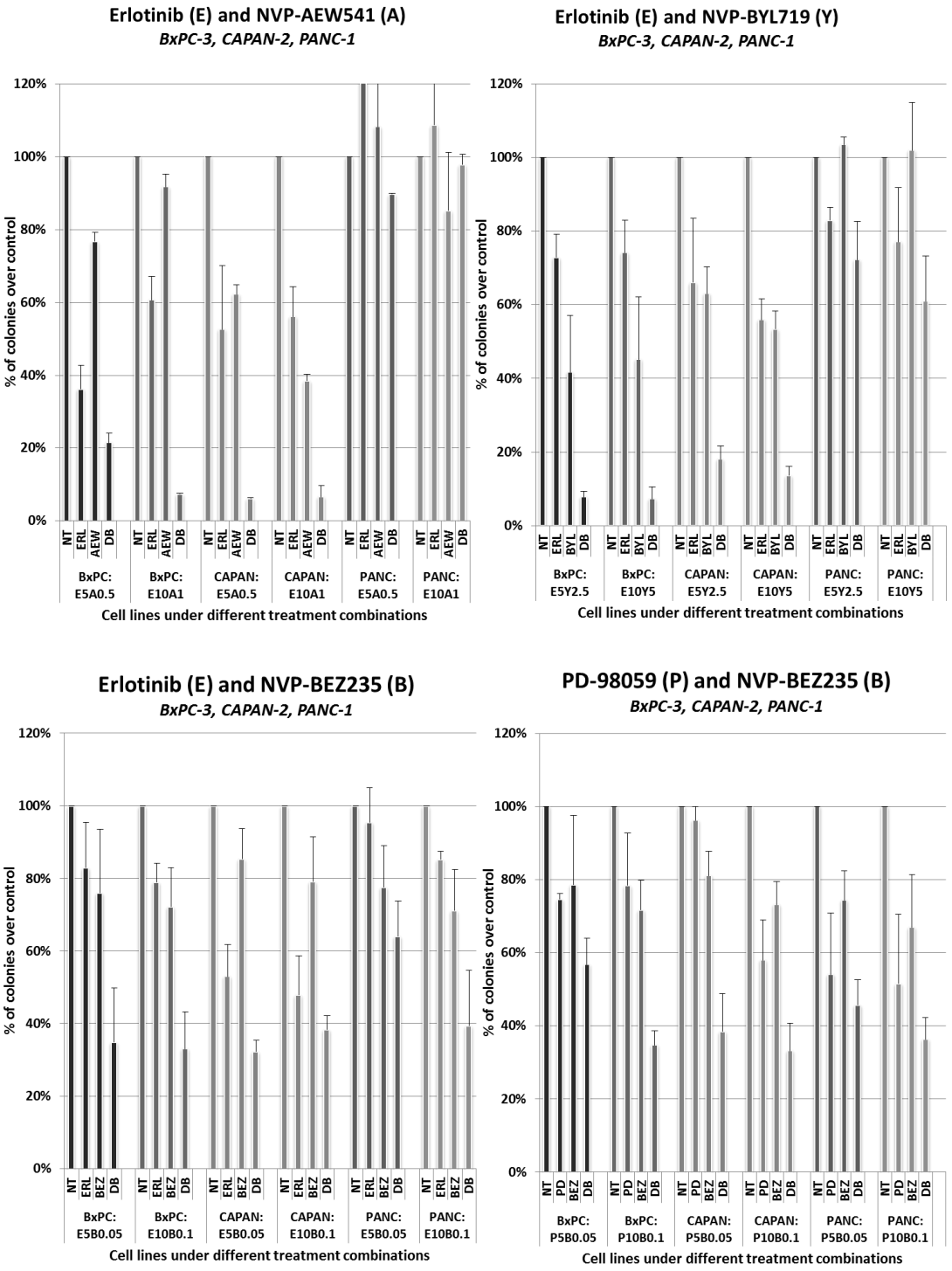

Figure 4.19: Summary results of the 4 CB Clonogenic Assay, average of 3 experiments.

Two patterns have emerged from the dense column graphs above. First of all, in all 4 combinations, a dose response pattern was followed, in that the higher dose of single or combined blockade treatment generally resulted in greater suppression of colony suppression. Secondly, the BxPC-3 and CAPAN-2 followed a different pattern of suppression as PANC-1. In the first two cell lines, EGFR/ IGF1R or EGFR/ PI3K co-inhibition were superior to SB and resulted in dramatic suppression of colony formation down to 10%, while the more downstream CBs with ERL or PD * BEZ resulted in slightly less marked suppression down to 30%. Conversely, PANC-1 was essentially resistant to the colony suppression effect of EGFR/ IGF1R co-inhibition, moderately resistant to EGFR/ PI3K co-inhibition (down to 60-70%), but much more sensitive to downstream blockades (down to 40-60%). These intriguing results may be explained by the constitutively active surface receptors (EGFR and IGF1R) in BxPC-3, and highly active PI3K downstream (especially Akt) observed in PANC-1 **(section 3.4)**. The observation that CAPAN-2 followed the same pattern as BxPC-3 was an interesting one. Although CAPAN-2 also had up-regulated PI3K/Akt pathways, this was nowhere as prominent as PANC-1 on gene and molecular levels, and pS6 expression was much higher in PANC-1 than CAPAN-2 in western blotting experiments. In summary, BxPC-3 and CAPAN-2 depend on upstream IGF1R and PI3K in mediating colony formation, whereas PANC-1 transduced this signal further downstream to PI3K, at the Akt and mTOR levels. The clonogenic assay results followed closely that of proliferation assay, suggesting that the effect of these CB to be long lasting, affecting cell lines long after the treatments were withdrawn.

4.3.1.2 CB combinations in Parent versus ER Cell Lines

Next, the four CB combinations were examined on the 2 parent and 2 ER cell lines. A representative photo is shown below:

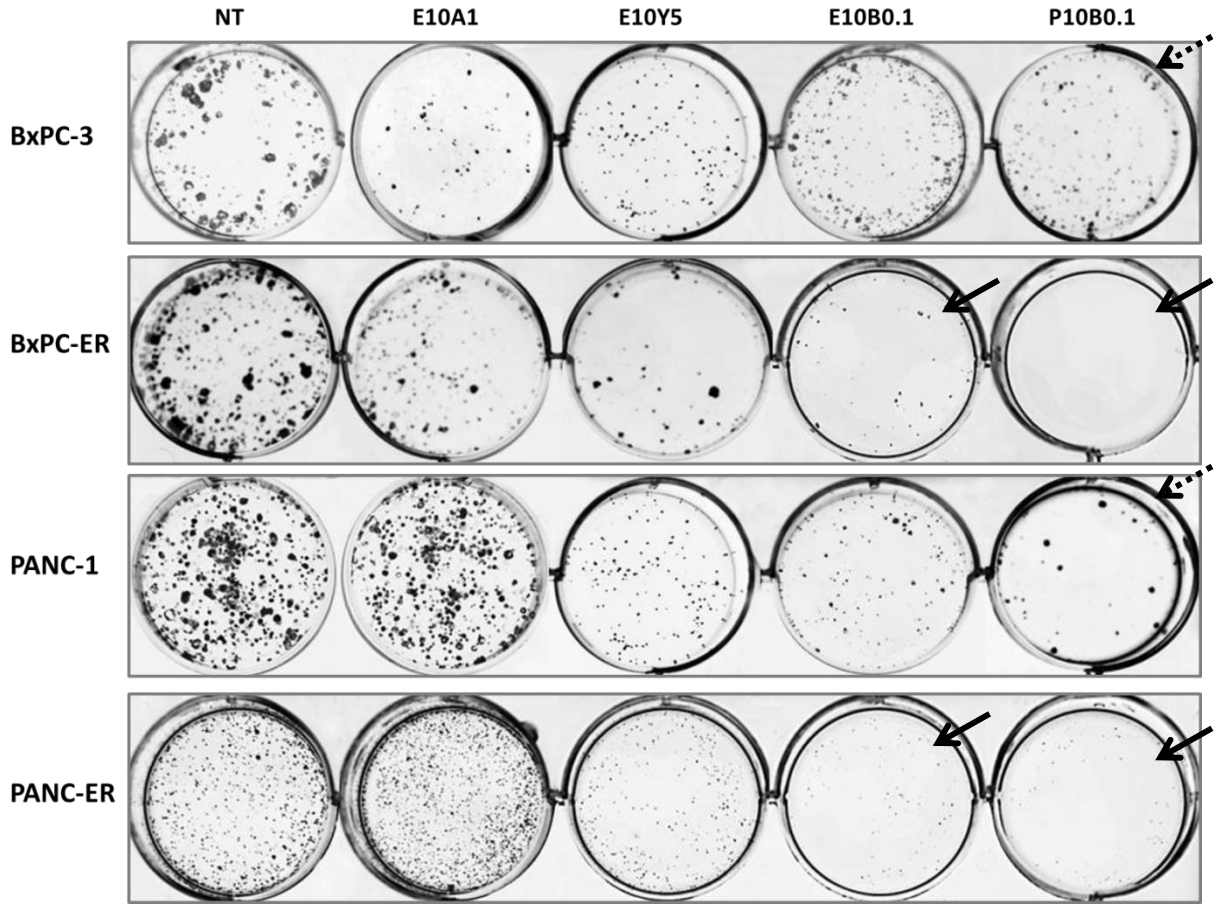

Figure 4.20: Representative photos of 4 CB combinations in parent versus ER cell lines.
E10B0.1 denotes erlotinib 10μM + BEZ-235 0.1μM, and P10B0.1 denotes PD-98059 10μM + BEZ-235 0.1μM

As before, BxPC-3 was very sensitive to the effect of E10A1, whereas PANC-1 was very resistant. As they progressed from upstream to downstream CB, the colony suppressing effect of PANC-1 increased and BxPC-3 decreased. At P10B0.1, the colony numbers for BxPC-3 and PANC-1 were roughly similar (dotted black arrows). Comparing the ER cell lines with the respective parent cell lines, they also responded better with downstream combined blockades. Importantly, they had dramatically decreased size and numbers of colonies compared to the parent counterparts upon exposure to E10B1 and P10B0.1 (straight black arrows). Results were summarised and statistics were shown in the next graph:

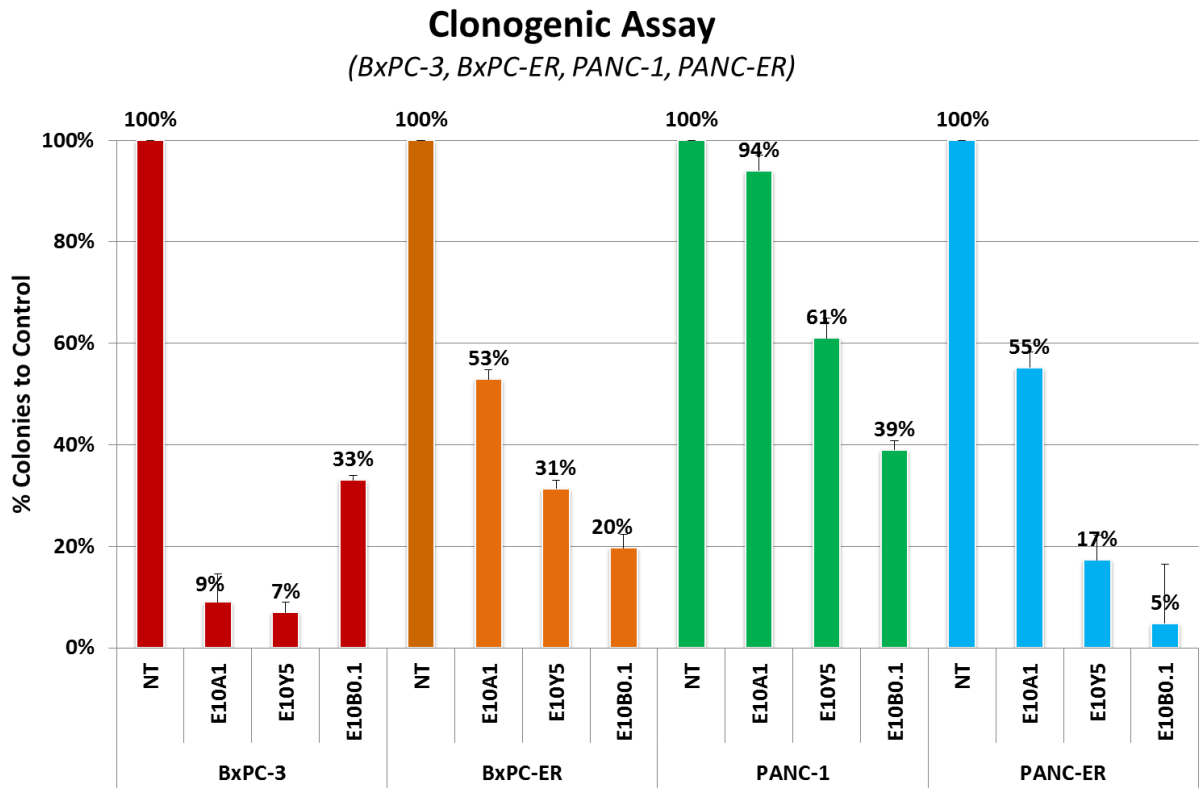

Figure 4.21: 4 CB combinations in parent versus ER cell lines, average of 3 experiments

	BxPC-ER: BxPC-3	PANC-ER: PANC-1
E10A1	**P=0.001**	P=0.95
E10Y5	**P=0.022**	**P=0.014**
E10B0.1	P=0.81	**P=0.004**
P10B0.1	**P=0.001**	**P<0.0001**

Table 4.5: Differential sensitivity between ER and parent cell line to CB, clonogenic assay

The reciprocal relationship between BxPC-3 and BxPC-ER was noted. BxPC-ER had significantly more colonies with E10A1 and E10Y5, and fewer colonies with P10B0.1 (all P<0.05). While PANC-1 and PANC-ER were resistant to E10A1, both were sensitive to PI3K or PI3K/mTOR-based CB. Intriguingly, like BxPC-ER, PANC-ER was increasingly more sensitive to progressive downstream CB compared to its parent counterpart (P=0.014, 0.004 and <0.0001). All in all, these provocative results fitted well with the synergy analysis that there was increased dependence of ER cell lines to PI3K/mTOR, and demonstrated EGFR/ PI3K co-inhibition as an effective strategy of colony suppression in these cell lines.

4.3.2 Cell Cycle Assay

***Key Finding*: PDAC cell lines depended on PI3K/Akt/mTOR in mediating multiple cell cycle checkpoints. PANC-ER was significantly hyperactive to this treatment than PANC-1**

Much attention was focused on cell cycle assay by flow cytometry, since it has been known for some time that the PI3K/Akt/mTOR/S6 pathway mediates G1 cell cycle progression in various cancer types.[325,326] Two methods were attempted to study cell cycle in pancreatic cancer: conventional propidium iodide (PI) assay and the more sophisticated BrDU/7AAD assay, which also allowed the study of cell cycle kinetics. Unfortunately, the BrDU/7AAD assay could not be optimised in these cell lines after multiple (>5) attempts. The PI assay, on the other hand, produced good and consistent results. In this sub-section, the focus is on the results produced from the PI assay. In the first set of experiments, 3 PDAC cell lines (BxPC-3, CAPAN-2, PANC-1) were tested for all 4 CB combinations and SB drugs that made up those combinations, with two dosing levels (low, medium) and two treatment times (24 hours, 48 hours). In the second set of experiments, the 4 CB and SB were performed simultaneously on BxPC-3, BxPC-ER, PANC-1 and PANC-ER, mostly on the optimal dosing and time point. Biological triplicate experiments were performed for each set.

After collecting information from the flow cytometer (on FLA-2 channel), DNA histograms were constructed and analysed using standard methods by Modfit.[327] Given the sheer amount of data, DNA histograms were only shown for noteworthy changes for illustration. A coefficient of variation (C.V.) <5% was considered acceptable for each histogram. Most results were summarised in column graphs or tables. The primary endpoint for cell cycle assay was the % of cells in S-phase or S-phase fraction (SPF), as it closely correlates with the actual proliferative behaviour of the cell population.[328] In each experiment, the SPF of each treatment was adjusted to control. The adjusted SPFs of three experiments are averaged, and where appropriate, paired t-test statistics iscalculated.

4.3.2.1 CB and SB on cell cycle for BxPC-3, CAPAN-2 and PANC-1

For illustration, CB /SB for the first combination ERL* AEW was shown for BxPC-3 and PANC-1. These DNA histograms were extracted from the low dose at 24 and 48 hours:

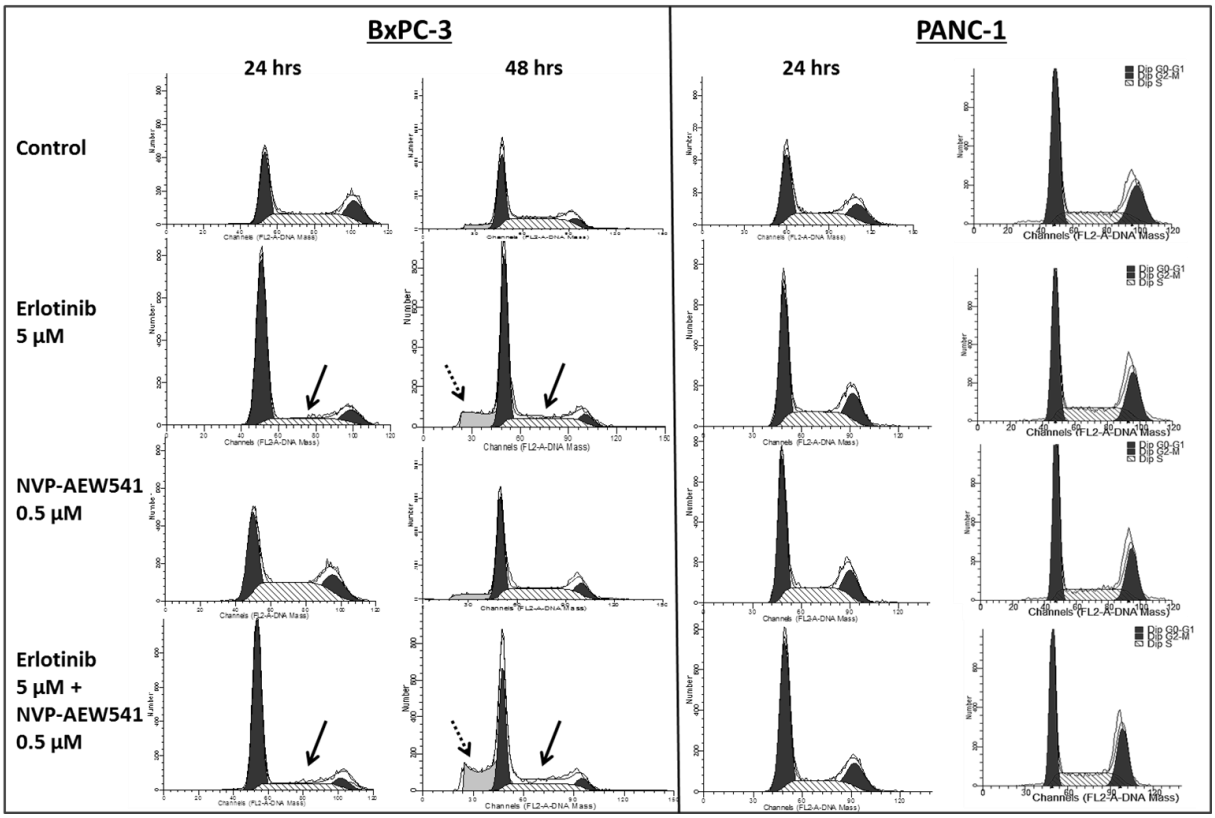

Figure 4.22: Representative DNA histograms forBxPC-3 and PANC-1 in response to Erlotinib and NVP-AEW541 SB and CB, 24 and 48 hours treatment

DNA histograms plot the DNA mass against event counts. The first taller peak corresponds to cells in G1 phase, the second shorter peak corresponds to cells in G2/ M phase, and the middle plateau section represents cells undergoing S phase. For BxPC-3, the relatively wide S-phase portion with control had become suppressed upon treatment with ERL or CB, accompanied by a taller G1 peak. This occurred in both 24 and 48 hours (**Figure 4.22**, left, straight arrows). In this particular experiment, there was also a large accumulation of cells lying to the left of G1 phase (Sub G1 Fraction). These cells had smaller DNA mass than cells in G1, and might represent cells undergoing aneuploidy or apoptosis (dotted arrows). IGF1R inhibitor did not cause any obvious suppression to S-phase compared to control. For PANC-1, neither SB nor CB caused a suppression of S-phase portion compared to control.

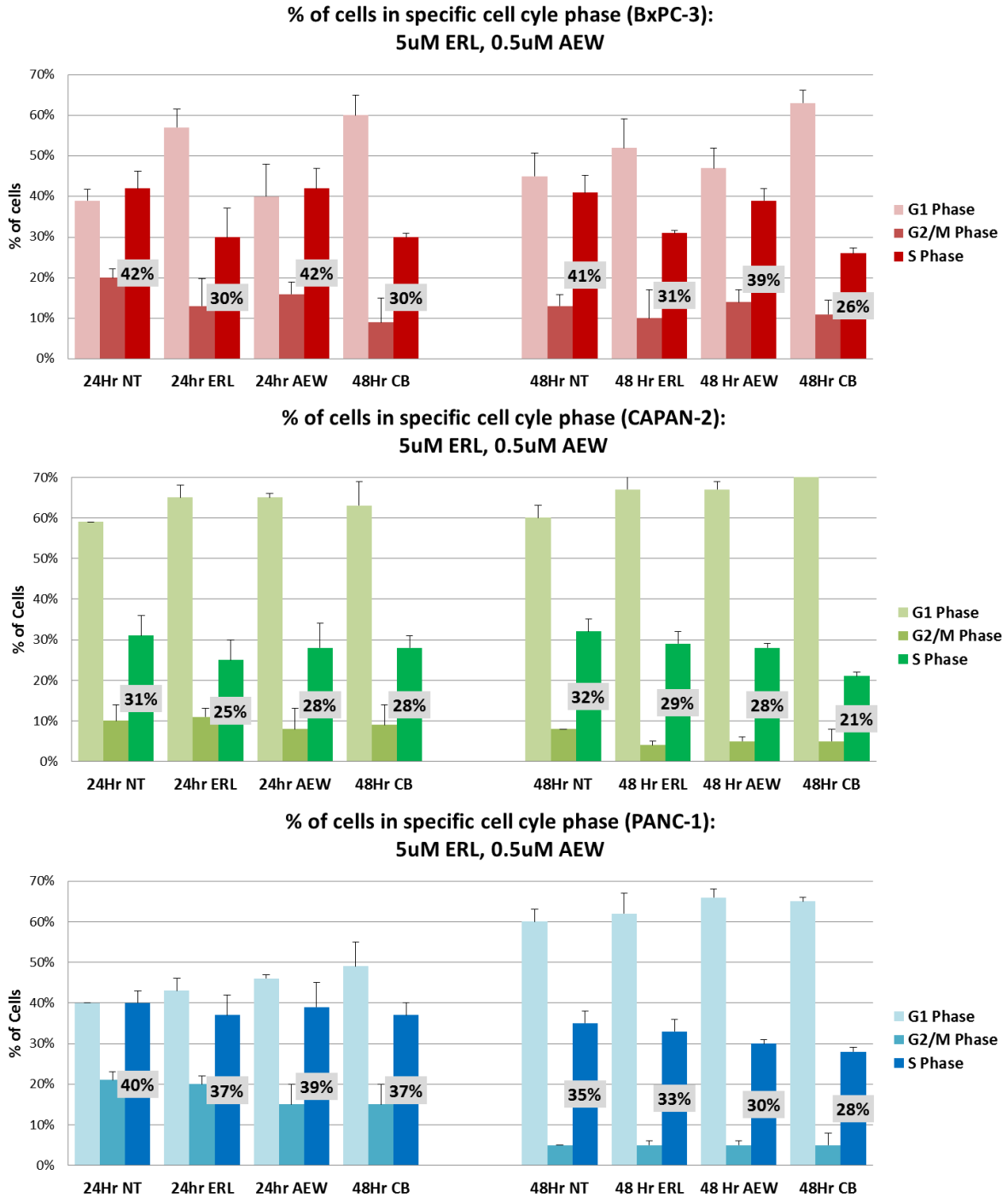

Figure 4.23: Cell Cycle analysis for BxPC-3, CAPAN-2 and PANC-1 with Erlotinib and NVP-AEW541 SB/CB

Next, the combined results of low dose CB for the 3 cell lines was analysed **(Figure 4.23)**.

The same pattern emerged in BxPC-3 for either treatment time point. At 24 hours, the SPF

decreased from 42% to 30% and 30% with Erlotinib 5μM and low dose CB. This was accompanied by an increase of cells in G1 phase, indicating that cells were prevented to enter from G1 into S-phase- *G1 arrest.* IGF1R inhibitor, on the other hand, did not cause any change in SPF. Thus, the active drug in this CB combination was clearly erlotinib in this cell line. In CAPAN-2, little changes were observed at 24 hours; at 48 hours of treatment, CB had reduced SPF from 32% to 21%. Lastly, in PANC-1, there was very slight decrease by CB at 24 and 48 hours. Clearly, BxPC-3 was a sensitive cell line whose cell cycle could be arrested by erlotinib alone. CAPAN-2 remained sensitive to CB but not SB alone, and PANC-1 was likely mediating its cell cycle further downstream of EGFR and IGF1R. Below is the analysis between the 4 CB combinations. The 48 hour (best) treatment time is shown, though both 24 and 48 hour treatments were performed:

BxPC-3	G1 (NT)	G1 (CB-L)	G1 (CB-M)	S (NT)	S (CB-L)	S (CB-M)
ERL*AEW541	45%	63% (140%)	68% (151%)	41%	26% (63% NT)	22% (54% NT)
ERL*BYL719	50%	69% (138%)	70% (140%)	42%	21% **(50% NT)**	20% **(48% NT)**
ERL*BEZ235	45%	55% (122%)	55% (122%)	42%	21% **(50% NT)**	20% **(48% NT)**
PD*BEZ235	43%	76% (177%)	77% (179%)	45%	13% **(29% NT)**	15% **(33% NT)**
CAPAN-2	**G1 (NT)**	**G1 (CB-L)**	**G1 (CB-M)**	**S (NT)**	**S (CB-L)**	**S (CB-M)**
ERL*AEW541	60%	73% (122%)	77% (128%)	32%	21% (66% NT)	17% (53% NT)
ERL*BYL719	57%	60% (105%)	63% (111%)	33%	31% (94% NT)	25% (76% NT)
ERL*BEZ235	60%	68% (113%)	71% (118%)	31%	26% (84% NT)	16% (62% NT)
PD*BEZ235	60%	69% (115%)	75% (125%)	33%	26% (79% NT)	21% (64% NT)
PANC-1	**G1 (NT)**	**G1 (CB-L)**	**G1 (CB-M)**	**S (NT)**	**S (CB-L)**	**S (CB-M)**
ERL*AEW541	60%	67% (112%)	61% (102%)	35%	28% (80% NT)	27% (77% NT)
ERL*BYL719	53%	57% (107%)	62% (117%)	37%	23% (62% NT)	10% **(27% NT)**
ERL*BEZ235	57%	64% (112%)	71% (125%)	37%	11% **(30% NT)**	14% **(38% NT)**
PD*BEZ235	55%	72% (131%)	75% (136%)	43%	14% **(33% NT)**	13% **(30% NT)**

Table 4.6: Cell Cycle analysis for BxPC-3, CAPAN-2 and PANC-1 with 4 CB combinations at 48 hours. CB-L denotes low dose CB, and CB-M denotes medium dose CB. Bracket shows % to control. Bolded indicates SPF less than or equal to 50% of control

G1 and S phase fractions were summarised in **Table 4.6** above. BxPC-3 and CAPAN-2 responded better with medium than low dose of ERL* AEW CB (10 and 1μM), with adjusted SPF 54% vs. 63% and 53% vs. 66% respectively. On the other hand, PANC-1 remained fairly resistant with a SPF 77% and 80% of control (low, medium CB). With downstream blockades, BxPC-3 and PANC-1 became increasingly susceptible. The adjusted SPF was 48% and 27% on medium dose of ERL* BYL, and both BEZ235-based CB were capable of reducing adjusted SPF to between 50-70% of control. This was almost invariably associated with increase in G1 fractions suggesting G1 arrest, and this increase was most prominent with PD *BEZ235 for these 2 cell lines. Interestingly, CAPAN-2 was only slightly affected by any CB combination, with the lowest adjusted SPF being 53% NT (ERL* AEW mod dose). However, one needs to be mindful that the S-phase fraction at control (NT) in CAPAN-2 was consistently lower than that for BxPC-3 and PANC-1. This was likely a technical artefact, relating to the the slow growing nature of CAPAN-2. The lower SPF at baseline might therefore underestimate the true effect of CB on cell cycle in this cell line.

4.3.2.2 4 CB Combinations on cell cycle in parent versus ER cell lines

CB and SB were performed on parent versus ER cell lines. All 4 CB and single agents that made up the CB were tested. For brevity, below shows a set of representative histograms for the 4 cell lines in response to Erlotinib (E10), Gemcitabine as a positive control (G0.05) –at 48 hours; and the 2 CB (E10Y5, E10B0.01) at 24 and 48 hours. The representative histograms for CB at were magnified for clarity. Reference to other CB and SB was made accordingly.

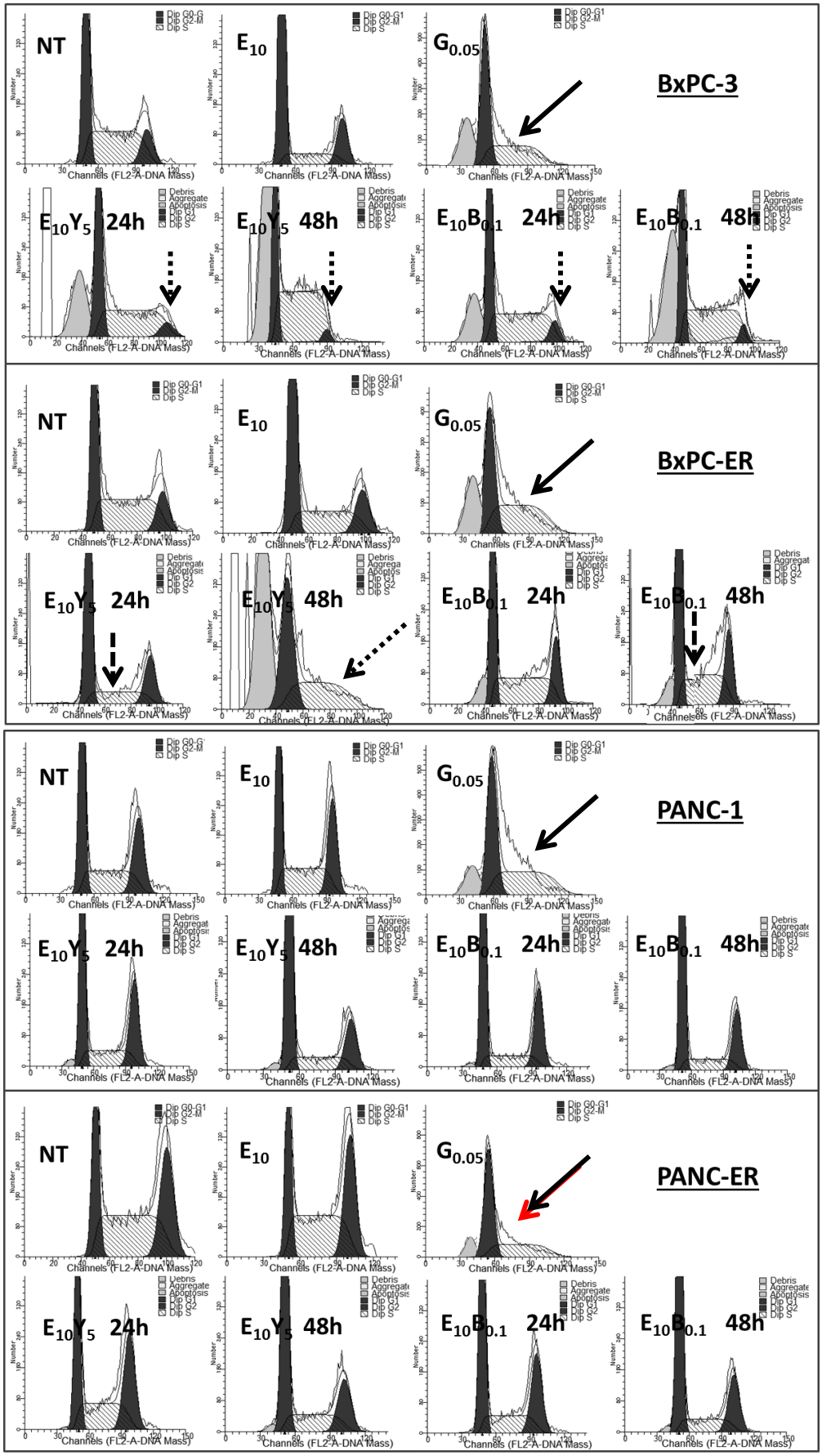

Figure 4.24: Representative DNA histograms for ER and Parent cell lines with CB at 24/ 48 hours

In all 4 cell lines, gemcitabine caused a *complete S-phase arrest*. Cells were prevented to enter into G2-phase, resulting in the disappearance of G2 peak (straight arrows). This closely reflects the mechanism of gemcitabine, an analogue of deoxycitidine that incorporates into DNA and prevents further DNA synthesis once phosphorylated into its active form.[329] While all 4 CB predominantly caused a G1 arrest in the 4 cell lines, PI3K or PI3K/mTOR inhibitor based CB also caused a variety of other disruptions to cell cycles. In a representative experiment, ERL*BYL and ERL*BEZ caused predominantly partial S phase or G2/M arrests in BxPC-3/ BxPC-ER. *Partial S-phase arrest* was evident with the greatly diminished G2 peak hiding in a plateau of S-phase (dotted arrows, BxPC-3), or a disappearance of G2 by 48 hours (dotted arrow, BxPC-ER). *G2/M arrest* appeared as a tight bottleneck just after G1 phase followed by a gradually rising slope into a larger G2 peak (dashed arrows, BxPC-ER). In the case of S-phase arrest (BxPC-3), this resulted in a G2 fraction reducing from 12.5% to 3% and 4% for BYL-719 and BEZ-235 combinations at 48 hours. In either cell line, this disruption in cell cycle resulted in accumulation of cells in pre-G1 phase more in 48 hours than 24 hours, which were likely apoptotic cells (shaded in dark grey). For PANC-1 and PANC-ER, a more common pattern was observed- G1 cycle arrest. Whilst it was harder to appreciate this given that DNA histograms were magnified, for PANC-1 G1 fraction increased from 53% to 68% (E10Y5) and 69% (E10B0.1) at 48 hour, accompanied by decrease of SPF from 32% to 17% (E10Y5) and 14% (E10B0.1). For PANC-ER, the changes were even more prominent. G1 fraction increased from 52% to 62% (E10Y5) and 73% (E10B0.1), with SPF decreased from 33% to 16% (E10Y5) and 5% (E10B0.1). In multiple experiments, G2/M and S-phase disruptions appeared to occur sometimes in ERL*BYL and frequently in ERL*BEZ or PD*BEZ, but were never evident in ERL*AEW. In all cases, SB with BYL-719 or BEZ-235 caused similar but lesser changes, implying that PI3K/Akt via mTOR was important in regulating multiple checkpoints in cell cycle. Finally, SPF was compared between ER and parent cells for the 4 CB at 48hr in 3 experiments:

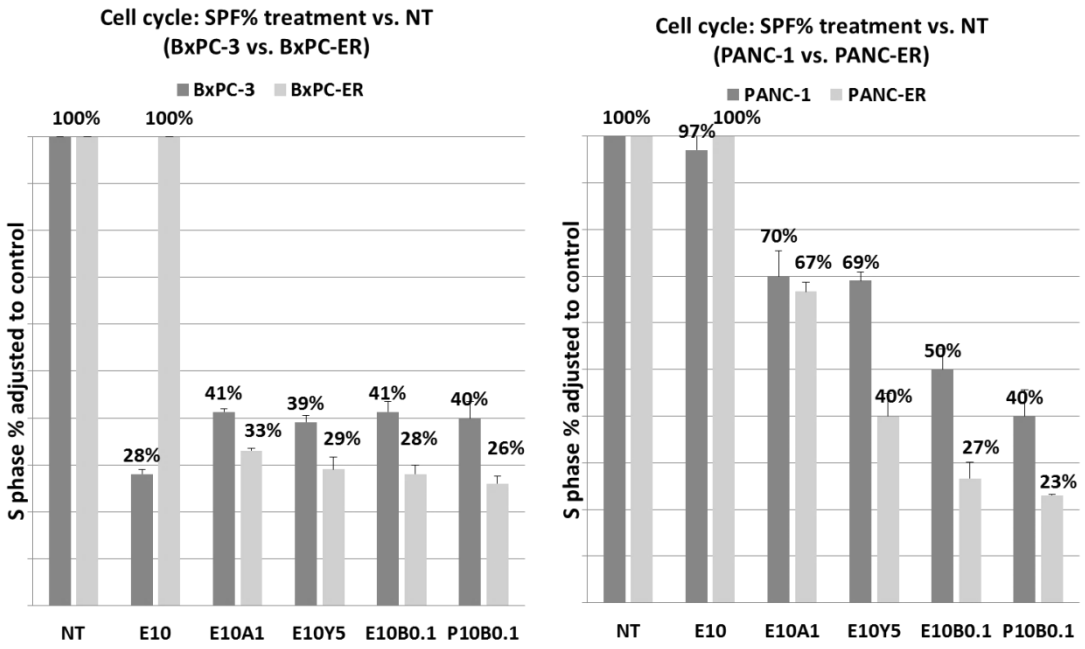

Figure 4.25: SPF% in parent versus ER cell lines for 4 CB combinations (48 hours)

	BxPC-3	BxPC-ER	PANC-1	PANC-ER	
E10A1 vs. NT	-27% t=-12.1, **P<0.0001**	-30% t=-8.5, **P<0.0001**	-10% t=-1.9, P=0.089	-10% t=-3.9, **P=0.003**	BxER vs. Bx: P=0.53 PaER vs. Pa: P=0.97
E10Y5 vs. NT	-28% t=-12.6, **P<0.0001**	-31% t=-8.9, **P<0.0001**	-14% t=-2.7, **P=0.02**	-23% t=-9.3, **P<0.0001**	BxER vs. Bx: P=0.26 PaER vs. Pa: P=**0.012**
E10B0.1 vs. NT	-26% t=-12.1, **P<0.0001**	-32% t=-9.1, **P<0.0001**	-21% t=-4.1, **P=0.002**	-30% t=-11.8, **P<0.0001**	BxER vs. Bx: P=0.15 PaER vs. Pa: P=**0.012**
P10B0.1 vs. NT	-27% t=-12.5, **P<0.0001**	-33% t=-9.3, **P<0.0001**	-25% t=-4.9, **P=0.0006**	-30% t=-11.8, **P<0.0001**	BxER vs. Bx: P=0.34 PaER vs. Pa: P=**0.043**

Table 4.7: Differential sensitivity between ER and parent cell line to CB, cell cycle

BxPC-3 was sensitive to erlotinib 10μM (E10) alone, with SPF reduced to 28% compared to control (P<0.0001). The cell cycle progression was unaffected by E10 in the three other cell lines, indicating erlotinib insensitivity/ resistance. In **figure 4.26 and table 4.7**, all 4 CB were more or less equally effective in BxPC-3 (40-41% SPF, -26 to -28% from NT). With the other 3 cell lines, downstream was more effective than upstream CB. This was particularly the case for PANC-1 and PANC-ER, where SPF was reduced by 10%, 14%, 21%, 25% (PANC-1) and

10%, 23%, 30% and 30% (PANC-ER) with E10A1, E10Y5, E10B0.1 and P10B0.1. To assess if there was a differential response between ER and parent cell lines to CB, t- statistics was calculated between each pair (ER: parent) after adjusting for each of the three experiments performed. There was a hint of higher efficacy on BxPC-ER than BxPC-3 for each CB, but the differential sensitivity between them was not significant (all $P>0.05$). On the other hand, PANC-ER was clearly more suppressed by BYL or BEZ-based CB compared to PANC-1 (-23 vs. -14%, -30% vs. -21%, -30% vs. -25%), and there was a significant difference between these lines in response to these 3 CB (all $P<0.05$).

Overall, downstream CB utilising PI3K or PI3K/mTOR inhibitors was especially effective causing a variety of G1, S or G2/ M arrests. In addition, **there was a more effective cell cycle inhibition by these downstream CB on ER cell lines, and significantly so in PANC-ER**. Thus, ER cell lines appeared to be dependent on the PAM pathway in cell cycle progression via multiple checkpoints, and these in turn appeared to be “actionable targets”. A Pre-G1 subpopulation with CB could represent apoptotic cells, but formal apoptotic assays are needed to assess for necrosis and apoptosis.

4.3.3 Apoptotic Assays

***Key Finding*: mTOR is important in regulating anti-apoptosis signals. PI3K /mTOR-based CB (+EGFR or MEK inhibition) were very effective in inducing necrosis and apoptosis, particularly in ER cell lines**

Apoptotic assays were studied next, since Akt is known to modulate anti-apoptosis and survival signals through Forkhead and BAD via Bcl-2 and FasL,[45] and a large fraction of cells were observed at pre-G1 phase in cell cycle assay when treated with CB, which was suggestive of apoptosis. An in-house protocol with PI and DiLC5 dye by flow cytometry was adopted.[265] All 4 CB were studied along with SB that made up the combinations. These drugs were first studied in BxPC-3 and PANC-1, with two treatment times (48, 72 hours) and 3 dosing levels (low, medium, high). Each experiment used negative (no treatment) and positive controls (super-saturated erlotinib 80 μM). The differences between parent and ER cell lines were studied, after choosing the optimal treatment time and dosing level. The endpoint was a cumulative measure of necrosis and apoptosis %, since dying cancer cells usually lied in a continuum from apoptosis to necrosis, and they were best studied together. Quadruplicate experiments were performed, to allow for paired t-test statistics to be calculated. For confirmation, cleaved caspase-3 was studied by western blotting and immunofluorescence. Shown below is a set of apoptotic plots for the two cell lines with ERL and/or AEW, at 48 hours.

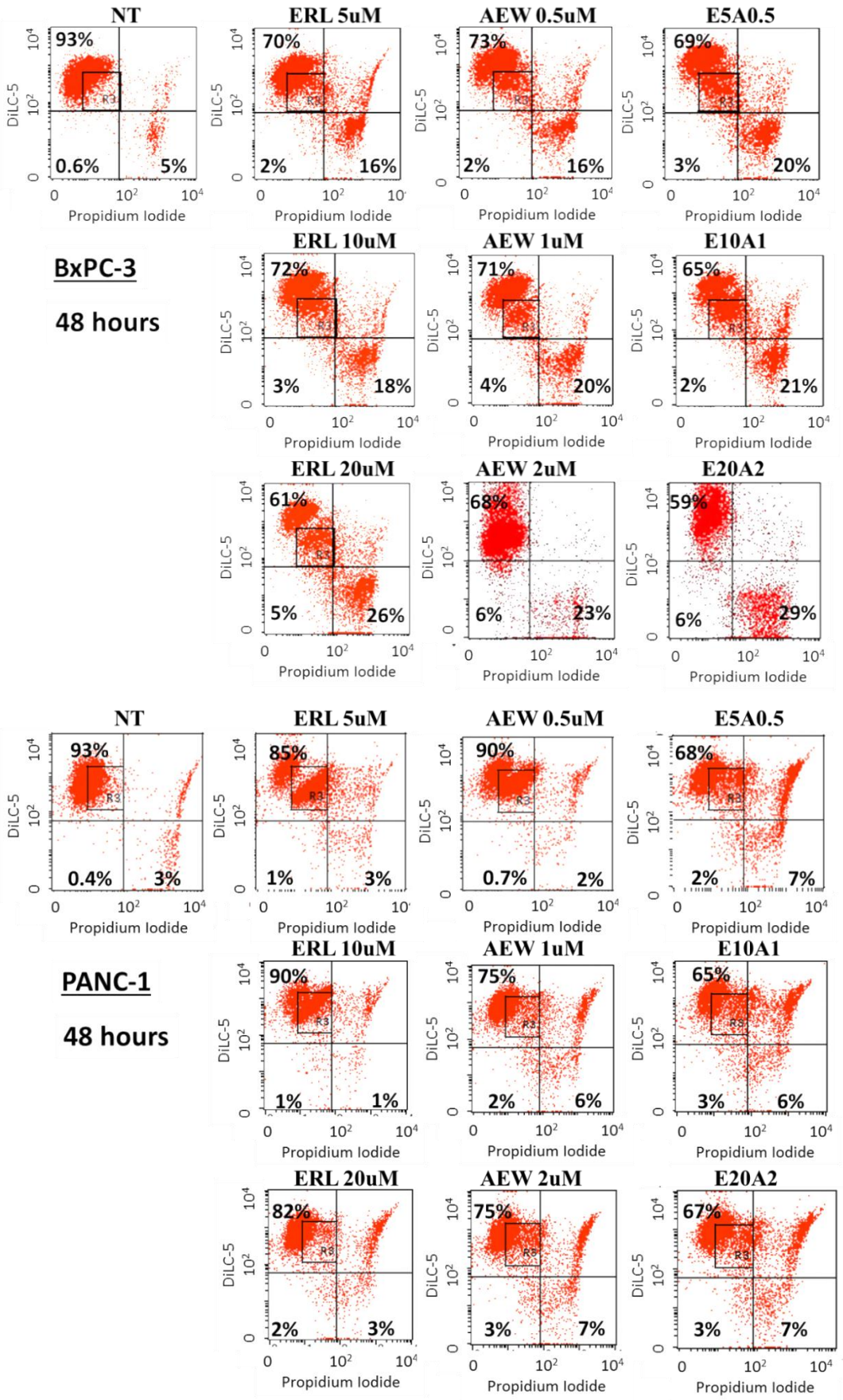

Figure 4.26: Representative Apoptosis plots for ERL* NVP-AEW541 CB in BxPC-3 and PANC-1

4.3.3.1 CB and SB on apoptosis and necrosis on BxPC-3 and PANC-1

DiLC5 is a mitochondrial dye that stains positive in live cells, whereas propidium iodide (PI) stains DNA when it is allowed to enter in a disrupted membrane. In the apoptosis plots, then, live cells are located on the upper left quadrant in the apoptotic scatterplot as they accumulate DiLC5 in the intact mitochondria but are not stained with PI because of intact membrane. Apoptotic cells have a clear loss of mitochondrial signal but retain an intact membrane, and are therefore located on the lower left quadrant. Necrotic cells have lost mitochondrial signal and are stained with PI because of disrupted membranes, and are hence located in the lower right quadrant. Finally, cells located at the upper right quadrant may be under "stress"; they have leaky membrane but remain active in their cellular machinery.[265]

For illustration, the apoptotic plots at 48 hour treatment were first shown above. In BxPC-3, both ERL and AEW SB alone were cytotoxic, with increasing necrosis (bottom right quadrant) proportional to dose response **(Figure 4.26)**. For all dosing levels, CB was superior to either drug alone, with necrosis rate of 20%, 21% and 29% for low, medium and high combined dosing respectively (bottom right quadrant, top figure). PANC-1, on the other hand, was very resistant to either SB or CB, at all dosing levels. Although there appeared a sub-population of cells that were under stress (upper right quadrant, bottom figure), there were very few cells that had undergone apoptosis (1-3%) or necrosis (6-7%). Thus, it appeared BxPC-3 was sensitive to dual upstream blockades, but not PANC-1.

Next, examples of 48-hour and 72-hour treatment in both cell lines in response to the other (downstream) CB are shown below. It was impossible to include all apoptotic plots for all treatments at both time points in this thesis. The following were included to illustrate some interesting mechanisms on apoptosis and necrosis by these downstream CB.

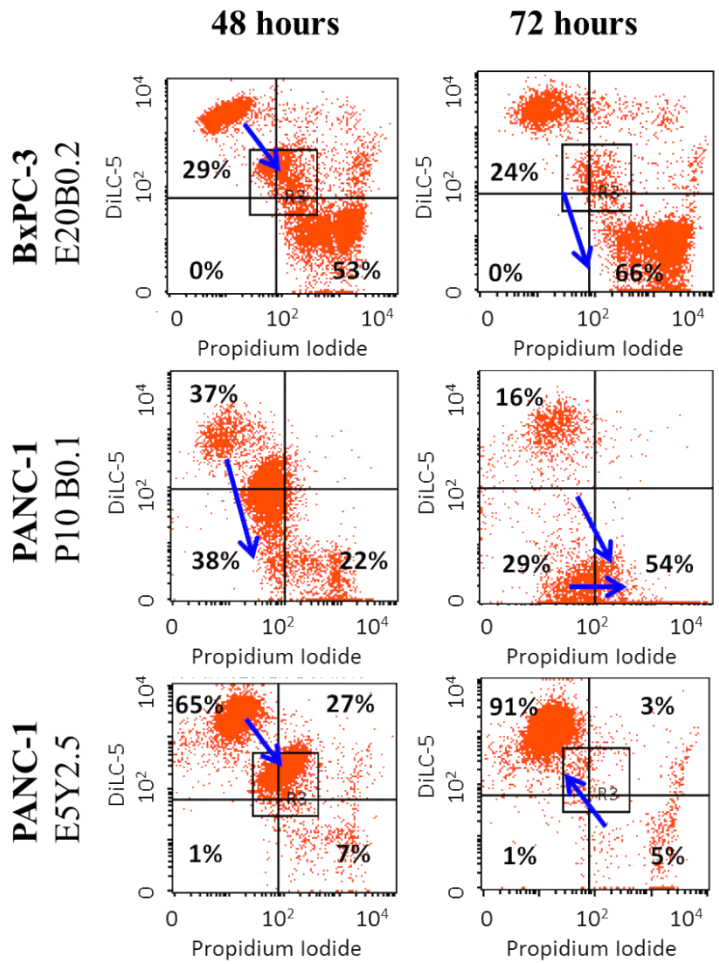

Figure 4.27: Representative Apoptosis plots of BxPC-3 and PANC-1 after 48 and 72 hours CB

In the first example, three subpopulations of cells were identified after 48 hours treatment of high dose CB with E20B0.2 on BxPC-3. By 72 hours, the middle cell population moved to the necrotic quadrant. In the second example, PANC-1 was treated with medium dose CB P10B0.1. At 48 hours, there were also 3 cell subpopulations, spreading over live, apoptotic and necrotic quadrants. By 72 hours, the apoptotic portions moved to the necrotic quadrant resulting in an increase from 22 to 54% necrosis. In the third example, PANC-1 was treated with low dose CB involving the PI3K inhibitor BYL719. In this case, 2 subpopulations separated early at 48 hours with no cells in apoptosis and necrosis; but by 72 hours, these all returned to the live quadrant. From these examples, 4 general observations were made: firstly, cells were affected by inhibitor as early as 48 hour treatment. Secondly, not all cells were equally affected by inhibitor combinations, resulting in different cell subpopulations in the apoptotic plots. Thirdly, whilst cell subpopulations separated early, not all were destined to

become apoptotic or necrotic. In the case of low dose combination in PANC-1 (example 3), cells under stress at 48 hours actually returned to the live quadrant at 72 hours. Finally, cells that were destined to die appeared to move down diagonally from upper left to bottom right, losing mitochondrial activity as well as increasing membrane permeability resulting in PI uptake. Whilst they might sink down to the apoptotic quadrant first (example 2), this was not always the case (example 1). Given the reasons above, **the 72 hour treatment results were considered more reliable and was primarily presented in subsequent series, and the cumulative measure of necrosis and apoptosis % were used as the study endpoint.**

The summary results for the 4 CB combinations in 4 experiments were shown below. Statistics were calculated between SB and CB, but not between CB and controls since nearly all treatment significantly induced necrosis and apoptosis compared to controls:

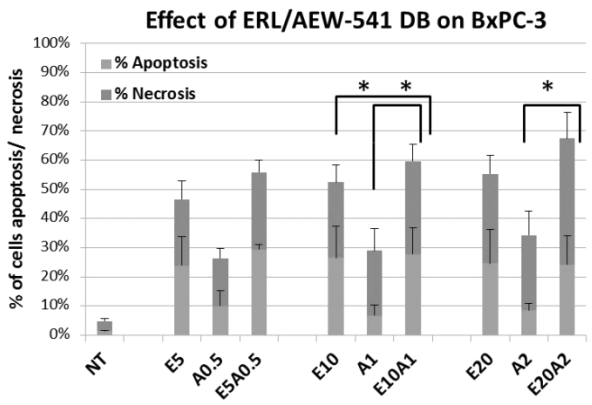
Effect of ERL/AEW-541 DB on BxPC-3
% Apoptosis
% Necrosis
% of cells apoptosis/ necrosis
NT
E5
A0.5
E5A0.5
E10
A1
E10A1
E20
A2
E20A2

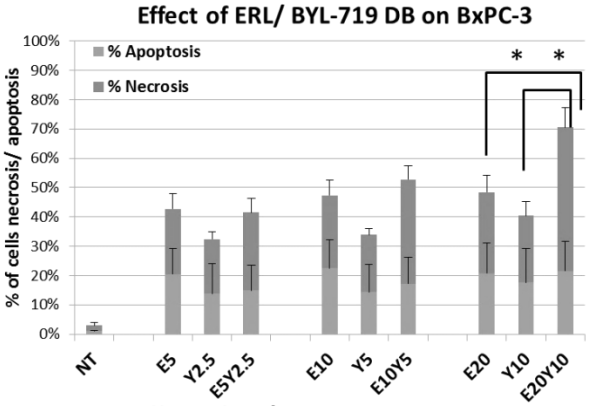
Effect of ERL/ BYL-719 DB on BxPC-3
% Apoptosis
% Necrosis
% of cells necrosis/ apoptosis
NT
E5
Y2.5
E5Y2.5
E10
Y5
E10Y5
E20
Y10
E20Y10

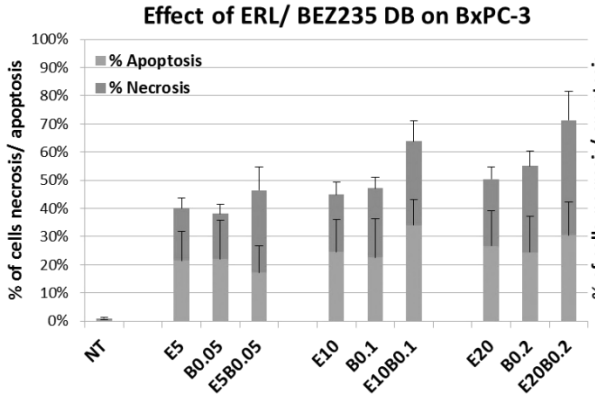
Effect of ERL/ BEZ235 DB on BxPC-3
% Apoptosis
% Necrosis
% of cells necrosis/ apoptosis
NT
E5
B0.05
E5B0.05
E10
B0.1
E10B0.1
E20
B0.2
E20B0.2

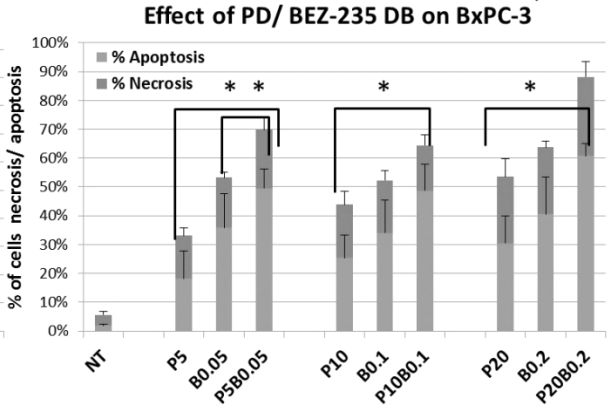
Effect of PD/ BEZ-235 DB on BxPC-3
% Apoptosis
% Necrosis
% of cells necrosis/ apoptosis
NT
P5
B0.05
P5B0.05
P10
B0.1
P10B0.1
P20
B0.2
P20B0.2

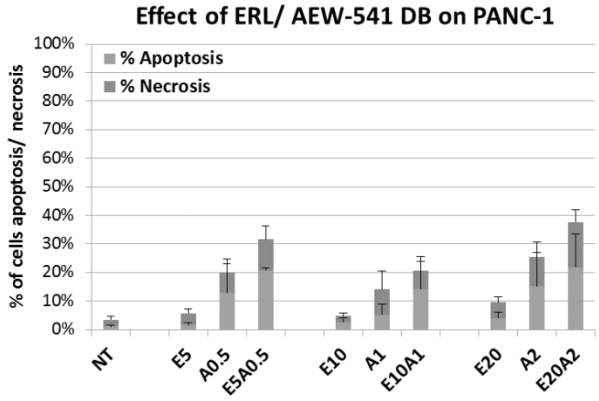
Effect of ERL/ AEW-541 DB on PANC-1
% Apoptosis
% Necrosis
% of cells apoptosis/ necrosis
NT
E5
A0.5
E5A0.5
E10
A1
E10A1
E20
A2
E20A2

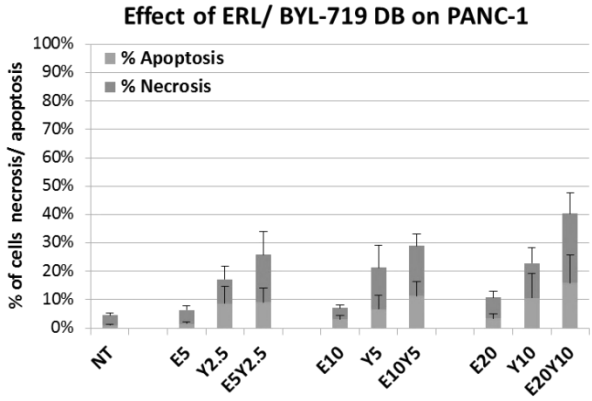
Effect of ERL/ BYL-719 DB on PANC-1
% Apoptosis
% Necrosis
% of cells necrosis/ apoptosis
NT
E5
Y2.5
E5Y2.5
E10
Y5
E10Y5
E20
Y10
E20Y10

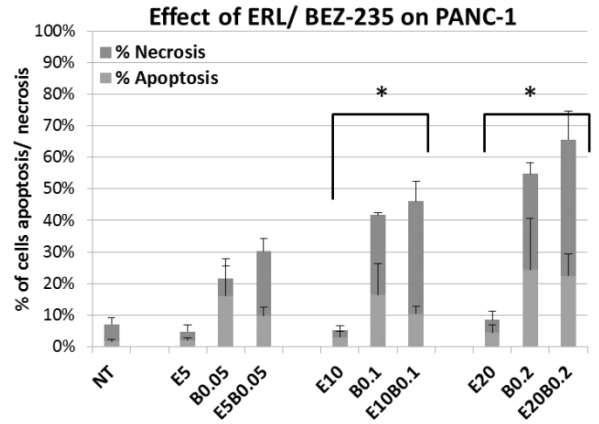
Effect of ERL/ BEZ-235 on PANC-1
% Necrosis
% Apoptosis
% of cells apoptosis/ necrosis
NT
E5
B0.05
E5B0.05
E10
B0.1
E10B0.1
E20
B0.2
E20B0.2

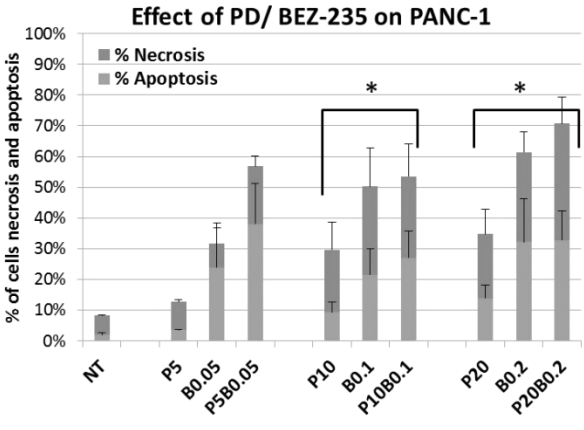
Effect of PD/ BEZ-235 on PANC-1
% Necrosis
% Apoptosis
% of cells necrosis and apoptosis
NT
P5
B0.05
P5B0.05
P10
B0.1
P10B0.1
P20
B0.2
P20B0.2

Figure 4.28: Summary Results of 4 CB on BxPC-3 and PANC-1 at 72 hours. * P<0.05

Here, all CB induced numerically higher necrosis and apoptosis than SB alone, and a dose response was observed for all SB and CB. Since each CB was analysed alongside the SB that made up the combination, the following important observations about SB could be made. In BxPC-3, ERL was probably the active drug of the first 2 CB, and is responsible for the significant differences between CB and SB observed. On the other hand, ERL was clearly the least active in PANC-1. Both AEW and BYL contributed little to apoptosis and necrosis, but they still produced slightly more apoptosis and necrosis in PANC-1 than ERL. BEZ had a substantial impact on apoptosis and necrosis in both cell lines (up to 60%); and was superior to ERL even in the erlotinib-sensitive BxPC-3. As for CB, the first two combinations (ERL* AEW, ERL* BYL) were effective in BxPC-3 (up to 70%), but not so effective in PANC-1 (only 30% maximum). The last two combinations (ERL* BEZ, PD* BEZ) were effective in both cell lines. In particular, PD*BEZ CB was statistically superior to PD alone in BxPC-3 for all doses and in PANC-1 for 2 of the 3 doses, inducing necrosis and apoptosis up to 90% in BxPC-3 and 70% in PANC-1. Thus, **BEZ-235 the dual PI3K/mTOR inhibitor was the active drug causing apoptosis and necrosis in both BxPC-3 and PANC-1, as was erlotinib in BxPC-3.** CB was better than SB in inflicting necrosis and apoptosis, with dual downstream inhibition (MEK and PI3K/mTOR) causing near-complete annihilation of cancer cells by 72 hours of treatment.

4.3.3.2 4 CB Combinations on apoptosis / necrosis in parent versus ER cell lines

Next, the 4 CB were compared between parent and ER cell lines together in 4 biological quadruplicate experiments. Below showed the representative apoptosis plots of the highest dose at 72 hr.

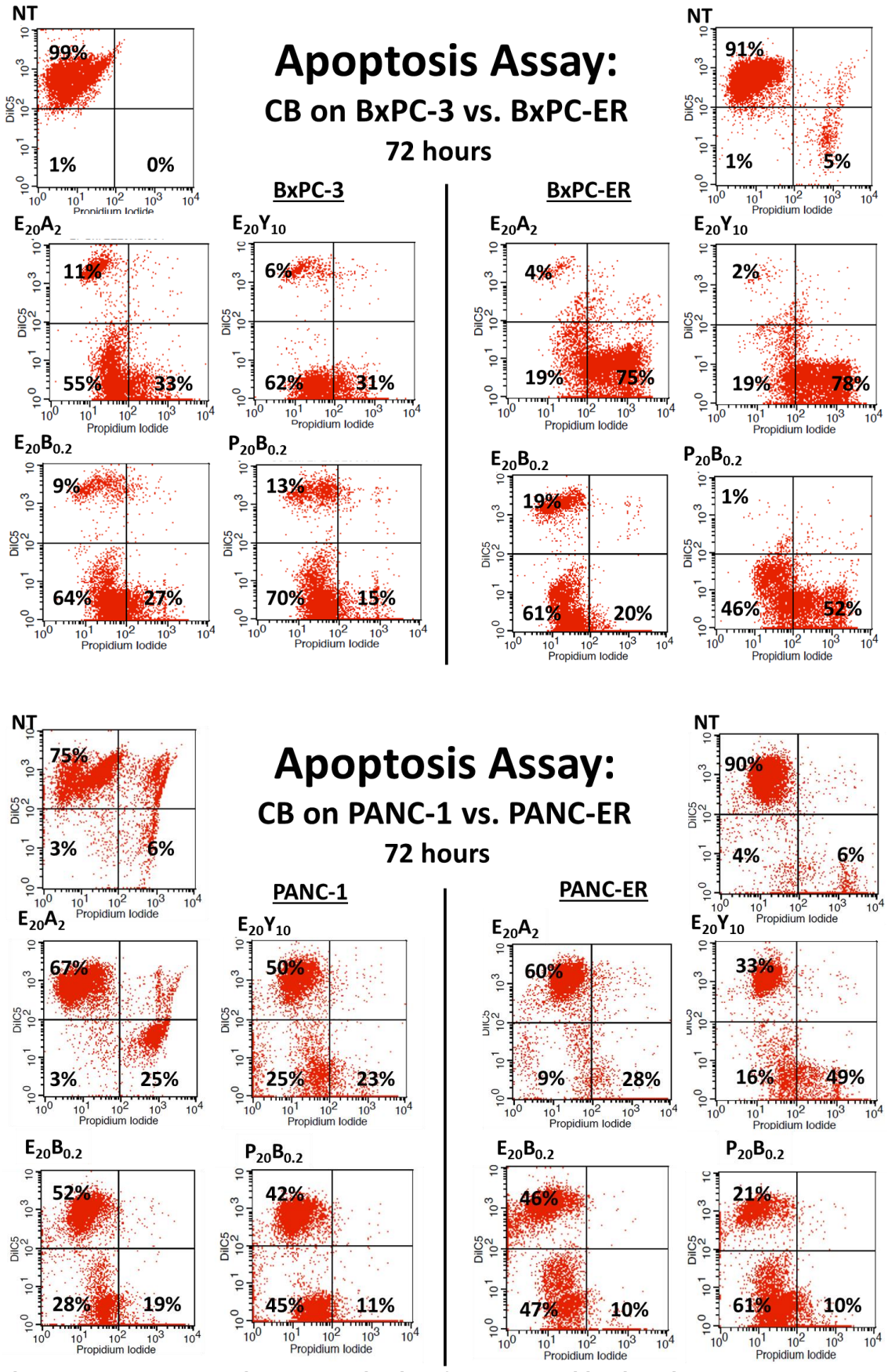

Figure 4.29: Representative Apoptosis plots for 4 CB combinations in ER versus parent cell lines

Shown above was the experiment with the extreme cases of apoptosis and necrosis on the highest dosing CB combinations. In this example, the highest dosing level of 4 CB were extremely effective against BxPC-3 and perhaps even slightly more so in BxPC-ER, with cumulative apoptosis and necrosis rate ranging from 81-99% in BxPC-ER compared to 85-93% in BxPC-3. For PANC-1 and PANC-ER, E20A2 appeared to be the least potent, inflicting a combined necrosis and apoptosis rate of 28% in PANC-1 and 37% in PANC-ER. The other three CB combinations were more cytotoxic, with the combined dual downstream blockade PD*BEZ being the most potent. There was also a suggestion that these three CB worked more effectively in PANC-ER (57-71%) than PANC-1 (48-56%).

4 experiments were also completed for the moderate dose of CB and SB. To maintain consistency with the cell cycle analysis **(table 4.7)**, this dosing was selected for statistical analysis for the parent and ER cell lines below, after adjusting to the 4 experiments.

VS. NT	BXPC-3	BXPC-ER	PANC	PANC-ER	
E10A1	t=3.62, 48% (P=0.001)	t=6.16, 58% (P<0.0001)	t=4.08, 32% (P=0.0003)	t=3.01, 27% (P=0.005)	BxER vs. Bx: P=0.57 PaER vs. Pa: P=0.24
E10Y5	t=3.67, 48% (P=0.001)	t=6.30, 57% (P<0.0001)	t=4.32, 34% (P=0.0002)	t=5.31, 46% (P<0.0001)	BxER vs. Bx: P=0.41 PaER vs. Pa: **P=0.048**
E10B0.1	t=3.73, 49% (P=0.001)	t=6.39, 65% (P<0.0001)	t=4.73, 49% (P<0.0001)	t=4.16, 56% (P=0.0002)	BxER vs. Bx: **P=0.046** PaER vs. Pa: **P=0.029**
P10B0.1	t=3.84, 51% (P=0.001)	t=7.54, 68% (P<0.0001)	t=4.80, 49% (P<0.0001)	t=6.22, 57% (P<0.0001)	BxER vs. Bx: **P=0.049** PaER vs. Pa: **P=0.043**

Table 4.8: Differential sensitivity between ER and parent cell line to CB, apoptosis assay

In BxPC-3, all moderate dose of CB appeared to cause similar amount of cumulative apoptosis and necrosis% (48-51%). BxPC-ER, on the other hand, showed increased sensitivity to each CB progressively downstream, with the greatest susceptibility for P10B0.1 (68%, P=0.0001). Statistically, there was a significant difference between BxPC-3 and BxPC-ER in their

responses to the last two combinations (P<0.05). PANC-1 was more sensitive to the last 2 CB than the first 2 CB, as described previously. PANC-ER showed higher resistance to E10A1, but E10Y5, E10B0.1 and P10B0.1 were all able to cause more necrosis and apoptosis, with the greatest susceptibility also for P10B0.1 (57%, P<0.0001). All of these three CB were significantly more effective in PANC-ER than PANC-1 (P<0.05) **(table 4.8)**. Therefore, along the same theme as cell cycle assays, apoptosis assays had demonstrated that EGFR/MEK and PI3K/mTOR cooperatively mediated anti-apoptosis signals. In particular, **mTOR appeared to be paramount to the regulation of this cellular function**. **Both ER cell lines became highly dependent on PI3K/Akt/mTOR resulting in increased apoptosis and necrosis with PI3K/mTOR-based combinations.**

4.3.3.3 Validation of Apoptosis Assay (microscopy and western blotting)

Apoptosis Assay was an in-house protocol that has been widely used in the Kolling Institute for many years. Since it was an unpublished protocol and the findings from the apoptosis assay were crucial for the purpose of this thesis (**discussion 4.5**), apoptosis needed to be validated by a number of standard methods. Western blotting and immunofluorescence of cleaved (activated) caspase-3, a protein that was intimately involved in the apoptosis process, were used as surrogate endpoints of apoptosis. Since the 4 CB had already been explored in detail in apoptosis assay, the aim of the validation was to demonstrate the superiority of CB over SB. ERL* BYL was chosen as the CB by default, as this was the main combination selected to take forward to *in-vivo* study.

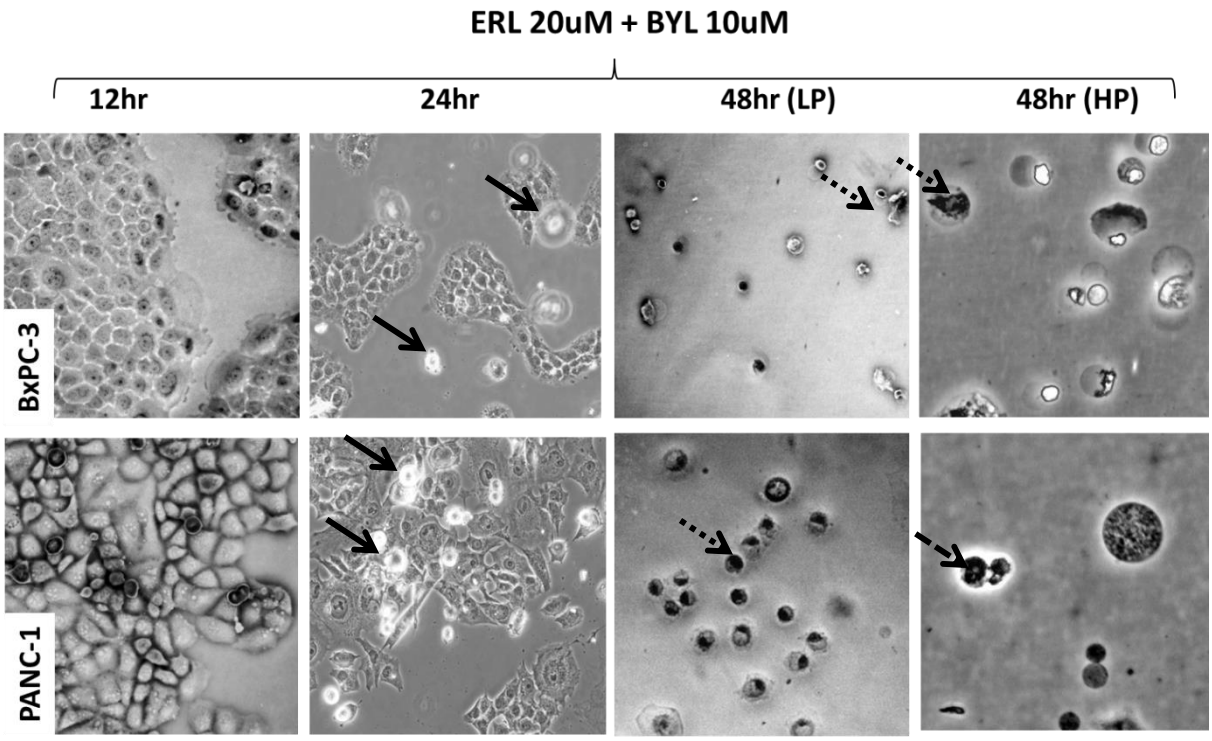

Figure 4.30: Cell microscopy of BxPC-3 and PANC-1 under E20Y10 CB. LP denotes low power; HP denotes high power

First, the time-lapsed response of cells under E20Y10 CB was studied under light microscopy **(Figure 4.33).** 12 hours into treatment, cells were relatively intact for both cell lines. After 24 hours of treatment, some cells were clearly detached from the flask (straight arrows), though morphology of these cells were difficult to appreciate since they were floating in the medium and became out of focus. By 48 hours, majority of cells that remained attached on the flask became shrivelled up with dense nuclei (dotted arrows) or disintegrated and formed debris (dashed arrows). These microscopic images were very typical to PDAC cell lines treated with PI3K or PI3K/mTOR-based CB. It often occurred with ERL* BYL and frequently occurred with BEZ or ERL* BEZ. However, it never occurred with CB involving IGF1R inhibitors.

Next, cleaved caspase-3 was examined using western blot. Shown below was one of two western blotting experiments optimising the treatment time for the study of cleaved caspase-3. This simple optimisation experiment involved treating BxPC-3 and PANC-1 with ERL or ERL* BYL at high dose, 24 and 48 hours. Protein concentrations were adjusted between cell lines, and they were blotted in two 10-well gels **(Figure 4.31)**.

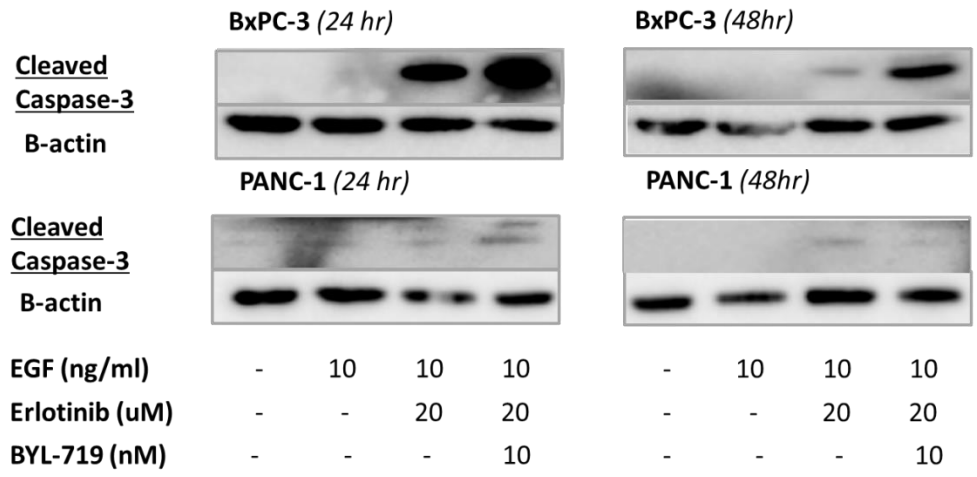

Figure 4.31: Cleaved caspase-3 treatment time optimisation (24 and 48 hours)

In both cell lines, cleaved caspase-3 intensity was higher with CB than SB, and was higher in the 24 hour than 48 hour treatment time point. Of note, the intensity of cleaved caspase-3 was higher in BxPC-3 than PANC-1, possibly suggesting that PANC-1 activated a different caspase for apoptosis or that this particular antibody was not ideal for wetern blotting study. The 4 cell lines were examined for cleaved caspase-3 with 24 hour treatment of CB and SB, and EGFR/IGF1R and EGFR/PI3K combinations were tested, in 2 experiments. Protein concentration was also adjusted, and each pair of parent and ER cell lines were studied together in the same blot **(Figure 4.32)**.

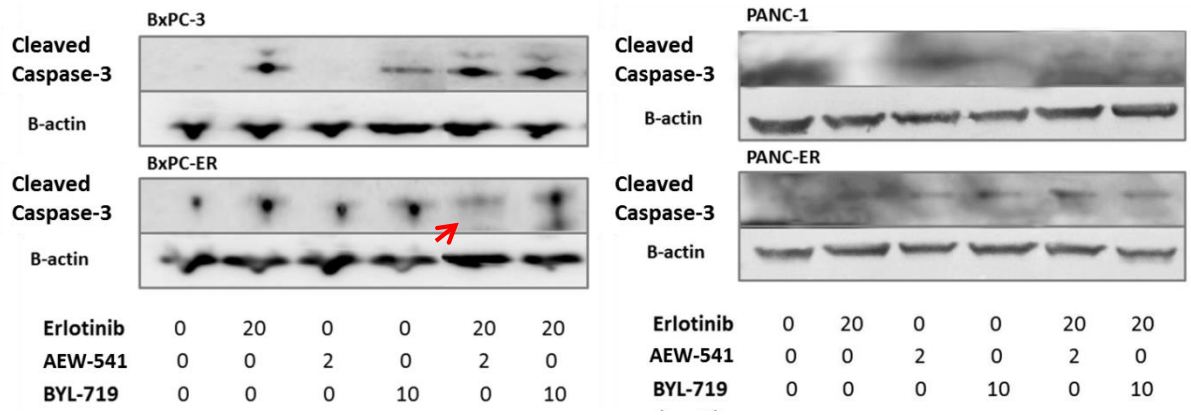

Figure 4.32: Cleaved caspase-3 treatment ERL*AEW and ERL*BYL CB/SB (24 hours)

In this representative blot, the signals for PANC-1/ PANC-ER were indeed much weaker than BxPC-3/ BxPC-ER, resulting in the detection of excessive background. Comparisons were

therefore difficult for PANC-1 and PANC-ER on western blotting given the weak caspase-3 signal. In BxPC-3 and BxPC-ER, CB generally appeared superior to SB. Erlotinib activated cleaved caspase-3 by 24 hour in BxPC-3, and the signal was less strong for BYL and not present for AEW. In BxPC-ER, a background cleaved caspase-3 signal was present at NT. Both ERL and BYL had similar levels of cleaved caspase-3; suggesting BYL had a stronger effect in BxPC-ER than BxPC-3. Whilst both CB showed strong cleaved caspase-3 signal in BxPC-3, ERL*AEW elicited a weaker signal in BxPC-ER. ERL* BYL, on the other hand, elicited the strongest signals in BxPC-ER implying superiority.

Unfortunately, the western blotting results were too weak, and microscopy results could only be regarded as supportive at best. In any case, these were insufficient as validation tools since the nature of these experiments could not allow for statistical analyses to be made. Cleaved caspsase-3 had to be studied by immunofluorescence instead.

4.3.3.4 Validation of Apoptosis Assay (immunofluorescence)

One of the difficulties studying cleaved caspase-3 by immunofluorescence was that individual cells activated caspase-3 at different treatment time points. To obtain caspase-3 staining in the largest number of cells under a high power field (63x by default), optimisation studies had to be carefully planned for the best treatment time. To do this, cleaved caspase-3 was examined over 5 treatment time points (6, 12, 18, 24, 30 hrs) based on the results of western blotting and microscopy. All 4 cell lines were independently optimised for the best condition. Higher dose - ERL 20 μM and BYL 10 μM – was chosen for confirmatory study.

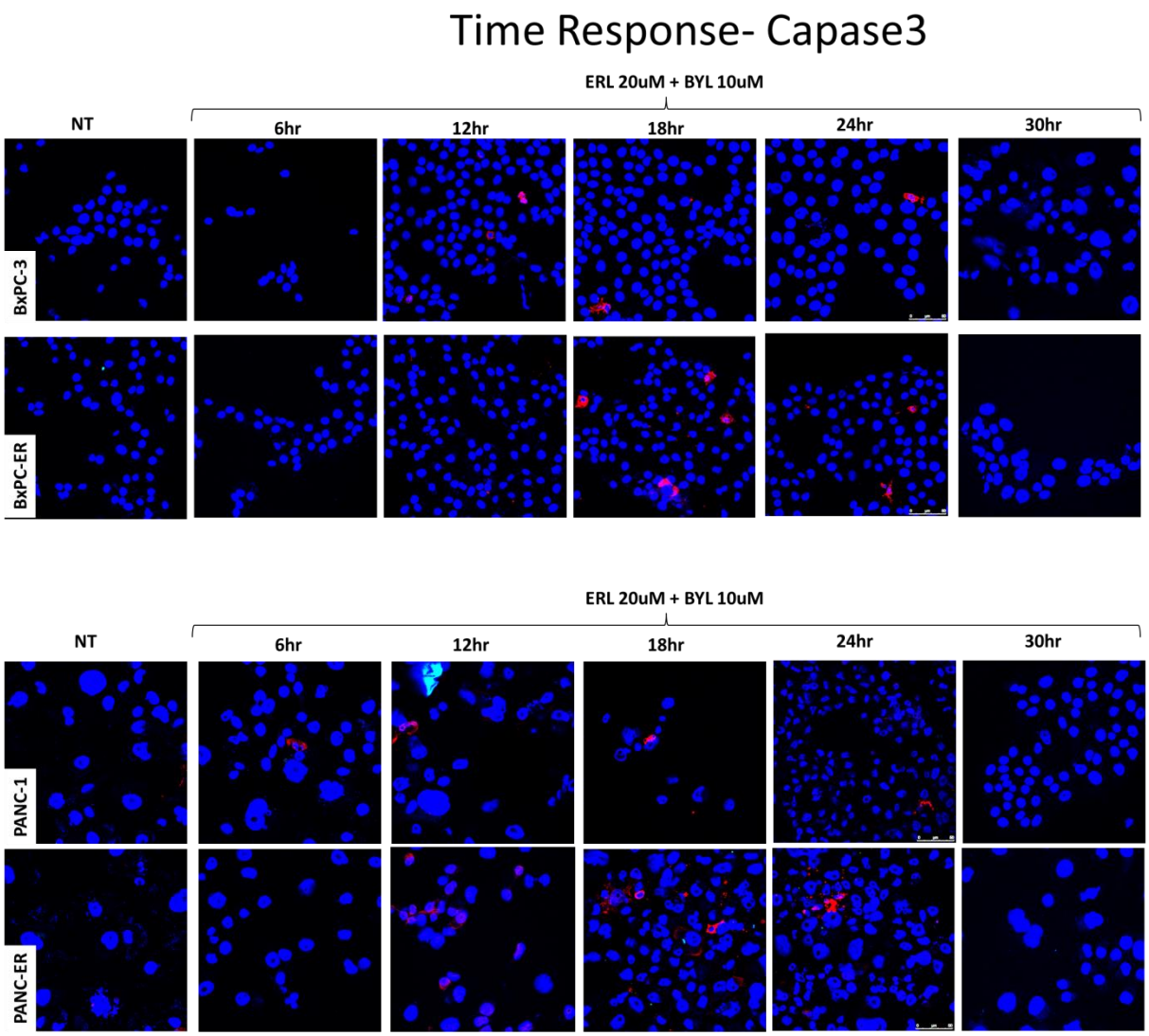

Figure 4.33: Optimisation experiment of activated caspase-3 immunofluorescence under E20Y10 CB treatment

Shown above were representative images of three optimisation experiments. Cleaved caspase-3 was essentially absent 6 hours into treatment, started to appear at 12 hours, was of the highest intensity from 18-24 hours, and disappeared altogether at 30 hours. This confirmed previous western blotting results of a higher cleaved caspase-3 expression at 24 hours. For subsequent experiments, **immunofluorescence was tested at 20-24 hours treatment.** In contrast to the weak signals in western blotting experiments in PANC-1/ PANC-ER, the same antibody produced good immunofluorescence signals for these cell lines. Thus, it was likely PANC-1/ PANC-ER also mediated apoptosis via caspase-3, only this particular antibody was better detected on immunofluorescence than western blotting.

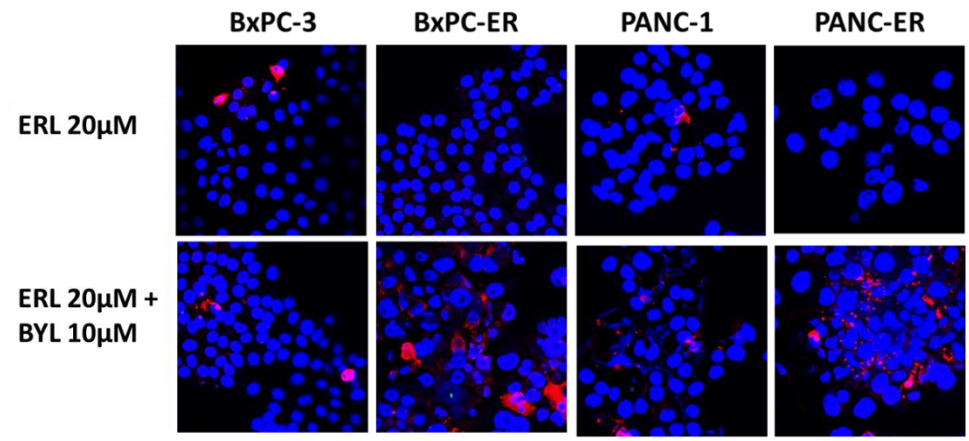

Figure 4.34: Activated caspase-3 immunofluorescence with E20 and E20Y10 at 20-24 hours

Representative photos of ER and parent cell lines treated with E20 and E20Y10 were shown **(Figure 4.34)**. Negative control (no treatment) were done for each experiment, but were not shown here since they essentially showed no staining. With E20, cleaved caspase-3 was of the highest intensity in BxPC-3, as expected. There were little caspase-3 staining in PANC-1 and essentially no staining for the ER cell lines. Conversely, the cleaved caspase-3 staining was much higher after treatment of E20Y10 CB in the ER cell lines than parent cell lines. These were in concordance with all the results observed thus far.

As per previous immunofluorescence studies, 4 independent experiments were performed and intensity was averaged from the 3 highest signals in each high power field taken from 5 random areas from each corner and the middle of the slides. Summary statistics and paired t-test were performed between ER and parent cell lines **(Figure 4.35)**.

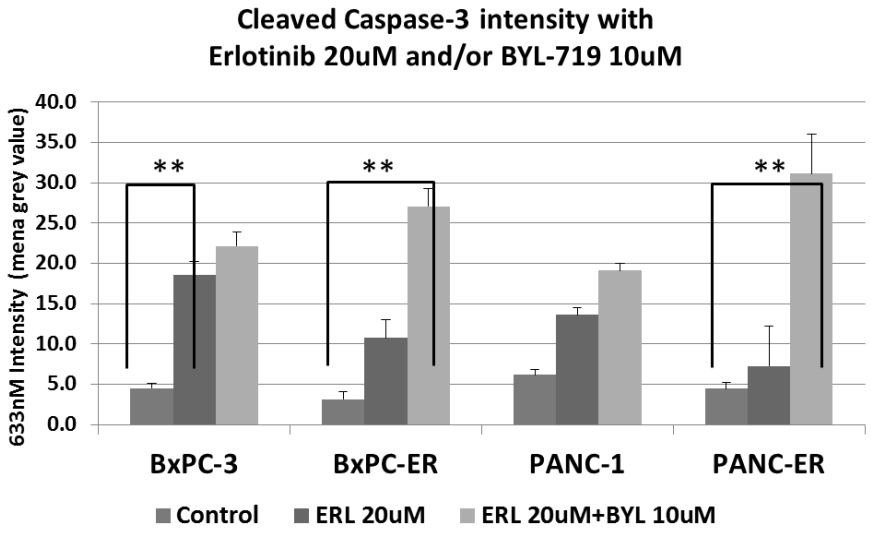

Figure 4.35: Summary statistics with E20 and E20Y10 at 20-24 hours treatment, 4 experiments, ** denotes P<0.001

Comparing between E20Y10 CB and E20 alone, cleaved caspase-3 activity was generally higher in CB than SB. Cleaved caspase-3 activity was significantly higher in E20 than control, but only for the BxPC-3 cell line. Cleaved caspase-3 was also significantly higher in CB than control, for the two ER cell lines. Comparing between ER and parent cell lines, paired t-test statistics showed that CB was significantly more effective in PANC-ER than PANC-1 (P=0.0001).

In summary, apoptosis assay and immunofluorescence showed high efficacy of PI3K inhibitor-based CB in inducing apoptosis and necrosis, whilst results of western blotting and microscopy were supportive. Additionally, interpreting these results together, the mechanism of apoptosis by these CB treatments was better understood: CB was cytotoxic to cancer cells, activating caspase-3 as early as 12 hours of treatment, with maximal signals at 20-24 hours **(Figure 4.33)**. Cell morphology began to change from 24-48 hours, with shrivelling of cells and condensation of nuclei **(Figure 4.30)**. Cells gradually shut down their mitochondrial activity at 48 hours, and finally approached the irreversible process of necrosis which was maximal by 72 hours **(Figure 4.27)**.

4.4.4 Migration Assays

***Key Finding:* All CB were equally effective in inhibiting migration, and there were no differential responses between ER and parent cell lines.**

Finally, the effect of CB combinations on cancer cell migration was studied. Cell migration was analysed in the incucyte imager after a uniform scratch wound was made on a 96 well plate. Mitomycin (10ug/ml) was previously optimised as an anti-proliferation agent, and was used to pre-treat and treat cells undergoing the migration process. Photos were taken at 2-hour intervals for 40-44 hours, and relative migration density was measured as the quantitative endpoint. A detailed methodology was described in chapter 2.

Cell imaging migration assays were performed for BxPC-3, BxPC-ER, PANC-1 and PANC-ER, in biological triplicate in each set of experiments. The first set of migration experiments compared all SB and CB between BxPC-3 and PANC-1. The second set of experiments compared the selected SB and CB combinations between parent and ER cell lines. Migration assays were not performed on the other 3 primary cell lines as the natural properties of these cell lines made them unsuitable for migration assay experiments: CFPAC-1 was too easily detachable, such that a uniform scratch could not be made; CAPAN-2 and MiaPACA-2 migrated way too slowly for meaningful migration density to be measured.

4.4.4.1 Migration Assays comparing all SB/ CB between BxPC-3 and PANC-1

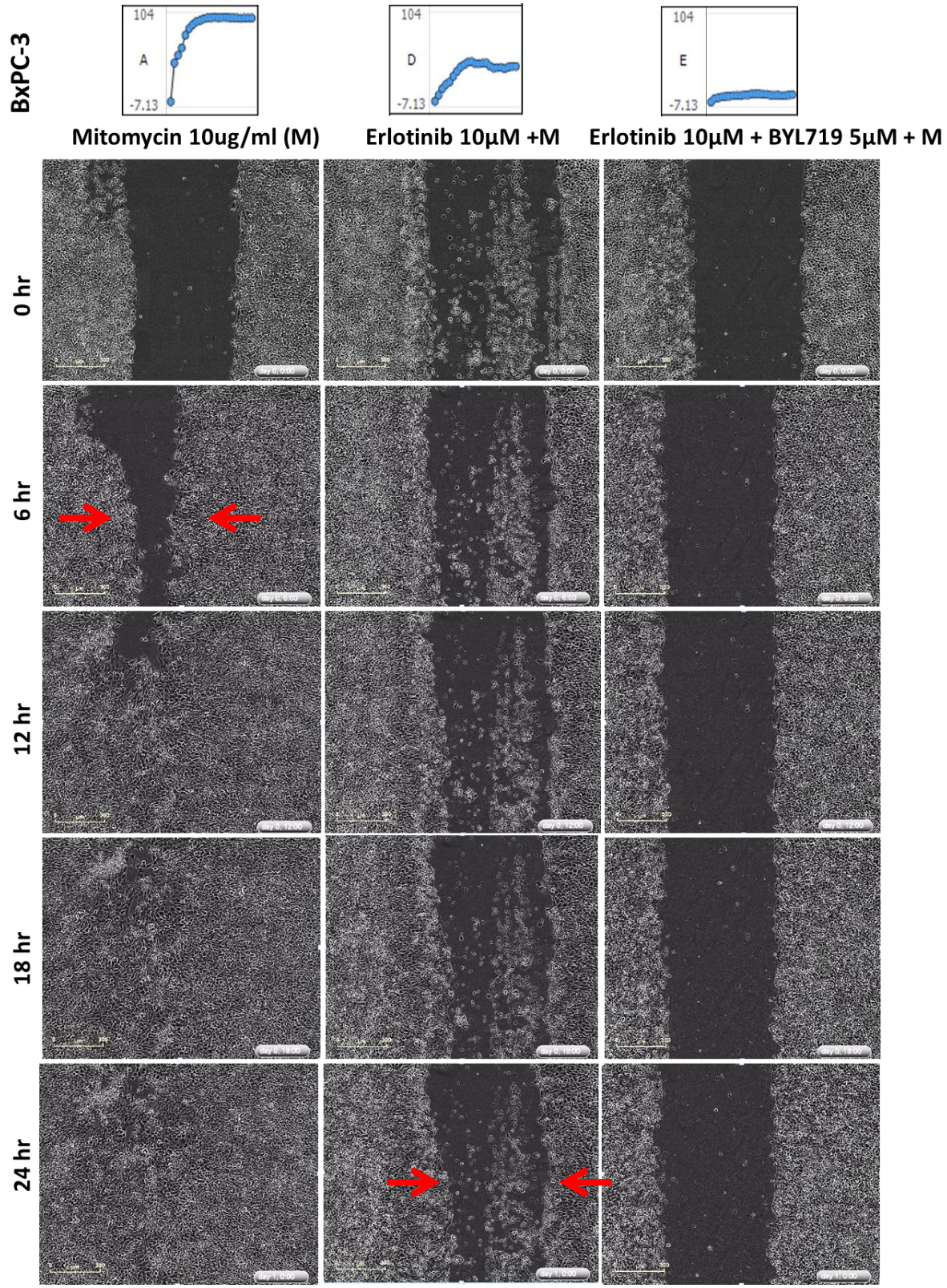

Figure 4.36: Representative photos of BxPC-3 undergoing SB and CB treatment (0-24hr)

The migration assay photos were converted into .avi movie files running at 2 frames per second for 40-44 hours. Excerpts of the movie of BxPC-3 undergoing ERL 10μM SB and E10Y5 were shown above to illustrate notable findings **(Figure 4.36)**.

Above, the migration rate for BxPC-3 in the absence of any inhibitor was exceedingly fast in the presence of mitomycin as an anti-proliferation agent. Cancer cells were well on their way of migrating towards each other by 6 hours, and at 12 hours the scratch wound had nearly closed in. With the addition of ERL 10 μM, the migration rate was retarded, but the migration process continued and was appreciated by 24 hours. Not shown here, the edges of the wound became apposed by 30 hours. For BxPC-3 undergoing E10Y5, the migration process was completely halted. There was no appreciable migration even at the termination of experiments (40 hours). Relative migration density is presented next:

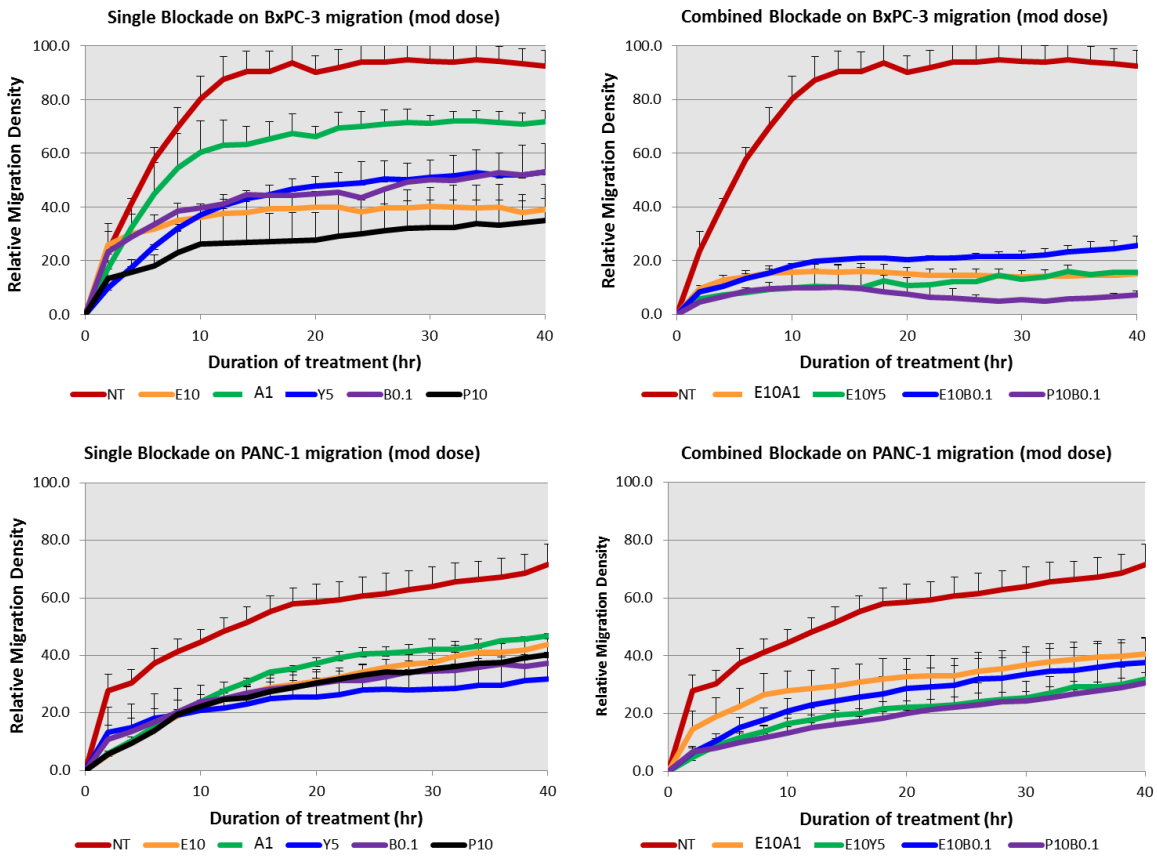

Figure 4.37: Migration Assay with SB and CB (mod dose) treatment in BxPC-3 and PANC-1

For brevity, only moderate inhibitor dosing results are shown since the low dosing results followed similar patterns. For BxPC-3, PD-98059 10 μM (P10) was the most effective in delaying and reducing relative migration density compared to control (**Figure 4.37,** top left diagram, orange and black lines compared to red line). IGF1R inhibitor (A1), PI3K inhibitor (Y5) and PI3K/mTOR inhibitor (B0.1) were less effective in reducing migration in this cell line (green, blue, purple lines). For PANC-1, all SB were similar in efficacy (bottom left diagram). Although it looked as though the migration density of treated cells was similar between BxPC-3 and PANC-1, these drugs were in fact more effective in BxPC-3 since BxPC-3 migrated much faster than PANC-1 at baseline (red lines, top left and bottom left diagrams). In BxPC-3, the best drugs E10 and P10 were able to reduce migration from 90% to 30% (33% of control); in PANC-1, the best drug Y5 was able to only reduce migration from 70% to 33% (47% of control). The different rates of migration between BxPC-3 and PANC-1 simply reflected the natural migration properties of the two cell lines, since optimisation experiments showed that the results at baseline remained the same regardless of whether mitomycin was added (not shown).

In BxPC-3, CB appeared more effective than SB (top right diagram). All CB reduced migration in a similar rate (down to 10-20%). CB was slightly more effective than SB (down to 20-40%). In both cell lines dual downstream blockades with PD-98059 plus NVP-BEZ (P10B0.1) were only slightly more effective (purple lines). Importantly, the contour of the trend was different in BxPC-3. CB completely retarded the migration rate in BxPC-3, resulting in almost flat migration curves.

Thus, it appeared that all pathways are involved in migration, with MAPK pathway (MEK) having a slightly more active role in BxPC-3. CB is effective in reducing migration in both cell lines compared to SB, especially in BxPC-3.

4.4.4.2 Migration Assays comparing SB/ CB between parent and ER cell lines

Migration assay was performed for SB and CB, and compared between parent and ER cell lines. Shown below are the results of 3 experiments ERL, AEW and BYL, as SB or CB **(Figure 4.38)**:

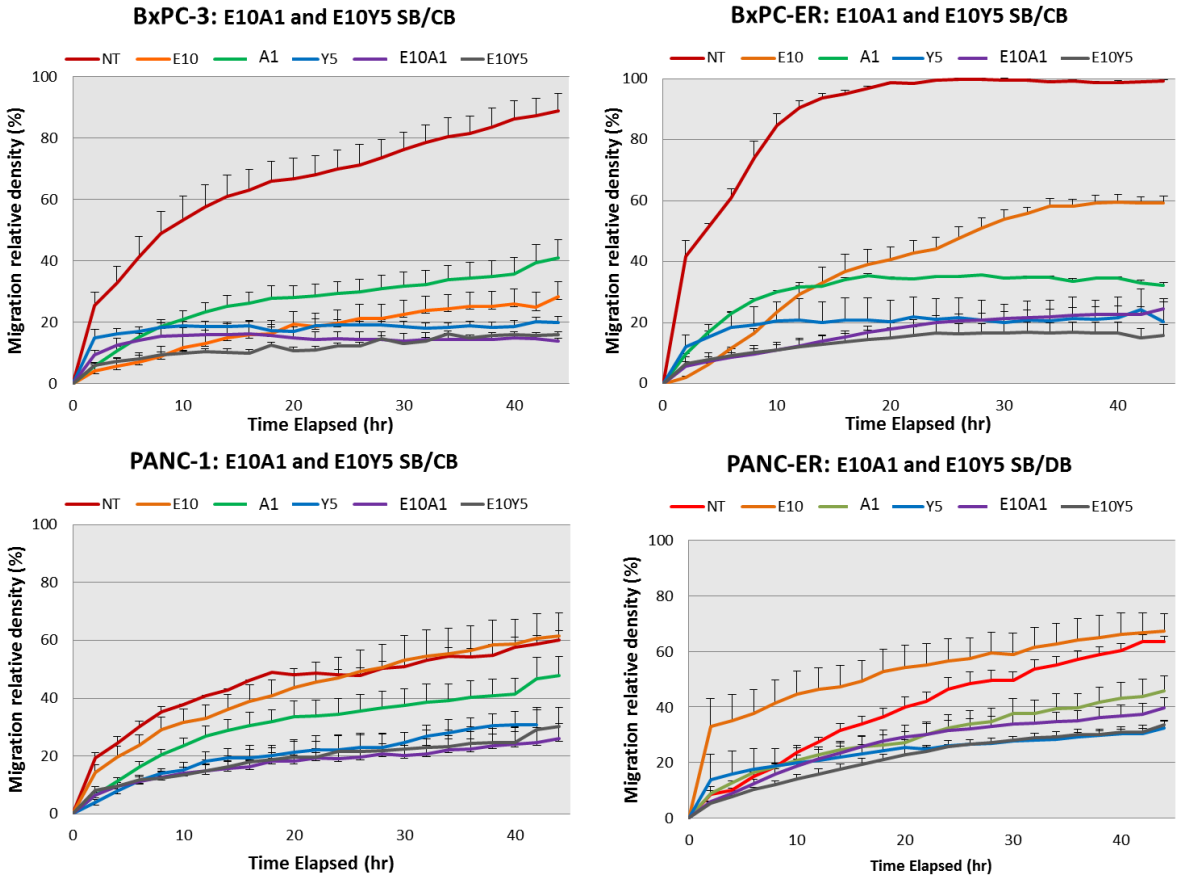

Figure 4.38: Migration Assay with E10A1 and E10Y5 SB/CB in parent versus ER cell lines

Comparing ER and parent cell lines, the trends showed BxPC-ER had a higher migration rate than BxPC-3 at baseline, whilst both PANC-1 and PANC-ER migrated at a similar rate (red lines). BxPC-ER had increased erlotinib resistance compared to BxPC-3, and both PANC-1 and PANC-ER were clearly resistant to the migration inhibitory effect of erlotinib (E10: orange lines). BYL (Y5: blue) was better than erlotinib and AEW (A1: green) in inhibiting migration in all 4 cell lines. Both E10A1 and E10Y5 CB (purple and grey) were equally effective. E10A1 was superior to ERL and AEW alone in all four cell lines. E10Y5 had similar effect of migration inhibition to BYL in all four cell lines, implying that this was the active agent. Different to the

clonogenic assay results, both CB were just as effective and there appeared little suggestion that ER cell lines were more hypersensitive to the effects of PI3Ki-based CB than parent cell lines. The 4 CB combinations were then compared side by side among the 4 cell lines **(Figure 4.39)**.

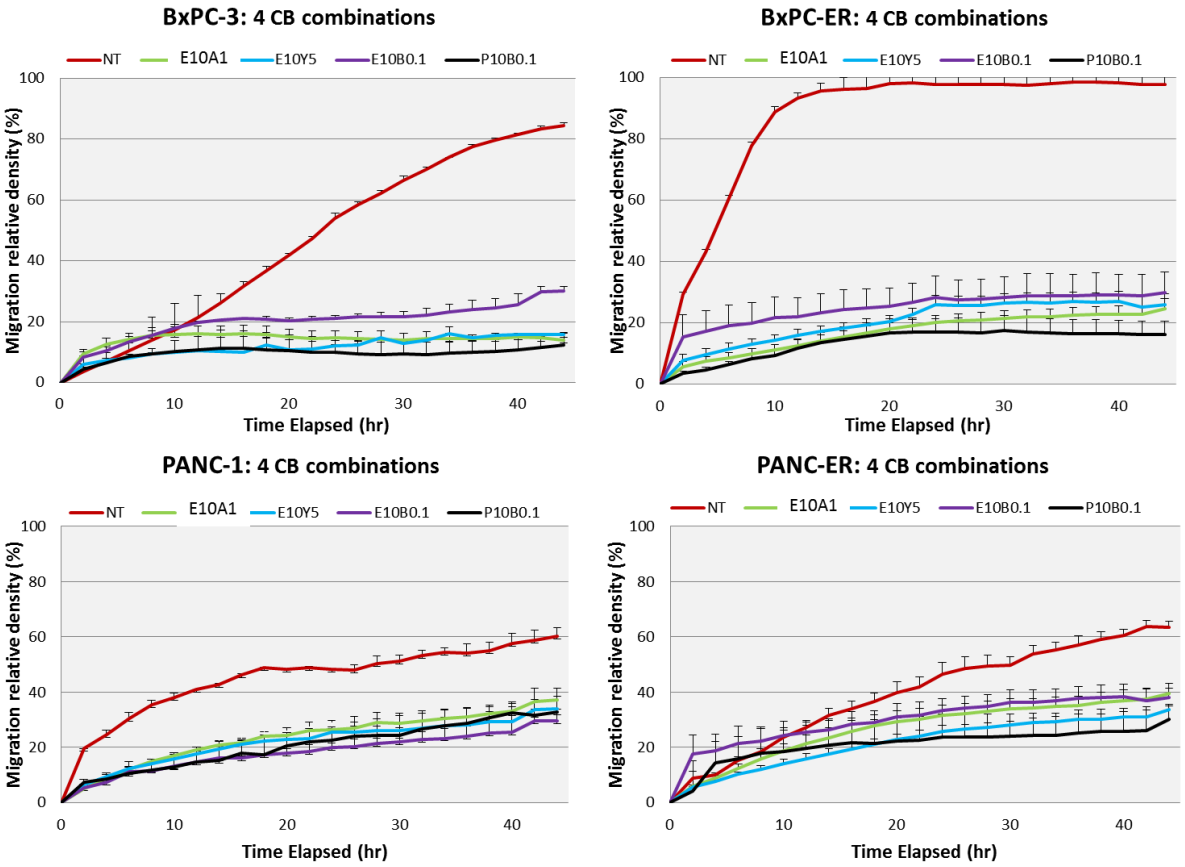

Figure 4.39: Migration Assay with 4 CB in parent versus ER cell lines

In all 4 cell lines, all 4 CB were equally effective in inhibiting the migration process down to 30% with variation of ±10%. This inhibition was very prominent in BxPC-3 and BxPC-ER, where the baseline migration rates were particularly high. There were no noticeable differences between parent cell lines and ER cell lines in their responses to a particular CB combination, suggesting that the **cancer migration is a complex process dependent on all molecular pathways at many levels, rather than on a specific molecular signal**.

4.4 Discussion

After discovering the important roles of downstream pathway up-regulation and in particular PI3K/Akt/mTOR activation in primary and acquired erlotinib resistance in chapter 3, this chapter set out three aims: 1) to study the effect of co-inhibition of the EGFR / MEK and PAM versus SB, 2) to find the most optimal combined blockade (CB) combination to take to *in-vivo* experiments, and 3) to explore oncogenic dependence of PI3K/Akt pathway – a concept that was suspected but largely left untouched in the previous chapter. To answer these 3 aims, 3 comparisons were made: 1) between CB and single blockade (SB), 2) between the 4 CB, and 3) examined any different responses to CB between parent and ER cell lines. This chapter was divided into two main sections: the study of synergy, and functional studies of combined blockade. For the purpose of discussion, results from these sections are combined, and presented under the two following headings.

4.4.1 Efficacy of Combined blockade Combinations *in-vitro*

The first aim was achieved relatively easily. By combining various inhibitors of EGFR /MEK and PAM pathways, **CB was found to be generally more effective than SB alone**. By complex mathematical and statistical approaches, cytotoxic and molecular synergy was demonstrated between erlotinib/ PD-98059 and BYL-719/ BEZ-235 in most cell lines. The endpoints, as measured by confluence (cell imaging proliferation assay), relative migration density (cell imaging migration assay), S-phase fraction (cell cycle assays) and cumulative apoptosis and necrosis rate (apoptosis assay) unanimously demonstrated superiority of CB to SB. In some cases, the effect of one agent dominated the combined effect of CB. For example, erlotinib caused a much higher necrosis and apoptosis rate than NVP-AEW541. Even so, ERL*AEW was slightly more cytotoxic than erlotinib alone, in all dosing levels (**Figure 4.27)**.

The second aim, to find the most optimal combined blockade in PDAC, was clearly a much more challenging task than the first. With so many possible targets in each respective

signalling pathway, there were innumerable drug combinations that could be tested. To systematically address this question, 4 CB combinations were scrutinised. The first two combinations (EGFR*IGF1R, EGFR*PI3K) were compared to determine the exact cross-talk mechanisms between IGF1R versus PI3K and EGFR. The third and fourth combinations (EGFR*PI3K/mTOR, MEK*PI3K/mTOR) covered further downstream signalling pathways, and were crucial in determining the exact role of the dual PI3K/mTOR inhibitor and which partner/s it interacted with. Given the large amount of data from the various assays, a table is constructed below to attempt to summarise the key findings:

	Erlotinib * NVP-AEW541 (ERL*AEW)	Erlotinib* NVP-BYL719 (ERL*BYL)	Erlotinib* NVP-BEZ235 (ERL*BEZ)	PD-98059* NVP-BEZ235 (PD*BEZ)
Cell Proliferation (MTT assays)	Highly synergistic in BxPC-3 and CFPAC-1, but antagonistic in MiaPACA-2, PANC-1	Antagonistic only in PANC-1, probably synergistic in other cell lines	Probably synergistic in all 5 cell lines	Probably synergistic in all 5 cell lines
Western blotting	Not synergistic in pERK, pAkt or pS6 inhibition	Synergistic in pS6 inhibition	Synergistic in pAkt (BxPC-3) and pS6 inhibition (both)	Difficult to assess since PD-98059 was a weak MEK inhibitor
Cell Proliferation (Imaging)	Same activity in BxPC-3/ PANC-1, but less active in ER lines (40-60% vs 10-30%)	High activity on all cell lines (BxPC-3, PANC-1, ER); results in cytostaticity	High activity on all cell lines (BxPC-3, PANC-1, ER); results in cytostaticity	High activity on all cell lines (BxPC-3, PANC-1, ER); results in cytostaticity
Clonogenic assay	Highly active in BxPC-3 only (85% reduction)	Highly active in BxPC-3 (88%), mod active (28-69%) in PANC-1 and ER lines	Highly active in BxPC-3 (78%), highly active (44-80%) in PANC-1 and ER lines	Highly active in all cell lines (65-96%)
Migration assay	Reduced to 20-30% migration density in Bx, Pan and ER lines	Reduced to 20-30% migration density in Bx, Pan and ER lines	Reduced to 20-30% migration density in Bx, Pan and ER lines	Reduced to 20-30% migration density in Bx, Pan and ER lines
Cell Cycle assay	20-50% reduction in SPF (Bx, PANC)	50-70% reduction in SPF (esp at med dose, PANC)	50-70% reduction with all dose (Bx, PANC)	50-70% reduction with all dose (Bx, PANC)
Apoptosis assay	High apo/necrosis for BxPC-3 and ER (48, 58%). Not effective in PANC-1 and ER	Similar apo/ necrosis for BxPC-3, BxPC-ER and PANC-1. Higher apo/ necrosis in PANC1 than ERL*AEW	Much higher apo/necrosis in BxPC-ER and PANC-ER (65%, 56%) than parents (49%, 49%)	Much higher apo/necrosis in BxPC-ER and PANC-ER (68%, 57%) than parents (51%, 49%)

Table 4.9: Comparison of 4 CB in various in-vitro assays

Whilst these experiments could not be performed on all PDAC cell lines given the immense work needed for each assay in optimising and adjusting for multiple variable factors (dose,

treatment time etc.), a number of general conclusions could be made nonetheless. Firstly, the best combination could be different depending on the cell lines. Given the vast genetic and molecular differences between PDAC cell lines, one would anticipate that one cell line would be more susceptible to one CB, and a different cell line to another. This was indeed the case: PANC-1 and the ER cell lines that had highly up-regulated PI3K were much more susceptible to dual downstream blockades PD*BEZ-235. On the other hand, for BxPC-3 - a *K-Ras* wild type cell line with up-regulated EGFR and IGF1R, co-EGFR-IGF1R inhibition by ERL*AEW was highly synergistic. Yet, even in this case, functional assays showed that this combination was only most active in inhibiting colony formation and causing necrosis/ apoptosis, but other CB combinations were superior in cell cycle disruptions, migration and proliferation (confluence) in this cell line **(Table 4.9)**. This suggests that multiple pathways remained at play even in the most erlotinib sensitive cell line.

Secondly, *synergy* is clearly not equivalent to superiority. Although not all data was shown, BEZ-235 was a very active agent on its own, in cell cycle disruptions and colony inhibition, as well as inhibiting migration and causing necrosis/ apoptosis. However, synergy indexes were only 1.12-1.50 when BEZ-235 was combined with Erlotinib or PD-98059, compared to 1.99 when erlotinib was combined with AEW541 in BxPC-3 **(Table 4.3)**. Synergy simply refers to positive interaction. If one drug is a highly potent drug on its own, it may not necessarily be synergistic when combined with another drug, since it would be difficult to demonstrate potency higher than an already high potency. Cell proliferation synergy experiments were carefully planned and executed with multiple equipotent dosing levels in a 6x6 matrix, but BEZ-235 remained such an active drug with nanomolar potency that it was hard to elicit synergy. Thus, synergy relates to mechanism, while superiority refers to efficacy- which was the focus for finding the optimal CB.

Thirdly, in terms of *efficacy,* any CB combination that included PI3K or PI3K/mTOR inhibitor (2^{nd}, 3^{rd}, 4^{th} combinations) appeared to be at least moderately to highly active to *all* cell lines tested, including erlotinib-sensitive (BxPC-3), insensitive (PANC-1) and resistant (ER) cell

lines alike. These 3 combinations were all equally and highly effective in inhibiting cell proliferation, cell cycle and migration; and there was a further increase in apoptosis/ necrosis and colony inhibition when comparing ERL*BYL to ERL*BEZ to PD*BEZ. In addition, the findings of multiple cell cycle arrests (G1, G2/M, S) and the shrivelled cells with dense nuclei on light microscopy were especially significant. These changes occurred mostly in BEZ-235 based CB, often in ERL*BYL, but never in ERL*AEW541 CB. This implies that PI3K is vital in proliferation and migration processes, whilst PI3K via downstream mTOR signalling is closely involved in the colony formation, survival/ anti-apoptosis and cell cycle functions via multiple checkpoints. This was illustrated with the figure below **(Figure 4.41)**, which added new information to the existing diagram **Figure 4.1**. By blocking both MAPK and PAM pathways downstream, reciprocal activation of collateral pathways was minimised. This, in turn, suggests that multiple pathways in fact converge rather than diverge at the level close to the nucleus.

Taking all the functional studies together, combined downstream blockade with **PD-98059 and BEZ-235 was the most effective CB combination**, affecting a variety of cellular functions in all cell lines. This appears consistent with current literature reporting strong synergy between MEK and PI3K in various cancer types.[191] Although this was considered the best of 4 CB, this did not end up being the CB combination used *in-vivo*. There were other considerations to the final choice such as toxicity, costs and drug availability. This will be discussed in more detail in the next chapter **(Chapter 5)**.

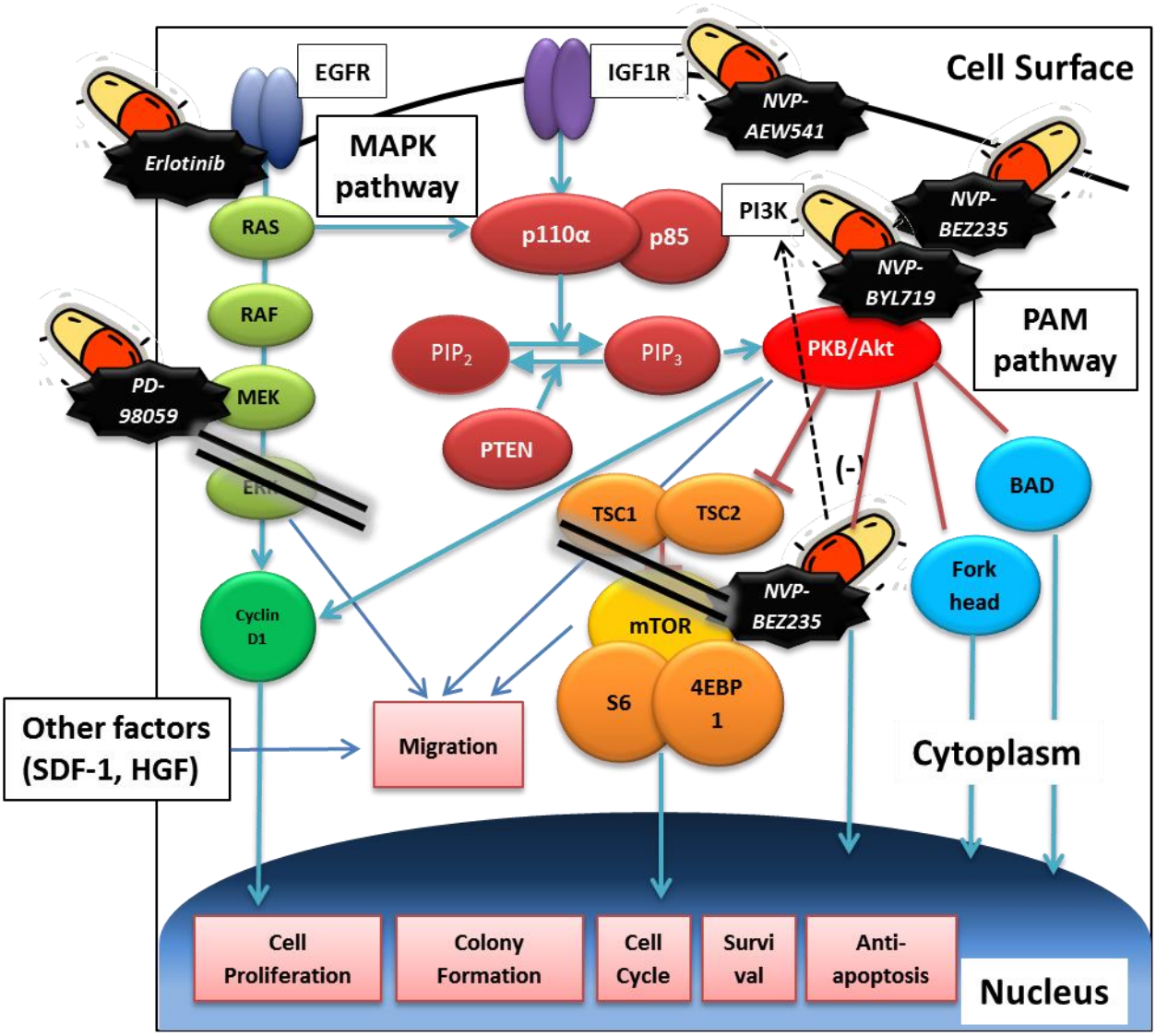

Figure 4.40: Cellular functions inhibited by CB in PDAC cell lines

4.4.2 Oncogenic Dependence to PI3K/Akt/mTOR pathway

Importantly, this study illustrates the possibility of oncogenic addiction/ dependence in pancreatic cancer, the third aim of this chapter. That is, cancers become dependent on the activity of specific oncogenes and hence display higher sensitivity to drugs targeting that particular cancer circuitry.[330] In the *in-vitro* model, the fact that both ER cell lines up-regulated the PAM pathway, made them susceptible to the effect of NVP-BYL719 or NVP-BEZ235 based treatment. The evidence for this was based on multiple functional studies and summarised in the table below:

Cellular Functions	Assays	Observations	Comments
Cell Proliferation^	MTT Assay	ERL*BYL was more synergistic and ERL*AEW less synergistic in both ER than parent cell lines	ER cell lines changed from dominant EGFR-IGF1R to EGFR-PI3K interactions
Molecular mechanisms	Western blotting	ERL*BYL and ERL*BEZ were more effective in inhibiting pAkt and pS6 in both ER cell lines	Molecular biological evidence that ER cell lines were depending on the PI3K in mediating downstream signals
Colony Formation	Clonogenic Assay	Both ER cell lines became hypersensitive to downstream DB, with PD*BEZ causing 88-96% colony inhibition (compared to 59-65% in parent cell lines)	ER cell lines depended on downstream EGFR/MAPK and PI3K/Akt/mTOR in mediating colony formation
Cell Cycle progression	Cell cycle assays	PANC-ER had significantly reduced SPF compared to PANC-1 in response to ERL*BYL and ERL*BEZ. A variety of cell cycle disruptions were observed for BYL and BEZ-based DB.	PI3K/Akt/mTOR was essential in multiple cell cycle checkpoints; PANC-ER significantly depended on this pathway at least for G1 progression
Apoptosis and necrosis	Apoptosis assay, Caspase-3 IF and WB	ERL*BEZ and PD*BEZ caused significantly more apoptosis and necrosis in ER cell lines, as was ERL*BYL in PANC-ER. ERL*BYL activated significantly more caspase-3 in PANC-ER than PANC-1	ER cell lines were highly dependent on mTOR in mediating survival and anti-apoptosis signals, making them highly susceptible to BYL or BEZ based DB
Migration Assay	Migration assay	All 4 cell lines were equally sensitive to all 4 DB, with relative migration density down to 20-40%	No differential sensitivity existed between ER and parent cell lines. Migration was propagated by multiple signals from both pathways

Table 4.10: Summary of 4 CB in various in-vitro assays. ^ Cell Proliferation assay was a crude measure of net cell proliferation minus cell death

Of note, the pattern of susceptibility correlated closely with the known normal cellular functions of the PI3K/Akt/mTOR system. BYL-719 or BEZ-235 based CB caused significant arrest in G1, a checkpoint normally regulated by Akt-driven cyclin D1. This combination also caused high levels of apoptosis and necrosis, and Akt is known to modulate anti-apoptosis and survival signals via Forkhead and BAD via Bcl-2 and FasL.[45] Lastly, it also substantially inhibited colony formation and cell proliferation, which depend on a number of pathways including Akt-driven mTOR, GSK3, p21 and p27.[45,178,323] These effects on ER cell lines in proliferation assays, cell cycle, apoptotic assays and clonogenic assays were above what was observed in the parent cell lines, and significantly so for PANC-ER **(Table 4.5, 4.7, 4.8)**. In contrast to proliferation and survival, migration was equally affected by all 4 CB, and there was no differential sensitivity observed between parent and resistant cell lines. Whilst the PI3K/Akt pathway has been linked to migration,[324] this is a complex process of cell-matrix-stroma

interaction orchestrated by many autocrine factors including stromal-cell-derived factor (SDF-1) and hepatocyte growth factor (HGF).[331] Possibly since migration is in part driven by other molecular pathways, oncogenic addiction of PI3K/Akt/mTOR pathway by erlotinib resistant cell lines did not display hyper-sensitivity to PI3K inhibitors **(Figure 4.40)**.

The study of oncogenic dependence was therefore a significant one, because like synthetic lethality, it provided a conceptual framework for developing cancer-specific cytotoxic treatment strategy, by exploiting the weakness of cancer cells to go down a specific pathway in the face of drug pressure.[200] Simply put, this study had found **that despite all the complex networks in PDAC cells, there was a single obligatory pathway of "least resistance" that was exploited by these cells to escape drug pressure (the PI3K/Akt/mTOR), which in turn make them targetable by combined targeted drug blockade strategies.** From this paradigm, there are multiple implications to ongoing research for pancreatic cancer, and these will be discussed in greater detail in **Chapter 6**.

In conclusion, combined blockade of the closely connected EGFR/MEK and PI3K/Akt/MAPK pathways were more effective than single blockade alone, and dual downstream blockade with MEK and PI3K/mTOR inhibitors appeared the most effective in all cell lines. Erlotinib resistant cell lines that were driven down this pathway became dependent on this for survival, making them hyper-sensitive to these treatments.

CHAPTER 5:

EGFR AND PI3K INHIBITORS CB *IN-VIVO*

5.1 Introduction

5.1.1 Chapter Background

So far, chapter 3 and 4 focused on *in-vitro* experiments and had elicited two intriguing properties about erlotinib resistance and pancreatic cancer: firstly, primary and acquired erlotinib resistance were both associated with downstream signalling pathway activation, especially via the PAM pathway. Secondly, erlotinib resistant PDAC cell lines were dependent on this obligatory pathway, making them highly susceptible to EGFR and PI3K co-inhibition. Putting these two concepts together, the hypothesis for translational study is that erlotinib resistance and/or PI3K/Akt over-activation may be potential predictive biomarkers for erlotinib plus PI3K inhibitors combined blockade. Therefore, initially the aim of this section was to study erlotinib resistance *in-vivo*. However, these objectives could not be definitively achieved *in-vivo* due to the challenges of developing an of erlotinib resistance animal model as well as statistical considerations. On the other hand, these objectives could be more easily and decisively studied in human studies. Since patient-derived xenograft model is an established method of testing anti-cancer drug activity, and has been shown to closely recapitulate clinical trial situation if developed appropriately,[332] the efforts were turned to developing and validating a suitable animal model and using it to establish *in vivo* efficacy of CB **(Chapter 5)**. The CB selected were ERL* BYL and ERL* BEZ. Although PD * BEZ was previously shown to be the most potent combination, PD-98059 was only used *in vitro* due to solubility issues,[192] and an appropriate MEK inhibitor could not be secured *in vivo* from pharma. As for the development of an *in-vivo* erlotinib resistant model and biomarkers for CB, these were attempted nonetheless with preliminary results presented in **section 5.4**. The ultimate proof of concept, however, will have to wait for human studies, whose study design is outlined in **Chapter 6**.

5.1.2 Chapter Aims

1. To establish and validate a pancreatic cancer xenograft model for drug testing
2. To test the *in-vivo* efficacy of EGFR and PI3K combined blockade

5.1.3 Chapter Methods- summary

The general animal study methods and design had been summarised in **section 2.2.14** and will be covered in more detail in the next section. Briefly, Patient-derived tumour tissue (PDTT) fresh from patients who underwent Whipple's surgery (JS) for resectable pancreatic cancer were removed, and transplanted in non-obese diabetic/severe combined immunodeficiency (NOD/SCID) mice. Whilst metastatic PDAC specimens would more closely resemble the *in-vitro* models of metastatic PDAC cell lines, this was not feasible as most metastatic PDAC patients only have fine-needle aspirate biopsies, and there would not be sufficient tissue for our animal model. Two models (sub-renal, subcutaneous) were established and validated independently for drug testing. Sub-renal was selected as the core model for the reasons described below. 2 drug combinations were used (ERL* BYL, ERL* BEZ); and these were compared against control, SB or gemcitabine (standard). BYL and BEZ were either purchased or provided for by Novartis Pharmaceuticals. MEK inhibitor such as PD-98059 was unfortunately not available in sufficient quantity for *in-vivo* testing. The primary endpoint for the core study was tumour volume. The secondary endpoints were kidney weight, metastatic disease and IHC of Ki-67. I had major involvement in the overall study design and methods, and the execution of the project was undertaken as a group work (RS, SJ, AX, SS, myself). The animal experiments were carried out conforming the Australian code of practice for the care and use of animals for scientific purposes (2004),[333] and were approved by local area ethics committee.

5.2 Study Methods and Design

5.2.1 Study Methods

5.2.1.1 Animals

NOD/SCID mouse is the most common murine xenograft model.[334] 6-8 week-old male NOD/SCID mouse were obtained from the Animal Resources Centre, Perth; and were housed at the Kearns Facility in the Kolling Medical Research Institute, Royal North Shore Hospital. They were housed for a week to familiarise with new environments before surgery.

5.2.1.2 Patient tumours

Patients were consented by the surgical team for donation of part of their cancer tissue for research. The donor tissue was obtained from patients with resectable pancreatic cancer undergoing Whipple's surgery in Royal North Shore Hospital. Within 30 minutes of surgical removal, the tumour specimens were preserved in DMEM supplemented with FBS and immediately transported in standard sterile transplant containers. Under sterile hood each tumour tissue was divided into two parts. One part was fixed in 10% formalin for histological analysis. The other part was cut into multiple 1 x 1 x 2 mm^3 pieces, and was kept in medium on a sterile petri dish at 4 ºC. Xenografts experiments were performed fresh on NOD/SCID mice inside Kearns facility within 2 hours. The tumours were examined and diagnosed independently by 2 senior pathologists (AG, CT).

The demographic details and histopathology of the tumours are presented in **Table 5.1**, In total, 21 human pancreatic cancer specimens were obtained. Median age was 59.5 years (range 49-79 years). 62% (13/21) were male. 6 patients had high grade (G3/G4) adenocarcinomas, and 15 patients had moderate grade adenocarcinoma (G2). 15 patients had pancreatic ductal adenocarcinoma. Among these, one tumour specimen (P009E7) was obtained from a pancreatic cancer metastatic lesion to the ribs. 4 patients had ampullary adenocarcinoma, 1 had duodenal cancer and 1 had gastric cancer. Since tumour biology of

these cancers could be very different to pancreatic cancer, these specimens of other pathologies were only used to develop the animal model. 18/21 patients were treatment naïve prior to surgery and had received gemicitabine treatment only after surgery. Only one patient (P010E8) received neoadjuvant gemcitabine and radiotherapy prior to tumour removal. 33% (7/21) had incomplete resection (R1), and would be expected to have poorer prognosis.[335]

Patient ID	Age/ sex	Pathologic Diagnosis[a]	Tumour Grade[b]	Tumour Stage[c]	Resection Margin*	Post-surgery treatment
P002E1	69/M	Amp	G2	T2N0M0	R0	Nil
P003E2	62/M	Amp	G2	T3N0M0	R0	Gemcitabine
P004E3	52/M	PDAC	G3	T2N1M0	R0	Gemcitabine
P005E4	62/F	PDAC	G2	T3N1M0	R1	Gemcitabine
P006E5	62/F	PDAC	G2	T3N0M0	R0	Gemcitabine
P007E6	66/M	PDAC	G4	T3N1M0	R1	Gemcitabine
P009E7	53/M	PDAC	G3	TxNxM1	N/A	Gemcitabine
P010E8	72/F	PDAC	G2	T3N1M0	R1	Gem& RT
P012E9	71/F	PDAC	G2	T3N1M0	R1	Gemcitabine
P013E10	46/M	PDAC	G3	T3N0M0	R0	Gemcitabine
P014E11	67/F	PDAC	G2	T3N1M0	R1	Gemcitabine
P021E15	79/M	PDAC	G2	T3N1M0	R1	Gemcitabine
P022E16	67/F	PDAC	G2	T1N0M0	R0	Gemcitabine
P025E17	57/F	Amp	G2	T2N1M0	R0	Gemcitabine
P026E18	58/M	Gastric	G2	T2N1M1	N/A	Gemcitabine
P027E19	58/M	PDAC	G2	T3N1M0	R0	Gemcitabine
P028E20	62/M	PDAC	G3	T3N1M0	R0	Gemcitabine
P029E21	72/M	Duodenal	G2	T3N0M0	R0	Nil
P030E22	49/F	PDAC	G3	T3N1M0	R0	Gemcitabine
P023E23	63/M	PDAC	G2	T3N1M1	R1	Gemcitabine
P024E24	79/M	Amp	G3	T3N1M0	R0	Gemcitabine

Table 5.1: Patient characteristics. Abbreviation: ***G2:*** *Moderately differentiated.* ***G3****: Poorly differentiated.* ***G4****: Undifferentiated.* ***M****: male.* ***F:*** *female.N/A.* ***Amp****: Ampullary adenocarcinoma.* ***PDAC****: Pancreatic ductal adenocarcinoma.* ***a****:WHO classification.* ***b****: TNM grading system.* ***c****:pTNM, AJCC 7th edition 2009.* ****Resection Margins:*** *R0, resection is defined as a grossly complete resection with microscopically negative margins; R1, resection is defined as a grossly complete resection with microscopically positive margins; and R2 resection is defined as a grossly incomplete resection N/A: no resection margin.* ***RT:*** *radiotherapy*

5.2.1.3 General care of animals

In accordance to the Australian Government National Health and Medical Research Council (NHMRC) Guidelines to promote the wellbeing of animals used for scientific purposes,[336] meticulous attention was given to apply high standards of quality and safety while ensuring animal rights of individual animal. Sterility was especially important for NOD-SCID immunocompromised mice.[337] This was controlled by providing ultra-violet sterilised water and food, completing procedures in clean and hooded work area, cleaning cages or transferring animals to new cages weekly, and using sterilised or pre-packaged instruments. Pain assessment and management was paramount, as disruption of animals' well-being frequently leads to variability and uncertainty of results.[336] Mice were evaluated for general appearance, ability to move normally around cage and reach food and water, ability to eat and drink, grooming habits, skin colour and lethargy. In addition to the standard monitoring, care was also taken to monitor signs of pilorection, hunched posture, changes in group behaviour and responses upon handling; as these could all represent signs of pain or distress. General anaesthetics 2% isoflurane mixed with NO_2 was used for all procedures including drug gavaging, to ensure the anaesthesia was quick and not distressing. Analgesia with pethidine was given post-op. Where mice were found to be dehydrated, nutrition gels were provided in the cages. Each week mice were weighed, and a log was kept for their serial weight and any concerning symptoms. Mice with loss of 20% body weight were euthanized. This was relatively uncommon, as mice at this age were observed to gain around 10% body weight per week, and cancer engraftment for 9 weeks caused cachexia unusually.

5.2.1.4 Surgical procedure

NOD/SCID mice were individually weighed and anesthetized with isoflurane, Nitrous oxide and Oxygen (2:1:1). The surgical field was cleaned with 70% alcohol and draped with sterile cloth, and surgical standard personal protective equipment (PPE) and instruments were used.

Sub-renal capsule grafting procedure was well established by Wang *et al* in Canada.[338] Whilst technically more challenging, this method was chosen as the core methods over subcutaneous model, since it resulted in high engraftment rate, allowed for quick assessment

(6-8 weeks) and resembled more closely to tumour histology and biology.[268,339] After prepping with betadine and shaving the dorsal surface of the back of the skin, a small incision was made along the midline. The back skin was lifted with a pair of sterile blunt forceps and the posterior body wall was cut with a pair of scissors creating an incision approximately 2 cm in length **(Figure 5.1)**. Each kidney was popped out by applying gentle pressure on either side of the abdomen using the forefinger. A pocket was then created between the capsule and kidney parenchyma by blunt dissection, and 1 - 2 grafts were inserted in the sub-renal capsule using a polished sterile glass pipette. The kidneys were gently eased back into body cavity. The abdominal wall and skin were closed with staples after both sides were completed.

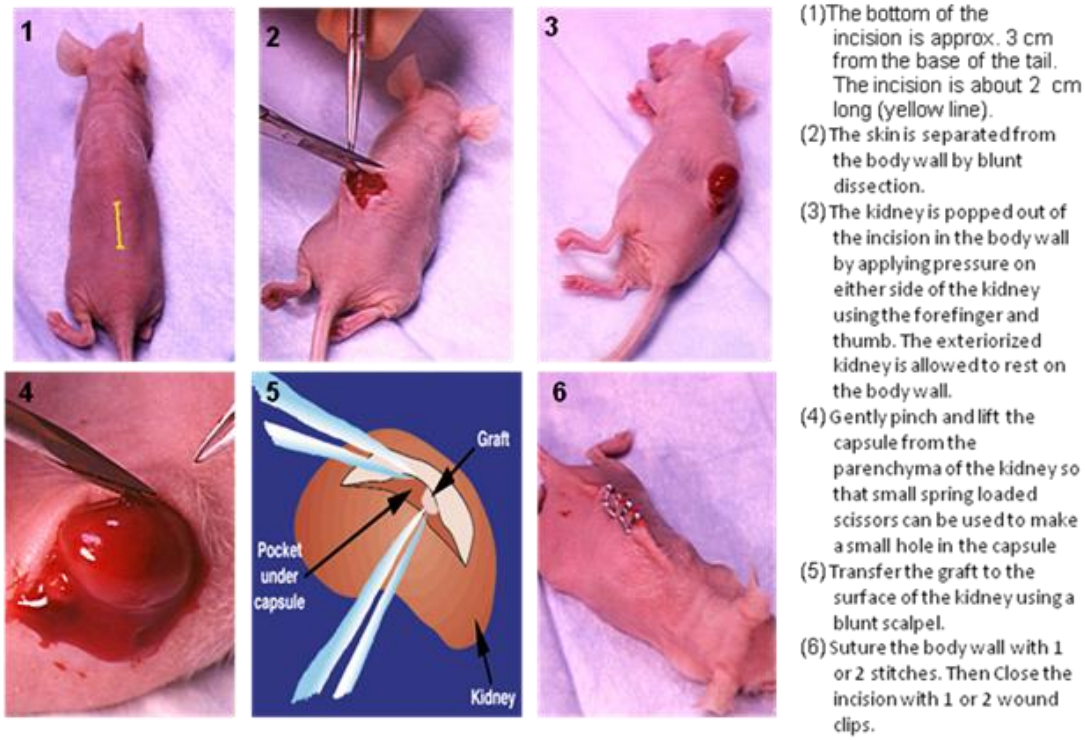

Figure 5.1 Sub-renal xenograft transplantation procedure.

Subcutaneous xenograft models were performed as previously described methods.[340] A smaller skin incision was made in the same way, and the adventitious tissue was dissected down by blunt forceps to create a subcutaneous pocket. Xenografts pieces were transplanted in the subcutaneous pockets on each side. Because of the smaller incisions, the skins were

apposed and glued instead of stapled. The mice were observed to recover more quickly post-operatively with this procedure than the sub-renal transplantation.

5.2.1.5 Post- operative Care and Monitoring

Standard post-operative care was provided for the animals. After surgery, the mice were allowed to recover under the warm condition (with heated mat) with one mouse per cage and free access to food and water. Pethidine 10-20mg/kg subcutaneously was given post-op. The animals' health was monitored daily after surgery for the first 5 days and then every second day until the wounds were healed. Twice weekly after operation, the wounds on the animals were examined and dressed with betadine. 10 days after surgery, staples were removed.

5.2.1.6 Drug Treatment

PDTT experiments were shown to be predictive of chemotherapeutic activity in humans, provided pharmcokinentically clinically equivalent doses were used.[332] Erlotinib 50mg/kg/day was used, as this *in-vivo* dose was expected to yield plasma concentrations near the clinically therapeutic levels in humans without causing cardiovascular and renal toxicities.[341] Intra-peritoneal injection of gemcitabine 100mg/kg twice weekly was the standard dose for pancreatic cancer *in-vivo* study, supported by a number of publications.[342,343] BYL-719 and BEZ-235 25mg/kg/day were chosen after demonstrating dose limiting toxicities with higher doses, and this was consistent with recommendations of the investigators' brochures. All inhibitors were homogenized in 6 mg/ml 0.5% methylcellulose prepared fresh twice weekly, whilst gemcitabine was diluted by sterile 0.9% normal saline into 10mg/ml solution. These dilutions were made based on the maximum gavage volume of 10ml/kg and maximum intraperitoneal bolus injection volume of 1% of animal weight.[336]

Gavaging of oral drug solution ensured the swallowing of drugs by animals. Standard 18-20 gauge plastic feeding tubes 1.5 inches long were used. The animal was first anaesthetised, restrained and gavaged by feeding tube using the other hand, after gently extending the neck.[344] Intraperitoneal (IP) injection was performed by holding the anaesthetised mouse in

the supine position with its posterior end slightly elevated. The needle was kept parallel to the vertebral column, and the injection was given at the abdominal surface of the lower quadrant of the abdomen at approximately 10^{o}.[345] Pre-packaged needles were used once only. All mice were monitored daily during drug treatment until termination of experiment.

5.2.1.7 Sacrifice of Animals

All mice will be euthanized on 60 days post grafting or 30 days post treatment. The last dose of treatment was given on day 28, and animals were given 2-day drug free holiday before sacrifice. The animals were killed by carbon monoxide inhalation instead of cervical dislocation to ensure a comfortable death.

5.2.1.8 End-of-study assessment and Tissue Collection

Animals were weighed at end of study. Kidneys were removed and also weighed. Tumours were directly visualized, photographed and measured using standard callipers. The tumours, lymph nodes, lungs, livers, kidneys, spleens, and bone (femur) of the hosts were removed, fixed and examined for metastases. Histopathology and IHC were performed on paraffin embedded slides using standard methods as described **(sub-section 2.2.15)**, and were reviewed and scored by a senior pathologist (AG).

5.2.1.9 Animal Ethics and Human Ethics Approval

All animal care and experiments were carried out in accordance with the guidelines of the Australia Council on Animal Care and the Royal North Shore Hospital Animal Care & Ethics Committee (Protocol number 1011-015A, Sydney, Australia). Pancreatic tumour surgical specimens were obtained from either Royal North Shore Hospital or North Shore Private Hospital (Sydney, Australia) following protocols approved by the Northern Sydney Health Human Research Ethics Committee (Protocol number: 0909-227M, Sydney, Australia).

5.2.2 Study Design

5.2.1.1 Development and validation of sub-renal model

For each experiment, one patient pancreatic cancer specimen could be dissected into sufficient graft pieces for 20 mice. 28 days after tumour engraftment, mice were randomised to IP gemcitabine or normal saline treatment for another 28 days. **The primary objective of the study was to demonstrate superiority of standard gemcitabine over control in end-of-study tumour volume**. **The secondary objective was to elicit similar histopathology and immunohistochemistry of proteins that were not expected to change with treatment, between pre-graft and post-graft tumour specimens**. Cytokeratin 7 and 20 (CK7) and (CK20) immunohistochemistry was selected, since the expressions of these markers were generally associated with specific cancer type, and pancreatic adenocarcinoma typically stained CK7+ and CK20+ or focally positive.[346] Two senior post-doc scientists (AX, SJ) had the principal roles in the development and validation of the sub-renal model. They had many years of animal study and immunohistochemistry experience. Other parts of the *in-vivo* project were undertaken by the research group (RS, SJ, AX, SS, myself) as described.

5.2.1.2 Drug testing using sub-renal model

For the ERL* BYL combination, this experiment was performed in 2 phases. In the first phase (pilot), animals were randomised to control, BYL and ERL* BYL. This was to establish superiority of CB over control that was not due to BYL alone. Importantly, The pilot study was also used to attain means and standard deviation statistics in order to calculate for the sample size for the core experiment. In the second phase (core), animals were randomised to 4 treatment arms: control, gemcitabine, ERL and ERL* BYL **(Figure 5.2)**. There was no BYL alone arm, since PI3K inhibitors were shown to produce modest single-agent efficacy at best.[47] **The primary objective was to demonstrate superiority of CB over control and non-inferiority of CB against standard gemcitabine. The secondary endpoints were kidney weight, metastatic disease and IHC of Ki-67 activity index**.

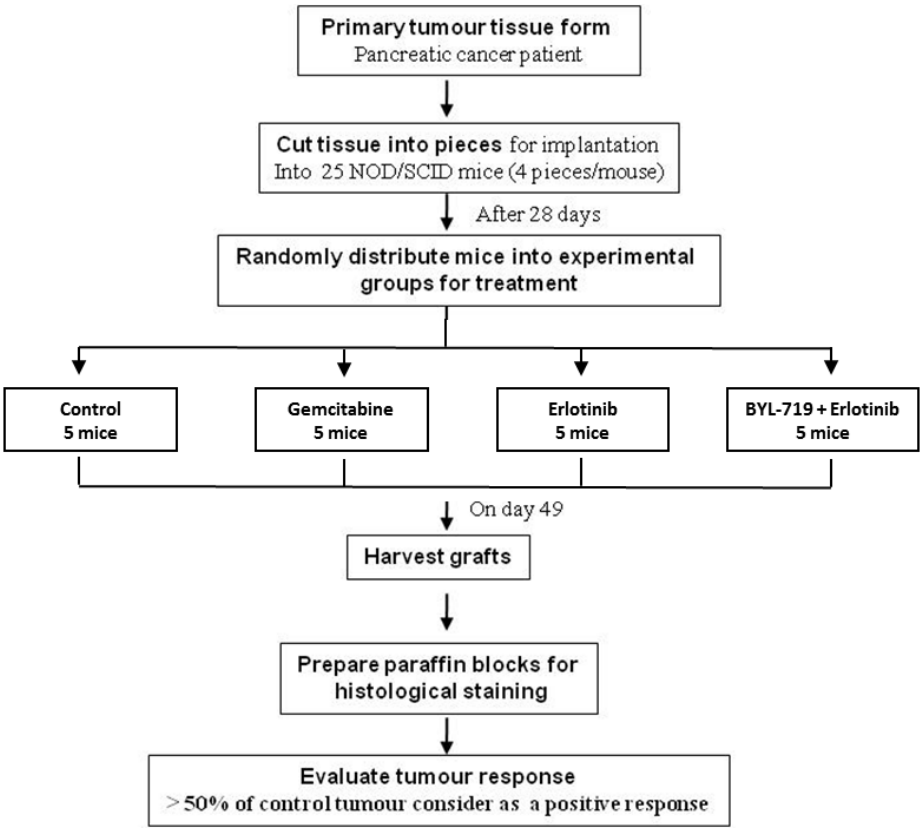

Figure 5.2: Study Design of the core sub-renal model experiments

For the ERL* BEZ combination, preliminary pilot experiments were performed for 4 treatment arms. Mice were randomised to control, gemcitabine, ERL and ERL* BEZ. This was different from the ERL* BYL study design, as there was difficiulty in the acquisition of sufficient BEZ drug for *in-vivo* testing. The study was closed early after only 2 experiments, due to a lack of efficacy observed and importantly, a safety issue of grade 5 toxicity as a result of ERL* BEZ CB. This will be discussed in detail in the results section.

5.2.1.3 Development and validation of subcutaneous model

Subcutaneous models have the advantage of being visible from the outside, thereby allowing direct visual monitoring and serial measurements.[347] Yet, the engraftment rate for subcutaneous model is typically low (40-60%), and it only succeeds in growing highly advanced malignancies, since it does not simulate the tumour microenvironment as the sub-

renal or orthotopic model do.[339] To circumvent this issue, serial transplantation of tumour xenograft was first performed in the sub-renal model to establish stable engraftment rate.[348,349] For each generation of mice, the tumour was divided and passaged to 3 to 4 mice at a time, and selected the mouse with the highest tumour burden for subsequent passages. In this way, the issue of tumour heterogeneity was overcome by means of natural selection. After serial passaging, the established xenograft was transplanted to the subcutaneous model. **The primary objective was to establish a xenograft which could grow and was measurable in the set timeframe of 28 days of study, with a high engraftment rate >75%. The secondary objective was to ascertain that tumours had not changed in morphology,** by examining the pre- and post-graft tumour histology of each new generation xenografts.

5.2.1.4 Drug testing using subcutaneous model

Once the tumour xenograft was validated for use in subcutaneous model, subcutaneous transplantation was performed and the mice were randomised to control, ERL, BYL and ERL* BYL. **The primary objective was to confirm sub-renal core study, and secondary objective was to demonstrate synergy with CB**. Thus, both ERL and BYL were studied as SB, but gemcitabine was not included. During the 28 days of study, tumour xenografts were palpated and measured by standard calipers weekly initially then twice weekly. The average tumour volumes for each group against time of study were presented as line graphs. The primary endpoint was comparison of tumour volume *trends* between CB, SB and control. Statistical analysis was performed but was limited by sample size.

5.2.1.5 Statistical and other Study Considerations

The 3 R's of code of practice in animal research (replacement, reduction, refinement) were advocated throughout the statistical considerations of our *in-vivo* study.[333] At each decision point, alternative study designs were considered to minimise the number of animals used. As mentioned, the sub-renal model experiments were divided into pilot and core studies. The pilot studies aimed to use a minimum number of animals to look for signals of efficacy and safety.

This had helped us apply early stopping of the ERL* BEZ experiments, after observing in excess of 2 deaths of animals due to CB toxicity. This pilot study design had also allowed for accurate statistical calculations to be made for the core study. For ERL* BYL, based on a δ (effect size) of -0.35, σ (standard deviation) of 0.55, standard α and β of 0.05 and 0.8, and a paired analysis, 21 animals were needed for each of the 4 treatment arms. This totalled to at least 84 animals in the core study (PS, version 3, 2009), and 90 animals were used. The subcutaneous model experiments used up 3-4 animals for each generation of passage, and it was meant to only complement and support the sub-renal model, particularly as statistics could not be performed for this study design. Therefore, the minimum number of animals (5 per treatment arm = 20 animals) was used to test the subcutaneous model. For statistical analysis, the data was log transformed since they did not conform to the normality assumption. Two-way ANOVA was used to analyse tumour volumes between treatment groups after adjusting to experiments (SAS 9.2), since the same xenograft was used for each experiment.

5.3 Study Results

5.3.1 Development and validation of sub-renal model: results

The sub-renal model was established from 21 patients, including 19 with pancreatic ductal adnocarcinoma. Of the total of 420 first-generation tissue implantations in 210 mice, 357 post-grafts were successfully grown under the sub-renal capsule, giving a net xenograft rate of 85%. **Figure 5.3** shows pancreatic tumour tissue xenografts after 8 weeks of growth in NOD/SCID mice. All grafts started as tiny 1x 1x 2 mm^3 grafts. By the end of 8 weeks, these successful grafts typically occupied 1/3 or 1/2 of the murine kidneys (~12mm^3, or 600% of original size), established neovascularisation and became locally invasive into the kidneys.

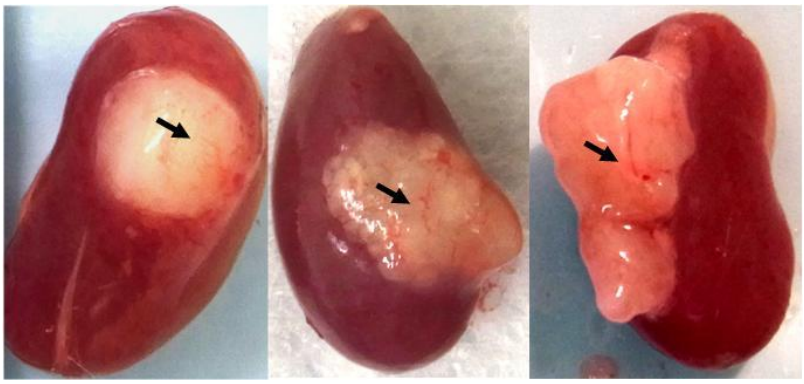

Figure 5.3: Sub-renal xenografts showing neovascularisation (black arrows)

The histopathology between the original tumours (pre-grafts) and the post-graft tissues were compared using H&E. Of the 21 pancreatic tumour specimens, 18 showed concordant histological morphology between the pre-graft and post-graft tissues. 3 of them only grew fibrous tissues. Among the 18 evaluable tumours, 12 were moderately differentiated (G2), 5 poorly differentiated (G3) and 1 undifferentiated (G4). In addition to grading and differentiation, the post-graft also carried over distinct morphological features such as ductal structures, loss of nuclear polarity, nuclear crowding and variation in nuclear size **(Figure 5.4)**. These 18 cases were further evaulated with immunohistochemistry (IHC).

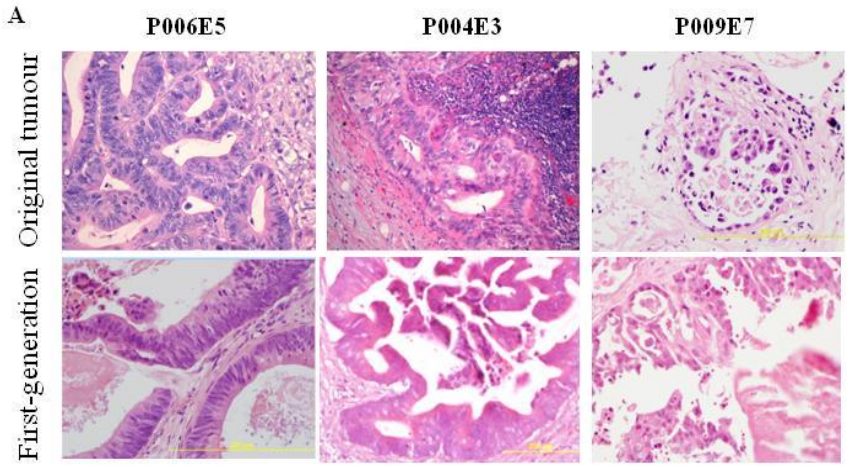

Figure 5.4: Similar histopathology between pre-graft and post-grafts tumour, in moderately differentiated (P006E5), poorly differentiated (P004E3) adenocarcinoma and metastasis lesion (P009E7).

The IHC of CK7, CK20 and Ki-67 were compared between pre-grafts and post-grafts tissue of animals undergoing gemcitabine versus control treatments. CK7 and CK20 are cytokeratins that define intrinsic properties of specific cancer types, so they were expected to be similar between pre-grafts and post-grafts with control.[346] Less is known about the changes of CK7 and CK20 with gemcitabine treatment, due to the paucity of literature. On the other hand, Ki-67 is a tumour activity index that has been shown to decrease with treatment in pre-clinical and clinical (mostly neoadjuvant) studies.[1,350,351] Indeed, no substantial differences in the IHC staining patterns was found between pre-grafts and post-grafts of animals treated with saline control, in all of the 18 specimens, indicating retention of tumour characteristics and reproducibility of this current sub-renal model. Moreover, post-grafts of animals treated with gemcitabine demonstrated reduced expression of Ki-67, CK7 and CK20 in 5 cases (P006E5, P012E9, P021E15, P029E21 and P030E22) **(Figure 5.5)**. Accordingly, in these cases the H&E showed low grade cells with less pleomorphism in these gemcitabine treated tumours. Importantly, these also happened to be the cases where there was a significant reduction in tumour volume in the gemcitabine treatment arm compared to control **(Figure 5.6, Table 5.3)**. Thus, these results supported the use of these IHC markers as surrogate endpoints of response in the subsequent core experiments.

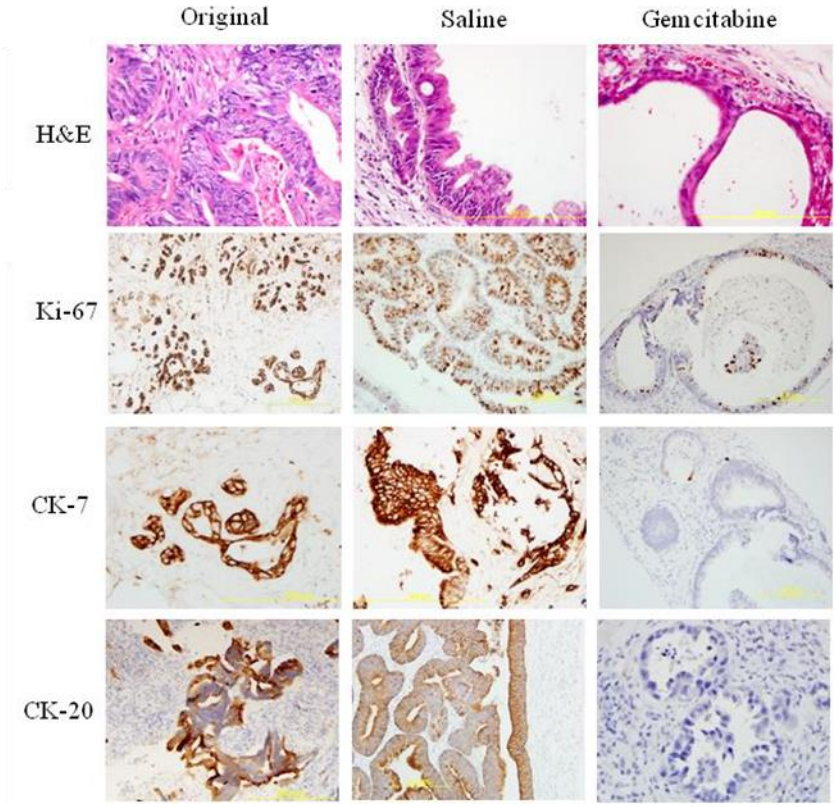

Figure 5.5: Representative IHC and H&E showing similarity of pre-grafts and post-grafts control, and response to gemcitabine

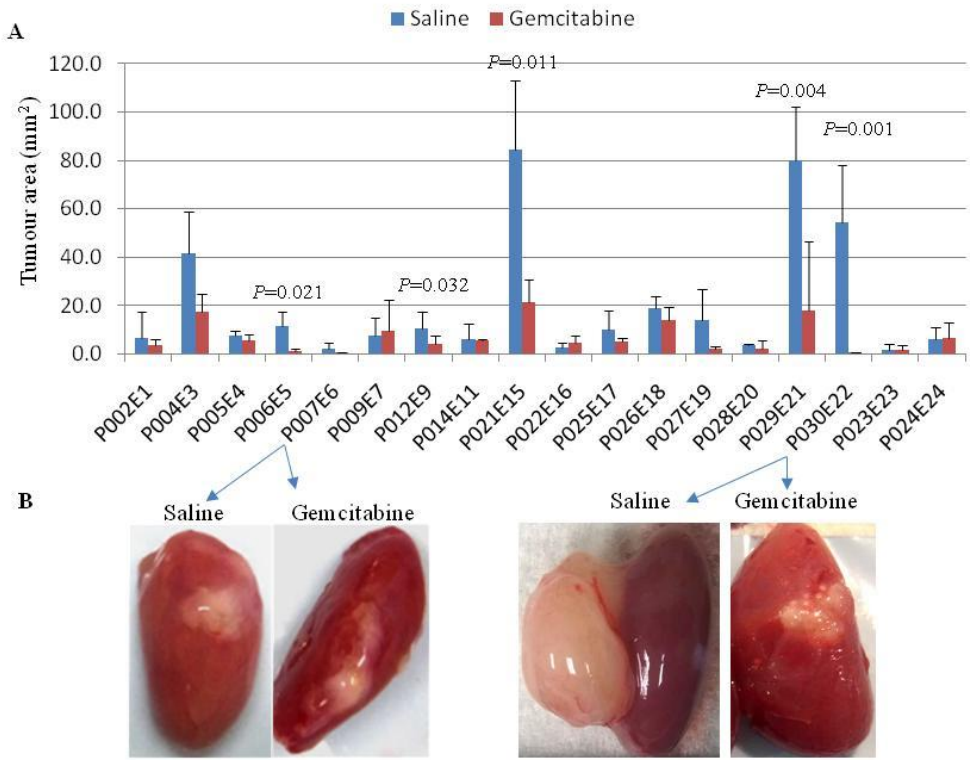

Figure 5.6: Significant responses in tumour volumes in 5 of 18 cases of sub-renal xenografts

Tumour area (mm^2) after treatment				
Patient ID	**Control**	**Gemcitabine**	**Inhibition%***	***P* value**
P002E1	6.81±10.47	3.58±2.64	47.43	0.290
P004E3	41.64±15.57	17.25±7.43	58.57	0.092
P005E4	7.79±1.70	5.62±2.38	28.85	0.134
P006E5	**11.66±6.03**	**1.36±0.72**	**88.34**	**0.021**
P007E6	2.27±2.45	0.68±0.27	70.04	0.155
P009E7	7.83±7.18	9.81±12.75	-25.29	0.413
P012E9	**10.69±7.01**	**3.96±3.74**	**62.96**	**0.032**
P014E11	6.29±6.28	5.67±0.58	9.86	0.436
P021E15	**84.3±28.81**	**21.2±9.65**	**75.90**	**0.011**
P022E16	2.83±2.02	4.48±3.28	-58.01	0.250
P025E17	9.92±8.23	5.14±1.66	48.19	0.110
P026E18	19.06±4.86	14.00±5.66	26.55	0.220
P027E19	13.88±12.76	2.00±1.37	85.58	0.079
P028E20	3.79±0.36	2.33±3.18	38.52	0.255
P029E21	**80.13±22.01**	**17.96±28.56**	**77.59**	**0.004**
P030E22	**54.42±23.5**	**0.58±0.20**	**98.90**	**0.001**
P023E23	1.916±2.04	1.75±1.88	9.70	0.453
P024E24	1.92±4.99	6.39±6.57	-0.07	0.255

Table 5.2: Tumour area inhibition rate in-vivo among 18 cases

In summary, the current sub-renal model was established with 21 xenografts (n=420). It produced a high engraftment rate of 85%, on par with other successful sub-renal models published in literature.[267,338] Importantly, it demonstrated high concordance in histology to the original tumour tissue. In this model, a response rate of 28% (5/18) to gemcitabine was demonstrated. This was slightly more than the 8-12% response rate observed in clinical studies,[108,109] but it certainly was within the expected range. Of interest, all 5 gemcitabine-responsive tumours consistently showed reduced Ki-67 with this treatment; suggesting a role of this as a surrogate marker for tumour response endpoints.

5.3.2 Drug testing using sub-renal model

5.3.2.1 ERL* BYL Combined blockade – Pilot study

In the pilot study involving 34 NOD/SCID mice in 3 separate PDTT experiments, animals treated with ERL 50 mg/day plus BYL 25 mg/day had smaller tumours (E50Y25) (8.0mm3, 95% CI: 4.3-14.8; n=11) compared with control (11.4mm3, 6.0-21.7; n=10) and BYL alone (10.4mm3, 6.2-17.4; n=12) **(Figure 5.7)**. The differences were not statistically significant due to the small sample size, but numerically there was a small increase in SB (Y25) versus control but a noticeable decrease in tumour volume in CB (E50Y25). This generated a hypothesis that PI3K inhibition alone was not sufficient to overcome pancreatic cancer, and supported the concept of CB as established by the *in-vitro* models in Chapter 4. In view of these results, BYL was therefore omitted but ERL was retained as a SB treatment arm for subsequent core studies.

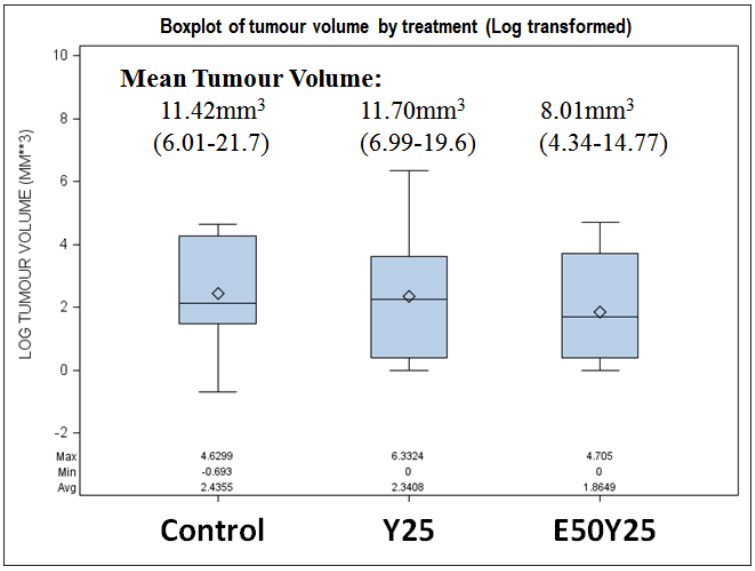

Figure 5.7: Boxplots of mean tumour volumes in control, Y25 and E50Y25 (Pilot sub-renal study)

This pilot study also provided the necessary statistical data for sample size to be calculated for the core experiment. Using the log transformed tumour volume data, a parameter estimate of 0.65 and standard error of 0.55 was estimated. The calculated sample size to demonstrate

a significant difference was at least 21 animals per treatment arm, or a minimum of 84 for 4 treatment arms in the core study.

5.3.2.2 ERL* BYL Combined blockade – Core Study

Dual treatment was further evaluated in six experiments, and compared with control, gemcitabine 100mg/kg twice weekly (G100) and ERL 50mg/day (E50) (n=90). The engraftment rate was 80%. Tumours treated with E50Y25 appeared to be smaller, flatter and less bulky than tumours treated with control vehicle, G100 and E50 **(Figure 5.8a)**. The adjusted mean tumour volumes for animals treated with E50Y25 was 3.5mm3 (95% CI: 2.2-5.8 mm3), compared to control (14.7 mm3, 9.9-21.9 mm3), G100 (2.6 mm3, 2.0-3.4 mm3) and E50 (5.8 mm3, 4.0-8.4 mm3) **(Figure 5.8b)**. Tumours in animals treated with E50B25 were significantly smaller than control (by 11.2 mm3, P=0.005). Tumours in gemcitabine-treated animals were also significantly smaller (by 12.7 mm3, P=0.001); and importantly, CB was non-inferior to standard G100 (P=0.54) **(Table 5.3a)**. The kidney weights for animals treated with E50Y25 and G100 were significantly lower than control (by 66 mg, P=0.002; by 70mg, P=0.002), and there were no significant differences between CB and G100 (P=0.86) **(Table 5.3b)**. The close correlation between tumour volume and kidney weight suggests the presence of a growing xenograft tumour had a significant impact on the weight of the organ on which it was engrafted. None of the animals had distant metastases on macroscopic inspection by the end of experiments (after 8 weeks of engraftment).

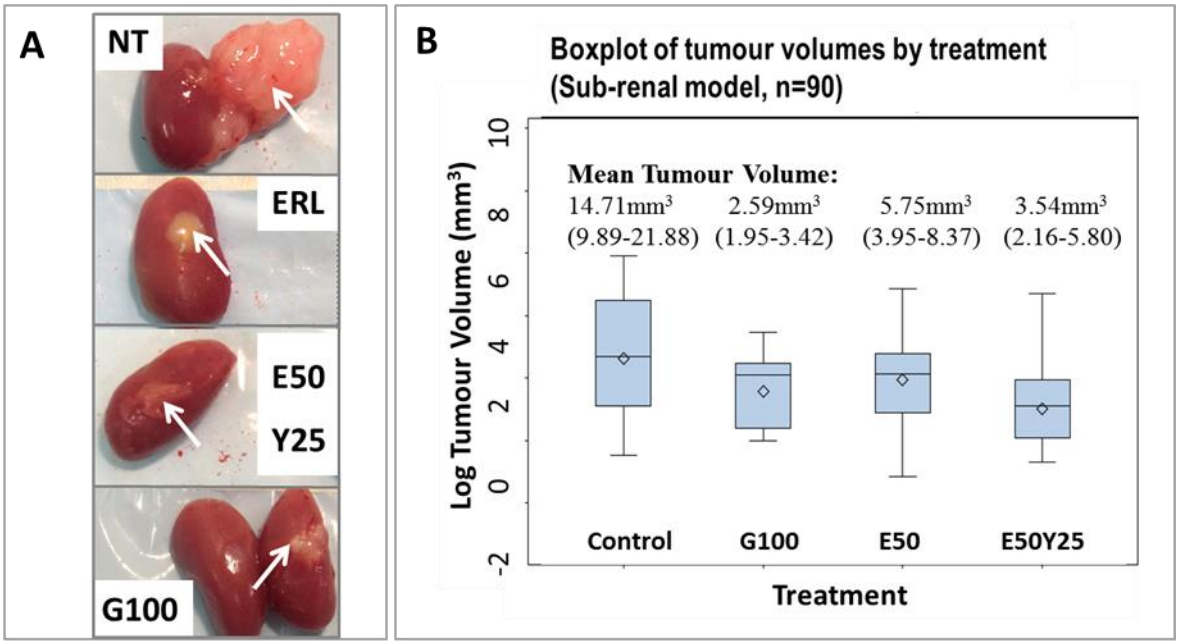

Figure 5.8: (A) Representative photos of tumours of animals undergoing treatment. (B) Boxplots of mean tumour volumes between control, Gem, E50 and E50Y25 (Core sub-renal study);

A

TUMOUR VOLUME, Difference in Mean Tumour Volume (mm³) (Sub-renal model: n=90)

Treatment Comparison	Estimate	Standard Error	t Value	Pr > |t|	95% Confidence Limits	
NT vs. G100	-12.13	0.498	-3.49	**0.001***	-13.75	-7.74
NT vs. E50	-8.96	0.505	-1.86	0.067	-12.61	1.02
NT vs. E50Y25	-11.17	0.488	-2.91	**0.005***	-13.37	-5.33
G100 vs. E50	3.16	0.520	1.54	0.129	-0.55	13.63
G100 vs. E50Y25	0.96	0.515	0.61	0.542	-1.32	7.30
E50 vs. E50Y25	-2.20	0.515	-0.94	0.350	-4.48	4.14

B

KIDNEY WEIGHT, Difference in weight (mg) (n=90)

Treatment Comparison	Estimate	Standard Error	t Value	Pr > |t|	95% Confidence Limits	
NT vs. G100	-70.4	21.69	-3.24	**0.002***	-113.8	-26.9
NT vs. E50	-40.7	20.50	-1.98	0.052	-81.7	0.3
NT vs. E50Y25	-66.3	20.50	-3.23	**0.002***	-107.4	-25.3
G100 vs. E50	29.7	21.98	1.35	0.18	-14.3	73.6
G100 vs. E50Y25	4.04	21.98	0.18	0.85	-40.0	48.0
E50 vs. E50Y25	-25.6	20.81	-1.234	0.22	-67.3	16.0

Table 5.3: 2-way ANOVA statistics of (A) tumour volumes and (B) kidney sizes in 4 treatment arms in core sub-renal study (ERL and BYL)

Histologically, the xenograft tumours of mice treated with E50Y25 appeared of lower grade with less Ki-67 and CK7 staining in 4 of the 6 experiments, compared with E50 and control **(Figure 5.9)**. In 2 other experiments, a small tumour subclone was more intensely stained for Ki-67 and CK7 in CB compared to control or G100, possibly reflecting tumour heterogeneity and/or early resistance to CB in these 2 cases. Nevertheless, there was intense staining to cleaved caspase-3 with CB, reinforcing the apoptotic or cytotoxic mechanism of these drugs. **(Figure 5.10)**. In all cases, pEGFR was decreased by erlotinib and more so with CB, indicating that the targeted drug treatment was hitting the target of interest.

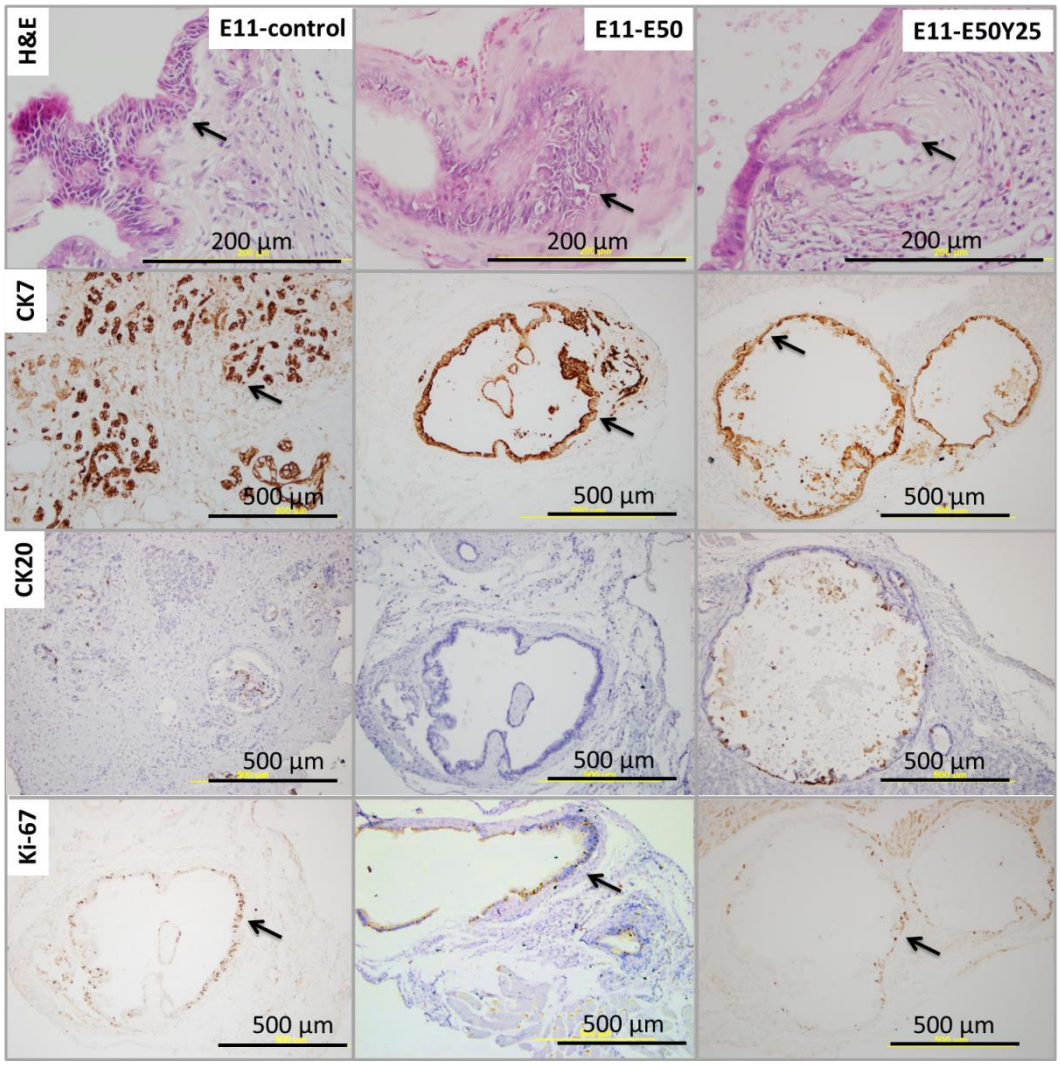

Figure 5.9: H&E and IHC between control, E50 and E50Y25 in a representative of 4 experiment responsive to CB

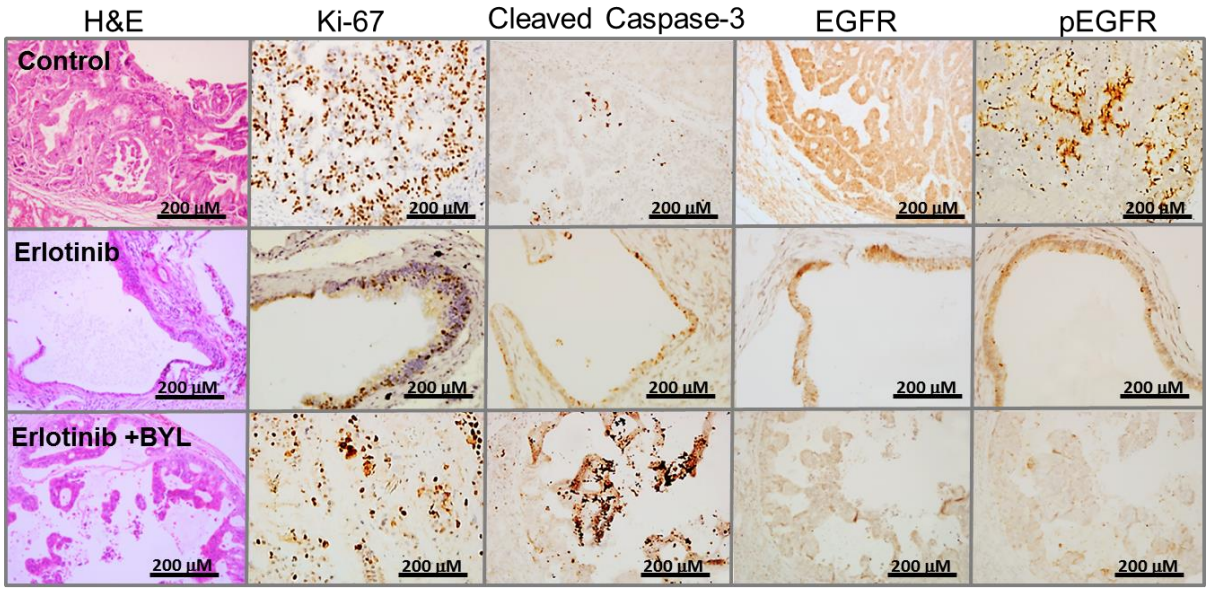

Figure 5.10: H&E and IHC between control, E50 and E50Y25 in a representative of 2 experiments unresponsive to CB

18 largest tumours representative of treatment arms (NT, erlotinib and CB) were stained with Ki-67 and cleaved caspase-3 IHC, and were analysed categorically in statistical analyses. Consistent with *in-vitro* studies, cleaved caspase-3 activation was significantly increased by CB (33.9% vs. 7.0%, P=0.049) whilst Ki-67 was unchanged (44.8 vs. 40.9%, P=0.63), indicating that this CB acted via cell apoptosis instead of reduced tumour proliferation **(Table 5.4)**.

Ki67%, IMMUNOHISTOCHEMISTRY (n=18)								
Treatment Comparison	**Ki67 <10%**	**Ki67 10-25%**	**Ki67 25-50%**	**Ki67 50-75%**	**Ki67 >75%**	**Adjusted mean (%)**	**t value**	**Pr > |t|**
NT	0%	14%	29%	14%	43%	40.9%	-	-
Erlotinib	25%	25%	0%	0%	50%	35.6%	-0.83	0.41
Erlotinib + BYL	20%	0%	0%	20%	60%	44.8%	-0.50	0.63

Caspase-3%, IMMUNOHISTOCHEMISTRY (n=18)								
Treatment Comparison	**Cas-3 <10%**	**Cas-3 10-25%**	**Cas-3 25-50%**	**Cas-3 50-75%**	**Cas-3 >75%**	**Adjusted mean (%)**	**t value**	**Pr > |t|**
NT	63%	13%	0%	25%	0%	7.0%	-	-
Erlotinib	83%	0%	17%	0%	0%	7.5%	0.01	1.00
Erlotinib + BYL	0%	20%	40%	40%	0%	33.9%	2.17	**0.049***

Table 5.4: 2-way ANOVA statistics of Ki-67% and caspase-3% grading between 4 treatment arms in core sub-renal study (ERL and BYL), as per standard grading classification[1]

5.3.2.3 ERL* BEZ Combined blockade – Core study

BEZ, the dual PI3K/mTOR inhibitor, demonstrated superiority to BYL in *in-vitro* studies (Chapter 4), particularly when combined with MEK inhibitor PD. Since PD or other MEK inhibitors were not available for *in-vivo* studies, ERL* BEZ was the next CB tested. Dosing was as per recommended doses in the investigators' brochure. Animals were randomised to control, G100, E50 and E50B25. Unfortunately, after 2 experiments it was found a high proportion of mice on E50B25 with moderate diarrhoea, and 3 mice were suspected to have died from the CB (2 from sepsis, 1 from severe diarrhoea). The study was stopped prematurely due to serious adverse events (SAE), but the data was analysed nonetheless. In 2 experiments (n=26), there was no significant differences in the 4 treatment groups, and the magnitude of effect of E50B25 on tumour volume and kidney weights was very small (-1.88mm^3, -7.14mg). Based on this and the SAE, a decision was made not to continue study of this drug on a lower dose.

A

TUMOUR VOLUME, Difference in Mean Tumour Volume (mm^3) (n=26)

Treatment Comparison	Estimate	Standard Error	t Value	Pr > |t|	95% Confidence Limits	
NT vs. G100	-1.25	0.968	-0.36	0.72	-3.87	18.96
NT vs. E50	0.45	0.874	0.16	0.88	-2.46	18.87
NT vs. E50B25	-1.88	0.874	-0.55	0.59	-4.42	14.16
G100 vs. E50	1.89	0.932	0.52	0.61	-2.32	31.96
G100 vs. E50B25	-0.39	0.932	-0.15	0.88	-2.64	15.72
E50 vs. E50B25	-2.27	0.833	-0.75	0.46	-4.44	10.32

B

KIDNEY WEIGHT, Difference in weight (mg) (n=26)

Treatment Comparison	Estimate	Standard Error	t Value	Pr > |t|	95% Confidence Limits	
NT vs. G100	5.36	22.11	0.24	0.81	-41.3	52.0
NT vs. E50	0.00	18.86	0.00	1.00	-39.8	39.8
NT vs. E50B25	-7.14	24.34	-0.29	0.77	-58.5	44.2
G100 vs. E50	-5.36	22.11	-0.24	0.81	-52.0	41.3
G100 vs. E50B25	-12.5	26.95	-0.46	0.65	-69.4	44.4
E50 vs. E50B25	-7.14	24.35	-0.29	0.77	-58.5	44.2

Table 5.5: 2-way ANOVA statistics of (A) tumour volumes and (B) kidney sizes in 4 treatment arms in core sub-renal model study (ERL and BEZ)

In conclusion, the core sub-renal xenograft study fulfilled its primary endpoint, demonstrating pre-clinical efficacy of ERL* BYL CB in reducing tumour volumes and providing a strong rationale for clinical development of BYL and ERL CB in pancreatic cancer. There was no early signal that BYL alone was effective in the pilot study, whilst erlotinib reduced tumour volume with borderline significance in the core study as a single agent (P=0.067). This implies that erlotinib remains the active agent in pancreatic cancer, with BYL producing additional benefits (or synergy) when added to erlotinib. BEZ, on the other hand, was found to have only a small non-significant effect on tumour volume. Whilst this may be due to inadequate sample size as a consequence of early stopping of the study, the significant toxicity of this drug hindered further drug development in the current study. Interestingly, the H&E and IHC results suggested a different mode of mechanism with these targeted therapies. There was a statistically significant increase in cleaved caspase-3 with CB (P=0.049), whilst Ki-67 remained unchanged. This suggested that CB was cytotoxic rather than cytostatic, and was certainly supported by the *in-vitro* apoptosis assay results **(Section 4.3.3)**. In 2 of 6 core ERL plus BYL experiments, a small sublone of aggressive dysplastic tumour cells was found even in CB treatment. This aligned with the current concept of tumour heterogeneity and acquired resistance to these drugs, and reinforced the need for treatment selection based on biomarkers to maximise effects.

5.3.3 Development and validation of subcutaneous model: results

The subcutaneous model was used to validate the sub-renal model results. Serial transplantation using 4 generations of sub-renal xenografts were performed, 3-4 mice per generation. Because of tumour heterogeneity, the small pieces of grafts (1x2x2 mm^3) used for each transplantation, and the slight differences in microenvironment of each NOD/SCID mouse, some variation in tumour sizes was anticipated in the same generation of mice. For each generation, the largest tumour for subsequent generation of xenografting was chosen.

After 4 generations of xenografts, the engraftment rate reached almost 100%. Comparing several generations of sub-renal xenografts upon sacrifice, the later generation grafts grew faster, and were larger and more solid or "fleshy" (white arrows, **Figure 5.11**). Specifically, the 3rd and 4th generation grafts were composed of more solid tissue, were more vascular and heterogenous in consistency and colour. In these examples, the 3rd generation graft on the right kidney was very locally aggressive and was wrapping around the kidney, though the one on the left kidney still remained small. On the other hand, all 4th generation grafts were large and invasive. This 4th generation graft even destroyed a kidney such that only liquefactive necrosis was found on dissecting this tumour (not shown).

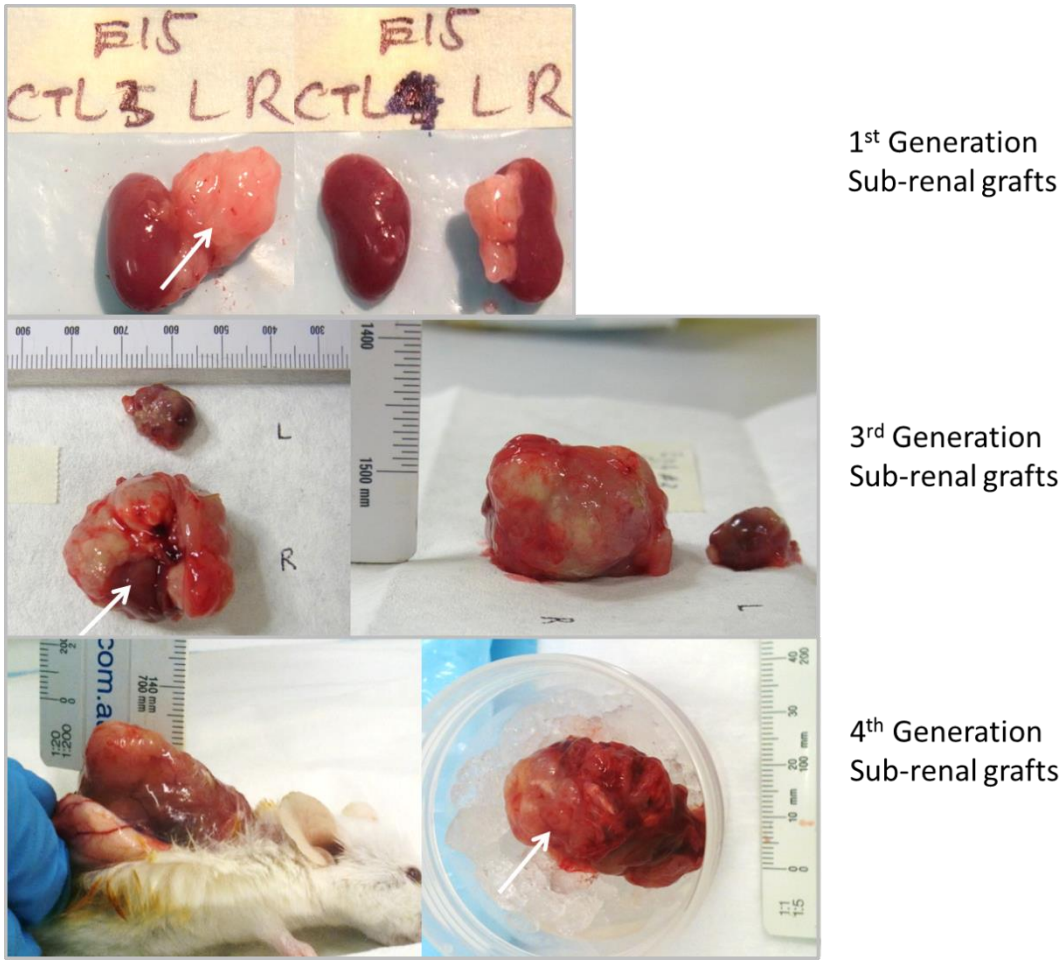

Figure 5.11: 1st versus 3rd versus 4th Generation sub-renal xenografts

The 3rd generation sub-renal xenograft on **Figure 5.11** was used to develop the subcutaneous model, whilst the remainder was passaged to the 4th generation sub-renal grafts in preparation of the core subcutaneous experiment. Tracking the 4 mice over 8 weeks post-transplantation,

the 4th generation subcutaneous tumour became palpable by 2 weeks and visible by 4 weeks **(Figure 5.12).** By 6-8 weeks, the tumour was certainly measurable even after the fur had grown back (red circles). Upon sacrifice of the mice after 8 weeks, the tumour palpated on examination corresponded well to the tumour found on dissection. In both examples on **Figure 5.13**, the subcutaneous tumour measured 10mm (note 1:5 ruler was used in the top and 1:1 ruler used in the bottom). The histology of several generations of xenografts tumour was compared: the ductal structures and morphology were similar between original tumour and the subsequent generation xenografts, except that tumour differentiation appeared of much higher grade in the 4th generation (black arrow, **Figure 5.14)**. All in all, subcutaneous model was established and validated, with good engraftment rate and growth rate to allow us perform drug testing in the core experiments.

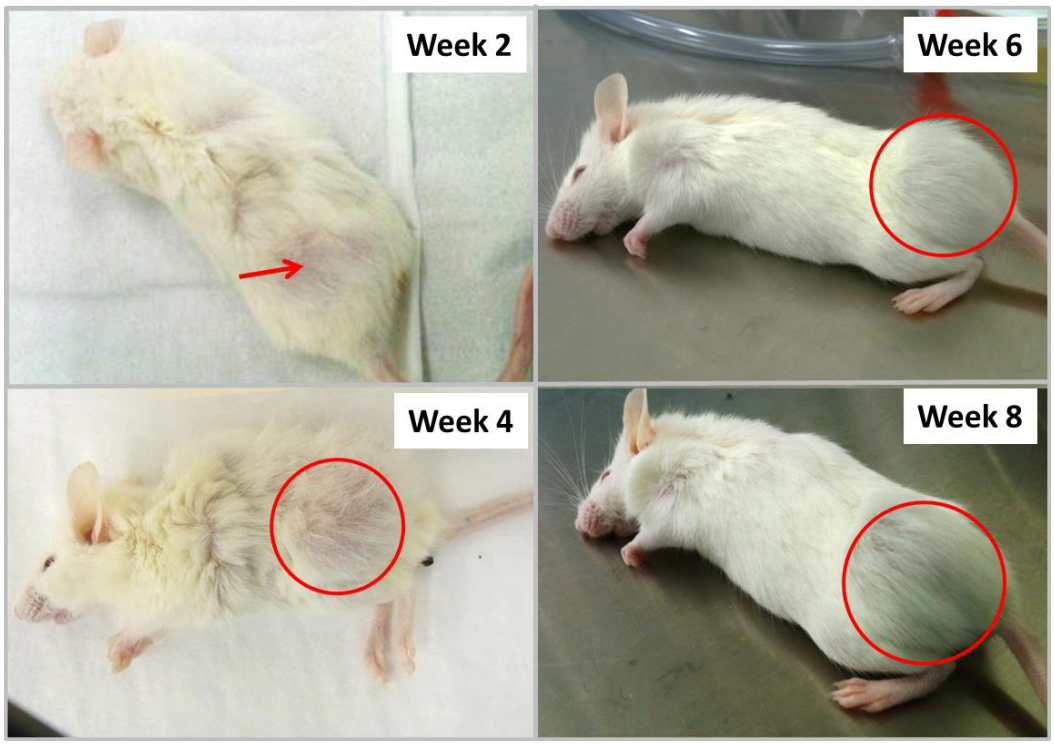

Figure 5.12: 4th generation subcutaneous model over 8 weeks post-transplantation

Figure 5.13: 4th generation subcutaneous xenografts models at end-of-study

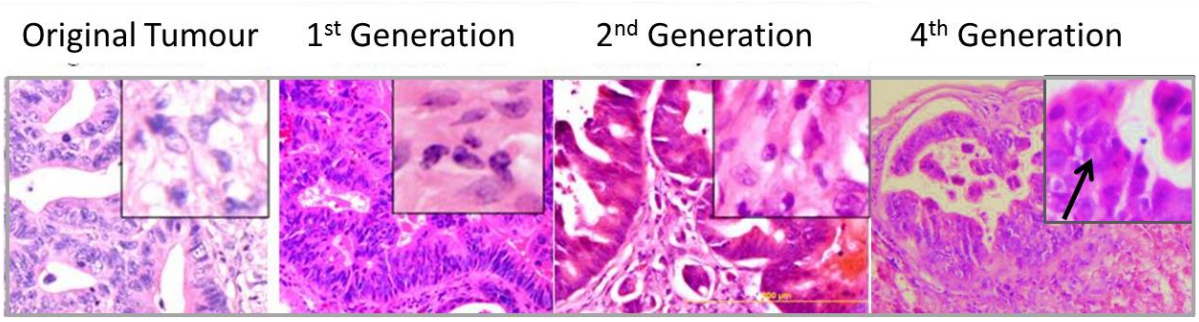

Figure 5.14: Histology comparison over 4 generations of xenografts tumour

5.3.4 Drug testing using subcutaneous model

The observation that the 4th generation tumour was more de-differentiated than xenografts from previous generations was somewhat beyond expectation, but it provided confidence of the utility of the 5th generation xenografts in the core subcutaneous model. The bulky tumour shown from **Figure 5.11** was dissected, and subcutaneous transplantation was performed on 17 mice simultaneously. The engraftment rate was 78%. This highly selected tumour was much more aggressive than the one in the pilot study, resulting in measurable tumours of an average 100mm^3 for nearly all animals only 4 weeks after transplantation. This was set as the baseline before treatment randomisation (control, E50, Y25 and E50Y25) **(Figure 5.15)**, All animals had fur reshaved as this point, and tumours were measured with calipers weekly in

the first 14 days and twice weekly thereafter. Overall the next 4 weeks of treatment, the tumour of mice receiving control treatment continued to grow exponentially (3000 mm^3 at 4 weeks). The tumours in animals receiving single agent treatment also grew in size – with BYL (1400 mm^3) much less effective than ERL (500 mm^3 at 4 weeks), as expected from the low single agent efficacy for PI3Ki. The tumours in animals treated with CB did not grow (still 100 mm^3 at 4 weeks) **(Figure 5.15)**. Multiple regression statistics showed significantly different trends between each treatment **(Table 5.5, A)**. The tumour doubling times for NT, Y25 and E50 were 7.1, 8.4 and 14.8 days respectively, and not reached for E50Y25. **Figure 5.16** showed the sizes of the tumours of mice two weeks into treatment. Mice on control treatment had very large tumours protruding from the skin with areas of necrosis and ulceration. Tumours on the Y25 mice were slightly smaller, and on the E50 mice were smaller still. In all 4 mice treated with CB, the tumours were as small as before treatment, and in 1 of 4 mice there was a complete response where the tumour completely disappeared.

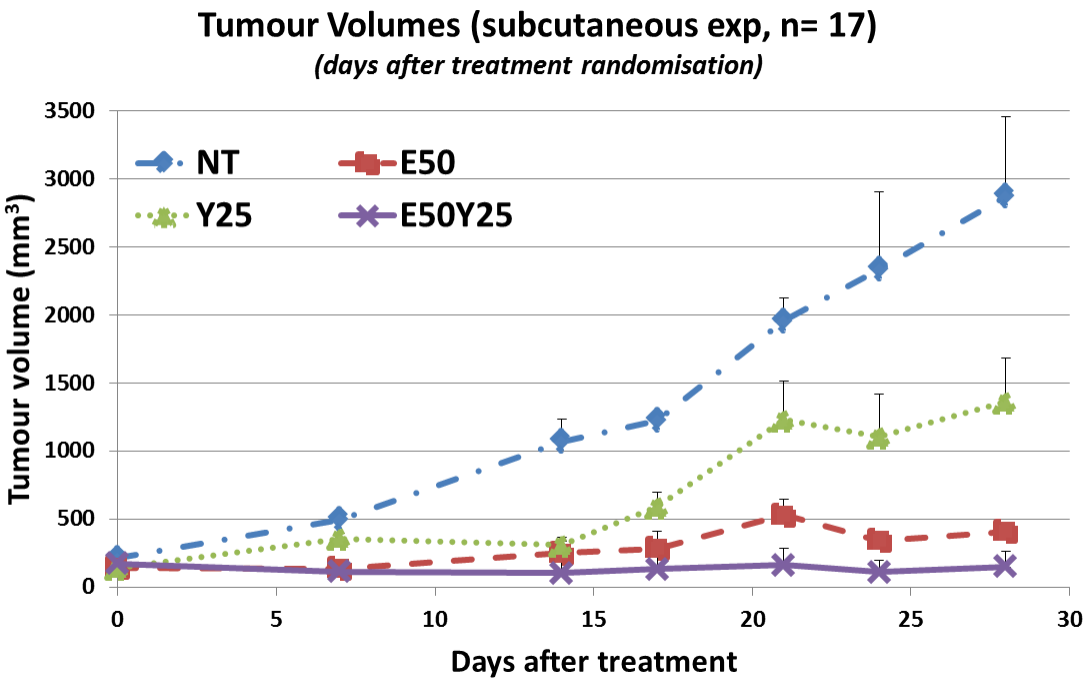

Figure 5.15: Tumour volumes over experiment time of core subcutaneous experiment

A

LOG TUMOUR VOLUME, LOG TREND STATISTICS (Subcutaneous model: n=17)					
TREATMENT	DF	Estimate	Standard Error	t Value	Pr > |t|
NT vs. E50	1	-1.784	0.364	-4.9	<0.0001*
NT vs. Y25	1	-0.480	0.148	-3.24	0.002*
NT vs. E50Y25	1	-1.663	0.240	-6.94	<0.0001*
E50 vs. Y25	1	0.827	0.300	2.75	0.008*
E50 vs. E50Y25	1	-1.563	0.269	-5.82	<0.0001*
Y25 vs. E50Y25	1	-4.021	0.498	-8.08	<0.0001*

B

LOG TUMOUR VOLUME, Difference in Log Mean Tumour Volume (mm^3) (Subcutaneous model: n=17)						
Treatment Comparison	Estimate	Standard Error	t Value	Pr > |t|	95% Confidence Limits	
NT vs. E50	-1.894	1.520	-1.250	0.241	-5.280	1.493
NT vs. Y25	-1.040	1.442	-0.720	0.487	-4.252	2.173
NT vs. E50Y25	-5.505	1.393	-3.950	0.003*	-8.609	-2.401
E50 vs. E50Y25	-3.611	1.216	-2.970	0.014*	-6.320	-0.902
Y25 vs. E50Y25	-4.465	1.117	-4.000	0.003*	-6.954	-1.977

Table 5.5: (A) TREND statistics at multiple measurements and (B) ANOVA statistics of LOG tumour volume at necropsy between control, E50, Y25 and E50Y25 in the core subcutaneous study

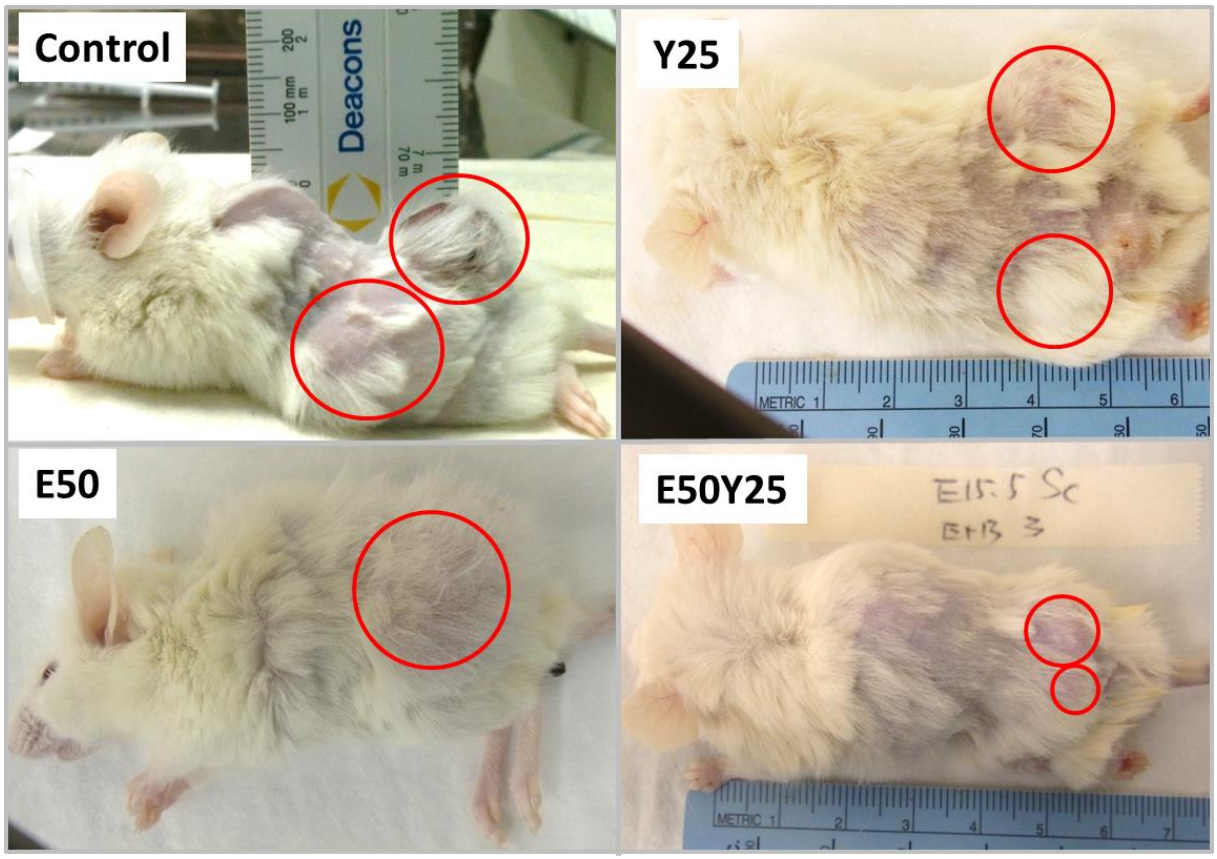

Figure 5.16: Representative of photos of animals treated with 4 treatment arms after 2 weeks in core subcutaneous study

In their weeks 8-12 of life during treatment, it was expected that mice would increase their body weight approximately 1 g per week.[352] In the control and SB treatment arm, the body weight of mice did not change. This was because the tumours had grown in size and weight, whilst the animals were observed to become more cachectic. The body weight of mice treated with CB paradoxically decreased, about 3g over 4 weeks **(Figure 5.17)**. There could be several reasons to this. These mice were fed 300 uL of drug solution each day, more than other mice, and this could result in lesser food intake. In 1 or 2 mice there was some intermittent mild diarrhoea from the CB treatment which could have resulted in dehydration. Also, the xenograft tumours did not grow, and did not contribute to increase in weight. In any case, where mice of the other 3 treatments were more hunched, slower and had lost their natural shine; the animals treated with CB were certainly much healthier despite loss of weight. 1 mouse treated with E50 died at day 24, without any obvious source of sepsis. This mouse had a 15% weight loss before it died, and it was concluded that it died from cancer complications.

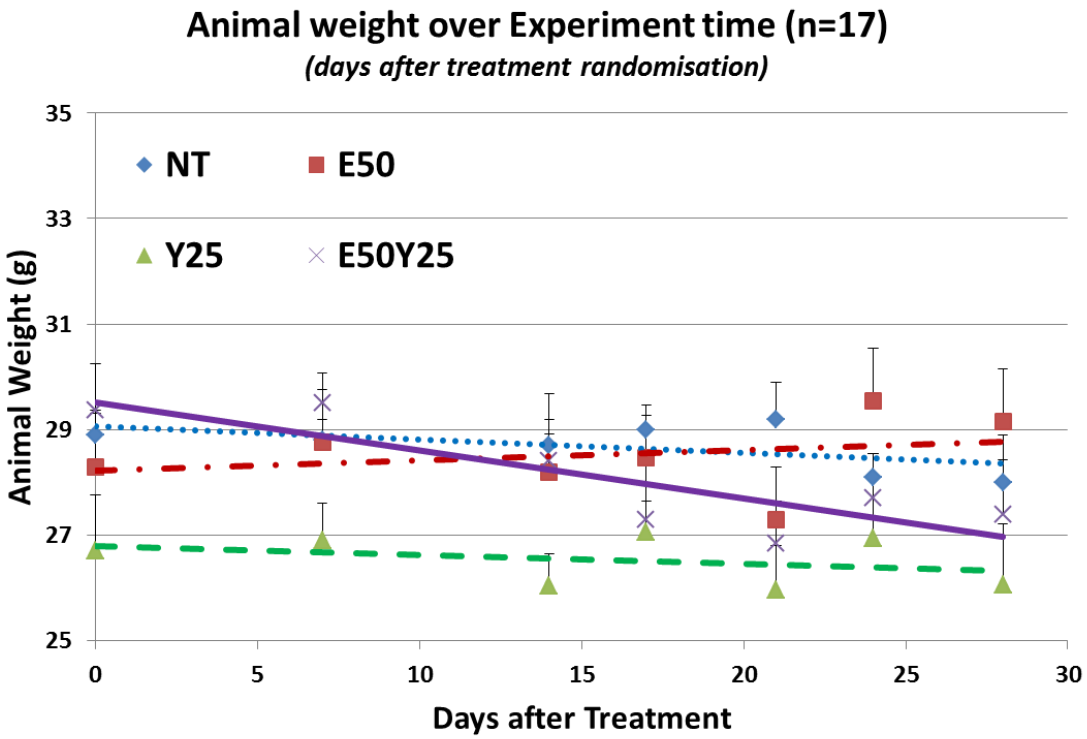

Figure 5.17: Animal weight over experiment time of core subcutaneous study

At necropsy, the subcutaneous tumour sizes on dissection corresponded to the measurement by external examination. The tumours were very large in control, still big in Y25, smaller in E50, and the smallest with E50Y25. In addition, the tumours on control treatment and SB were hyper-vascular and solid, compared to the small pale necrotic tumour in mice treated with E50Y25 **(Figure 5.18)**, The end-of-study tumour volume of tumours in the 4 treatment arms were analysed further with ANOVA after log transformation, to evaluate if this supported the statistical findings in the sub-renal model. The statistics in **table 5.5 (B)** had to be presented in log transformed values because of the vast differences in volumes between control (3000 mm^3) with E50Y25 (100 mm^3) as described earlier. In this small study of 17 mice, animals treated with SB alone had no significant reduction in tumour size than NT (E50: P=0.24, Y25: P=0.49). Yet, despite this small study, animals treated with E50Y25 had significantly smaller tumours than control (P=0.003), E50 (P=0.014) and Y25 (P=0.003).

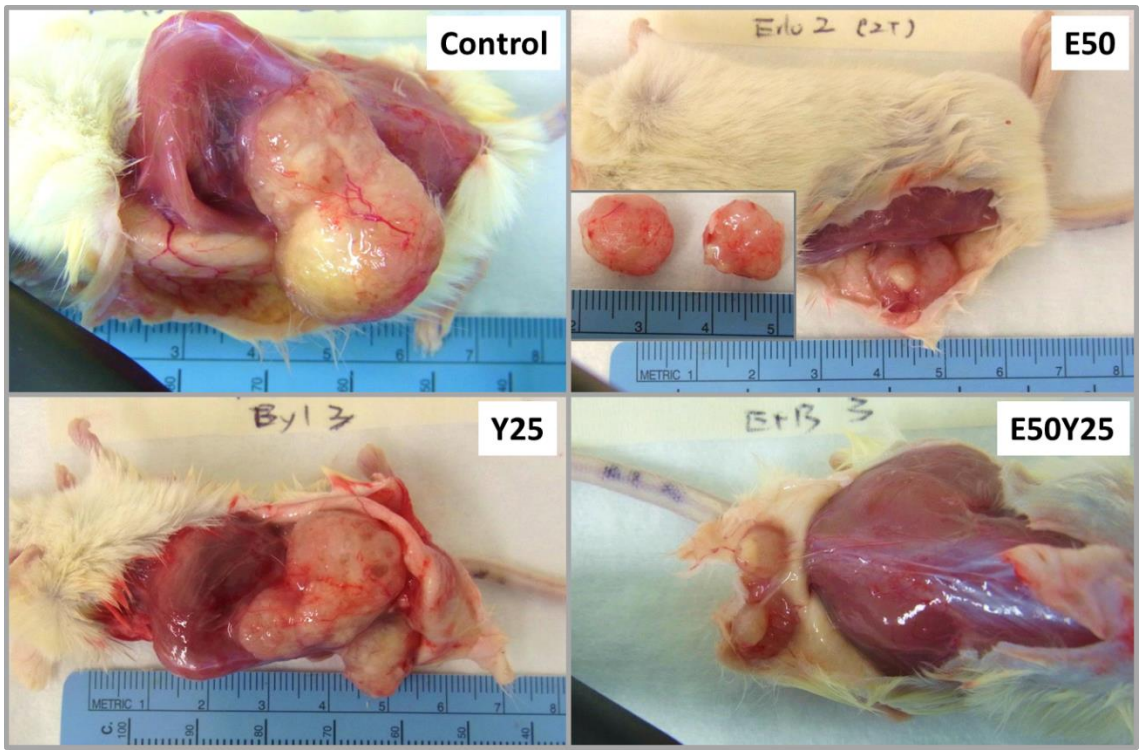

Figure 5.18: Representative end-of-study photos of animals treated with 4 treatment arms in core subcutaneous study

The objective of the core subcutaneous model was thus achieved; the superiority of CB over control was validated in the sub-renal model, and demonstrated its superiority over even SB alone. Further study of this model was deemed unnecessary and not indicated, given the highly significant results, the number of animals needed to sacrifice for serial passaging (15-20), and the distress caused by the highly selective and invasive tumour on these animals.

5.4 *In-vivo* Sub-studies

Given the theme of this thesis on erlotinib resistance and PI3K/Akt driving mechanism in PDAC, it was desirable to study these topics further *in-vivo*. These were attempted, basing the study design from previously reported models. There are, however, specific challenges associated with developing *in-vivo* resistant model and *in-vivo* study of PI3K/Akt markers. In particular, the statistical power required to draw definitive conclusion *in-vivo* is too large to be accomplished through *in-vivo* study alone, and is best studied in clinical trials. Whilst proposals for these will be explored further in **chapter 6 ongoing studies**, the preliminary *in-vivo* results for erlotinib resistant model and PI3K/Akt/mTOR biomarkers are presented here.

5.4.1 Biomarkers in erlotinib insensitive and resistant tumour

In-vivo, there are many ways to study biomarkers of the PI3K/Akt/mTOR pathway, including phosphorprotein array, western blotting, immunohistochemistry, qRT-PCR, and fluorescence in situ hybridization (FISH).[353-355] However, in clinical practice biomarker assay methods are much more limited. For example, the routine testing of standard biomarkers EGFR, *K-Ras*, B-raf mutations and HER2 amplification are essentially limited to slide-based IHC, FISH and qRT-PCR methodologies due to their convenience and reproducibility.[356-358] To complicate matters further, bringing biomarkers from bench top to bedside has been hampered by the exceedingly complex biology and roadmap of PI3K/Akt/mTOR. A large number of genes

including PIK3CA, PTEN, PDK1, AKT1,2,3, TSC1,2, mTOR, Rheb genes; as well as PTEN, PIK3CA, pAkt and pS6 proteins have been implicated as key potential biomarkers of this pathway. Aside from these, mRNA and epigenetics may also be involved.[359,360] There is currently no consensus of the approach of development of these novel biomarkers.[359]

The objective in this *in-vivo* sub-study was to study key molecular differences between animals that had good and poor response to erlotinib (that is, erlotinib insensitivity); as well as between erlotinib resistant and primary tumour (erlotinib resistance). For erlotinib insensitivity, this study was underpowered. Due to the study design using patient-derived xenografts, only 6 primary tumours were used in sub-renal transplantation and subsequently studied of 90 animals in the core study. From discussion with biostatistician, at least 15 primary tumours (or 225 mice) would be required to show statistical significance. For erlotinib resistance, the preliminary experiments were unfortunately unsuccessful **(Sub-section 5.4.2)**. The development of further resistant tumours was limited by the expense of continued supply of the drug and the lack of tumour monitoring by imaging. It was therefore impossible for any statistically meaningful conclusions to be drawn from this study.

Here the preliminary findings of this sub-study focusing on the PI3K/Akt pathway is reported; but due to the lack of statistical power, this could only serve as a proof of principle. In **chapter 6** the clinical trial proposal to answer this research question definitively will be discussed.

5.4.1.1 Study of AKT/ pAkt and EGFR/ pEGFR in Erlotinib insensitivity

From the *in-vitro* studies, a consistent correlation of phosphorylated Akt and S6 protein to erlotinib resistance was found. From the gene expression point of view, downstream gene signals including NF-κB1A and c-fos were found up-regulated in PCR array. However, none of the aforementioned biomarkers were found to be correlated to erlotinib resistance except for *AKT-2,* which was only modestly up-regulated **(sub-section 3.5.6)**. Whilst the focus had been immunofluorescence and western blotting for the assessment of the total and

phosphorylated proteins *in-vitro*, these methods are operator-dependent, inconvenient and not always reproducible. They are also not standard methods for ongoing human studies. IHC, on the other hand, is a common and standard way of evaluating molecular markers, and is highly reproducible. A variety of stains including p/EGFR, p/AKT, p/S6, SMAD4, vimentin and FAP was used, in consultation with a senior pathologist. Like in immunofluorescence, S6 and pS6 antibodies were inconsistent in IHC. For other stains, no consistent patterns were found except for p/EGFR and p/Akt. The results for these markers will be presented here.

Based on previous studies, AKT/ EGFR and pAkt/ pEGFR primary antibodies were tested at dilutions of 1:200-800 and 1:50-200 respectively.[54,354] After optimisation, the best dilution for all 4 markers was chosen to be 1:150. The results of p/EGFR were illustrated already in **figure 5.10**. For p/Akt, The original tumours (pre-graft) of experiments E11 and E15 were first stained **(Figure 5.19)**. IHC for AKT was not useful because of the abundance of tissue AKT and the non-specific staining pattern of cancer versus normal tissues. Similar to other publications, abundant total AKT was found in both tumour and the adjacent normal tissues,[361] and there were no differences in total AKT expression between E11 and E15 pre-grafts. Phosphorylated Akt, on the other hand, had more specific staining pattern in tumour tissue. Of interest, the tumour with low erlotinib response (E11) tended to have higher pAkt than tumour with higher response (E15).

Currently, there is no standard of biomarker cut-offs for AKT and pAkt. Various research groups attempted to categorise IHC scoring, using a composite score called the H- score. [360,362] This equals to percentage of positive cells (PP) by staining intensity (SI) on a high-power field: SI was scored 0 = negative, 1 = weak, 2 = moderate, and 3 = strong. The H-score value ranges from 0 to 300%; and a H-score more than 50% is considered positive. Based on the IHC scoring system, the pAkt H-score was 110% (/300%) for the low erlotinib response E11 and 13% (/300%) for the high erlotinib response E15. This suggests that basal or pre-treatment AKT activity (pAkt), but not total AKT, appeared to be associated with erlotinib insensitivity. This is in concordance in the *in-vitro* study results.

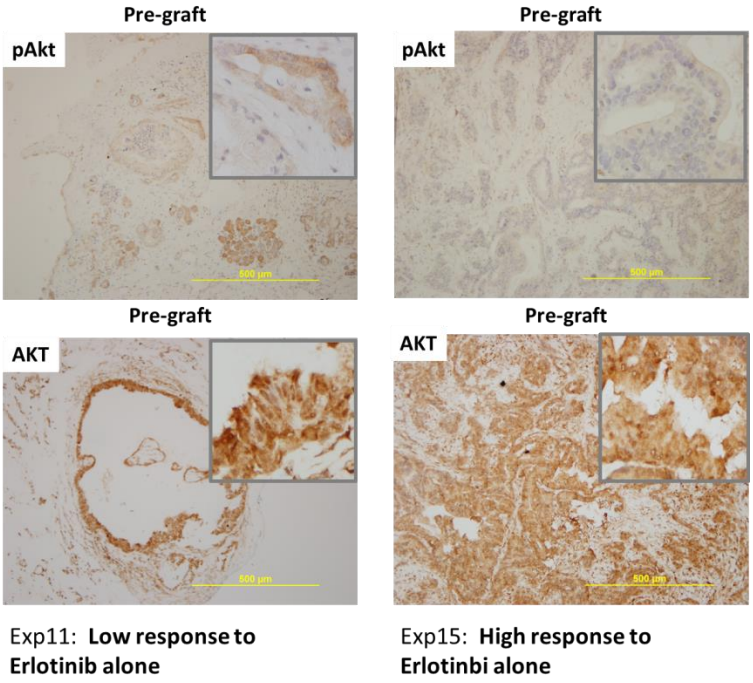

Figure 5.19: AKT and pAkt IHC on erlotinib-sensitive and less sensitive tumour (pre-graft)

pAkt and pEGFR were then examined in the primary tumours and correlated with tumor responses for each of the 6 xenograft experiments **(Figure 5.20)**. By RECIST 1.1,[363] partial response was observed in only 2 of the 6 experiments with erlotinib alone, but was observed in all 6 experiments with E50Y25, with the highest tumour response observed in experiment 9 (E9) (-66%) **(Figure 5.20)**. pEGFR was scored 2+ and 3+ in E9 and E15, whilst pAkt was scored 2+ and 3+ in the primary tumours of E19 and E11 respectively **(Figure 5.21)**. Of interest, E9 and E15 were among the experiments with the highest magnitude of response to both SB and CB, whereas E11 and E19 were among the lowest responses. That said, E11 and E19 showed equivocal tumour responses (stable disease) with erlotinib alone (-3% and -9%), but partial responses with the CB (-32% and -38%). The differential responses to SB and CB for these two experiments were among the highest with an absolute difference of 29% in both cases **(Figure 5.20)**. This study therefore suggests the roles of pEGFR as positive and pAkt as negative predictive biomarkers for erlotinib SB or erlotinib plus BYL CB. This supports the concept that Akt over-expression as a negative prognostic factor,[54] as well as a negative predictive factor for single blockade of EGFR.[132] Importantly, despite pAkt being a negative predictive factor of erlotinib, this can still be overcome by EGFR-PI3K co-inhibition.

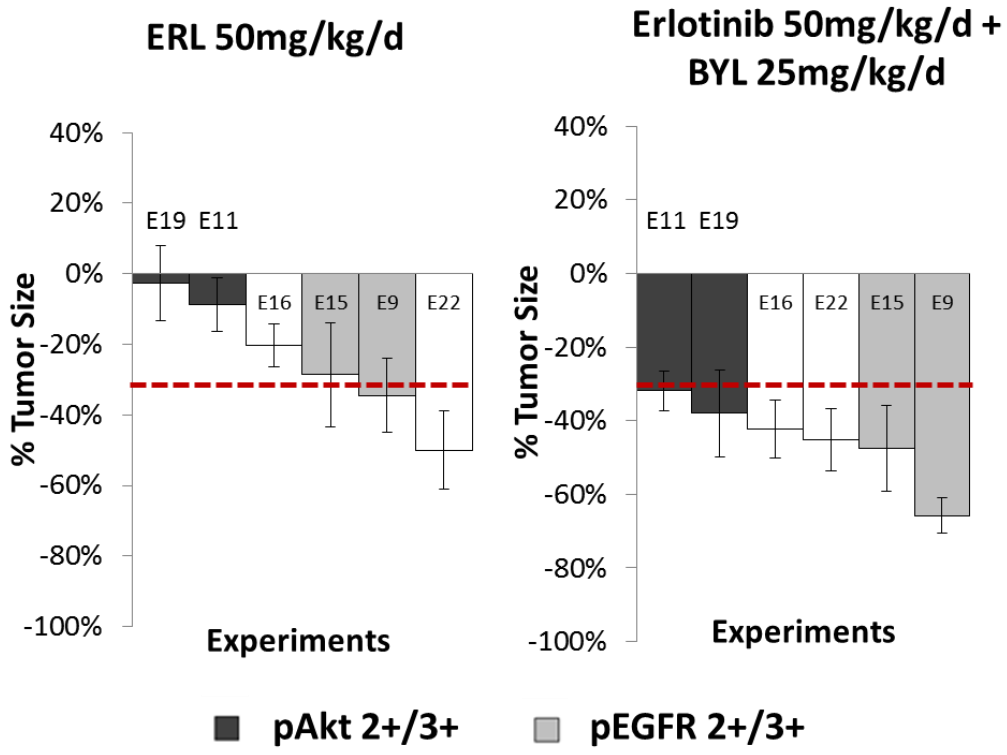

Figure 5.20: Tumour responses to SB and CB by RECIST 1.1

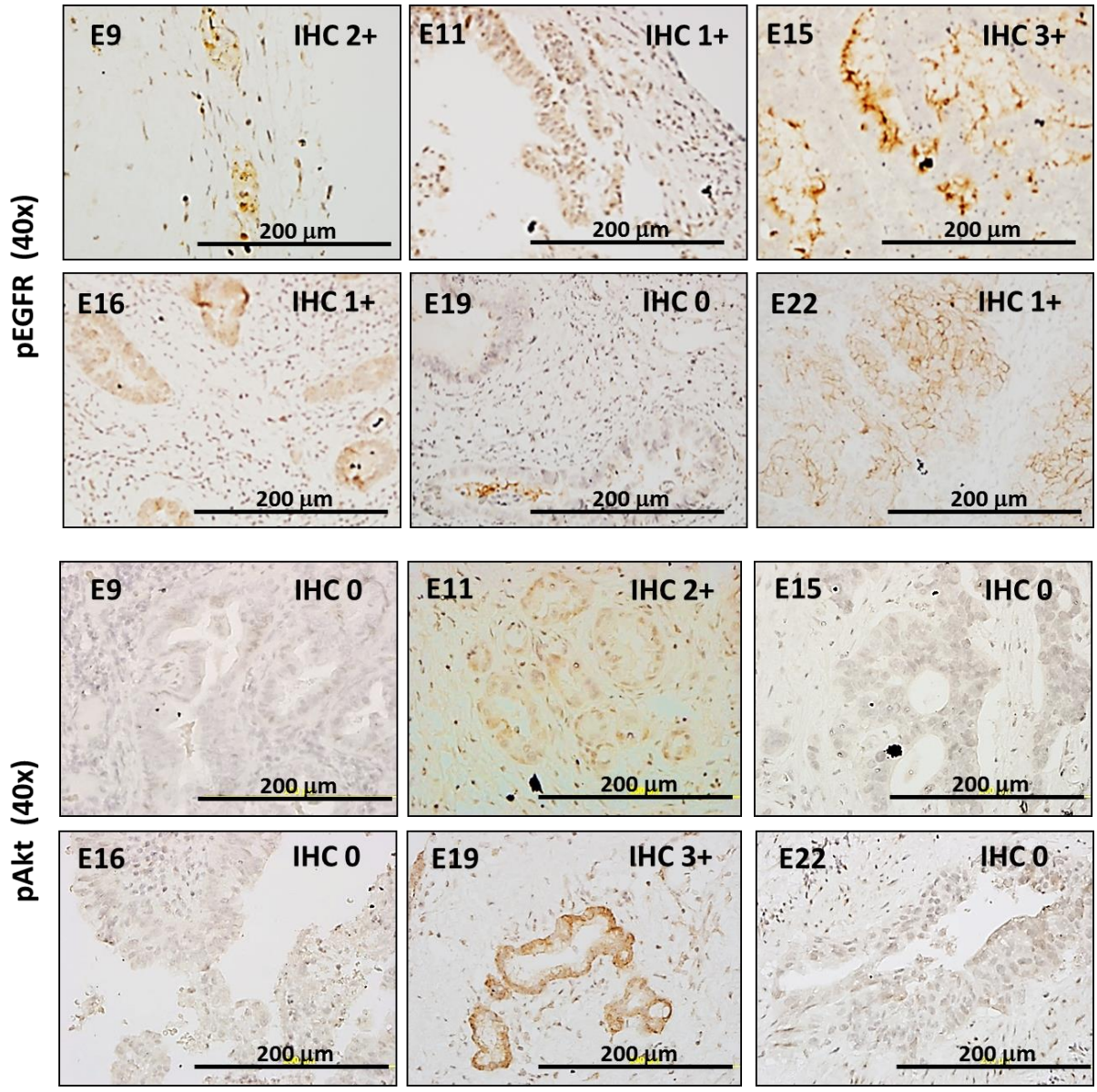

Figure 5.21: pEGFR and pAkt staining for all 6 experiments

To study the downstream effects of *in-vivo* drug inhibition further, two experiments were stained and stained the end-of-study tumour xenografts treated with control, E50 and E50Y25, with AKT and pAkt for 2 of the experiments. Total AKT IHC slide photos were not shown as these showed abundant staining similar to pre-grafts. For both E11 and E15, pAkt was different among tumours undergoing different treatments, even though they originated from the same pre-grafts. This suggested that pAkt staining pattern was affected by residual treatment effect. All mice were off-treatment for at least 3 days before necropsy, but since the half-life of erlotinib was 36 hours, it was likely that the treatment still exerted some systemic

effect at necropsy. In both high-response and low-response experiments, the pAkt activity was increased for tumours undergoing SB (E50), but decreased for tumours undergoing CB (E50Y25) **(Figure 5.22)**. The pAkt H-scores were 12% (NT), 33% (E50) and 1% (E50Y25) for E11; and 19% (NT), 35% (E50) and 11% (E50Y25) for E15. This preliminary experiment suggests that erlotinib alone increases pAkt, possibly similar to the oncogenic shift mechanism observed in *in vitro* studies, but that CB reduces pAkt expression. Importantly, the experiment that showed low response to erlotinib had the complete disappearing of pAkt signal with CB, supporting the concept of PI3K/Akt oncogenic dependence.

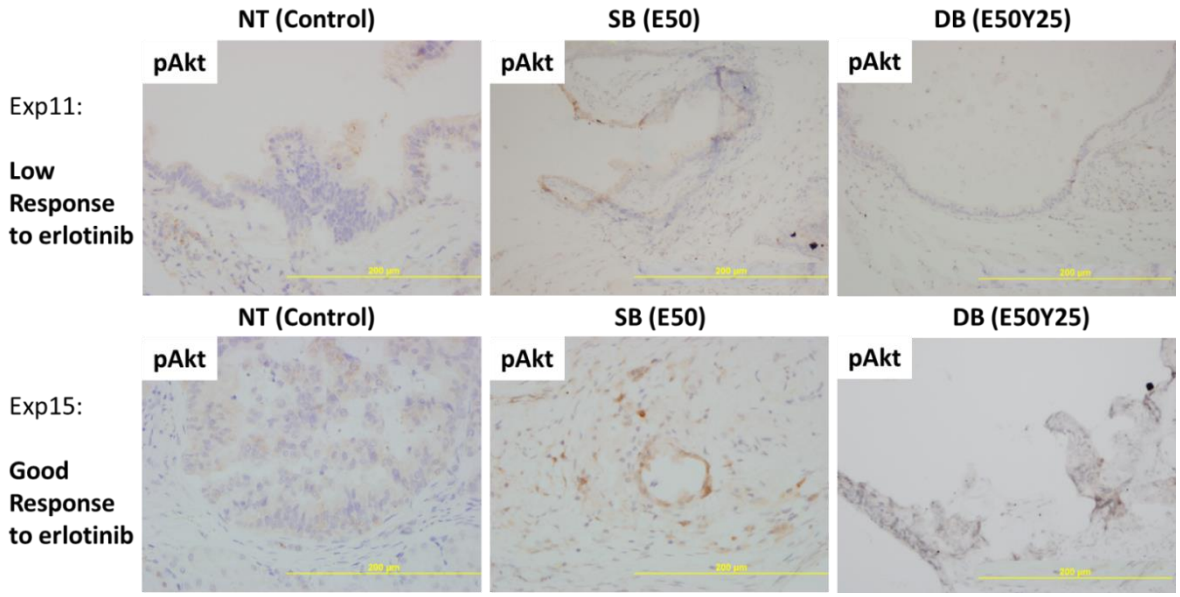

Figure 5.22: pAkt IHC response on erlotinib-sensitive and less sensitive tumours

In conclusion, there is suggestion that tumours that have up-regulated pAkt confer resistance to single agent erlotinib, whereas up-regulated pEGFR conversely confers sensitivity. Regardless, there was an improved response rate observed for CB versus SB in all experiments. Interestingly, there were substantial differences in the magnitude of response for the two experiments with strong pAkt staining, suggesting that CB could overcome this negative predictive marker. From another point of view, pAkt could therefore act as a differential biomarker for CB treatment selection over SB.

5.4.2 *In-vivo* Erlotinib Resistant Model

The study design for this sub-study was based on a research paper on developing an erlotinib resistant orthotopic lung cancer murine model.[364] In this study, the authors produced transgenic mice models using using vectors transfection or transgene insertion (EGFR, K-Ras mutation, P53 loss), and treated a total of 13 mice with several treatment regime of erlotinib 25 mg/kg/day 5 days a week. They examined continuous versus intermittent protocol, the use of doxycycline to ensure continued expression of transgene, and treatment from 5 to 8 months. To confirm the presence of lung tumour and to monitor tumour growth, they used MRI on the mice every 4 weeks. The authors found that the intermittent protocol supplemented by doxycycline on "off-treatment" period was the best strategy, with most apparent tumour growth from 4 months onwards.

One major hurdle in developing the erlotinib resistant model was the inadequate imaging modality for monitoring tumour growth in our animal house facility. Based on the group's experiences and results with both subcutaneous and sub-renal models, sub-renal model with the higher engraftment and growth rates was chosen for development of erlotinib resistant moddue to its high vascularity. Whilst tumours that were passaged a number of generations would be aggressive enough to be palpable even as sub-renal xenografts, the concept of developing a drug resistant model was to simulate the human environment as closely as possible, and in this sense only first-generation xenografts should be employed. Thus, the only way to monitor tumour growth internally was to perform regular imaging as the previous study described.

Unfortunately, the animal house was not equipped with a PET or MRI imaging facility. Whilst our group has affiliations with CSIRO and a number of nuclear medicine physicians, the rule from our animal house is that animals once taken outside cannot be brought back to the facility. Our animal house was equipped with the Carestream in-vivo MS FX PRO (Carestream, Toronto), a multispectral fluorescent, luminescent and radioisotopic high-resolution x-ray system which are increasingly used in *in-vivo* studies.[365,366] A fluorescent dye (DID) was used,

and multiple attemps were made to optimise conditions for the best imaging results. Briefly, varying concentration of the dye, varying times of tail injection and imaging (4, 24, 48 hours) was explored, and both *in-vivo* and *ex-vivo* studies undertaken. A multimodality animal rotation system was utilised to generate 3-dimensional pictures.

Below showed a montage of x-ray images taken 48 hours after injection of DID dye on 3 mice that had sub-renal tumours xenografted 8 weeks prior. On necropsy, all 3 mice had viable tumours. In 1 of the 3 mice, the tumour was localised well (white arrow) where it was transplanted, but this did not display on the other 2 mice **(Figure 5.23)**. Thus, although the carestream imaging system was specific in tumour localisation, the sensitivity rate was too low to be used for routine tumour monitoring in the erlotinib resistant model. Attempts are made to combine DID dye with over-expressed proteins in pancreatic cancer, and this is a current subject of another student's PhD.

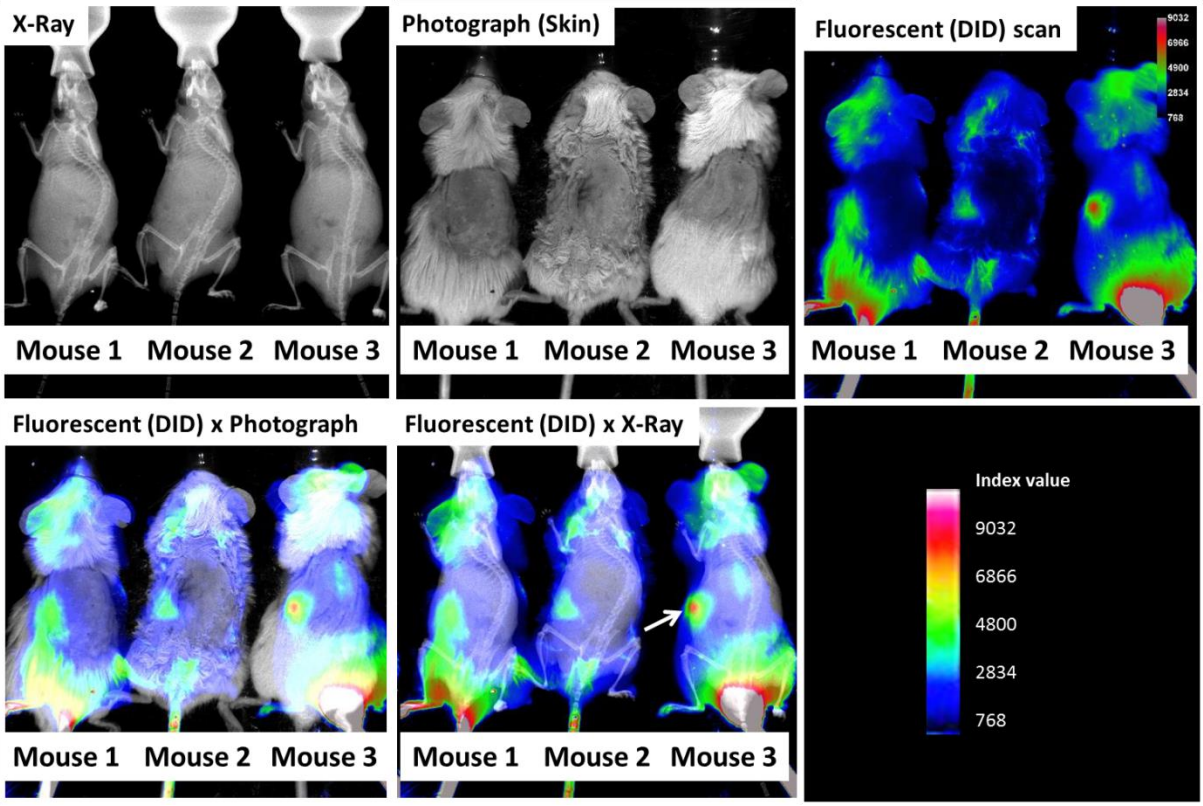

Figure 5.23: Carestream imaging for tumour localisation

Due to the uncertainty of current imaging for tumour monitoring, and the drug expense for long-term animal feeding of erlotinib, a pilot study of only 3 animals was performed, where sub-renal transplantation was used for two mice (M1, M3); and subcutaneous approach was used in another (M2) **(Figure 5.24)**. The mice were allowed to grow for 8 weeks (sub-renal) and 12 weeks (subcutaneous) respectively before starting erlotinib treatment. M1 was treated with erlotinib 25 mg/kg/day, and M2 and M3 treated with 50 mg/kg/day. An on-off schedule was implemented as recommended to allow for tumour regrowth.[364] For M1 and M2 Doxycycline was supplemented with food in the off-treatment period. This was used to ensure expression of the transgene.[364] M1 and M2 had a 4-week-on 4-week-off schedule, whereas M3 had a 4-week-on 2-week off schedule.

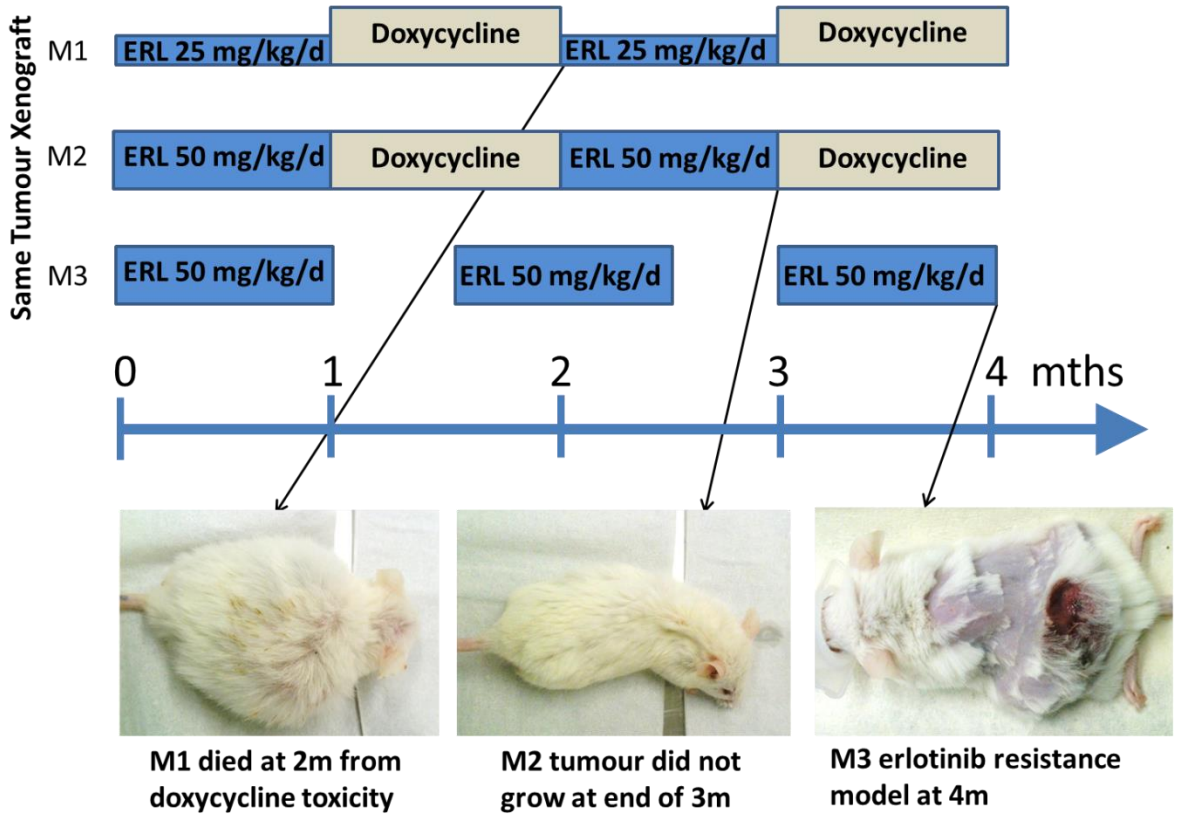

Figure 5.24: Erlotinib resistant xenograft models- study design

M2 was a mouse that had subcutaneous transplantation of xenografts. The tumour did not grow and was not present when the study was terminated at 3 months. The tumour did grow in M1 and M3, but M1 unexpectedly died at 2 months. It was on its treatment-off period, and

no other interventions were given at the time except for doxycycline. No sources of sepsis were found on the animal at autopsy. Doxycycline was not gavaged in mice, and was merely supplemented in the water. It was possible that by chance the mouse drank excessive water supplemented doxycycline and became overdosed. M3 was different to the other 2 mice where doxycycline was not given, and only a 2-week treatment-off period was allowed. The tumour on this mouse was palpable by 3 months, with ulcerations by 4 months. This tumour was removed upon necropsy 3 days after stopping treatment and fixed for histopathological diagnosis. Unfortunately, there were extensive necrosis but no viable tumours were identified in M3 **(Figure 5.24)**.

All in all, development of *in-vivo* model was not successful. It was limited by the absence of tumour imaging for monitoring, the lack of continued supply of the erlotinib targeted therapy and the underpowered statistics. Overall it was deemed too high a risk and costs to continue undertaking this sub-study in animal experiments. Instead plans are made to study this in the setting of a clinical trial.

5.5 Discussion

Following the success of combined blockade *in-vitro* in pancreatic cancer in chapter 4, this was further evaluated *in-vivo* in this chapter. The objectives here were to develop and validate an animal model for drug testing, and then to use this to evaluate a number of CB combinations. Other sub-objectives of the *in-vivo* study were to develop an erlotinib resistant animal model and to assess for candidate predictive biomarker/s for erlotinib resistance and for CB combination. A full assessment would not be possible for this thesis, and thus these were only intended as preliminary assessments (sub-studies) foreshadowing larger clinical confirmatory trials, to be discussed in chapter 6.

5.5.1 Patient derived tumour tissue model (PDTX)

Patient derived tumour xenograft (PDTX) model is more demanding and requires close collaboration between surgeons, pathologists and scientists to ensure immediate transplantation of fresh viable tumour tissue into immunocompromised mice. However, there are many advantages of over traditional cell line *in vivo* model. Cell line *in vivo* models have long been criticised for not "sufficiently representing clinical cancer characteristics, especially with regard to metastasis and drug sensitivity".[339] PDTX model, on the other hand, better reflects human tumour biology, can be transplanted in various modes, and through generations of passaging provides a virtually unlimited source of tumour tissue for therapeutic testing.[339] Whilst not perfect or standard by any means compared to patient study, PDTX models have significant roles in drug sensitivity screening, biomarker developments, and can also produce useful pharmacokinetic/ dynamic and resistance models **(Figure 5.25, 5.26)**[367,368]. In this project, a close resemblance of PDTX to patient histology was found, and sufficient tissue were generated to evaluate drug testing *in vivo* as well as attempt at biomarker discovery and generation of a drug resistance model.

Aspects	Cell line *in vivo*	PDTX *in vivo*	Patient study
Resembling to tumour tissue	No	Yes	-
Transplantation	Sub-cutaneous mostly	Sub-cutaneous, sub-renal, orthotopic	-
Tissue available	Unlimited	Potentially unlimited	Limited
Drug sensitivity screening	Many, but not realistic	Many, more realistic	Limited
Biomarkers discovery	Limited	Possible	Standard (Phase II/III translational study)
Pharmacodynamic/ kinetic model	Not possible	Possible	Standard (Phase I study)
Resistance model	Not realistic	Realistic	Standard

Figure 5.25: Characteristic of PDTX model

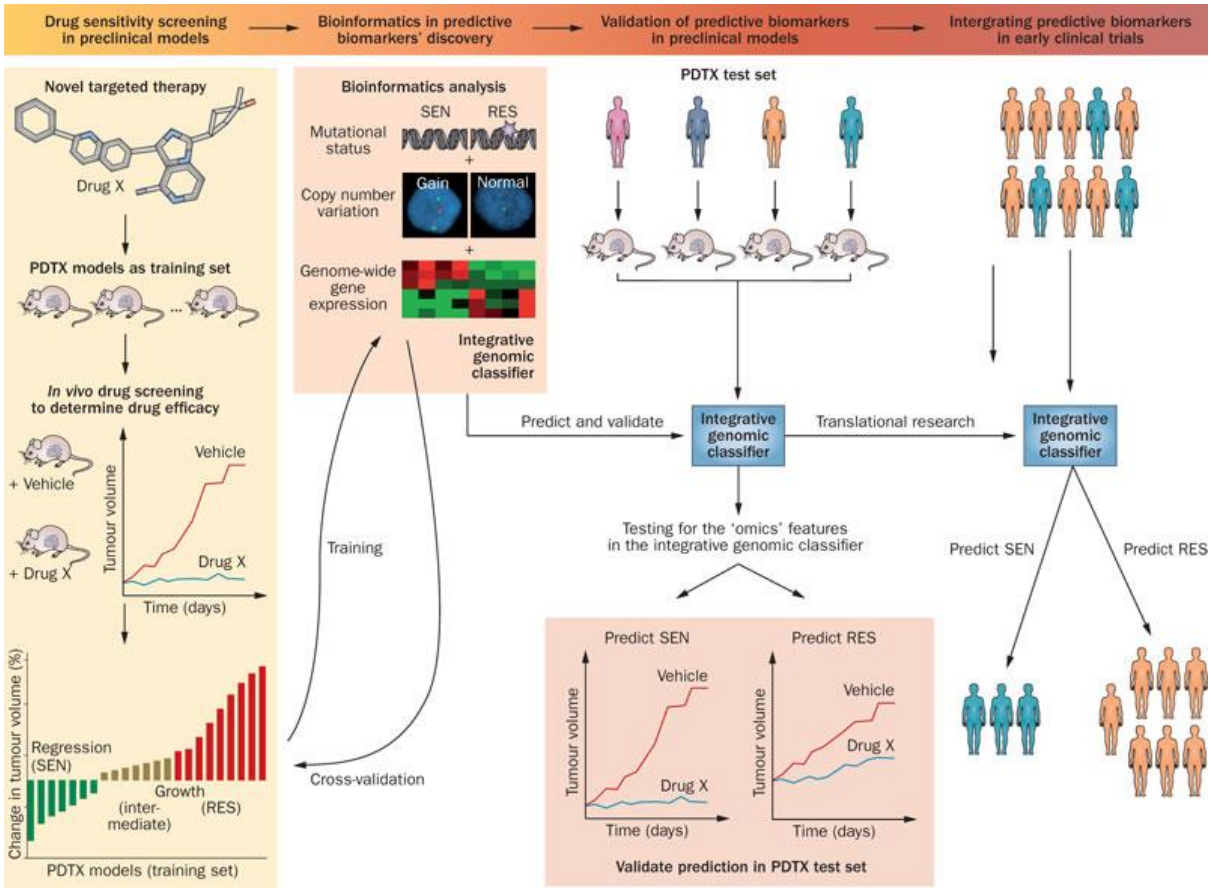

Figure 5.26: Uses of PDTX model in drug development. Courtesy of Tentler et al. 2012.[367]

5.5.2 Sub-renal versus subcutaneous transplantation models

Two models were used to evaluate drug efficacy in this project: sub-renal and subcutaneous models. Orthotopic models had also been considered, but xenograft transplantation directly into the pancreas of small mice only 30g in weight proved exceedingly difficult. The pros and cons for the sub-renal and subcutaneous models are listed below:

Aspects	Sub-renal	Subcutaneous
Animals needed	20 per experiment (total 90 for ERL * BYL core)	17 + 20 (for passaging) per experiment
Preparation	Easy (1st Generation xenografts)	Difficult (4th-5th Generation xenografts)
Technicality	Difficult	Easy
Engraftment Rate	80-90%	50%^
Growth Rate	6-8 weeks	6 months*
Multiple measurement	No	Yes
Statistical power	High	Low
Use for our study	**Primary model**	**Supportive model**

Table 5.6: Comparison between sub-renal and subcutaneous models for our in-vivo studies. ^ Engraftment rate improved to 80%, and * growth rate improved to 8 weeks with 4-5 passages of first generation primary tumour

There were several reasons for choosing both models: sub-renal was an efficient and cost-effective model. Due to the high vascularity in the sub-renal capsule, the engraftment and growth rates were consistently high, and robust statistics could be calculated. However, only one measurement could be used in the absence of adequate imaging: the end-of-study measurement of tumour volume. Subcutaneous model, on the other hand, allowed multiple measurements of tumour by calipers once established. This allowed for tumour doubling time and growth trend statistics to be calculated.[273] However, it required several generations of tumour passaging to establish a stable engraftment and growth rate. Even then, the engraftment rate was inferior to that of sub-renal model. This resulted in missing values, and

the statistical power was thus relatively lower for the same number of mice to be used. As our group constantly sought to comply with the NHMRC code of practice for minimisation and refinement of animal studies, the sub-renal model was chosen as the primary model based on the smaller number of animals required, and subcutaneous model as a supportive method.

5.5.3 Combined blockade efficacy *in-vivo*

Table 5.7 below summarised the sample sizes and statistical findings of the sub-renal and subcutaneous experiments. The P-values were calculated by 2-way ANOVA after adjusting for each experiment (SAS 9.2). Both erlotinib plus BEZ-235 and erlotinib plus BYL-719 CBs were tested, but the former was abandoned due to high levels of toxicity, which was also reported by other research groups in our institution. Possibly due to premature study termination, no significant differences were observed between E50B25, E50 and NT. The pilot study for the latter CB (E50Y25) was also not significantly different to E50 and NT; but the magnitude of difference was greater than that between E50 and NT. This pilot study therefore showed some early signs of efficacy, and provided the effect estimate that was used to calculate the true sample size for an adequately powered study. After 6 experiments with 90 animals, the sub-renal core study achieved its objective by showing superiority over control (P=0.0005) and non-inferiority over gemcitabine (P=0.54). A subsequent follow-up subcutaneous study not only confirmed superiority of E50Y25 over NT (P=0.003), but also superiority over E50 (P=0.014) and Y50 (P=0.003). CB essentially halted tumour growth, such that the tumour doubling time was not reached in CB. Interestingly, BYL was not as effective as ERL as single agent, echoing current literature that these drugs are best used in combination with other targeted therapies for continuing clinical development.[47]

Experiment	n=	E50Y25 vs.			
		NT	G100	E50	Y50
Sub-renal (Pilot)	34	0.45	-	-	0.55
Sub-renal (Core)	90	**0.0005**	0.54	0.35	-
Subcutaneous (Core)*	17	**0.003**	-	**0.014**	**0.003**

Experiment	n=	E50B25 vs.			
		NT	G100	E50	Y50
Sub-renal (Pilot)	-	-	-	-	-
Sub-renal (Core)	26	0.59	0.88	-	0.46

Experiment	n=	G100 vs.			
		NT	E50	Y50	E50Y25
Sub-renal (Pilot)^	215	Associated with clinical response	-	-	-
Sub-renal (Core)	90	**0.0001**	0.13	-	0.542

Table 5.7: Summary of P-values from ANOVA statistics of sub-renal and subcutaneous experiments. * based on end-of-study measurement. ^part of a larger study that established our current sub-renal model

There is now therefore sufficient pre-clinical evidence (both *in-vitro* and *in-vivo*) to take the concept of combined blockade with erlotinib plus PI3Kα inhibitor NVP-BYL719 to clinical trials. The abbreviated findings of this combination were presented in a National meeting (Australasian Pancreatic Club 2013) and now published (CCR. 2014), and the proposal for clinical trials submitted to the two respective pharamaceutical for global evaluation. I believe that co-targeting MEK and PI3K warrants further evaluation given its strong *in-vitro* data and emerging clinical profile in other cancer types.[207] One approach for further *in-vivo* and clinical development may be combining a novel MEK inhibitor such as AZD-6244 with BYL-719 in the future.

5.5.4 Biomarkers for erlotinib resistance and CB response

Current literature implicates Akt over-activation and K-Ras mutation as negative prognostic markers,[44,54] and quasi-mesenchymal status as negative predictive markers for erlotinib treatment.[212] In chapter 3 and 4, erlotinib resistance is shown to be associated with up-regulation of PI3K/Akt pathway via mTOR. This *in-vivo* study, though by no means definitive, suggests the roles of pEGFR as positive and pAkt as negative predictive biomarkers for erlotinib SB or erlotinib plus BYL CB. This is consistent with the current PDAC literature since mutant K-Ras still employs EGFR to some extent, and it is also shown to increase GSK-3β of the PI3K/Akt system contributing to tumor cell proliferation and survival.[65,212] Although tumours with high pAkt immunostaining were correlated with lower response to CB compared to experiments with primary tumours expressing 0/1+ pAkt, partial responses were nonetheless observed in CB whilst no response was evident in SB. Hence, pAkt may also have a differential role in guiding CB treatment over SB. Whilst preliminary results were supportive of current literature, the clinical development of these biomarkers remained challenging, and a number of ongoing issues must be addressed in ongoing studies:

1) **Target selection**: pEGFR and pAkt were chosen as the candidate biomarkers for response for erlotinib and BYL-719, given the previous *in-vitro* studies and that it is directly downstream of PI3Kα. However, EGFR and PI3K/Akt pathways are exceedingly complex and multiple targets may be involved. At present, no single gene or molecular target has been demonstrated to predict efficacy for PI3K inhibitors reliably in published literature, which may be because of co-existing alterations in this pathway.[47] Whilst phospho-RTK or PCR array may be of some use in biomarker discovery, genome wide screening platform will likely be required to look for genetic signatures predicting the efficacy of this treatment in clinical studies.[359]

2) **Combined platforms**: Current approaches to biomarker development are "one-dimensional" relying on single modality assay such as IHC, FISH or mRNA profiling. Early

biomarker studies on the PAM inhibitors are unfortunately flawed by improper, inappropriate or insensitive assays.[47] In the PI3K signalling pathway where multiple mechanisms may be dysregulated, an integrated approach with combined analysis of DNA, RNA, protein and epigenetics is recommended.[359] For further development of pAkt or pEGFR as biomarkers, this target must be tested on other platforms to correlate gene, molecular levels with patient outcomes.

3) **Study Design:** One of the most frequently overlooked aspects of biomarker study by researchers is statistical power. In particular, two common errors are seen: arbitrarily setting biomarker cut-offs, and performing multiple testing without adjustment.[359] Current practice in IHC is to score staining patterns in a dichotomous covariate (0, 1+, 2+, 3+).[369] However, it is increasingly recognised that biomarkers should be evaluated as a continuous outcome in multivariate analyses in research setting, rather than as a dichotomous outcome in univariate analysis. Studies that are inappropriately designed based on unadjusted dichotomous statistics are often underpowered, and resulted in false acceptance of insignificant biomarkers (type II error).[359,369] This sub-study attempted to utilise H-score, developed by McCarty and modified by Allred,[370] and validated in 137 breast cancer patients.[360] H-scores have been evaluated in PDAC in the study of SGLT1, Bcl-2 and p53 as prognostic markers and hedgehog as predictive markers.[371,372] Although currently not specifically validated in PAM pathway in PDAC, it should be optimised in ongoing studies.

In conclusion, this chapter has succeeded in achieving the aims that were set out: to develop 2 animal models for drug testing and establish the *in-vivo* efficacy for PI3K/ EGFR co-inhibition in pancreatic cancer. The findings of the last three chapters (3, 4, 5) have together put forward a strong case for clinical development of this combination in pancreatic cancer. Nonetheless, additional translational research is still urgently needed to develop “robust biomarkers for clinical decision making and for patient selection”.[373] The implications of these results are discussed in the next chapter, and the study design for an ongoing clinical trial will also be presented.

CHAPTER 6:

THESIS DISCUSSION

6.1 Summary of Thesis backgrounds

6.1.1 Background of the thesis

This thesis was planned in 2010 and undertaken from 2011 to 2013. At the time FOLFIRINOX and gemcitabine-abraxane data had not been published yet, and gemcitabine was the only standard of care for advanced or metastatic pancreatic cancer. The only positive phase III drug combination clinical trial was the PA.3 in 2007, demonstrating that gemcitabine plus EGFR inhibitor erlotinib improved survival compared to gemcitabine.[108] At the time, the PA.3 trial was strongly criticised for its limited clinical significance (improving survival of only 10 days) despite its statistical significance. Our group identified the importance of combining targeted therapies and identifying biomarkers in pancreatic cancer, before the embarrassment of the riches in literature over the last 3-4 years.

Until mid-2010, there was a high level of enthusiasm with IGF1R antibody in the treatment of cancer. IGF1R antibodies have nanomolar potency, long half-lives allowing for 3-weekly infusion and have relatively few side effects except for hyperglycemia.[374] In addition, there was a strong rationale combining IGF1R antibodies with chemotherapy, and this strategy has been shown to have activity in NSCLC in phase I and early phase II studies.[374] From 2008 to 2010, there had been a series of pre-clinical studies demonstrating synergy of EGFR and IGF1R inhibitors in various cancers.[86,375,376] Later, it was also shown that IGF1R antibodies plus chemotherapy were active even in gastrointestinal carcinomas with *K-Ras* mutation.[377,378]

My interests in experimenting with IGF1R inhibitors stemmed from pre-clinical studies establishing the role of IGF1R over-expression in mediating proliferation, survival, angiogenesis and invasion in pancreatic cancer.[379,380] One of our prior studies of EGFR, IGF1R and urokinase pathways in 46 pancreatic cancer specimens also found an importance of IGF system in tumour progression. In addition, it also demonstrated significant association between *EGFR* and *IGF1R*-related genes, suggesting extensive cross-talks between the 2

pathways.[63] I therefore made a hypothesis that erlotinib insensitivity or resistance in pancreatic cancer may be overcome by adding IGF1R inhibitors to erlotinib.

In 2010, I attended the Australia and Asian Pacific Clinical Oncology Research Development Workshop (ACORD), and designed and completed a 100-page phase II clinical trial protocol with the aim of randomising 42 patients to erlotinib or erlotinib plus IGF1R antibody CP-751,871 (figitumumab). This was the first manufactured antibody, and was also the drug with the highest level of evidence. I also designed a translational component with our proposed study, with mandatory collection of tissue for gene and IHC analysis of IGF-related biomarkers. At the time, combined blockade strategy was not yet popularised, and the study design was therefore considered novel. The proposal was endorsed by the Australasian Gastro-Intestinal Trials Group (AGITG) and submitted to Pfizer for consideration.

Unfortunately, in the American Society of Clinical Oncology (ASCO) meeting in mid-2010, a large international phase III clinical trial NSCLC (n=820) was stopped early after showing chemotherapy plus figitumumab resulted in significantly worse survival compared to chemotherapy alone (HR 1.6, P=0.006). Combination therapy resulted in serious adverse events including dehydration, hyperglycemia and haemoptysis, and no subgroups had been found to derive more benefits from combination therapy.[176] Subsequent studies showed conflicting data of whether IGF-1 or IGF1R was predictive to IGF1R combination therapies.[177,381] The significantly harmful findings of this study had essentially closed off further development of this class of agents in various companies over the next 2 years. My proposal of phase II trial was rejected in early 2011. I received figitumumab from Pfizer for pre-clinical studies, though the preliminary studies *in-vitro* also showed limited activity of this drug in pancreatic cancer.

Due to these unforseen circumstances, I had to radically alter my PhD research project in early 2011. I performed a literature review, and found a number of interesting molecular biology facts of the EGFR and IGF1R pathways, including the role of downstream PI3K

pathways over-activation in cancer progression in pancreatic cancer, and cross-talks between downstream EGFR/ MAPK and PI3K pathways. These will be discussed further in the next section. In contrast to the comprehensive development program of IGF1R inhibitors, PI3K and PI3K/mTOR inhibitors drug development were very new at the time, and little clinical data of these drugs existed at the time. Despite several discussions with managing directors and international experts, I could not acquire the drugs or funding for a clinical trial without further pre-clinical evidence. I therefore changed from clinical trial and translational research to basic science research.

Initially, we purchased our own drugs from manufacturing companies. Later, when I had established effects of these drugs, I requested BYL-719 and BEZ-235 from Novartis. In the first year of my research project, I explored the mechanisms of erlotinib resistance and initially tested drug combinations of IGF1R inhibitors (NVP-AEW541, OSI-906) or PI3K inhibitors (BYL-719) and erlotinib *in-vitro* (Chapter 3, part of chapter 4). In my second year, I progressively studied the synergy and effects of downstream blockade using 4 CB combinations (chapters 4), after demonstrating superior effect of PI3K inhibitors over IGF1R inhibitors. With the encouraging results, I requested Novartis for BYL-719 and BEZ-235 for *in-vivo* testing, and carried out the *in-vivo* experiments between 2012 and 2013 (chapter 5).

6.1.2 Summary of known facts and evidence

The facts and evidence have been comprehensively described in **Chapter 1: introduction**. Below is a summary of known facts, and the research questions that arise.

The hypotheses or research questions for the research project were based on a number of scientific facts. *Mechanistically*, PAM pathway is often over-expressed in PDAC. In contrast to NSCLC, *EGFR* mutations in pancreatic cancer are rare and typically silent, and EGFR tyrosine kinase activity is highly conserved.[58,213] Whilst *EGFR* gene may be up-regulated in 50%, EGFR protein is only over-expressed in 30% of PDAC.[213,382] On the other hand, IGF1R, PI3K and

Akt proteins are found to be over-expressed in 50%, 70% and 50% by IHC.[61] Cross-talks between EGFR and IGF1R are known to exist for various cancer types.[86] In PDAC, significant cross-talks also exist between downstream signalling pathways. For example, oncogenic activation of Ras has been demonstrated to increase PI3K and GSK3 beta (downstream of Akt),[65,68] and the Ras-induced PI3K/ mTOR signal transduction is shown to be sufficient to lead to tumourigenesis in pancreatic cancer.[80] Since *K-Ras* mutation is highly prevalent in PDAC,[20] and *K-Ras* mutation is associated with EGFR antibody resistance at least in colorectal cancer,[137,305] the obvious question is whether erlotinib resistance in PDAC is also mediated by over-activation of PAM pathway, possibly by *K-Ras*.

Therapeutically, there are to date no current clinical data of PI3K inhibitors in pancreatic cancer. Two clinical trials exist exploring the effect of erlotinib and EGFR antibody cetuximab. The marginal benefits of erlotinib in improvement of overall survival have already been described numerous times in this thesis. Yet, it is important to note the disease control rate (58%) and improvement in PFS (HR 0.77, P=0.0004) exceeded that may be expected from an absolute survival benefit of 10 days.[108] This same pattern was also noted in another targeted therapy trial randomising patients to gemcitabine plus cetuximab versus gemcitabine alone, yielding a disease control rate of 51% and highly significant improvement in PFS (P=0.006).[124] Despite the effect of EGFR inhibition in disease stabilisation and delay in progression the absolute benefit in survival is small. Given the extensive molecular cross-talk in pancreatic cancer, the therapeutic question proposed is whether dual targeting of EGFR and IGF1R or PI3K may be more effective than EGFR inhibition alone.

Translational data based on clinical trials is extensive in metastatic NSCLC and CRC. EGFR mutation and *K-Ras* wild type have long been established and now adopted in clinical practice, as predictive factors for EGFR inhibitors and EGFR antibodies.[137,138,144,145] Biomarkers for the use of erlotinib have not been fully established in PDAC however, with *K-Ras* mutation status implicated in one study but not the other.[121,213] One of the research questions was to explore

predictive biomarkers for sensitivity to SB versus CB. Given the limitation in statistical power in *in vivo* study design, the aim here is proof of concept to take to clinical translational study.

Mechanistic	Therapeutic	Translational
	Summary of known facts	
EGFR is over-expressed in 30% of PDAC[61]	**Gem+ Erlotinib > Gem in overall survival (HR 0.82, P=0.038)** (PA.3)	**In mNSCLC, EGFR mutation was predictive of EGFR TKI response[144,145]**
***K-Ras* is mutated in 90% of PDAC[20]**	**The absolute benefits was only 10 days** (PA.3)	**In mCRC, *K-Ras* wild type was predictive of EGFR antibody response[137,138]**
PI3K and Akt are over-expressed in 70% and 50% respectively[48,54]	**Gem + Erlotinib > Gem in PFS (HR 0.77, P=0.0004)** (PA.3)	**K-Ras may be negative predictive for erlotinib response in PDAC[121]**
Multiple levels of interactions exist (EGFR/IGF1R, *K-Ras*/ PI3K)[68]	**Disease control rate with dual agent =58%** (PA.3)[108]	**Only positive predictive "marker" for erlotinib appeared to be grade 2-3 rash** (PA.3)[108]
	Research Questions arisen	
What is/ are the key driver/s for erlotinib resistance? (Ch 3)	***Can combined blockade strategy increase efficacy of targeted treatment (Ch 4, 5)***	***Can a marker be identified for dual targeted therapy strategy? (Ch 5, 6)***

Table 6.1: Summary of known facts and research questions

6.1.3 Summary of aims and methods

The chapters and chapter aims are summarised below. Chapter 3 and 4 are *in-vitro* studies and chapter 5 continues onto *in-vivo* studies. Chapter 3 aims to characterise the genetic and molecular profile or primary and acquired resistance by means of 5 PDAC cell lines and 2 pairs of parent and ER cell lines. Chapter 4 aims to compare CB versus SB, and to test the best of 4 upstream/ downstream CB combinations. Chapter 5 aims to take the two best CB combinations into animal studies, after establishing and validating a xenograft model. Note that the translational sub-studies (e.g. pAkt/ AKT and *in-vivo* resistance model) were not included in part of the chapter 5 aims. These preliminary studies were only meant to demonstrate feasibility but could not be definitively studied *in-vivo.*

Chapters	Chapter Aims
Chapter 3: genetic and molecular characterisation of primary and acquired erlotinib resistance **(initial stage)**	1. To assess erlotinib sensitivity in 5 PDAC cell lines 2. To develop PDAC cell lines with acquired resistance to erlotinib 3. To study molecular properties for primary and acquired erlotinib resistance 4. To propose treatment strategies that may exploit the knowledge of erlotinib resistance
CHAPTER 4: combined blockade versus single blockade of EGFR and PI3K/mTOR in-vitro **(testing stage)**	1. To compare the effect of combined blockade (CB) versus single blockade (SB), and to establish synergy 2. To propose the "best" CB combination for pancreatic cancer to take to in-vivo study 3. To explore onocogenic dependence by comparing differential response to CB between parent and resistant cell lines
CHAPTER 5: combined blockade of EGFR and PI3K in-vivo **(validation stage)**	1. To establish and validate a pancreatic cancer xenograft model for drug testing 2. To test the in-vivo efficacy of EGFR and PI3K dual blockade

Table 6.2: Summary of chapters and chapter aims

The summarised methods were illustrated below. This was divided into initial stages, testing stages and validation stages. Ongoing experiments will comprise of clinical and translational stages **(Figure 6.1)**.

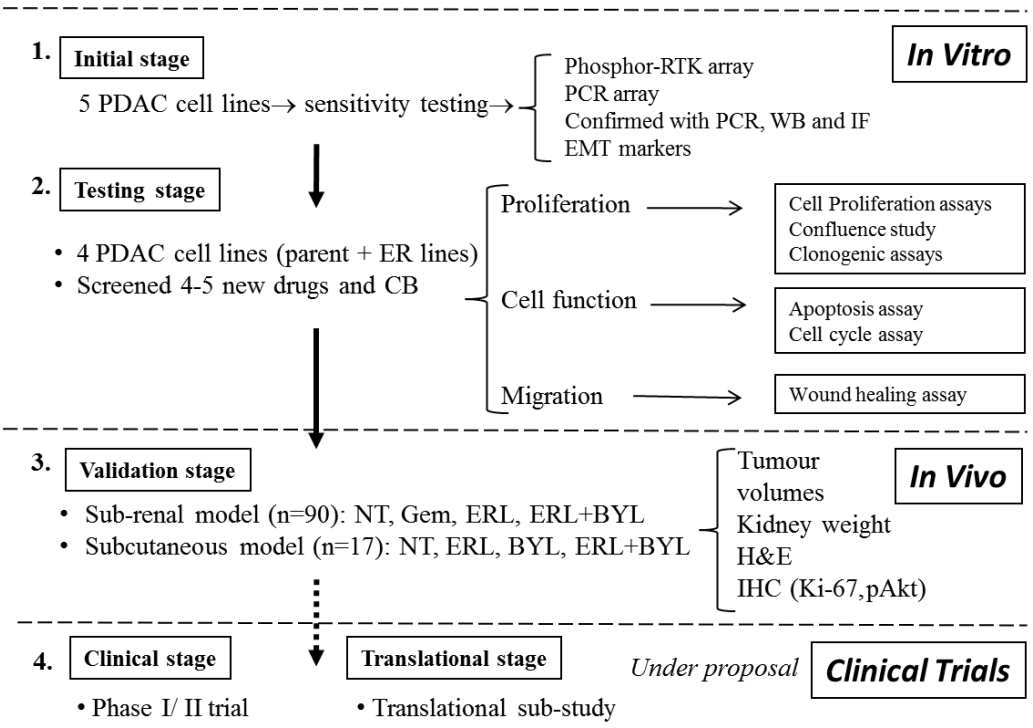

Figure 6.1: Summary of Methods in the Research Program

Briefly, in the initial stage, 5 PDAC cell lines which differ in their sensitivity to erlotinib were used. The most erlotinib sensitive (BxPC-3) and insensitive (PANC-1) were used to develop 2 erlotinib resistant cell lines (BxPC-ER, PANC-ER). Phospho-RTK and PCR arrays were used on the 2 pairs of parent and ER cell lines to compare their molecular and genetic differences that attributed to *erlotinib resistance* (acquired resistance). qRT-PCR, western blotting (WB) and immunofluorescence (IF) were used to study the EGFR, IGF1R and MAPK/PAM pathways that attributed to *erlotinib insensitivity* (primary resistance) in the 5 PDAC cell lines, as well as to validate the screening array results. After demonstrating stability of erlotinib resistance, the differences between each pair of cell lines were assessed based on the status of erlotinib resistance only, thus making it a powerful model.

In the CB testing stage, 4 CB combinations were used (EGFR/ IGF1R, EGFR/ PI3Kα, EGFR/ PI3K/mTOR, MEK/PI3K/mTOR) and compared these to single agents that made up the CB. 6 *in-vitro* assays (cell proliferation assays, confluence/ incucyte study, clogenic assays, apoptosis assays, cell cycle assays, wound healing/ migration study) were used to study 3 cellular functions- cell proliferation, cell function and migration. These are particularly important functions in tumour progression and metastasis. Both synergy and efficacy of these drugs were studied. These experiments allowed us to fully assess the effects of CB, and to interrogate the roles of upstream and downstream MAPK and PAM pathways in PDAC.

The *in-vivo* studies were regarded as the validation stage. Due to the expense and complexity of *in-vivo* experiments, it was not possible to test all 4 CB combinations in animal study. Two models (sub-renal, subcutaneous) were used to evaluate two best CBs (ERL+ BYL, ERL+ BEZ), and studied the primary endpoint of tumour volumes and secondary endpoints of kidney weight, H&E and IHC (Ki-67). The sample sizes were based on a 2-sided α of 0.05, β of 0.8 and an expected 36% decrease in tumour volumes by CB from pilot study. The objectives were to demonstrate superiority of CB over control and non-inferiority (or equivalence) to standard gemcitabine chemotherapy.

The thesis currently ends with the validation stage, having confirmed the efficacy, safety and dosing of erlotinib plus BYL-719 CB pre-clinically. The next phase will be clinical and translational stages in a first-in-man phase I/ II trial. The concept has been submitted to Novartis for further review, and the proposal was presented in the AGITG/ Australasian Pancreatic Club Workshop (Oct 2013). This will be discussed further in **section 6.3**.

6.2 Results and Clinical significance

Whilst the results and discussion have been described at the end of each chapter, the pertinent findings and the significance or implications for the thesis as a whole are presented here. The research project combines mechanistic, therapeutic and translational findings to answer the research question, and is illustrated in the same way as the background facts.

Mechanistic	Therapeutic	Translational
	Results	
Downstream pathways are up-regulated in erlotinib insensitivity	***In-vitro*, dual PI3K/mTOR and MEK blockade was most effective**	***In-vitro,* pAkt up-regulation predicts EGFR/ PI3K/ mTOR CB efficacy**
PI3K/Akt via mTOR is "exploited" in erlotinib resistance	***In-vivo,* dual PI3K/mTOR and EGFR blockade was too toxic**	***In-vitro*, oncogenic dependence to pAkt is demonstrated in erlotinib resistance**
NF-kb and Fos genes over-expression are implicated in erlotinib resistance	***In-vivo,* dual PI3K and EGFR blockade was superior to control and equivalent to gemcitabine chemotherapy**	**ER cell lines were hyper-sensitive to PI3K-based CB**
Erlotinib insensitivity and resistance are likely associated with EMT	***In-vivo,* CB appeared more cytotoxic (↓ tumour vol, ↑ cleaved caspase-3) than cytostatic (↓ Ki67)**	***In-vivo,* preliminary results showed pEGFR to be positive predictive and pAkt as negative predictive; pAkt may act as differentiating biomarker of CB over SB**
	Significance	
Significant cross-talks exist between MAPK and PI3K/Akt pathways in PDAC	***Combination strategy, e.g. Erlotinib plus BYL-719, should be evaluated in PDAC in clinical trial***	***pAkt and pEGFR may be candidate predictive biomarkers, and should be further evaluated in translational study***

Table 6.3: Summary of chapters results and significance

6.2.1 Mechanisms of erlotinib resistance

6.2.1.1 Mechanisms of primary erlotinib resistance

Primary erlotinib resistance is associated with increased expression of downstream pathways, in PI3K/Akt (CAPAN-2, PANC-1) more so than MAPK (ERK) (MiaPACA-2) in PDAC cell lines. There also appears to be significant interaction between the EGFR/ ERK and IGF1R/PI3K **(sub-section 3.4.3, 3.4.4)**. This is demonstrated by activation of downstream Akt and ERK by either EGF or IGF stimulation, and paradoxical increases in pAkt in response to erlotinib, and pERK in response to AEW in PANC-1. When a stressor is applied to one downstream pathway, cancer cells can rapidly switch to an escape route, a process that has been termed "oncogenic shift".[132] There is a trend of *MAPK1*, *PIK3CA* and *AKT-2* gene up-regulation in concordance to molecular over-activation in erlotinib insensitive cell lines **(table 3.8)**. Vimentin is also implicated in primary erlotinib resistance, being expressed in all 3 erlotinib-insensitive cell lines CAPAN-2, MiaPACA-2 and PANC-1, though only MiaPACA-2 is truly mesenchymal in morphology **(sub-section 3.4.2)**.

6.2.1.2 Mechanisms of acquired erlotinib resistance

For acquired erlotinib resistance, there appear to be at least three mechanisms at play. Firstly, as demonstrated by phospho-RTK screening array and validated by western blotting and immunofluorescence, erlotinib resistance is associated with further exploitation of PI3K/Akt pathway, mediating via mTOR **(sub-sections 3.5.2-3.5.4)**. This shift to the dominant PAM pathway may enable cancer cells to escape the EGFR blockade by erlotinib. Secondly, ER cell lines also activate the downstream ERK pathway, though not as strongly as PI3K/Akt **(sub-sections 3.5.3-3.5.4)**. This would explain why PANC-ER showed especially high levels of cross-resistance to MEK inhibition, upstream of ERK **(table 3.3)**. Finally, both ER cell lines had likely undergone EMT into mesenchymal morphology, and characterised by a significant increase in vimentin expression **(sub-section 3.5.1)**. EMT results in decreased cell-cell adherence, increased motility, invasiveness and anchorage-independent survival.[160] This is

particularly important as PI3K/Akt axis activation is emerging as a central player in EMT.[383] These observed mechanisms are likely related and together they confer a survival advantage for acquired ER cell lines when treated with erlotinib alone.

Of interest, PI3K/Akt molecular over-activation in erlotinib resistance is not necessarily associated with the over-expression of these genes. screening PCR array found that only several gene expressions were different between parent and ER cell lines. Among these, *NF-κB* and *Fos* genes were the most highly over-expressed genes in BxPC-ER and PANC-ER respectively **(sub-sections 3.5.5-3.5.6)**. Both these genes lie further downstream to PI3K/Akt/mTOR, almost to the nuclear levels. Yet, they were associated with up-regulation of PI3K/Akt upstream molecular pathway. These findings therefore suggest a negative feedback mechanism of downstream genes to PI3K/Akt molecular signalling.

All in all, in this study of primary and acquired erlotinib resistance, the two are thought to be fairly similar. In either setting, PI3K/Akt has a dominant role, and there is an intricate cross-talk between Ras/RAF/MEK/ERK and PI3K/Akt/mTOR pathways are involved, likely on several levels, with inputs from both EGFR and IGF1R. These cross-talk pathways were examined further with single and combined blockade therapeutic strategies.

6.2.2 Single and Combined blockade therapeutic strategies

6.2.2.1 Single targeted blockade

Single targeted blockade yielded valuable information about these pathways in pancreatic cancer. Whilst erlotinib and AEW are potent EGFR and IGF1R inhibitors respectively, the use of these drugs alone resulted in paradoxical activation of the reciprocal pathway in erlotinib-insensitive PANC-1 **(sub-section 3.4.2.3)**. Likewise, pan-PI3K inhibitor LY-294002 also resulted in paradoxical activation of pERK, whereas class I PI3Kα inhibitor NVP-BYL719 was able to appropriately attenuate both pAkt [IC_{50} 4.6μM (3.8-5.3)] and pERK signals [IC_{50} 22.8μM (21.5-24.2)] **(table 3.4)**. Importantly, BYL is a potent PI3Kα inhibitor with high affinity to P110α

subunit (IC_{50} = 5nM), which is 50-fold more specific than other subunits.[384] In contrast, LY is much less specific and less potent, with an IC_{50} range of 1-50 μM for all PI3K-kinase subunits.[385] In these experiments, BYL was shown to be 4 times more potent than LY in pAkt and pERK inhibition in both erlotinib sensitive and insensitive cell lines **(table 3.4)**. Class I PI3K is highly over-expressed in 70% of PDAC, and is known to interact with Ras and p85 regulatory units to activate Akt.[48] My observation of paradoxical activation with erlotinib, AEW and LY, but not BYL which has an extremely high affinity to PI3Kα, suggests a crucial role of PI3Kα in the cross-talk mechanism. It supports the theory of *K-Ras* driven PI3K/Akt over-activation via the α-subunit as a mechanism of oncogenic shift in these *K-Ras* mutant cancers **(Figure 6.2)**.[386,387]

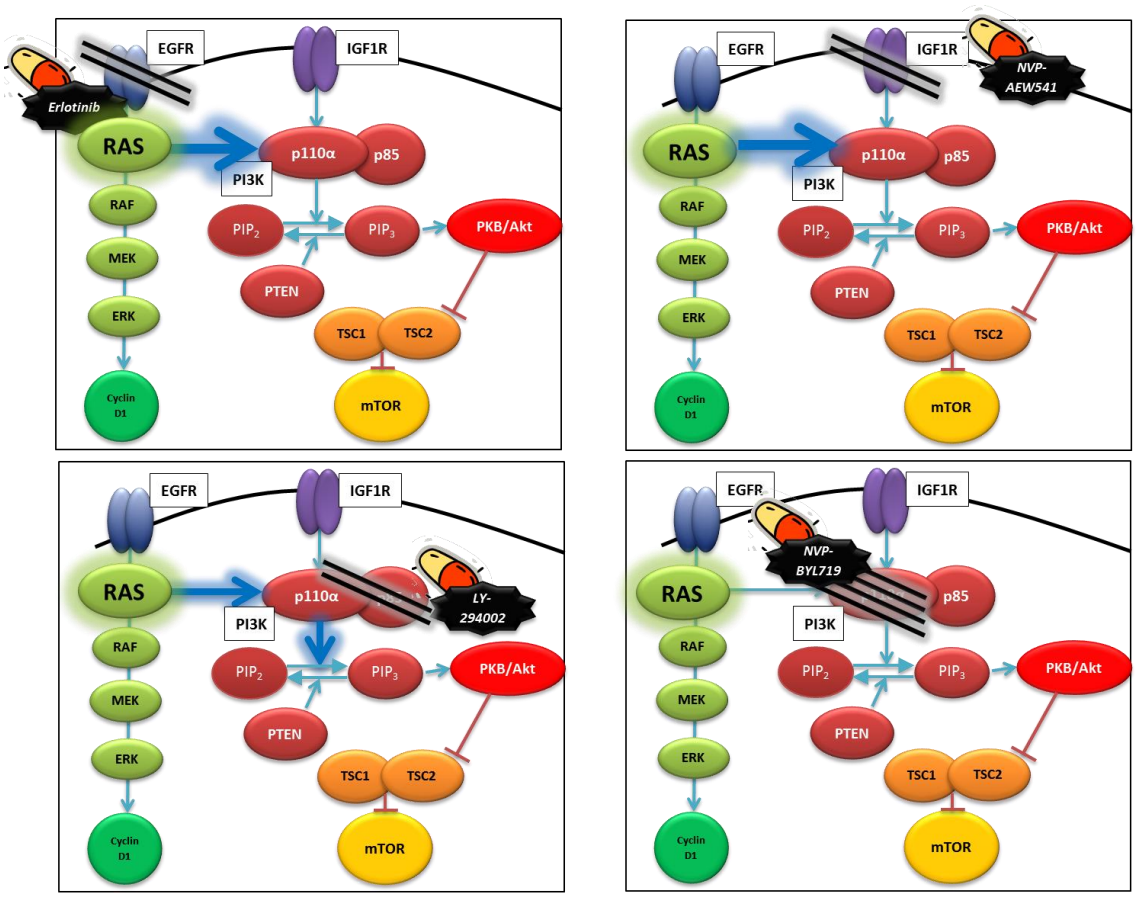

Figure 6.2: K-Ras to PI3Kα interaction leading to oncogenic shift with single blockade of EGFR, IGF1R or PI3K, but not with specific PI3Kα inhibitors

BEZ-235 is an interesting drug with dual properties of PI3Kα and mTOR, with IC_{50} of 5nM to P110α subunit of PI3K and 6.5nM to RPS6, the effector of mTORC-1 complex. It is also important to note that BEZ-235 is only specific to these 2 molecular signals but inactive to most other kinases.[183] In western blotting, BEZ-235 was shown to abrogate pERK, pAkt and pS6 signals as a single agent **(Figure 4.13)**. In the comparison of BYL-719 with BEZ-235, BEZ-235 was found to be 88-fold, 7-fold and 260-fold more potent than BYL-719 in inhibiting pERK, pAkt and pS6 in BxPC-3, and 39-fold, 41-fold and 118-fold more potent in PANC-1 **(table 4.2)**. Given that both drugs have similar nanomolar potency to PI3Kα and only differ in the dual activity to mTOR for BEZ-235, the only logical conclusion appears to be that mTOR is also involved in cross-talks between pathways as well as negative feedback to upstream signalling pathways. Together with the previous results, these findings challenge the "classical cascade" transmitting molecular signals from surface receptors (e.g. EGFR, IGF1R) to downstream effectors (ERK, Akt, mTOR). Instead, these suggest that each molecule has positive and negative feedbacks to both upstream and downstream targets. The analogy is that of a complex metro network where commuters can take many different routes across different train lines to arrive from A to B. Given this intricate molecular network in pancreatic cancer, the hypothesis is that dual targeted therapy blockade will likely be superior to single therapy, and the research question hence becomes whether there is significant difference between upstream and downstream combined blockades.

6.2.2.2 Combined blockade versus single blockade

When comparing dual to single blockade, the effect of two drugs together is assumed to be at least as good as the combined effects of each drug alone (additivity effect). To concretely prove the hypothesis, multiple assays were undertaken to evaluate two endpoints: synergy **(section 4.2)** and efficacy **(section 4.3)**. The synergy studies were dividd into "cytotoxic synergy" cell proliferation assays and "molecular synergy" western blotting analyses, and examined these by means of well-grounded statistical models such as contour plots,

isobolograms and bliss formula (synergy index). In the *cytotoxic synergy* studies, EGFR-IGF1R co-inhibition was found to be highly synergistic for erlotinib sensitive cell lines such as BxPC-3 and CFPAC-1 but antagonistic for erlotinib insensitive cell lines including MiaPACA-2 and PANC-1. On the other hand, PI3K/mTOR inhibitor was synergistic with either erlotinib or MEK inhibitor PD-98059 for all 5 parent cell lines **(table 4.1)**. Of particular interest, erlotinib and AEW-541 became less synergistic, and erlotinib and BYL-719 became more synergistic in both BxPC-ER and PANC-ER cell lines **(figure 4.9)**. This reinforced the findings of high EGFR-PI3K and low EGFR-IGF1R interaction in erlotinib insensitive or resistant cell lines. Importantly, western blotting demonstrated BYL and BEZ were capable of effective inhibition of both PI3K/Akt/mTOR and EGFR/ERK pathways when combined with erlotinib, with near-complete abrogation of pAkt, pERK and pS6. The *molecular synergy* analysis by isobolograms revealed that the highest level of synergy was located at the pS6 level for BYL-719* Erlotinib and at pAkt and pS6 levels for BEZ-235-based combinations (**figure 4.14)**. To establish *efficacy* of CB, parent cell lines were tested with ERL* AEW and ERL* BYL as representative combinations, and demonstrated that CB was indeed far superior to the effect of single agent alone, in confluence studies **(figure 4.10)**, clonogenic assays **(figure 4.19)**, cell cycle assays **(figure 4.23)**, apoptosis assays **(figure 4.27)**, caspase-3 studies **(figure 4.35-36)** and migration studies **(figure 4.37)**. Taken together, both synergy and efficacy of CB were proven, and the results confirmed the important role of pS6 and pAkt in the EGFR- PI3K pathway cross-talks.

6.2.2.3 The best combined blockade combination/s

To understand more about the mechanism of the EGFR/PI3K pathways cross-talks and to select the best CB combinations for *in-vivo* studies, 4 upstream versus downstream CB combinations were systematically studied on 2-3 parent cell lines, using clonogenic assays **(figure 4.20)**, cell cycle assays **(table 4.4)**, apoptosis assays **(figure 4.29)** and migration assays **(figure 4.40)**. In these experiments, the overall pattern was that CBs involving PI3Kα or PI3K/mTOR inhibitors were more effective. Downstream CB appeared more effective than

upstream CB, and MEK/ PI3K/mTOR inhibition appeared the most potent. The exception to this rule was migration assay, where all CB were equally effective **(figure 4.40)**.

After establishing the superiority of PI3K or PI3K/mTOR-based CB, ERL * BYL-719 and ERL * BEZ-235 CB were taken into *in-vivo* study with patient-derived tumour xenograft. The development and validation of the two models (sub-renal, subcutaneous) were described in **section 5.3.1** and **5.3.3**, and the drug doses were taken from the Novartis's investigator brochure based on previous publications. Unfortunately, the study on ERL * BEZ-235 had to be discontinued as this combination caused excessive treatment-related deaths in animals. ERL * BYL-719, on the other hand, was better tolerated and was superior to control (P=0.005) and non-inferior to standard gemcitabine chemotherapy (P=0.542) in the sub-renal study **(Table 5.3)**. In subcutaneous xenograft experiments, this combination was also shown to be far superior to control or single drugs alone for the 28-day duration of treatment **(Figure 5.15)**. Of interest, whilst this CB significantly reduced tumour volumes, it had no effect on tumour activity as measured by Ki-67, as opposed to chemotherapy **(Table 5.4)**. This suggests that CB is cytotoxic but is not as effective as chemotherapy in halting DNA synthesis and cell proliferation.

The results in totality comprehensively explored the mechanism of EGFR – PI3K pathways cross talks and the pre-clinical efficacy of CB drug combination. It demonstrates that downstream CBs are more synergistic and effective in pancreatic cancer, although all CB involving PI3K appeared effective. *In-vivo*, ERL + BYL significantly reduced tumour volumes. In particular, this TKI may have a different focus of action to standard chemotherapy, with more focus on apoptosis/necrosis than proliferation. This study thus provides a strong rationale for clinical development of BYL-719 and erlotinib combination for the treatment of pancreatic cancer.

6.2.3 Candidate biomarkers for combined blockade treatment

Using targeted therapies in unselected cancer population has limited success. Enriching treatment population based on clinical biomarkers (e.g. young, Asian female non-smoker in NSCLC) saw the beginning of personalising medicine, whilst the effects of treatment selection based on molecular biomarkers (e.g. EGFR mutation in mNSCLC patients treated with EGFR inhibitors, or *K-Ras* wild type status in mCRC patients treated with EGFR antibodies, or B-Raf mutation in melanoma patients treated with B-Raf inhibitors) were far reaching.[138,144,149,388] A comprehensive biomarker study could not be properly conducted in small-scale pre-clinical studies, but a search for early signals was attemped anyway in the preparation of launching CB strategy to clinical trial phase.

6.2.3.1 Erlotinib resistance and pEGFR / pAkt as biomarkers to CB

The first "biomarker" that was discovered was, in fact, erlotinib resistance. In the *in-vitro* model, both ER cell lines were more sensitive to EGFR/ PI3K-based CB than parent cell lines. A molecular screening approach using phospho-RTK array identified pS6 and pAkt as the differential factors **(figure 3.35, 3.36)**. In other words, the fact that ER cell lines upregulated the PI3K/Akt/mTOR pathway made them susceptible to the effect of BYL-based treatment. Of note, the pattern of susceptibility correlated closely with the known normal cellular functions of the PI3K/Akt/mTOR system **(figure 4.22, figure 4.26, figure 4.30)**. These effects, observed in proliferation, cell cycle, apoptosis and clonogenic assays, were greater than those in the parent cell lines, significantly so in one of the two ER cell lines studied (PANC-ER) **(tables 4.3, 4.5, 4.6)**. In contrast to proliferation and survival, migration was dramatically but equally affected by all 4 CB, and no differential sensitivity was observed between parent and ER cell lines **(figure 4.40)**. Whilst the PI3K/Akt pathway has been linked to migration, this is a complex process of cell-matrix-stroma interaction orchestrated by many autocrine factors.[331] Possibly since migration is driven by many molecular pathways, these PI3K-dependent ER cell lines did not display hyper-sensitivity to PI3K inhibitors in migration inhibition.

To study this further *in-vivo*, 2 sub-studies were conducted: developing *in-vivo* erlotinib resistance model, and to explore pEGFR and pAkt as an IHC marker **(subsections 5.41 and 5.42)**. Unfortunately, as already mentioned, the development of *in-vivo* resistant model was unsuccessful. The IHC study, while preliminary, showed that xenograft with high basal pEGFR had high tumour response to erlotinib alone. Tumours with high pAkt tended to have tumour response to erlotinib * BYL-719 CB but not to erlotinib alone. Therefore, this suggests that subjects treated with erlotinib will probably do well if tumour had high basal pEGFR. Conversely, subjects with tumour high in basal pAkt should probably be treated with EGFR/ PI3K CB.

From the mechanistic point of view, these data suggested oncogenic dependence of PI3K in PDAC. That is, cancers become dependent on the activity of specific oncogenes and hence display higher sensitivity to drugs targeting that particular cancer circuitry.[330,389] In this case, pancreatic cancer cell lines that are chronically exposed to erlotinib shunt its molecular signals down the PI3K/Akt pathway (oncogenic shift), and even relying on it thus making them highly susceptible to EGFR /PI3K co-inhibition (oncogenic dependence or addiction). This, therefore, challenges the complexity posed by the concept of genomic heterogeneity, in that there remains obligatory pathways operating in a predictable pattern in cancer despite extensive genetic alterations in cancers, and these pathways as a whole (not single signals) are in turn actionable. It therefore supports a strategic use of combined horizontal blockade of multiple obligatory pathways for pancreatic cancer.

6.2.2.3 K-Ras mutation as a biomarker?

It is possible that mutated *K-Ras* gene is the marker that precedes these other surrogate markers mentioned above. As outlined before, *K-Ras* functions upstream of PI3K by directly binding the catalytic subunit p110 of PI3K [68], and *K-Ras* mutant tumors have been implicated in resistance to EGFR and MEK inhibition via PI3K activaton [53,387]. This could not be determined in the current study, as sequencing studies had not yet been performed. However,

circumstantial evidence from the experiments seemed to support this hypothesis. CAPAN-2, MiaPACa-2 and PANC-1- all of which are *K-Ras* mutant,[228] behaved very differently to BxPC-3 which is *K-Ras* wild type. Also, a slightly higher susceptibility of PANC-ER to EGFR-PI3Kα or EGFR-PI3K/mTOR co-inhibition than BxPC-ER was observd. And lastly, as already discussed, oncogenic shift occurred in PANC-1 with EGFR, IGF1R and PI3K single blockade, but not in specific PI3Kα blockade **(figure 6.2)**. If indeed *K-Ras* mutation is the driver mutation and predictive marker for CB, this may have significant implications to the treatment over 90% of pancreatic cancer patients with K-Ras mutated tumour.

6.3 Future directions

After completing *in-vitro* and *in-vivo* study of MAPK and PI3K/Akt/mTOR pathways blockades in pancreatic cancer, essentially we have come back a full circle to where I started my project, only this time my clinical research proposal is that for erlotinib plus BYL-719 instead of erlotinib plus IGF1R inhibitor figitumumab. With the strong pre-clinical evidence, I am proposing a phase I and II clinical trial with a built-in translational sub-study. The proposal has already been submitted to pharma company (Novartis) on the global level, and has been presented and endorsed by Australian Pancreatic Club and Australasian Gastro-Intestinal Trial Group (AGITG). Minor changes has been made to the proposal since. Briefly, the original research trial protocol and proposal are summarised below:

6.3.1 Clinical Trial- Aims

1. To assess safety of dual inhibitors in pancreatic cancer, to establish recommended phase II dose (phase I)
2. To assess an early efficacy signal of erlotinib plus BYL-719 in pancreatic cancer (phase II)
3. To evaluate pAkt, *K-Ras* mutation and other biomarkers that may predict good outcomes for this treatment (translational sub-study)
4. To evaluate quality of life of patients on single-blockade or dual-blockade or best supportive care (quality of life sub-study)

6.3.2 Clinical Trial- Methods

6.3.2.1 Phase Ib clinical Trial

Phase I cohort utilizes a fixed standard dose for erlotinib (100mg daily), and a Beysian approach to dose-escalation of BYL-719, with starting dose chosen based on pharmaceutical IB recommendations for patients with advanced biliary and pancreatic cancers. Patients will be studied in classic n=3 cohorts. Dose escalation will occur if 0 out of 3 patients reach dose-

limiting toxicity (DLT), stop if more than 2 out of 3 reach DLT and expanded to 6 patients if 1 out of 3 reach DLT. Erlotinib will be started at 100mg daily, the standard dose in clinical practice in pancreatic cancer. BYL-719 will be started at 90mg daily. The n+1 dose-escalation is ERL 100mg/d, BYL 180mg/d; n-1, n-2 and N-3 dosing de-escalations are ERL 100mg/d, BYL 60mg/d; ERL 75mg/d, BYL 60mg/d; and ERL 75mg/d, BYL 30mg/d respectively). Recommended phase II dose (RP2D) is determined as the next lower dose level from DLT **(Figure 6.3)**. This model ensures safety while maximises study efficiency.

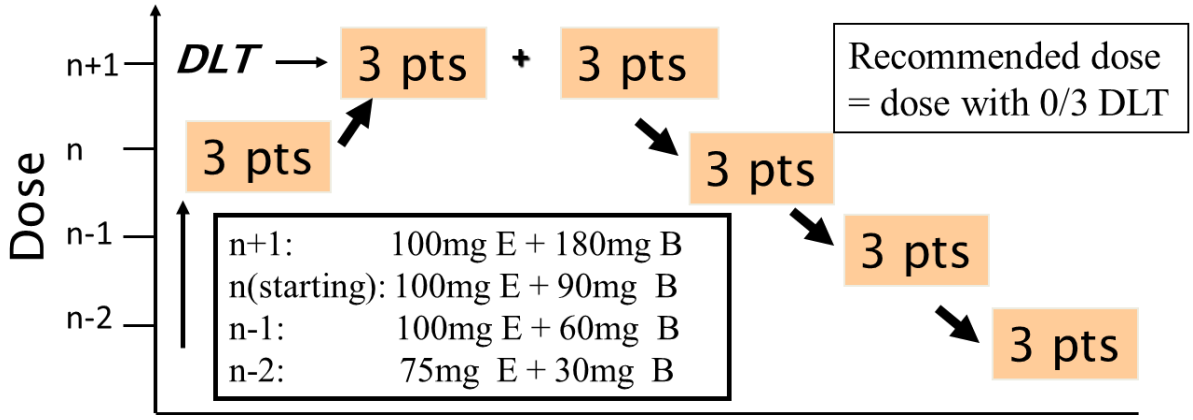

Figure 6.3: Proposed phase I clinical trial design- Beysian model for dose escalation.

6.3.2.2 Phase II clinical Trial

The phase II study randomises patients to second or third-line erlotinib plus BYL-719 or placebo in a 2:1 ratio, with a planned cross-over of patients on placebo to combined blockade upon progression. Patients will be stratified by known prognostic factors in pancreatic cancer: age, ECOG; and lines of therapy. The primary study endpoint is progression-free survival. The secondary endpoints are 3 month PFS rate, response rate, overall survival, toxicity and quality of life **(Figure 6.4)**. Patient will be followed up every week with routine bloods for chemotherapy, every 4 weeks with examination and tumour marker CA19.9; and CT imaging every 6 weeks for 12 months. Estimated accrual period is 12-18 months. Other study details including study screening, inclusion and exclusion criteria are illustrated in **figure 6.5**. There are a number of features in this study design that are of importance:

1) **Second or third-line study**: gemcitabine-based chemotherapy (gem-abraxane) or FOLRINOX remains the standard first-line treatment. On the other hand, no standard second-line treatments currently exist. [118,119] Patients have a 2:1 chance to be randomised to the active treatment, with planned cross-over of patients who progressed on placebo.

2) **Placebo control:** Measurement bias is inherent for endpoints of AE and QoL, and may also bias investigator-rated PFS and RR. It is therefore important that patients on control arm be offered an identical placebo. Since both targeted therapies are oral drugs, it is more feasible and ethical to offer oral placebo than if it were IV placebo.

3) **PFS as primary endpoint:** a phase II study with its limited sample size will not be powered sufficiently to study overall survival (OS). In contrast to OS, progression-free survival (PFS) is less affected by cross-over and subsequent treatments. This is why PFS should be the primary study endpoint in this study.

4) **Secondary endpoints:** Most patients will be expected to progress in the first 3 months. Since CT scans will only be performed every 6 weeks unless there is clinical progression, the proportion of patients who have not progressed by 3 months serve as a good surrogate marker for PFS. Other endpoints are typical for pancreatic cancer trial: response rate (expected to be at least 10% in unselected population, similar to gemcitabine), CA19.9 response (>50% decrease), overall survival, adverse events and quality of life as measured by the FHSI-18.

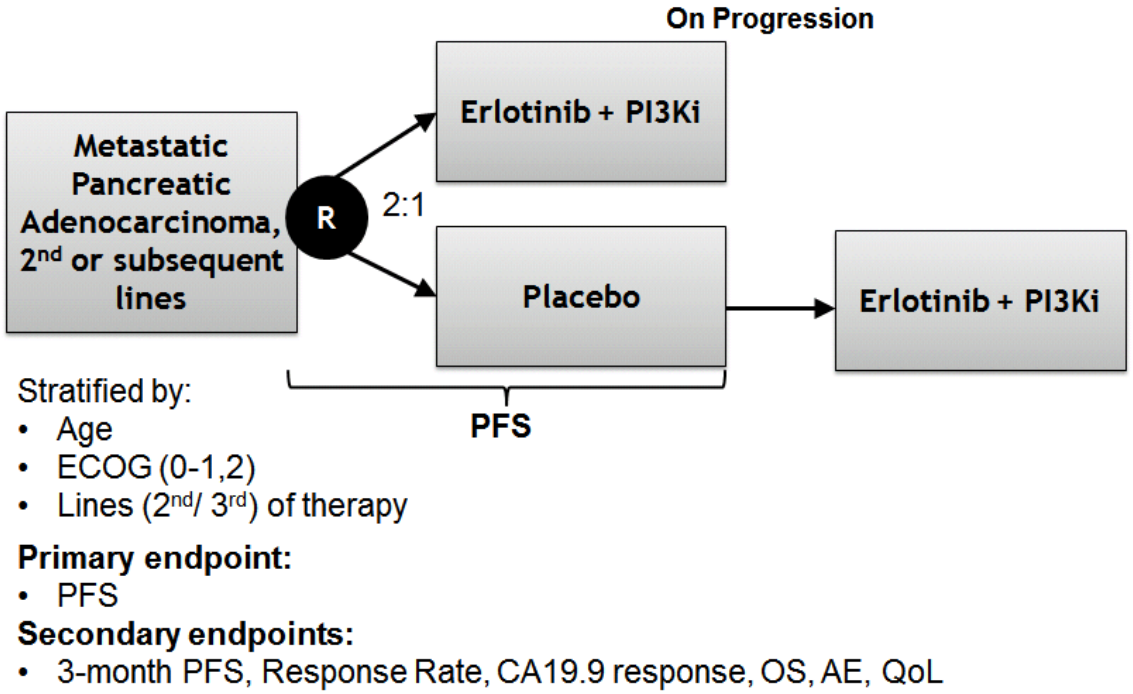

Figure 6.4: Proposed randomised phase II trial study design

Phase II study - Study details

Study screening

- Complete history and exam
- FBC, UEC, LFT, CEA, CA19-9
- CT or MRI evidence of metastatic disease

Inclusion criteria

- ECOG 0-2
- Neut > 1.5, Plt >100
- Bilirubin <1.5x ULN
- Measurable lesions radiologically

Exclusion criteria

- History of other major cancers
- Uncontrolled diabetes
- Previous molecular targeted therapies
- Pregnancy or breast-feeding

Assessment

- H/E, bloods (CEA, CA19.9) **4-weekly**
- **FHSI-18 QoL** scale 4-weekly
- CT restaging scans **6-weekly**

Follow up

- 18 months or until death

Translational sub-study

Tissue collection

- Biopsy mandated before enrolment
- Previous whipple's surgical specimen allowed if progression to metastatic disease within last 3 months
- FNA and core biopsies allowed

Translational endpoints

- IHC analysis of pAkt, pEGFR
- FISH analysis of *AKT-1, 2, 3, pEGFR*
- PCR and direct sequencing of K-ras mutation
- Core biopsies, if available, are archived for gene sequencing

Figure 6.5: Proposed randomised phase II trial study details

6.3.2.2 Translational sub-study

The translational sub-study aims at confirming the roles of pAkt, pEGFR over-expression and exploring *K-Ras* mutation as predictive markers for dual targeted therapies. Biopsy is mandated before enrolment in study, but a practical approach is adopted to ensure feasibility. For most patients initially diagnosed with metastatic pancreatic cancer, FNA or endoscopic ultrasound (EUS) biopsy of primary or metastases will be available for tissue collection. Both FNA and core biopsies are allowed. For practical reasons, the study also allows for previous whipple's surgical specimen if the metastatic disease progresses recently (within last 3 months), since patients in this situation are assumed to have progressed from pancreatic cancer and tissue biopsy is not required.

Based on the preliminary studies, both pAkt and pEGFR genes and proteins will be studied as potential markers. In humans, pEGFR protein over-expression could be studied with IHC, and appeared to correlate with *EGFR* gene amplification with FISH and PCR.[390,391] IHC for demonstrating pAkt activation and FISH for demonstrating *AKT* related genes amplification appear to be the most robust techniques studied.[54,355,361] Conversely, PCR studies of *AKT* related genes in human studies are based on older techniques and may not be reproducible.[392,393] For *K-Ras* mutation testing, current standard PCR techniques use probes that detect common mutations on codon 12 and 13, but may miss other variant mutations. Direct sequencing, on the other hand, is capable for detecting all possible mutations in exons 2 and 3 but lack sensitivity.[394] In order to fully capture the role of *K-Ras* mutation, both standard PCR and direct sequencing will be used. Other biomarkers that have been studied for PI3K inhibitors include PIK3CA mutation and PTEN loss, which will also be included here. For core biopsies where more tissue are available, patient consent will be requested to archive tissues for gene sequencing later on.

6.3.2.3 Quality of Life sub-study

Quality of Life (QoL) is an important endpoint, as survival of patients with metastatic PDAC is short (6-10 months) and quality of life with or without treatment is paramount. QoL will be assessed every 4 weeks for the duration of the study, and every 8 weeks after second progression (PFS2). The 18-item FHSI-18 index is derived from FACT-G and FACT-H sub-scales and developed by the FACIT group; it has been validated for patients with pancreatic and hepato-biliary cancers with high internal validity and reliability.[395-397] It is easily administered (only 5 minutes for patients), and the item wording is of a 12 year-old reading level. It has a standard scoring system, making it well suited for administration in this setting.

6.3.3 Clinical Trial- statistical considerations

For the phase I study, between 9-18 patients will be recruited. For the randomized phase II study, prior data indicates that the median PFS on the best-supportive care (BSC) in second-line setting is 1.5 months.[398] The proposed treatment should have comparable rate of PFS to the "standard" second-line OFF (fluouracil and oxaliplatin) regimen, with the median survival times of 3.5 months.[118,119,398] To demonstrate a change from median PFS from 1.5 to 3.5 months in this single arm phase II study, **60 subjects** will be needed with an alpha of 0.05 and power of 0.8 and allowing for 10% drop out rate.

6.3.4 Clinical Trial- feasibility

The phase I study will be undertaken in Royal North Shore Hospital (RNSH), a tertiary cancer care hospital. The primary investigator (PI) will be myself and phase I expert medical oncologist A/Prof Nick Pavlakis. The aim for phase II is a multi-centred clinical trial with RNSH and Gosford Hospital as lead sites. The translational sub-study will be undertaken in the Cansur Group, Kolling Institute (headed by Prof Ross Smith). The study proposal has been submitted to Novartis and Roche, and funding is requested from the pharmaceutical companies as well as NHMRC.

6.4 Thesis Conclusion

The MAPK (RAS/ RAF/ MEK/ ERK), and PAM (PI3K/Akt/mTOR) signalling cascades are integral pathways with strong input from EGFR and IGF1R, and they together mediate cancer cell growth, survival and progression. This research project has demonstrated extensive cross-talks through multiple levels, and established the involvement of PI3K/Akt/ mTOR on multiple levels in the mechanism of both primary and acquired erlotinib resistance. Further, this cross-talk was shown to be disrupted by dual targeting of both pathways, and downstream combined blockade was more effective and synergistic than upstream combined blockades. *In-vivo*, erlotinib plus BYL-719 significantly reduced tumour volumes in both subcutaneous and sub-renal tumour model. Importantly, pancreatic cancer was shown to develop onocogenic dependence to PI3K/Akt pathway, and pEGFR and pAkt in turn may both act as surrogate markers predicting efficacy of single and combined blockade strategy. Thus, this pre-clinical study shows strong biological rationale to the clinical development of co-inhibition of EGFR and PI3K in phase I and II trials, and suggests the evaluation of pAkt, *pEGFR* over-expression; and *K-Ras* mutation as potential biomarkers. It also suggests that MEK and PI3K co-inhibition warrants further evaluations. It is anticipated that the results of this project will rekindle interests of studying targeted therapies in pancreatic cancer, and assist in developing the personalising treatment strategy in this deadly disease.

References

1. Nishimura R, Osako T, Okumura Y, et al: Ki-67 as a prognostic marker according to breast cancer subtype and a predictor of recurrence time in primary breast cancer. Exp Ther Med 1:747-754, 2010
2. AIHW: Cancer in Australia: an overview, 2008. Canberra, Case Series 46, AIHW, 2008
3. NCI: SEER Stat Fact Sheets: Pancreas. Bethesda, SEER, 2013
4. Creighton N, Baker D, Bishop J: Pancreatic cancer in New South Wales. Sydney. Sydney, Cancer Institute NSW, 2010
5. Ferlay J, Shin H, Bray F, et al: GLOBOCAN 2008 v2.0, Cancer Incidence and Mortality Worldwide. Lyon, France IARC, 2010
6. AIHW: Australian Cancer Incidence and Mortality (ACIM) books: Pancreatic Cancer, Australian Government: Australian Institute of Health and Welfare, 2012
7. Jemal A, Siegel R, Ward E, et al: Cancer statistics 2008. CA Cancer J Clin 58:71-96, 2008
8. Curado M, Edwards B, Shin H, et al: Cancer Incidence in Five Continents volume 9 report, IARC Scientific Publications, No. 160. Lyon, 2007
9. Lowenfels AB, Maisonneuve P: Risk factors for pancreatic cancer. J Cell Biochem 95:649-56, 2005
10. CanTreat I: Scaling up cancer diagnosis and treatment in developing countries: what can we learn from the HIV/AIDS epidemic? Ann Oncol 21:680-2, 2010
11. Lowenfels AB, Maisonneuve P, Lankisch PG: Chronic pancreatitis and other risk factors for pancreatic cancer. Gastroenterol Clin North Am 28:673-85, x, 1999
12. Lowenfels AB, Maisonneuve P, Whitcomb DC: Risk factors for cancer in hereditary pancreatitis. International Hereditary Pancreatitis Study Group. Med Clin North Am 84:565-73, 2000
13. Kim DH, Crawford B, Ziegler J, et al: Prevalence and characteristics of pancreatic cancer in families with BRCA1 and BRCA2 mutations. Fam Cancer 8:153-8, 2009
14. Zheng W, McLaughlin JK, Gridley G, et al: A cohort study of smoking, alcohol consumption, and dietary factors for pancreatic cancer (United States). Cancer Causes Control 4:477-82, 1993
15. Ridolfo B, Stevenson C: The quantification of drug-caused mortality and morbidity in Australia. Canberra, AIHW, 2001
16. Muscat JE, Stellman SD, Hoffmann D, et al: Smoking and pancreatic cancer in men and women. Cancer Epidemiol Biomarkers Prev 6:15-9, 1997
17. Raimondi S, Maisonneuve P, Lowenfels AB: Epidemiology of pancreatic cancer: an overview. Nat Rev Gastroenterol Hepatol 6:699-708, 2009
18. Ahlgren JD: Epidemiology and risk factors in pancreatic cancer. Semin Oncol 23:241-50, 1996
19. Lowenfels AB, Maisonneuve P, Cavallini G, et al: Pancreatitis and the risk of pancreatic cancer. International Pancreatitis Study Group. N Engl J Med 328:1433-7, 1993
20. Schneider G, Schmid RM: Genetic alterations in pancreatic carcinoma. Mol Cancer 2:15, 2003
21. Sakorafas GH, Tsiotou AG, Tsiotos GG: Molecular biology of pancreatic cancer; oncogenes, tumour suppressor genes, growth factors, and their receptors from a clinical perspective. Cancer Treat Rev 26:29-52, 2000
22. Fukushige S, Waldman FM, Kimura M, et al: Frequent gain of copy number on the long arm of chromosome 20 in human pancreatic adenocarcinoma. Genes Chromosomes Cancer 19:161-9, 1997
23. Furukawa T, Sunamura M, Horii A: Molecular mechanisms of pancreatic carcinogenesis. Cancer Sci 97:1-7, 2006

24. Simone D, Maitra A: Molecular Genetics of Pancreatic Cancer. New York, Springer, 2013
25. van Heek NT, Meeker AK, Kern SE, et al: Telomere shortening is nearly universal in pancreatic intraepithelial neoplasia. Am J Pathol 161:1541-7, 2002
26. Sato N, Goggins M: The role of epigenetic alterations in pancreatic cancer. J Hepatobiliary Pancreat Surg 13:286-95, 2006
27. International Cancer Genome C, Hudson TJ, Anderson W, et al: International network of cancer genome projects. Nature 464:993-8, 2010
28. APGI: The Australian Pancreatic Cancer Genome Initiative (APGI), Quensland centre of medical genomics, 2013
29. Biankin AV, Waddell N, Kassahn KS, et al: Pancreatic cancer genomes reveal aberrations in axon guidance pathway genes. Nature, 2012
30. Campbell PJ, Yachida S, Mudie LJ, et al: The patterns and dynamics of genomic instability in metastatic pancreatic cancer. Nature 467:1109-13, 2010
31. Yachida S, Jones S, Bozic I, et al: Distant metastasis occurs late during the genetic evolution of pancreatic cancer. Nature 467:1114-7, 2010
32. Caldas C: Cancer sequencing unravels clonal evolution. Nat Biotechnol 30:408-10, 2012
33. Hou Y, Song L, Zhu P, et al: Single-cell exome sequencing and monoclonal evolution of a JAK2-negative myeloproliferative neoplasm. Cell 148:873-85, 2012
34. Xu X, Hou Y, Yin X, et al: Single-cell exome sequencing reveals single-nucleotide mutation characteristics of a kidney tumor. Cell 148:886-95, 2012
35. Gerlinger M, Rowan AJ, Horswell S, et al: Intratumor heterogeneity and branched evolution revealed by multiregion sequencing. N Engl J Med 366:883-92, 2012
36. Stratton MR, Campbell PJ, Futreal PA: The cancer genome. Nature 458:719-24, 2009
37. Peifer M, Fernandez-Cuesta L, Sos ML, et al: Integrative genome analyses identify key somatic driver mutations of small-cell lung cancer. Nat Genet 44:1104-10, 2012
38. Tamborero D, Gonzalez-Perez A, Perez-Llamas C, et al: Comprehensive identification of mutational cancer driver genes across 12 tumor types. Sci Rep 3:2650, 2013
39. Gonzalez-Perez A, Perez-Llamas C, Deu-Pons J, et al: IntOGen-mutations identifies cancer drivers across tumor types. Nat Methods 10:1081-2, 2013
40. Bardeesy N, DePinho RA: Pancreatic cancer biology and genetics. Nat Rev Cancer 2:897-909, 2002
41. Jones S, Zhang X, Parsons DW, et al: Core signaling pathways in human pancreatic cancers revealed by global genomic analyses. Science 321:1801-6, 2008
42. Hanahan D, Weinberg RA: Hallmarks of cancer: the next generation. Cell 144:646-74, 2011
43. Steelman LS, Chappell WH, Abrams SL, et al: Roles of the Raf/MEK/ERK and PI3K/PTEN/Akt/mTOR pathways in controlling growth and sensitivity to therapy-implications for cancer and aging. Aging (Albany NY) 3:192-222, 2011
44. Chen H, Tu H, Meng ZQ, et al: K-ras mutational status predicts poor prognosis in unresectable pancreatic cancer. Eur J Surg Oncol 36:657-62, 2010
45. Fresno Vara JA, Casado E, de Castro J, et al: PI3K/Akt signalling pathway and cancer. Cancer Treat Rev 30:193-204, 2004
46. Paez J, Sellers WR: PI3K/PTEN/AKT pathway. A critical mediator of oncogenic signaling. Cancer treatment and research 115:145-67, 2003
47. Rodon J, Dienstmann R, Serra V, et al: Development of PI3K inhibitors: lessons learned from early clinical trials. Nat Rev Clin Oncol 10:143-53, 2013
48. Edling CE, Selvaggi F, Buus R, et al: Key role of phosphoinositide 3-kinase class IB in pancreatic cancer. Clin Cancer Res 16:4928-37, 2010
49. Hay N, Sonenberg N: Upstream and downstream of mTOR. Genes Dev 18:1926-45, 2004
50. Huang J, Manning BD: A complex interplay between Akt, TSC2 and the two mTOR complexes. Biochem Soc Trans 37:217-22, 2009

51. Paez J, Sellers WR: PI3K/PTEN/AKT pathway. A critical mediator of oncogenic signaling. Cancer Treat Res 115:145-67, 2003
52. Jin Q, Esteva FJ: Cross-talk between the ErbB/HER family and the type I insulin-like growth factor receptor signaling pathway in breast cancer. J Mammary Gland Biol Neoplasia 13:485-98, 2008
53. Bondar VM, Sweeney-Gotsch B, Andreeff M, et al: Inhibition of the phosphatidylinositol 3'-kinase-AKT pathway induces apoptosis in pancreatic carcinoma cells in vitro and in vivo. Mol Cancer Ther 1:989-97, 2002
54. Yamamoto S, Tomita Y, Hoshida Y, et al: Prognostic significance of activated Akt expression in pancreatic ductal adenocarcinoma. Clin Cancer Res 10:2846-50, 2004
55. Xu Z, Zhang Y, Jiang J, et al: Epidermal growth factor induces HCCR expression via PI3K/Akt/mTOR signaling in PANC-1 pancreatic cancer cells. BMC Cancer 10:161, 2010
56. Roberts PJ, Der CJ: Targeting the Raf-MEK-ERK mitogen-activated protein kinase cascade for the treatment of cancer. Oncogene 26:3291-310, 2007
57. Tobita K, Kijima H, Dowaki S, et al: Epidermal growth factor receptor expression in human pancreatic cancer: Significance for liver metastasis. Int J Mol Med 11:305-9, 2003
58. Tzeng CW, Frolov A, Frolova N, et al: Epidermal growth factor receptor (EGFR) is highly conserved in pancreatic cancer. Surgery 141:464-9, 2007
59. Tzeng CW, Frolov A, Frolova N, et al: EGFR genomic gain and aberrant pathway signaling in pancreatic cancer patients. J Surg Res 143:20-6, 2007
60. Boeck S, Jung A, Laubender RP, et al: EGFR pathway biomarkers in erlotinib-treated patients with advanced pancreatic cancer: translational results from the randomised, crossover phase 3 trial AIO-PK0104. Br J Cancer 108:469-76, 2013
61. Ueda S, Hatsuse K, Tsuda H, et al: Potential crosstalk between insulin-like growth factor receptor type 1 and epidermal growth factor receptor in progression and metastasis of pancreatic cancer. Mod Pathol 19:788-96, 2006
62. Nair PN, De Armond DT, Adamo ML, et al: Aberrant expression and activation of insulin-like growth factor-1 receptor (IGF-1R) are mediated by an induction of IGF-1R promoter activity and stabilization of IGF-1R mRNA and contributes to growth factor independence and increased survival of the pancreatic cancer cell line MIA PaCa-2. Oncogene 20:8203-14, 2001
63. Xue A, Scarlett CJ, Jackson CJ, et al: Prognostic significance of growth factors and the urokinase-type plasminogen activator system in pancreatic ductal adenocarcinoma. Pancreas 36:160-7, 2008
64. Morgillo F, Woo JK, Kim ES, et al: Heterodimerization of insulin-like growth factor receptor/epidermal growth factor receptor and induction of survivin expression counteract the antitumor action of erlotinib. Cancer Res 66:10100-11, 2006
65. Zhang JS, Koenig A, Harrison A, et al: Mutant K-Ras increases GSK-3beta gene expression via an ETS-p300 transcriptional complex in pancreatic cancer. Oncogene 30:3705-15, 2011
66. Chow JY, Quach KT, Cabrera BL, et al: RAS/ERK modulates TGFbeta-regulated PTEN expression in human pancreatic adenocarcinoma cells. Carcinogenesis 28:2321-7, 2007
67. Eser S, Reiff N, Messer M, et al: Selective requirement of PI3K/PDK1 signaling for Kras oncogene-driven pancreatic cell plasticity and cancer. Cancer Cell 23:406-20, 2013
68. Yang HW, Shin MG, Lee S, et al: Cooperative Activation of PI3K by Ras and Rho Family Small GTPases. Mol Cell, 2012
69. Kalluri R, Weinberg RA: The basics of epithelial-mesenchymal transition. J Clin Invest 119:1420-8, 2009
70. Zavadil J, Bottinger EP: TGF-beta and epithelial-to-mesenchymal transitions. Oncogene 24:5764-74, 2005
71. Hamada S, Satoh K, Masamune A, et al: Regulators of epithelial mesenchymal transition in pancreatic cancer. Front Physiol 3:254, 2012
72. Maier HJ, Wirth T, Beug H: Epithelial-Mesenchymal Transition in Pancreatic Carcinoma. Cancers 2:2058-2083, 2010
73. Kubiczkova L, Sedlarikova L, Hajek R, et al: TGF-beta - an excellent servant but a bad master. J Transl Med 10:183, 2012

74. Hotz B, Arndt M, Dullat S, et al: Epithelial to mesenchymal transition: expression of the regulators snail, slug, and twist in pancreatic cancer. Clin Cancer Res 13:4769-76, 2007
75. Maitra A, Hruban RH: Pancreatic cancer. Annu Rev Pathol 3:157-88, 2008
76. Giehl K, Seidel B, Gierschik P, et al: TGFbeta1 represses proliferation of pancreatic carcinoma cells which correlates with Smad4-independent inhibition of ERK activation. Oncogene 19:4531-41, 2000
77. Giehl K, Imamichi Y, Menke A: Smad4-independent TGF-beta signaling in tumor cell migration. Cells Tissues Organs 185:123-30, 2007
78. Hao K, Tian XD, Qin CF, et al: Hedgehog signaling pathway regulates human pancreatic cancer cell proliferation and metastasis. Oncol Rep, 2012
79. Ellenrieder V, Hendler SF, Boeck W, et al: Transforming growth factor beta1 treatment leads to an epithelial-mesenchymal transdifferentiation of pancreatic cancer cells requiring extracellular signal-regulated kinase 2 activation. Cancer Res 61:4222-8, 2001
80. Agbunag C, Bar-Sagi D: Oncogenic K-ras drives cell cycle progression and phenotypic conversion of primary pancreatic duct epithelial cells. Cancer Res 64:5659-63, 2004
81. Singh A, Greninger P, Rhodes D, et al: A gene expression signature associated with "K-Ras addiction" reveals regulators of EMT and tumor cell survival. Cancer Cell 15:489-500, 2009
82. Singh A, Settleman J: EMT, cancer stem cells and drug resistance: an emerging axis of evil in the war on cancer. Oncogene 29:4741-51, 2010
83. Yauch RL, Januario T, Eberhard DA, et al: Epithelial versus mesenchymal phenotype determines in vitro sensitivity and predicts clinical activity of erlotinib in lung cancer patients. Clin Cancer Res 11:8686-98, 2005
84. Buck E, Eyzaguirre A, Barr S, et al: Loss of homotypic cell adhesion by epithelial-mesenchymal transition or mutation limits sensitivity to epidermal growth factor receptor inhibition. Mol Cancer Ther 6:532-41, 2007
85. Shah AN, Summy JM, Zhang J, et al: Development and characterization of gemcitabine-resistant pancreatic tumor cells. Ann Surg Oncol 14:3629-37, 2007
86. Buck E, Eyzaguirre A, Rosenfeld-Franklin M, et al: Feedback mechanisms promote cooperativity for small molecule inhibitors of epidermal and insulin-like growth factor receptors. Cancer Res 68:8322-32, 2008
87. Zhao H, Desai V, Wang J, et al: Epithelial-mesenchymal transition predicts sensitivity to the dual IGF-1R/IR inhibitor OSI-906 in hepatocellular carcinoma cell lines. Mol Cancer Ther 11:503-13, 2012
88. Wang Z, Li Y, Kong D, et al: Acquisition of epithelial-mesenchymal transition phenotype of gemcitabine-resistant pancreatic cancer cells is linked with activation of the notch signaling pathway. Cancer Res 69:2400-7, 2009
89. Das S, Becker BN, Hoffmann FM, et al: Complete reversal of epithelial to mesenchymal transition requires inhibition of both ZEB expression and the Rho pathway. BMC Cell Biol 10:94, 2009
90. Dangi-Garimella S, Krantz SB, Shields MA, et al: Epithelial-mesenchymal transition and pancreatic cancer progression, in Grippo P, Munshi H (eds): Pancreatic Cancer and Tumor Microenvironment. Transworld Research Network, India, 2012
91. Dosch JS, Pasca di Magliano M, Simeone DM: Pancreatic cancer and hedgehog pathway signaling: new insights. Pancreatology 10:151-7, 2010
92. Berman DM, Karhadkar SS, Maitra A, et al: Widespread requirement for Hedgehog ligand stimulation in growth of digestive tract tumours. Nature 425:846-51, 2003
93. Thayer SP, di Magliano MP, Heiser PW, et al: Hedgehog is an early and late mediator of pancreatic cancer tumorigenesis. Nature 425:851-6, 2003
94. Kelleher FC: Hedgehog signaling and therapeutics in pancreatic cancer. Carcinogenesis 32:445-51, 2011
95. Yauch RL, Gould SE, Scales SJ, et al: A paracrine requirement for hedgehog signalling in cancer. Nature 455:406-10, 2008
96. Harrison DA: The Jak/STAT pathway. Cold Spring Harb Perspect Biol 4, 2012
97. Rawlings JS, Rosler KM, Harrison DA: The JAK/STAT signaling pathway. J Cell Sci 117:1281-3, 2004

98. Steelman LS, Pohnert SC, Shelton JG, et al: JAK/STAT, Raf/MEK/ERK, PI3K/Akt and BCR-ABL in cell cycle progression and leukemogenesis. Leukemia 18:189-218, 2004
99. Quintas-Cardama A, Verstovsek S: Molecular pathways: Jak/STAT pathway: mutations, inhibitors, and resistance. Clin Cancer Res 19:1933-40, 2013
100. Smith CA, Fan G: The saga of JAK2 mutations and translocations in hematologic disorders: pathogenesis, diagnostic and therapeutic prospects, and revised World Health Organization diagnostic criteria for myeloproliferative neoplasms. Hum Pathol 39:795-810, 2008
101. Palagani V, Bozko P, El Khatib M, et al: Combined inhibition of Notch and JAK/STAT is superior to monotherapies and impairs pancreatic cancer progression. Carcinogenesis 35:859-66, 2014
102. Sharma N, Shankar S, Srivastava R: STAT3 as an emerging molecular target in pancreatic cancer. Gastrointestinal Cancer: Targets and Therapy 4:115-122, 2014
103. Gilabert M, Calvo E, Airoldi A, et al: Pancreatic cancer-induced cachexia is Jak2-dependent in mice. J Cell Physiol 229:1437-43, 2014
104. Hurtwiz H, Uppal N, Wagner A, et al: A randomized double-blind phase 2 study of ruxolitinib (RUX) or placebo (PBO) with capecitabine (CAPE) as second-line therapy in patients (pts) with metastatic pancreatic cancer (mPC). J Clin Oncol 32:5s, 2014 (suppl; abstr 4000), 2014
105. Philip PA: Locally advanced pancreatic cancer: where should we go from here? J Clin Oncol 29:4066-8, 2011
106. Burris H, Moore M, Andersen J, et al: Improvements in survival and clinical benefit with gemcitabine as first-line therapy for patients with advanced pancreas cancer: A randomized trial. J Clin Oncol 15:2403-2413, 1998
107. Tempero M, Plunkett W, Ruiz Van Haperen V, et al: Randomized phase II comparison of dose-intense gemcitabine: thirty-minute infusion and fixed dose rate infusion in patients with pancreatic adenocarcinoma. J Clin Oncol 21:3402-8, 2003
108. Moore MJ, Goldstein D, Hamm J, et al: Erlotinib plus gemcitabine compared with gemcitabine alone in patients with advanced pancreatic cancer: a phase III trial of the National Cancer Institute of Canada Clinical Trials Group. J Clin Oncol 25:1960-6, 2007
109. Cunningham D, Chau I, Stocken DD, et al: Phase III randomized comparison of gemcitabine versus gemcitabine plus capecitabine in patients with advanced pancreatic cancer. J Clin Oncol 27:5513-8, 2009
110. Conroy T, Desseigne F, Ychou M, et al: FOLFIRINOX versus gemcitabine for metastatic pancreatic cancer. N Engl J Med 364:1817-25, 2011
111. Von Hoff DD: Final results of a randomized phase III study of weekly nab-paclitaxel plus gemcitabine versus gemcitabine alone in patients with metastatic adenocarcinoma of the pancreas. , ASCO GI 2013, LBA #148, 2013
112. Jacobs A, Burris HA, Rivkin SE, et al: A randomized Phase III study of rubitecan (ORA) vs. best choice (BC) in 409 patients with refractory pancreatic cancer. Report from a North-American multi-center study. J Clin Oncol 2004;22:14s [abstract 4013].
113. Oettle H, Pelzer U, Stieler J, et al: Oxaliplatin/folinic acid/5-fluoruracil [24 h] (OFF) plus best supportive care versus best supportive care alone (BSC) in second-line therapy of gemcitabine-refractory advanced pancreatic cancer (CONKO 003). J Clin Oncol 2005;23:315s [abstract 4031]
114. Heinemann V, Quietzsch D, Gieseler F, et al: Randomized phase III trial of gemcitabine plus cisplatin compared with gemcitabine alone in advanced pancreatic cancer. J Clin Oncol 24:3946-52, 2006
115. Berlin JD, Catalano P, Thomas JP, et al: Phase III study of gemcitabine in combination with fluorouracil versus gemcitabine alone in patients with advanced pancreatic carcinoma: Eastern Cooperative Oncology Group Trial E2297. J Clin Oncol 20:3270-5, 2002
116. Conroy T, Gavoille C, Samalin E, et al: The role of the FOLFIRINOX regimen for advanced pancreatic cancer. Curr Oncol Rep 15:182-9, 2013
117. Tempero M, Behrman S, Herman J, et al: NCCN Guidelines Pancreatic Adenocarcinoma, version 1, 2013
118. Custodio A, Puente J, Sastre J, et al: Second-line therapy for advanced pancreatic cancer: a review of the literature and future directions. Cancer Treat Rev 35:676-84, 2009

119. Gounaris I, Zaki K, Corrie P: Options for the treatment of gemcitabine-resistant advanced pancreatic cancer. JOP 11:113-23, 2010
120. Pelzer U, Kubica K, Stieler J: A randomized trial in patients with gemcitabine refractory pancreatic cancer. Final results of the CONKO 003 study. J Clin Oncol 2008;26(15s):217s [abstract 4508].
121. Heinemann V, Vehling-Kaiser U, Waldschmidt D, et al: Gemcitabine plus erlotinib followed by capecitabine versus capecitabine plus erlotinib followed by gemcitabine in advanced pancreatic cancer: final results of a randomised phase 3 trial of the 'Arbeitsgemeinschaft Internistische Onkologie' (AIO-PK0104). Gut 62:751-9, 2013
122. Groner B: Introduction: the rationale for the development of targeted drugs in cancer therapy. Recent Results Cancer Res 172:1-3, 2007
123. Kindler H, Niedzwiecki D, Hollis D, et al: A double-blind, placebo-controlled, randomized phase III trial of gemcitabine (G) plus bevacizumab (B) versus gemcitabine plus placebo (P) in patients (pts) with advanced pancreatic cancer (PC): a preliminary analysis of Cancer and Leukemia Group B (CALGB). . J Clin Oncol 2007; 25:199s (Abstract 4508).
124. Philip PA, Benedetti J, Corless CL, et al: Phase III study comparing gemcitabine plus cetuximab versus gemcitabine in patients with advanced pancreatic adenocarcinoma: Southwest Oncology Group-directed intergroup trial S0205. J Clin Oncol 28:3605-10, 2010
125. Van Cutsem E, van de Velde H, Karasek P, et al: Phase III trial of gemcitabine plus tipifarnib compared with gemcitabine plus placebo in advanced pancreatic cancer. J Clin Oncol 22:1430-8, 2004
126. Bramhall SR, Schulz J, Nemunaitis J, et al: A double-blind placebo-controlled, randomised study comparing gemcitabine and marimastat with gemcitabine and placebo as first line therapy in patients with advanced pancreatic cancer. Br J Cancer 87:161-7, 2002
127. Kindler H, Richards D, Stephenson J, et al: Placebo-controlled, randomized phase II study of conatumumab (C) or AMG 479 (A) or placebo (P) plus gemcitabine (G) in patients (pts) with metastatic pancreatic cancer. J Clin Oncol 28:15s, 2010 (suppl; abstr 4035)
128. Kindler HL, Richards DA, Garbo LE, et al: A randomized, placebo-controlled phase 2 study of ganitumab (AMG 479) or conatumumab (AMG 655) in combination with gemcitabine in patients with metastatic pancreatic cancer. Ann Oncol 23:2834-42, 2012
129. AMGEN: Amgen Announces Termination Of Ganitumab Phase 3 Study For Futility In Metastatic Pancreatic Cancer. 08/08/2012,
130. Huang ZQ, Saluja AK, Dudeja V, et al: Molecular targeted approaches for treatment of pancreatic cancer. Curr Pharm Des 17:2221-38, 2011
131. Mackenzie RP, McCollum AD: Novel agents for the treatment of adenocarcinoma of the pancreas. Expert Rev Anticancer Ther 9:1473-85, 2009
132. Wheeler DL, Dunn EF, Harari PM: Understanding resistance to EGFR inhibitors-impact on future treatment strategies. Nat Rev Clin Oncol 7:493-507, 2010
133. Fojo T, Parkinson DR: Biologically targeted cancer therapy and marginal benefits: are we making too much of too little or are we achieving too little by giving too much? Clin Cancer Res 16:5972-80, 2010
134. Chong CR, Janne PA: The quest to overcome resistance to EGFR-targeted therapies in cancer. Nat Med 19:1389-400, 2013
135. Sequist LV, Yang JC, Yamamoto N, et al: Phase III study of afatinib or cisplatin plus pemetrexed in patients with metastatic lung adenocarcinoma with EGFR mutations. J Clin Oncol 31:3327-34, 2013
136. Vervenne W, Bennouna J, Humblet Y, et al: A randomized, double-blind, placebo (P) controlled, multicenter phase III trial to evaluate the efficacy and safety of adding bevacizumab (B) to erlotinib (E) and gemcitabine (G) in patients (pts) with metastatic pancreatic cancer. Journal of Clinical Oncology 26:4507, 2008
137. Karapetis CS, Khambata-Ford S, Jonker DJ, et al: K-ras mutations and benefit from cetuximab in advanced colorectal cancer. N Engl J Med 359:1757-65, 2008
138. Van Cutsem E, Kohne CH, Hitre E, et al: Cetuximab and chemotherapy as initial treatment for metastatic colorectal cancer. N Engl J Med 360:1408-17, 2009

139. Kyriazis AA, Kyriazis AP, Sternberg CN, et al: Morphological, biological, biochemical, and karyotypic characteristics of human pancreatic ductal adenocarcinoma Capan-2 in tissue culture and the nude mouse. Cancer Res 46:5810-5, 1986

140. Shepherd FA, Rodrigues Pereira J, Ciuleanu T, et al: Erlotinib in previously treated non-small-cell lung cancer. N Engl J Med 353:123-32, 2005

141. Pirker R, Pereira JR, Szczesna A, et al: Cetuximab plus chemotherapy in patients with advanced non-small-cell lung cancer (FLEX): an open-label randomised phase III trial. Lancet 373:1525-31, 2009

142. Pirker R, Pereira JR, von Pawel J, et al: EGFR expression as a predictor of survival for first-line chemotherapy plus cetuximab in patients with advanced non-small-cell lung cancer: analysis of data from the phase 3 FLEX study. Lancet Oncol 13:33-42, 2012

143. Cappuzzo F, Ciuleanu T, Stelmakh L, et al: Erlotinib as maintenance treatment in advanced non-small-cell lung cancer: a multicentre, randomised, placebo-controlled phase 3 study. Lancet Oncol 11:521-9, 2010

144. Mok TS, Wu YL, Thongprasert S, et al: Gefitinib or carboplatin-paclitaxel in pulmonary adenocarcinoma. N Engl J Med 361:947-57, 2009

145. Zhou C, Wu YL, Chen G, et al: Erlotinib versus chemotherapy as first-line treatment for patients with advanced EGFR mutation-positive non-small-cell lung cancer (OPTIMAL, CTONG-0802): a multicentre, open-label, randomised, phase 3 study. Lancet Oncol 12:735-42, 2011

146. Zhou C, Wu Y, Liu X, et al: Overall survival (OS) results from OPTIMAL (CTONG0802), a phase III trial of erlotinib (E) versus carboplatin plus gemcitabine (GC) as first-line treatment for Chinese patients with EGFR mutation-positive advanced non-small cell lung cancer (NSCLC). J Clin Oncol 30S:abstr 7520, 2012

147. Rosell R, Carcereny E, Gervais R, et al: Erlotinib versus standard chemotherapy as first-line treatment for European patients with advanced EGFR mutation-positive non-small-cell lung cancer (EURTAC): a multicentre, open-label, randomised phase 3 trial. Lancet Oncol 13:239-46, 2012

148. Herbst RS, Giaccone G, Schiller JH, et al: Gefitinib in combination with paclitaxel and carboplatin in advanced non-small-cell lung cancer: a phase III trial--INTACT 2. J Clin Oncol 22:785-94, 2004

149. Shepherd FA, Rodrigues Pereira J, Ciuleanu T, et al: Erlotinib in previously treated non-small-cell lung cancer. N Engl J Med 353:123-32, 2005

150. Thatcher N, Chang A, Parikh P, et al: Gefitinib plus best supportive care in previously treated patients with refractory advanced non-small-cell lung cancer: results from a randomised, placebo-controlled, multicentre study (Iressa Survival Evaluation in Lung Cancer). Lancet 366:1527-37, 2005

151. Van Cutsem E, Vervenne WL, Bennouna J, et al: Phase III trial of bevacizumab in combination with gemcitabine and erlotinib in patients with metastatic pancreatic cancer. J Clin Oncol 27:2231-7, 2009

152. Ludwig JA, Lamhamedi-Cherradi S-E, Lee H-Y, et al: Dual Targeting of the Insulin-Like Growth Factor and Collateral Pathways in Cancer: Combating Drug Resistance. Cancers 3:3029-54, 2011

153. Guix M, Faber AC, Wang SE, et al: Acquired resistance to EGFR tyrosine kinase inhibitors in cancer cells is mediated by loss of IGF-binding proteins. J Clin Invest 118:2609-19, 2008

154. Engelman JA, Zejnullahu K, Mitsudomi T, et al: MET amplification leads to gefitinib resistance in lung cancer by activating ERBB3 signaling. Science 316:1039-43, 2007

155. Chakravarti A, Loeffler JS, Dyson NJ: Insulin-like growth factor receptor I mediates resistance to anti-epidermal growth factor receptor therapy in primary human glioblastoma cells through continued activation of phosphoinositide 3-kinase signaling. Cancer Res 62:200-7, 2002

156. Erjala K, Sundvall M, Junttila TT, et al: Signaling via ErbB2 and ErbB3 associates with resistance and epidermal growth factor receptor (EGFR) amplification with sensitivity to EGFR inhibitor gefitinib in head and neck squamous cell carcinoma cells. Clin Cancer Res 12:4103-11, 2006

157. Pao W, Wang TY, Riely GJ, et al: KRAS mutations and primary resistance of lung adenocarcinomas to gefitinib or erlotinib. PLoS Med 2:e17, 2005

158. Jackman D, Pao W, Riely GJ, et al: Clinical definition of acquired resistance to epidermal growth factor receptor tyrosine kinase inhibitors in non-small-cell lung cancer. J Clin Oncol 28:357-60, 2010

159. Ayoola A, Barochia A, Belani K, et al: Primary and acquired resistance to epidermal growth factor receptor tyrosine kinase inhibitors in non-small cell lung cancer: an update. Cancer Invest 30:433-46, 2012

160. Eyzaguirre A, Buck E, Iwata K, et al: Mechanisms of resistance to EGFR tyrosine kinase inhibitors: implications for patient selection and drug combination strategies. Targeted oncology 3:235-243, 2008

161. Mateo J, Ong M, Yap T, et al: Opportunities and Pitfalls of Targeted Therapeutic Combinations in Solid Tumors, 2012 Education Book: Tumour biology, 2012

162. Wu YL, Lee JS, Thongprasert S, et al: Intercalated combination of chemotherapy and erlotinib for patients with advanced stage non-small-cell lung cancer (FASTACT-2): a randomised, double-blind trial. Lancet Oncol 14:777-86, 2013

163. Buck E, Eyzaguirre A, Haley JD, et al: Inactivation of Akt by the epidermal growth factor receptor inhibitor erlotinib is mediated by HER-3 in pancreatic and colorectal tumor cell lines and contributes to erlotinib sensitivity. Mol Cancer Ther 5:2051-9, 2006

164. Frolov A, Schuller K, Tzeng CW, et al: ErbB3 expression and dimerization with EGFR influence pancreatic cancer cell sensitivity to erlotinib. Cancer Biol Ther 6:548-54, 2007

165. Navas C, Hernandez-Porras I, Schuhmacher AJ, et al: EGF receptor signaling is essential for k-ras oncogene-driven pancreatic ductal adenocarcinoma. Cancer Cell 22:318-30, 2012

166. Markman B, Atzori F, Perez-Garcia J, et al: Status of PI3K inhibition and biomarker development in cancer therapeutics. Ann Oncol 21:683-91, 2010

167. Ueda S HK, Tsuda H, Ogata S et al. : Potential crosstalk between insulin-like growth factor receptor type 1 and epidermal growth factor receptor in progression and metastasis of pancreatic cancer. Modern Pathology 19:788-796, 2006

168. Hakam A, Fang Q, Karl R, et al: Coexpression of IGF-1R and c-Src proteins in human pancreatic ductal adenocarcinoma. Dig Dis Sci 48:1972-8, 2003

169. Freeman JW, Mattingly CA, Strodel WE: Increased tumorigenicity in the human pancreatic cell line MIA PaCa-2 is associated with an aberrant regulation of an IGF-1 autocrine loop and lack of expression of the TGF-beta type RII receptor. J Cell Physiol 165:155-63, 1995

170. Moser C, Schachtschneider P, Lang SA, et al: Inhibition of insulin-like growth factor-I receptor (IGF-IR) using NVP-AEW541, a small molecule kinase inhibitor, reduces orthotopic pancreatic cancer growth and angiogenesis. Eur J Cancer 44:1577-86, 2008

171. Momose I, Kunimoto S, Osono M, et al: Inhibitors of insulin-like growth factor-1 receptor tyrosine kinase are preferentially cytotoxic to nutrient-deprived pancreatic cancer cells. Biochem Biophys Res Commun 380:171-6, 2009

172. Hartog H, Wesseling J, Boezen HM, et al: The insulin-like growth factor 1 receptor in cancer: old focus, new future. Eur J Cancer 43:1895-904, 2007

173. Chi K, Gleave M, Fazli L, et al: Phase II study of preoperative figitumumab (F) in patients (pts) with localized prostate cancer (PCa). J Clin Oncol 28:15s, 2010 (suppl; abstr 4662)

174. Schmitz S, Kaminsky-Forrett MC, Henry S, et al: Phase II study of figitumumab in patients with recurrent and/or metastatic squamous cell carcinoma of the head and neck: clinical activity and molecular response (GORTEC 2008-02). Ann Oncol 23:2153-61, 2012

175. Karp DD, Paz-Ares LG, Novello S, et al: Phase II study of the anti-insulin-like growth factor type 1 receptor antibody CP-751,871 in combination with paclitaxel and carboplatin in previously untreated, locally advanced, or metastatic non-small-cell lung cancer. J Clin Oncol 27:2516-22, 2009

176. Jassem J, Langer CJ, Karp DD, et al: Randomized, open label, phase III trial of figitumumab in combination with paclitaxel and carboplatin versus paclitaxel and carboplatin in patients with non-small cell lung cancer (NSCLC). J Clin Oncol 28:15s, 2010 (suppl; abstr 7500), 2010

177. Gualberto A, Hixon ML, Karp DD, et al: Pre-treatment levels of circulating free IGF-1 identify NSCLC patients who derive clinical benefit from figitumumab. Br J Cancer 104:68-74, 2011

178. Workman P, Clarke PA, Guillard S, et al: Drugging the PI3 kinome. Nat Biotechnol 24:794-6, 2006
179. Ma J, Sawai H, Matsuo Y, et al: IGF-1 mediates PTEN suppression and enhances cell invasion and proliferation via activation of the IGF-1/PI3K/Akt signaling pathway in pancreatic cancer cells. J Surg Res 160:90-101, 2010
180. Workman P, Clarke PA, Raynaud FI, et al: Drugging the PI3 kinome: from chemical tools to drugs in the clinic. Cancer Res 70:2146-57, 2010
181. Baselga J, Campone M, Piccart M, et al: Everolimus in postmenopausal hormone-receptor-positive advanced breast cancer. N Engl J Med 366:520-9, 2012
182. Beaver JA, Park BH: The BOLERO-2 trial: the addition of everolimus to exemestane in the treatment of postmenopausal hormone receptor-positive advanced breast cancer. Future Oncol 8:651-7, 2012
183. Maira SM, Stauffer F, Brueggen J, et al: Identification and characterization of NVP-BEZ235, a new orally available dual phosphatidylinositol 3-kinase/mammalian target of rapamycin inhibitor with potent in vivo antitumor activity. Mol Cancer Ther 7:1851-63, 2008
184. Santiskulvong C, Konecny GE, Fekete M, et al: Dual targeting of phosphoinositide 3-kinase and mammalian target of rapamycin using NVP-BEZ235 as a novel therapeutic approach in human ovarian carcinoma. Clin Cancer Res 17:2373-84, 2011
185. Cho DC, Cohen MB, Panka DJ, et al: The efficacy of the novel dual PI3-kinase/mTOR inhibitor NVP-BEZ235 compared with rapamycin in renal cell carcinoma. Clin Cancer Res 16:3628-38, 2010
186. Cao P, Maira SM, Garcia-Echeverria C, et al: Activity of a novel, dual PI3-kinase/mTor inhibitor NVP-BEZ235 against primary human pancreatic cancers grown as orthotopic xenografts. Br J Cancer 100:1267-76, 2009
187. Brunner-Kubath C, Shabbir W, Saferding V, et al: The PI3 kinase/mTOR blocker NVP-BEZ235 overrides resistance against irreversible ErbB inhibitors in breast cancer cells. Breast Cancer Res Treat 129:387-400, 2011
188. Wang WJ, Long LM, Yang N, et al: NVP-BEZ235, a novel dual PI3K/mTOR inhibitor, enhances the radiosensitivity of human glioma stem cells in vitro. Acta Pharmacol Sin 34:681-90, 2013
189. McCubrey JA, Steelman LS, Abrams SL, et al: Emerging MEK inhibitors. Expert Opin Emerg Drugs 15:203-23, 2010
190. Rusconi P, Caiola E, Broggini M: RAS/RAF/MEK inhibitors in oncology. Curr Med Chem 19:1164-76, 2012
191. Chappell WH, Steelman LS, Long JM, et al: Ras/Raf/MEK/ERK and PI3K/PTEN/Akt/mTOR inhibitors: rationale and importance to inhibiting these pathways in human health. Oncotarget 2:135-64, 2011
192. Wang D, Boerner SA, Winkler JD, et al: Clinical experience of MEK inhibitors in cancer therapy. Biochim Biophys Acta 1773:1248-55, 2007
193. Solit DB, Garraway LA, Pratilas CA, et al: BRAF mutation predicts sensitivity to MEK inhibition. Nature 439:358-62, 2006
194. Hatzivassiliou G, Haling JR, Chen H, et al: Mechanism of MEK inhibition determines efficacy in mutant KRAS- versus BRAF-driven cancers. Nature 501:232-6, 2013
195. Flaherty KT, Robert C, Hersey P, et al: Improved survival with MEK inhibition in BRAF-mutated melanoma. N Engl J Med 367:107-14, 2012
196. Akinleye A, Furqan M, Mukhi N, et al: MEK and the inhibitors: from bench to bedside. J Hematol Oncol 6:27, 2013
197. LoRusso PM, Canetta R, Wagner JA, et al: Accelerating cancer therapy development: the importance of combination strategies and collaboration. Summary of an Institute of Medicine workshop. Clin Cancer Res 18:6101-9, 2012
198. Kummar S, Chen HX, Wright J, et al: Utilizing targeted cancer therapeutic agents in combination: novel approaches and urgent requirements. Nat Rev Drug Discov 9:843-56, 2010
199. Dancey JE, Chen HX: Strategies for optimizing combinations of molecularly targeted anticancer agents. Nat Rev Drug Discov 5:649-59, 2006

200. Kaelin WG, Jr.: The concept of synthetic lethality in the context of anticancer therapy. Nat Rev Cancer 5:689-98, 2005
201. Sosman JA, Puzanov I, Atkins MB: Opportunities and obstacles to combination targeted therapy in renal cell cancer. Clin Cancer Res 13:764s-769s, 2007
202. Aad G, Abbott B, Abdallah J, et al: Search for diphoton events with large missing transverse energy in 7 TeV proton-proton collisions with the ATLAS detector. Phys Rev Lett 106:121803, 2011
203. Baselga J, Cortes J, Kim SB, et al: Pertuzumab plus trastuzumab plus docetaxel for metastatic breast cancer. N Engl J Med 366:109-19, 2012
204. Hecht JR, Mitchell E, Chidiac T, et al: A randomized phase IIIB trial of chemotherapy, bevacizumab, and panitumumab compared with chemotherapy and bevacizumab alone for metastatic colorectal cancer. J Clin Oncol 27:672-80, 2009
205. Tol J, Koopman M, Cats A, et al: Chemotherapy, bevacizumab, and cetuximab in metastatic colorectal cancer. N Engl J Med 360:563-72, 2009
206. Haller DG: Cetuximab plus FOLFIRI as a first-line therapy in metastatic colorectal cancer. Community Oncology 9:302-304, 2012
207. Britten CD: PI3K and MEK inhibitor combinations: examining the evidence in selected tumor types. Cancer Chemother Pharmacol 71:1395-409, 2013
208. Sos ML, Fischer S, Ullrich R, et al: Identifying genotype-dependent efficacy of single and combined PI3K- and MAPK-pathway inhibition in cancer. Proc Natl Acad Sci U S A 106:18351-6, 2009
209. Sheikh R, Walsh N, Clynes M, et al: Challenges of drug resistance in the management of pancreatic cancer. Expert Rev Anticancer Ther 10:1647-61, 2010
210. Ritzel MW, Ng AM, Yao SY, et al: Recent molecular advances in studies of the concentrative Na+-dependent nucleoside transporter (CNT) family: identification and characterization of novel human and mouse proteins (hCNT3 and mCNT3) broadly selective for purine and pyrimidine nucleosides (system cib). Mol Membr Biol 18:65-72, 2001
211. Greenhalf W, Ghaneh P, Neoptolemos JP, et al: Pancreatic Cancer hENT1 Expression and Survival From Gemcitabine in Patients From the ESPAC-3 Trial. J Natl Cancer Inst, 2013
212. Collisson EA, Sadanandam A, Olson P, et al: Subtypes of pancreatic ductal adenocarcinoma and their differing responses to therapy. Nat Med 17:500-3, 2011
213. da Cunha Santos G, Dhani N, Tu D, et al: Molecular predictors of outcome in a phase 3 study of gemcitabine and erlotinib therapy in patients with advanced pancreatic cancer: National Cancer Institute of Canada Clinical Trials Group Study PA.3. Cancer 116:5599-607, 2010
214. Lee J, Jang KT, Ki CS, et al: Impact of epidermal growth factor receptor (EGFR) kinase mutations, EGFR gene amplifications, and KRAS mutations on survival of pancreatic adenocarcinoma. Cancer 109:1561-9, 2007
215. Oliveira-Cunha M, Hadfield KD, Siriwardena AK, et al: EGFR and KRAS mutational analysis and their correlation to survival in pancreatic and periampullary cancer. Pancreas 41:428-34, 2012
216. Pryczynicz A, Guzinska-Ustymowicz K, Kemona A, et al: Expression of EGF and EGFR strongly correlates with metastasis of pancreatic ductal carcinoma. Anticancer Res 28:1399-404, 2008
217. Nguyen Q, Perumel M, Waldman T, et al: Glucose Metabolism Measured by [18F]Fluorodeoxyglucose Positron Emission Tomography Is Independent of PTEN/AKT Status in Human Colon Carcinoma Cells. Translational Oncology 4:241-248, 2011
218. Kinross KM, Brown DV, Kleinschmidt M, et al: In vivo activity of combined PI3K/mTOR and MEK inhibition in a Kras(G12D);Pten deletion mouse model of ovarian cancer. Mol Cancer Ther 10:1440-9, 2011
219. Janku F, Tsimberidou AM, Garrido-Laguna I, et al: PIK3CA mutations in patients with advanced cancers treated with PI3K/AKT/mTOR axis inhibitors. Mol Cancer Ther 10:558-65, 2011
220. Duffy A, Kummar S: Metastatic pancreatic adenocarcinoma: current standards, future directions. Am J Ther 17:79-85, 2010

221. Tan MH, Nowak NJ, Loor R, et al: Characterization of a new primary human pancreatic tumor line. Cancer Invest 4:15-23, 1986
222. ATCC: American Type Culture Collection, 2012
223. Cullen JJ, Weydert C, Hinkhouse MM, et al: The role of manganese superoxide dismutase in the growth of pancreatic adenocarcinoma. Cancer Res 63:1297-303, 2003
224. Malicet C, Lesavre N, Vasseur S, et al: p8 inhibits the growth of human pancreatic cancer cells and its expression is induced through pathways involved in growth inhibition and repressed by factors promoting cell growth. Mol Cancer 2:37, 2003
225. Schoumacher RA, Ram J, Iannuzzi MC, et al: A cystic fibrosis pancreatic adenocarcinoma cell line. Proc Natl Acad Sci U S A 87:4012-6, 1990
226. Moore PS, Sipos B, Orlandini S, et al: Genetic profile of 22 pancreatic carcinoma cell lines. Analysis of K-ras, p53, p16 and DPC4/Smad4. Virchows Arch 439:798-802, 2001
227. Dahiya R, Kwak KS, Byrd JC, et al: Mucin synthesis and secretion in various human epithelial cancer cell lines that express the MUC-1 mucin gene. Cancer Res 53:1437-43, 1993
228. Deer EL, Gonzalez-Hernandez J, Coursen JD, et al: Phenotype and genotype of pancreatic cancer cell lines. Pancreas 39:425-35, 2010
229. Yunis AA, Arimura GK, Russin DJ: Human pancreatic carcinoma (MIA PaCa-2) in continuous culture: sensitivity to asparaginase. Int J Cancer 19:128-35, 1977
230. Fujita M, Otsuka Y, Yamada S, et al: X-ray irradiation and Rho-kinase inhibitor additively induce invasiveness of the cells of the pancreatic cancer line, MIAPaCa-2, which exhibits mesenchymal and amoeboid motility. Cancer Sci 102:792-8, 2011
231. Lieber M, Mazzetta J, Nelson-Rees W, et al: Establishment of a continuous tumor-cell line (panc-1) from a human carcinoma of the exocrine pancreas. Int J Cancer 15:741-7, 1975
232. Haque I, Mehta S, Majumder M, et al: Cyr61/CCN1 signaling is critical for epithelial-mesenchymal transition and stemness and promotes pancreatic carcinogenesis. Mol Cancer 10:8, 2011
233. MIMS Australia: Monthly Index of Medical Specialties, Australia, 2013
234. Department of Health and Aging Commonwealth of Australia: Pharmaceutical Benefits Scheme, 2013
235. Wakeling AE, Guy SP, Woodburn JR, et al: ZD1839 (Iressa): an orally active inhibitor of epidermal growth factor signaling with potential for cancer therapy. Cancer Res 62:5749-54, 2002
236. Ciardiello F, Caputo R, Bianco R, et al: Antitumor effect and potentiation of cytotoxic drugs activity in human cancer cells by ZD-1839 (Iressa), an epidermal growth factor receptor-selective tyrosine kinase inhibitor. Clin Cancer Res 6:2053-63, 2000
237. Zhou X, Zheng M, Chen F, et al: Gefitinib inhibits the proliferation of pancreatic cancer cells via cell cycle arrest. Anat Rec (Hoboken) 292:1122-7, 2009
238. Garcia-Echeverria C, Pearson MA, Marti A, et al: In vivo antitumor activity of NVP-AEW541-A novel, potent, and selective inhibitor of the IGF-IR kinase. Cancer Cell 5:231-9, 2004
239. Piao W, Wang Y, Adachi Y, et al: Insulin-like growth factor-I receptor blockade by a specific tyrosine kinase inhibitor for human gastrointestinal carcinomas. Mol Cancer Ther 7:1483-93, 2008
240. Hewish M, Chau I, Cunningham D: Insulin-like growth factor 1 receptor targeted therapeutics: novel compounds and novel treatment strategies for cancer medicine. Recent Pat Anticancer Drug Discov 4:54-72, 2009
241. Chaussade C, Rewcastle GW, Kendall JD, et al: Evidence for functional redundancy of class IA PI3K isoforms in insulin signalling. Biochem J 404:449-58, 2007
242. Semba S, Itoh N, Ito M, et al: The in vitro and in vivo effects of 2-(4-morpholinyl)-8-phenyl-chromone (LY294002), a specific inhibitor of phosphatidylinositol 3'-kinase, in human colon cancer cells. Clin Cancer Res 8:1957-63, 2002
243. Gharbi SI, Zvelebil MJ, Shuttleworth SJ, et al: Exploring the specificity of the PI3K family inhibitor LY294002. Biochem J 404:15-21, 2007
244. Hartmann W, Kuchler J, Koch A, et al: Activation of phosphatidylinositol-3'-kinase/AKT signaling is essential in hepatoblastoma survival. Clin Cancer Res 15:4538-45, 2009

245. Hu L, Zaloudek C, Mills GB, et al: In vivo and in vitro ovarian carcinoma growth inhibition by a phosphatidylinositol 3-kinase inhibitor (LY294002). Clin Cancer Res 6:880-6, 2000
246. Novartis: BYL-719: investigator's brocheure (ed 3rd), 2011
247. Dudley DT, Pang L, Decker SJ, et al: A synthetic inhibitor of the mitogen-activated protein kinase cascade. Proc Natl Acad Sci U S A 92:7686-9, 1995
248. Simon C, Juarez J, Nicolson GL, et al: Effect of PD 098059, a specific inhibitor of mitogen-activated protein kinase kinase, on urokinase expression and in vitro invasion. Cancer Res 56:5369-74, 1996
249. Dufourny B, Alblas J, van Teeffelen HA, et al: Mitogenic signaling of insulin-like growth factor I in MCF-7 human breast cancer cells requires phosphatidylinositol 3-kinase and is independent of mitogen-activated protein kinase. J Biol Chem 272:31163-71, 1997
250. Alessi DR, Cuenda A, Cohen P, et al: PD 098059 is a specific inhibitor of the activation of mitogen-activated protein kinase kinase in vitro and in vivo. J Biol Chem 270:27489-94, 1995
251. Simon C, Hicks MJ, Nemechek AJ, et al: PD 098059, an inhibitor of ERK1 activation, attenuates the in vivo invasiveness of head and neck squamous cell carcinoma. Br J Cancer 80:1412-9, 1999
252. Ghayad SE, Vendrell JA, Ben Larbi S, et al: Endocrine resistance associated with activated ErbB system in breast cancer cells is reversed by inhibiting MAPK or PI3K/Akt signaling pathways. Int J Cancer 126:545-62, 2010
253. Holcomb B, Yip-Schneider MT, Matos JM, et al: Pancreatic cancer cell genetics and signaling response to treatment correlate with efficacy of gemcitabine-based molecular targeting strategies. J Gastrointest Surg 12:288-96, 2008
254. Kim WY, Prudkin L, Feng L, et al: Epidermal growth factor receptor and K-Ras mutations and resistance of lung cancer to insulin-like growth factor 1 receptor tyrosine kinase inhibitors. Cancer, 2012
255. Zhang YJ, Tian XQ, Sun DF, et al: Combined inhibition of MEK and mTOR signaling inhibits initiation and progression of colorectal cancer. Cancer Invest 27:273-85, 2009
256. Franken NA, Rodermond HM, Stap J, et al: Clonogenic assay of cells in vitro. Nat Protoc 1:2315-9, 2006
257. Yao E, Zhou W, Lee-Hoeflich ST, et al: Suppression of HER2/HER3-mediated growth of breast cancer cells with combinations of GDC-0941 PI3K inhibitor, trastuzumab, and pertuzumab. Clin Cancer Res 15:4147-56, 2009
258. Murray JM: Methods for imaging thick specimens: confocal microscopy, deconvolution, and structured illumination. Cold Spring Harb Protoc 2011:1399-437, 2011
259. Rasmussen R: Rapid Cycle Real-Time PCR Methods and Applications. Heidelberg, Springer Press, 2001
260. Mergny JL, Lacroix L: Analysis of thermal melting curves. Oligonucleotides 13:515-37, 2003
261. Livak KJ, Schmittgen TD: Analysis of relative gene expression data using real-time quantitative PCR and the 2(-Delta Delta C(T)) Method. Methods 25:402-8, 2001
262. Karlen Y, McNair A, Perseguers S, et al: Statistical significance of quantitative PCR. BMC Bioinformatics 8:131, 2007
263. Hotz MA, Gong J, Traganos F, et al: Flow cytometric detection of apoptosis: comparison of the assays of in situ DNA degradation and chromatin changes. Cytometry 15:237-44, 1994
264. Kallioniemi OP, Visakorpi T, Holli K, et al: Automated peak detection and cell cycle analysis of flow cytometric DNA histograms. Cytometry 16:250-5, 1994
265. Best G, Peters L: Apoptosis Assay DiLC5 and PI. Flow Cytometry Core factility. Sydney, Australia, Kolling Institute, 1999
266. Wei N, Liu SS, Chan KK, et al: Tumour suppressive function and modulation of programmed cell death 4 (PDCD4) in ovarian cancer. PLoS One 7:e30311, 2012
267. Lee CH, Xue H, Sutcliffe M, et al: Establishment of subrenal capsule xenografts of primary human ovarian tumors in SCID mice: potential models. Gynecol Oncol 96:48-55, 2005

268. Dong X, Guan J, English JC, et al: Patient-derived first generation xenografts of non-small cell lung cancers: promising tools for predicting drug responses for personalized chemotherapy. Clin Cancer Res 16:1442-51, 2010
269. Euhus DM, Hudd C, LaRegina MC, et al: Tumor measurement in the nude mouse. J Surg Oncol 31:229-34, 1986
270. Tomayko MM, Reynolds CP: Determination of subcutaneous tumor size in athymic (nude) mice. Cancer Chemother Pharmacol 24:148-54, 1989
271. Lopez T, Hanahan D: Elevated levels of IGF-1 receptor convey invasive and metastatic capability in a mouse model of pancreatic islet tumorigenesis. Cancer Cell 1:339-53, 2002
272. Whitehead A, Whitehead J, Todd S, et al: Fitting models for the joint action of two drugs using SAS. Pharm Stat 7:272-84, 2008
273. Heitjan DF, Manni A, Santen RJ: Statistical analysis of in vivo tumor growth experiments. Cancer Res 53:6042-50, 1993
274. Shiao YH, Palli D, Caporaso NE, et al: Genetic and immunohistochemical analyses of p53 independently predict regional metastasis of gastric cancers. Cancer Epidemiol Biomarkers Prev 9:631-3, 2000
275. Charafe-Jauffret E, Tarpin C, Bardou VJ, et al: Immunophenotypic analysis of inflammatory breast cancers: identification of an 'inflammatory signature'. J Pathol 202:265-73, 2004
276. Mendoza MC, Er EE, Blenis J: The Ras-ERK and PI3K-mTOR pathways: cross-talk and compensation. Trends Biochem Sci 36:320-8, 2011
277. Hylander BL, Repasky EA, Gibbs J, et al: Pancreatic tumors show variable sensitivity to Erlotinib: characterization of the response of cell lines in vitro and patient derived xenografts grown in SCID mice. Proc Amer Assoc Cancer Res 46:abst 3396, 2005
278. Sylvester PW: Optimization of the tetrazolium dye (MTT) colorimetric assay for cellular growth and viability. Methods Mol Biol 716:157-68, 2011
279. Lu YY, Jing DD, Xu M, et al: Anti-tumor activity of erlotinib in the BxPC-3 pancreatic cancer cell line. World J Gastroenterol 14:5403-11, 2008
280. Durkin AJ, Bloomston PM, Rosemurgy AS, et al: Defining the role of the epidermal growth factor receptor in pancreatic cancer grown in vitro. Am J Surg 186:431-6, 2003
281. Hak AM, Offerijns FG, Verheul CC: Toxic effects of DMSO on cultured beating heart cells at temperatures above zero. Cryobiology 10:244-50, 1973
282. Turksen K: Embryonic Stem Cell Protocol. New Jersey, Humana Press, 2006 pp. 378-9
283. Maioli E, Torricelli C, Fortino V, et al: Critical appraisal of the MTT assay in the presence of rottlerin and uncouplers. Biol Proced Online 11:227-40, 2009
284. Li J, Kleeff J, Giese N, et al: Gefitinib ('Iressa', ZD1839), a selective epidermal growth factor receptor tyrosine kinase inhibitor, inhibits pancreatic cancer cell growth, invasion, and colony formation. Int J Oncol 25:203-10, 2004
285. Salomon DS, Brandt R, Ciardiello F, et al: Epidermal growth factor-related peptides and their receptors in human malignancies. Crit Rev Oncol Hematol 19:183-232, 1995
286. Perez-Plasencia C, Duenas-Gonzalez A: Can the state of cancer chemotherapy resistance be reverted by epigenetic therapy? Mol Cancer 5:27, 2006
287. Micalizzi DS, Farabaugh SM, Ford HL: Epithelial-mesenchymal transition in cancer: parallels between normal development and tumor progression. J Mammary Gland Biol Neoplasia 15:117-34, 2010
288. Xue M, Cao X, Zhong Y, et al: Insulin-like growth factor-1 receptor (IGF-1R) kinase inhibitors in cancer therapy: advances and perspectives. Curr Pharm Des 18:2901-13, 2012
289. Roudabush FL, Pierce KL, Maudsley S, et al: Transactivation of the EGF receptor mediates IGF-1-stimulated shc phosphorylation and ERK1/2 activation in COS-7 cells. J Biol Chem 275:22583-9, 2000
290. LifeTechnologies: TaqMan® Chemistry vs. SYBR® Chemistry for Real-Time PCR, 2013
291. Gudnason H, Dufva M, Bang DD, et al: Comparison of multiple DNA dyes for real-time PCR: effects of dye concentration and sequence composition on DNA amplification and melting temperature. Nucleic Acids Res 35:e127, 2007

292. Matsenko NU, Rijikova VS, Kovalenko SP: Comparison of SYBR Green I and TaqMan real-time PCR formats for the analysis of her2 gene dose in human breast tumors. Bull Exp Biol Med 145:240-4, 2008
293. Bustin SA, Benes V, Garson JA, et al: The MIQE guidelines: minimum information for publication of quantitative real-time PCR experiments. Clin Chem 55:611-22, 2009
294. Invitrogen: Real Time PCR: from Thoery to Practice. Carlifornia, Invitrogen, 2008
295. CellSignaling: PathScan® RTK Signaling Antibody Array Kit (chemiluminescent readout), 2010
296. Skorski T: BCR/ABL regulates response to DNA damage: the role in resistance to genotoxic treatment and in genomic instability. Oncogene 21:8591-8604, 2002
297. Shendure J, Ji H: Next-generation DNA sequencing. Nat Biotechnol 26:1135-45, 2008
298. Heller MJ: DNA microarray technology: devices, systems, and applications. Annu Rev Biomed Eng 4:129-53, 2002
299. Wieczorek D, Delauriere L, SchagatT: Methods of RNA Quality Assessment, Promega Corporation, 2012
300. Nishikori M: Classical and Alternative NF-kB Activation Pathways and Their Roles in Lymphoid Malignancies. Journal of Clinical Experimental Haematopathology 45:15-24, 2005
301. Park S, Zhao D, Hatanpaa KJ, et al: RIP1 activates PI3K-Akt via a dual mechanism involving NF-kappaB-mediated inhibition of the mTOR-S6K-IRS1 negative feedback loop and down-regulation of PTEN. Cancer Res 69:4107-11, 2009
302. Zhang X, Zhang L, Yang H, et al: c-Fos as a proapoptotic agent in TRAIL-induced apoptosis in prostate cancer cells. Cancer Res 67:9425-34, 2007
303. Engelman JA, Janne PA, Mermel C, et al: ErbB-3 mediates phosphoinositide 3-kinase activity in gefitinib-sensitive non-small cell lung cancer cell lines. Proc Natl Acad Sci U S A 102:3788-93, 2005
304. Lange F, Rateitschak K, Kossow C, et al: Insights into erlotinib action in pancreatic cancer cells using a combined experimental and mathematical approach. World J Gastroenterol 18:6226-34, 2012
305. Lopez-Chavez A, Carter CA, Giaccone G: The role of KRAS mutations in resistance to EGFR inhibition in the treatment of cancer. Curr Opin Investig Drugs 10:1305-14, 2009
306. Ascierto PA, Kirkwood JM, Grob JJ, et al: The role of BRAF V600 mutation in melanoma. J Transl Med 10:85, 2012
307. Yoon J, Koo KH, Choi KY: MEK1/2 inhibitors AS703026 and AZD6244 may be potential therapies for KRAS mutated colorectal cancer that is resistant to EGFR monoclonal antibody therapy. Cancer Res 71:445-53, 2011
308. Meng F, Liu L, Chin PC, et al: Akt is a downstream target of NF-kappa B. J Biol Chem 277:29674-80, 2002
309. Chang F, Lee JT, Navolanic PM, et al: Involvement of PI3K/Akt pathway in cell cycle progression, apoptosis, and neoplastic transformation: a target for cancer chemotherapy. Leukemia 17:590-603, 2003
310. Zahorowska B, Crowe PJ, Yang JL: Combined therapies for cancer: a review of EGFR-targeted monotherapy and combination treatment with other drugs. J Cancer Res Clin Oncol 135:1137-48, 2009
311. Tallarida RJ, Lamarre N, Benamar K: Combinations of drugs that produce opposite effects. International Journal of Pure and Applied Mathematics 71:415-425, 2011
312. Tallarida RJ: Drug synergism: its detection and applications. J Pharmacol Exp Ther 298:865-72, 2001
313. Chou TC: Theoretical basis, experimental design, and computerized simulation of synergism and antagonism in drug combination studies. Pharmacol Rev 58:621-81, 2006
314. Teicher BA: Tumor models for efficacy determination. Mol Cancer Ther 5:2435-43, 2006
315. Tallarida RJ: An overview of drug combination analysis with isobolograms. J Pharmacol Exp Ther 319:1-7, 2006

316. Cokol M, Chua HN, Tasan M, et al: Systematic exploration of synergistic drug pairs. Mol Syst Biol 7:544, 2011
317. Bliss CI: The toxicity of poisons applied jointly. Annals of Applied Biology 26:585–615, 1939
318. Han M, Lei JF, Tan Q, et al: Limitations of the use of MTT assay for screening in drug discovery. Journal of Chinese Pharmaceutical Sciences 19:195-200, 2010
319. Appledorn D: Live Content Imaging : Innovative Paradigm for Cell-Based Assays. Genetic Engineering & Biotechnology News 32:34, 2012
320. Zeng FY, Dong H, Cui J, et al: Glycogen synthase kinase 3 regulates PAX3-FKHR-mediated cell proliferation in human alveolar rhabdomyosarcoma cells. Biochem Biophys Res Commun 391:1049-55, 2010
321. Bruyere E, Jonckheere N, Frenois F, et al: The MUC4 membrane-bound mucin regulates esophageal cancer cell proliferation and migration properties: Implication for S100A4 protein. Biochem Biophys Res Commun 413:325-9, 2011
322. Beltran PJ, Chung YA, Moody G, et al: Efficacy of ganitumab (AMG 479), alone and in combination with rapamycin, in Ewing's and osteogenic sarcoma models. J Pharmacol Exp Ther 337:644-54, 2011
323. Nguyen KT, Zong CS, Uttamsingh S, et al: The role of phosphatidylinositol 3-kinase, rho family GTPases, and STAT3 in Ros-induced cell transformation. J Biol Chem 277:11107-15, 2002
324. Huang CY, Fong YC, Lee CY, et al: CCL5 increases lung cancer migration via PI3K, Akt and NF-kappaB pathways. Biochem Pharmacol 77:794-803, 2009
325. Gao N, Zhang Z, Jiang BH, et al: Role of PI3K/AKT/mTOR signaling in the cell cycle progression of human prostate cancer. Biochem Biophys Res Commun 310:1124-32, 2003
326. Gao N, Flynn DC, Zhang Z, et al: G1 cell cycle progression and the expression of G1 cyclins are regulated by PI3K/AKT/mTOR/p70S6K1 signaling in human ovarian cancer cells. Am J Physiol Cell Physiol 287:C281-91, 2004
327. Ormerod M: Flow Cytometry - A Basic Introduction. LA, USA, De Novo, 2008
328. Taubert G, Krug H: Flow cytometric DNA histograms and type of growth. J Cancer Res Clin Oncol 114:559-64, 1988
329. Plunkett W, Huang P, Xu YZ, et al: Gemcitabine: metabolism, mechanisms of action, and self-potentiation. Semin Oncol 22:3-10, 1995
330. Weinstein IB: Cancer. Addiction to oncogenes--the Achilles heal of cancer. Science 297:63-4, 2002
331. Ilina O, Friedl P: Mechanisms of collective cell migration at a glance. J Cell Sci 122:3203-8, 2009
332. Kerbel RS: Human tumor xenografts as predictive preclinical models for anticancer drug activity in humans: better than commonly perceived-but they can be improved. Cancer Biol Ther 2:S134-9, 2003
333. NHMRC: Australian code of practice for the care and use of animals for scientific purposes (7th edition), Australian Governement, 2004
334. Dao MA, Nolta JA: Immunodeficient mice as models of human hematopoietic stem cell engraftment. Curr Opin Immunol 11:532-7, 1999
335. Neoptolemos JP, Stocken DD, Dunn JA, et al: Influence of resection margins on survival for patients with pancreatic cancer treated by adjuvant chemoradiation and/or chemotherapy in the ESPAC-1 randomized controlled trial. Ann Surg 234:758-68, 2001
336. NHMRC: Guidelines to promote the wellbeing of animals used for scientific purposes The assessment and alleviation of pain and distress in research animals, Australian Government, 2008
337. Ito M, Hiramatsu H, Kobayashi K, et al: NOD/SCID/gamma(c)(null) mouse: an excellent recipient mouse model for engraftment of human cells. Blood 100:3175-82, 2002
338. Wang Y, Revelo MP, Sudilovsky D, et al: Development and characterization of efficient xenograft models for benign and malignant human prostate tissue. Prostate 64:149-59, 2005
339. Jin K, Teng L, Shen Y, et al: Patient-derived human tumour tissue xenografts in immunodeficient mice: a systematic review. Clin Transl Oncol 12:473-80, 2010

340. Presnell SC, Werdin ES, Maygarden S, et al: Establishment of short-term primary human prostate xenografts for the study of prostate biology and cancer. Am J Pathol 159:855-60, 2001
341. EMA: Assessment report of Tarceva, European Medicines Agency 2010
342. Jimeno A, Feldmann G, Suarez-Gauthier A, et al: A direct pancreatic cancer xenograft model as a platform for cancer stem cell therapeutic development. Mol Cancer Ther 8:310-4, 2009
343. Baker CH, Trevino JG, Summy JM, et al: Inhibition of PDGFR phosphorylation and Src and Akt activity by GN963 leads to therapy of human pancreatic cancer growing orthotopically in nude mice. Int J Oncol 29:125-38, 2006
344. Oregon: ORAL GAVAGE IN MICE AND RATS, Laboratory Animal Resources Center, Oregon University, 2011
345. Shimizu S, Hirota J: Chapter 5.2: Routes of Administration, in Hedrich H, Bullock G (eds): The Laboratory Mouse. London, Elsevier, 2012
346. Chu P, Wu E, Weiss LM: Cytokeratin 7 and cytokeratin 20 expression in epithelial neoplasms: a survey of 435 cases. Mod Pathol 13:962-72, 2000
347. Bryan WR: Quantitative studies on the latent period of tumors induced with subcutaneous injections of the agent of chicken tumor I; estimation of the latent period. J Natl Cancer Inst 6:373-7, 1946
348. Jin K, He K, Han N, et al: Establishment of a PDTT xenograft model of gastric carcinoma and its application in personalized therapeutic regimen selection. Hepatogastroenterology 58:1814-22, 2011
349. Jin K, Li G, Cui B, et al: Assessment of a novel VEGF targeted agent using patient-derived tumor tissue xenograft models of colon carcinoma with lymphatic and hepatic metastases. PLoS One 6:e28384, 2011
350. Nishimura R, Osako T, Okumura Y, et al: Clinical significance of Ki-67 in neoadjuvant chemotherapy for primary breast cancer as a predictor for chemosensitivity and for prognosis. Breast Cancer 17:269-75, 2010
351. Albert JM, Cao C, Kim KW, et al: Inhibition of poly(ADP-ribose) polymerase enhances cell death and improves tumor growth delay in irradiated lung cancer models. Clin Cancer Res 13:3033-42, 2007
352. Jax: Body Weight information: NOD-CB17-SCID: The Jackson Laboratory, 2013
353. Sangai T, Akcakanat A, Chen H, et al: Biomarkers of response to Akt inhibitor MK-2206 in breast cancer. Clin Cancer Res 18:5816-28, 2012
354. Radhakrishnan P, Baraneedharan U, Veluchamy S, et al: Inhibition of rapamycin-induced AKT activation elicits differential antitumor response in head and neck cancers. Cancer Res 73:1118-27, 2013
355. Kirkegaard T, Witton CJ, Edwards J, et al: Molecular alterations in AKT1, AKT2 and AKT3 detected in breast and prostatic cancer by FISH. Histopathology 56:203-11, 2010
356. Ross JS: Breast cancer biomarkers and HER2 testing after 10 years of anti-HER2 therapy. Drug News Perspect 22:93-106, 2009
357. Duffy MJ, Lamerz R, Haglund C, et al: Tumor markers in colorectal cancer, gastric cancer and gastrointestinal stromal cancers: European group on tumor markers (EGTM) 2013 guidelines update. Int J Cancer, 2013
358. Roengvoraphoj M, Tsongalis GJ, Dragnev KH, et al: Epidermal growth factor receptor tyrosine kinase inhibitors as initial therapy for non-small cell lung cancer: Focus on epidermal growth factor receptor mutation testing and mutation-positive patients. Cancer Treat Rev, 2013
359. Bartlett JM: Biomarkers and patient selection for PI3K/Akt/mTOR targeted therapies: current status and future directions. Clin Breast Cancer 10 Suppl 3:S86-95, 2010
360. Esteva FJ, Guo H, Zhang S, et al: PTEN, PIK3CA, p-AKT, and p-p70S6K status: association with trastuzumab response and survival in patients with HER2-positive metastatic breast cancer. Am J Pathol 177:1647-56, 2010
361. Al-Bazz YO, Underwood JC, Brown BL, et al: Prognostic significance of Akt, phospho-Akt and BAD expression in primary breast cancer. Eur J Cancer 45:694-704, 2009

362. Mazieres J, Brugger W, Cappuzzo F, et al: Evaluation of EGFR protein expression by immunohistochemistry using H-score and the magnification rule: Re-analysis of the SATURN study. Lung Cancer 82:231-7, 2013
363. Eisenhauer EA, Therasse P, Bogaerts J, et al: New response evaluation criteria in solid tumours: revised RECIST guideline (version 1.1). Eur J Cancer 45:228-47, 2009
364. Politi K, Fan PD, Shen R, et al: Erlotinib resistance in mouse models of epidermal growth factor receptor-induced lung adenocarcinoma. Dis Model Mech 3:111-9, 2010
365. Gammon S, Leevy W, Loechner M: Carestream Molecular Imaging: imaging of cancer biology and relevant pathways in-vivo. Nature Methods 6, 2009
366. Pizzonia J, Holmberg J, Orton S, et al: Multimodality animal rotation imaging system (Mars) for in vivo detection of intraperitoneal tumors. Am J Reprod Immunol 67:84-90, 2012
367. Tentler JJ, Tan AC, Weekes CD, et al: Patient-derived tumour xenografts as models for oncology drug development. Nat Rev Clin Oncol 9:338-50, 2012
368. Siolas D, Hannon GJ: Patient-derived tumor xenografts: transforming clinical samples into mouse models. Cancer Res 73:5315-9, 2013
369. Gown AM: Current issues in ER and HER2 testing by IHC in breast cancer. Mod Pathol 21 Suppl 2:S8-S15, 2008
370. Shousha S: Oestrogen receptor status of breast carcinoma: Allred/H score conversion table. Histopathology 53:346-7, 2008
371. Casneuf VF, Fonteyne P, Van Damme N, et al: Expression of SGLT1, Bcl-2 and p53 in primary pancreatic cancer related to survival. Cancer Invest 26:852-9, 2008
372. Von Hoff DD, Kim B: Vismodegib Blocks Hedgehog-Expressing Pancreatic Cancer in Mahoney D (ed): The Oncology Report, 2012
373. Saini KS, Loi S, de Azambuja E, et al: Targeting the PI3K/AKT/mTOR and Raf/MEK/ERK pathways in the treatment of breast cancer. Cancer Treat Rev, 2013
374. Gualberto A: Figitumumab (CP-751,871) for cancer therapy. Expert Opin Biol Ther 10:575-85, 2010
375. Kaulfuss S, Burfeind P, Gaedcke J, et al: Dual silencing of insulin-like growth factor-I receptor and epidermal growth factor receptor in colorectal cancer cells is associated with decreased proliferation and enhanced apoptosis. Mol Cancer Ther 8:821-33, 2009
376. Zhou X, Yuan Y, Song J, et al: Dual silencing of epidermal growth factor and insulin-like growth factor 1 receptors significantly limits growth of nasopharyngeal carcinoma in nude mice. J Laryngol Otol 123:208-22, 2009
377. Cohen BD, Baker DA, Soderstrom C, et al: Combination therapy enhances the inhibition of tumor growth with the fully human anti-type 1 insulin-like growth factor receptor monoclonal antibody CP-751,871. Clin Cancer Res 11:2063-73, 2005
378. Ii M, Li H, Adachi Y, et al: The efficacy of IGF-I receptor monoclonal antibody against human gastrointestinal carcinomas is independent of k-ras mutation status. Clin Cancer Res 17:5048-59, 2011
379. Kwon J, Stephan S, Mukhopadhyay A, et al: Insulin receptor substrate-2 mediated insulin-like growth factor-I receptor overexpression in pancreatic adenocarcinoma through protein kinase Cdelta. Cancer Res 69:1350-7, 2009
380. Tomizawa M, Shinozaki F, Sugiyama T, et al: Insulin-like growth factor-I receptor in proliferation and motility of pancreatic cancer. World J Gastroenterol 16:1854-8, 2010
381. Wynes MW, Ekman S, Asuncion BR, et al: Insulin-like growth factor 1 (IGF-1R) protein expression (PE) and gene copy number (GCN) for discrimination of response and outcome to figitumumab in NSCLC. J Clin Oncol 30, 2012 (suppl; abstr 7597), 2012
382. Ueda S, Ogata S, Tsuda H, et al: The correlation between cytoplasmic overexpression of epidermal growth factor receptor and tumor aggressiveness: poor prognosis in patients with pancreatic ductal adenocarcinoma. Pancreas 29:e1-8, 2004
383. Larue L, Bellacosa A: Epithelial-mesenchymal transition in development and cancer: role of phosphatidylinositol 3' kinase/AKT pathways. Oncogene 24:7443-54, 2005
384. Furet P, Guagnano V, Fairhurst RA, et al: Discovery of NVP-BYL719 a potent and selective phosphatidylinositol-3 kinase alpha inhibitor selected for clinical evaluation. Bioorg Med Chem Lett 23:3741-8, 2013

385. Foster FM, Traer CJ, Abraham SM, et al: The phosphoinositide (PI) 3-kinase family. J Cell Sci 116:3037-40, 2003
386. Castellano E, Downward J: RAS Interaction with PI3K: More Than Just Another Effector Pathway. Genes Cancer 2:261-74, 2011
387. Wee S, Jagani Z, Xiang KX, et al: PI3K pathway activation mediates resistance to MEK inhibitors in KRAS mutant cancers. Cancer Res 69:4286-93, 2009
388. Chapman PB, Hauschild A, Robert C, et al: Improved survival with vemurafenib in melanoma with BRAF V600E mutation. N Engl J Med 364:2507-16, 2011
389. Weinstein IB, Joe AK: Mechanisms of disease: Oncogene addiction--a rationale for molecular targeting in cancer therapy. Nat Clin Pract Oncol 3:448-57, 2006
390. Hanawa M, Suzuki S, Dobashi Y, et al: EGFR protein overexpression and gene amplification in squamous cell carcinomas of the esophagus. Int J Cancer 118:1173-80, 2006
391. Yang YL, Xu KL, Zhou Y, et al: Correlation of epidermal growth factor receptor overexpression with increased epidermal growth factor receptor gene copy number in esophageal squamous cell carcinomas. Chin Med J (Engl) 125:450-4, 2012
392. Bellacosa A, de Feo D, Godwin AK, et al: Molecular alterations of the AKT2 oncogene in ovarian and breast carcinomas. Int J Cancer 64:280-5, 1995
393. Ruggeri BA, Huang L, Wood M, et al: Amplification and overexpression of the AKT2 oncogene in a subset of human pancreatic ductal adenocarcinomas. Mol Carcinog 21:81-6, 1998
394. Wang HL, Lopategui J, Amin MB, et al: KRAS mutation testing in human cancers: The pathologist's role in the era of personalized medicine. Adv Anat Pathol 17:23-32, 2010
395. Yount S, Cella D, Webster K, et al: Assessment of patient-reported clinical outcome in pancreatic and other hepatobiliary cancers: the FACT Hepatobiliary Symptom Index. J Pain Symptom Manage 24:32-44, 2002
396. Cella D, Butt Z, Kindler HL, et al: Validity of the FACT Hepatobiliary (FACT-Hep) questionnaire for assessing disease-related symptoms and health-related quality of life in patients with metastatic pancreatic cancer. Qual Life Res 22:1105-12, 2013
397. Heffernan N, Cella D, Webster K, et al: Measuring health-related quality of life in patients with hepatobiliary cancers: the functional assessment of cancer therapy-hepatobiliary questionnaire. J Clin Oncol 20:2229-39, 2002
398. Li J, Merl MY, Saif MW: Any second-line therapy for advanced pancreatic cancer? Highlights from the "2010 ASCO Gastrointestinal Cancers Symposium". Orlando, FL, USA. January 22-24, 2010. JOP 11:151-3, 2010